AD-A133 310 BEAM PROPAGATION EXPERIMENTAL STUDY(U) MISSION RESEARCH 1/
CORP ALBUQUERQUE NM R J ADLER ET AL. APR 83 AMRC-R-466
AFOSR-TR-83-0743 F49620-81-C-0016

UNCLASSIFIED F/G 20/7 NL

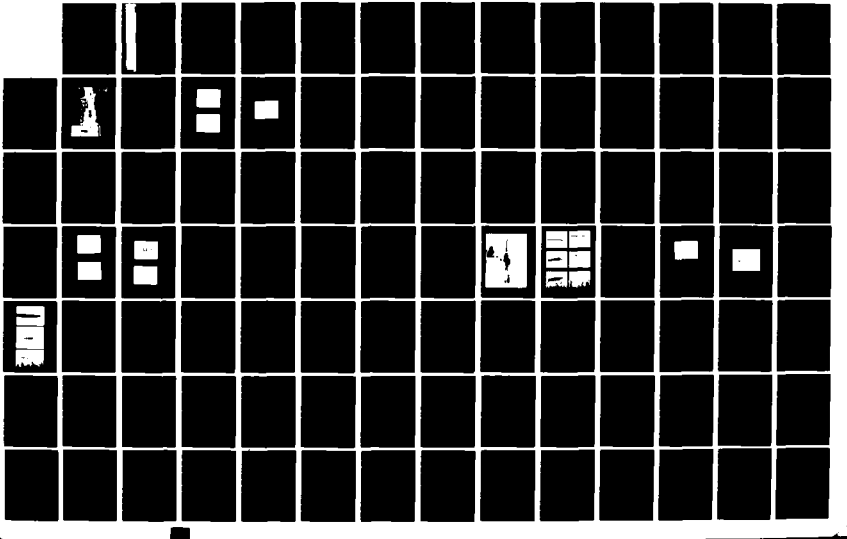

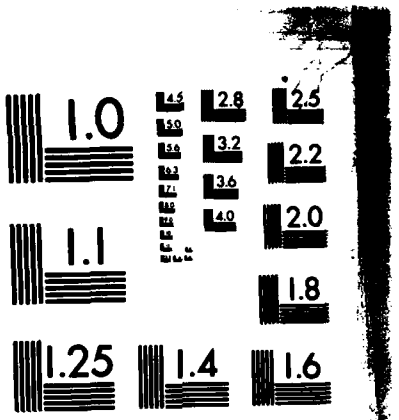

AMRC-R-466
Copy 5

FINAL REPORT

BEAM PROPAGATION EXPERIMENTAL STUDY

R. J. Adler
G. F. Kiuttu
B. A. Sabol
W. Bostick
C. A. Ekdahl
L. A. Wright
B. B. Godfrey
T. P. Hughes
N. F. Roderick
D. J. Sullivan

April 1983

Prepared for: Air Force Office of Scientific Research
Physics Directorate
Bolling Air Force Base
Washington, DC 20332

Under Contract: F49620-81-C-0016

Prepared by: MISSION RESEARCH CORPORATION
1720 Randolph Road S.E.
Albuquerque, New Mexico 87106

Research sponsored by the Air Force Office of Scientific Research (AFSC), under contract F49620-81-C-0016. The United States Government is authorized to reproduce and distribute reprints for governmental purposes notwithstanding any copyright notation herein.

DISCLAIMER NOTICE

THIS DOCUMENT IS BEST QUALITY PRACTICABLE. THE COPY FURNISHED TO DTIC CONTAINED A SIGNIFICANT NUMBER OF PAGES WHICH DO NOT REPRODUCE LEGIBLY.

UNCLASSIFIED

SECURITY CLASSIFICATION OF THIS PAGE (When Data Entered)

REPORT DOCUMENTATION PAGE		READ INSTRUCTIONS BEFORE COMPLETING FORM
1. REPORT NUMBER AFOSR-TR- 83-0743	2. GOVT ACCESSION NO.	3. RECIPIENT'S CATALOG NUMBER
4. TITLE (and Subtitle) BEAM PROPAGATION EXPERIMENTAL STUDY		5. TYPE OF REPORT & PERIOD COVERED Final Report
		6. PERFORMING ORG. REPORT NUMBER AMRC-R-466
7. AUTHOR(s) R. J. Adler, W. Bostick, B. B. Godfrey, G. F. Kiuttu, C. A. Ekdahl, T. P. Hughes, B. A. Sabol, L. A. Wright, N. F. Roderick, D. J. Sullivan		8. CONTRACT OR GRANT NUMBER(s) F49620-81-C-0016
9. PERFORMING ORGANIZATION NAME AND ADDRESS Mission Research Corporation 1720 Randolph Road, S.E. Albuquerque, New Mexico 87106		10. PROGRAM ELEMENT, PROJECT, TASK AREA & WORK UNIT NUMBERS 61102F 2301/A7
11. CONTROLLING OFFICE NAME AND ADDRESS Air Force Office of Scientific Research Physics Directorate Bolling AFB, Washington, D.C. 20332		12. REPORT DATE April 1983
		13. NUMBER OF PAGES 209
14. MONITORING AGENCY NAME & ADDRESS(if different from Controlling Office)		15. SECURITY CLASS (of this report) Unclassified
		15a. DECLASSIFICATION DOWNGRADING SCHEDULE

16. DISTRIBUTION STATEMENT (of this Report)

Approved for Public Release; Distribution Unlimited.

17. DISTRIBUTION STATEMENT (of the abstract entered in Block 20, if different from Report)

18. SUPPLEMENTARY NOTES

19. KEY WORDS (Continue on reverse side if necessary and identify by block number)

Electron Beams
Beam Propagation
Resistive Hose Instability
Electron Beam Erosion
Plasma Conductivity

20. ABSTRACT (Continue on reverse side if necessary and identify by block number)

A program of extensively diagnosed experiments to investigate the physics of intense relativistic electron beam propagation in air has been performed using beam generators at the Air Force Weapons Laboratory. The primary objectives of this research were to measure the rate of erosion of the head of the beam, and to investigate resistive instabilities, such as the hose and hollowing modes, that limit the transport of beam energy over significant distances.

DD FORM 1 JAN 73 1473 EDITION OF 1 NOV 65 IS OBSOLETE

UNCLASSIFIED

SECURITY CLASSIFICATION OF THIS PAGE (When Data Entered)

Block 20 Concluded.

The first year tasks of delineating the pressure range for maximum energy transport and measuring the temporal evolution of the current density profile were accomplished on the FX-100 and FX-25 accelerators. Maximum energy transport (measured calorimetrically) of the FX-100 beam (~1.5 MeV, ~40 kA, 120 ns) occurred at 0.3-0.5-Torr air pressure. This air-pressure window for maximum energy transport was defined by loss of the tail of the beam at high pressures and by erosion of the beam head at low pressures. Propagation in the window was characterized by a high degree of current neutralization (~80% or more), by intense light emission, suggestive of strong avalanche breakdown, and by the onset of a virulent hollowing instability that resulted in as much as 80% of the beam current being carried in a thin annular shell at a radius about twice the Bennett radius characterizing the initially injected current distribution. Space- and time-resolved measurements of the current distribution with a fast-risetime subminiature charge collector array showed that the thin-shell hollowing instability developed late (~20 ns or more) into the beam pulse. Spectroscopic measurements of the visible emission suggest that the air near the axis of the beam may have been hotter and more highly ionized in this pressure regime, which may have resulted in a conductivity profile more centrally concentrated than that of the beam.

The second year tasks of investigating nose erosion and the hose instability were performed on the 1 MeV, 25 kA VISHNU accelerator. A low pressure beam preparation (conditioning) cell was used to reduce the level of transverse beam perturbations. Best operation (lowest transverse displacement) was found at 0.7 Torr and in this mode, propagation of a 5-6 kA beam was studied. Beam characterization measurements showed that the 1.0 cm radius beam propagated in a well-confined pinch over the first 25 cm. Plasma monopole decay times over this distance were measured and peak decay times were found to be in the range 20-90 nanoseconds over the pressure range 630-5 Torr. Nose erosion was measured and was found to be extremely nonuniform. Beam front velocities were found to be as low as ~0.30 v ($v \cong 0.9$ c is the electron streaming velocity) were observed over the first 50 cm with velocities increasing up to 0.85 v over a 1.3 m propagation distance.

Hose instability measurements on the beam indicated that both frequencies and growth rates were in good agreement with present models. A correlation between hose frequency and measured dipole decay time was found as $f \sim 0.14/\tau_D$ where τ_D was the measured dipole decay time. Measurements also indicate that over ~1.5 m propagation distance the beam nose can become unstable resulting in zero energy propagation.

Simulations performed at 630 Torr showed good agreement with experiments.

ACKNOWLEDGEMENTS

The authors would like to thank Tom Montoya for careful and patient work in setup and operation of the experiments. The experiments would not have been possible without the continuous cooperation and support of AFWL personnel including M. C. Clark, J. Clifford, D. C. Straw, and R. L. Copeland. We also thank R. B. Miller and M. G. Mazzarakis for useful discussions. Finally, we thank Sid Putnam for his continuous advice on beam characterization.

EXECUTIVE SUMMARY

Directed energy weapons have the potential to revolutionize modern warfare and greatly affect national defense policies. The application of high-energy particle beams as directed energy weapons is particularly promising because of their ability to penetrate targets. The realization of this concept is dependent on the solution of major technical issues in the areas of pulse power, particle accelerators and beam-target interactions.[1] These technical problems can probably be overcome with the expenditure of sufficient technical effort.

The physics of beam propagation may, however, prevent delivery of sufficient energy over the distances required to make beams practical as weapons. Endoatmospheric propagation remains a key issue that may not yield to a massive research effort. Basic physics questions about the growth rates and nature of instabilities encountered during beam pulse transmission through the atmosphere remain unresolved. The complexity of beam propagation physics and air chemistry makes the prediction of beam behavior difficult. Theoretical analysis has used broad assumptions regarding the beam current distribution and plasma channel evolution and equilibrium in order to make the problem more tractable.[2-5] Clearly, the issue of propagation will not be fully resolved until full-scale experiments with accelerators having weapons-grade parameters are performed. It is also clear that one cannot wait for the advent of such experiments, because beam propagation will have a significant role in determining the optimal weapon accelerator parameters. It is desirable, therefore, to address the scaling of propagation phenomena with beam parameters by conducting experiments using presently available accelerators.

With this goal in mind, Mission Research Corporation has performed a detailed study of beam propagation phenomena. In our two year study, we have investigated a variety of significant propagation phenomena, including

the hose[2,3] and hollowing effects,[4,5] net energy transport, plasma response to the electron beam, evolution of the beam nose,[6] time dependent plasma optical emission, beam conditioning, and beam RF emission.[7] Particular emphasis has been placed on the effect of beam nose evolution on the hose instability, and the effect of this interaction on general propagation physics. First year studies were performed on the FX-100 and FX-25 accelerators. When both of these machines were removed, experiments continued on the VISHNU accelerator once it became operational.

Diagnostics and equipment used during the experiment are outlined in Sec. I. New diagnostics and techniques implemented include radial 'penny probes' for beam front velocity determination, miniature Faraday cup arrays for time-resolved beam profile measurements, a triangle detector to monitor beam hollowing and hose behavior, and a technique to infer plasma current decay rates.

First year experiments addressed fundamentals such as propagation windows, beam profile evolution, and optical emission. The second year experiments concentrated on propagation in a large diameter cell, and included the fast-rise and nose-coupled hose instability experiments. In November, experiments using the 4.5 cm conditioning cell began, and detailed hose, plasma decay time, radial probe, and nose-hose experiments continued (often in two shifts) until the end of February 1983.

The first task performed was determination of the stable propagation pressure window of the FX-100 electron beam. In general, the window was found between 0.3 and 0.6 Torr in air for a 3 m propagation distance. This result is in good agreement with the accepted phenomenology of beam propagation. At very low pressures, the beam front velocity is limited by the rate at which the gas can be ionized. The first portion of the beam is lost due to radial electric fields, reducing the transported beam energy. Above 0.6 Torr, particle loss occurs due to the resistive hose instability,

and possibly a hollowing instability late in time. While the hose instability is a definite cause of energy loss, the hollowing effect appears to produce a hollow but stable beam with an outer current shell.

Beam distribution evolution was studied using the FX-25. At the anode foil the beam distribution was found to be well defined with a sharp outer cutoff. Both anode foil scattering (16° RMS) and phase mixing contributed to the beam evolution to a 1 cm radius Bennett profile at 3 m from the diode. The difference in the propagation window pressure between the various experiments is noteworthy--for the FX-25 beam in a 5 cm drift tube the pressure was 1.6 Torr, for the FX-100 it was 0.5 Torr, and for VISHNU it was 1.0 Torr--approximately inversely proportional to pulse length. The FX-100 and FX-25 data are presented in Appendix A.

The initial set of VISHNU experiments (Sec. II) investigated propagation in a large cell after conditioning in a smaller drift tube. Energy transport measurements were made to define the propagation window, and the nose-coupled hose effect was observed. Observation of this effect was made with Faraday cups, calorimetry, and open shutter photography. Further measurements also demonstrated the deleterious effect of beam mismatch on the injection process.

Nose erosion studies were performed as a necessary adjunct to the nose-hose coupling studies. The beam front velocity was measured and was found to be spatially nonuniform--low near the injection point, and increasing to near the beam velocity as propagation continued. This effect contributes to one of the more important effects we observed--a 1 ns beam risetime. Our present understanding is that the onset of the fast beam front propagation can be exceedingly rapid, leading to fast beam rise times.

After the initial survey, a detailed set of runs was made with a 'conditioned' electron beam. A total of approximately 20 kA was injected into a small tube which acted to center the beam. Phase mixing resulted in damping of transverse motion, and particle losses resulted in a final current of approximately 5 kA. The optimum point for conditioning cell operation was found to be approximately 0.70 Torr. This value of conditioning cell pressure was used almost exclusively for subsequent experiments.

The initial beam state was characterized in several ways at an axial position 25 cm beyond the end of the conditioning cell. In particular, the radial profile was measured using a 7-port Faraday cup array, and detailed plasma decay time measurements were performed. The Faraday cup data exhibited hose-type motion for higher pressures. These measurements are presented in Sec. III. In general, the beam has a 1 cm radius Bennett-type profile at this axial position.

Measurements of beam hose growth using $\dot{B}$ probes were made with the same beam parameters as the characterization measurements (Sec. IV). These measurements are in good qualitative agreement with present hose theories. The hose oscillation frequency is observed to decrease with time into the pulse, consistent with the observed increase in decay time. It varies from 15 MHz or less for 10 Torr to of order 100 MHz in the body of a 230 Torr shot. Typical hose instability growth lengths are found to be approximately 15 cm at 10-20 Torr. Note that the betatron wavelength was approximately 10-15 cm for our parameters. Faraday cup array displacements were also consistent with < 1 cm displacements at an axial position of 25 cm--within a factor of two of the magnetic probe data results. An important hose parameter--the relative motion of the beam and magnetic axes--has also been observed.

Studies of this beam after injection into the large propagation tank are also is discussed in Sec. IV. A novel 'triangular' detector was used to measure beam parameters--both the hollowing and hose effects were

observed using this diagnostic. The hollowing and hose instabilities were sometimes observed simultaneously below 100 Torr. Beam nose evolution was also studied in detail in this configuration. After 1.2 m of propagation, beam head transverse motion is severe and the beam is considered to be nose-hose *unstable*. The time duration of the beam head on the detector decreased with axial position, demonstrating the development of the hose-hose effects due to erosion.

Several other measurement series were performed. Radial electron collector results indicate the existence of an unexplained radial current loss. Potentially, the most important result of the study is the observation of hose stable beam propagation in full pressure air for a rotating beam.

Other topics are discussed in the appendices, including the FX-100 experiments, channel temperature measurements, considerations for design of a transverse beam perturbation device or "tickler", beam dynamics in the small Faraday cup collectors, and optical diagnostics considerations.

In general, we conclude that at least one nose-hose coupling effect exists. It is found to be associated with slow propagation near the beam injection point. This results in matching of the nose velocity and the hose convection velocity. Transverse position monitor measurements indicate that the hose instability frequency is in agreement with the usual models[2] [3] in the body of the beam. We find that $f = .13\ \tau_d$ where f is the hose frequency, and τ_d is the dipole decay time.

CONTENTS

Section		Page
	EXECUTIVE SUMMARY	ii
I	FACILITIES AND DIAGNOSTICS	1
	A. FACILITIES	1
	B. DIAGNOSTICS	7
II	INITIAL MEASUREMENTS	28
	A. CONDITIONING	28
	B. LARGE CELL OBSERVATIONS	35
	C. BEAM BLOW-UP OBSERVATIONS	39
III	BEAM CHARACTERIZATION	45
	A. TRANSVERSE MOTION	45
	B. BEAM PROFILE	45
	C. PLASMA DECAY TIME	62
IV	NOSE EROSION AND HOSE RESULTS	69
	A. BEAM FRONT MEASUREMENTS	69
	B. HOSE STUDIES	76
	C. NOSE-HOSE DEVELOPMENT	87
V	NUMERICAL SIMULATIONS OF ELECTRON BEAM HOLLOWING AND NOSE EROSION IN LOW DENSITY AIR	96
VI	CONCLUSIONS	108
	REFERENCES	109

CONTENTS (Continued)

Appendices

APPENDIX A - FX-100 and FX-25 EXPERIMENTS

APPENDIX B - OPTICAL EMISSIONS FROM INTENSE RELATIVISTIC ELECTRON BEAM EXCITED AIR

APPENDIX C - CHANNEL TEMPERATURE DETERMINATION

APPENDIX D - TICKLER ANALYSIS

APPENDIX E - PARTICLE SIMULATIONS OF FX-100 BEAM PROPAGATION AND COMPARISON WITH EXPERIMENT

APPENDIX F - ELECTRON BEAM TRANSPORT IN A SMALL APERTURE FARADAY CUP

APPENDIX G - MONTE CARLO ELECTRON BEAM TRANSPORT IN AIR

I. FACILITIES AND DIAGNOSTICS

A. FACILITIES

The VISHNU Accelerator is a reconditioned Physics International Pulserad 415 flash X-radiography accelerator. From the 1960's until 1976, it was used for various pulsed high voltage projects such as Kerr optical effect measurements, and ion diode design studies. In early 1981, the decision to reactivate the machine for intense electron beam vacuum propagation studes was made.

The diode, main switch and insulator were lost during the storage period, so a new diode was designed by R. Adler of MRC and H. Ives, then of AFWL. J. Thorne of AFWL took charge of turning building 910 from a storage area into a laboratory facility. In the spring of 1982, R. Copeland of AFWL reconfigured the Marx generator and designed a new trigger system for the accelerator. Successful operation of the accelerator began in June of 1982 when the inner transmission line was hung from nylon rods. Diode diagnostics were implemented that same month by R. Adler and G. Kiuttu of MRC. Diode prepulse, the last remaining difficulty in machine operation, was eliminated using shunt resistors in July of 1982.

The first experiments using the rebuilt accelerator were performed by R. Adler, G. Kiuttu, and B. Sabol in the area of rotating beam propagation. These experiments ended in September when hardware for the large propagation chamber, which was designed in June, became available and AFOSR supported propagation experiments began.

A photograph of the machine front end and the large propagation cell is shown in Fig. 1.

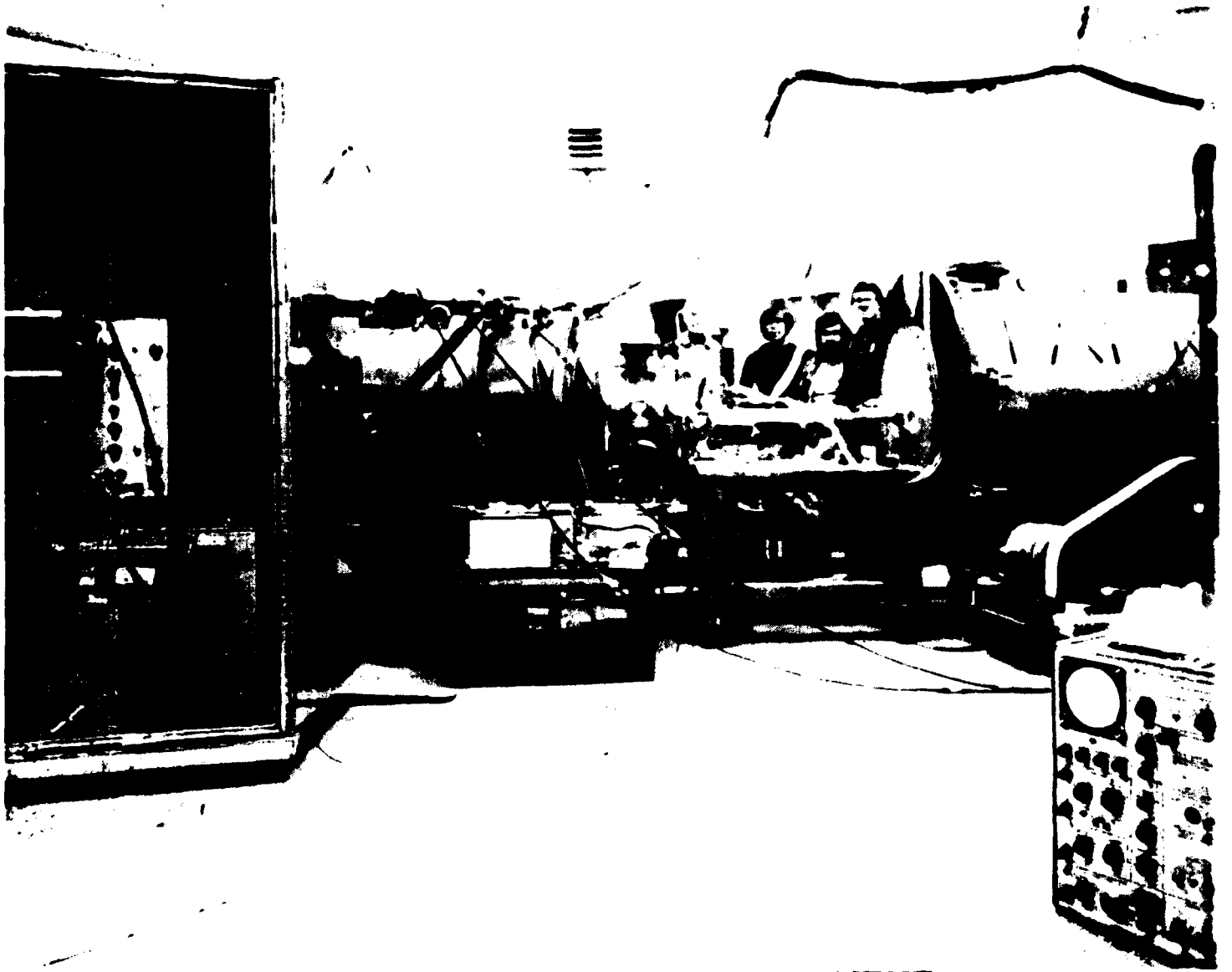

VISHNU PROPAGATION EXPERIMENT

Figure 1. The accelerator front end is shown on the left with the large propagation cell on the right. The conditioning cell and experimental team (except Gerry Kiuttu who took the picture) are shown in the center.

i) VISHNU

Typical VISHNU voltage and current waveforms are shown in Fig. 2. The diode impedance of 30-40 Ω was much greater than the 10 Ω line impedance resulting in a step-type exponential voltage characteristic for t > 40 ns. Reproducibility was excellent for the first 75 nanoseconds of the pulse as shown for the 8-shot diode voltage overlay of Fig. 3. (Note that the jitter later in the pulse is due to diode flashover, which was usually corrected by cleaning the diode as in the shot of Fig. 2.)

The machine prepulse voltage was negligible due to the implementation of resistors shunting the diode capacitance. The machine operated without serious breakdowns during the experimental run. Routine maintenance consisted of cleaning the diode insulator approximately once every 100 shots. The diode vacuum was typically maintained below 10^{-4} Torr.

A schematic of the electron beam diode is shown in Fig. 4. A 3.1 cm diameter flat carbon disc was used as the cathode and centered to within 1 mm using a ball joint 30 cm back along the shank. Kapton foils coated with Aerodag were used for the anode. Later in the experiments, the foil changer shown in Fig. 4 was implemented. Thus, foils destroyed by beam damage could be replaced rapidly. The foil changer works reliably, and is perhaps one of the least expensive ($800 including design, machining, materials, welding and personnel salaries and overhead) ever built.

ii) Large Propagation Cell

The large cell was 2.2 m in length, 1.2 m in diameter, and had a 15 cm wide lucite window along the side. This window was covered with screen to make the electrical path complete. It was connected to a 10 cm radius drift tube preceded by either a 4.5 cm I.D. conditioning cell, or further 10 cm radius tubes and could be evacuated to as low as 0.060 Torr with available pumping. It is shown on the right hand side of Fig. 1.

DIODE VOLTAGE 1.2 MV/cm

DIODE CURRENT 53 ka/cm

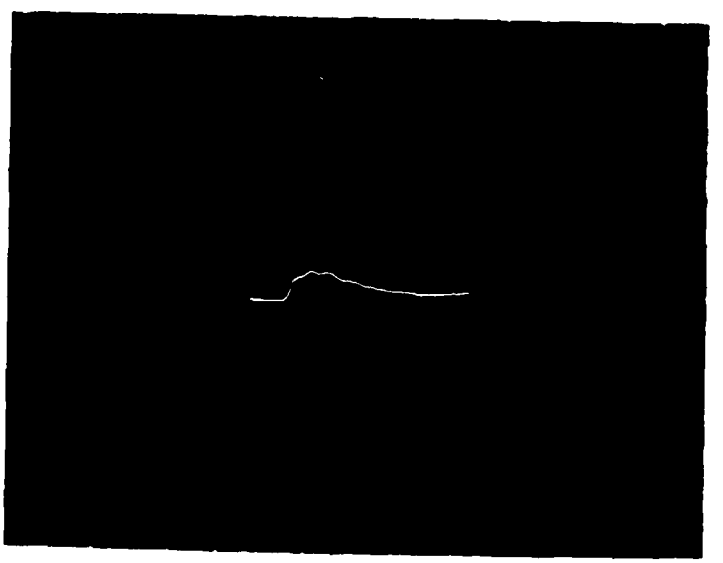

80 ns/cm

Figure 2. Typical VISHNU diode voltage and current waveforms.

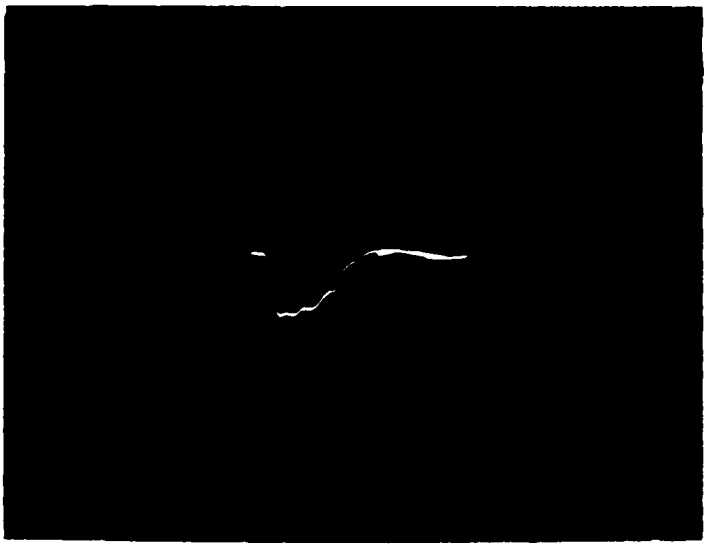

Figure 3. 8 shot overlay of VISHNU diode voltage.

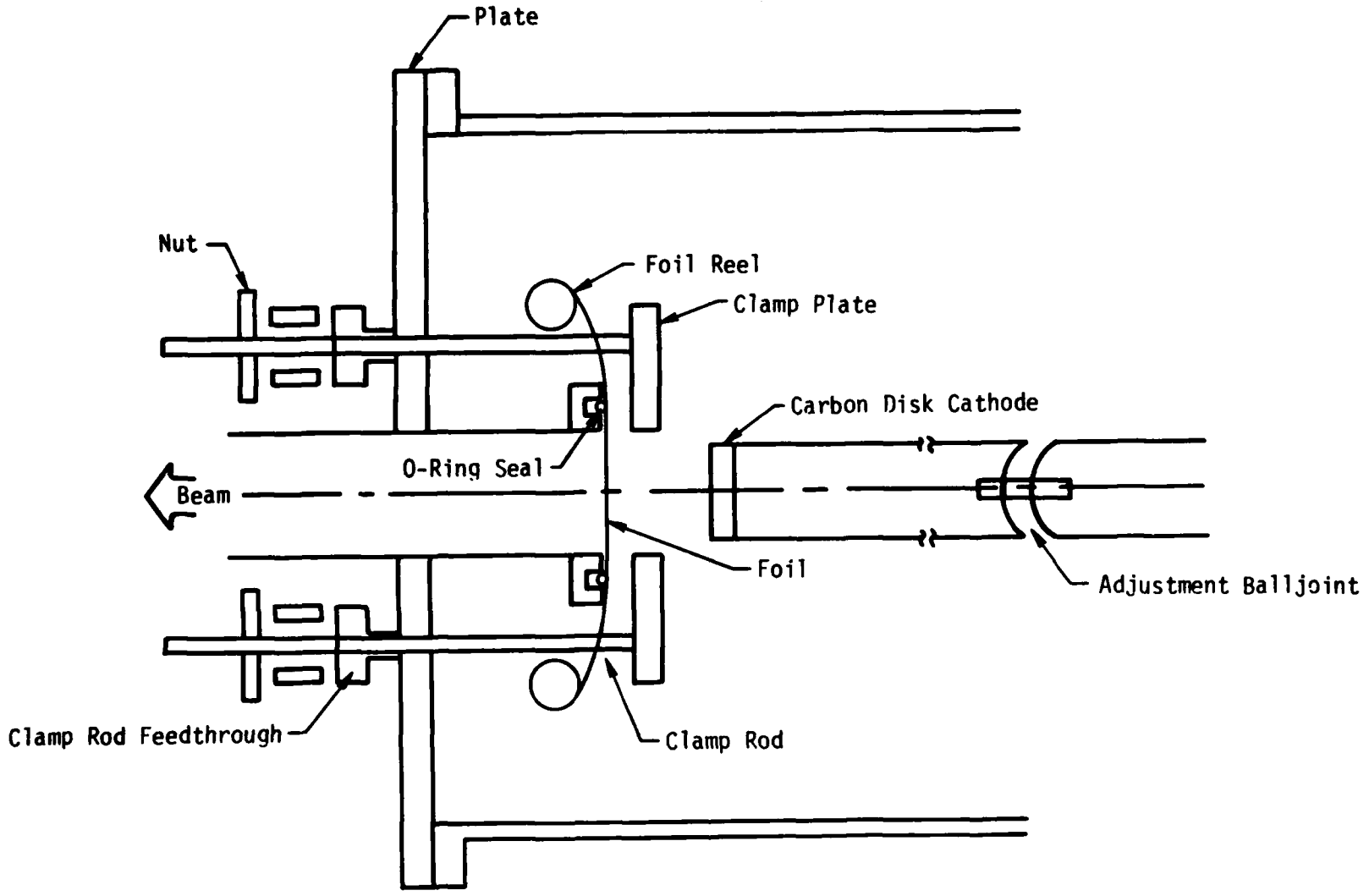

Figure 4. VISHNU diode showing the foil changer - the beam propagates to the left.

B. DIAGNOSTICS

i) Data Acquisition

VISHNU is located in AFWL building 910, more than 100 feet from the main facility in building 909. Signals from the experimental area propagate via RG-214 cable and are acquired on Tektronics 7700 and 7900 series oscilloscopes in the main screen room in building 909. Due to the long cable run, signals are limited to 2 nanosecond risetimes. In some phases of the experiments, faster oscilloscope rise times were required. When necessary, Tektronix 519 oscilloscopes were placed in a shielded enclosure within 3 m of the diode, resulting in a system risetime of < 0.5 nanoseconds.

The oscilloscopes were supplied by AFWL and numbered no less than 8 at any time. Signals were recorded on Polaroid Type 612 film at a typical sweep speed of 20 nanoseconds/division. Waveforms of particular interest were digitized on the AFWL PDP11/60 computer system and could be further processed by the computer. The diode voltage was recorded on all shots with allocation of the other channels dependent on the particular experiment.

ii) Machine Diagnostics

The machine output characteristics were measured with resistive and capacitive voltage monitors, B_θ field loops in the diode, and a resistive voltage monitor at the output of the Marx Generator.

The resistive monitors are simply $CuSO_4/H_2O$ solution resistive dividers of the standard Sandia National Laboratories design.[8] The virtue of these monitors is that the resistive ratio remains fixed even if the solution resistivity changes. The capacitive monitor operated in 'V-dot' mode, (i.e., the RC time constant of the probe was much less than 1 nanosecond) so the monitor output represented the derivative of the diode voltage.

Capacitive monitor signals were then integrated using a passive RC network to produce a voltage waveform. The resistive and capacitive voltage monitor signals agreed very well.

iii) Inductive Current Shunts

One of our primary research objectives is a study of the beam-head erosion[6] process, which can lead to rapid net-current risetimes in the drift tube. For these measurements we designed and constructed inductive net-current detectors that had substantially faster response times than the available Rogowski loops.

The inductive-shunt current monitors consisted of epoxy-filled annular channels machined in an Aluminum flange that was inserted between two sections of the drift tube. As can be seen in Fig. 5, the return current flowing on the drift-tube inner surface was forced to flow around the inside surface of the annular channel. A voltage was thus induced across the insulating gap by the time-varying magnetic field in the annular channel. In the limit of time-scales short compared with the magnetic diffusion time into the Alumiunum shunt, the voltage appearing around the channel is purely inductive and can be detected by completing a flux loop as shown in Fig. 5. The inductive component of the voltage that appears at the pick-up point is given by:

$$V = -\frac{d\phi}{dt} = -\mu_o \frac{dI}{dt} \int \frac{drdz}{r} \quad , \tag{1}$$

Substituting the inductance, L, for the shunt geometry into this equation gives

$$V = -\frac{\mu_o w}{2\pi} \ln \frac{r_o}{r_i} \frac{dI}{dt} \quad , \tag{2}$$

where r_o is the outer radius of the channel, r_i, is the inner radius, and w is the flux loop axial length.

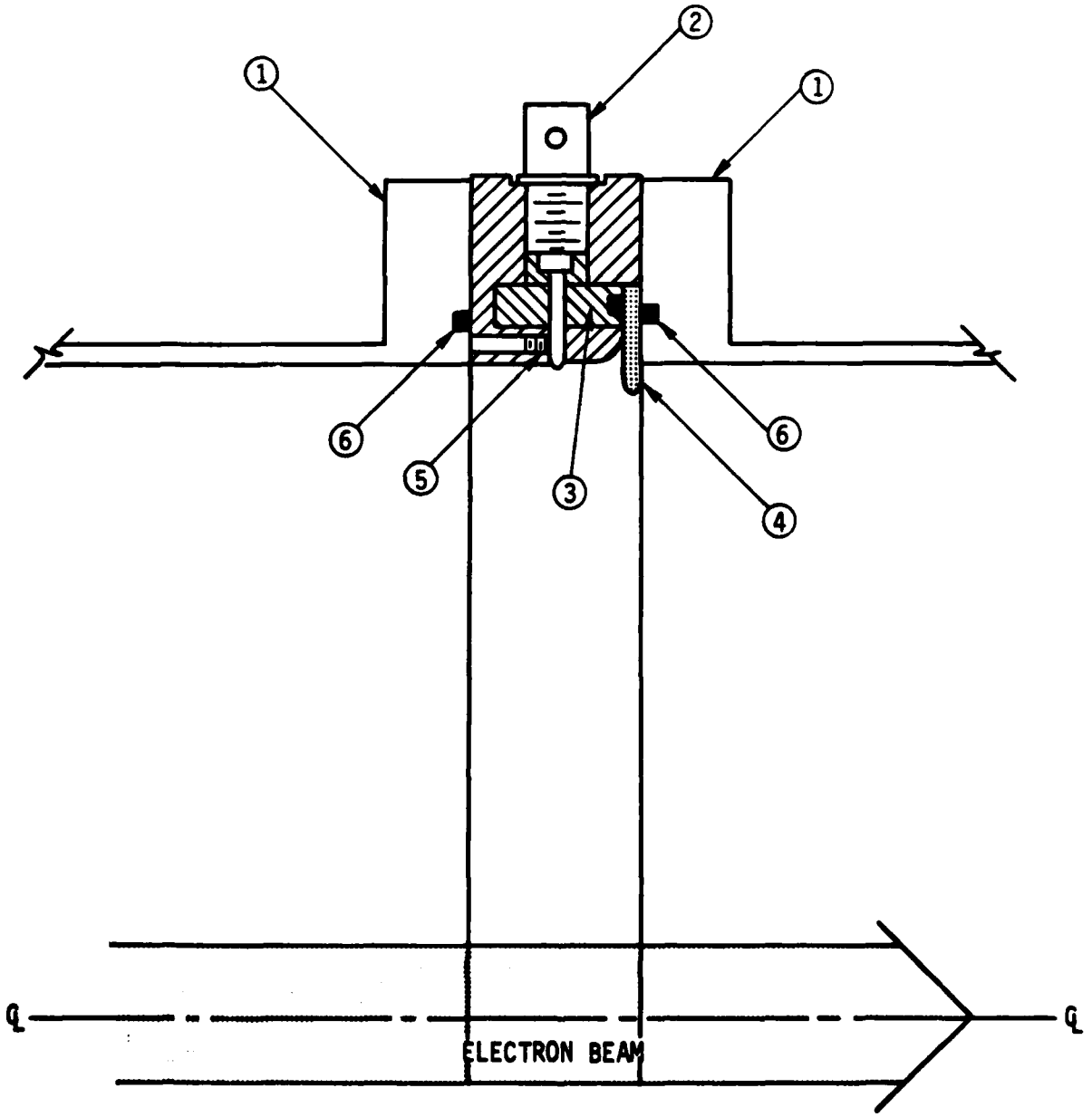

Figure 5. Fast-risetime inductive-shunt current monitor installed between two sections of drift tube (1). (2) is the BNC signal-output. (3) is the epoxy filled annular channel. (4) is the polyethylene insulating gasket. (5) is the set screw to provide electrical contact for the detector pin. (6) are 'O' ring vacuum seals.

An advantage of this type of current monitor is that it provides a simple penetration of the conducting drift tube that results in a well-shielded coaxial signal-transmission geometry. In addition, the narrow insulating gap is a wave guide beyond cutoff for low-frequency modes other than the TEM mode that is excited by the time-varying axial current, and thus provides shielding from unwanted electromagnetic noise. Furthermore, although a single voltage pickup is sufficient for an azimuthally symmetric system such as a coaxial transmission line, asymmetric current channels can be accurately measured by summing the signals from several voltage pick-ups separated by equal increments of angle. In this respect, the inductive-shunt monitor can be thought of as the well-shielded limit of a Rogowski belt current monitor.[9] Finally, the achievable risetime of an inductive-shunt monitor is substantially faster than for a Rogowski coil because the output signals are summed in parallel rather than in series, thus significantly reducing the inductance and L/R risetime.

These net current monitors were positioned at various axial positions during the different phases of the program. They provided reliable, low-noise measurements of the net current in the drift tube.

iv) Subminiature Faraday Cup Array

An array of fast-response Faraday charge collectors was developed to measure the time-resolved current distribution. The data from this array provided a picture of the evolution of the radial current profile at a particular axial location without relying on shot-to-shot reproducibility. Each detector in the array consisted of a length of Uniform Tubes Co. UT-47 rigid coaxial transmission line that was embedded in a massive graphite block, as shown in Fig. 6. The initial radial spacing of the detectors was chosen to be 1.25 cm. However, our early discovery of significant beam current carried outside of the Bennett radius caused us to modify the array by increasing the detector density at large radii. The collectors were

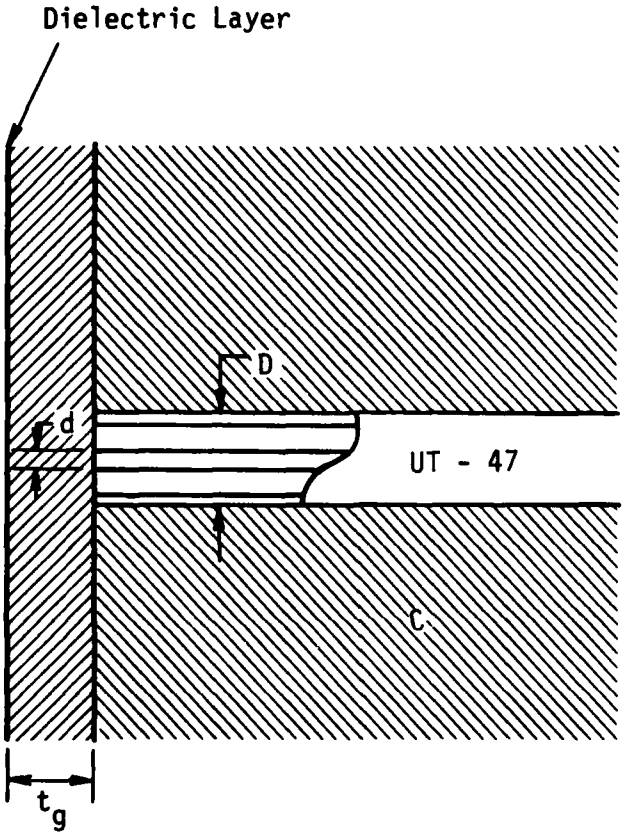

Figure 6. Small Faraday cup.

shielded from the ionized-gas electrons and low-energy secondaries by a thin graphite sheet in the original array developed during the FX-25 experiments. The array that we constructed for the FX-100 propagation experiments used a 125 μm thick Titanium foil plasma shield that was insulated from the collectors with 25 μm thick Kapton film. During the VISHNU experiments, the Kapton was replaced by a 500 μm thick vinyl absorber on a smaller array. A schematic of this two-dimensional array is shown in Fig. 7. Of all dielectric materials that we have experimented with, Kapton (a polyimide) exhibits the most resistance to the intense beam irradiation. Although we replaced the shielding and insulating foils on a regular basis as a precaution, we had few problems with insulator breakdown in this detector configuration.

Electron scattering in the array materials results in an energy-sensitive effective collection area. The reason is that the more energetic electrons have a higher probability of scattering into the collector because of their greater depth of penetration. We studied this effect by using the Monte Carlo radiation transport code CYLTRAN to obtain the energy sensitivity of the effective collection area. Details of this study are reported in Appendix C. The energy sensitivity appears to be modest over a wide range of energies around the peak energy of the FX-100 beam, but the collection area for these high-energy electrons is significantly (factor of ~2) enhanced over the geometrical area.

The experiments using the FX-25 beam demonstrated that the risetime for these coaxial collectors driving a matched and properly terminated signal cable was limited only by the cable dispersion and oscilloscopes. In those experiments 1 ns risetimes were observed, and faster risetimes were observed in the VISHNU experiments. The combination of the high level signal generated by these collectors and the unbroken coaxially shielded construction resulted in a high signal-to-noise ratio on the oscillograms.

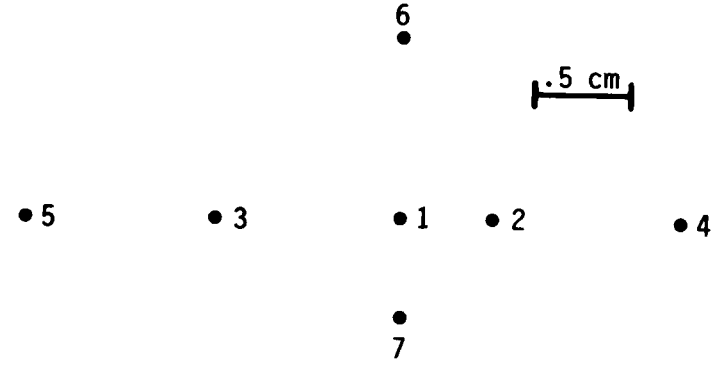

Figure 7. Two-dimensional Faraday cup array pattern - #1 is on the system axis.

v) Carbon Calorimetry

The graphite block containing the array of Faraday collectors was also used as a beam calorimeter by measuring the temperature rise with a thermocouple. Because carbon calorimetry integrates over time, space, and the beam-energy distribution, it is impossible to distinguish beam-electron energy losses from loss of transported charge without simultaneous, precise measurements of beam current. The carbon calorimeter is quite simple to field in this kind of experiment, and it is the traditional diagnostic for definition of the propagation pressure window. Our use of a thermistor sensor simplified the measurements. The thermistor was found to be insensitive to radiation, and when calibrated, it was found to have a linear response over the restricted temperature range of this application.

Incorporation of the charge-collector array into the calorimeter block enabled us to simultaneously determine the beam energy transport and the temporal evolution of the radial current profile at any given axial location. A limited number of measurements were made with the calorimeter in vacuum, and isolated from the ionized-gas channel by a Titanium foil. The results of these measurements indicated that the energy deposited on the calorimeter from the plasma was not a significant fraction of the beam energy.

vi) Open Shutter Photography

Time-integrated open-shutter photographs of the beam and ionized-channel excited air emission were obtained at a number of viewing ports over the course of the experiment. The symmetry properties of the drift tube were not disrupted by the ports because a return-current carrying screen was incorporated in each. The exposures with these cameras were recorded with Polaroid Type 52, 57 or 58 film. Both color and black and white films were used depending on the beam light output.

Because the observed light is a result of beam effects on the gas, rather than direct beam effects, open shutter results should be evaluated with care. A discussion of many of the issues involved in interpretation of the data obtained in this experiment with optical emission diagnostics is contained in Appendix B.

A point not covered in Appendix B is the following. As shown in the Appendix, the excitation of the upper level of the radiative transitions by the low-energy plasma electrons is $\sim(kT_e)^{1/2}(1 + kT_e/E_0)\exp(-kT_e/E_0)$, where T_e is the temperature of the cold electrons, and E_0 is the threshold of the excitation cross-section, $E_0 \gg kT_e$. The radiation is, therefore, very sensitive to the population of the high-energy tail of the electron distribution. It is well known that high electric fields can significantly distort the tail of the distribution. For example, a modest E/p of about 100 V/cm/Torr can increase the effective temperature of the tail of the distribution by a factor of 5 or more. As a consequence, the visible emission can be vastly different from regions having the same gas temperature and plasma electron density, but having widely disparate values of E/p. This may be the cause of some of the more spectacular effects seen in both open-shutter and time-resolved photographs.

vii) 'Penny' Probes and the Erosion Rate Measurement Technique

Radial beam current densities are typically much less than axial current densities. As a result larger collectors are required for radial beam current density measurements. Five probes of the type shown in Fig. 8 were fabricated for the measurement of radial electron currents. A penny was drilled and soldered to a type HN vacuum feedthrough. Copper foil was soldered to the vacuum side to form a cylindrical 'can' which was at least 2 mm from the penny. The can was filled with epoxy, after which the penny was covered with 0.5 mm thick vinyl, and then covered with 0.025 mm of

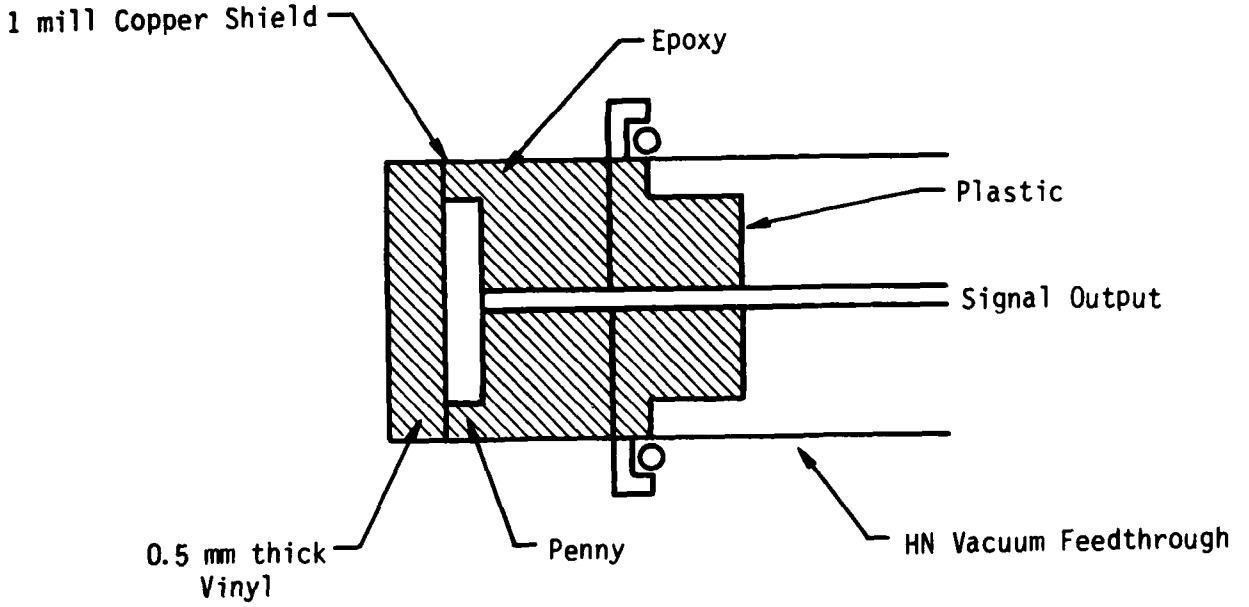

Figure 8. 'Penny Probe'.

Copper foil on the top. The minimum energy of electrons striking the penny is dictated by electron range-energy[10] relations and is > 200 keV. All signals monitored by the probes were negative, and we expect that the absolute magnitude of the current is within 20% of the current expected based on area. The signals were found to go to zero at times in the pulse consistent with a diode voltage of 200-300 keV.

Penny probe signals may be used to infer the axial beam propagation velocity if the beam current and effective probe area are known. If the beam particle velocity is v, and the front velocity is v_f, then the total charge per unit time lost radially in an infinitely long tube is $I_b(1 - v_f/v) = I_r$. For simplicity assume a linear beam current rise time τ behind the front. At any time, $t < \tau$ after the start of the beam front passes, the radial current density is

$$J_r = \frac{I_b\left(1 - \frac{v_f}{v}\right)}{2\pi a v_f \tau} \tag{3}$$

or equivalently

$$\int_0^\tau J_r dt = \frac{I_b\left(1 - \frac{v_f}{v}\right)}{2\pi a v_f} \tag{4}$$

which implies

$$\frac{v_f}{v} = \frac{I_b}{I_b + \left[\int_0^\tau J_r dt\right] 2\pi a v} \tag{5}$$

Thus, the erosion velocity

$$v_e = v - v_f = \frac{\int_0^\tau J_r dt \; 2\pi a v}{I_b + \int_0^\tau J_r dt \; 2\pi a v} \tag{6}$$

is found directly without subtraction, or measurement of small (few ns) time differences. The fact that subtraction is not required for erosion rate determination makes this technique particularly sensitive and reliable.

viii) B-dot Monitors

The B-dot monitors used in our experiments work on the same principle as the so-called 'inductive shunt' monitor discussed in Sec. I.B.iii. The rate of change of flux through the loop induces a voltage which is either displayed directly or integrated at the scope and then displayed directly. Subtraction of signals from loops placed on opposite sides of the drift tube nulls out axisymmetric current and results in signals dependent on both current and transverse position. In general, for systems with integration time constant τ, a drift tube radius b, and current I, the signal is

$$V = \frac{k}{\tau} \frac{I}{[(b + x)^2 + y^2]^{1/2}} \qquad (7)$$

where (x, y) is the position of the beam with respect to the system axis and k is the axisymmetric current monitor calibration. Subtraction of opposing loop signals gives rise to

$$V \sim \frac{2kI}{\tau} \frac{x}{b} \qquad \text{for x, y small} \qquad (8)$$

A correction factor for nonlinearities in (7) is given in Fig. 9.

With loops supplied by M. C. Clark of AFWL, our subtraction error was found to be less than 2%. Thus, the upper bound to the systematic error in position measurement is less than 2 mm.

Subtraction of the beam and net currents gave us a direct measure of the plasma current. This measurement was also accurate to ~2% of the beam current magnitude, typically 5-10% of the plasma current.

ix) Vacuum Current Measurements

A number of current measurements were made in vacuum in order to eliminate plasma current contributions and get direct beam current values. B-dot monitor signals described above were summed and integrated, a technique which resulted in signals which were independent of position in the small displacement limit.

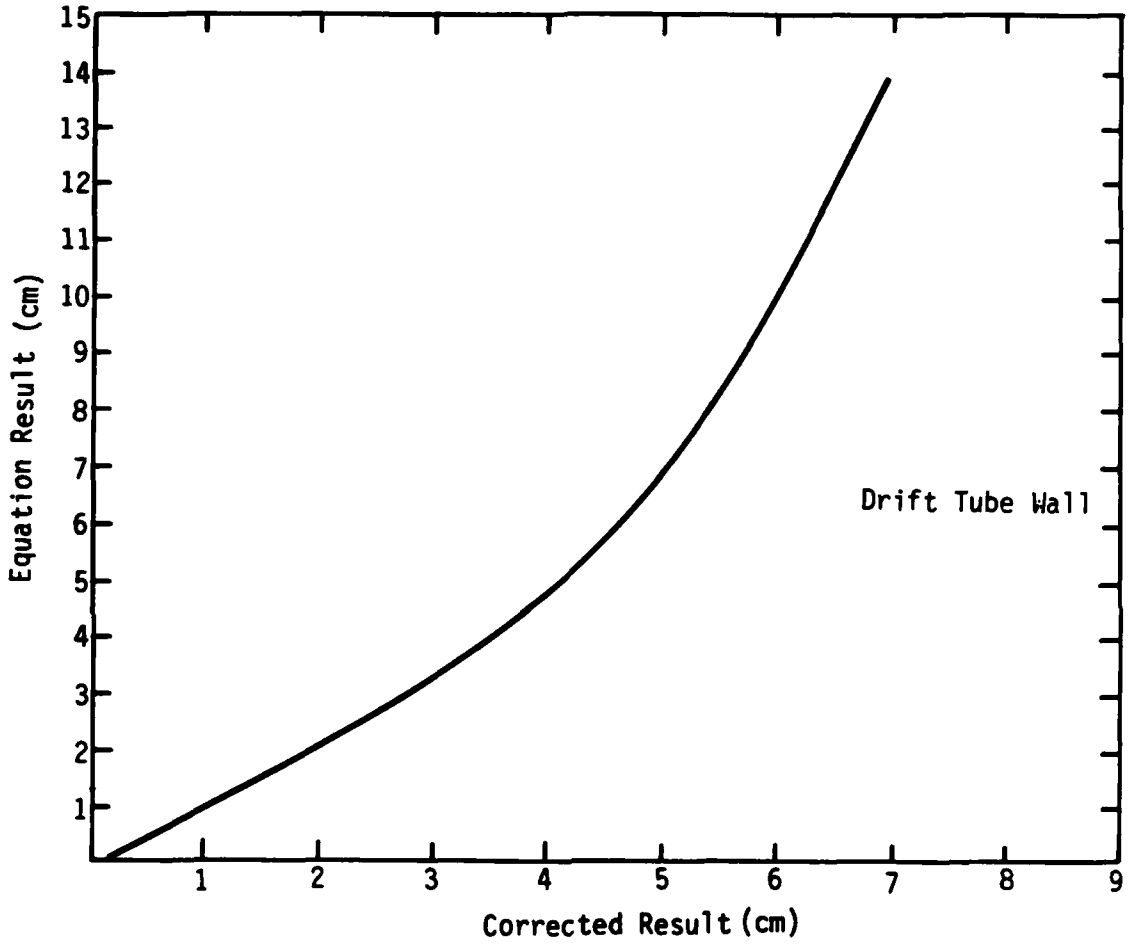

Figure 9. Relation between the equation (8) result and for displacement x (vertical axis) and true displacement (horizontal axis), for a 10 cm radius drift tube.

Initial tests indicated that plasma currents were still generated for pressures as low as 5×10^{-3} Torr. In order to keep the pressure sufficiently low in the vacuum cell, an air-cooled diffusion pump was placed in close proximity to the vacuum cell, and measurements were taken at pressures below 10^{-3} Torr. At these low pressures a vacuum beam collector was required to prevent virtual cathode formation.

x) Triangle Detector

A face-on view of the 'triangle' detector implemented in our experiment is shown in Fig. 10. We developed this detector array geometry for a variety of reasons. The number of oscilloscope channels available to us was limited to ~12, so that after standard current and voltage measurements only ~8 were available. We needed to maximize the data available from any array, and we wanted convenient signal amplitudes of order 10-100 Volts. The most important physics consideration in the design choice was the ability to distinguish between hose and hollowing motions simultaneously.

In order to take advantage of tomagraphic[11] techniques we chose an array of long, narrow detectors, which approximate line integrals of the distribution. A regular array has special geometric properties which can aid in data analysis. In particular, equilateral triangles have useful properties. Hollowing is detected by comparing a second, nested parallel equilateral triangle to the first. The difference between the signals in the two arrays is a measure of hollowing. Finally, a central circular detector was included for completeness. Each long narrow strip is a Faraday collector, and the whole array is covered by 125 μm Kapton and Ti foils to prevent plasma current contributions to the signals.

A technique for analyzing the data can be developed in a straightforward manner if we assume that the collectors are much longer than a beam radius, if we assume a particular radial distribution, if we assume that a circular beam is displaced, and if we assume that the beam is not hollow. As discussed above, comparison of the signals should indicate hollowing.

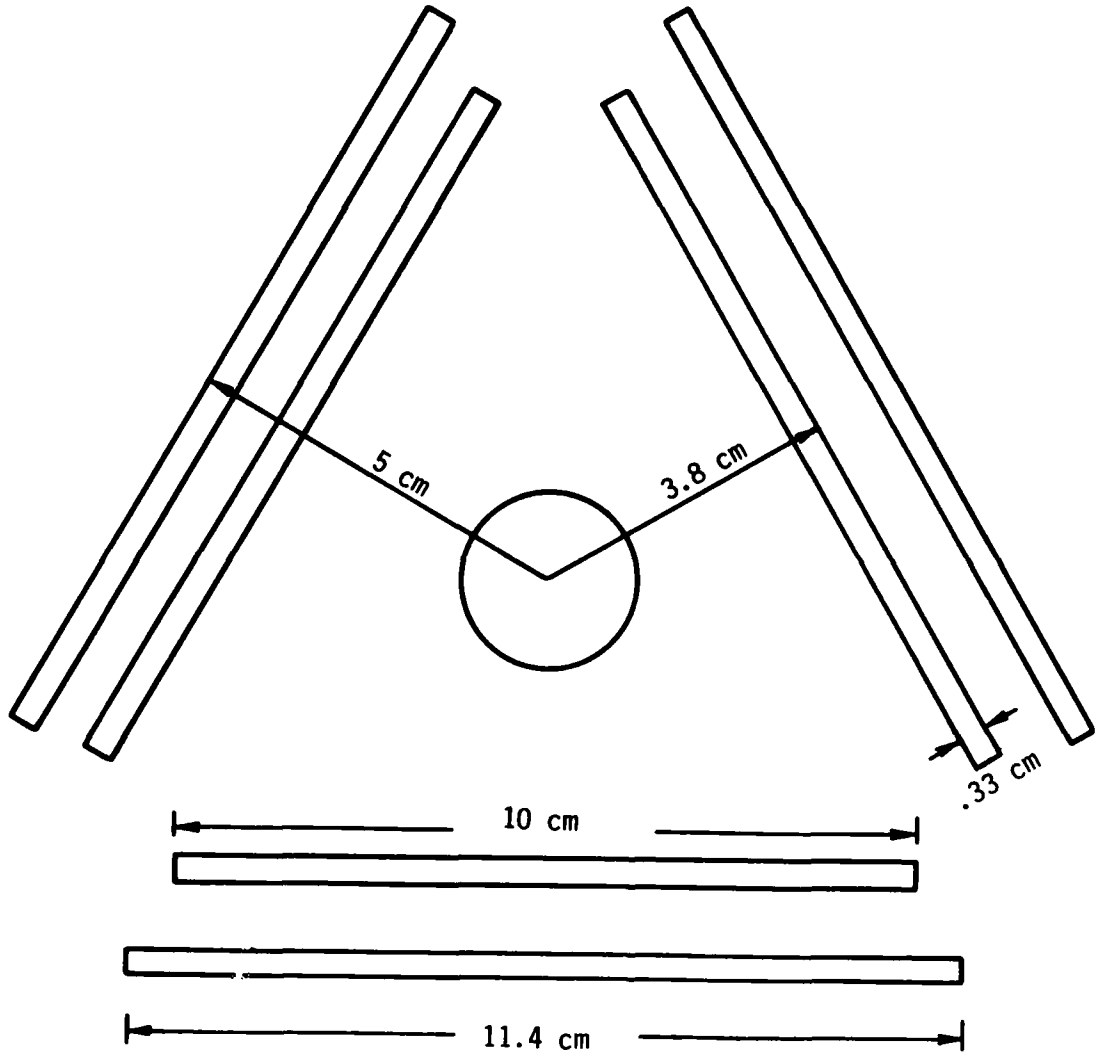

Figure 10. Triangle detector configuration used in the experiment.

As a first example, assume a profile of the type

$$J_b = \frac{I_b}{\pi a^2 \left(1 + \frac{r^2}{a^2}\right)^2} \tag{9}$$

If the beam centroid falls within the triangle, we find

$$I_n = \frac{\delta\, a^2 I_b}{2(a^2 + x_n^2)^{3/2}}$$

$$x_1 + x_2 + x_3 = \frac{\sqrt{3}}{2} L \tag{10}$$

where the meaning of x_n is shown in Fig. 11, and I_n is the current intercepted by the nth strip.

Assuming I_b is known or can be estimated to reasonable accuracy, we normalize the equation using the following variables:

$$\xi_1 + \xi_2 + \xi_3 = \frac{\sqrt{3}}{2} \frac{L}{a} \; ; \qquad \xi_n = \frac{x_n}{a}$$

$$1 + \xi_n^2 = \left(\frac{\delta I_b}{2aI_n}\right)^{2/3} \tag{11}$$

We find the parameter 'a' from the equation

$$\sum_{n=1}^{3} \left[\left(\frac{\delta I_b}{2aI_n}\right)^{2/3} - 1\right]^{1/2} = \frac{\sqrt{3}}{2} \frac{L}{a} \tag{12}$$

which may or may not have a solution. A bound on the solution is

$$\frac{\delta I_b}{2\, aI_n} > 1 , \qquad \text{or} \qquad a < \frac{\delta I_b}{2\, I_n} \tag{13}$$

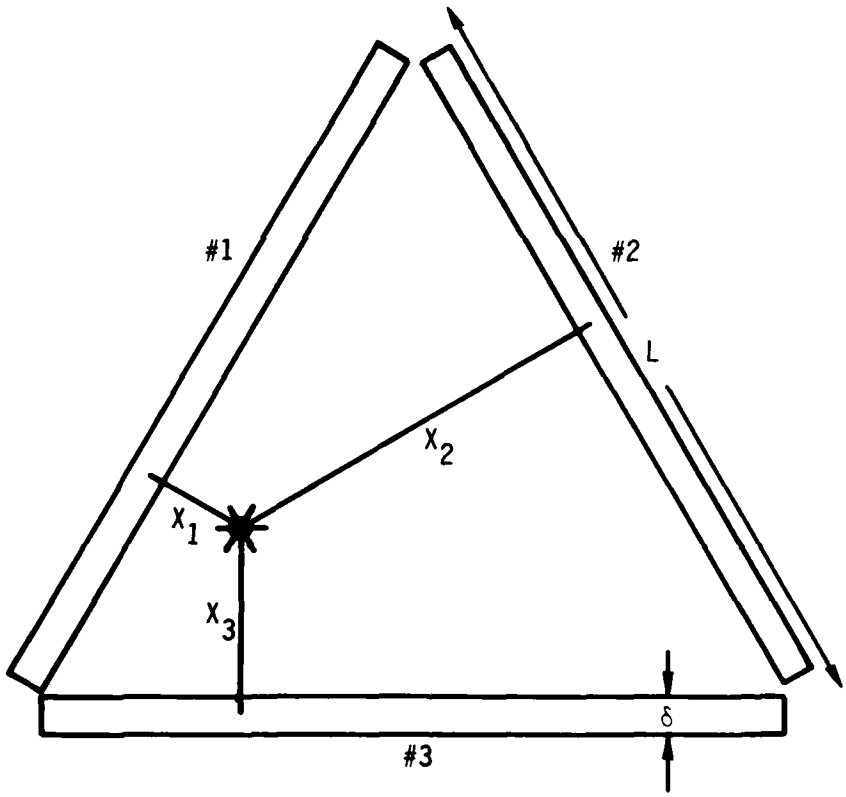

Figure 11. Triangle detector geometry used for calculations.

This is a necessary but not sufficient condition for solution. The procedure above should give a technique for finding the centroid position and Bennett radius given data from the detectors. Note that this detector is actually most useful when the beam is slightly displaced.

Another distribution of interest is

$$J_b = \frac{I_b\, a}{2\pi\,(r^2 + a^2)^{3/2}} \tag{14}$$

for which

$$I_n = \frac{2\delta a}{(a^2 + x^2)}\; I_b \tag{15}$$

Once again

$$\xi_1 + \xi_2 + \xi_3 = \frac{\sqrt{3}}{2} L \tag{16}$$

$$\frac{I_n}{I_b} = \frac{2\delta}{a}\; \frac{1}{(1 + \xi_n^2)} \quad \text{or} \quad \xi_n = \left(\frac{2\delta I_b}{a I_n} - 1\right)^{1/2} \tag{17}$$

so that

$$\sum_{n=1}^{3} \left[\left(\frac{2\delta I_b}{a I_n}\right) - 1\right]^{1/2} = \frac{2}{\sqrt{3}}\; \frac{L}{a} \tag{18}$$

Note that in the limit $\frac{I_n}{I_b} \ll \frac{2\delta}{a}$

$$\left(\frac{2\delta I_b}{a}\right)^{1/2} \left(\frac{1}{I_1^{1/2}} + \frac{1}{I_2^{1/2}} + \frac{1}{I_3^{1/2}}\right) = \frac{\sqrt{3}}{2}\; \frac{L}{a} \tag{19}$$

This same approximation procedure can be invoked for the Bennett distribution (previous case), and it provides a useful starting point for finding an iterative solution.

We have applied these techniques successfully in several cases. In general, the method appears to give the best results when the maximum difference in signal magnitudes is a factor of ~5. For higher energy accelerators, this technique would be useful if thin insulated tungsten wires were used 2-3 Bennett radii away from the beam centroid.

xi) Plasma Decay Time Measurement Technique

The most crucial parameter governing the hose instability is the dipole decay time τ_d, which depends on the beam channel conductivity and current density profiles. The dipole decay time is approximately eight times the plasma monopole decay time τ_m, which governs the axisymmetric plasma response to changing beam current:

$$\frac{d(I_{plasma})}{dt} = -\frac{d}{dt}(I_{beam}) - \frac{1}{\tau_m} I_{plasma} \qquad (20)$$

Since plasma current is the difference between net current and beam current, τ_m may be determined from the directly measurable quantities $I_{beam}(t)$, $I_{net}(t)$, and $\dot{I}_{net}(t)$:

$$\tau_m(t) = [I_{net}(t) - I_{beam}(t)]/\dot{I}_{net}(t). \qquad (21)$$

The form of Eq. (21) may be generalized to include the effects of changing radius $\dot{a}$. From a simple calculation, the effect of changing radius is found to be less than that of current variations, except for very rapid pinching. A comparison of the electric field from pinching E_p and current variation E_I for the Bennett profile is

$$\frac{E_p}{E_I} = \frac{\frac{r}{r^2+a^2} + \frac{1}{a}\tan^{-1}\frac{r}{a} - \frac{\pi}{2}}{\ln\frac{r^2}{r^2+a^2}} \left(\frac{2\dot{a}}{a} \quad \frac{I}{\dot{I}}\right)$$

$$\simeq \frac{.7\,\dot{a}}{a} \quad \frac{I}{\dot{I}} \qquad .2 < \frac{r}{a} < 2$$

$$\sim 0 \qquad r > 2 \qquad (22)$$

We performed these measurements for gas cell pressures ranging from 1 Torr to 630 Torr, and for beam currents of approximately 5 kA and 15 kA. The configuration for these experiments is depicted in Fig. 12. B_θ dot monitors were summed from the gas cell ($\dot{I}_{net}$) and from the vacuum cell with reverse polarity ($-\dot{I}_{beam}$) in a four-port transformer adder at the machine, a technique which reduced timing errors. The resultant $\dot{I}_{plasma}$ signal was RC integrated. Separate $\dot{I}_{net}$ signals from the gas cell were recorded without integration. The vacuum beam currents and plasma currents were corrected for radial current losses between the upstream and downstream detectors to provide more accurate estimates of the plasma decay time. The results of these experiments are presented in Sec. III.c.

xii Pressure

Pressures for most of the experiments were measured with a McLeod gauge which gives absolute pressure from .1-150 Torr. Above this pressure, or when the McLeod gauge was not available, the pressure was measured using Granville-Phillips pressure gauges calibrated from .01-760 Torr.

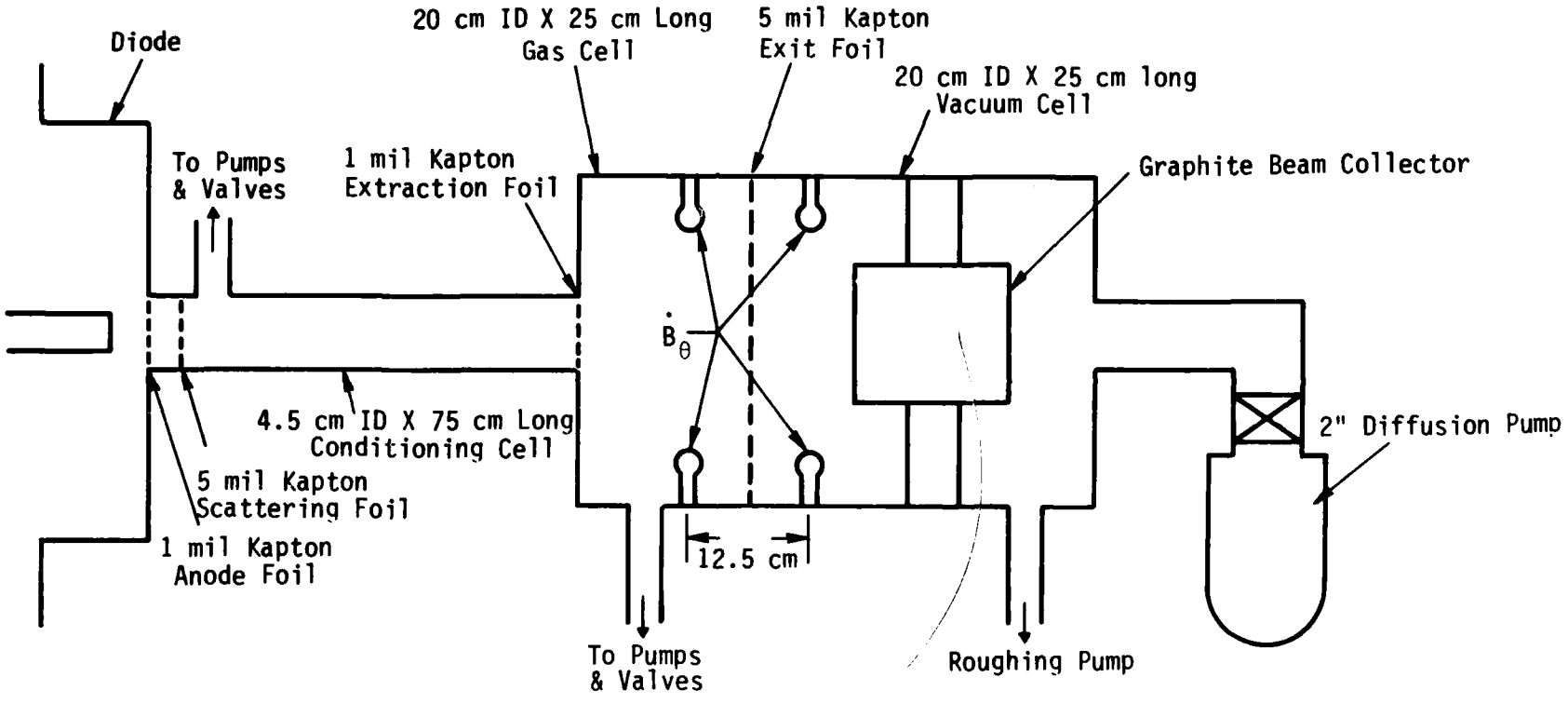

Figure 12. Configuration for plasma decay rate measurements.

II. INITIAL MEASUREMENTS

The first experimental series was a survey of parameter space using the large propagation cell. Measurements were also made to characterize the beam as it exits the conditioning cell. Much of the experiment was performed using the configuration shown in Fig. 13 in which a 10 cm radius, 1 m long conditioning cell was followed by a 25 μm Kapton foil, 25 cm of 10 cm radius tubing, and the large propagation cell.

A. CONDITIONING

The first task was to choose an appropriate conditioning cell pressure. We wished to decrease the beam rise time and center the beam using the natural centering properties of the image currents in the walls.[12] The beam current was monitored with $\dot{B}$ loops, and our objective was to find the operating pressure which maximized dI/dt, and minimized transverse displacements.

At low pressure ($P < 0.5$ Torr), high frequency (0.8-1.5 GHz) signals were observed on the loop traces. Examples of these signals are shown in Fig. 14. Our observations of this phenomena are summarized below.

1) E-fields > 25 kV/cm are associated with the oscillation.

2) The oscillations are not shielded by plasma currents (the plasma monopole decay time is > 100 ns during the oscillations).

3) The electric fields are large over significant (40 cm) distances.

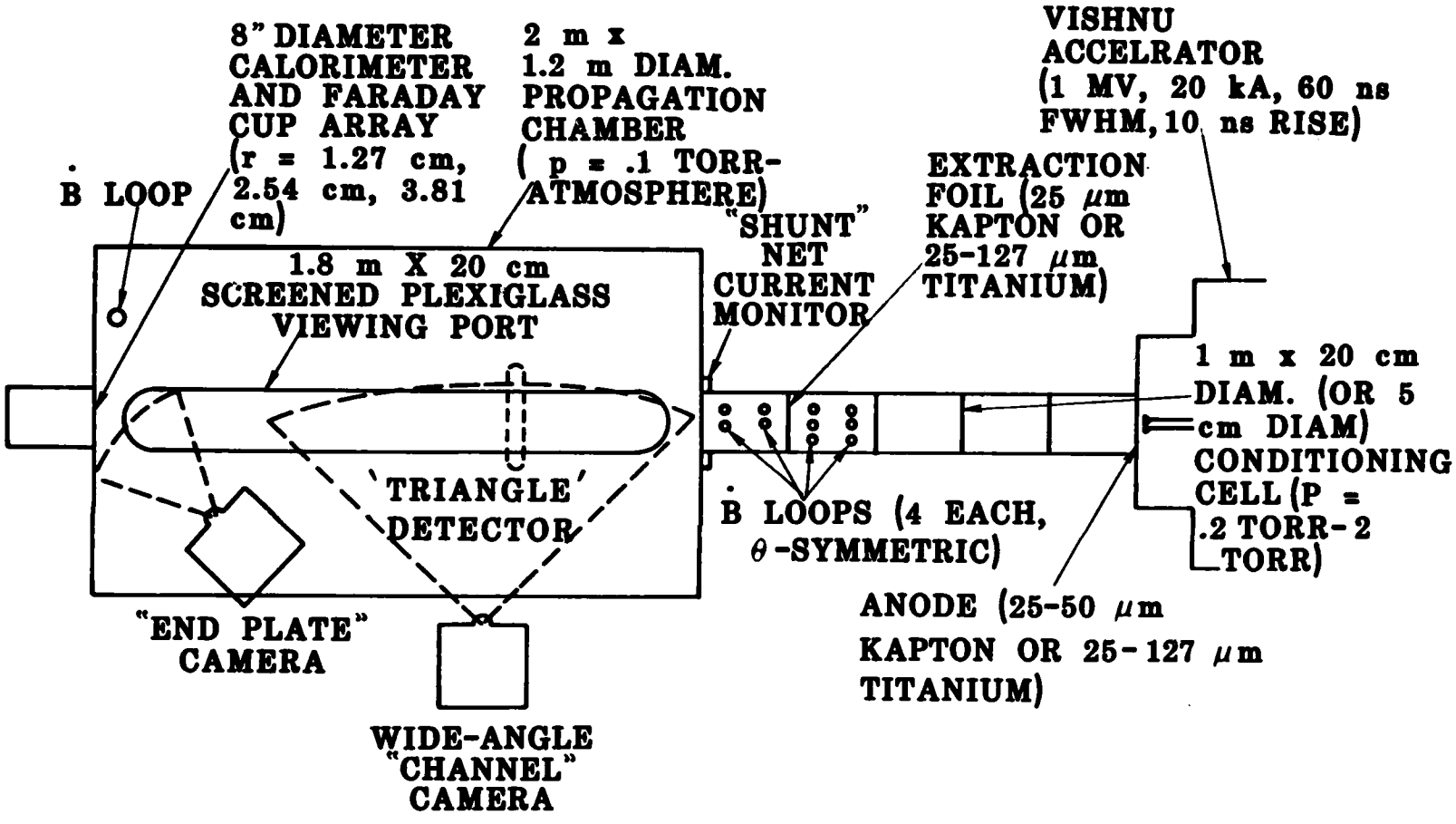

Figure 13. Propagation Experiment Schematic.

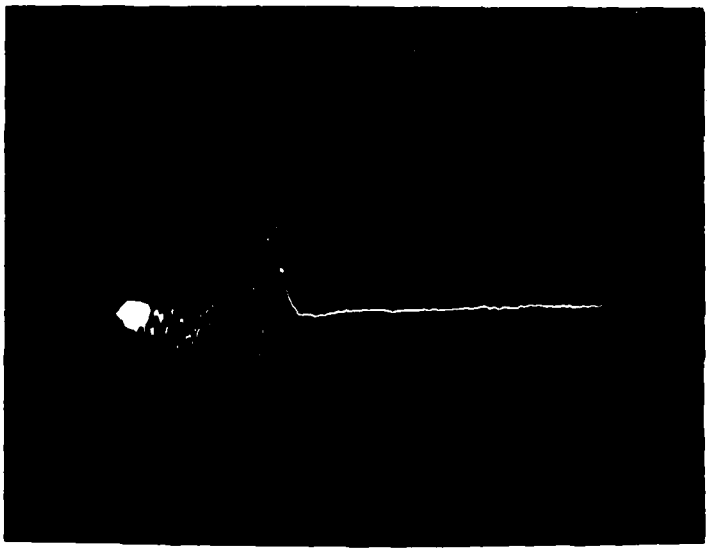

a)

0.12 TORR

0.08 TORR 34 DEGREE BEAM SCATTER

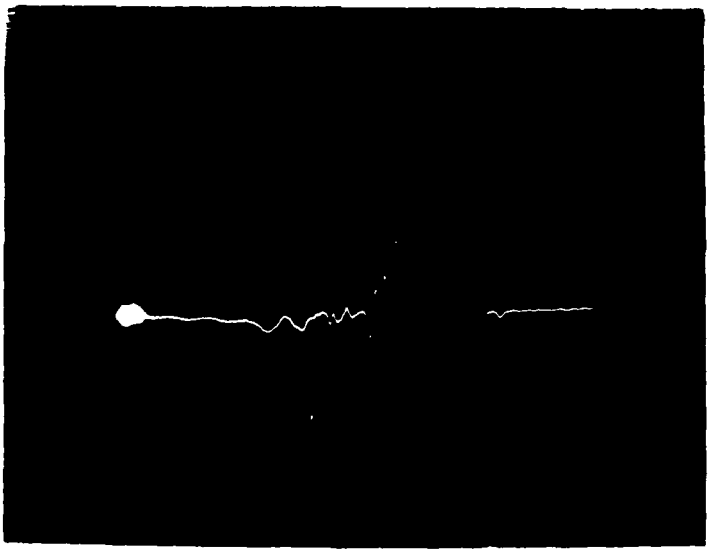

b)

1 ns/mm

Figure 14. RF signals for various conditions as marked.

B DOT SIGNALS 4 DEGREE SCATTERING

c)

2 TORR

d)

0.5 TORR

2 ns/mm

Figure 14. Continued.

4) Increasing the beam emittance using a 127 μm Ti foil does not suppress the oscillations.

5) The oscillation frequency is near the axial beam plasma frequency $(4\pi ne^2/\gamma^3 m)^{1/2}$.

6) The plasma electrons are magnetized in this parameter regime (see Fig. 15).

Similar oscillations were observed in earlier propagation experiments in the 10 GHz range at $\gamma \sim 1.8$.[7] Note that we expect $f \propto (\beta V)^{-3/2}$ for axial beam plasma frequency oscillations, so that both RF observations may be due to axial beam modulations.

In the absence of a clear understanding of the oscillation effect we chose to run the conditioning cell at a pressure of 0.4 Torr, where the oscillation effect is relatively minor. Studies of the beam dI/dt at the beam head, indicated that this quantity seldom exceeded 5×10^{12} in the conditioning cell, aside from oscillations. Further, we found that dI/dt was much lower after the transition through the foil than in the conditioning cell. Thus, low pressure conditioning is not necessarily a useful technique for increasing the beam head electric field, which is proportional to dI/dt.

The beam radial current density profile was observed 25 cm beyond the conditioning cell, at the entrance to the large propagation chamber. Current density profiles at various times are shown in Fig. 16. The beam is found to have a larger current density at large radii than is consistent with a Bennett profile. The effective radius for this configuration is observed to be a minimum 10 nanoseconds into the pulse.

The initial conditions for injection into the large propagation chamber were a radius of 1.5 cm, injected beam current of 14 kA, risetime of 5 nanoseconds and a peak beam energy of 1 MeV.

SCALAR CONDUCTIVITY MAY NOT BE VALID UNTIL HIGH PRESSURE

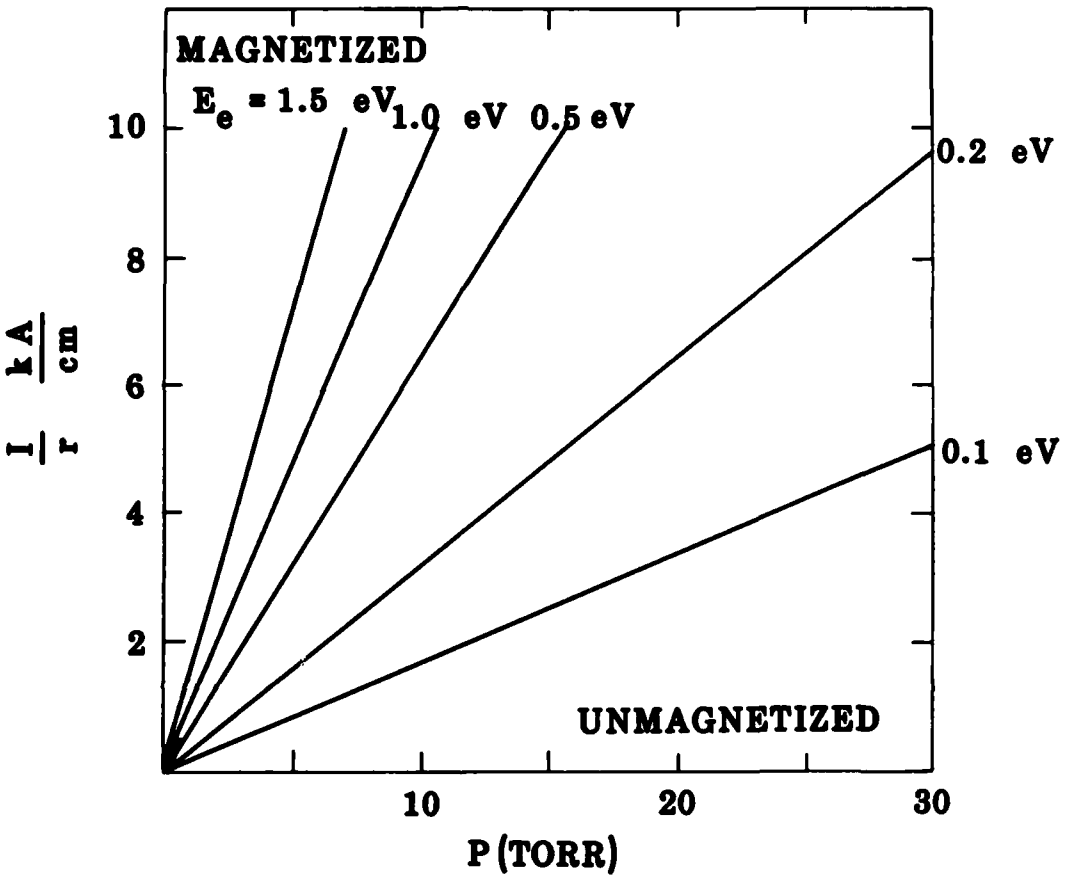

Figure 15. PLOTS ABOVE INDICATE $\omega_c = \nu_m$ FOR VARIOUS ELECTRON ENERGIES

ν_m = MOMENTUM TRANSFER COLLISION FREQUENCY

ω_c = PLASMA ELECTRON CYCLOTRON FREQUENCY

(ν_m FROM PHELPS, et. al.)

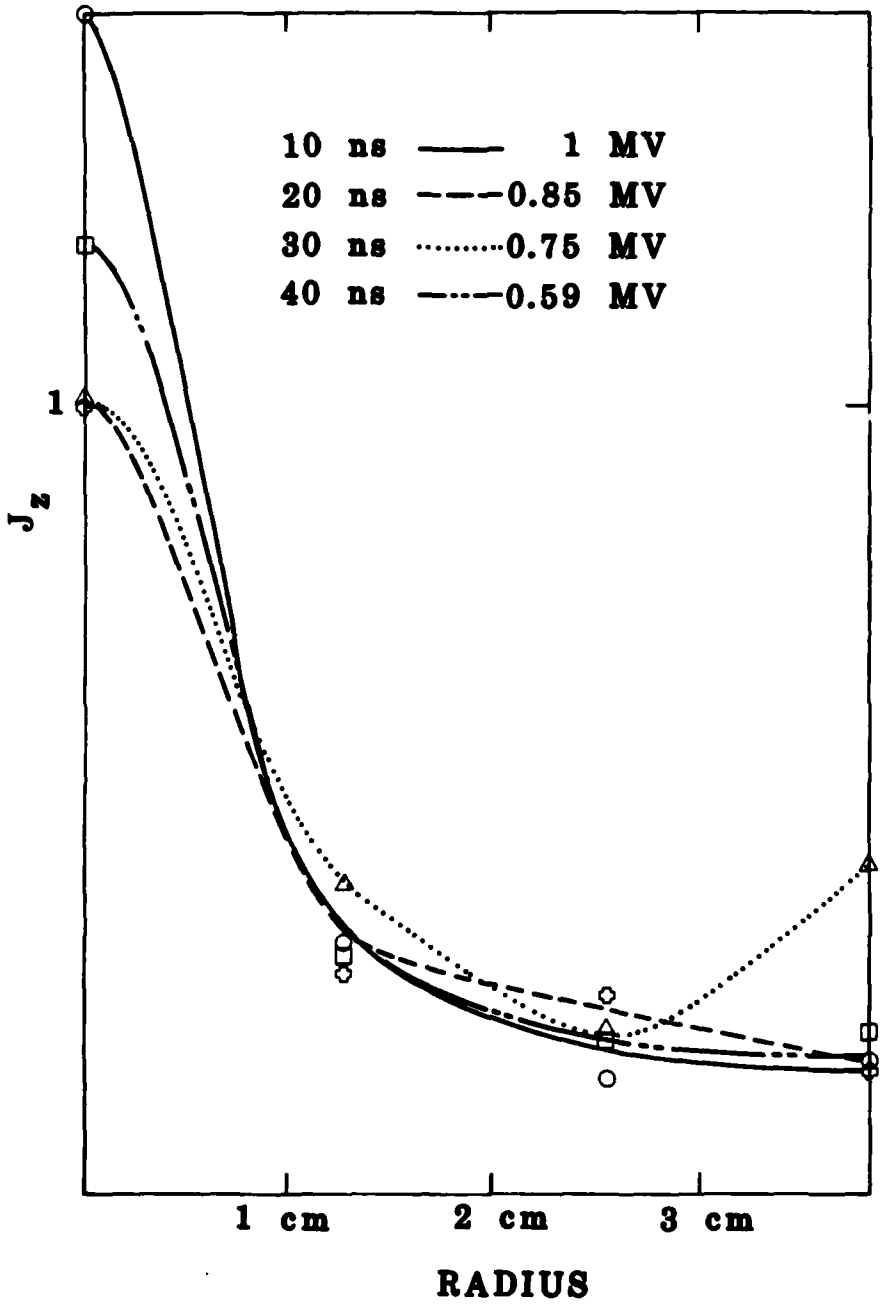

Figure 16. **TYPICAL RADIAL PROFILE 25 cm BEYOND THE CONDITIONING CELL.**

B. LARGE CELL OBSERVATIONS

Propagation in the large chamber was monitored with open shutter photography, the carbon calorimeter, and the Faraday cup array. It is interesting to compare FX-100 beam energy propagation in 10 cm radius tubes to VISHNU propagation results in a 60 cm radius tube. This is shown in Fig. 17.

The best propagation is found below 1 Torr for both experiments--~0.5 Torr for the FX-100 experiment, and ~0.8 Torr for the VISHNU experiments. In the FX-100 case, significant energy propagation is observed for pressures of 3 Torr and above--a factor of 6 higher in pressure than the center of the propagation window. The VISHNU case is quite different as no energy is observed on the calorimeter above 2 Torr. We conjecture that this difference is due to the different drift tube radii used in the two cases. The effect of a smaller diameter tube is illustrated by Fig. 18. An open shutter photograph of beam propagation in the smaller tube is shown in which the beam is clearly reflected from the drift tube walls several times. This demonstrates the effect of wall stabilization on the hose instability, and the importance of performing hose instability experiments in large diameter propagation chambers. Further, wall stabilization may account for inferred hose stability at 2 Torr in previous experiments. In the 20 Torr case shown in Fig. 18, the beam nose was observed to propagate to the detector, in contrast to the large propagation cell case. Clearly wall stabilization increases the amount of beam which is transported.

For the large diameter chamber VISHNU experiments, the question which must be addressed is: what is the reason for zero energy propagation above 2 Torr? Open shutter photographs of a 0.8 Torr shot with 295 Joules propagated energy, a 1 Torr shot with 72 Joules propagated and a 5 Torr shot with virtually no propagated energy are shown in Fig. 19, in order to illustrate the differences. All beams appear to be well-confined, so that hollowing can be ruled out as a cause of non-propagation. The 0.8 Torr beam propagates nearly straight and strikes the target within 8 cm, while

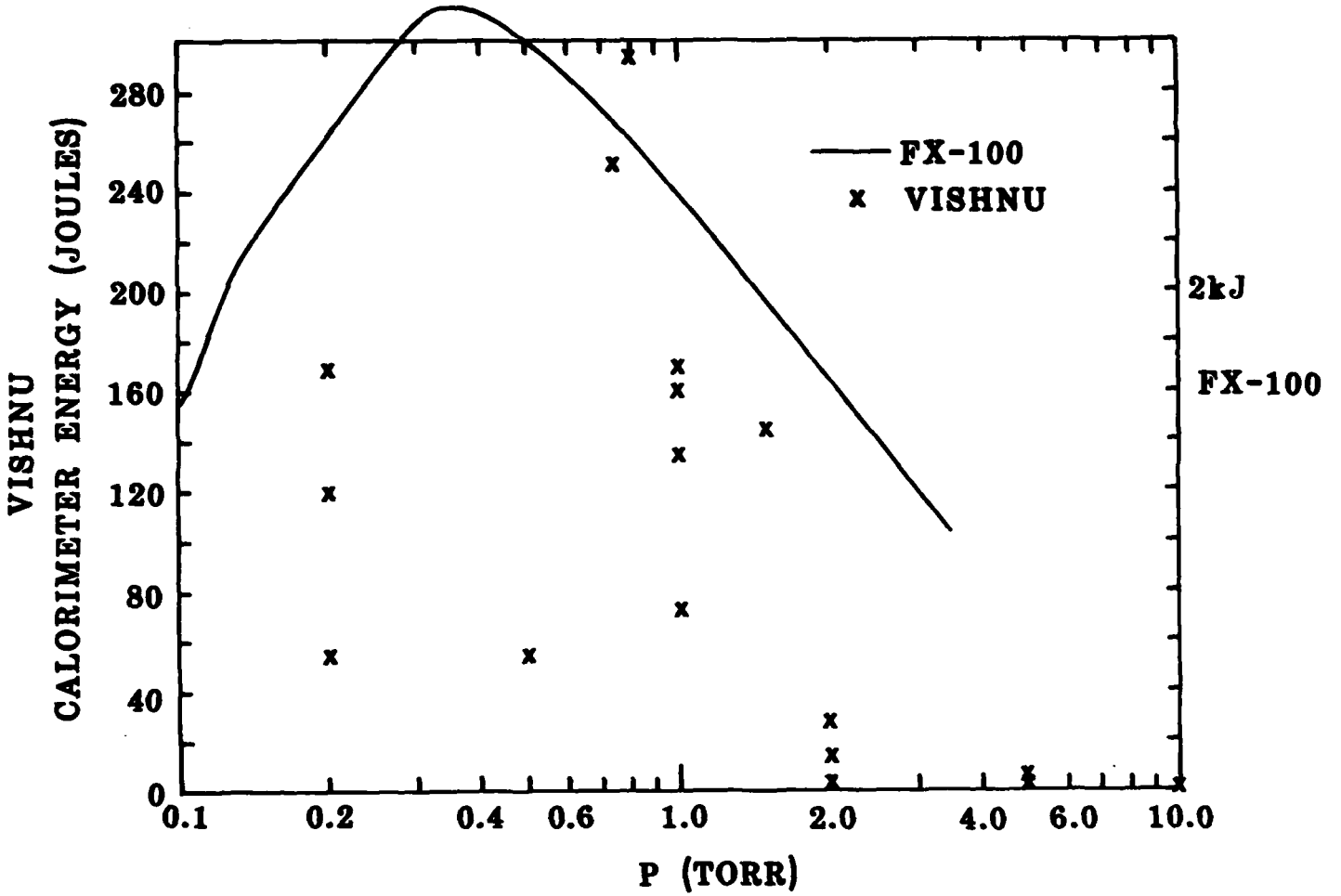

Figure 17. **TRANSPORTED ENERGY vs. PROPAGATION PRESSURE FOR 15 kA INJECTED CURRENT FROM 120 cm X 20 cm DIAM. .4 TORR CONDITIONING CELL**

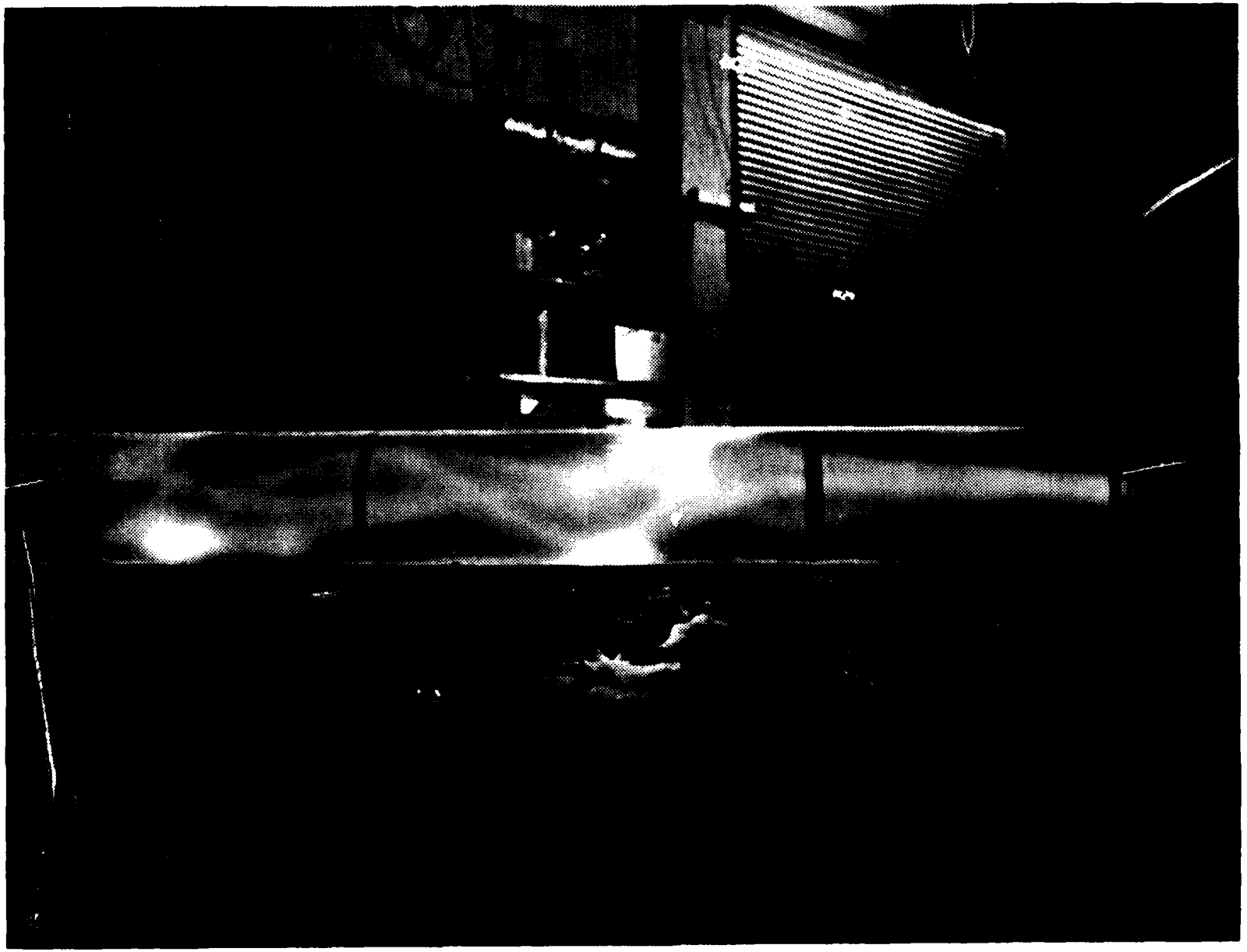

Figure 18. Beam propagation at 20 Torr in a narrow drift tube showing the effect of the wall in recentering the beam.

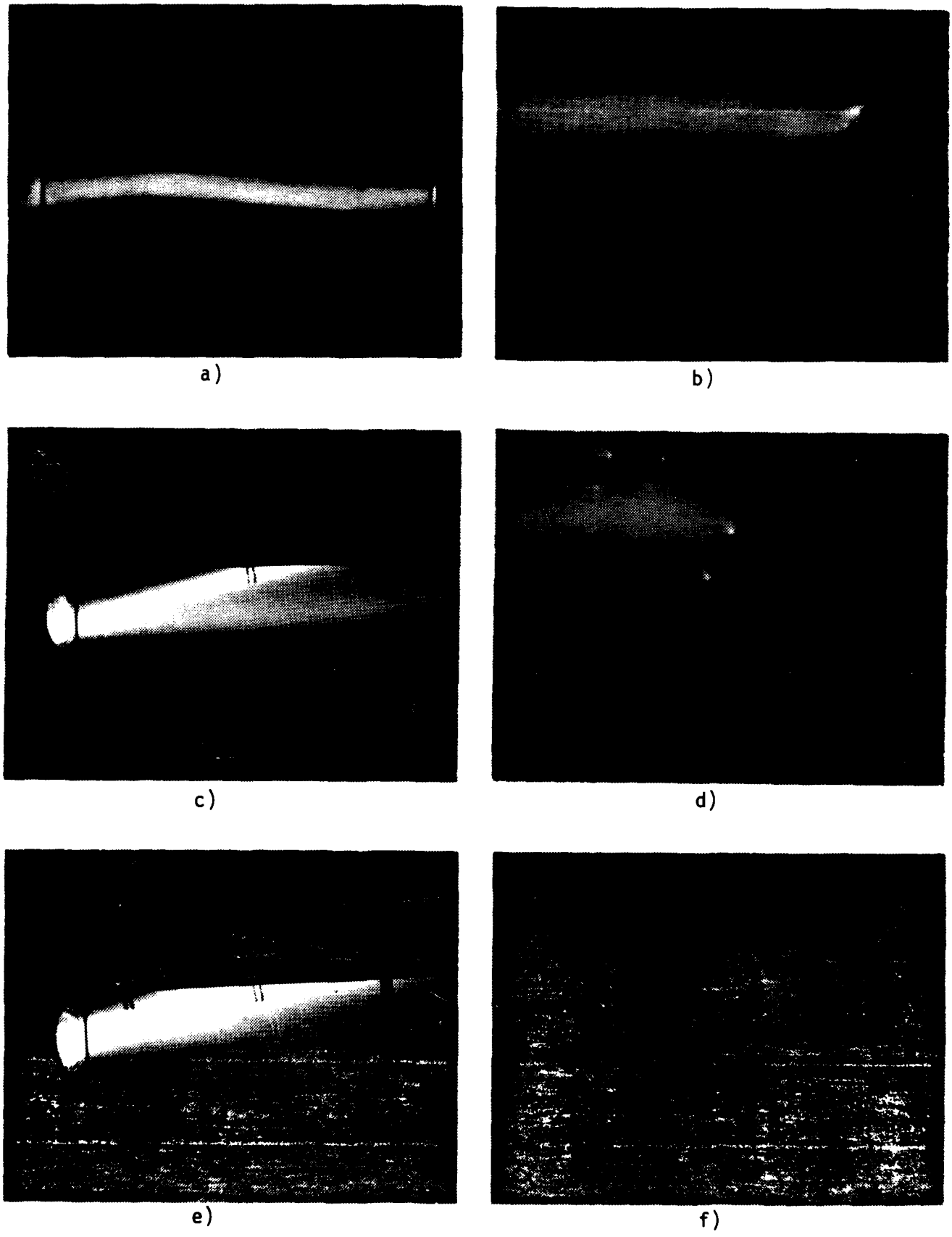

Figure 19. a), b) = .8 Torr; c), d) = 1.0 Torr; e), f) = 5.0 Torr. a), c), and e) are shots of the first 1.2 m, while b), d), and f) are end plate photos.

no portion of the 5 Torr beam strikes the target. The transition case of the 2 Torr beam is most illustrative. In this case the nose strikes the target (this was verified by Faraday cup signals), and at later times the beam is deflected due to the hose instability.

We suggest that the nose of the beam is eroded at a rate such that the hose instability is absolute in the frame of the nose.[13] This is the so-called 'nose coupled hose' instability. In order to test at least part of this conjecture, the time required for the beam to propagate from the conditioning cell exit to the back plate of the large chamber was measured. The shunt current monitor signal was summed near the source on the same channel with the Faraday cup so that the delay measurement was not dependent on detailed timing measurements of long cables. The result was a measured average beam front velocity of 0.50 ± 0.05 c for pressures between 0.7 and 2 Torr. Note that we are actually comparing current rise time in an r = 10 cm area to current density rise time. The rise time of the current density is observed to be very rapid--of order 1 nanosecond or less as shown in Fig. 20. The implications of these results will be discussed in Sec. IV.c, along with the later nose-hose measurements.

C. BEAM BLOW-UP OBSERVATIONS

The 10 cm radius conditioning cell was replaced by a 2.25 cm radius cell in order to further reduce the initial beam transverse oscillation level.

In one series of experiments in this set, a 25 μm thick Ti foil was used to scatter the electron beam. A typical photograph is illustrated in Fig. 21. An outer halo is observed to diverge as the beam propagates away from the injection point. This divergence was found to be dependent on conditioning cell current, as shown in Fig. 22. For low conditioning cell currents, the divergence angle approaches zero, while for high conditioning cell currents, the divergence angle is large. As illustrated in Fig. 23, placing the Ti foil at the anode foil position, rather than at the end of the conditioning cell results in apparently well-confined propagation for the majority of the beam.

2 ns/mm

Figure 20.

FAST FARADAY CUP MEASUREMENTS ON AXIS SHOW CURRENT DENSITY RISETIMES $\tau_r < 1$ ns, IN AGREEMENT WITH CPROP SIMULATIONS (2 METER PROPAGATION IN 2 TORR AIR, 1.1 TORR CONDITIONING CELL PRESSURE).

DIVERGENCE FOR A 1.0 TORR CONDITIONING CELL PRESSURE

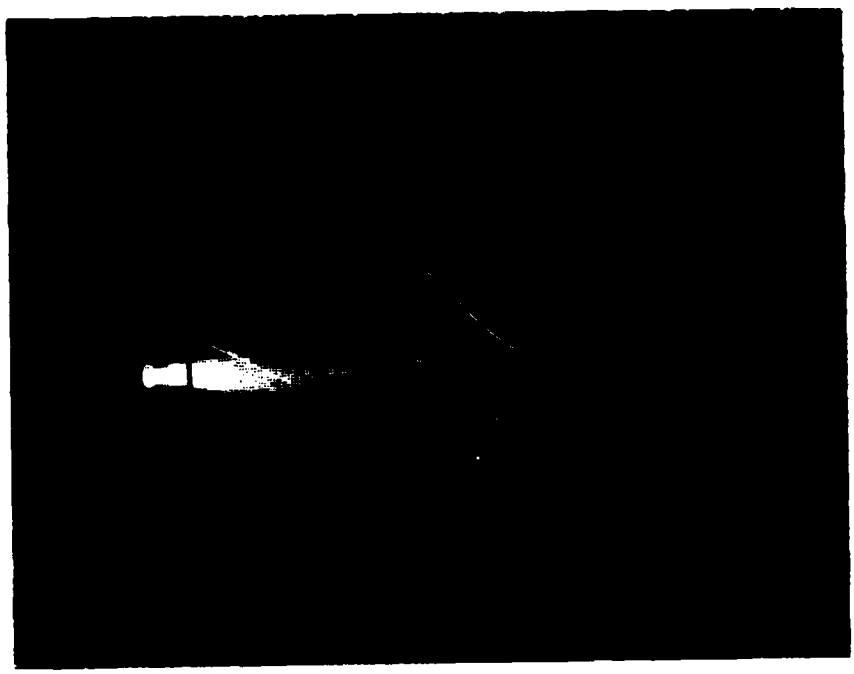

Figure 21.

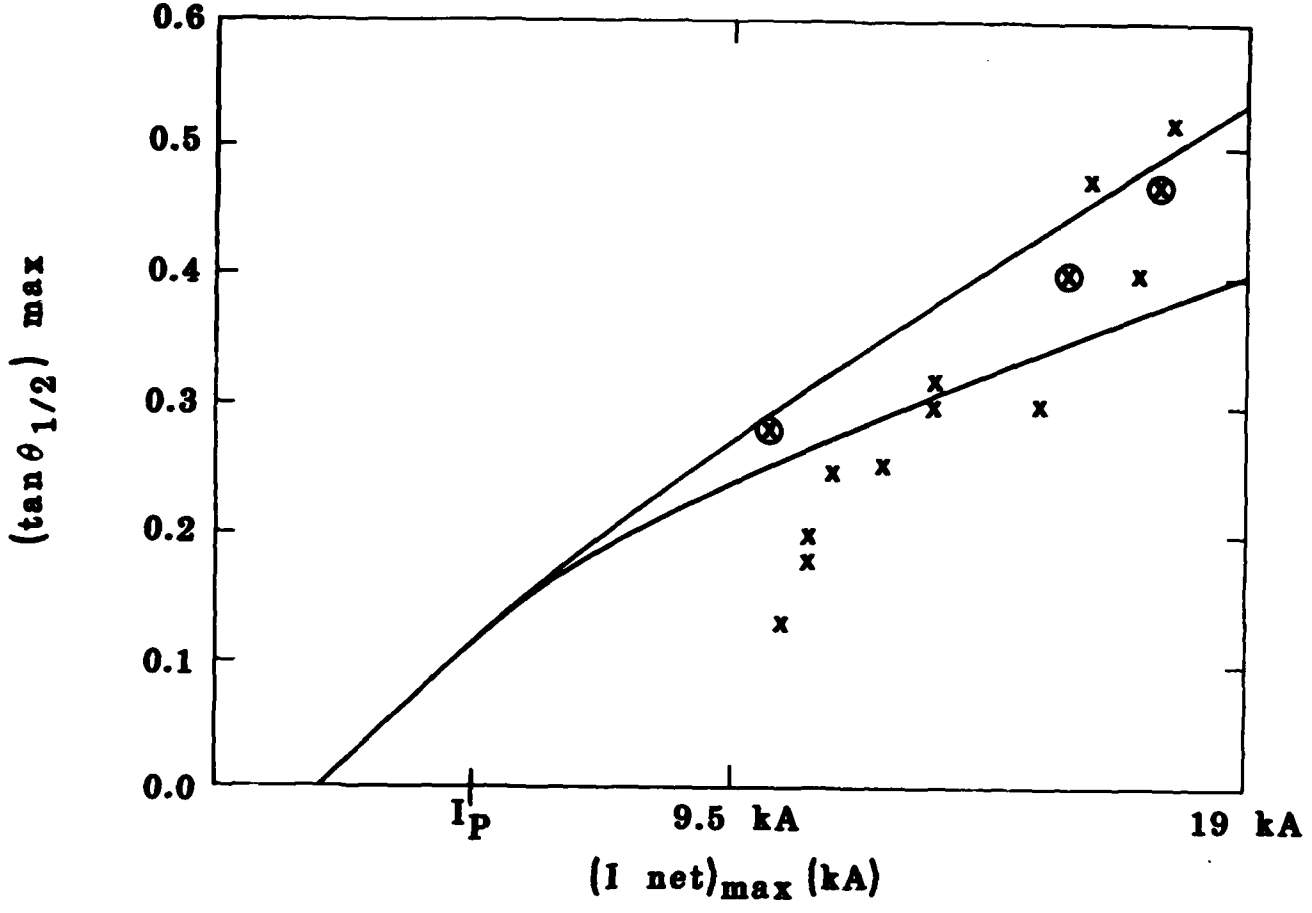

Figure 22. **BEAM DIVERGENCE IN 2 TORR AIR AS A FUNCTION OF CONDITIONING (P≤2 TORR) CELL PEAK NET CURRENT**

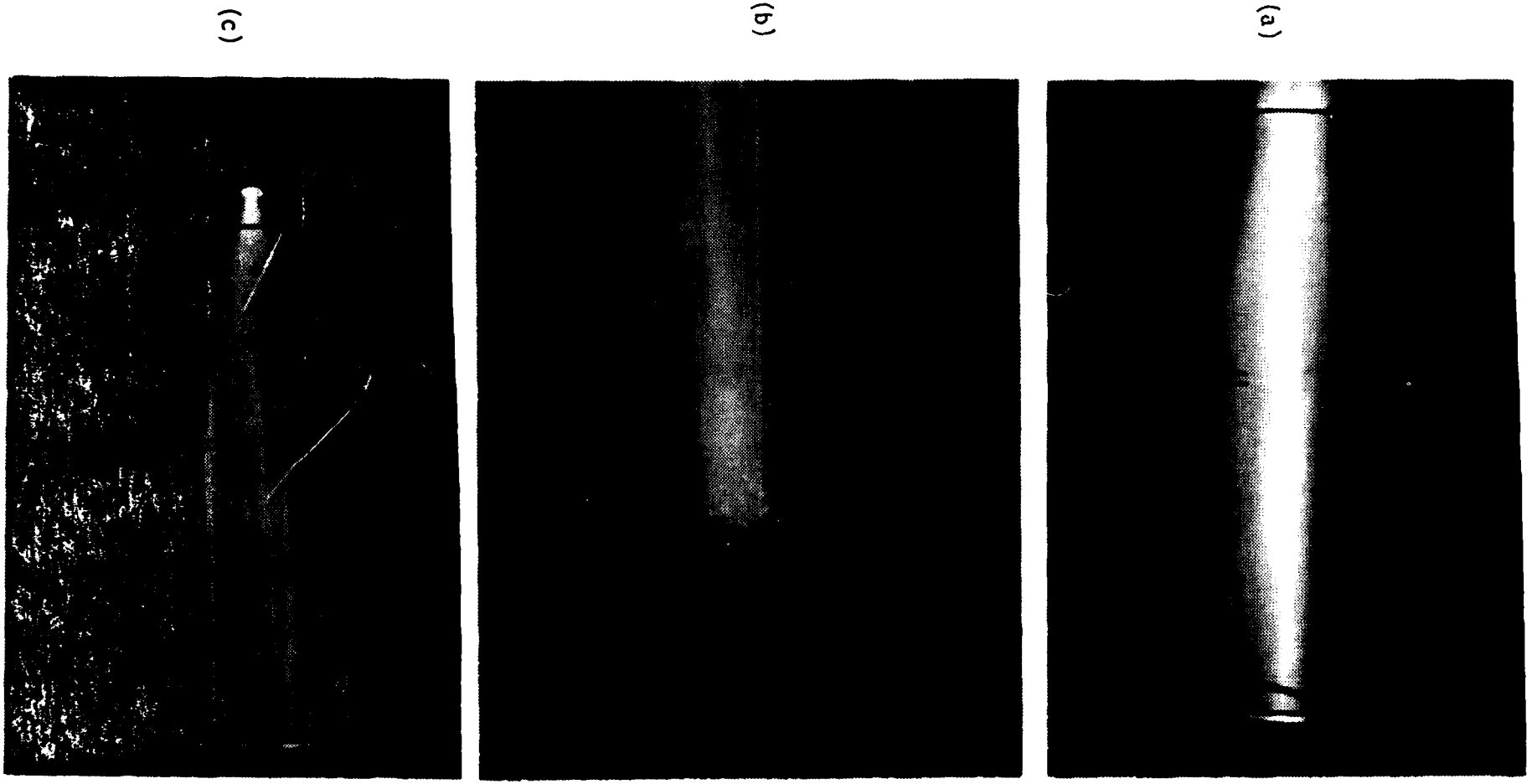

Figure 23. Beam propagation with emittance foil at anode (a,b) and at the end of the conditioning cell (c), demonstrating improved propagation.

This effect is well explained by the combination of increased emittance due to the Ti foil, and reduced net current observed in the large diameter chamber. In the limit of zero net current I_n, the divergence would be a combination of the maximum betatron oscillation angle in the conditioning cell ~ $\sqrt{2I_c/I_A}$ (I_c = conditioning cell current $I_A = \gamma mc^3/e$ = Alfven current) and the foil divergence angle of ~0.3 radians. Addition of the two by quadrature and making an ad-hoc correction for focusing due to I_p results in an angle

$$\theta \sim \left(0.09 + \frac{2I_c}{I_A}\right)^{1/2} - \left(\frac{2I_p}{I_A}\right)^{1/2} \qquad (23)$$

which is also plotted in Fig. 22. This is a gross example of the effect of increasing the emittance between the conditioning cell and main cell.

One other phenomenon observed in our experiments (and certainly many others) deserves note. In Fig. 19, for example, one observes high intensity light spots at the end plate. These are almost certainly 'cathode' spots[14]--that is, a high density plasma region in which electrons can be extracted from a metal due to locally enhanced temperatures. Such spots occur at the end plate early in the pulse, and at the injection point late in the pulse. Their existence and location may affect beam propagation because they act as a source for the plasma current.

III. BEAM CHARACTERIZATION

The initial survey measurements demonstrated that interesting phenomena were occurring in the large propagation chamber experiments. In order to get more quantitative results, we undertook careful characterization of the beam in the configuration of Fig. 24. The extracted current was 5-6 kA, of which almost 100% propagated to z = 25 cm. The beam energy was ~ 1.1 MeV.

A. TRANSVERSE MOTION

Our objective was to produce a beam with a very low transverse displacement and velocity at the exit of the conditioning cell. Average beam offset was monitored with witness foils and with unintegrated, subtracted B-dot detectors. In unintegrated mode, a perfectly balanced B-dot pair monitors the quantity $\dot{B} \sim \dot{I}x + \dot{x}I$, so that $\dot{B}/I$ is a good measure of both the initial transverse velocity and position in units of velocity. This quantity is plotted in Fig. 25a, and the same data after passing through bandpass filters is shown in Fig. 25b. Clearly, 0.70 Torr should be our operating point. Blue cellophane witness foils verified that at lower pressures the beam was offset by as much as 3 mm. Although the bandpass filter data cannot be easily quantified, it qualitatively indicates that growth is stronger at lower (i.e., 30 MHz) frequencies. If we assume a freqeuncy of 20 MHz, the typical displacement is ~0.7 mm.

Our present understanding is that the rapid increase of transverse noise above 0.8 Torr is due to hose instability growth in the conditioning cell combined with increases in the magnitude of the net current. The witness plates also indicated that the beam at the extraction foil had a nominal 0.5 cm radius and was offset no more than 1 mm at P = 0.70 Torr.

B. BEAM PROFILE

Because our intention was to make measurements relevant to the propagating beam state in the large diameter drift chamber, we decided to

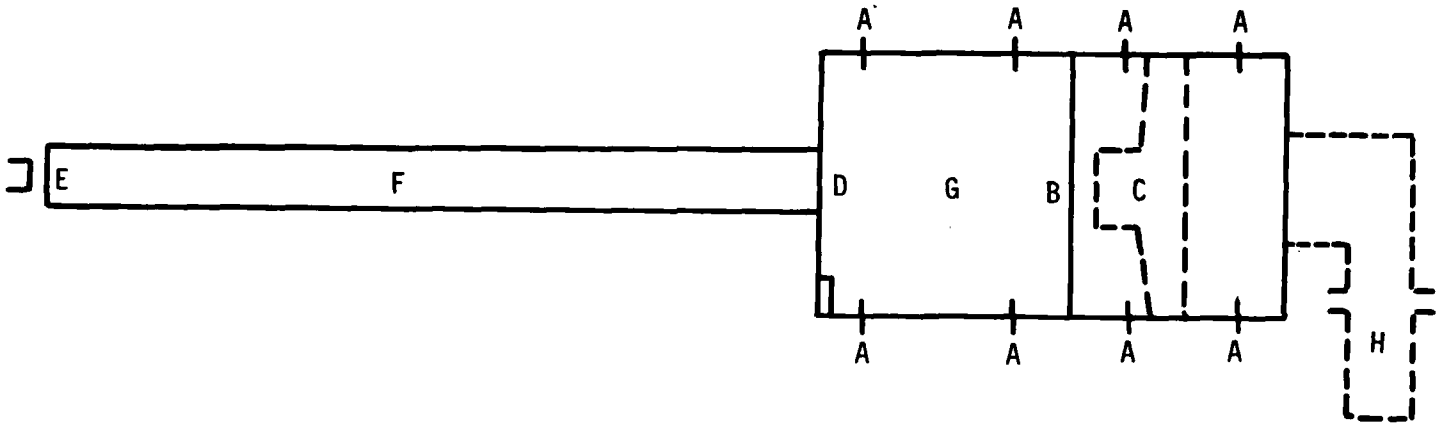

Figure 24. Experimental Configuration showing:

(A) B-dot or Penny probe position
(B) Vacuum/gas interface foil or Faraday cup position
(C) Vacuum current collector
(D) 25 μm Kapton extraction foil
(E) 125 μm Kapton entrance foil
(F) Conditioning cell
(G) Propagation cell
(H) Diffusion Pump

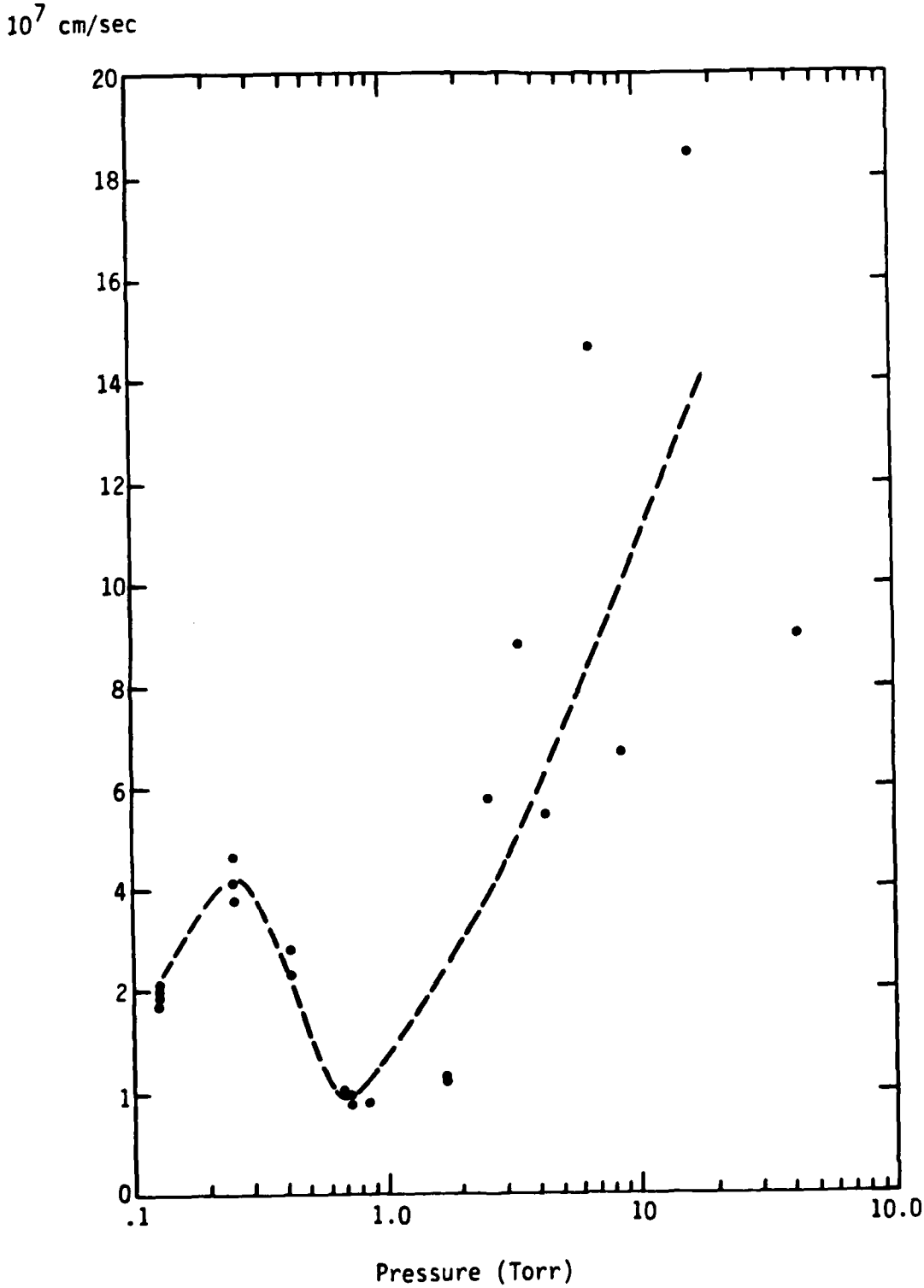

Figure 25a. Conditioning cell exit transverse velocity as a function of pressure.

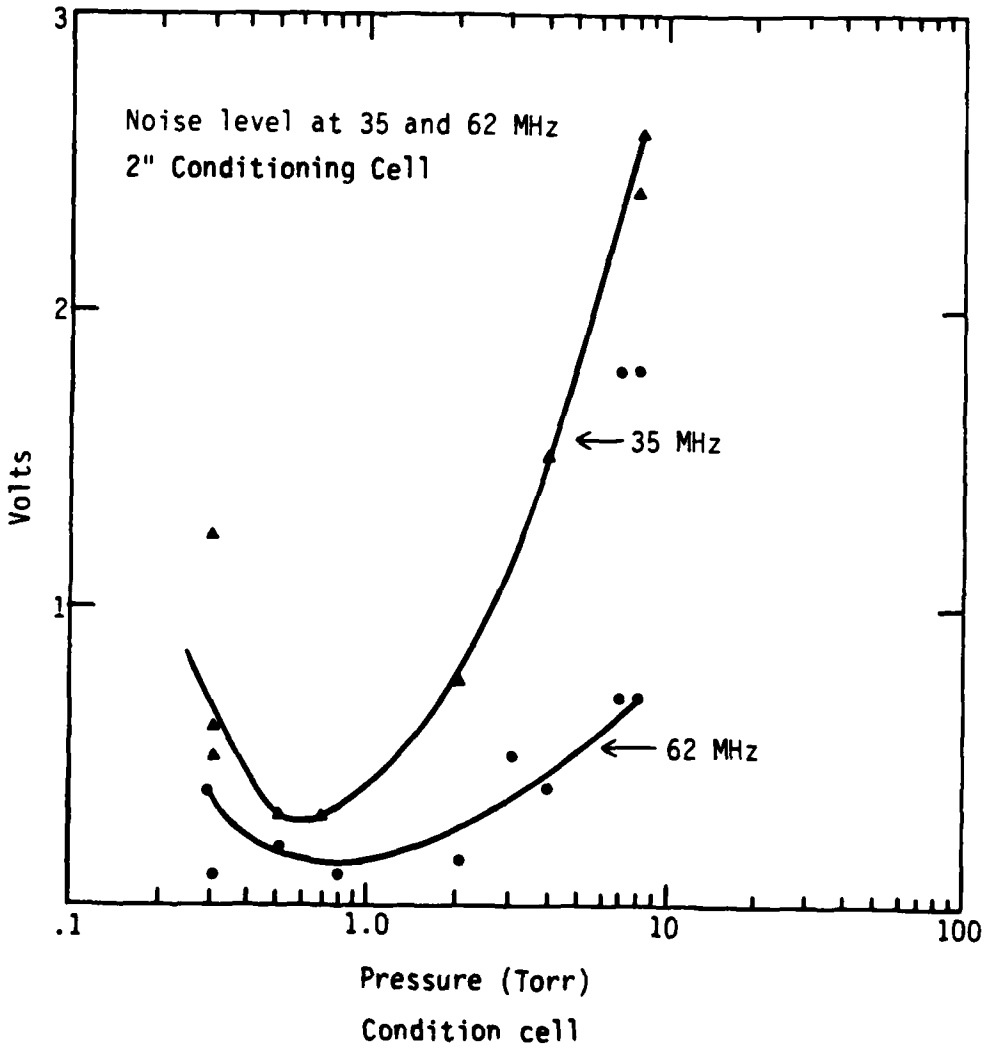

Figure 25b. Data broken into frequency bands.

measure the beam radial profile as a function of time at a position 25 cm (more than 2 betatron wavelengths) beyond the extraction foil.

The Faraday cup array of Fig. 7 was used to make time dependent measurements of the beam radial profile. The motion of the beam centroid was evident on this detector. In Fig. 26, a representation of radial profile data at a hose stable pressure of 3 Torr is shown. This profile indicates that the Bennett radius is ~0.9-1.0 cm between 30 and 50 nanoseconds. During the 0-30 nanosecond time period, the radius is undergoing significant changes. We also note that although the beam is stable in this particular case, it appears to be slightly off axis (~1 cm) at z = 25 cm. Two other cases are shown in Figs. 27, 28. Note the quasi-three-dimensional technique used to plot data in the transverse plane. The 50 Torr data of Fig. 27 indicates that the beam undergoes several oscillations, peaking at probes (sequentially) 7-2-6-2-1-1-7, in 8 nanosecond intervals. We ascribe this motion to the hose instability. The 15 Torr case demonstrates an apparently monotonically increasing displacement in the direction of probe 6 from probe 7. These observations are in qualitative agreement with the B-dot hose data of Sec. IV.

Most hose oscillations observed appear to be continuous in space. Cases do exist however, where the motion is discontinuous between two channels. This type of motion would not be easily observed on magnetic probes due to the plasma current contribution.

In general, the Bennett radius can be taken from the profile data at some representative time for each shot and one can attempt to arrive at general scaling information. The beam profile is affected by hose motion, and this effect was observed in the Astron experiments.[15] Our studies indicate that sweeping of the beam a distance of 2 cm results in a 50% increase in the beam diameter. In general, the Bennett radius was found to be 1.0 ± 0.2 cm independent of pressure.

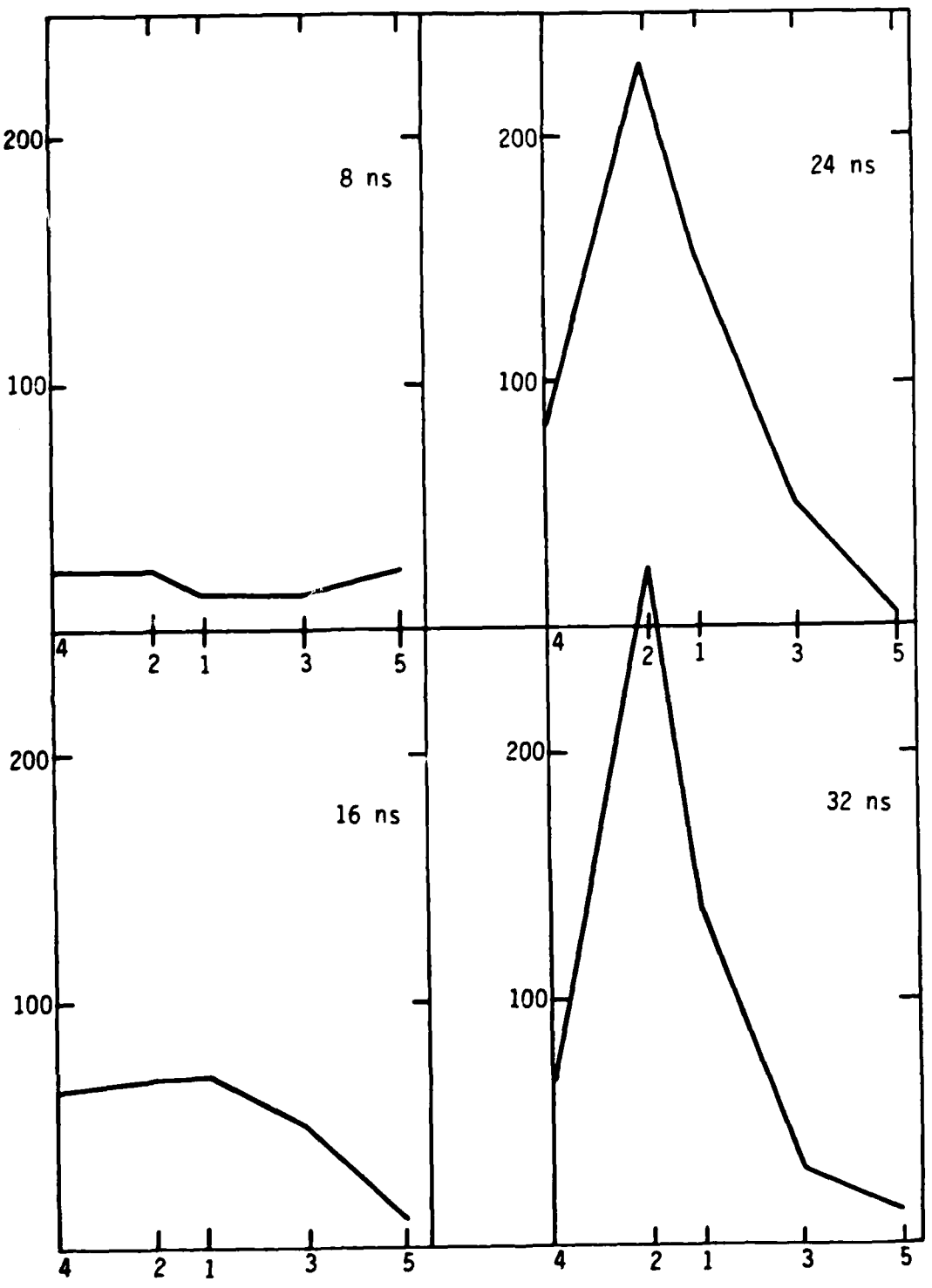

Figure 26a. Beam profile at 3 Torr where the probe number is indicated on the horizontal axis and the relative current density on the vertical. Probe 1 is center and probes 1,2 are separated .5 cm, and probes 1,3; 3,5; and 4,2 are separated 1 cm.

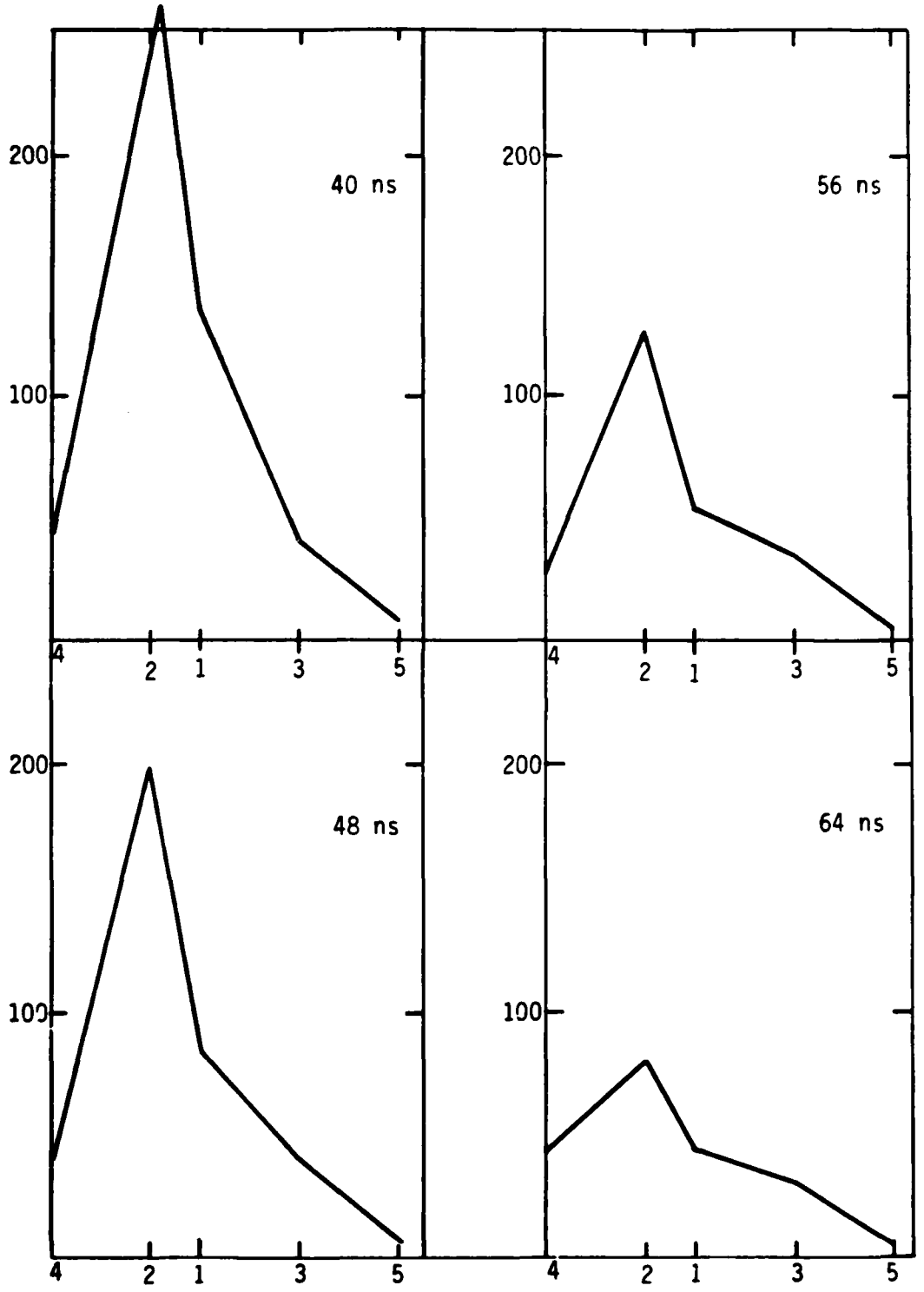

Figure 26. Continued.

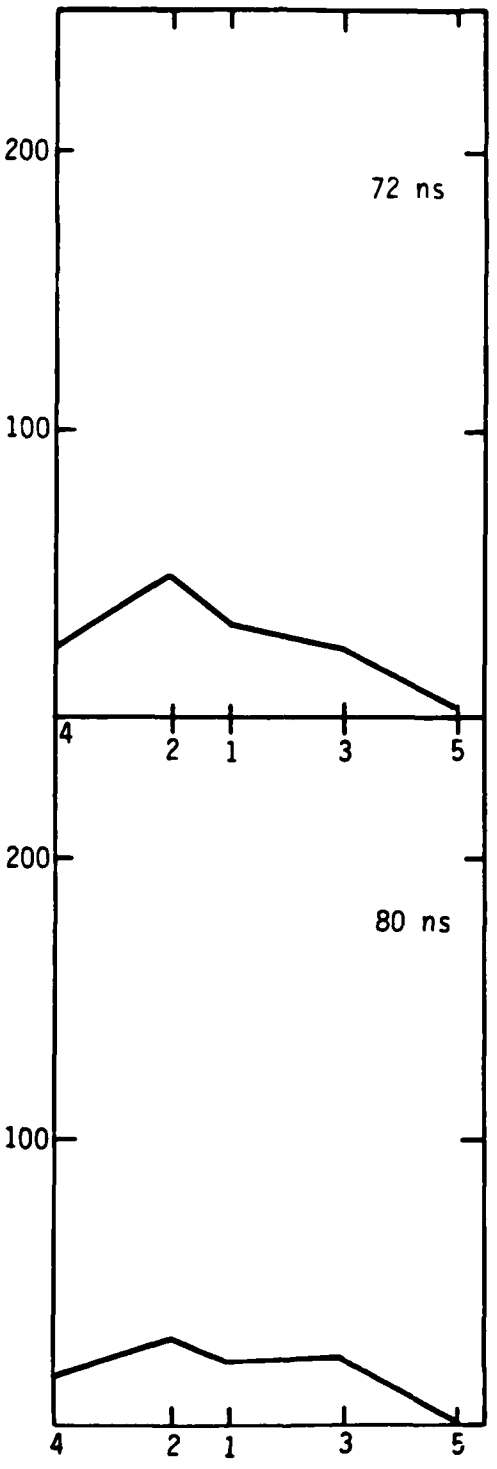

Figure 26. Concluded.

Beam Profile at 3 Torr

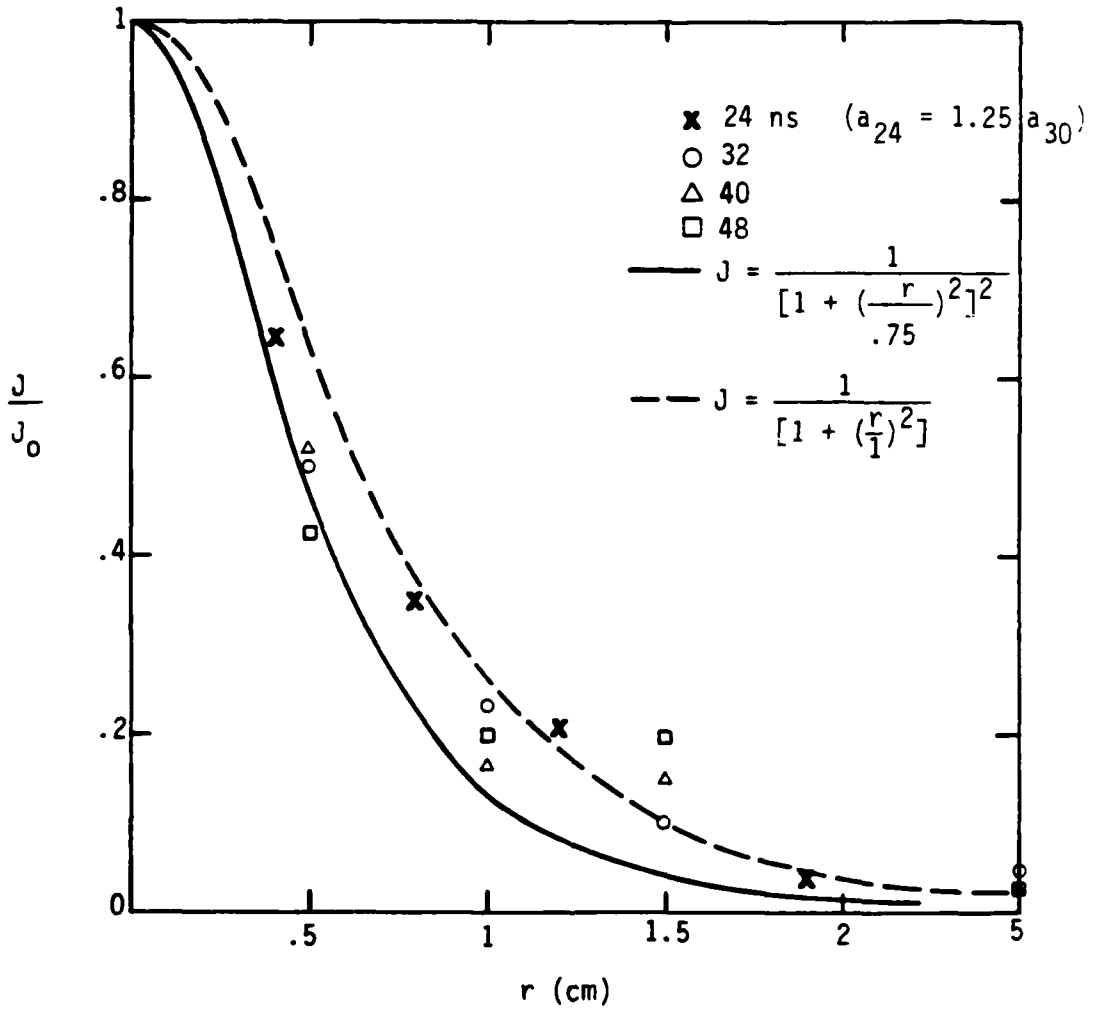

Figure 26b. Radial beam profile from the data of Fig. 26a.

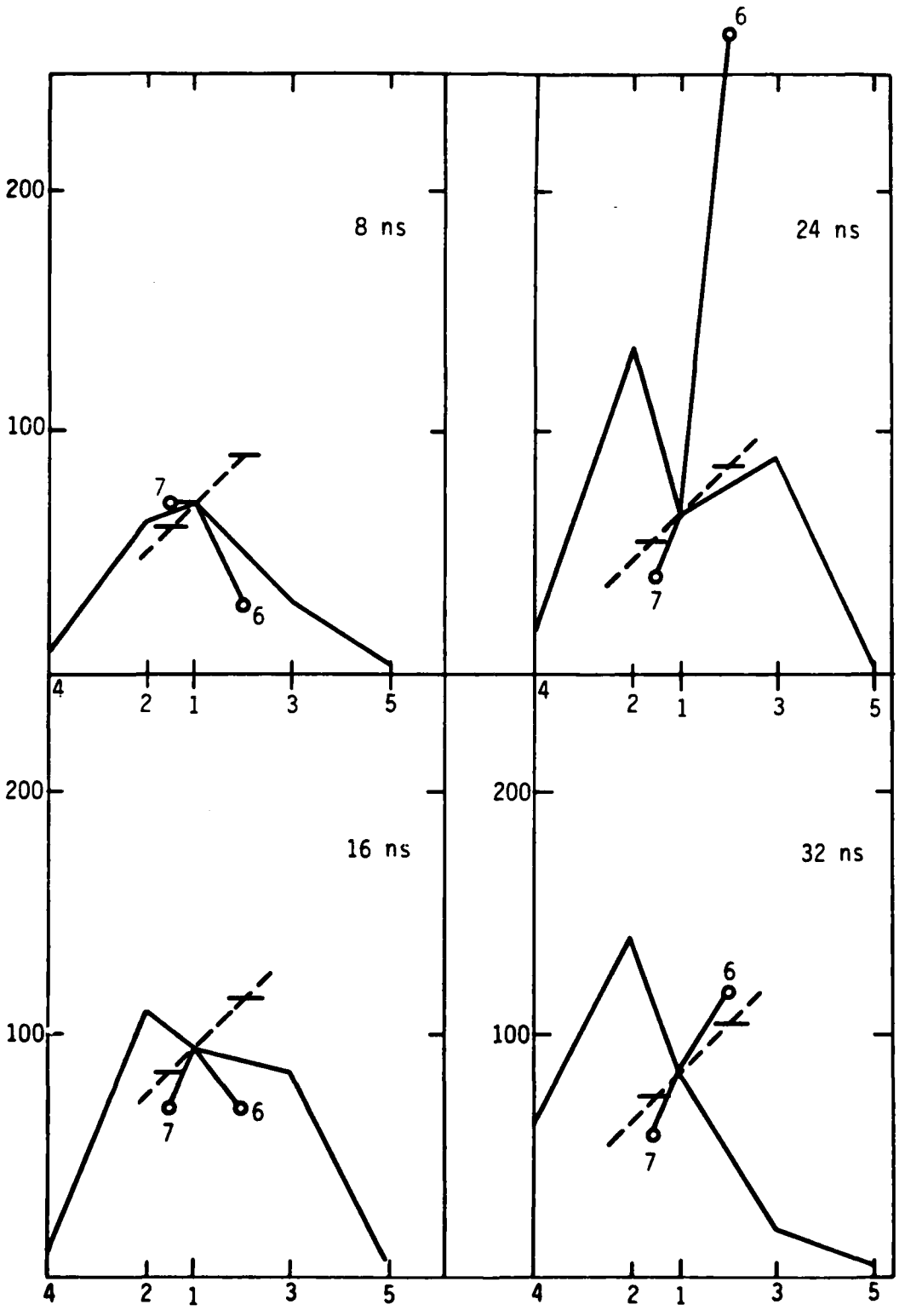

Figure 27. Beam profile evolution for 50 Torr. Transverse probes 6,7 are plotted relative to probe 1 at a 45° angle. Thus, the dashed line represents the probe 1 signal relative to 6 and 7.

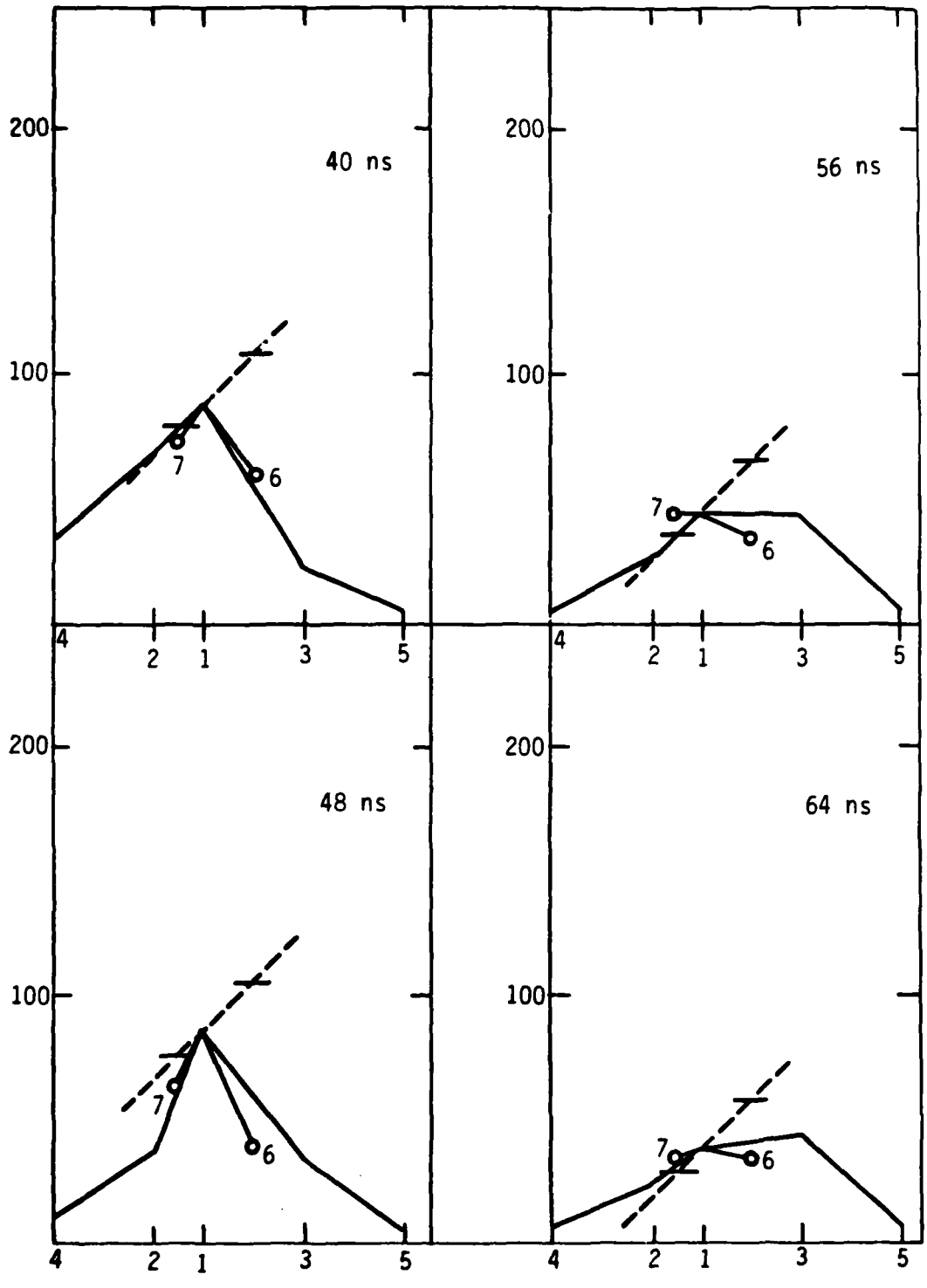

Figure 27. Continued.

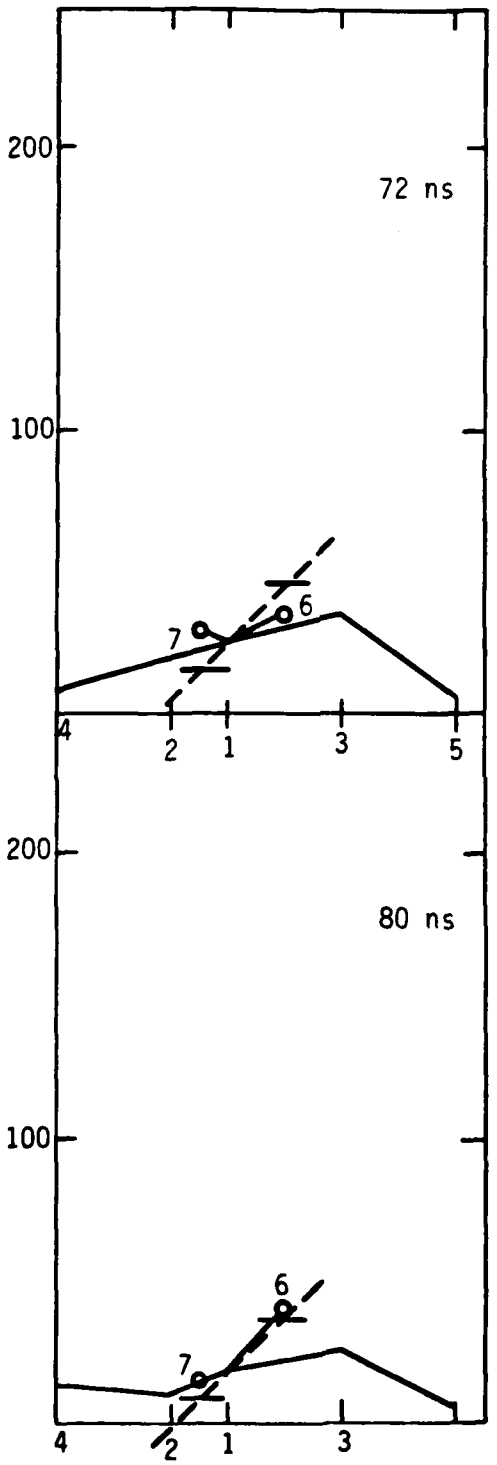

Figure 27. Concluded.

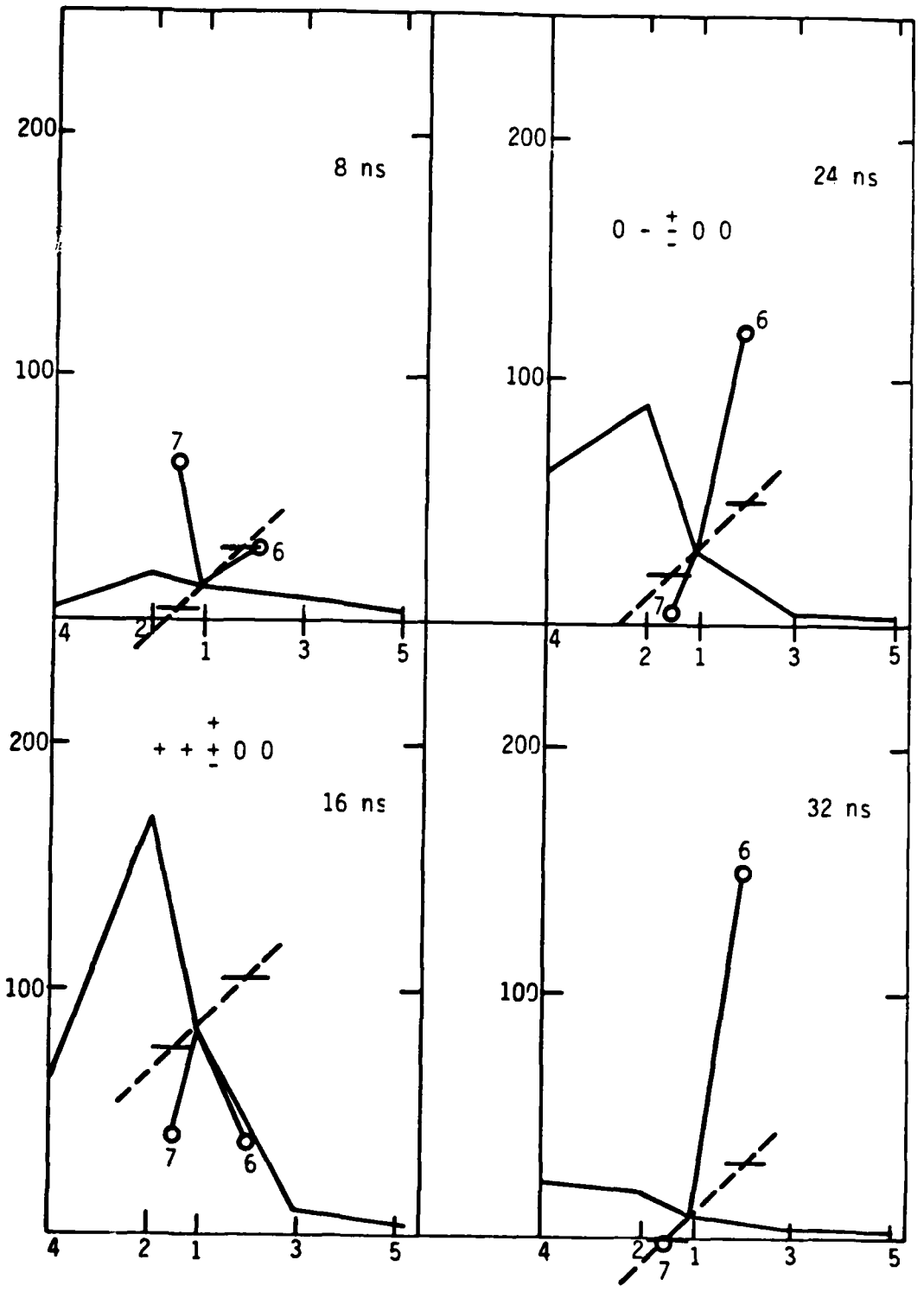

Figure 28. 15 Torr Faraday cup data.

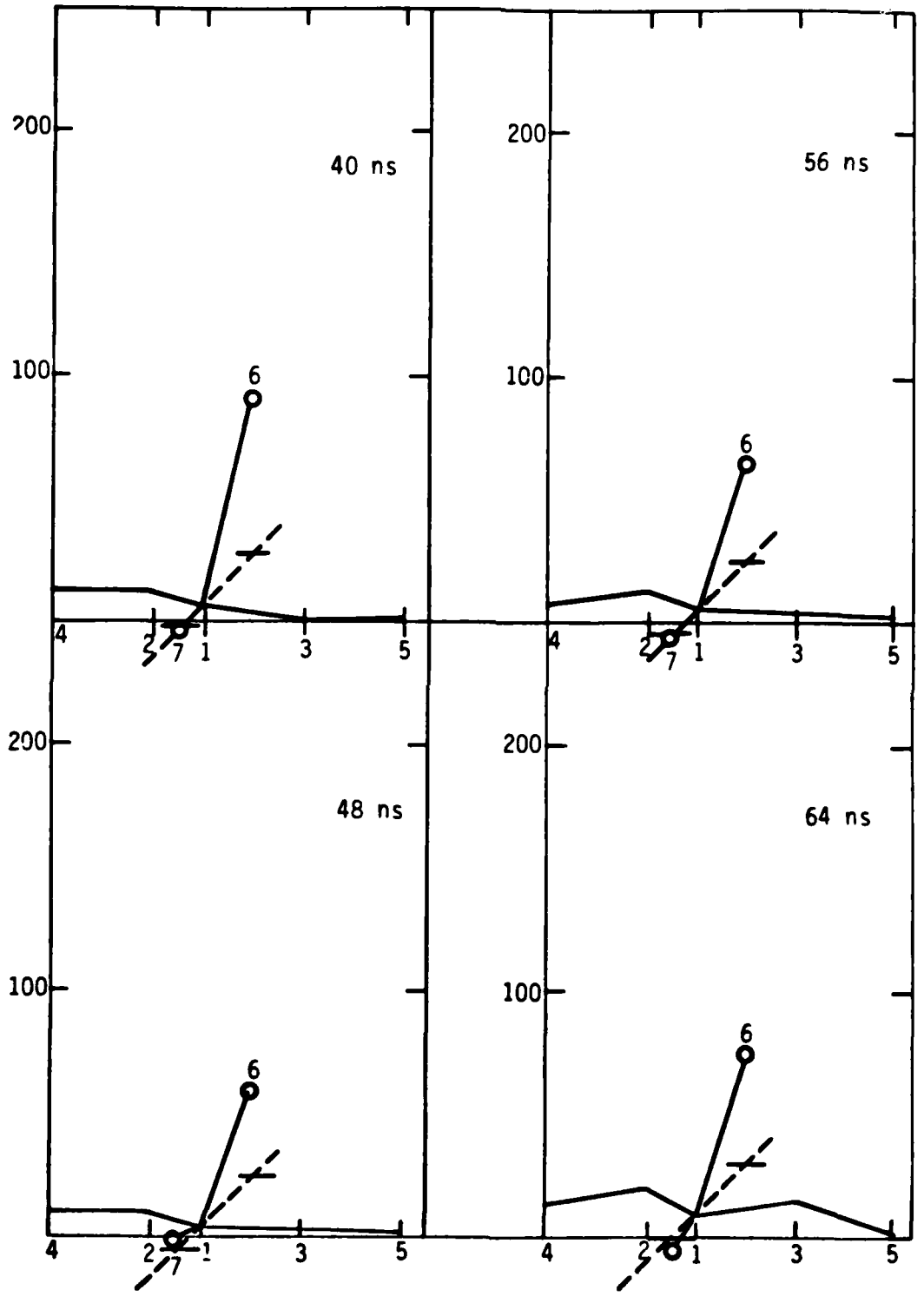

Figure 28. Continued.

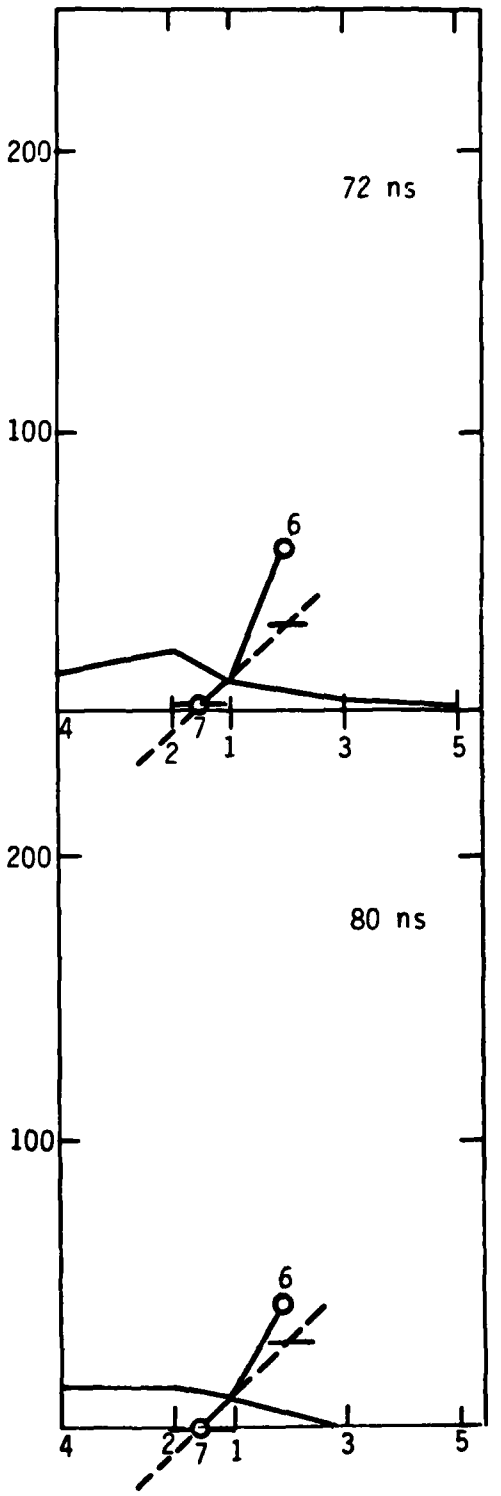

Figure 28. Concluded.

As we vary the pressure and observe the beam profile temporal evolution, we find a significant change at P = 15 Torr. For P < 15 Torr, the beam does not evolve into a well-pinched profile until ~20 ns into the pulse. For P > 15 Torr, the beam is found to be in a well-defined, pinched state for times earlier than 8 ns. For the marginal 15 Torr case, the beam is found to be in its pinched state at t ≈ 10 nanoseconds. This effect can tentatively be ascribed to the low net current which is observed at low pressures. The equilibrium radius varies as $I_n^{-1/2}$, and it is this fact which is reflected in the data.

Although it is tempting to ascribe some minimum net current requirement for pinched propagation based on this data, no one value results. The net current criterion based on the data is 2.8 kA for 3 Torr, 4.5 kA for 10 Torr, and 2 kA for 15 Torr. If we speculate that the differences in net current at 'pinch time' are due to variations in the return current profile, then it is possible that the results can be explained by plasma return currents which differ from inside to outside the beam. These effects may also be the result of axisymmetric beam hollowing which is a result of avalanche ionization. This correlates well with the observed upper pressure for avalanche ionization of 5-15 Torr found in Sec. III.c.

The apparent fixed value of the Bennett radius may also be a result of return currents flowing outside the beam at low pressure. Based on this data the half-current density point is found to be ~0.65 cm. For fixed emittance, we would expect this quantity to depend on time into the pulse, and on current. The current in turn depends on pressure, but the radius is independent of pressure between 2 and 100 Torr. The current variation between 1 and 150 Torr is shown in Fig. 29. The relatively constant radius may tentatively be explained by the combination of hose-induced beam broadening at 10 Torr and above where the net current exceeds 4 kA.

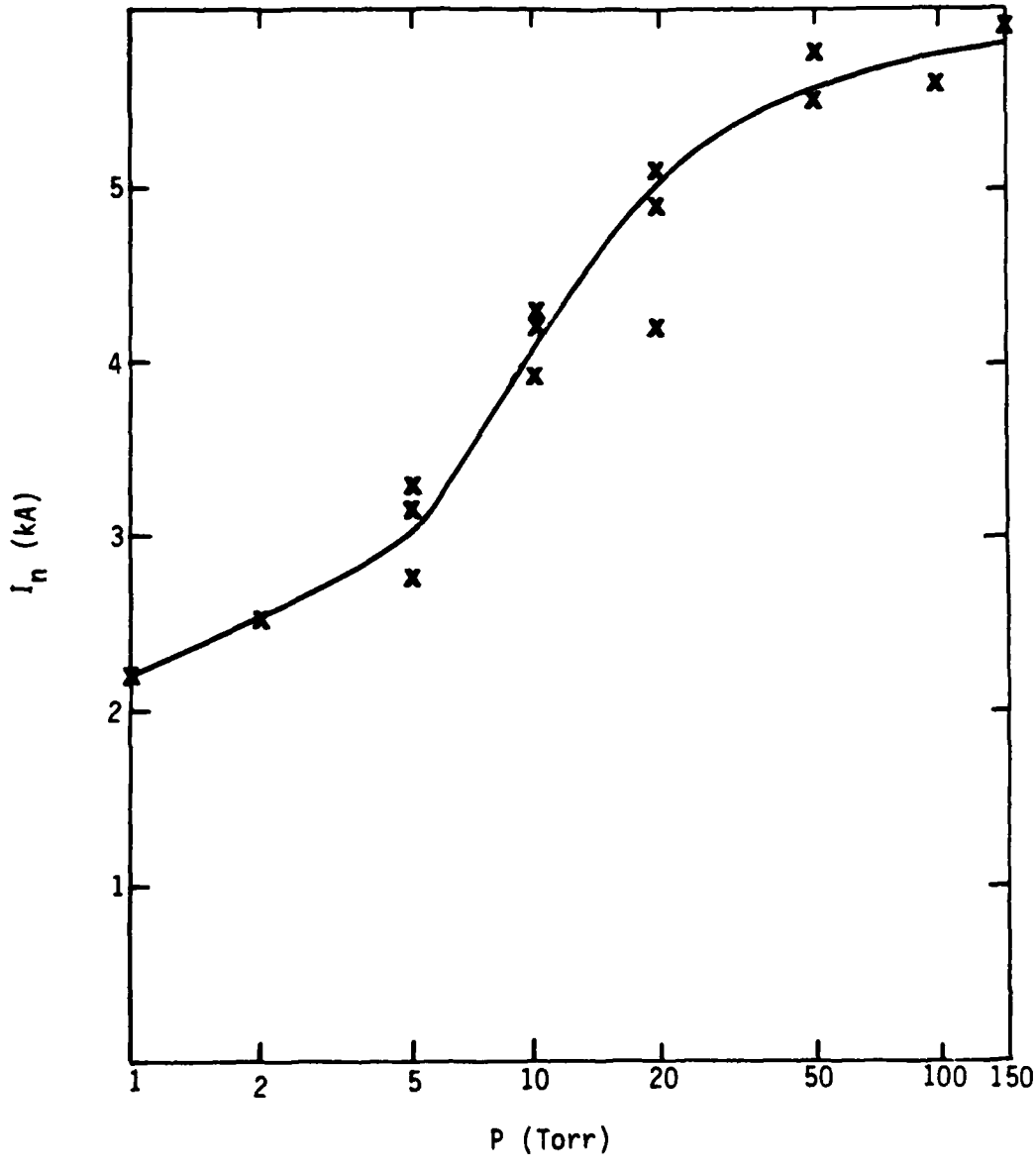

Figure 29. Net currents as a function of pressure.

C. PLASMA DECAY TIME

The most important plasma parameter in the hose instability problem is the plasma dipole decay time, τ_d. This quantity is well approximated by the variational expression[15]

$$\tau_d = \left\{ \int \frac{dr}{r} \sigma(r) \left[\frac{I_n}{c}\right]^2 \right\} / \left\{ \int \pi dr \left[j(r)\right]^2 \right\} , \qquad (24)$$

where I(r) is the net current within radius r. The approximate value of τ_d is

$$\tau_d \approx \frac{1}{8} \tau_m = \frac{1}{8} \left(\frac{4\pi\sigma a^2}{c^2} \right) = \frac{1}{8} \frac{\sigma a^2}{6c^2} \quad ; \quad \sigma = \frac{ne^2}{m\nu} \qquad (25)$$

for Lee's spread mass model of the hose instability. The equation above assumes that the beam drift tube is infinite. In our case, b ≈ 10a, and this should be a good approximation. The technique used for analyzing the data to arrive at τ_m is discussed in some detail in Sec. I.xi. We simply note here that the decay time includes contributions due to changes in the beam and channel radii. These decay time measurements are still the most detailed measurements of this type of which we are aware, and provide the basis for comparisons of hose theory and experiment.

Three representative decay time plots are shown in Figs. 30, 31, 32. The peak decay time τ_m is found to be 90, 40, and 20 nanoseconds at 5, 100, and 620 Torr, respectively corresponding to average peak conductivities of 3×10^{13}, 1×10^{13}, and 6×10^{12} sec^{-1}. The general nature of the time dependence varies with pressure. At 5 Torr there is a rapid increase in τ during the first 10 nanoseconds, followed by a slower rise during the next 50 nanoseconds. At this time the beam current begins to fall, and so, as a result, does the decay time. The rapid rise is indicative of avalanche ionization. Some variations in τ_m early in the pulse are probably a consequence of variations in the beam radius a. For 15, 100 and 620 Torr, we find τ to be increasing approximately linearly during the pulse. Analysis of τ_d for a higher current shot (15 kA versus 5 kA) at 20 Torr showed

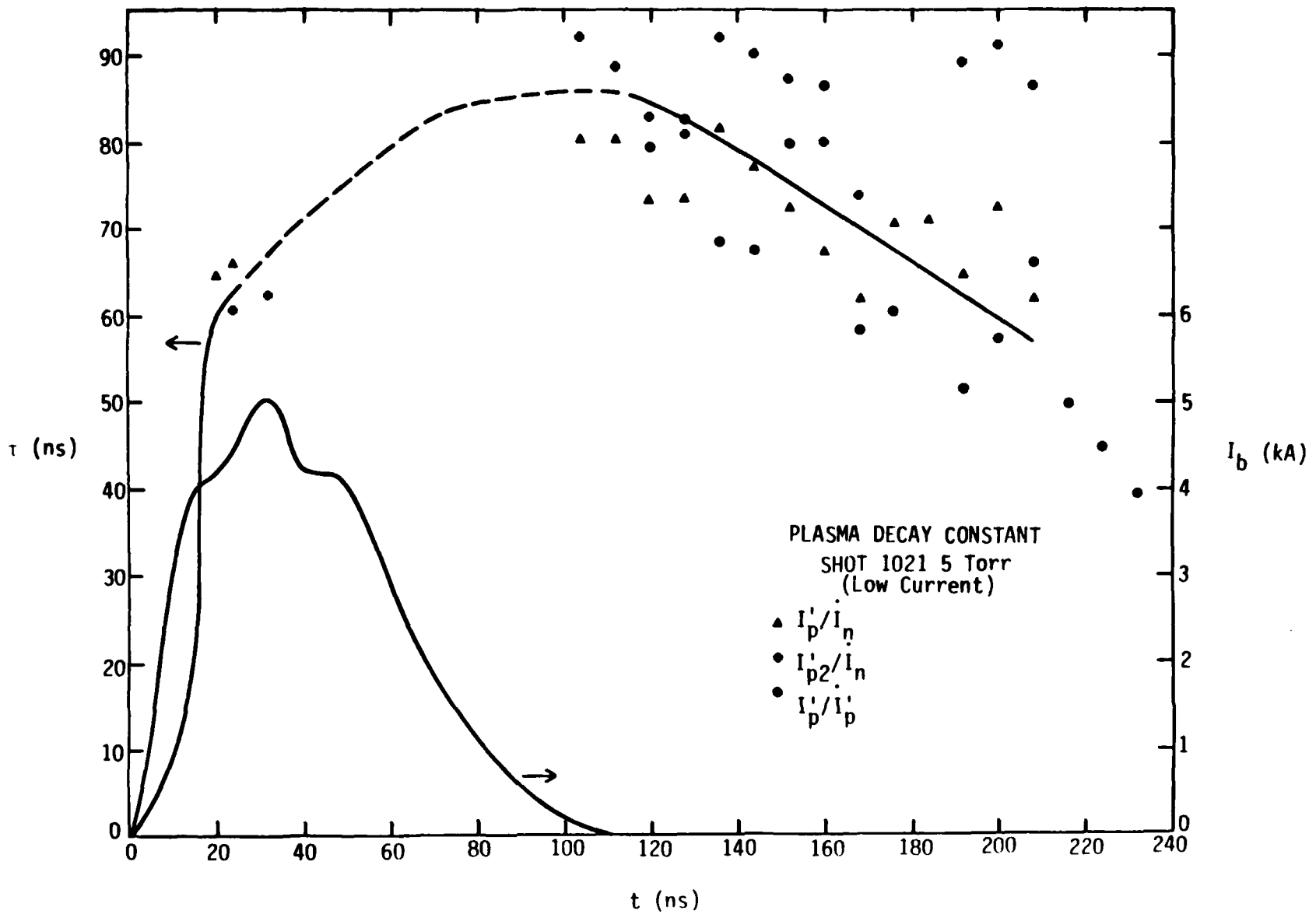

Figure 30. Plasma decay time τ_m for 5 Torr.

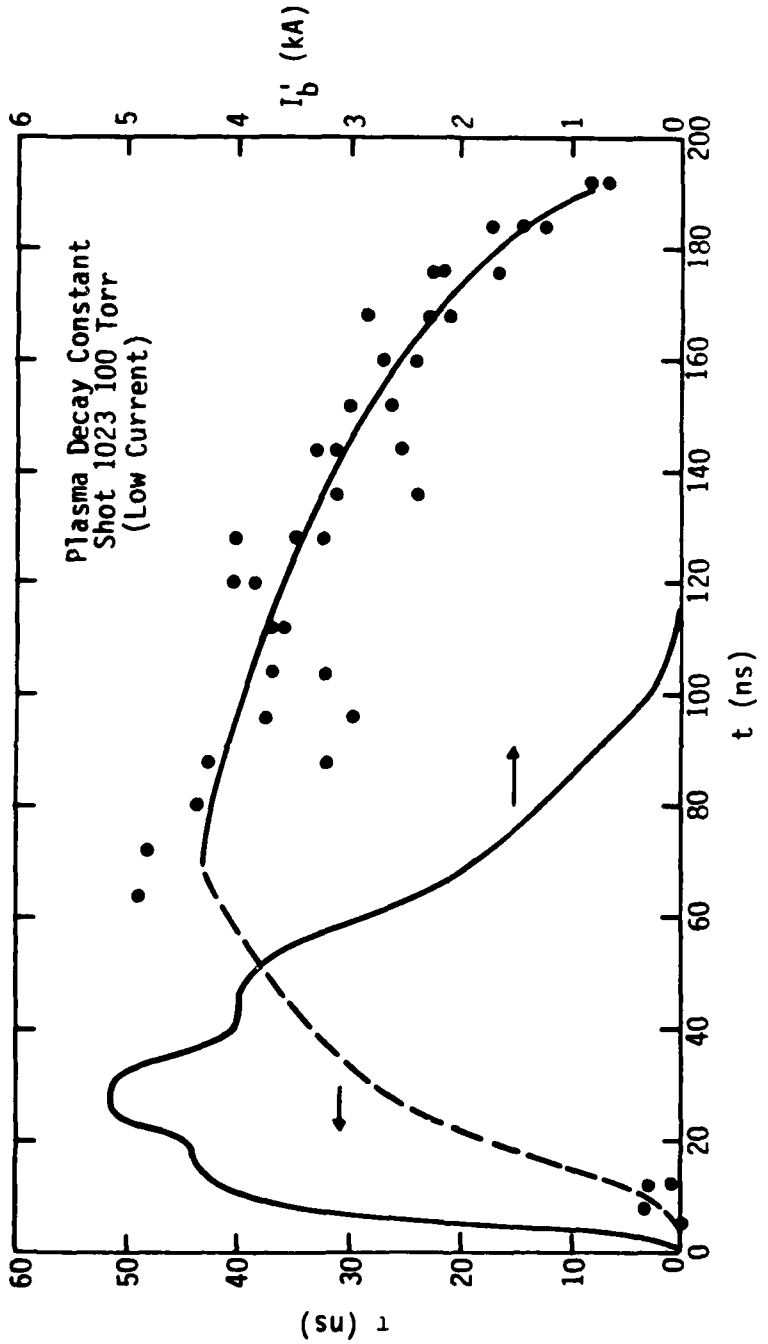

Figure 31. Decay time for 100 Torr.

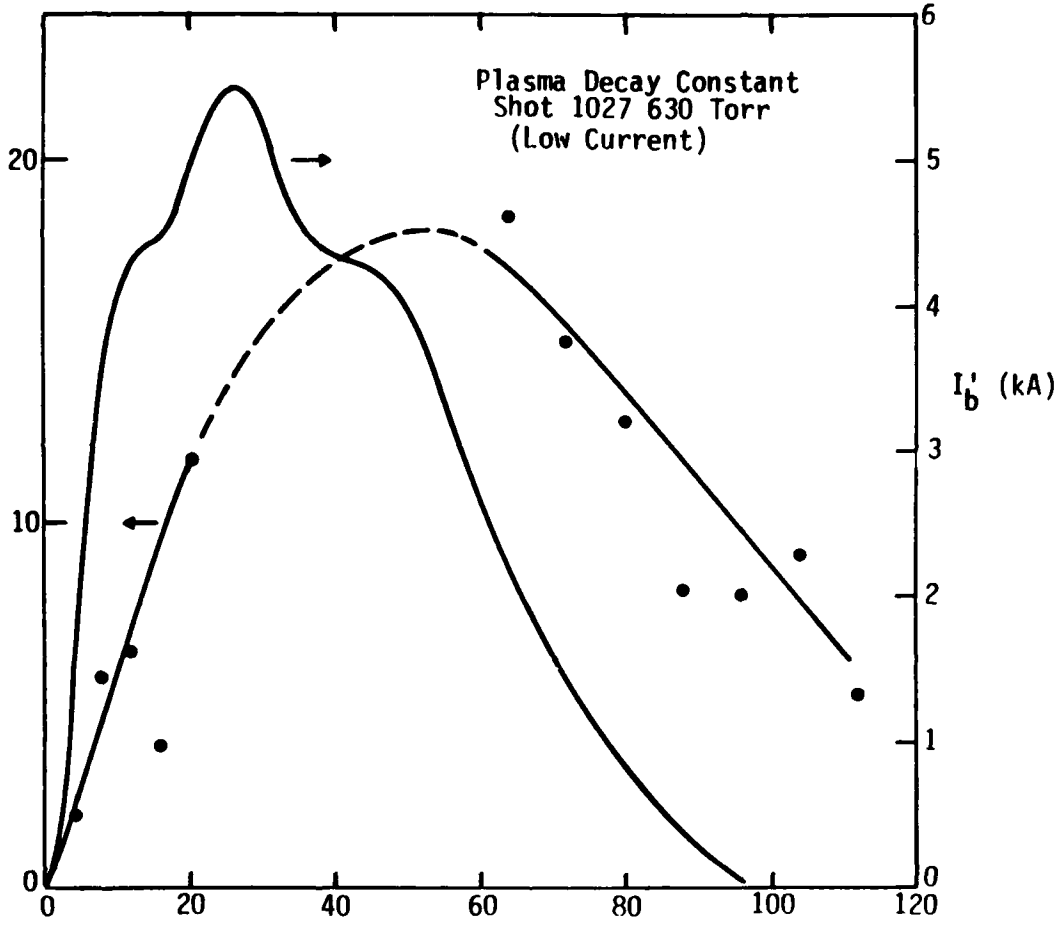

Figure 32. Decay time for 630 Torr.

no significant differences from the corresponding low current shot (Figs. 33, 34). There appears, based on the data, to be a transition between avalanche and impact ionization at ~15 Torr. This corresponds to E/P ~15 V/cm-Torr.

The decay time changes by a factor of only five where the variation in pressure is a factor of 120 (5 Torr to 620 Torr). This results because lower temperatures and higher collision frequencies at high pressures have counteracting effects. As the neutral density, n, is increased, the electron temperature falls and the electron collision frequency, which varies as nT increases only slowly.

A convenient formula relating τ_m to the electron density per unit length may be derived from the relation between the collision frequency and temperature, and Eq. (24)

$$N = \pi a^2 n = 3\times10^{12}\ P(\text{Torr})\ T(\text{eV})\ \tau_m \qquad (26)$$

These measurements are particularly valuable if some other relation between n and T is known. If we assume that the Saha relation is valid at full pressure, and that error is due only to uncertainty in the thermodynamic pressure P, we find that T_e ~ 0.6 eV ± 10% for full pressure air. This number appears to be eminently reasonable in light of the number of assumptions (such as channel diameter) required to calculate it.

The plasma decay time results are particularly important in allowing us to predict hose frequency behavior, and in providing a benchmark for numerical work (see Sec. V.B). A general observation relevant to all the results in this section is that the decay time does not vary wildly with changes in pressure or current, in the absence of avalanching. It would be possible to produce a useful empirical model for τ given more data on decay times for more varied currents and pulse lengths.

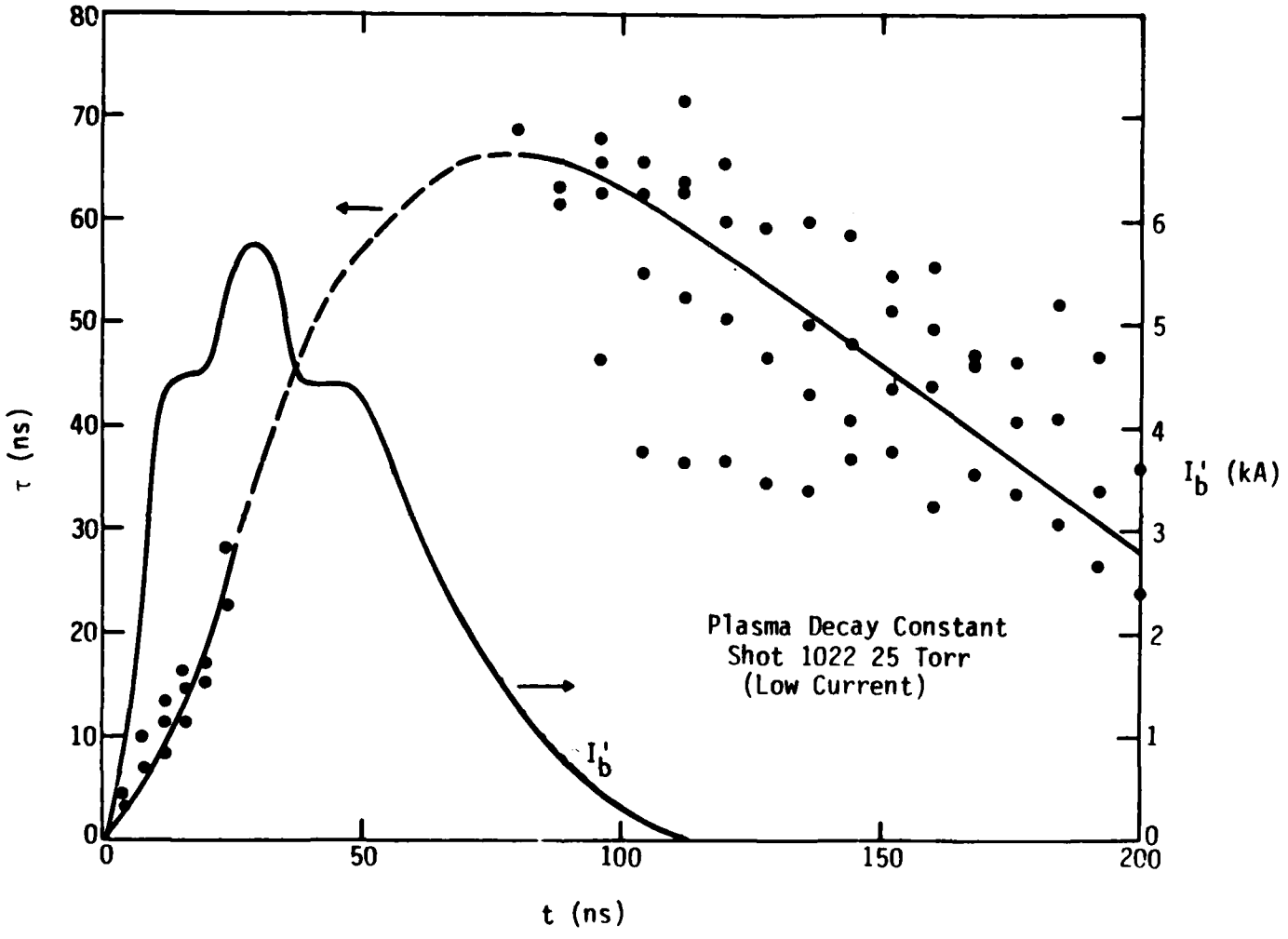

Figure 33. Decay time (20 Torr, low current).

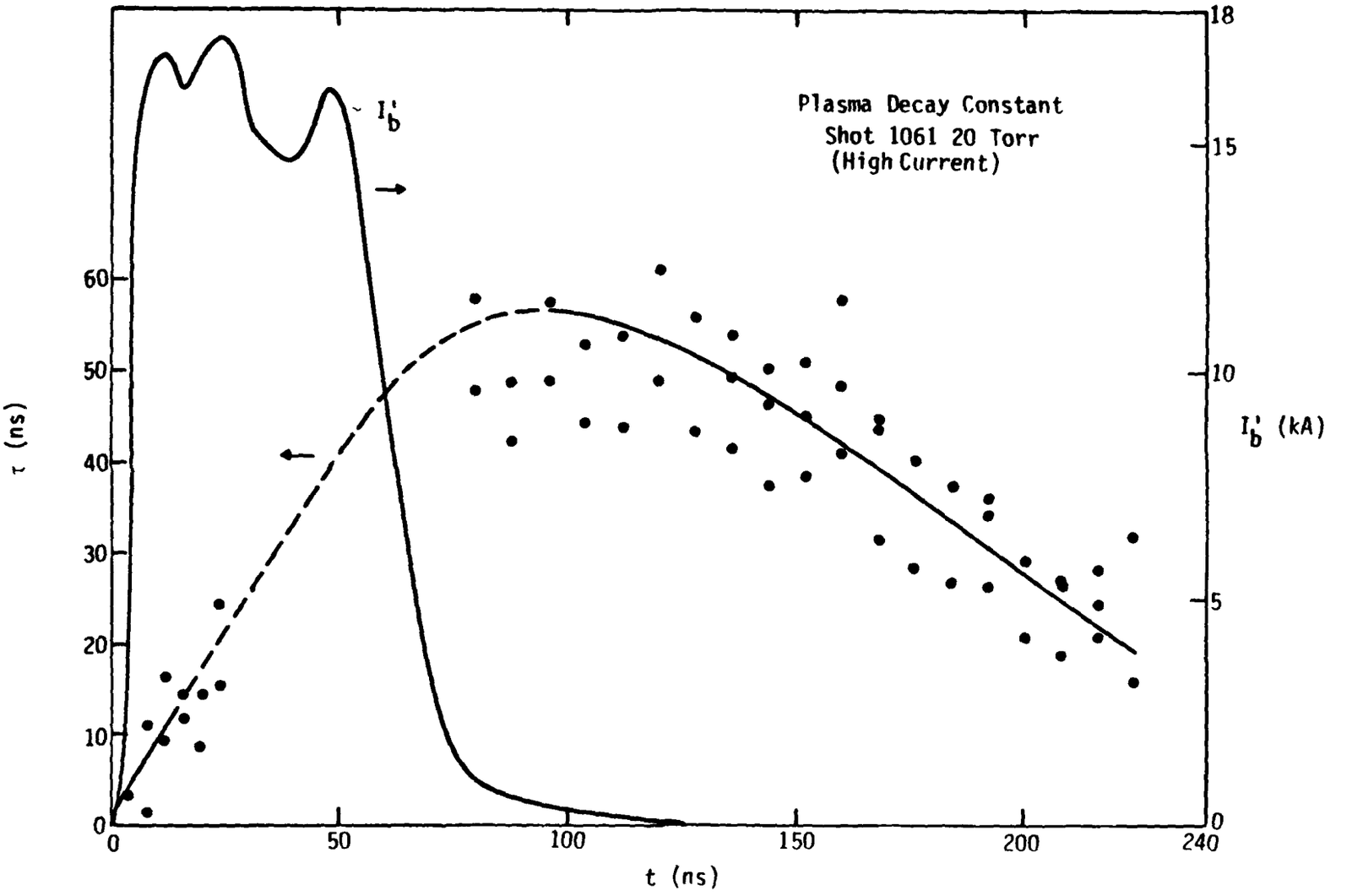

Figure 34. Decay time (20 Torr, high current).

IV. NOSE EROSION AND HOSE RESULTS

In this section we will discuss our beam front propagation measurements, the hose growth measurements in the r = 10 cm chamber, and finally, the nose coupled hose instability measurements. Where applicable, we will attempt to compare these results with theory.

A. BEAM FRONT MEASUREMENTS

Using the penny probes and the beam front velocity measurement technique outlined in Sec. I.B.vii, along with differential B-dot probes, we have characterized beam front propagation in detail. Our experimental setup is shown in Fig. 35, where 4 penny probes and the specific B-dot summing network are outlined, along with an aperture used on some shots, and an intermediate net current monitor. Several major results are evident:

1) The beam front velocity is extremely nonuniform with the velocity generally increasing as a function of propagation distance to 85 cm, and decreasing beyond.

2) Extremely fast (< 1 ns) rise times can be produced with the aperture plate inserted in the drift tube.

3) The erosion rate increases with increasing net current.

4) Anomalous radial losses occur during the pulse.

As discussed in Sec. IIb, the average beam front velocity in the large propagation cell was observed to be relatively slow--0.45-0.55 c. This value results from comparing the time at which the first net current is observed at a B-dot current monitor to the time the first current is

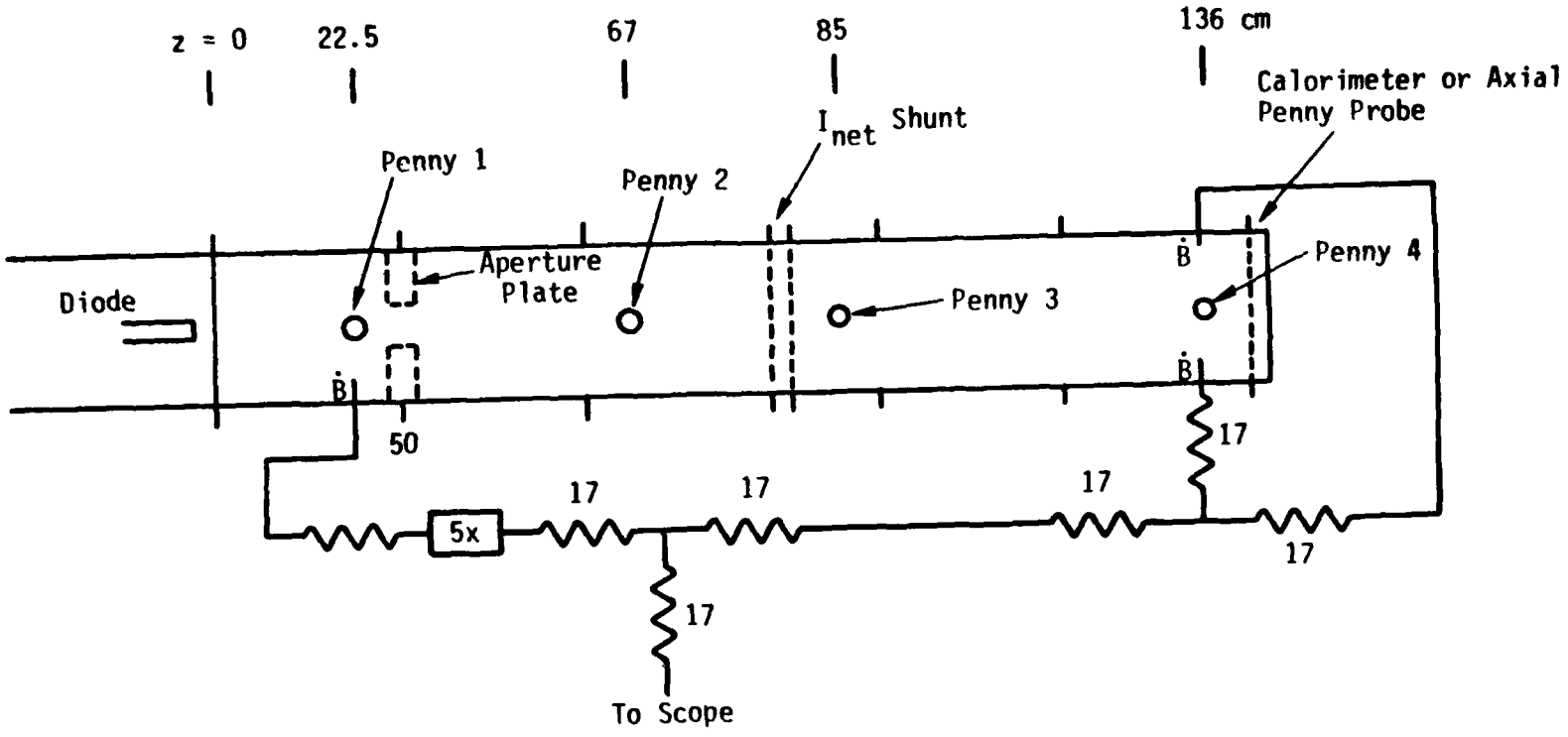

Figure 35. Beam front analysis setup.

observed in the central Faraday cup detector. Similar measurements have been made for the same nominal beam current (~15 kA), in the r = 10 cm tube. A typical data set is shown in Fig. 36 for a beam current of 15 kA. The dashed lines indicate the time assigned to the beam front propagation phase of the penny probe signals. The net current undergoes considerable spatial variation for this particular case, as shown by Figs. 36a-c. At 67 cm and beyond, the penny probe signals show radial beam currents which result from both beam front radial emission, and an anomalous radial loss process. The penny probe beam front phase duration was chosen by noting local minima in the signals. Net current traces indicate an upper bound of 12 ns at 22 cm, and 6 ns at 136 cm for the beam front phase. In general a rise-time reduction is always observed on the net current signals. Between 22 and 85 cm, the first, low current portion of the beam is lost. This is consistent with Fig. 36c where P_{22} is seen to have a 5 nanosecond duration. Indications from the z > 25 cm signals is that the 5 nanosecond rise-time is observed beyond this point. The early portion of the I_{85} signal shows a faster rise time, however, this is not observed at the end of the drift tube.

A series of experimental measurements was performed where the pressure was varied for the same 15 kA injection parameter. The hose instability and its effects dictated an upper pressure for reasonable results of ~20 Torr (see Fig. 18). The beam front velocity as a function of axial position <u>for all pressures</u> $1 \leq P \leq 20$ Torr is shown in Fig. 37, where v_f/v_b is the ratio of front to beam velocity, and the beam electron axial velocity is nominally 0.88 c. The quantity v_f/v is found to average to 0.76 for the last three probes. The slow front velocity at z < 50 cm contributes to the total propagation time, and reduces the average front velocity to ~0.6 v_f.

The beam front "length" $\ell \sim v_f/\tau_r$ (τ_r = rise time) is typically longer than the drift tube for the parameters of the experimental series described above. In the course of the experiments an aperture plate was placed at z = 25 cm, as shown in Fig. 35. In addition to reducing the propagated current, we found that this plate resulted in a much reduced

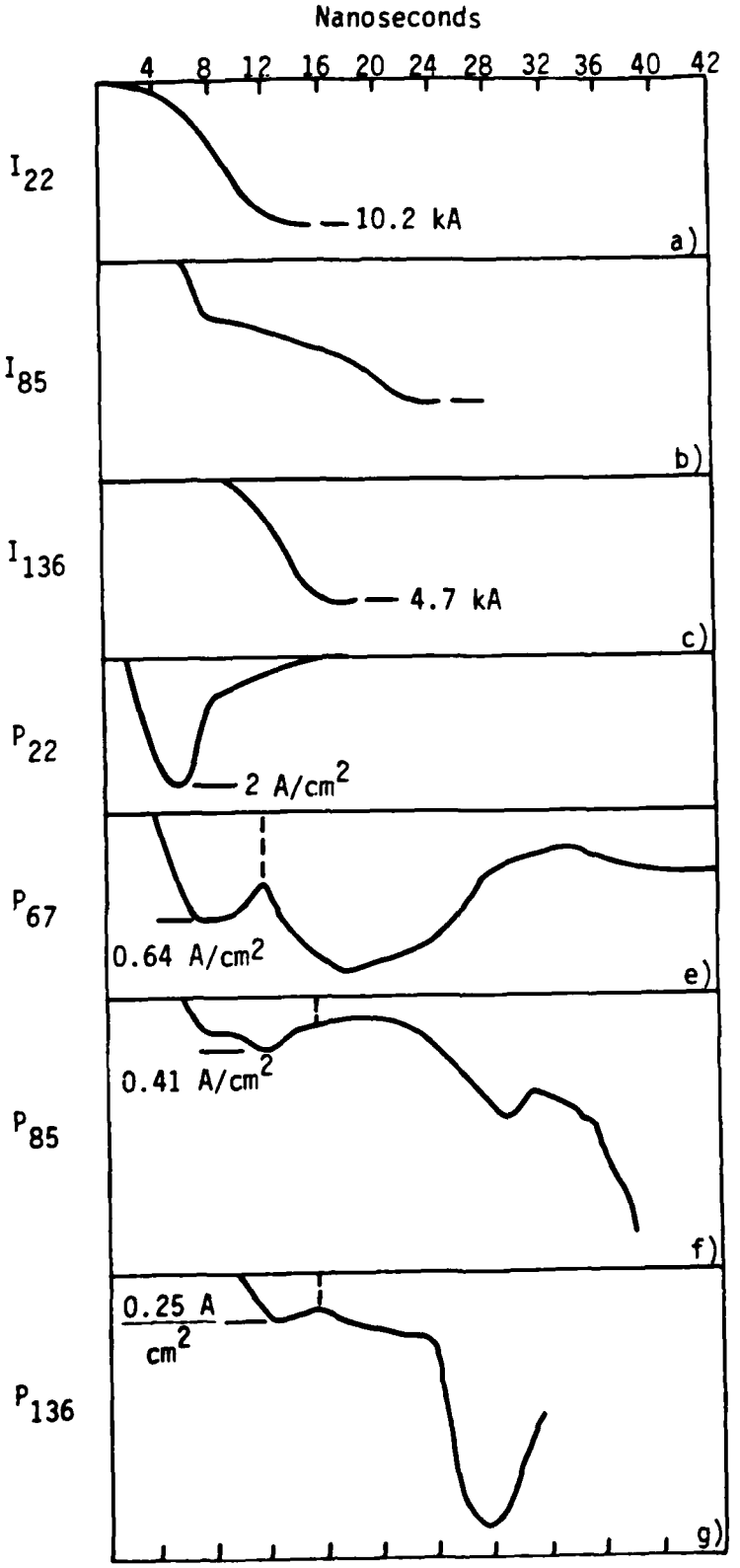

Figure 36. Net currents at a) 22 cm, b) 80 cm, c) 136 cm and penny probe signals at d) 22, e) 67, f) 85, and g) 136.

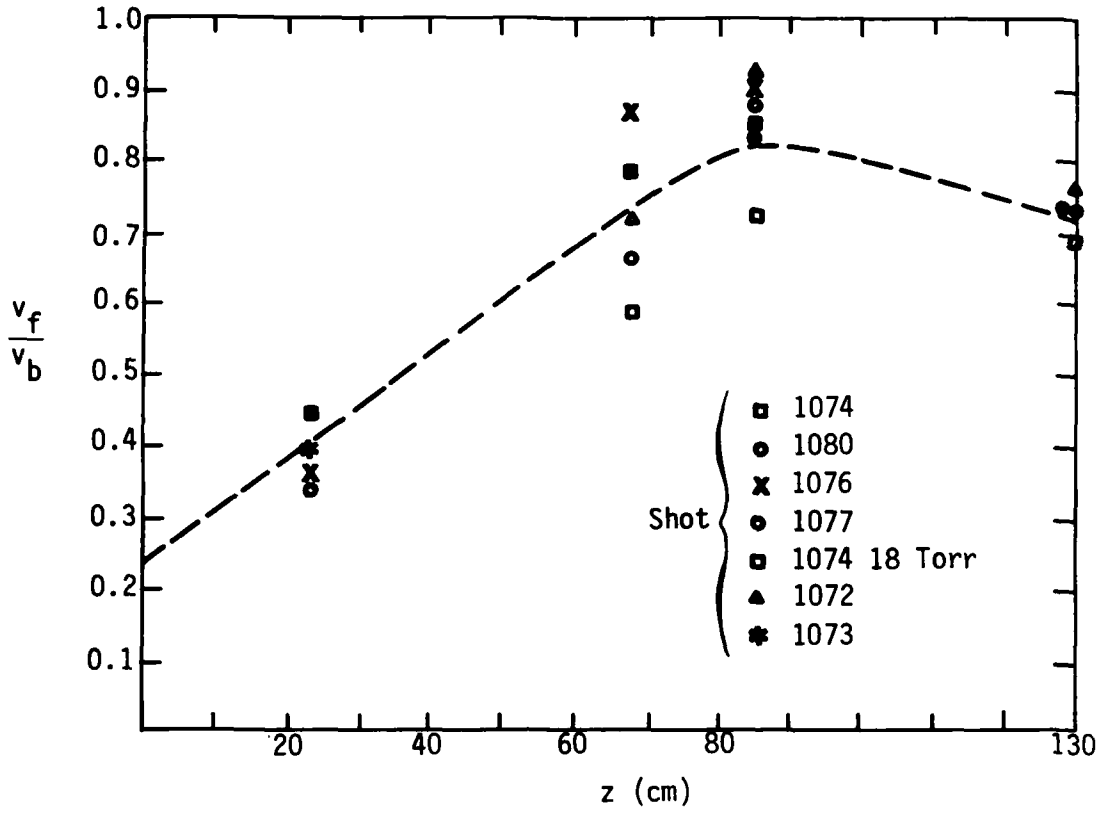

Figure 37. Beam front velocity as a function of axial position. The highest net current and pressure is shot 1074.

rise time, and hence, enhanced dI/dt. A typical set of waveforms for a 1.8 cm diameter aperture is shown in Fig. 38, for an 18 Torr propagation pressure. The $\dot{I}$ exceeded 10^{13} A/sec with the exact value dependent on corrections for the system time response. The penny probe signals are also consistent with a subnanosecond rise time. The existence of significant RF oscillations at 600 MHz during the first 20 nanoseconds at 18 Torr is significant, and may indicate that oscillations are associated with fast rise times. These oscillations are probably of the same type as those discussed in Sec. II.

Based on the penny probe signals, a beam front velocity of v_f/v ~0.85 ± 0.03 v is observed for the second half of the drift tube. The present theoretical prediction for the steady state beam front velocity is[20]

$$\frac{v_f}{v} \sim 1 - \frac{1}{1 + \frac{mc^3}{2e} \frac{\gamma - 1}{I_b \, \ell n(b/a)}} \tag{27}$$

where b/a is the ratio of tube to beam radius. This equation predicts $v_f/v \sim 0.5$ c for the case of b/a ~ 2.7. Clearly, the present analytical theories are inapplicable or must be modified since v_f/v is typically ~0.85 in our data. One area in which the theoretical model is in error is its direct dependence on I_b. The effect of magnetic slowing, which varies as the net current is clear in our data--high I_n is observed to slow the beam front by as much as 0.1 c in the case of Fig. 37, shot 1079.

Previous workers in a similar parameter regime (15 kA, 1.5 MV, 2 Torr) also measured a somewhat higher front velocities than predicted by Eq. (27). Fessenden et al.[16] measured $v_f \sim 0.77$ v in a detailed series of experiments utilizing the FX-25 accelerator. This value is in reasonable agreement with the assymptotic value of ~0.82 v_f we measure over the last 50 cm of the drift tube.

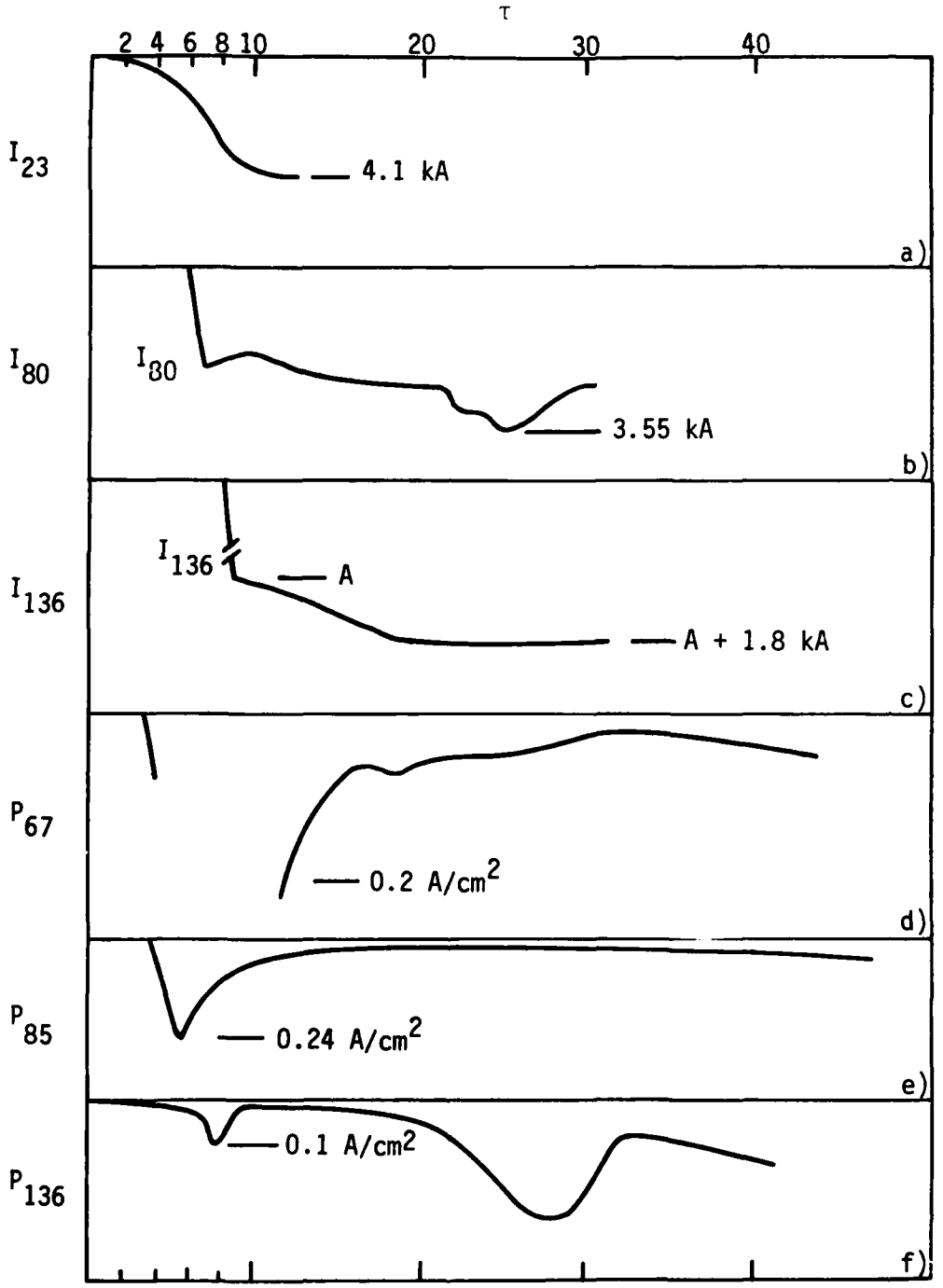

Figure 38. Apertured current traces for 18 Torr. The I_{136} current is unknown because of attenuation of the very fast dI/dt.

The presence of high frequency electric fields may also affect beam front propagation as suggested in Ref. 7. In the r = 10 cm drift tube, the cutoff frequency for TM01 is 1.14 GHz, so the first harmonic of the 600 MHz signal we observe is above cutoff.

The origin of the fast rise time in the aperture case has not yet been elucidated. It may be associated with rapid transition between unpinched and pinched propagation observed in the Faraday cup data. As shown in Fig. 26 the beam radius shows a rapid change at ~20 ns into the pulse. Thus, the rapid risetime effect may be correlated to the transition between unpinched and pinched flow observed in the Faraday cup measurements of Sec. II.A.

B. HOSE STUDIES

A series of position monitor measurements were made using the beam which comes out of the 4.5 cm ID conditioning cell in order to gain an understanding of the hose instability for our particular beam parameters. The experimental setup is similar to that shown in Fig. 23, with a propagation distance of 50 cm. The data was taken at a series of pressures, with, as discussed in Sec. III, a 5 kA beam. Position monitor signals were acquired without integration so that more detailed high frequency data could be obtained. Differential signals such as the direct subtracted B-dot output weight frequency components by a factor ω where ω is the angular frequency of a hose oscillation. The main component of an unintegrated signal is proportional to $\dot{x}I$ after the rise time, where x is the transverse position. As such, if the instability is in the linear regime, $\dot{x}$ is a linear parameter and linear growth rates can be computed.

Conversely, the frequency components observed if the instability is in the nonlinear regime are probably the dominant linear modes. This conjecture is based on the idea that in the nonlinear state, the beam moves ballistically (i.e., in a straight line path) at an angle to the axis determined by the nonlinear instability amplitude.

Typical direct B-dot data is shown in Fig. 39. Note that these are subtracted signals on one plane (both planes were monitored). The signals in the transverse (vertical) plane were somewhat smaller, indicating a systematic source of noise in the horizontal plane in the conditioning cell, which we did not attempt to isolate.

We note a number of features in the raw data. The most important is the frequency content: The frequency increases with pressure at a fixed time in the pulse. It also decreases with time for a fixed pressure. High frequencies are typically observed at the beginning of a trace. The "average" hose velocity assuming a fixed net current of 5 kA is shown as a function of pressure in Fig. 40, although we note that the net current is somewhat lower, particularly at low pressures of 1 and 2 Torr. In general the hose velocity increases slowly with pressure as shown in the data corrected for net current in Fig. 41. The hose velocity correlates well with the peak net current as is also shown in Fig. 41.

We plot the position data derived from Fig. 39 in Fig. 42. Oscillation periods from Fig. 39 have been used to attempt to quantify the observed hose frequency dependences. The period data is compiled as shown in the Fig. 39 bar lines and is admittedly subjective. As a standard for comparison we use the conductivity data from Sec. III.c and assume τ_d = 1/8 τ_m (Bennett profile results), and also assume linear decay time growth as observed, so that $\tau_m \sim (t/70\ ns)\ \tau_m\ (70)$.

The results are shown in Fig. 43, where the curve $\omega\tau_d = 0.85$ is plotted for comparison. The agreement is better than one would expect based on the accuracy of the data, and the extrapolations made. The frequencies chosen were based on the (d/dt) (Ix) data and so tend to indicate higher frequencies than would the position monitor data.

A great deal of theoretical work has been performed on the hose instability and we will limit ourselves to comparisons with the models of

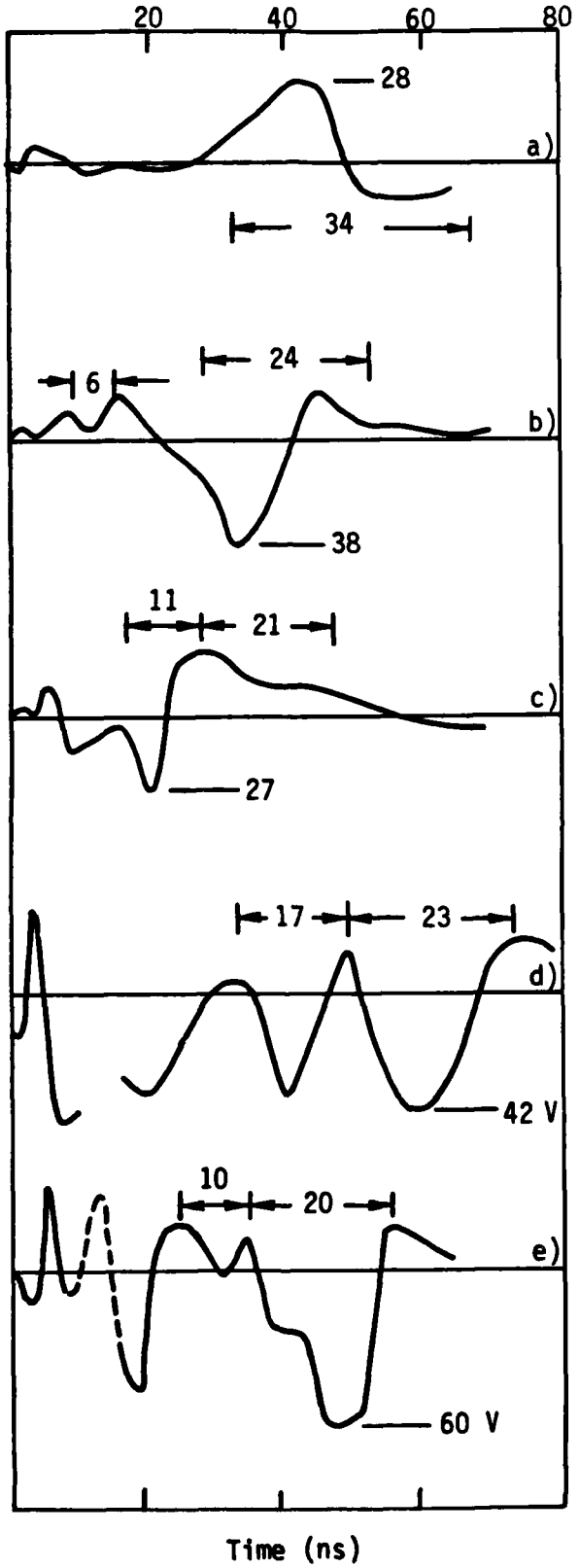

Figure 39. B-dot for pressures of a) 10, b) 20, c) 70, d) 150, and e) 230 Torr.

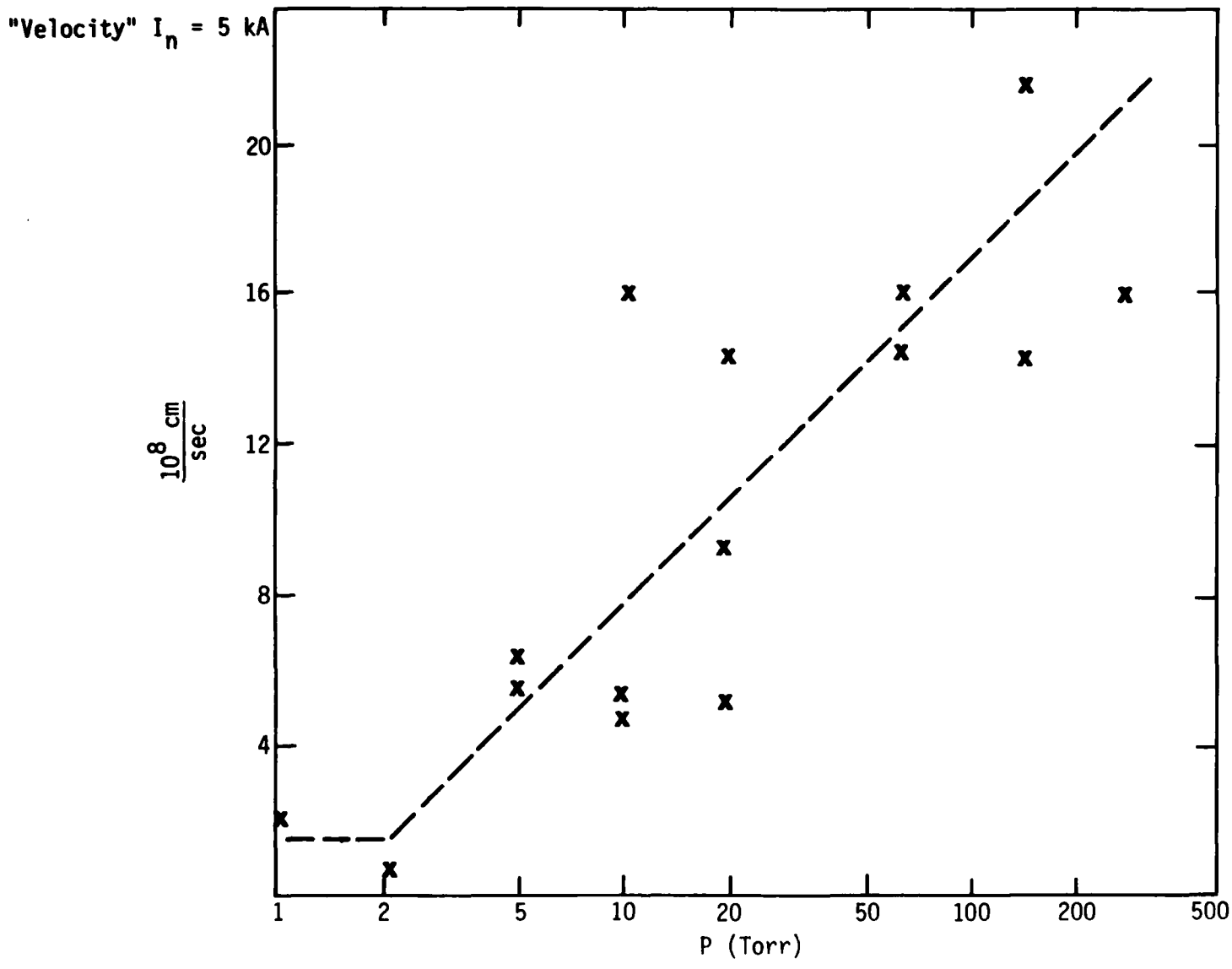

Figure 40. Hose velocity at 54 cm as a function of pressure.

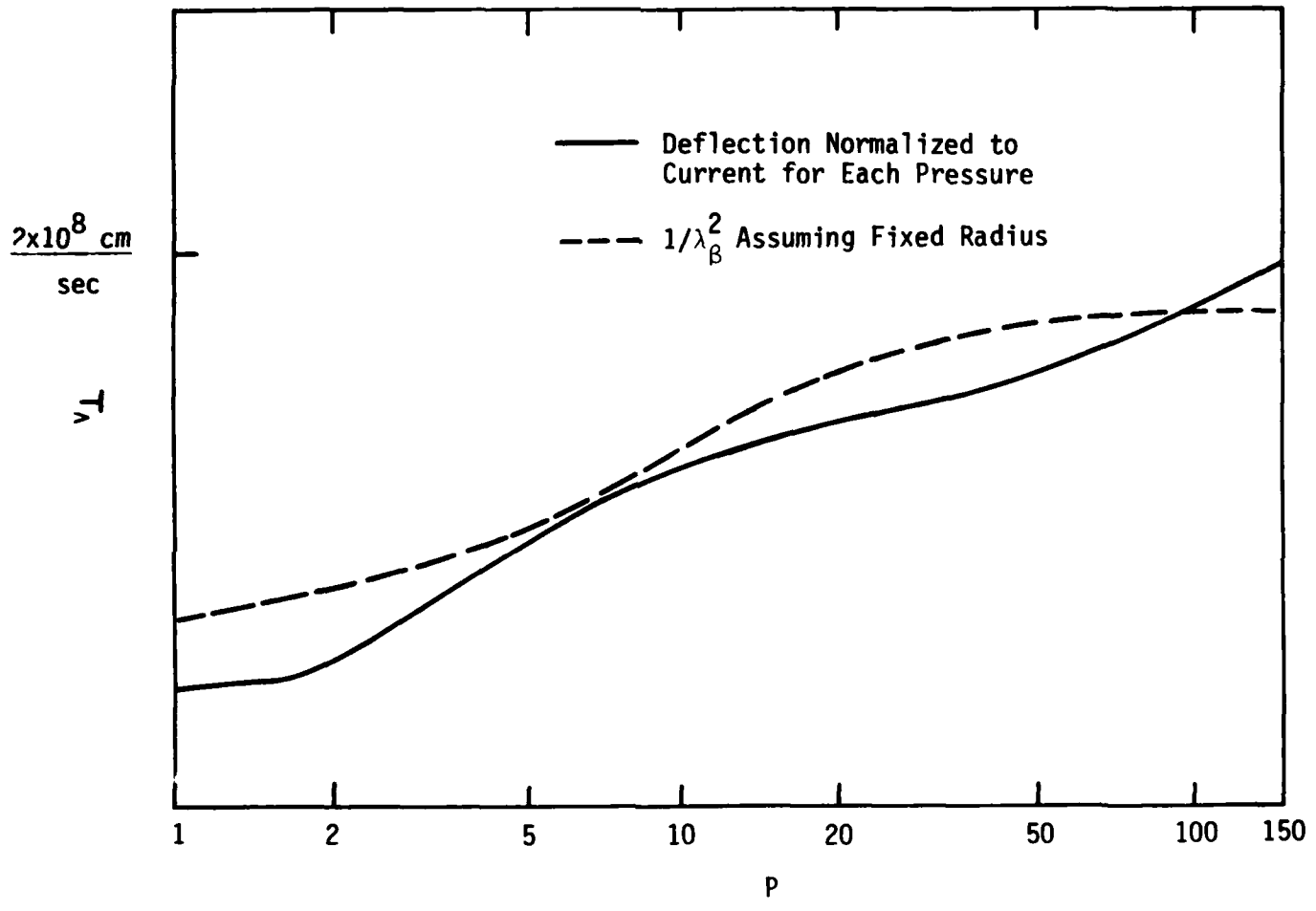

Figure 41. Hose velocity data corrected for the net current dependence compared to the betatron wavelength squared.

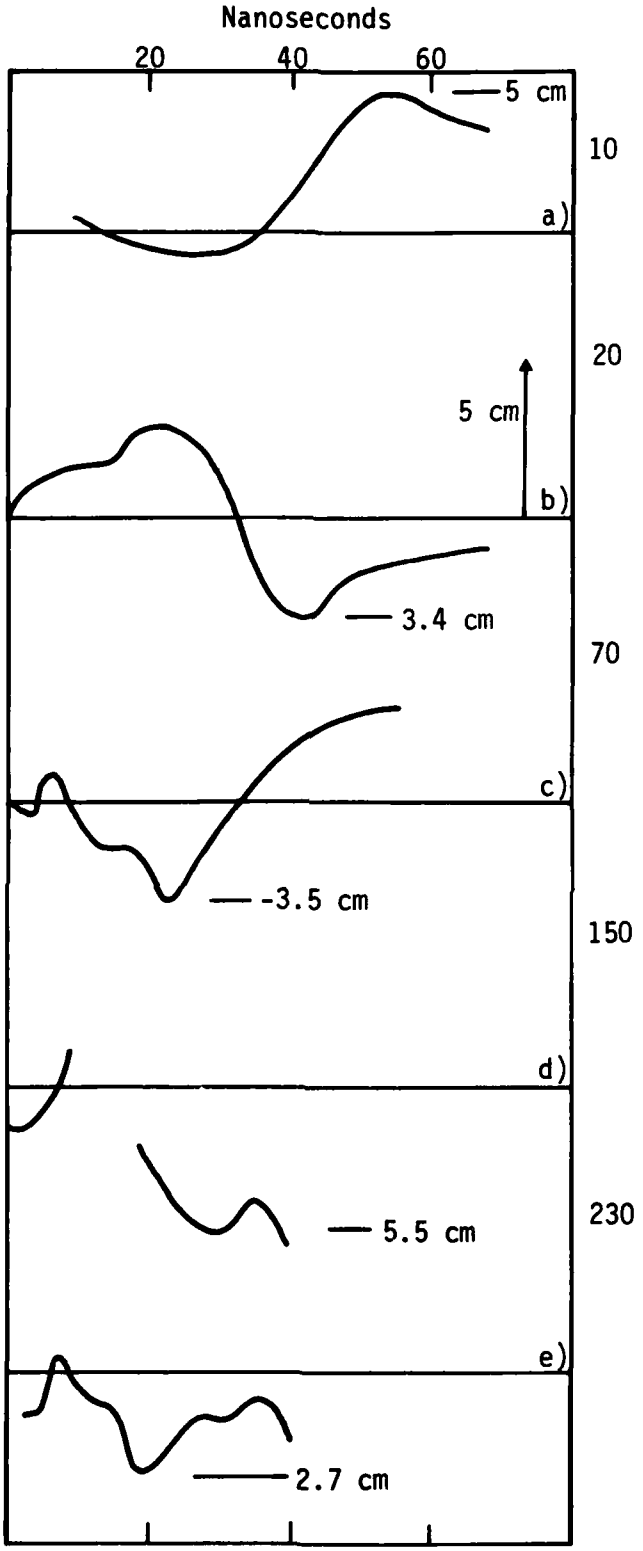

Figure 42. Position data corresponding to Fig. 39 for pressures of a) 10 Torr, b) 20 Torr, c) 70 Torr, d) 150 Torr, and e) 230 Torr.

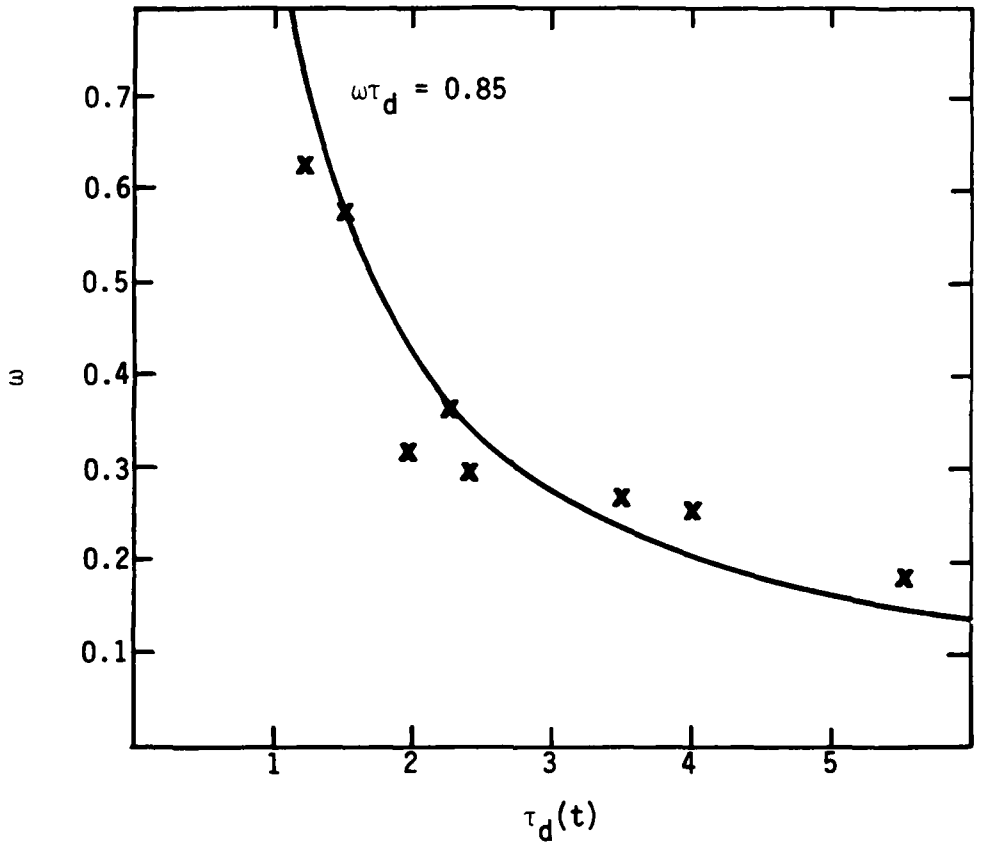

Figure 43. Hose frequency dependence on plasma decay time $\tau_d = \tau_m/8$.

Lee, and of Uhm and Lampe.[4] Given the assumption of real frequency ω in the lab frame, most theoretical work concentrates on growth in the beam frame, which is characterized by the real and imaginary lab frame frequencies Ω_r and Ω_i. The prediction of Lee's analysis in the absence of damping due to phase mixing is that Ω_i/k_β (k_β = betatron wavenumber) is maximized for $\omega\tau_d \sim 0.57$. The spread mass model predicts maximum growth for $\omega\tau_D \sim 0.5$. Uhm and Lampe's model includes monopole plasma currents, and indicates that $\omega\tau_d \sim 0.7$ for maximum growth. From these results we conclude that our result is in good qualitative, and even passable quantitative agreement with theory for the relationship between growth frequency and decay time.

Our hose growth data is consistent with the following interpretation:

1) The pulse length is much longer than the beam propagation distance and the hose convection time in the system.

2) Under the situation above we observe spatial growth from an approximately fixed amplitude noise source.

3) The main parameter changing during the pulse is τ, and the frequency varies according to the variation of τ.

4) Due to 1) the hose frequency can vary since the unstable waves convect out of the measurement volume.

To our knowledge, this analysis represents the first experimental correlation between the hose frequency and plasma decay time.

Spatial hose growth lengths may also be calculated from the data. Our input noise differs from the linear theory case--in our case, a beam

with some fixed noise enters the plasma, and the plasma response dictates the amplitude of magnetic axis perturbations. In linear theory, the two are coupled by the time delay of a fixed sinusoidal input. For this reason, we can define two growth rates--the magnetic axis growth rate which ignores the plasma response problem, or the growth for a fixed transverse beam motion.

The growth rate computed from the ratio of magnetic probe signals relies on determination of the exact frequency components of the two signals. We attempted to do this with some success using bandpass filters, as in the conditioning cell run.

For the data run typified by Fig. 39, we find a spatial e-folding length of 16 ± 8 cm. We compare this to the peak value predicted by the rigid beam model of ~$5/k_\beta$, ~$0.8\ \lambda_\beta$, ~12 cm for a 1 cm radius beam.

An example of a particularly good spatial correlation is shown in Fig. 44, where signals from probes spaced 42 cm are shown and the growth length was ~12 cm. This growth length is also in reasonable agreement with theory.

One interesting feature which may be discerned from Fig. 44 and other similar data is that at early times in the pulse, high frequency signlas are more evident on the downstream pictures than on the upstream, indicating faster growth at high frequencies.

A quick survey of magnetic versus beam position was performed using the vacuum cell. A limitation of the measurements was that they were separated by half a betatron wavelength. An example is shown in Fig. 45. Further investigation of relative motion is essential for further hose studies since it will give the instability phase. In addition, comparison of the two signals gives a <u>direct</u> measure of τ_d.

AD-A133 310 BEAM PROPAGATION EXPERIMENTAL STUDY(U) MISSION RESEARCH 2/4
CORP ALBUQUERQUE NM R J ADLER ET AL. APR 83 AMRC-R-466
AFOSR-TR-83-0743 F49620-81-C-0016

UNCLASSIFIED F/G 20/7 NL

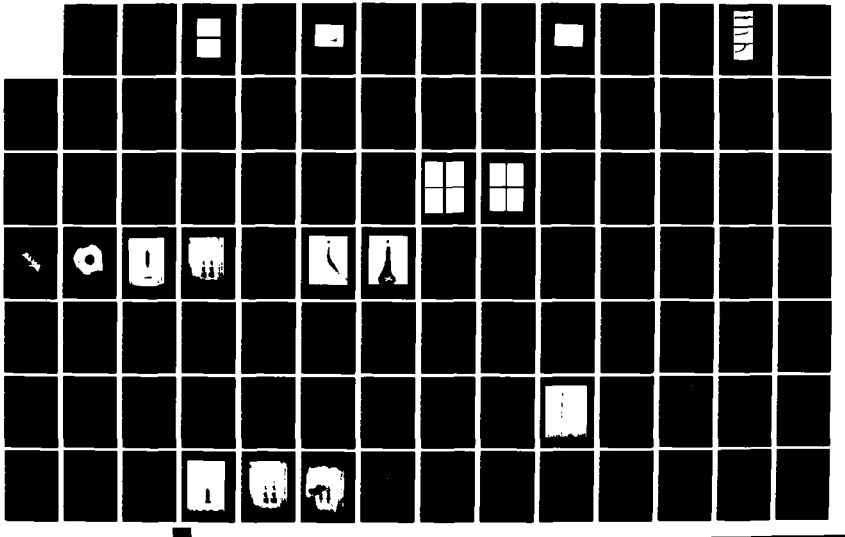

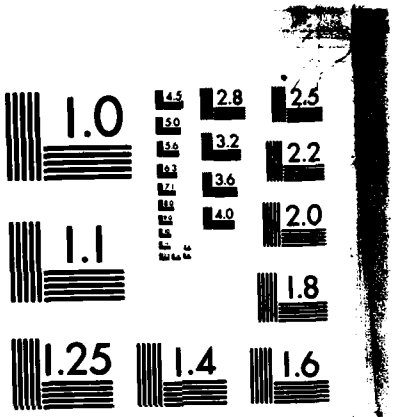

MICROCOPY RESOLUTION TEST CHART
NATIONAL BUREAU OF STANDARDS-1963-A

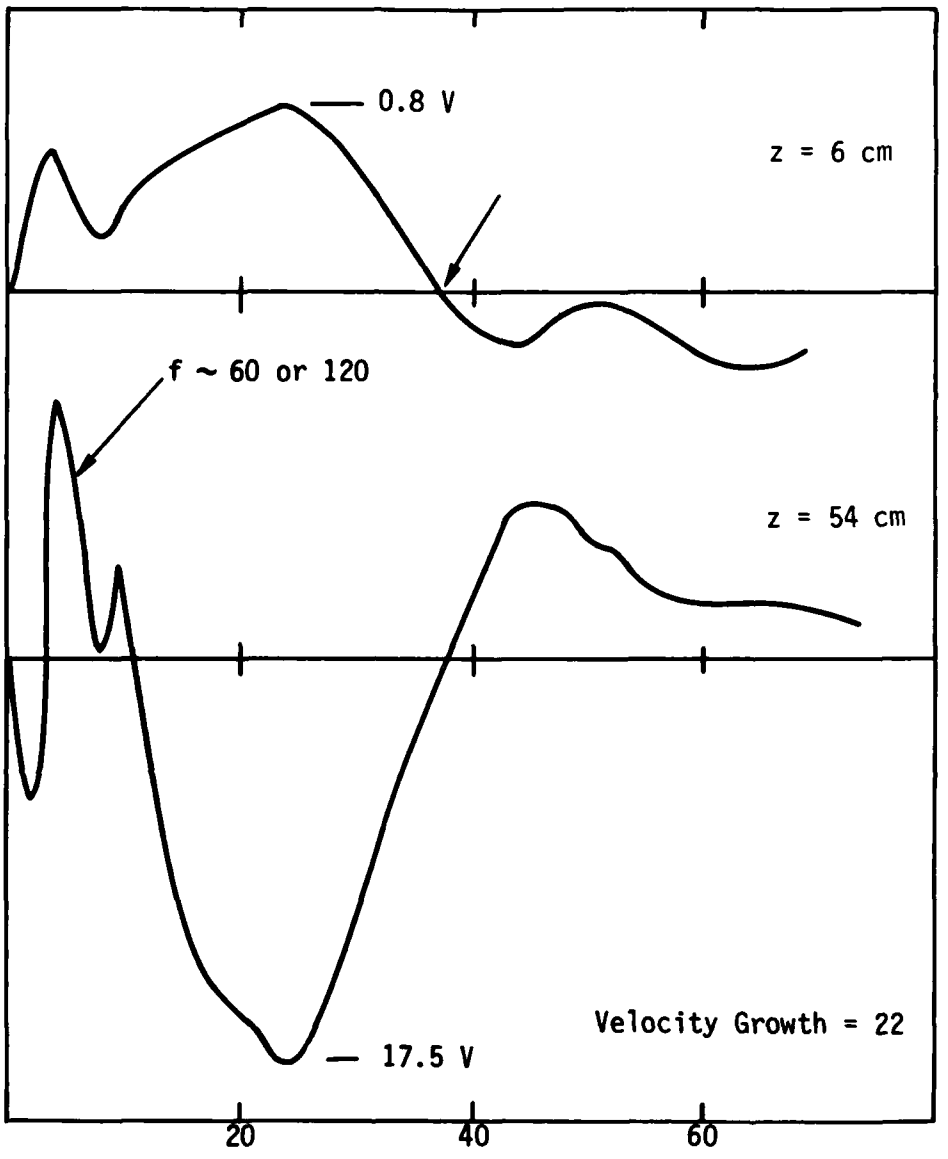

Figure 44. Spatial growth of the hose velocity for P = 20 Torr.

a)

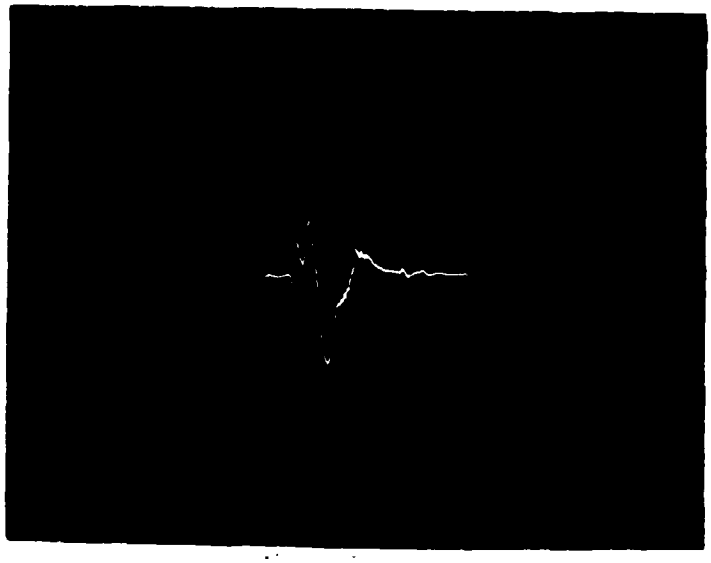

b)

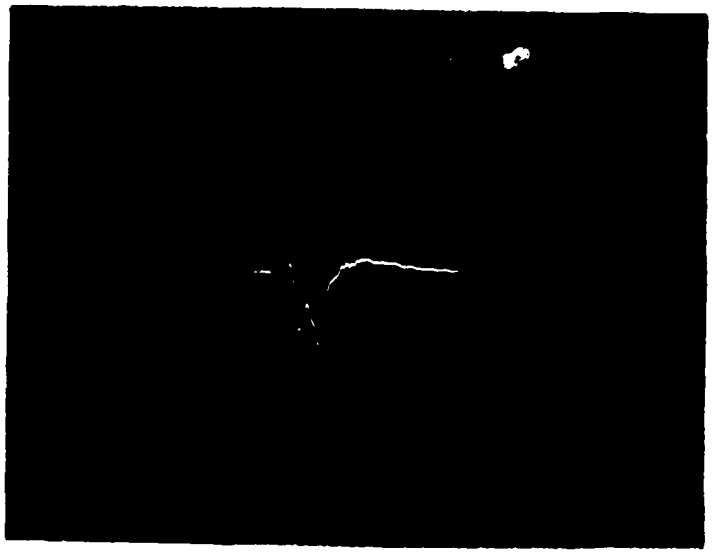

Figure 45. Comparison of transverse velocitv for a) magnetic centroid and b) beam centroid.

C. NOSE-HOSE DEVELOPMENT

Using the triangle detector, beam propagation in the large cell was measured as a function of axial position. The measurements of the previous section have established the existence and magnitude of the hose instability in the body of the beam. The purpose of the measurements outlined in this section was to take a more detailed look at beam hose during the first few nanoseconds of propagation evolution. In addition we wished to study a larger range of pressures than we used in Sec. II. Pressures of 10, 50, 100, 200 and 620 Torr were used in the experimental setup of Fig. 12, and the 4.5 cm conditioning cell. Some of the most striking results were obtained at a pressure of 50 Torr--an open shutter photograph of propagation over 1.2 m to the triangle detector is shown in Fig. 46. Summing all triangle detector channels gives an approximate beam current measurement. Triangle currents for z = 0.30, 0.60, and 1.2 m from the injection point are shown in Fig. 47. The duration of a stable beam is ~16 nanoseconds at 0.30 m, 4 nanoseconds at 0.60 m, and 0 nanoseconds at 1.2 m. Examination of the individual signals indicates that propagation is unstable even in the nose at 2 nanoseconds. The hose convection velocity near the nose appears comparable to the beam front propagation velocity. We observe that over 30 cm, there is a dramatic reduction in current transport. This can be explained if the hose is moving at least as fast as the beam front while simultaneously growing in the beam front frame. Note that it is possible for different frequency components to propagate at different phase and group velocities.

The first 60 cm of propagation distance was observed to have anomalously slow propagation (Sec. III.A), consistent with the picture above. Also note that the CPROP simulations (Sec. V) suggest that the beam front velocity is significantly slower at 76 Torr than at 15 Torr (where our beam front measurements were performed). The rapid rise of the beam current--which occurs at the system limited value of 2 ns in Fig. 47. is consistent with the evolution of beam front propagation as observed in the apertured beam study of Sec. IIIa. In Sec. IIIa., rapid beam front motion was associated with the onset of the pinch which ended the slow propagation phase.

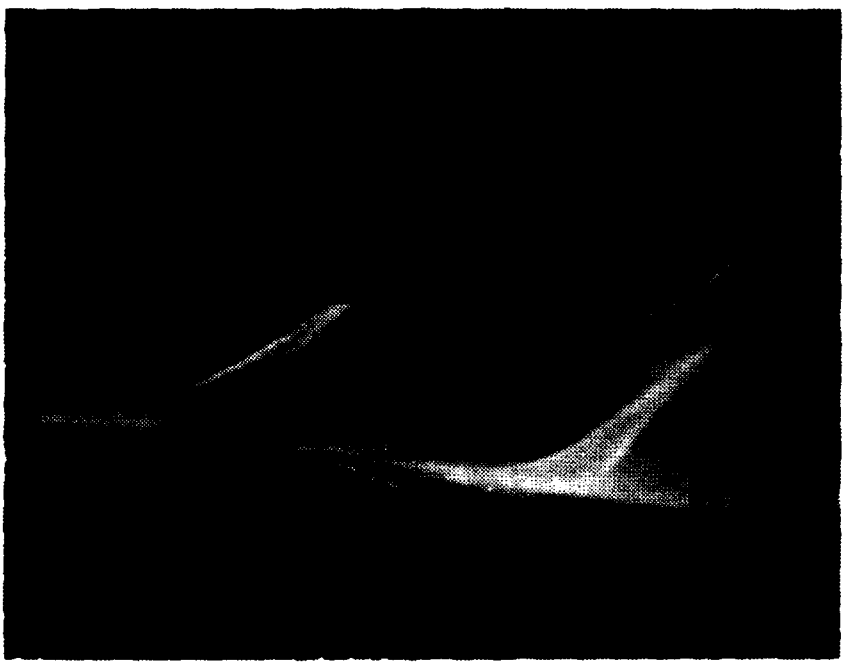

Figure 46. Open shutter photograph of a hose unstable beam propagating 1.2 m in the large propagation cell.

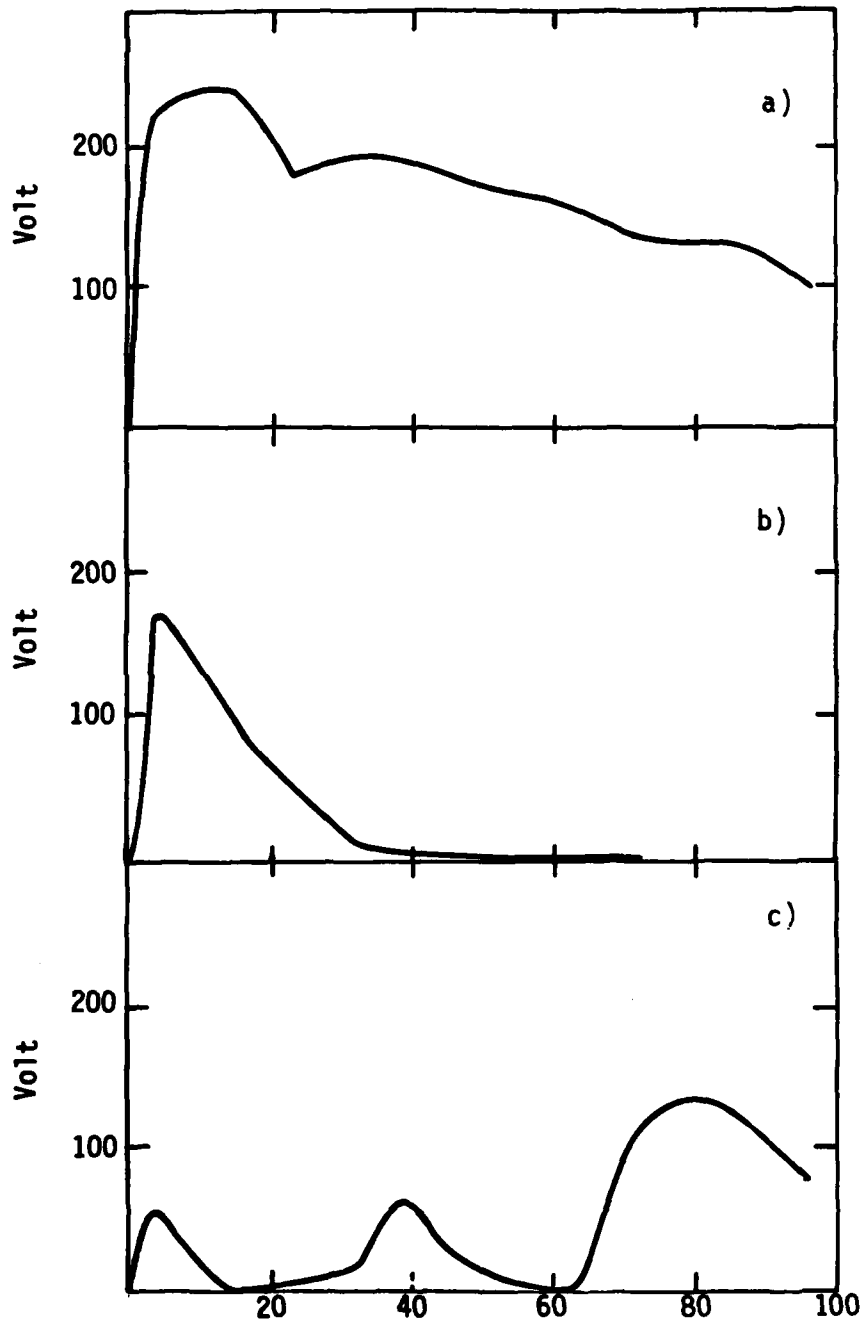

Figure 47. Approximate beam current at a) 30 cm, b) 60 cm, c) 120 cm for 50 Torr.

Similar data taken at 200 Torr is shown in Fig. 48. The same beam front evolution is observed in this case as in the 50 Torr case.

By far the most stable propagation is observed at 630 Torr (Albuquerque atmospheric pressure). In this case, the beam is expected to undergo Nordseick expansion, and this is in fact observed optically as shown in Fig. 49. The Nordsieck length observed in our optical measurements is approximately 50 ± 10 cm. The Nordsieck length predicted based on our peak value of γ (~0.63) is 60 cm for Moliere scattering, and ~30 cm for Rossi-Greisen scattering. The light pattern is expected to be an underestimate since there is a contribution due to the portions of the beam at lower power. Also note that there is a significant (1.27 keV/cm) direct energy loss by the beam in air, which further reduces the Nordsieck length. Based on these considerations, our experiment indicates that the true Nordsieck length is given by the Moliere scattering formalism.[17]

The stability of the beam for at least 0.90 m in this case is also of interest. At injection, the number of betatron wavelengths per Nordsiek length is ~3, and some hose unstable motion was observed in some of the 1.2 m propagation cases. Thus, we conclude that three betatron wavelengths per Nordsieck length is the case for marginal stability for a beam with a 1 mm offset.

Since we have observed unstable beam nose propagation, it is instructive to calculate the expected hose convection rate. Lee has performed this calculation,[2] and the result is that the forward convection velocity is

$$v_c \sim \frac{v_b}{\alpha + v_b} \qquad (28)$$

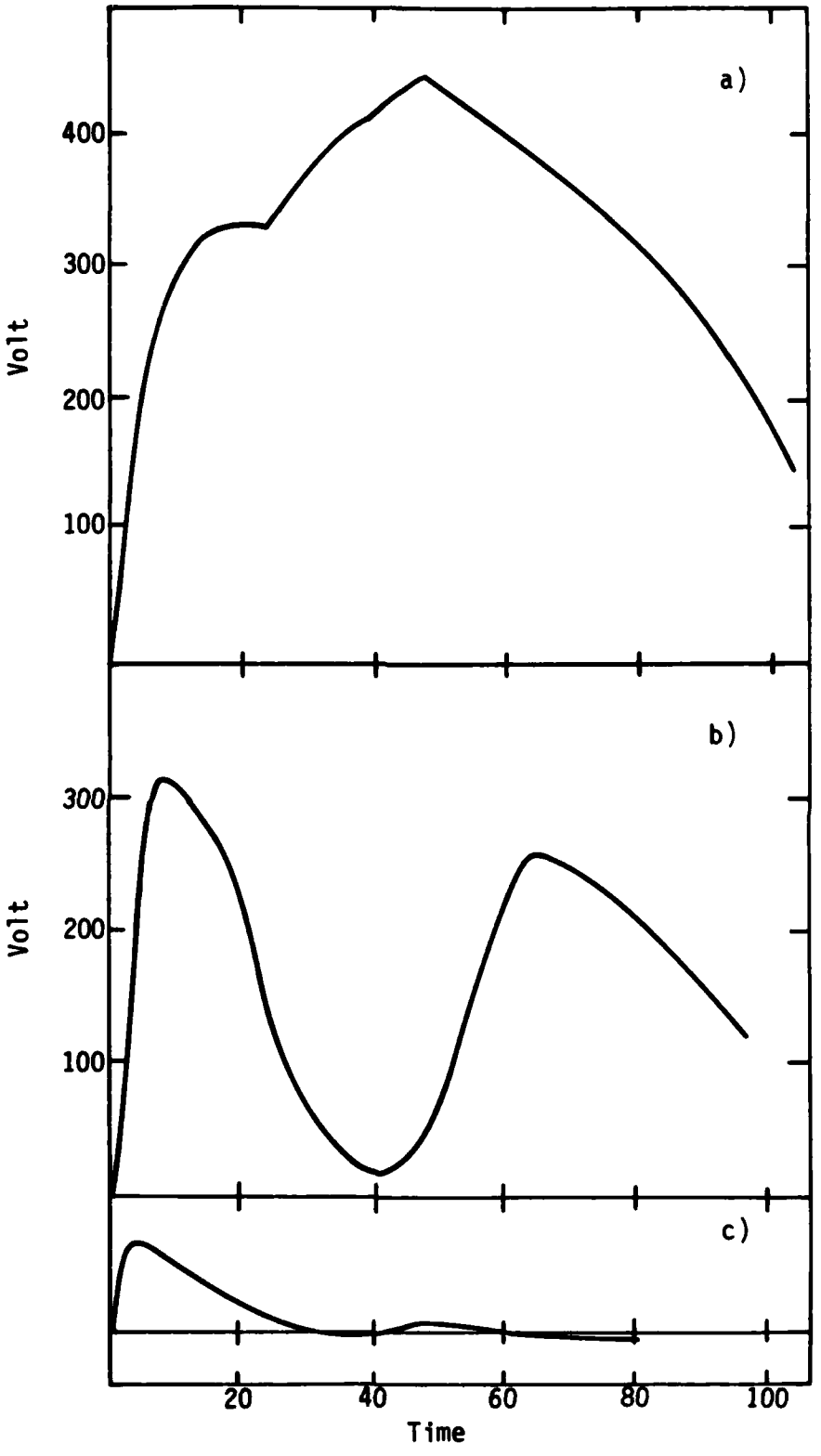

Figure 48. Approximate beam current at a) 30 cm, b) 60 cm, and c) 120 cm for 200 Torr.

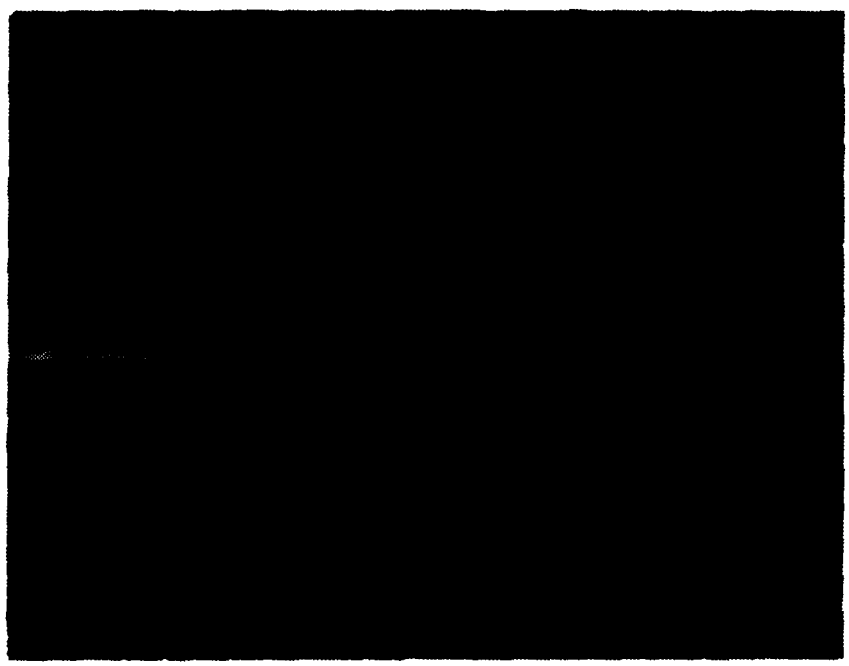

Figure 49. Open shutter photograph of a beam undergoing Nordsieck expansion.

$$\alpha \sim \frac{\lambda\beta}{\tau_d} \tag{29}$$

We have observed unstable nose propagation in a variety of circumstances. the nose velocity has been observed to be nonuniform--varying between ~0.3 and 0.8 c. We have measured τ_d near the beam head for several sets of parameters. Referring to the data of Sec. II, we had $\lambda_\beta > 15$ cm, and $\tau_m = 4$ ns at $t = 4$ ns into a 15 Torr pulse. The resulting convection velocity is ~c/2 from Eq. (29), so that observation of nose-coupled hose is consistent with the fast erosion rates observed for the first 60 cm of propagation.

The decay time data for 100 Torr propagation, on the other hand, indicates that the hose convection velocity for the set of experiments discussed in this section does not reach c/2 until ~10 nanoseconds into the pulse. In order to explain our observations we must therefore conclude that either the theory is wrong, or nose-erosion is more rapid at higher pressures as suggested by the CPROP simulations. Based on the simulations we expect that the beam front velocity will be as low as 0.35 c.

Another possibility exists. If we assume that impact ionization is the dominant conductivity-generating mechanism, a certain minimum length of beam must precede (in time) the unstable point in order to raise τ_D and hence v_c. Particles which receive transverse displacements at the foremost unstable point move forward in the nose frame to disrupt the front, since no mechanism exists to damp their transverse motion (note that by assumption τ_D is so small ahead of the unstable point that the magnetic and beam axes are nearly coincident). This amounts to saying that ahead of the unstable point, no hose theory applies since $\tau_D \sim 0$, and so ballistic electron motion results in the unstable nose.

A final significant discovery of our research is the observation of hose stable propagation of a rotating electron beam over a length of 4-6 λ_β as shown in Fig. 50. The distance shown is approximately 1 Nordsieck length, and rotation was introduced by a small magnetic field on the cathode.

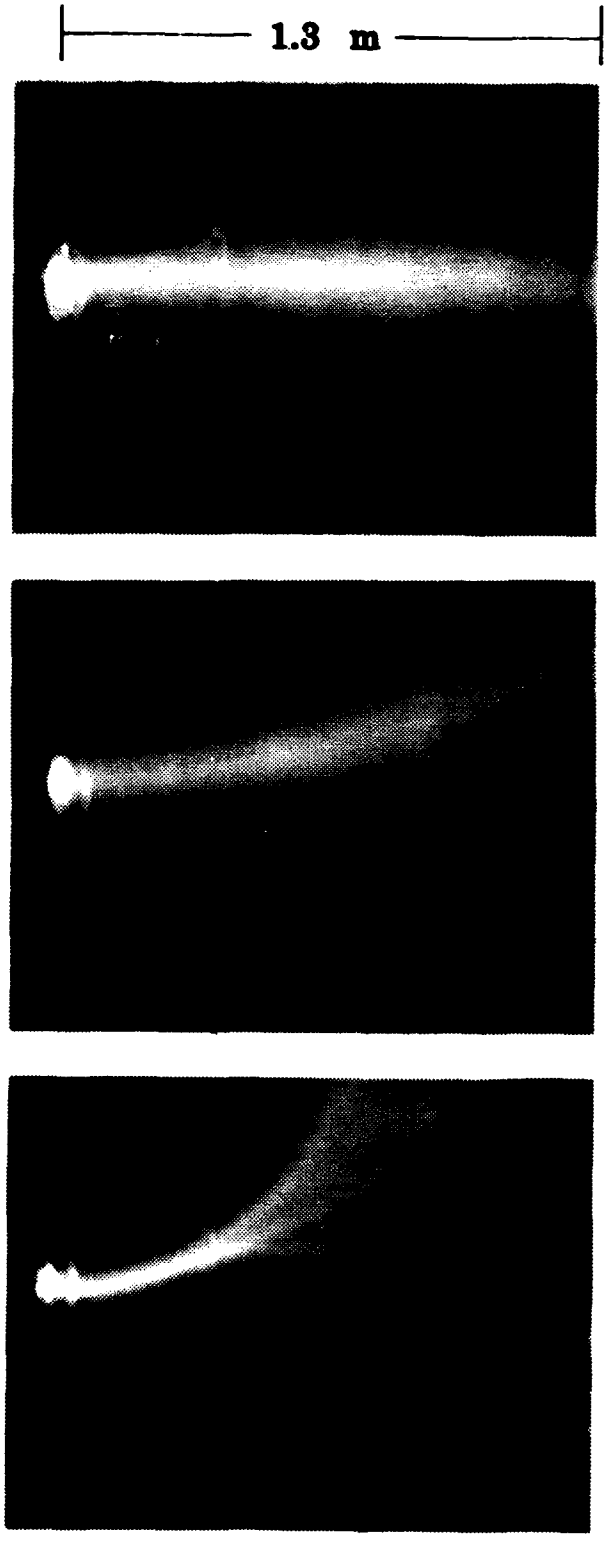

Figure 50. **BEAM PROPAGATING IN FULL DENSITY AIR EXHIBIT ENHANCED HOSE STABILITY WITH ROTATION (B_{zo})**

V. NUMERICAL SIMULATIONS OF ELECTRON BEAM HOLLOWING AND NOSE EROSION IN LOW DENSITY AIR

Four two-dimensional axisymmetric computer simulations of VISHNU beam propagation in low density air were carried out at about the time that the corresponding experiments were beginning. The computations were performed not for the purpose of detailed comparisons with or interpretations of the experiments, but rather to provide a preview of what axisymmetric phenomena might be expected. Issues of particular interest included the radial profile of the VISHNU beam in low density air, the rate of nose erosion and associated rise-time reduction, and the air density of onset of the hollowing instability. The simulations also were intended to uncover possible surprises.

The computations modeled VISHNU electron beam transport in a 10 cm radius drifttube at air densities of 1/2, 1/10, and 1/50 standard atmosphere. Runs were made in both the beam and laboratory frames. In the former the tube was of arbitrary length, while in the latter it was terminated by metal endplates 150 cm apart. The beam itself was taken to have a 20 kA current and 1 MeV energy. The current axial profile was initialized to a hyperbolic tangent rise with a 2.5 nsec scale factor, corresponding to a 10-90% current riselength of 4 nsec. Only the first 5-10 nsec of the beam pulse was followed, and this duration was quite adequate for the purpose. The beam was loaded with a Bennett radial profile of radius 1.5 cm, truncated at three Bennett radii.

Simulations were carried out using the particle-in-cell beam propagation code CPROP.[18] Although at least three other propagation codes exist, CPROP is the best suited to relatively low energy beams, such as the VISHNU beam, because it does not employ the usual paraxial particle motion or frozen field approximations. Additionally, the code's Moliere scattering algorithm is important for properly treating Nordsieck expansion of the VISHNU beam at higher air densities.[17]

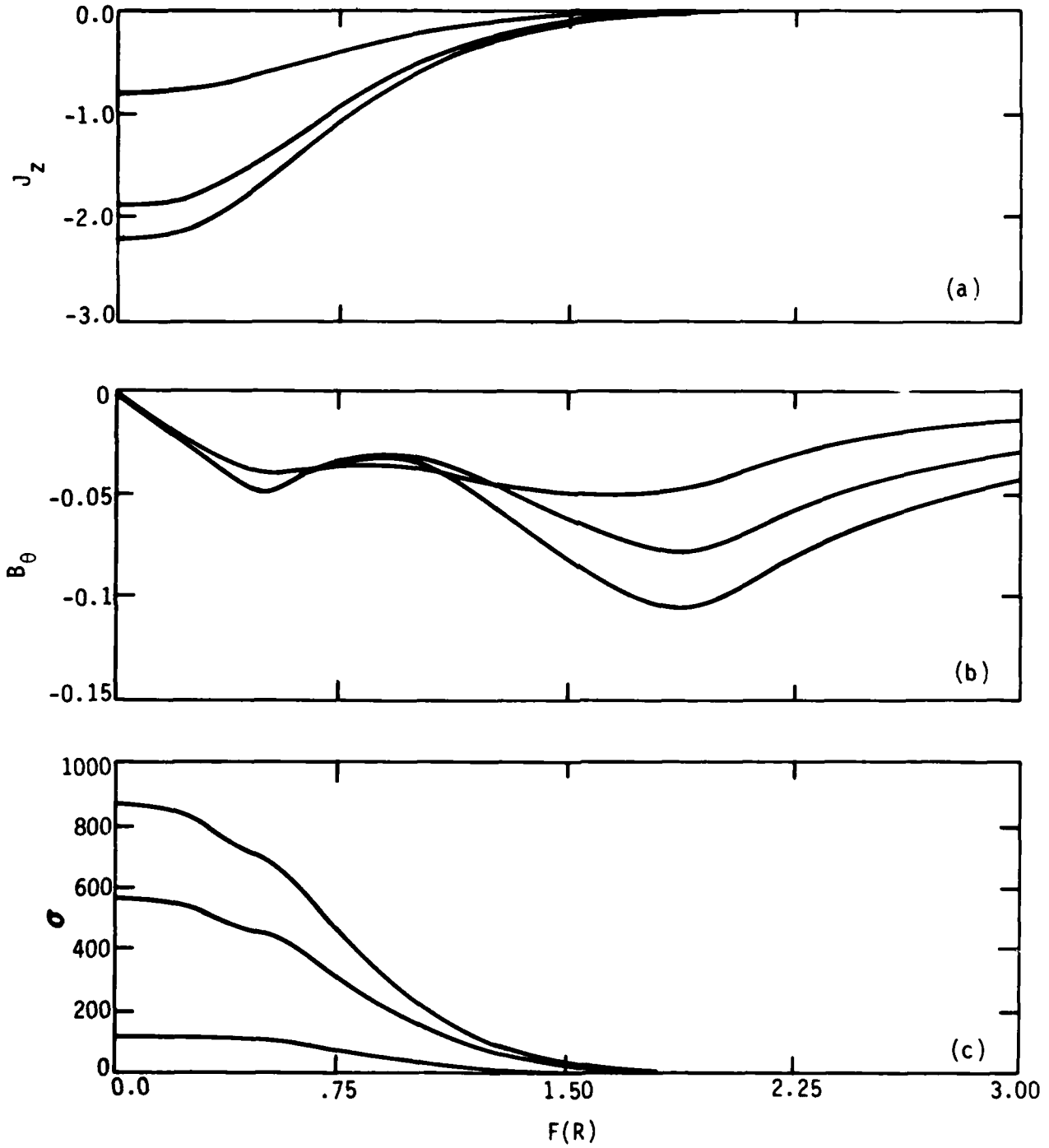

Figure 51. Three crossections of initial (a) beam current, (b) magnetic field, and (c) air conductivity from 1/50 atmosphere simulation showing field modification due to broad conductivity profile. (Exponential zoning in radius)

Properly modeling conductivity generation in air below 1/10 atmosphere is a serious problem in all propagation codes. The Lawrence Livermore National Laboratory PHOENIX package (including recombination) was utilized in these simulations despite its acknowledged limitations at very low densities.[19] Subsequently, we modified the Science Applications, Inc. BMCOND routines for use in CPROP,[20] and we hope to repeat a few of these VISHNU runs to see what differences occur. Nonetheless, quantitative agreement between experimentally and computationally determined conductivities in low density air should not be expected until non-local ionization and secondary electron transport phenomena are properly included.[21-23]

Co-moving beam frame simulations of the first 150 cm of the beam were carried out at the three densities listed above primarily to investigate the threshold for hollowing instabilities in the beam nose and secondarily to obtain the rate of nose erosion. Although at each density a Bennett profile was loaded, at the two lower densities the beam rearranged itself radially, passing through a state in which the net current reversed direction near the nominal Bennett radius in the well pinched part of the beam. Apparently, the early-time current reversal resulted from a high return current fraction and a conductivity profile wider than the beam profile. Figure 51 shows typical crossections of the beam current, plasma conductivity, and azimuthal magnetic field at 1/50 atmosphere. The broadened conductivity profile was in turn due to a combination of avalanche and recombination. The beam soon settled down to a slightly wider profile in the 1/10 atmosphere run. This same evolution appeared to be developing in the 1/50 atmosphere run as well, but before a steady state could be reached a strong instability occured in the beam nose, soon disrupting the entire 150 cm beam segment.

TABLE 1. Beam front velocity, inductive field strength, and net current from simulations of 20 kA, 1 MeV VISHNU beam at reduced air density.

Run	Density (atm)	v_f/v_b (theo)	v_f/v_b (sim)	E/P (kV/cm-atm)	I_n/I
1A	0.5	0.38	0.28	50	0.5
1B	0.1	0.62	0.41	160	0.5
1C	0.02	0.82	0.77	1300	0.3

The nose erosion rate was large in all three cases. Table 1 summarizes our findings, comparing the beam front velocity as determined from the simulations with an analytical estimate[6]

$$\frac{v_f}{v_b} = \left(1 + L\ \frac{\nu_N}{\gamma}\right)^{-1} - \frac{\nu_N}{2\gamma} \qquad (30)$$

where $v_b = 0.94$ is the single particle velocity. The net current ν_N is taken from just behind the pinch point in the simulations. The inductance

$$L = 1 + 2\ \ell n\ (R_c/R_b) \qquad (31)$$

is based on the Bennett and drifttube radii, L=4.7. Typically, L ~ 6 in an infinite medium.[24] The dominant, first term on the right side of (30) takes account of inductive energy loss at the pinch point, while the second term is a small correction due to betatron oscillations. This erosion rate expression has no contribution due to scattering. The effect of scattering on erosion has been estimated analytically only in the limit of low rates ($L\ \nu_N/\gamma \ll 1$),[24] which certainly does not pertain here. Comparison of analytical and computational predictions for beam front velocity shows that the former systematically exceeds the latter. At higher densities this discrepancy undoubtedly is due to neglect of scattering in (30). At lower densities particle bunching near the pinch point may increase the erosion rate slightly in the simulations. (Experience with ETA beam simulations indicates that electron bunching can increase the erosion rate by as much as 20%.[23]) Agreement between theory and computation is satisfactory in view of these uncertainties.

Good experimental data is available to contrast with the 1/50 atmosphere simulation only, due to severe hose instabilities at the two higher densities. The measured beam front velocity, as discussed thoroughly elsewhere in this report, was very low while the beam propagated the first few

ten's of cm. Whether this was caused by blowoff of low energy electrons at the beginning of the pulse or by other, unknown reasons is unclear. In any event, the relative beam velocity reaches 0.65-0.70 for propagation distances beyond 80 cm. The source of this discrepancy between experiment and simulation almost certainly is the conductivity model. Consistant with this supposition, CPROP predicts a return current fraction of about 0.3 in the beam body, while a value approaching 0.5 is measured experimentally. Indeed, extrapolating the higher return current fraction to the nose region gives a front velocity agreeing much better with the experimental figure.

Nose erosion reduces not only the beam front velocity but also the current risetime. After 100 cm of propagation the risetime had dropped to about 0.5 and 1.0 nsec for the 1/10 and 1/2 atmosphere cases, respectively. Over the same distance the risetime in the 1/50 atmosphere run decreased to of order 0.2 nsec, this smaller value presumably due to reduced scattering and the associated axial bunching of particles. Note, however, that the effective risetime entering into inductive field estimates is bounded from below by the transit time across the conductivity channel, R_c in (32). The riselength of the azimuthal magnetic field in the simulations never was less than about 2 R_c^{-1}. This estimate is supported by VISHNU experiments, for which magnetic field probes gave 1 nsec risetimes after some propagation distance, while Faraday cups gave lower values.

Only the 1/50 atmosphere simulation was unstable. Strong hollowing developed in the beam nose after about 100 cm of propagation and moved back into the pulse at roughly the beam velocity. Within an additional 200 cm of propagation the entire 150 cm beam segment being simulated became severely distorted. The unstable wave frequency was initially 0.071 cm^{-1} but steadily increased in time for fixed positions in the beam. Figure 52 illustrates this. The monopole decay length was about 170 cm at a position 30 cm behind the pinch point at early times, but varied dramatically in

space and time as the instability developed. Although there was some tendency for the magnetic field to reverse most strongly somewhat off axis, it was insufficient to break the beam into multiple annuli.

Table 1 also lists the ratios of peak axial field to air density and of net to beam current. According to the standard criterion, E/P>130 kV/cm-atm and $I_n/I<0.5$,[5] the 1/10 atmosphere simulation was at the instability threshold. The rapid erosion may have had a stabilizing influence. Overall, the simulation results support the emperical criterion.

Actual experiments are, of course, performed within drift chambers of finite length, stationary in the laboratory. The 1/50 atmosphere case was, therefore, repeated in the lab frame with a 150 cm long drifttube. Results agreed qualitatively with the beam frame simulation at early times. Instability developed after about 100 cm of propagation,leaving a single large amplitude standing wave near the far end of the tube. The wavenumber, 0.12 cm^{-1}, was somewhat larger than expected, 0.08 cm^{-1}, but may have been influenced by the proximity of the metal endplate. The standing wave decayed very slowly after the beam head left the chamber; the monopole decay length at that time was about 800 cm. Also, at about that same time a gentle hollowing developed throughout the first half of the drifttube. (This is qualitatively similar to the unpinched phase of propagation observed below 15 Torr.) Whether the final state of the beam is better described as a saturated weak instability or as a change in the equilibrium is unclear and perhaps irrelevant. After 10 nsec the final profile was moderately hollow, as shown in Figure 53. Some of the experimental data suggest similiar behavior.

Figures 54, 55 and 56 are snapshots of the beam electron distribution and magnetic field contours at 3.33, 6.67, and 10.0 sec. (Recall that non-uniform radial zoning is employed in the plots, as well as in the computations.) The late-time hollowing, stationary in the lab frame, probably is the most interesting aspect of these simulations; additional investigations seem warranted.

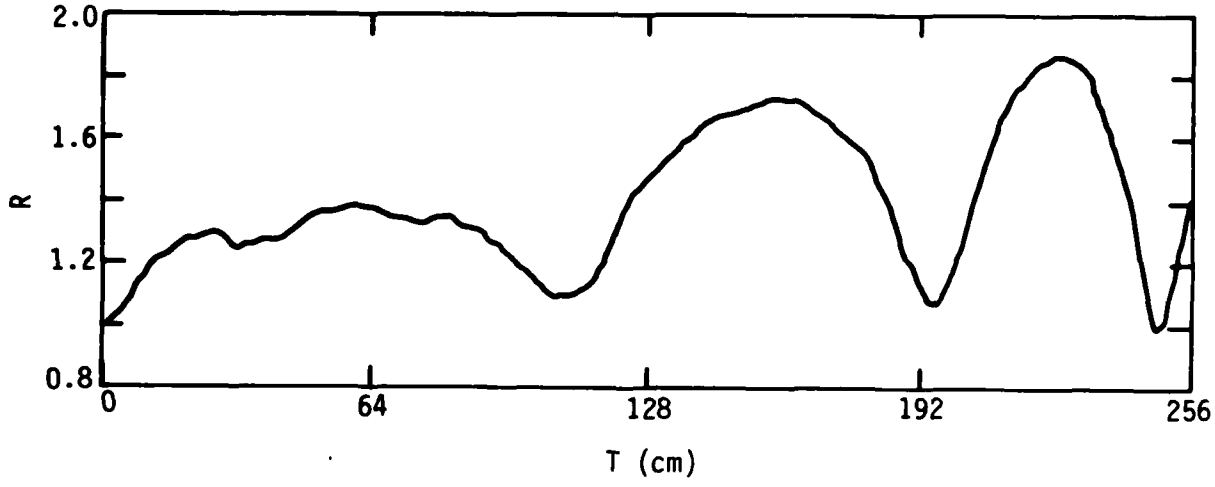

Figure 52. Oscillation of beam half-radius at a point 100 cm behind nose in 1/50 atmosphere simulation.

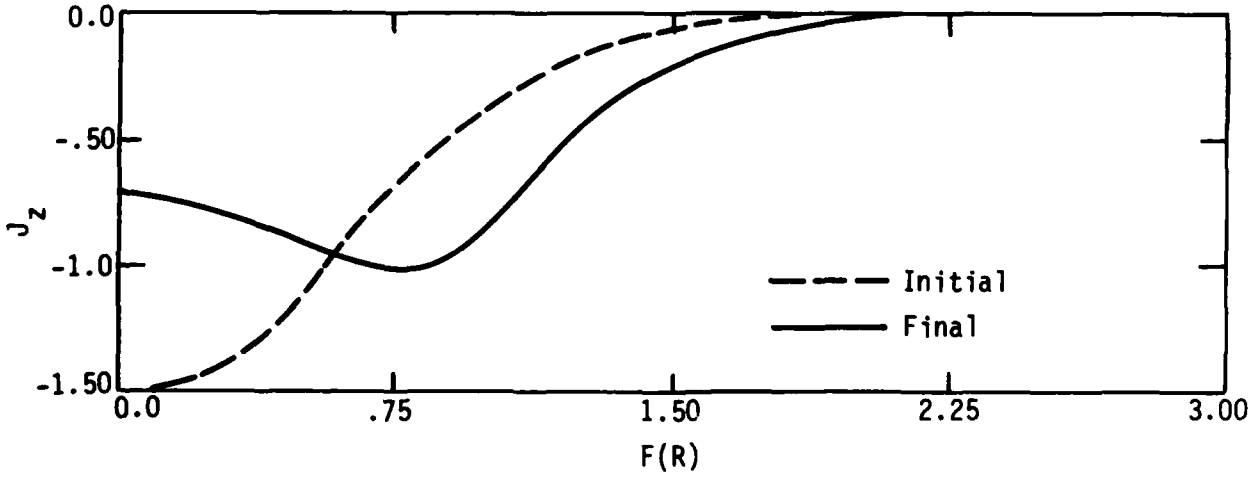

Figure 53. Initial (dashed curve) and final (solid curve) beam current profiles from low density laboratory frame simulation. (Exponential in radius)

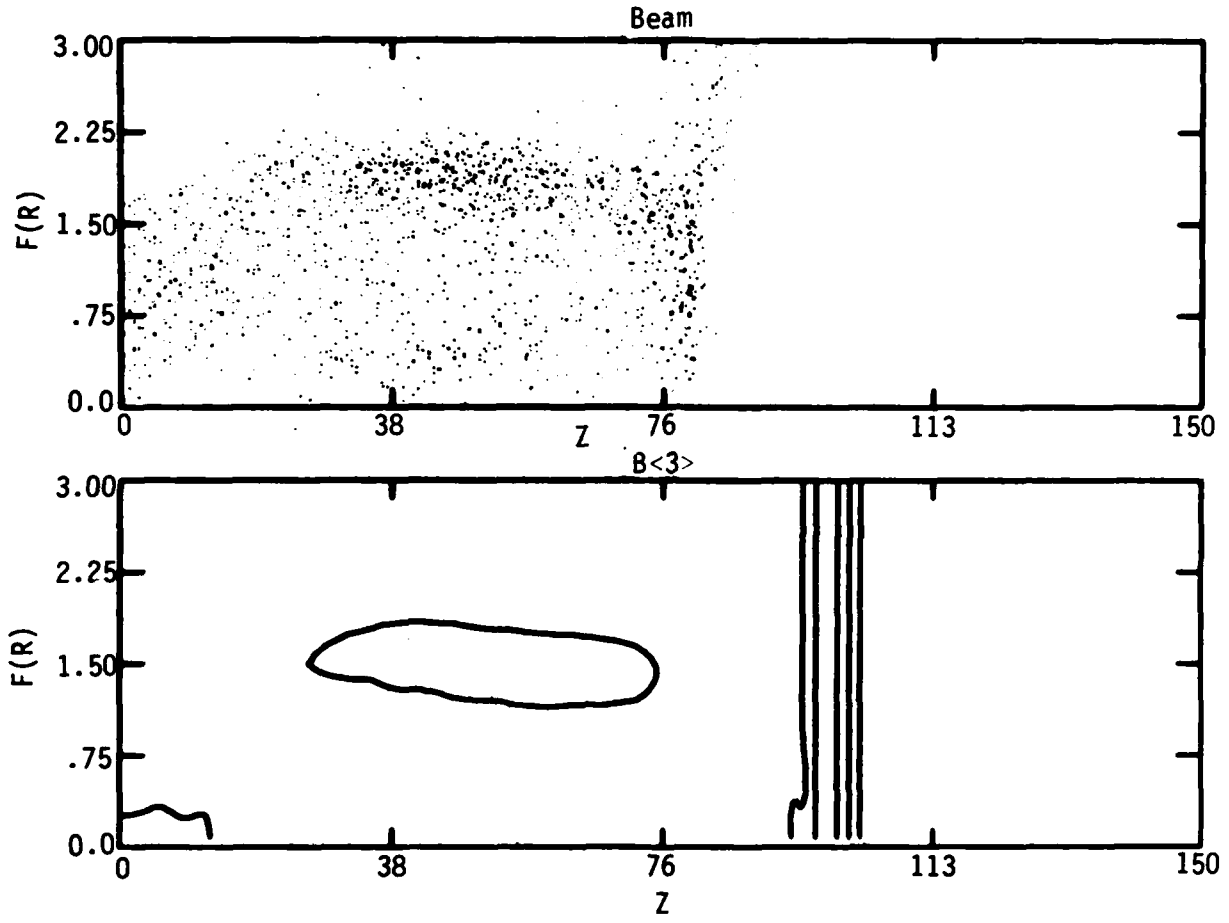

Figure 54. Beam particle configuration and magnetic field contours 3.33 nsec after beam injection in low density laboratory frame simulations.

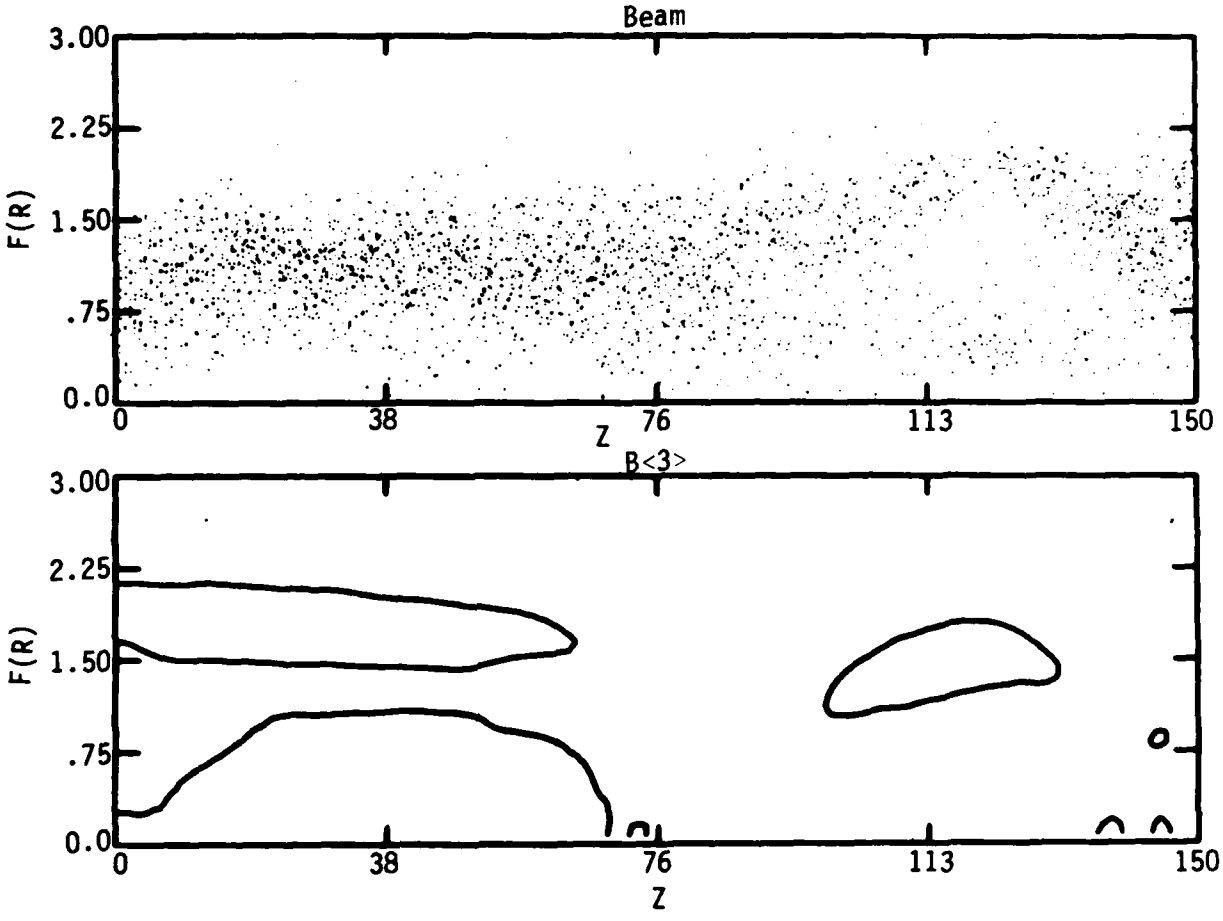

Figure 55. Beam particle configuration and magnetic field contours 6.67 nsec after beam injection in low density laboratory frame simulations.

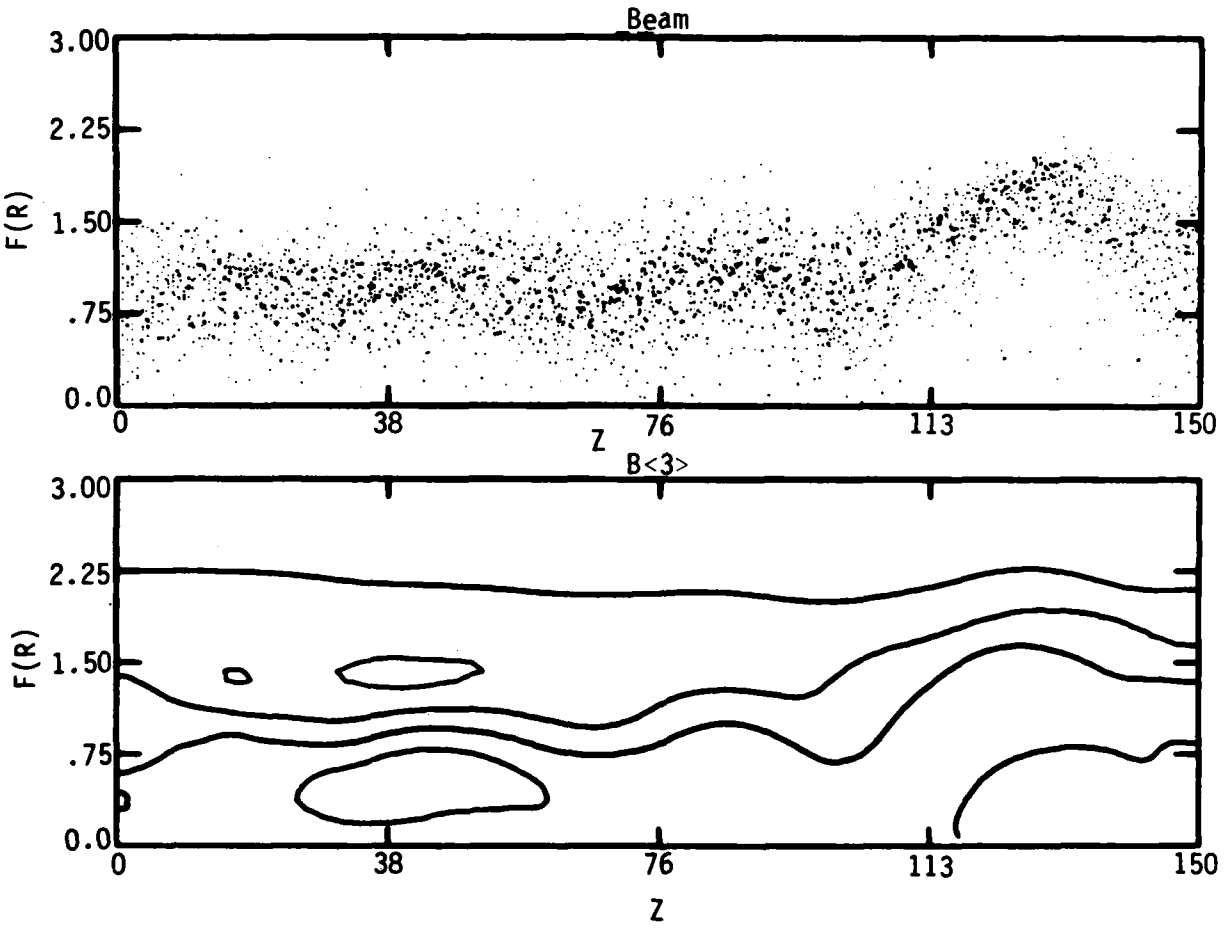

Figure 56. Beam particle configuration and magnetic field contours 10.0 nsec after beam injection in low density laboratory frame simulations.

One two-dimensional numerical simulation was conducted to compare plasma decay times based on a frequently used air chemistry model with experiment. The calculation was performed using the fully relativistic code described previously. This initial investigation was conducted using full density Albuquerque air at low current. In this regime the air chemistry models should be most accurate. Experimental data obtained in this regime showed a generally well behaved beam in the propagation cell which exhibited reasonably two-dimensional behavior.

To make the comparison a 1.0 MeV beam with a 0.5 cm Bennett radius truncated at 2 Bennett radii was injected into a propagation chamber 25 cm long and 10.05 cm in diameter. Air pressure was set at 630 Torr. The air chemistry model used was the Lawrence Livermore National Laboratory PHOENIX package. Beam current was approximated using simple functional relations to model the experimentally measured values. The simulation was run for the first 34 ns of the beam pulse. A hyperbolic tangent with a 7.5 ns risetime was used to initiate the pulse. This was followed by a sine squared pulse beginning at 16 ns and rising to a peak current of 5.5 kA. The quarter cycle time for this portion of the pulse was 9 ns.

Beam behavior was very similar to that observed in experiment. The beam radius at the endplate started at larger than 1 cm then pinched to approximately 0.5 cm as the beam current increased. Beam current and net current measured at 18.8 cm from injection are shown in Fig. 57 along with the corresponding experimental traces. As can be easily seen agreement between simulation and experiment is quite good through the first 30 ns of the beam pulse.

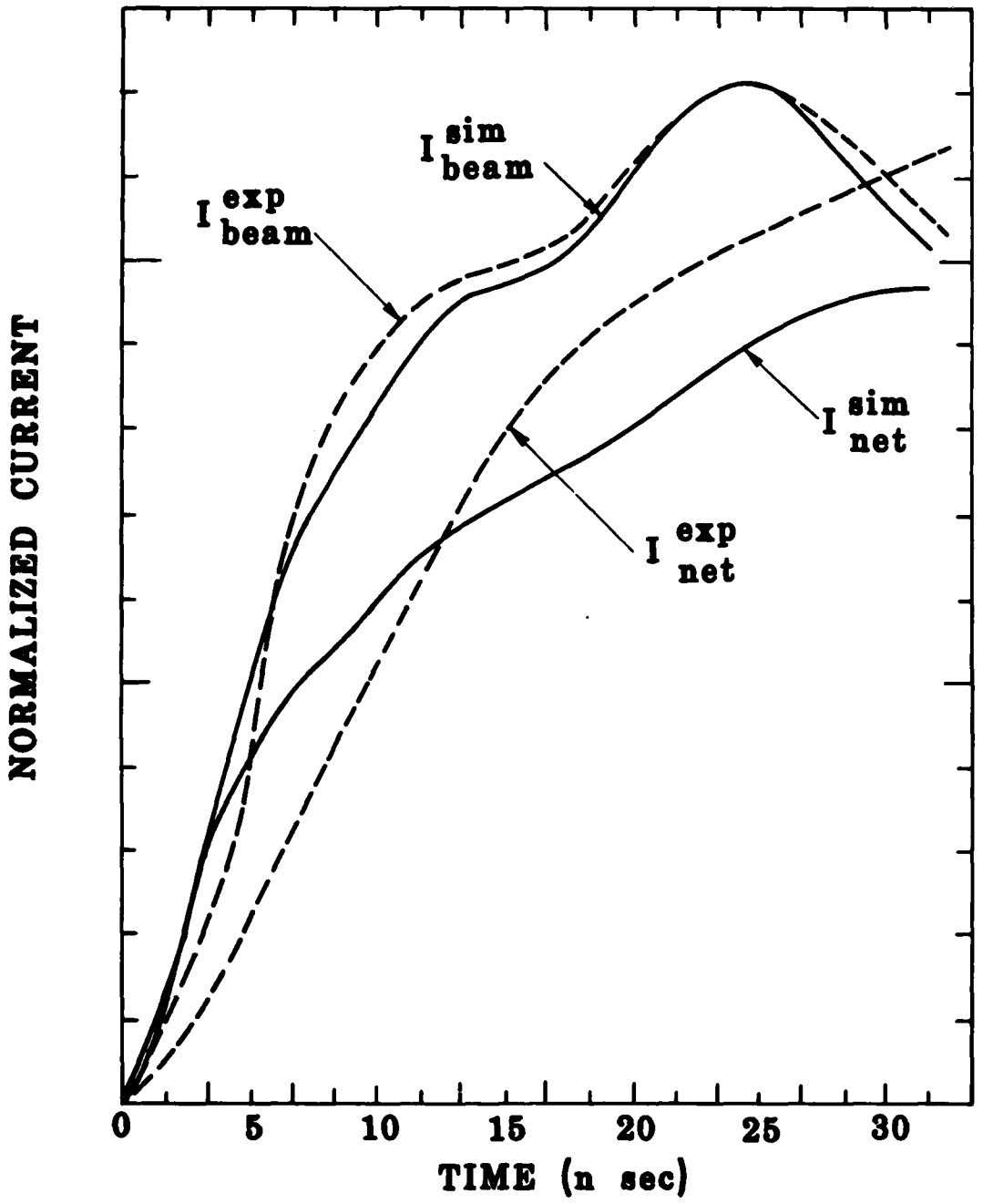

Figure 57. **COMPARISON OF CPROP AXISYMMETRIC CODE RESULTS AND EXPERIMENT FOR ATMOSPHERIC AIR PROPAGATION (Z = 18.75cm)**

VI. CONCLUSION

The goal of the study was to observe the beam nose propagation, resistive hose instability and their interaction. We have completed these tasks. The main results are:

1) The nose-coupled hose effect exists and its existence is correlated with nonuniform or slow beam front velocities ($v < 0.5\ v_b$).

2) Beam front motion exhibits nonuniform features, and is slow near the injection point.

3) Fast rise (1 nanosecond) beams can be generated in a number of ways and generation of such beams appear to be associated with the slow front velocity phase.

4) The plasma decay time can be conveniently measured--it is found to increase linearly throughout the pulse.

5) The dominant hose frequency is controlled by the plasma decay time according to $\omega \sim 0.85\ \tau_D$. This result is within reasonable range of the theoretical value of $\omega \sim 0.6/\tau_D$.

6) Hose growth lengths are in good agreement with theory.

7) A number of new and useful diagnostic techniques have been developed including the "penny" probes, triangle detectors, and plasma decay measurement.

8) A rotating beam has intriguing hose stability properties.

9) CPROP simulations are in good agreement with experiment at 630 Torr.

REFERENCES

1. B. D. Guenther, R. Lontz, and J. L. May, "Particle Beam Research Issues," Proceedings of Particle Beam Research Workshop, US Air Force Academy, 9-11 January 1980.

2. E. P. Lee, Phys. Fluids 21, 1327 (1978).

3. W. M. Sharp, M. Lampe, and H. S. Uhm, Phys. Fluids 25, 1456 (1982).

4. H. S. Uhm and M. Lampe, Phys. Fluids 25, 1444 (1982).

5. G. Joyce and M. Lampe, "Numerical Simulation of the Axisymmetric Hollowing Instability," to be published.

6. W. M. Sharp and M. Lampe, Phys. Fluids 23, 2383 (1980).

7. J. A. Nation and W. Garner, Nuc. Fusion 11, 5 (1971).

8.

9. W. Rogowski and W. Steinhaus, Arch. Elektrotech 1, 141 (1912).

10. L. Pages, et. al., Atomic Data 4, 1 (1972).

11. J. H. Williamson and D. E. Evans, IEEE Trans. Plasma Sci. PS-10, 82 (1982).

12. E. Ott and R. V. Lovelace, Phys. Fluids 16, 2029 (1973).

13. E. P. Lee, Unpublished.

14. G. Ecker, IEEE Trans Plasma Sci. PS-4, 218 (1976).

15. E. P. Lee, et al., UCID-19639, Lawrence Livermore National Laboratory, Livermore, and E. J. Lauer, et. al., Phys. Fluids 21, 1344 (1978).

16. T. Fessenden, et al., UCID-17840, Lawrence Livermore National Laboratory, Livermore.

17. T. P. Hughes and B. B. Godfrey, "Improved Treatment of Multiple Scattering of Intense Charged Particle Beams," AMRC-R-389, Mission Research Corporation, Albuquerque, 1982.

18. B. B. Godfrey, "High Current Beam Propagation Study," AMRC-R-367, Mission Research Corporation, Albuquerque, 1982.

19. F. W. Chambers and D. M. Cox, "Standard Test Case Runs for the EMPULSE Monopole Field Solver and Conductivity Generation Model," unpublished, Lawrence Livermore National Laboratory, Livermore, 1981.

20. R. L. Feinstein, "BMCOND Model," SAI-U-080-8203, Science Applications, Inc., Palo Alto, 1982.

21. S. S. Yu and R. E. Melendez, "Nonlocal Boltzman Theory of Plasma Channels," UCID-19731, Lawrence Livermore National Laboratory, Livermore, 1983.

22. N. J. Carron and W. R. Wortman, "Nonlocal Ionization in Charged Particle Beams," MRC-R-649, Mission Research Corporation, Santa Barbara, 1981.

23. R. R. Johnston, et. al., to be published.

24. W. M. Sharpe and M. Lampe, "Steady-State Treatment of Relativistic Electron Beam Erosion," Phys. Fluids 23, 2383 (1980).

APPENDIX A

APPENDIX A
FX-100 and FX-25 EXPERIMENTS

A. Propagation Experiments

The FX-100 low pressure air propagation experiments were performed in several different experimental runs, each with the specified diagnostics needed to address a limited set of particular issues. This strategy was necessary because of the limited number of data channels that were available for our use. Furthermore, the impending demise of the FX-100 generator was always foremost in our thinking, and in many cases we hurried through an experimental run more rapidly than we would have liked, in order to complete all the baseline measurements before the accelerator was decommissioned.

Our first set of experimental runs was designed to delineate the stable-propagation pressure window with carbon calorimetry, while at the same time accumulating meaurements of the spatial current distribution with the charge-collector array. Other diagnostics fielded to provide corroboration of the current distribution included radiochromic-film dosimetry, TLD arrays, and open-shutter photography. Because of our discovery of the unexpected "halo" of current surrounding the central beam, we devoted a number of shots to extensive investigation into its cause. These included the use of a series of carbon collimators at the anode foil in order to eliminate the possibility that shank emission in the diode was causing the halo current. It was not.

Because the propagation pressure window is also delineated by a minimum in the net current,[1] we devoted a limited number of shots to measurements of net and beam currents at various axial positions. The importance of the channel conductivity and the possibility of using visible light emitted to obtain information about the parameter led us to design an

extensive series of runs devoted to optical diagnostics, for example, spectroscopy and time-resolved streak and framing photography. Finally, a limited test of a compact magnetic beta-spectrometer designed and constructed at Los Alamos National Laboratory was made in order to test the feasbility of using this design in other low-pressure propagation experiments.

The diagnostics used and pressures surveyed in these experiments is tabulated in Appendix B. These experiments produced a large bank of data, all of which has not been fully analyzed.

B. Simulations

Under a separate contract a linearized, three-dimensional, fully electromagnetic particle-in-cell code (KMRAD) was written to investigate resistive instabilities. KMRAD was used to predict instability growth and convection rates in the beam body for the parameters of the FX-100 experiments. Under yet another contract MRC developed a propagation code, CPROP, based on the two-dimensional, relativistic, electromagnetic, particle-in-cell beam simulation code CCUBE. CPROP is being used to investigate the physics of the nose-coupled hollowing instability, including the effects of nose blowoff at injection, ohmic energy losses, conductivity generation, and return current formation. This code treats blowoff, ohmic losses, beam hollowing, and return currents by direct self-consistent numerical integration of the Maxwell equations and the single particle relativistic equations of motion. Conductivity has been based on models developed at Lawrence Livermore National Laboratory. Improved models more appropriate for the low-pressure experiments at AFWL are now being developed at MRC for DARPA and will be added to CPROP in due course. Details of the comparisons between KMRAD and CPROP simulations and the experiments are to be found in Appendix E.

C. Experimental Results and Discussion

In both the FX-25 and FX-100 experiments the energy deposition in a calorimeter at the end of the drift tube was used to define the propagation window in pressure. This measurement integrates over both particle energy and current and is not necessarily indicative of electron kinetic energy loss. For example, we found in our experiments that the low and high pressure limits of the propagation window were largely determined by loss of particles from the beam, rather than by beam-electron kinetic energy loss. Figure 1 shows the beam-current density measured on axis at the end of the FX-25 drift tube at different pressures. Here one can clearly see the definition of the propagation window at high pressures through the erosion of the beam head. The current history measured at the diode can be overlaid on these data as an envelope, but has been omitted for clarity. It is also evident that there is a regime of pressure in which both nose-erosion and tail-loss are simultaneously limiting the beam charge transport through the 3 m drift tube. The propagation window for the FX-100 is shown in Fig. 2. Two measurements of net current for pressures on either side of the window "center" for the FX-100 beam are shown in Fig. 3. It appears that nose-erosion was not so significant for this beam as for the FX-25; however, it must be remembered that the FX-100 pulsewidth was ~6 times that of the FX-25 to begin with, and, therefore, the loss of calorimetrically measured transported energy resulting from equivalent erosion of transported charge would not be so large a fraction of the total in the FX-100 experiments as in the FX-25 experiments. The fact that erosion of the FX-100 beam did not play so large a role as for the FX-25 beam resulted in the comparatively gentle decrease on the low-energy side of the window. The erosion of the beam head can be seen in streak photographs taken at pressures lower than the window center. These are shown in Fig. 4. In Fig. 5 we show streak photographs taken at pressures on the high side of the window, and here it is clearly seen that the loss of the beam tail is the result of hosing of the beam into the wall prior to its reaching the observation port at 4.5 m.

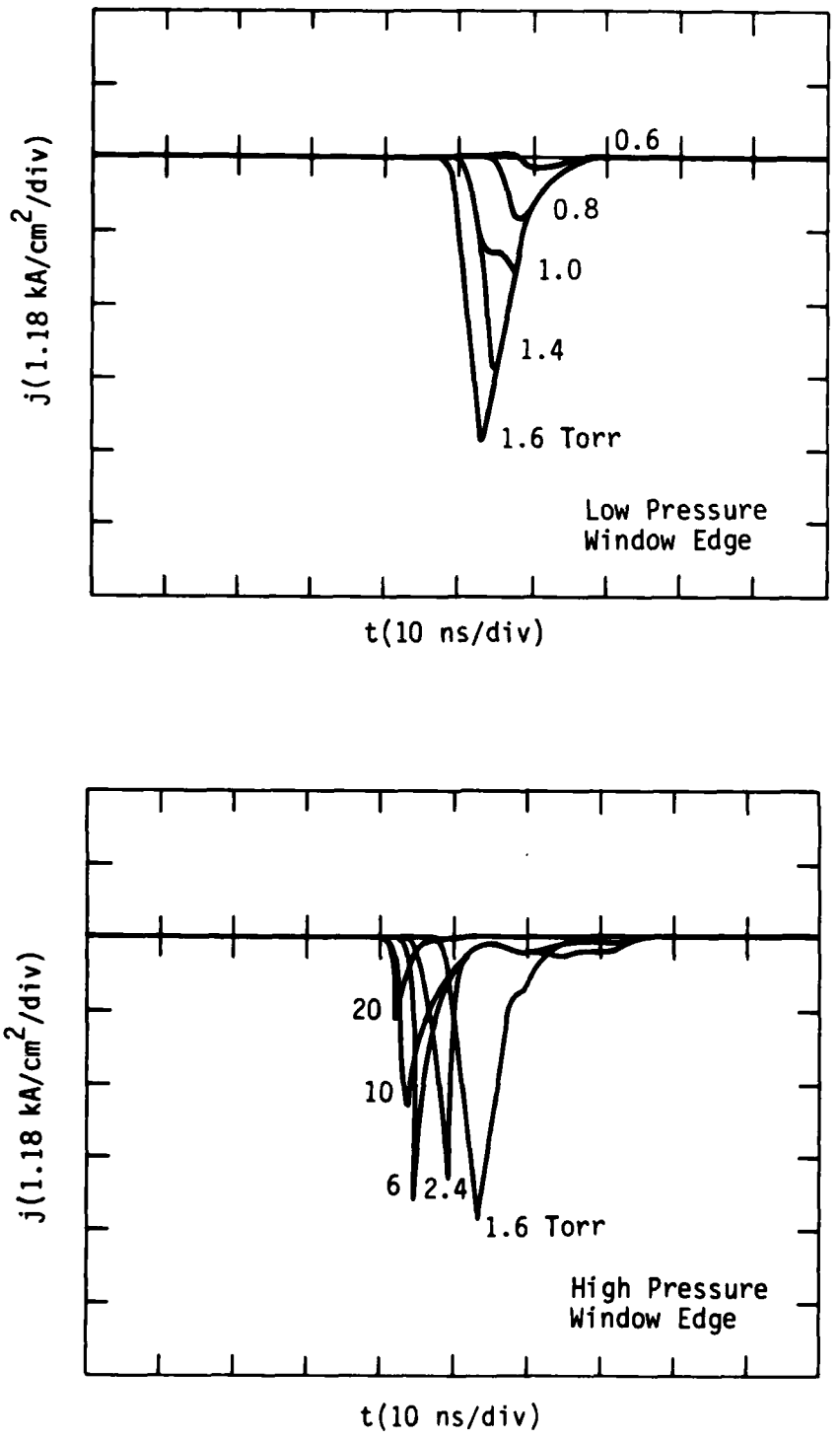

Figure 1. FX-25 beam current density on axis for different pressures. Maximum energy transport was at 1.6 Torr. The current density near the diode had a waveform that approximated the envelope of these signals. The erosion of the beam nose is clearly evident at pressures below 1.6 Torr (upper). At higher pressures both nose erosion and tail loss resulting from hosing are evident (lower).

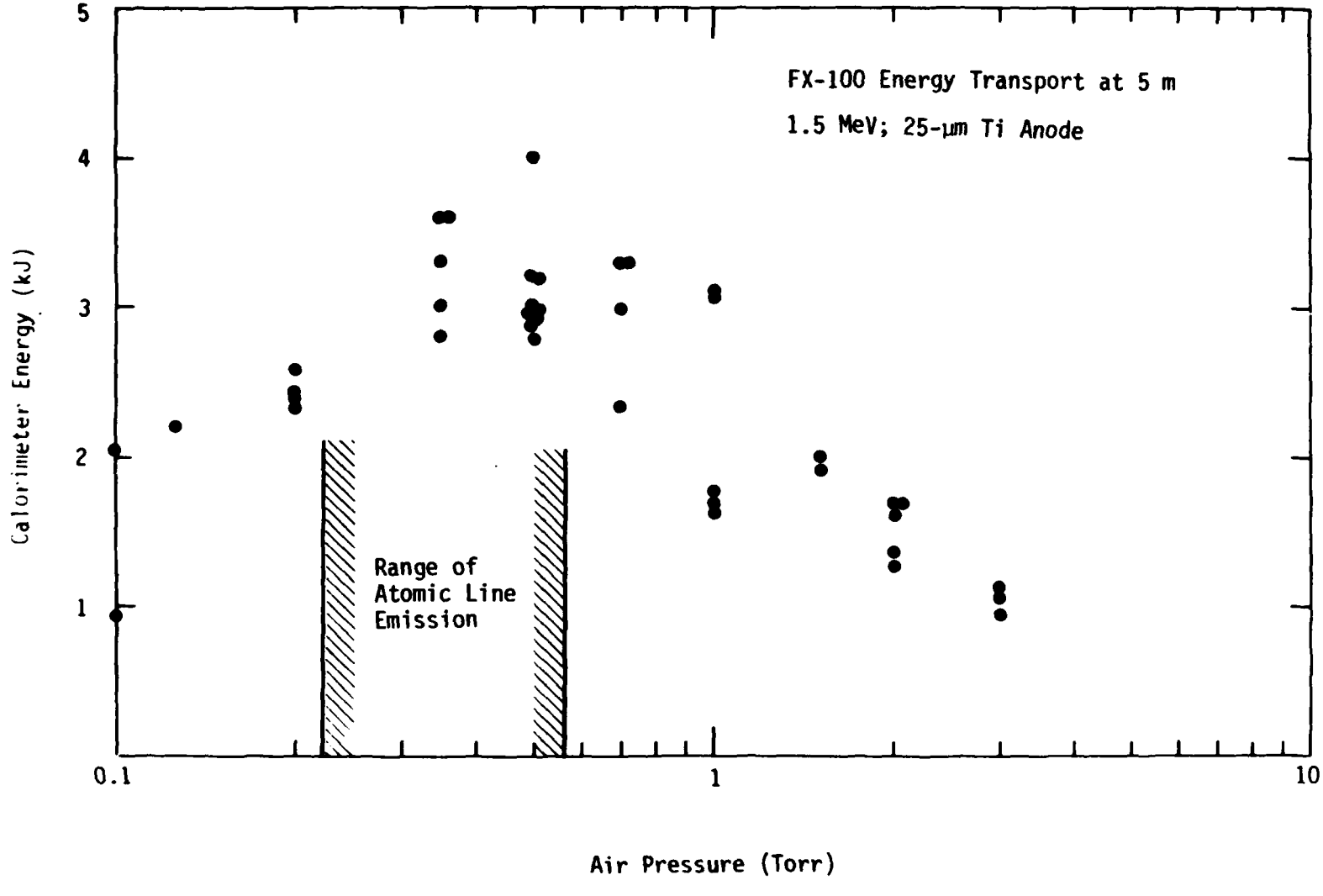

Figure 2. FX-100 propagation window in air for 5-m propagation length. In the range indicated there was intense emission of atomic line radiation as well as the characteristic molecular band emission.

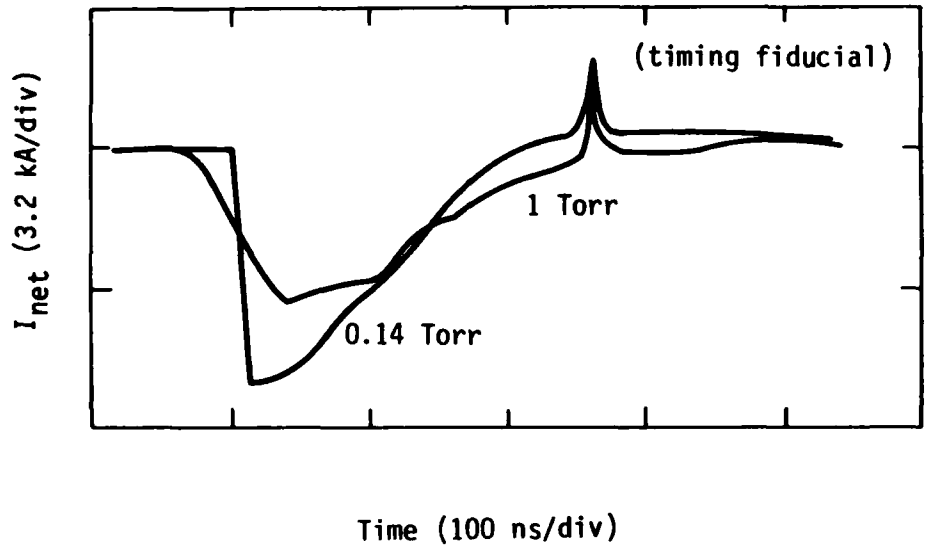

Figure 3. Net current measured in FX-100 propagation experiments at high and low air pressures in the propagation window. The pulse sharpening seen at pressures lower than that for maximum energy transport (~ 0.5 Torr) is thought to result from rapid loss of the beam front and subsequent slow erosion.

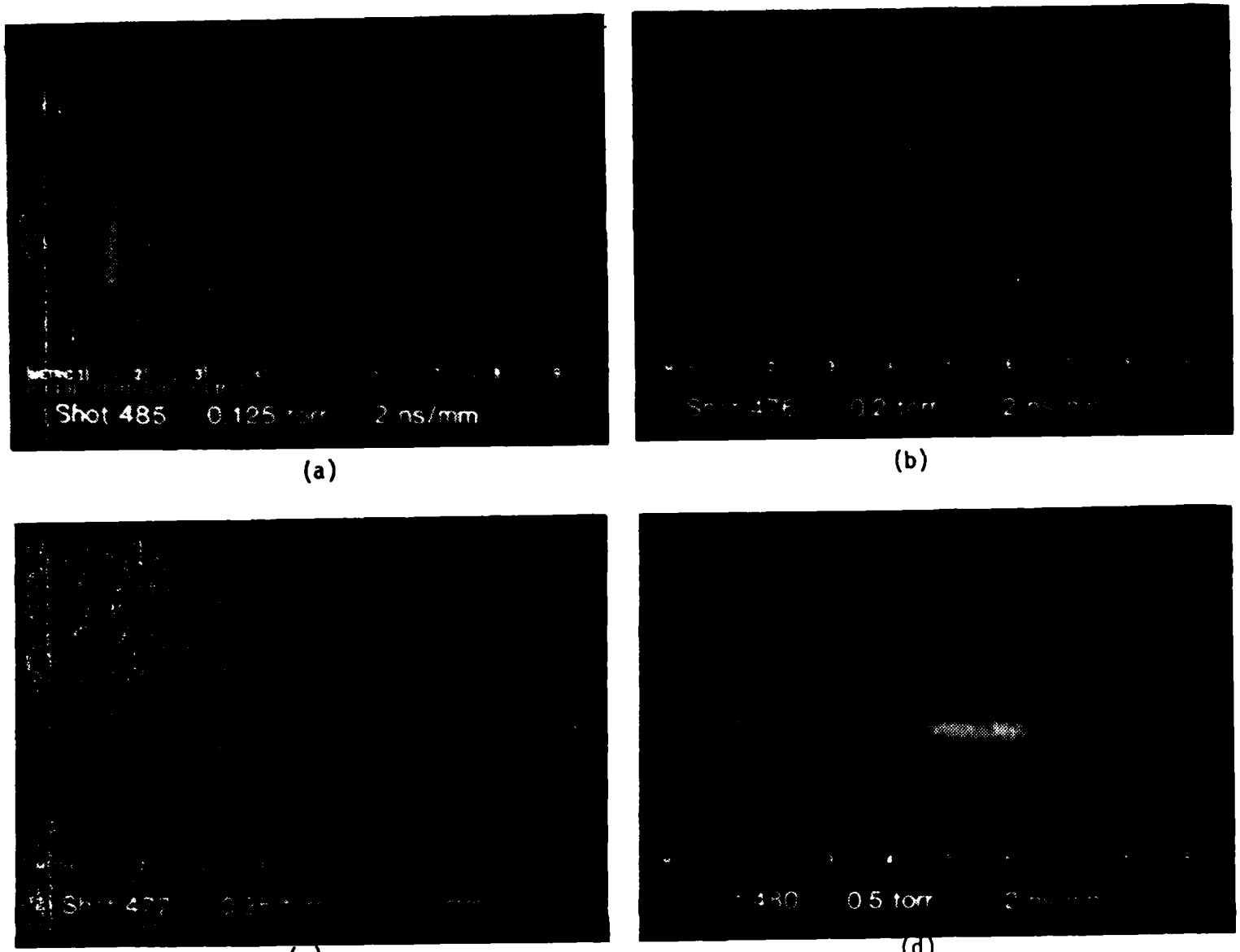

Figure 4. Streak-camera photographs of the beam-excited air emission at Z = 4.5-m as pressure is increased from below the propagation pressure window (a) to the center of the window (d). (Ignore the image converter-tube blemish in the far left of each photograph.) The beam head is at the left of each streak (taken through a vertical slit. The delay in start of emission in (a) as compared with (d) is presumably the result of erosion at lower pressures.

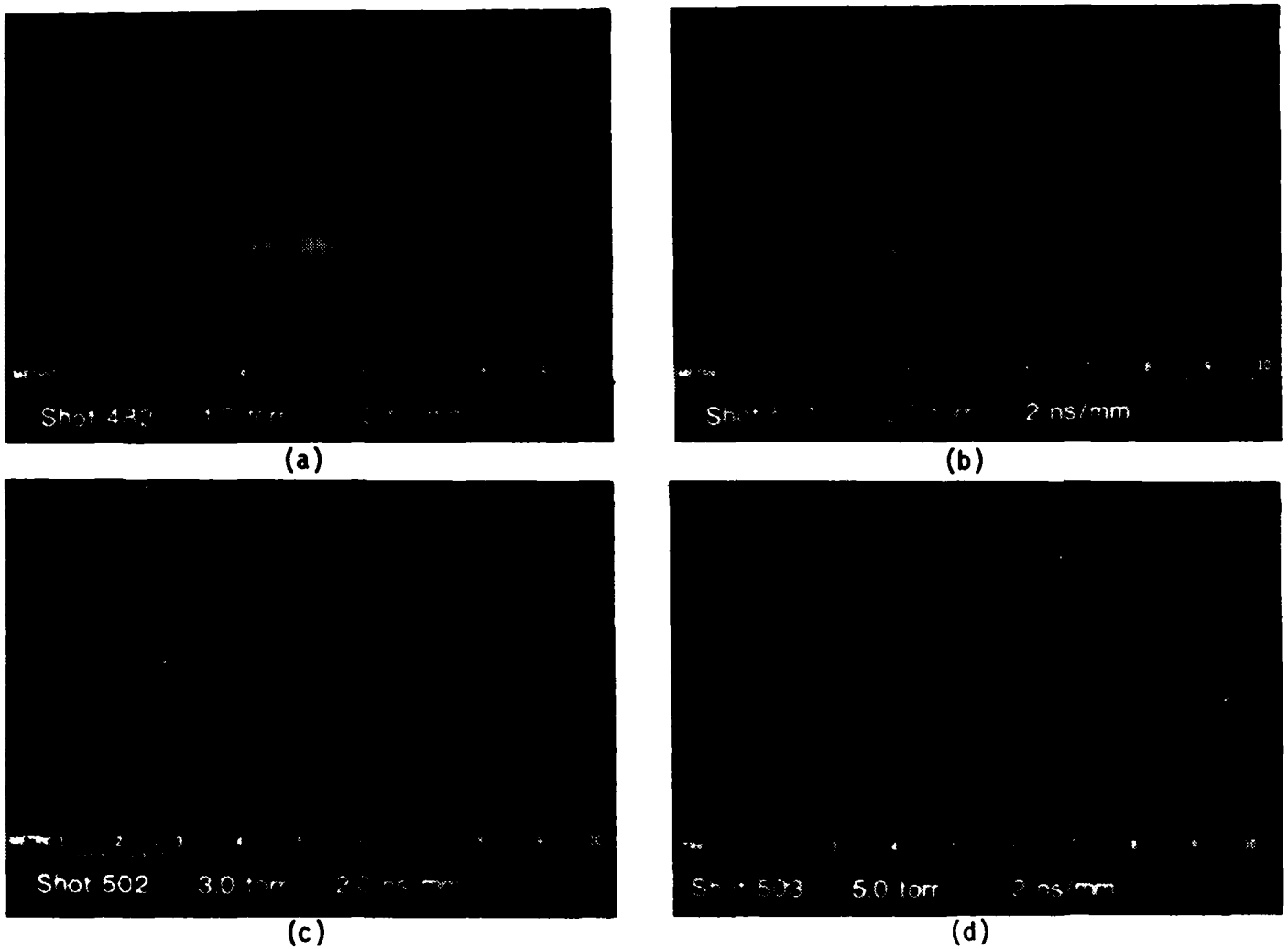

Figure 5. Streak-camera photographs of the FX-100 beam at 4.5-m as air pressure is increased above the propagation window showing loss of the tail of the beam. Figures (b) and (c) show especially clear evidence of hosing in the tail.

Note especially that the beam in Fig. 5b appears to be convective, and that in Fig. 5c a piece of the beam has been detached from the head by the extreme motion of the hose. We should appreciate that we always detected a small piece of the beam head transported to the end of the tube even in the presence of the most violent hosing at pressures in excess of 20 Torr. A small piece of the beam head propagating significant distances on axis has apparently been observed in full density air propagation experiments[2,3] on the large accelerators, and there was some circumstantial evidence for this in our full density FX-25 experiments. This was true for both FX experiments, and may be an initial indication of the lack of nose-hose coupling at these experimental parameters. It should be mentioned that this effect has been observed in many prior propagation experiments.[1 2 3]

In the FX-100 experiments the pressure window for propagation was also delineated by vivid displays of visible emission as is illustrated by the open-shutter photographs in Fig. 6. Spatially resolved spectral measurements of the light emitted showed that in a concentrated region near the axis much of the emission was from dissociated and ionized nitrogen (Fig. 7). Because it requires ~2.4 eV to form this species, we infer a high energy density for the ionized gas on axis. The radial extent of the high energy region is much less than the radius characteristic of the Bennett-like beam current profile (a~3 cm). Although these spectra do not constitute a direct measurement of the channel conductivity, they are suggestive of a hotter and hence more highly-ionized and conductive gas on the axis.

The propagation window was also characterized by the appearance of a virulent azimuthally symmetric instability that caused a large fraction of the beam current to be expelled from the central channel into an annular "halo" region. This thin shell of current then propagated with the residue of the central core to the end of the drift tube. This phenomenon was observed with radiochromic foils, open-shutter photography, streak photography, and our array of fast risetime subminiature charge collectors. The

Figure 6. FX-100 open shutter photographs at Z = 4.5 m and pressures spanning the propagation window showing the molecular band emission at high and low pressures and atomic (O) line emission at intermediate pressures. (Beam propagating left to right, circular aperture 17.5 cm diameter). Note the apparent annular halo of emission surrounding the beam.

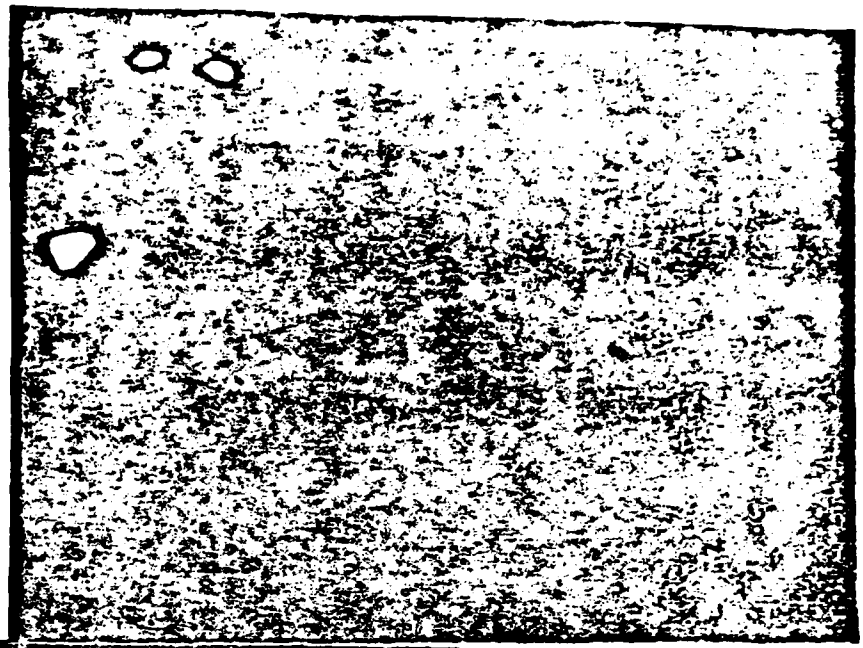

0.7 Torr

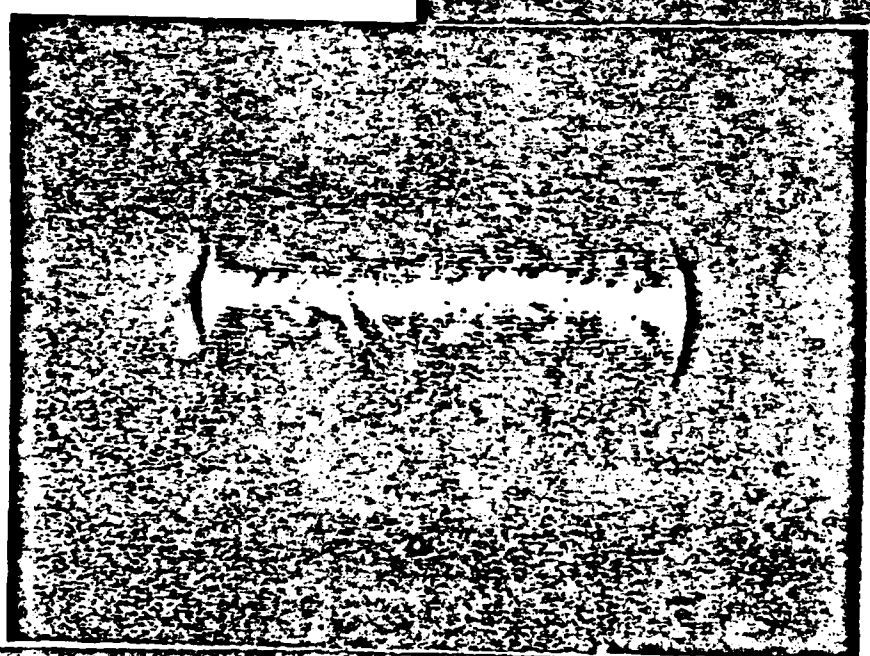

0.25 Torr

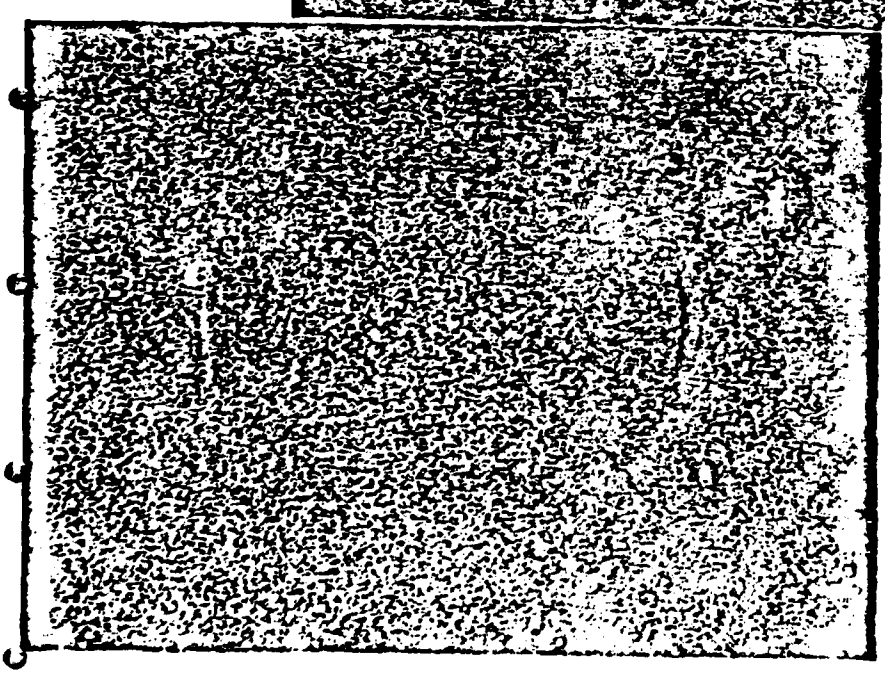

0.13 Torr

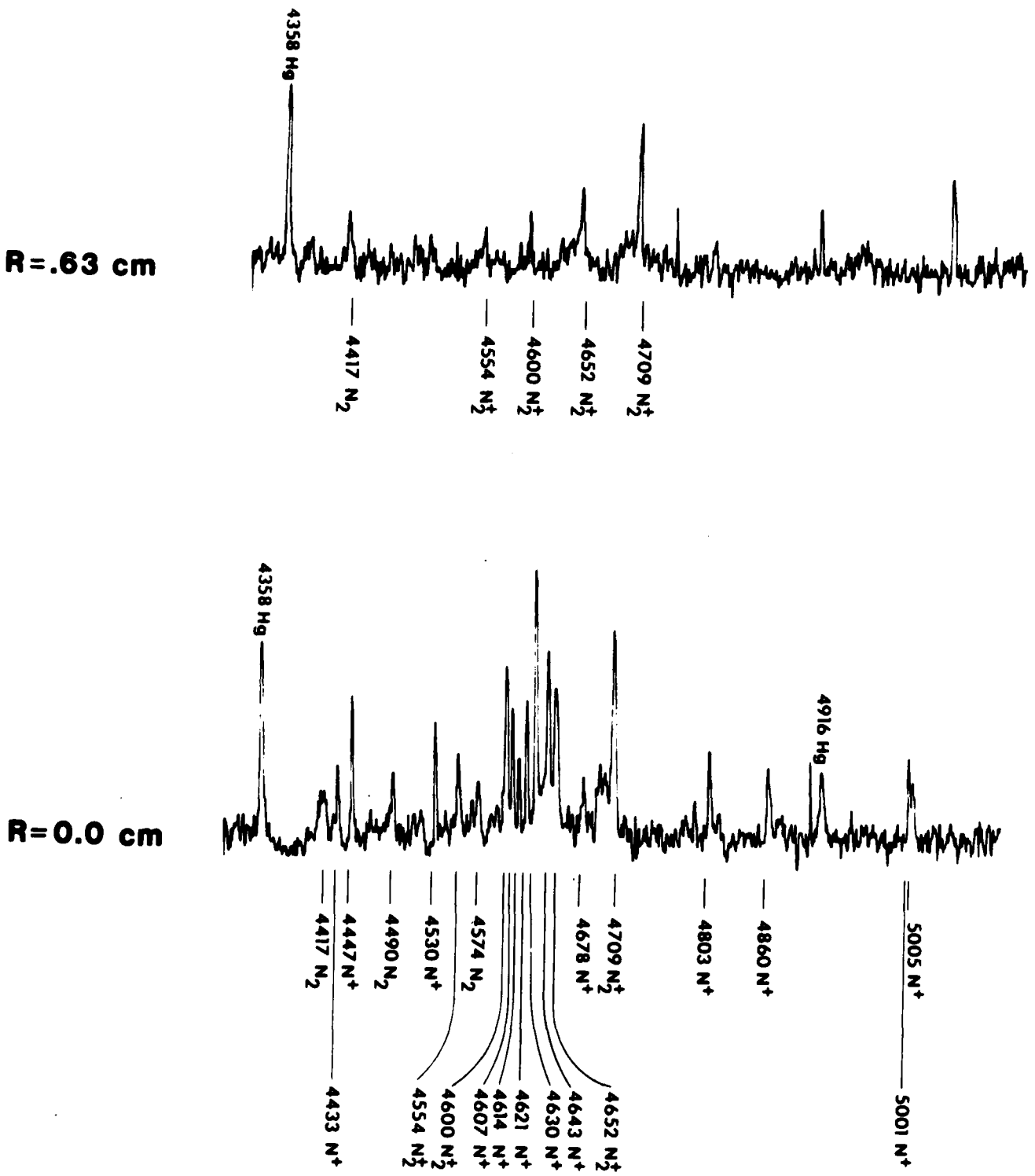

Figure 7. Atomic emission observed in the propagation window (p = 0.35 Torr) is confined to region near the beam axis well inside of the beam Bennett radius (a ~ 3 cm).

radiochromic (blue cellophane) film measurements were made with 125 μm Ti foils shielding the film from exposure to any electrons with kinetic energy below ~180 keV. The same titanium foil thickness was used to shield the array of charge collectors. A time and space resolved plot of the current density at a distance less than 1 m from the diode is shown in Fig. 8. The data plotted in this figure clearly show the evolution of the annular shell at a time late in the beam pulse. An example of a radiochromic exposure can be seen in Fig. 9. Many other examples of the time history of the spatial distribution of current associated with this thin-shell hollowing instability can be found throughout the appendices. The hollow current carrying shell is also evident in both time-integrated and time resolved photographs. It is seen in the open-shutter photograph in Fig. 6 that was taken at 0.25 Torr and in the photograph taken at 0.7 Torr. Figure 10 is a streak photograph showing a well developed shell of current. The open shutter photographs show other rather spectacular effects in addition to the hollowing. It is of interest to resolve these in time to try to understand their causes. In particular, the intense atomic emission concentrated near the axis persists for very long times after the passage of the beam, as seen from the framing camera sequence in Fig. 11. The time integration of this afterglow radiation accounts for the "hot spots" seen in the open shutter pictures. The most likely explanation for the persistence of this afterglow radiation is the extremely slow deionization rates for the ionized atomic nitrogen in the central core. Also evident in Fig. 10 is the apparent formation of the "streamers" during the latter part of the beam pulse. Additional observations about the streamers are that they always open in the direction of beam propagation, as if they were ejected from the channel by primaries, and the opening angle is more acute near the diode. These might be particle tracks "exposed" by the high E/P environment, they could be instabilities in the beam, or they could be low-energy electron exposures of electromagnetic-field effects. Which of these, or other, causes is responsible for the vivid streamer displays is highly speculative at this juncture. The streamers may be masked at earlier times

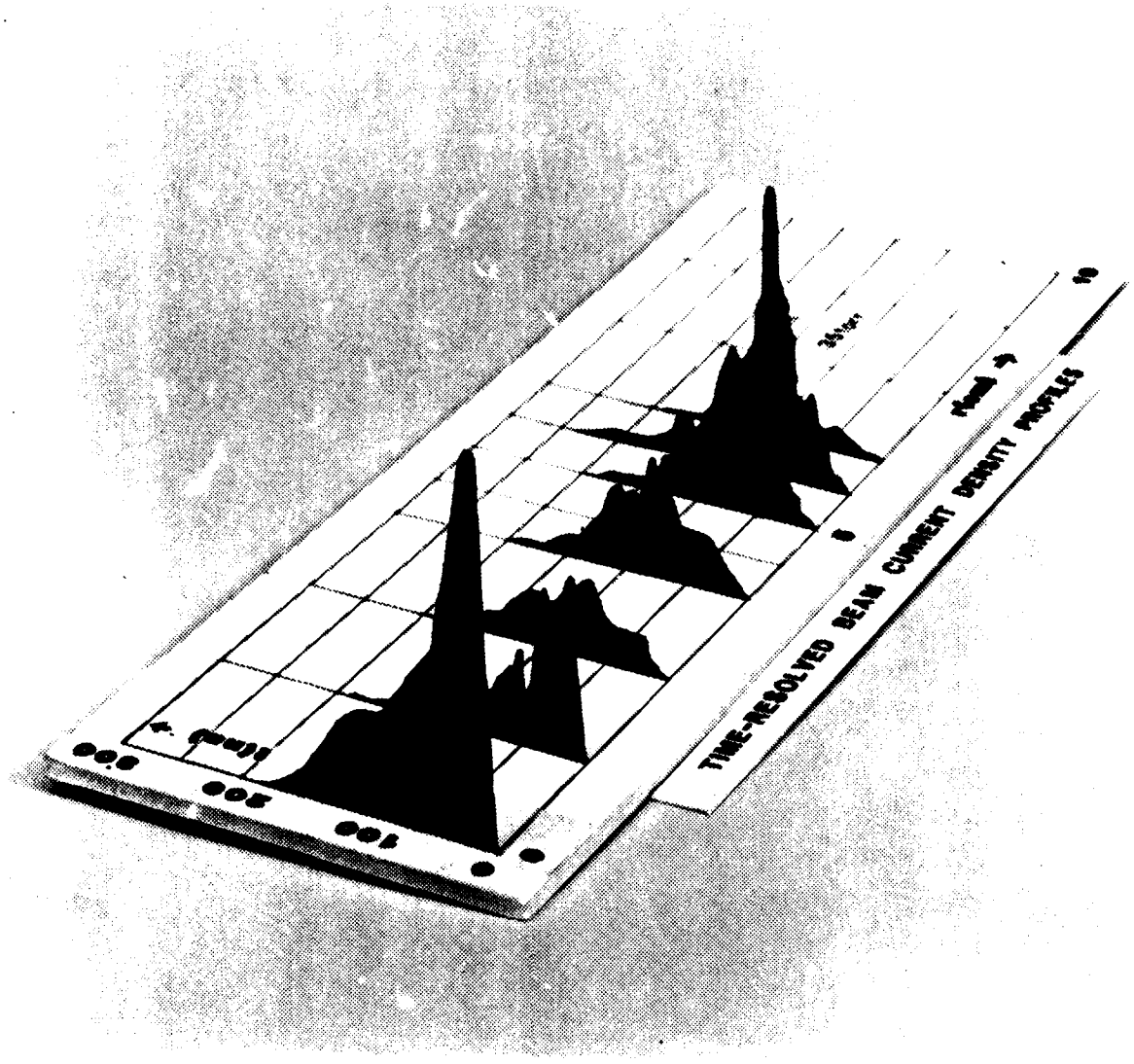

Figure 8. Time-resolved beam current density profile at Z = 0.81-m. p_o = 0.35 Torr. Note development of "halo" current of high energy ($\gtrsim$ 150 keV) electrons at late time in beam pulse.

Radiochronic (blue cellophane) foil exposed to FX-100 beam after propagating 5 m in 0.5-Torr air. Note the bleaching at large radii resulting from annular "halo" of electrons.

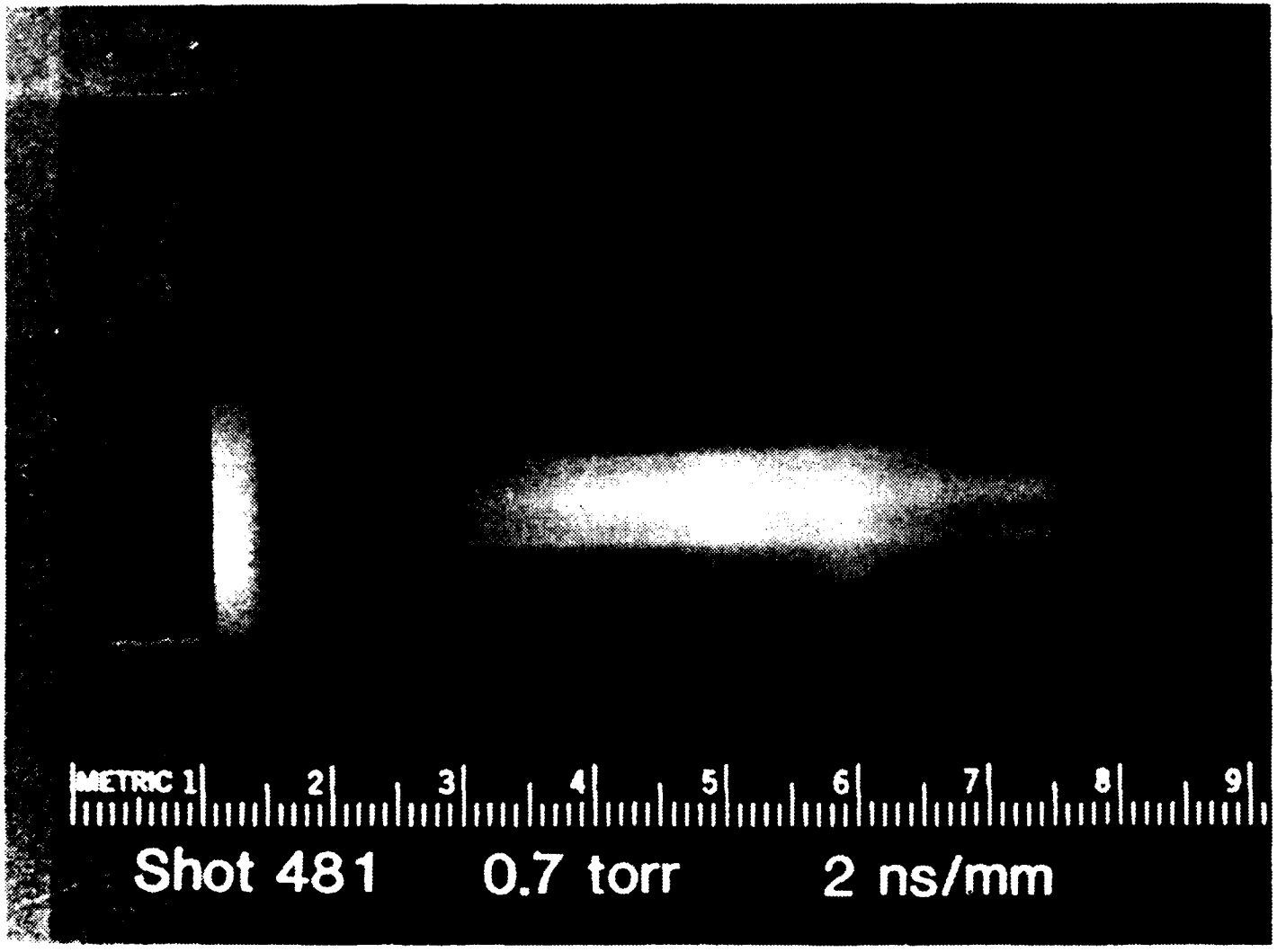

Figure 10. Imacon streak-camera picture taken through a vertical slit at 4.5 m showing emission from fully developed annular halo.

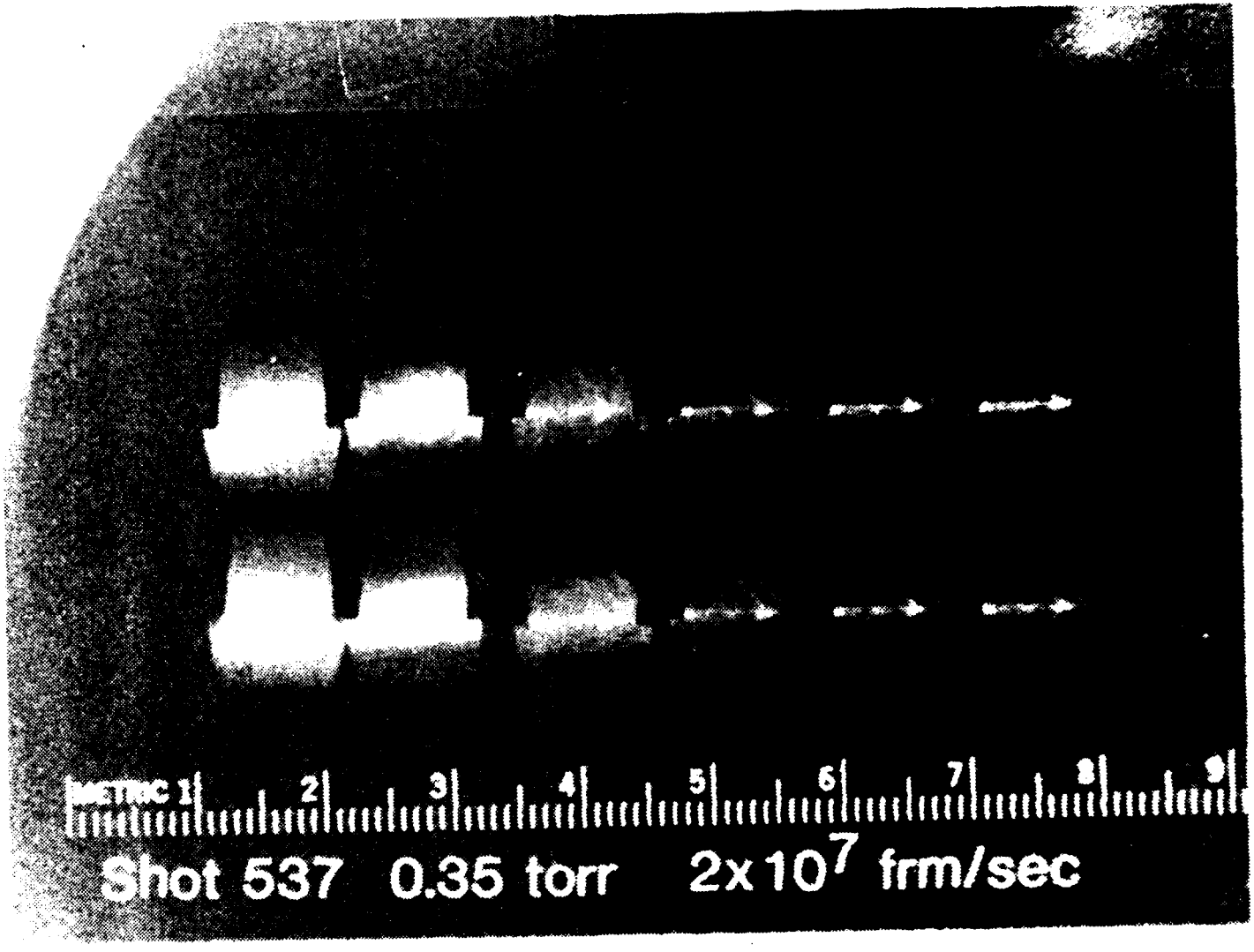

Figure 11. Framing-camera photograph of FX-100 beam at Z = 4.5-m. The exposure time for each frame is 10 ns. This shows the apparent development of a hollowing instability late in the beam pulse, and the persistence of the emission on axis, compared with the rapidly quenched emission from the beam body.

by direct beam excited emission, but on the basis of these photographs one cannot be certain that they are not formed during the switching off of the space-charge neutralized beam current, which may lead to pinching of the remaining unbalanced charge channel.

The appearance of a thin-shell hollowing instability in the pressure regime where avalanching provides an important contribution to the conductivity, which may have a profile more peaked than the beam, and where the current is highly neutralized is in qualitative agreement with existing theory and simulations. However, the > 20 ns delay into the beam pulse before the instability onset is not clear. It may be that this is simply the delay for the conductivity to form the required profile for instability, or the result of a pathological change in the diode characteristics late in the pulse.

Finally, a word about out FX-25 beam extraction experiments is in order. A marked threshold for the stabilization of the full density air hose instability was observed when the preparation cell pressure was reduced below 1 Torr. Because there appeared to be no associated threshold in the erosion-caused pulse sharpening in the drift tube, it is unlikely that this was the dominant mechanism for stabilization, although it may be a necessary ingredient. The same may be said for phase-mixed damping of initial oscillations that are shock-excited at the diode. The probable reason for the threshold is the matching of λ_β inside the cell and just outside of the extraction foil in full density air. This implies matching both the beam radius and net current. Our diagnostics were insufficient to provide conclusive evidence for matching at the stabilization threshold in this limited set of exploratory tests of the use of a beam conditioning cell. The effect is shown in the open shutter photographs in Fig. 12 (3 Torr in preparation cell), and Fig. 13 (0.6 Torr in preparation cell). Note that even when violently unstable in Fig. 12, there is evidence for a part of the beam transporting straight to the wall (as indicated by the

Figure 12. Open shutter photograph of the FX-25 beam extracted into full-density air (630 Torr) through a 25 m Kapton foil after drifting through 3 m of 3 Torr air.

Figure 13. Open shutter photograph of the FX-25 beam extracted into full density air after drifting through 3 m of 0.6 Torr air.

fluorescence of the wall on axis). In Fig. 13 the stable propagation length is limited by the wall to about 5 or 6 betatron wavelengths. These experiments show that there is great promise for the use of the preparation cell technique for providing greater control of the beam stability properties.

REFERENCES

1. T. J. Fessenden, R. J. Briggs, J. C. Clark, E. J. Lauer, and D. U. Trimble, Lawrence Livermore National Laboratory Report UCID-17840, 1979.

2. R. B. Miller, private communication.

3. M. C. Clark, private communication.

APPENDIX B

APPENDIX B

UNCLASSIFIED

SECURITY CLASSIFICATION OF THIS PAGE (When Data Entered)

REPORT DOCUMENTATION PAGE		READ INSTRUCTIONS BEFORE COMPLETING FORM
1. REPORT NUMBER	2. GOVT ACCESSION NO.	3. RECIPIENT'S CATALOG NUMBER
4. TITLE (and Subtitle) Optical Emissions from Intense Relativistic Electron Beam Excited Air		5. TYPE OF REPORT & PERIOD COVERED Topical Report 6. PERFORMING ORG. REPORT NUMBER AMRC-R-326
7. AUTHOR(s) L. A. Wright, C. A. Ekdahl, R. F. Benjamin and T. P. Starke		8. CONTRACT OR GRANT NUMBER(s) F49620-81-C-0016
9. PERFORMING ORGANIZATION NAME AND ADDRESS MISSION RESEARCH CORPORATION 1400 San Mateo Blvd., S.E. Suite A Albuquerque, New Mexico 87108		10. PROGRAM ELEMENT, PROJECT, TASK AREA & WORK UNIT NUMBERS
11. CONTROLLING OFFICE NAME AND ADDRESS Air Force Office of Scientific Research Bolling Air Force Base Washington, DC 20332		12. REPORT DATE November 1981 13. NUMBER OF PAGES 41
14. MONITORING AGENCY NAME & ADDRESS(if different from Controlling Office)		15. SECURITY CLASS (of this report) Unclassified 15a. DECLASSIFICATION/DOWNGRADING SCHEDULE

16. DISTRIBUTION STATEMENT (of this Report)

Approved for Public Release; Distribution Unlimited.

17. DISTRIBUTION STATEMENT (of the abstract entered in Block 20, if different from Report)

18. SUPPLEMENTARY NOTES

19. KEY WORDS (Continue on reverse side if necessary and identify by block number)

Relativistic electron beam diagnostics
Molecular Spectra
Atomic Spectra

20. ABSTRACT (Continue on reverse side if necessary and identify by block number)

During recent low-pressure air propagation experiments with the FX-100 electron beam (E ~ 1.5 MeV, I ~ 40 kA, Δt ~ 120 ns, p ≈ 0.1 - 20 Torr) several diagnostics that used visible light emission were employed. These included time-integrated (open-shutter) photography, time-resolved (streak and framing) photography, and time-integrated spectroscopy. In this report we develop a theoretical framework for interpretation of these diagnostics and discuss the results of the measurements.

(Continued)

DD FORM 1 JAN 73 1473 EDITION OF 1 NOV 65 IS OBSOLETE

UNCLASSIFIED

SECURITY CLASSIFICATION OF THIS PAGE (When Data Entered)

We find that for propagation experiments in general there may be large contributions to the observed emission from both delta rays and the ionized-channel electrons. The plasma electron contribution is sensitive to temperature and to distortion of the tail of the distribution through high E/p effects. The emitted light can be used to observe the beam current in regions not dominated by high E/p because of the proportionality of the descendent electron density to the beam electron density. However, radial resolution of the current density profile may be blurred by the contribution of delta rays ejected at large angles. The temporal response of the emitted light can be expected to faithfully reproduce the beam current history only when the pressure is higher than a minimum, which depends on the highest frequency of interest in the beam current.

From the spectral measurements we have identified observed red emission to be atomic oxygen at 6157A, we have identified a large number of N_2, N_2^+, and N^+ emissions, and we have shown the atomic line radiation to emanate from a region of limited radial extent. In the streak photographs we have seen some results of the magnetic field collapse at the end of the beam. We have observed that the molecular emissions temporally track the beam and that the atomic emission persists at late times, after the beam has passed. The framing photos also show the collapse of the field and radiating volume, and the long time history of the atomic emissions.

ABSTRACT

During the low-pressure air propagation experiments with the FX-100 electron beam (E~ 1.5 MeV, I ~ 40 kA, Δt ~ 120 ns, p ~ 0.1 - 20 Torr) several diagnostics that used visible light emission were employed. These included time-integrated (open shutter) photography, time-resolved (streak and framing) photography, and time-integrated spectroscopy. In this report we develop a theoretical framework for interpretation of these diagnostics and discuss the results of the measurements.

We find that for propagation experiments in general there may be large contributions to the observed emission from both delta rays and the ionized-channel electrons. The plasma electron contribution is sensitive to temperature and to distortion of the tail of the distribution through high E/p effects. The emitted light can be used to observe the beam current in regions not dominated by high E/p because of the proportionality of the descendent electron density to the beam electron density. However, radial resolution of the current density profile may be blurred by the contribution of delta rays ejected at large angles. The temporal response of the emitted light can be expected to faithfully reproduce the beam current history only when the pressure is higher than a minimum, which depends on the highest frequency of interest in the beam current.

From the spectral measurements we have identified observed red emission to be atomic oxygen at 6157Å, we have identified a large number of N_2, N_2^+ and N^+ emissions, and we have shown the atomic line radiation to emanate from a region of limited radial extent. In the streak photographs we have seen some results of the magnetic field collapse at the end of the beam. We have observed that the molecular emissions temporally track the beam and that the atomic emission persists at late times, after the beam has passed. The framing photos also show the collapse of the field and radiating volume, and the long history of the atomic emissions.

CONTENTS

Section		Page
	ABSTRACT	i
I.	INTRODUCTION	1
II.	THEORY OF VISIBLE EMISSION FROM ELECTRON BEAMS PROPAGATING IN AIR	3
III.	EXPERIMENTAL RESULTS AND DISCUSSION	12
	REFERENCES	37

I. INTRODUCTION

Observation of visible light emission is a commonly used diagnostic technique in high-intensity relativistic electron-beam propagation experiments. Photography is an obvious and useful way of observing the behavior of self-luminous experiments, and much information has been obtained from both high-speed and time-integrated photography. For example, estimates of the hose-instability growth length, betatron wavelength, and beam radius have been obtained from photographic records.[1-3] Visible light emitted in beam experiments has also been observed by other methods such as wavelength-filtered fast photodetectors measuring the total light emitted from a region of limited axial extent.[4] For some beam and air pressure parameter regimes, these measurements were found to be correlated with the total beam current, which suggests that this technique could be employed as a nonperturbing beam-current monitor ("optical Faraday-cup").[5-6] Furthermore, if the excitation of air fluorescence by primary beam electrons is indeed the dominant source of light, then the analysis of high-speed streak or framing camera photographs would be a convenient method for obtaining time-resolved details of the beam current density distribution.

As indicated, there is a wealth of information to be gained from the proper interpretation of optical emissions. The purpose of this report is two-fold: to develop a rough theoretical basis for such an interpretation, and to present the results of optical measurements from recent FX-100 experiments. In Section II the underlying assumptions about optical emissions are reviewed, excitation mechanisms other than by the primary beam identified and the importance of these mechanisms estimated.

We will show that for propagation experiments in general there may be significant contributions to the emitted light resulting from delta rays (knock on electrons) and ionized-channel electrons. The contribution from the channel-plasma electrons is sensitive to the temperature and can be enhanced by distortions of the high-energy tail of the distribution by large electric fields. We will develop the necessary conditions on the air pressure that must be met in order to reproduce the beam current temporal history with high fidelity. We will conclude that because of the proportionality of the descendent-electron distribution to the beam electron distribution, reproduction of the beam current is possible within these constraints, although delta rays can lead to a blurring of the radial current profile. In Section III experimental results are presented and discussed. These results include spectra, streak photographs and framing photographs. Observed red emission from the low-pressure FX-100 experiments was spectrally identified as an atomic oxygen line. Additionally, we identified a large number of singly ionized nitrogen lines confined in a region much smaller than the beam radius, as well as the typical beam-excited molecular nitrogen bands seen over the entire radial extent of the beam. The atomic emissions were seen to persist for times much longer than the passage of the beam, leading to an "over-exposure" of persistent stationary structure in the time-integrated open-shutter photographs.

II. THEORY OF VISIBLE EMISSION FROM ELECTRON BEAMS PROPAGATING IN AIR

In high-density air propagation experiments with p_o greater than a few Torr the emission is dominated by the molecular nitrogen purple-blue light emissions.[7] Of these, the N_2^+ first negative (1^-) band emission at 3914 A and the N_2 second positive (2^+) band emission at 3371 A are transitions that have been suggested as useful for beam diagnostics. The excited states of these transitions are rapidly quenched and it is assumed that the time history of these transitions accurately reflects the time history of the electron density that excites the molecules. With this assumption and if the emission results from only the beam primaries, the light emitted from an axially limited region measures the beam current and accurately maps the radial distribution of the high-energy beam.

Possible sources of error in these interpretations can result if there is significant excitation of the molecular states by the secondary (delta-ray) electron population or by the weakly-ionized channel electrons. The cross sections for excitation generally have thresholds of about 5- 20 eV, have maxima near 70-90 eV, and fall off as $\ell nE/E$ in the high energy limit.[8] Figure 1 presents the excitation cross section for the N_2^+ first negative band. The delta-ray distribution, which extends outside of the beam radius, will provide a significant contribution to the excitation because of the large proportion of delta-rays with energies near the excitation cross-section maximum. This is evident from inspection of the delta-ray distribution[9] presented in Figure 2. Furthermore, light emitted from a particular axial location is to some degree dependent on delta rays created at a different axial position. Thus, the spatial dependence of the emission intensity is highly dependent on the spatial distribution of delta-ray secondaries, which tends to mask the correlation with primary beam excitation. Finally, the weakly-ionized channel electrons can contribute strongly to the observed light; as a result of high E/p (electric-field to pressure ratio) distortion of the channel-plasma electron distribution, there may be a significant number of electrons with energies greater than the threshold or near the peak of the excitation

cross section. As seen in Figure 3, without the high E/p effects the overlap of the plasma electron distribution and the excitation cross-section is inconsequential for temperatures less than 1 eV. These secondary electrons can produce a light intensity competitive with that produced by primary beam excitation and correct interpretation of visible observations thus depends on an understanding of these effects.

Thus, the problems of interpreting measurements of visible light emission are somewhat analogous to the problems that arise in attempts to interpret measurements of currents using Rogowski belts or B-dot probes. These inductive current diagnostics are sensitive only to the net current (sum of primary beam and secondary return currents)and additional diagnostics must be employed to resolve each component . The light emission diagnostics are, in turn, also sensitive to a weighted net current (sum of primary beam and secondary currents weighted by effective excitation factors).

There are two steps in unfolding beam parameters from the observed emission. The first is to determine the position dependent excited state population density from the given visible intensity. The intensity of visible radiation emitted by an optically-thin line radiator with thickness z is

$$I = \frac{h\nu}{4\pi} A \int_0^z N_{ex} dZ \quad , \tag{1}$$

where $h\nu$ is the photon energy, $A(s^{-1})$ is the spontaneous emission transition probability, and N_{ex} (cm^{-3}) is the position dependent excited state population density. The spatial variation of N_{ex} can be obtained by tomographic inversion techniques (eg. Abel inversion for cylindrically symmetric systems such as beams). Photography can thus provide an accurate measurement of the time-integrated spatial distribution of excited states if an optical filter at wavelength $\lambda = c/\nu$ is used. Time resolution can be obtained with a streak or framing camera. The remaining question is that of establishing beam parameters through a knowledge of N_{ex}.

For the optically thin radiator, radiative excitation can be neglected, and the excitation to the upper state by collisions occurs at a rate given by $\langle \sigma n_e v \rangle$, where σ is the (velocity dependent) excitation cross section. The average is taken over the electron distribution in velocity space, n_e. The total density distribution is composed of n_b (primary-beam electrons), n_δ (delta-ray secondary electrons) and n_p (ionized-channel plasma electrons); each has a very different velocity distribution. The upper state of the transition can be de-excited collisionally (in addition to radiating) and the rate for this process is $q_0 N_0$, where N_0 is the density of air molecules, and q_0 is the quenching coefficient in air.

Including these processes and neglecting other means of populating the upper level (such as recombination) one gets the rate equation for the excited state population,

$$\dot{N}_{ex} = \langle \sigma n_e v \rangle N_0 - A N_{ex} - q N_{ex} N_0 \quad . \tag{2}$$

Equation (2) can be rewritten as

$$\dot{N}_{ex} + N_{ex}/\tau = \langle \sigma n v \rangle N_0 \quad , \tag{3}$$

which has the solution

$$N_{ex} = \exp[-t/\tau] \int^{t} \exp[t'/\tau] \langle \sigma n_e v \rangle N_0 dt' + C \exp[-t/\tau], \tag{4}$$

The time constant, τ, in equations (3) and (4) is

$$\tau = [A + q N_0]^{-1} \tag{5}$$

Several features of Equations (2)-(5) that relate to the applicability of optical emission diagnostics are worth pointing out. The lower pressure

for practical use of this radiation diagnostic is the pressure at which quenching first dominates τ. For pressure greater than this minimum and time variations of the electron density much larger than τ, the density of excited states is independent of air pressure and is given by

$$N_{ex} \sim \langle \sigma n_e v \rangle / q \tag{6}$$

As an example, we will use the first negative emission of N_2(3914 A); for this transition the spontaneous emission coefficient is $A = 1.24 \times 10^7$ s^{-1} and the quenching coefficient in air is $q = 5.1 \times 10^{-10}$ cm^3 s^{-1} (Ref. 10). Therefore, quenching dominates τ for air densities $N_0 > A/q = 2.4 \times 10^{16}$ cm^{-3} ($p_0 > .74$ Torr at 20°C). For full atmospheric pressure, $\tau = 78$ ps, which is much faster than the time variations in present experiments. For comparison the second positive emission of N_2(3371 A) ($A = 1.1 \times 10^7$ s^{-1} and $q = 6.6 \times 10^{-11}$ cm^3 s^{-1})[11] has a minimum useful pressure of ~5.1 Torr ($\tau \sim .60$ ns for 3371 A emission in full density air).

Equation (5) can be solved for N_0, the minimum neutral number density required to assure a required response time t_r.

$$N_0 = \frac{1}{q t_r} - \frac{A}{q}$$

For $N_2^+(1-)$ and $N_2(2^+)$ this becomes, respectively,

$$p = \frac{59.4}{t_r(ns)} - .74 \text{ Torr} \tag{7a}$$

$$p = \frac{459.}{t_r(ns)} - 5.05 \text{ Torr} \tag{7b}$$

Equations (7) are plotted in Figure 4. This figure is useful for the determination of the minimum pressure for which the emission intensity can be expected to faithfully follow an experimental density variation.

Furthermore, this figure indicates the expected delay time between the onset of a rapid electron density increase at low pressures (where the density rise time is much less than t_r given by Eq. (7)) and the appearance of the optical emission. For example, at pressures less than 1 Torr, the emission from density increases occurring in less than ~ 10 ns would have a rise time of ~ 20 - 30 ns. This lack of temporal fidelity is a further limitation on the pressure range for use of emission diagnostics.

To summarize, to be assured that the emission intensity faithfully reproduces the electron density variation, one is restricted to pressures greater than given in Fig. 4 for any expected time variation of the electron density, and to insure independence of the emission from the neutral gas density the pressure must be greater than 0.7 Torr (for 3914 A light) or 5.1 Torr (for 3371 A).

Assuming that the density variations in the experiment satisfy the foregoing restrictions, then the observed emission intensity will be proportional to $\langle \sigma n_e v \rangle$ (Equation (1) and Equation (6)). However, n_e is composed of n_b, n_δ and n_p; the beam, secondary and plasma electron distributions; each with its own widely differing energy distribution. The observed fluorescence is a combination (both temporaly and spatially) of these, and any information about n_b (or $j_b = \langle n_b v \rangle$) must be further unfolded.

To unfold the observed fluorescence first consider the plasma electrons. At the higher pressures a significant fraction of the plasma electrons result from direct ionization and, therefore, have a density proportional to the beam density. These electrons cannot distort the optical measurements unless there exists a mechanism for locally distorting the light intensity resulting from their excitation of the molecular levels. Such a mechanism is found in high E/p effects. For high electric field-

to-pressure ratios (E/p) a large number of particles go into the high energy tail of the distribution raising the effective temperature of the electrons.[12] For E/p = 10 V cm^{-1} $Torr^{-1}$ in air, T_e^{eff}/T_{gas} ~ 50 (Ref. 13). Because of high effective temperature electrons with more than the threshold for excitation (~11eV for $N_2(2^+)$) will be present. The large number of plasma electrons relative to the beam electrons (~10^3) could contribute greatly to the observed emission. Because of the time dependent fields and skewed distribution, a simple but accurate estimate of these effects cannot be made here.

However, a rough estimate of $\langle n\sigma v\rangle$ can be made for both the plasma and the beam. The ratio of these gives the relative amount of excitation due to both sources. The average for the plasma electrons can be done by using a Maxwellian distribution and a linear fit for the excitation cross section near its threshold, if the Maxwellian temperature is much less than the threshold energy. Then,

$$\begin{aligned} \sigma &= aE + b \qquad && E > E_o \\ &= 0 \qquad && E \leq E_o \quad . \end{aligned} \tag{8}$$

For $N_2^+(1-)$, E_o ~ 18.8 eV and $a = 10^{-18}$ cm^2 eV^{-1} and $b = 1.88\times10^{-17}$ cm^2. The average for beam electrons was calculated from a monoenergetic distribution. The result is

$$\frac{\langle n\sigma v\rangle_p}{\langle n\sigma v\rangle_b} \sim \left(\frac{n_p}{n_b}\right)\left(\frac{8kT}{\pi mc^2}\right)^{1/2} \frac{a(E_o + 2kT)}{\sigma(E_b)}\, e^{-E_o/kT} \quad , \tag{9}$$

where the subscripts p or b refer to plasma or beam electrons, n is the particle density, kT the plasma temperature, E_b the beam electron energy, mc^2 the electron rest mass, $\sigma(E_b)$ the excitation cross section at the beam energy, E_0 the threshold energy for excitation, and b is the slope of the cross section at threshold. For the $N_2^+(1-)$ band, assuming that $n_p/n_b = 10^3$ and 1.5 MeV beam electrons,

$$\frac{\langle n\sigma v\rangle_p}{\langle n\sigma v\rangle_b} \sim 37.2(kT)^{1/2}\,(18.8 + 2kT)\,e^{-18.8/kT} \quad . \tag{10}$$

For 20 MeV beams

$$\frac{\langle n\sigma v\rangle_p}{\langle n\sigma v\rangle_b} \sim 27.9(kT)^{1/2}\,(18.8 + 2kT)\,e^{-18.8/kT} \quad . \tag{11}$$

The 1.5 MeV result is plotted on Figure 5. For plasma temperatures greater than 2.6 eV, the excitation from plasma electrons is greater than from beam electrons. The curve is very steep between 1 and 3 eV and probably quite sensitive to the model. The curve is, therefore, intended only as a rough guideline and an indication of the magnitude of possible plasma electron effects. What is clearly evident is that the light resulting from the plasma electron distribution can equal that resulting from beam primaries if the effective plasma temperature is only slightly increased by high E/p effects. That is, the emission resulting from plasma electrons is greatly and non-linearly enhanced in regions of high E/p. A 20 MeV curve could be similar to the 1.5 MeV curve only scaled in magnitude by .75. On the scale of Figure 5 the two would be almost indistinguishable.

Next we examine the delta-ray (knock-on) secondary electrons. Bombarding N_2 with 1.5 MeV electrons and monitoring the $N_2^+(1-)$ emissions, Hirsch, et al., found that roughly 1/3 of the emission was due to primaries and 2/3 due to secondaries. A theoretical estimate of $\langle n\sigma v\rangle_\delta / \langle n\sigma v\rangle_b$ can be made to compare to the experimental results. Again $\langle n\sigma v\rangle_b$ is calculated by characterizing the distribution as monoenergetic and using the cross section evaluated at the beam energy. The number of particles, n, is left unspecified,

$$\langle n\sigma v\rangle_b \sim 1.8\times10^{-19} n_b \quad . \tag{12}$$

For every n_b that forms N_2^+, there are n_b delta electrons formed and a total of secondaries, tertiaries, etc. of ~ 3 n_b. By integrating over the electron distribution and cross section

$$\langle n\sigma v\rangle_\delta \sim 3.9\times10^{-19} n_b \quad . \tag{13}$$

This gives 32% of the emission due to primaries and 68% due to secondaries, in very close agreement with experimental results. At 20 Mev these fractions are 38% and 62%, respectively.

Considering the case of a 20 MeV beam of .1 cm radius in full density air, neglecting the fields gives half the energy of the secondaries deposited within a radius of .1 cm (in the beam) and half outside of the beam. Considering only primaries and secondaries, 1/3 of the $N_2^+(1^-)$ emission is due to primaries, 1/3 due to secondaries in the beam and 1/3 due to secondaries outside the beam. The effect of the delta-ray secondaries is, therefore, to blur the radial spatial resolution. The time history of the total light from a region of limited axial extent will, however, not be significantly different than the time history of the beam current as a result of delta ray effects because of the proportionality of

n_b and n_δ. Thus, an optical Faraday cup based on this principle should not be affected by delta-ray electrons. Indeed, the additional signal resulting from delta ray secondaries helps to enhance the wanted signal (proportional to n_b) compared with the "noise" (proportional to n_p, for example).

In summary, there are large contributions to the observed emission from both delta rays and the plasma electrons. The contribution from the plasma is very sensitive to the temperature and high energy tail of the distribution and the delta ray contribution differs spatially from the beam contribution. Although much information must be decoupled to obtain beam parameters from optical emissions, the emissions do appear to be good monitors of total energy deposition. In regions not dominated by high E/p effects, the total (radially integrated) light from a region of limited axial extent can probably be used as an "optical Faraday cup" to measure $I_b(t)$ because of the proportionality of the descendent electron density to n_b. The temporal response of such a diagnostic can be expected to follow I_b only at pressures higher than a minimum determined by the most rapid fluctuations of I_b.

III. EXPERIMENTAL RESULTS AND DISCUSSION

To this point the discussion has centered on the interpretation of observed emissions, primarily $N_2(2^+)$ and $N_2^+(1^-)$. Also important, and of future diagnostic use, is the understanding of the gross features of open shutter and high-speed photographs. In this section we will attempt to understand some of these features by examining optical measurements made during the course of propagation experiments using the AFWL FX-100 accelerator. The parameters of these experiments appear in Table 1.

Two striking features on some open-shutter photographs are color changes (red and/or green-blue) and feathering (see Figure 6 for this effect). Time integrated spectra were obtained to identify the source of this emission. Streak and framing photographs give both a temporal history of the emissions and an indication of feathering.

Spectral measurements were taken at 0.35 Torr (near the 0.5 Torr air pressure for maximum energy transport; i.e., "middle" of the propagation window). Because of time constraints spectra at other pressures could not be taken. The spectra were taken after propagating 4.5 m. They were integrated over 10 shots. The dispersing instrument used for these data was a Jarell-Ash 1/2-meter Fastie-Ebert spectrometer with a 1200 groove/mm (5500 Å blaze wavelength) grating. The recording medium was Polaroid type 47 film.

Figures 7-11 display densitometer scans of the photographs of the spectral lines, and Table 2 lists the identified lines and bands and their designations. There are three major wavelength regions where emission are observed: 3750-4450Å, 4600-4710Å, and 6157Å. Lower wavelengths were not recorded because the acrylic windows used have a sharp cutoff at

- 3500A. The lowest wavelength region is the characteristic purple-blue emissions and is dominated by N_2 and N_2^+. The band emission intensity in these regions was probably sufficient to saturate the film response. The wavelength region 4600-4710A is dominated by singly ionized atomic nitrogen (N^+). Emission in the red wavelength range is dominated by a line at 6157A.

The red (6157 A) emission appears only in a narrow range of pressures. In the FX-100 experiments the red emission is observed between - 0.1 → 0.8 Torr, and is not observed at any pressure in pure N_2 experiments. At higher and lower air pressures the emission is the characteristic purple-blue from N_2 and N_2^+.

The 6157A emission line is from atomic oxygen, and was the only neutral atomic emission observed. The oxygen transition is $4d^5D$ - $3p^5P$ while the ground state is $2p^3P$. Although forbidden transitions such as $^3P \rightarrow {}^5D$ frequently occur through scattering, it seems unlikely that for the most intense oxygen transition the upper state would be populated in this manner. Probably, the beam produces O^+, which recombines with electrons to form oxygen in the ^5D state. This interpretation is also consistent with no emission being observed at higher pressures. O^+ would be lost through charge exchange to O_2 which is exoergic, so there would be no recombination to form $O(^5D)$. Similarly, at very low pressures, recombination would not be as likely because of the reduced collision frequency. Figure 12 is a more detailed densitometer scan for this oxygen line, actually 3 lines at 6156.0, 6156.8 and 6158.2A corresponding to J = 1, 2 and 3.

Figure 13 shows two densitometer scans over the same portion of the spectra. The bottom one was taken along the axis of the beam as were all the earlier scans. The upper scan corresponds to a radial position 0.63 cm off axis. At this radial position the atomic nitrogen (N^+) lines were no longer apparent. This was a general characteristic of the

spectra. The spatial extent of the atomic lines was much smaller than for the molecular lines. The molecular emission had a radius of ~ 30 mm, the atomic emission ~ 2.4 mm, and the radius of the beam was ~ 30 mm. This is indicative of a very high electron-distribution average energy near the axis, because the electron energy needed to dissociate and ionize the N_2 molecules is ~ 24.3 eV.

An Imacon 790 image-converter camera was used to obtain streak and framing pictures of the emission. These observations were made through the same window used for the spectrometer but were not simultaneous with spectral measurements. The image-converter camera had a rather long delay after triggering, and in order to record the head of the beam it was necessary to delay the emission light by folding the optical path through 2.2 m and locating the camera next to the FX-100 output switch. The camera trigger was derived directly from the light emitted by the FX-100 output switch. This physical arrangement provided the required delay of the beam emission signal through the beam vacuum-diode delay, beam-propagation delay, and optical-path delay. A 1200-mm Questar collection lens used at the camera provided adequate magnification and light intensity without the use of intermediate field or relay lenses.

Figure 14 is a streak photograph taken at 0.35 Torr. The abrupt decrease in the diameter of the emission is at ~ 120 ns, the length of the beam pulse. It is clear from this photograph that the intense emission near the axis persists in stationary patterns for long times after the beam has passed through the region. The radial contraction is probably due to the collapse of the magnetic field set up by the beam. Because the spectra had shown the spatial depedence of the atomic and molecular emissions to be different, streak photographs were made with wavelength filters with passbands at typical molecular and atomic emission wavelengths. One filter had a passband centered at the N^+ band at 4278Å and these photographs showed that the molecular emission turned off at 120 ns (at the same time that the beam turned off). This light was observed to originate over the larger

radial extent previously observed in the time-integrated spectral measurements. The other filter allowed for the transmission of the atomic nitrogen lines between 4607Å and 4643Å. In agreement with the spectra, the atomic emissions were of limited radial extent. Unfortunately, the intensity of the atomic emissions was low and the starting time for these could not be accurately determined. They appear to start ~ 100 ns after the beam head and continue for more than 800 ns after the beam passage.

Although plasma currents continue to flow in the gas long after the beam passage, the L/R decay of these currents is too rapid (100 - 200 ns) to explain the observed afterglow emission from excited atomic states, which persists for more than 800 ns. Another possible mechanism for the continued excitation of these states is the collisional transfer of energy initially stored as molecular vibrational energy (T_v) by beam or delta-ray electron excitation. However, the most likely explanation for the persistance of atomic states such as N^+ after their initial formation is simply the extremely slow deionization rate at the low air pressures of these experiments. To show this, the deionization times for the various collisional reactions[14] as well as radiative recombination [15] are graphed for a wide range of dry air pressures in Fig. 17. Also given is the scaling of this time with neutral gas and electron density and temperature.

For calculation of the N^+ deionization times that are graphed in Figure 17 the gas temperatures (T_g), electron temperature (T_e) and electron density, n_e, were chosen to give the fastest rates for realistic values of these parameters. That is, it is unreasonable to assume that the N^+ concentrate could be depleted more rapidly than indicated by the graph. It is clear from this figure that the observed afterglow from N^+ states for > 500 ns in 0.35 Torr air is not surprising. Note that, although deionization of high pressure and weakly ionized air is controlled by neutral association, deionization at pressures higher than ~ 2 Torr

can be dominated by three-body recombination if the fractional ionization ($f = n_e/n_a$) is great enough. However, at the pressures relevant to the FX-100 experiments reported here the rate determining reactions for N^+ deionization are $N^+ + O_2$ reactions. All deionization times increase with temperature and even with an air temperature as cold as 1/40 eV, deionization by these reactions in 0.35 Torr air is slow enough that N^+ ions would persist in the afterglow for several hundred ns, in agreement with the observations.

Framing photographs are shown in Figures 15 and 16. Each frame is integrated over 10 ns and the interval between frames is 40 ns. The sequence in which the frames were taken alternates between the lower and upper rows, left to right (in the N shaped sequence characteristic of the Imacon camera). These photographs clearly show the formation of the feather patterns seen earlier in the open shutter photographs (Fig. 6). The feathering appears to occur at the end of the beam (Frames 3 and 4), possibly as the fields (and thus E/p) are rapidly changing. However, the feathering may be present at all times and masked by other intense emissions. As the region of emission collapses at the end of the beam, the vertices of the feathers remain in the same location and continue to radiate for long times (the last frame is ~ 600 ns in Fig. 16, and ~ 700 ns in Fig. 17). The integration of the radiation from these vertices is responsible for the intense exposure previously seen near the axis of the open shutter pictures. Thus, the "hot spots" previously seen in open shutter photographs do not result from extremely intense emission for a short duration, but rather are the result of long time exposure compared with the remainder of the emission.

In summary, from the spectral measurements we have identified the observed red emission to be atomic oxygen at 6157Å, we have identified a large number of N_2, N_2^+ and N^+ emissions, and we have shown the

atomic line radiation to emanate from a region of limited radial extent. In the streak photographs we have seen some results of the magnetic field collapse at the end of the beam. We have observed that the molecular emissions temporally track the beam and that the atomic emission persists at late times, after the beam has passed. The framing photos give the first hint of the feathering process, show the collapse of the field and radiating volume, and the long time history of the atomic emissions. Further development of these techniques (i.e., time-resolved spectroscopy) holds great promise for providing much information on beam-air chemistry (and hence conductivity) and on basic beam parameters.

This research was sponsored by the Air Force Office of Scientific Research (AFSC) under contract F49620-81-C-0016. The authors wish to acknowledge the assistance of Winston Bostick in performing these experiments. Professor Bostick was a senior research physicist in the University Residency Program sponsored by the Air Force Office of Scientific Research under IPA-905-79-01016C. Finally, the authors are deeply indebted to the following members of the Dynamic Testing Division (M Division) at Los Alamos National Laboratory for the time-resolved photography of the FX-100 propagation experiments: Lee Builta, Dave Moir, and Steve Schmidt. Starke.

TABLE 1. FX-100 BEAM PROPAGATION EXPERIMENT PARAMETERS

Maximum Beam Energy,	E_b = 1.5 - 2.0 MeV
Maximum Beam Current,	I_b = 35 - 40 kA
Beam Pulse Duration,	Δt = 120 ns
Beam 1/e-radius at injection,	r_{bo} = 3 cm
Propagation Chamber Radius,	R_w = 10 cm
Observation Port Position,	z_o = 4.5 m
Air Pressure,	p_o = 0.1 - 20 Torr

TABLE 2. IDENTIFICATION OF OBSERVED LINES AND BANDS.

WAVELENGTH Å	ATOM/MOLECULE	TRANSITION (band) (v', v")
3755	N_2	(2+) (1,3)
3805	N_2	(2+) (0,2)
3858	N_2	(2+) (4,7)
3884	N_2^+	(1-) (1,1)
3914	N_2^+	(1-) (0,0)
3943	N_2	(2+) (2,5)
3998	N_2	(2+) (1,4)
4059	N_2	(2+) (0,3)
4095	N_2	(2+) (4,8)
4142	N_2	(2+) (3,7)
4167	N_2^+	(1-) (3,4)
4200	N_2	(2+) (2,6)
4236	N_2^+	(1-) (1,2)
4270	N_2	(2+) (1,5)
4278	N_2^+	(1-) (0,1)
4344	N_2	(2+) (0,4)
4417	N_2	(2+) (3,8)
4433	N+	$3d\ ^3p^o$-$4f$ D(5/2)
4447	N+	$3p\ ^3D - 3d\ ^3D^o$
4490	N_2	(2+) (2,7)
4530	N+	$3d\ ^1F - 4f$ G(9/2)
4554	N_2^+	(1-) (3,5)
4574	N_2	(2+) (1,6)
4600	N_2^+	(1-) (2,4)
4607	N+	$3s\ ^3p^o - 3p\ ^3P$
4614	N+	$3s\ ^3p^o - 3p\ ^3P$
4621	N+	$3s\ ^3p^o - 3p\ ^3P$
4630	N+	$3s\ ^3p^o - 3p\ ^3P$
4643	N+	$3s\ ^3p^o - 3p\ ^3P$
4652	N_2^+	(1-) (1,3)
4678	N+	$3d\ ^1p^o - 4f$ D(3/2)
4709	N_2^+	(1-) (0,2)
4803	N+	$3p\ ^3D - 3d\ ^3D^o$
4860	N+	$3p\ ^3D - 3d\ ^3D^o$
5001	N+	$3p\ ^3D - 3d\ ^3F^o$
5005	N+	$3s\ ^5p - 3p\ ^5p^o$
		$3p\ ^3D - 3d\ ^3F^o$
5667	N+	$3s\ ^3p - 3p\ ^3D$
5680	N+	$3s\ ^3p - 3p\ ^3D$
5686	N+	$3s\ ^3p - 3p\ ^3D$
5711	N+	$3s\ ^3p - 3p\ ^3D$
6157	O	$3p\ ^5p - 4d\ ^5D^o$

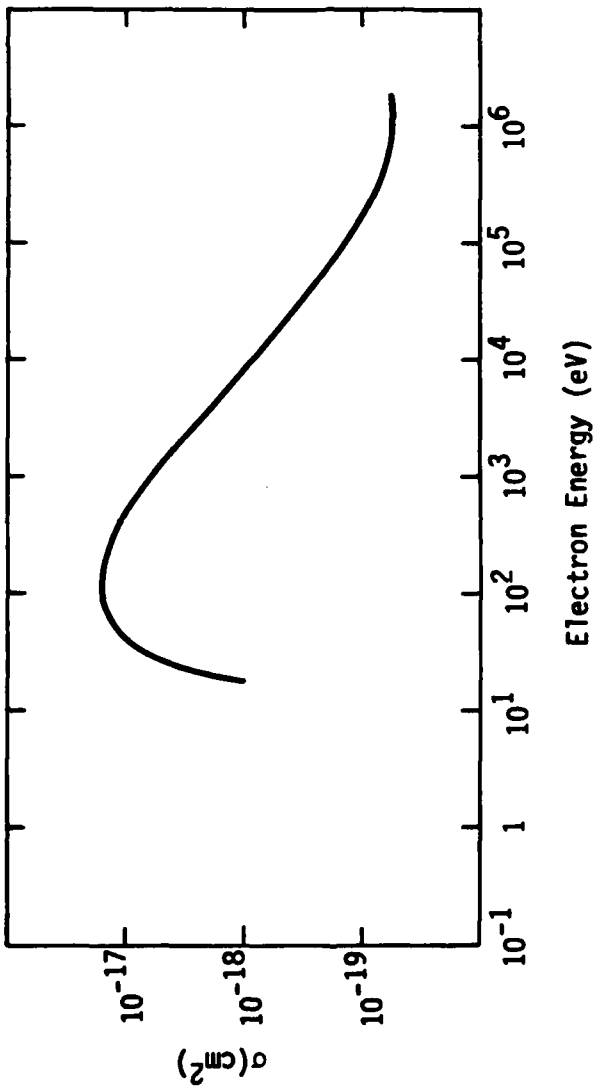

Figure 1. Excitation cross section for $N_2^+(1^-)$.
(Data from Ref. 8)

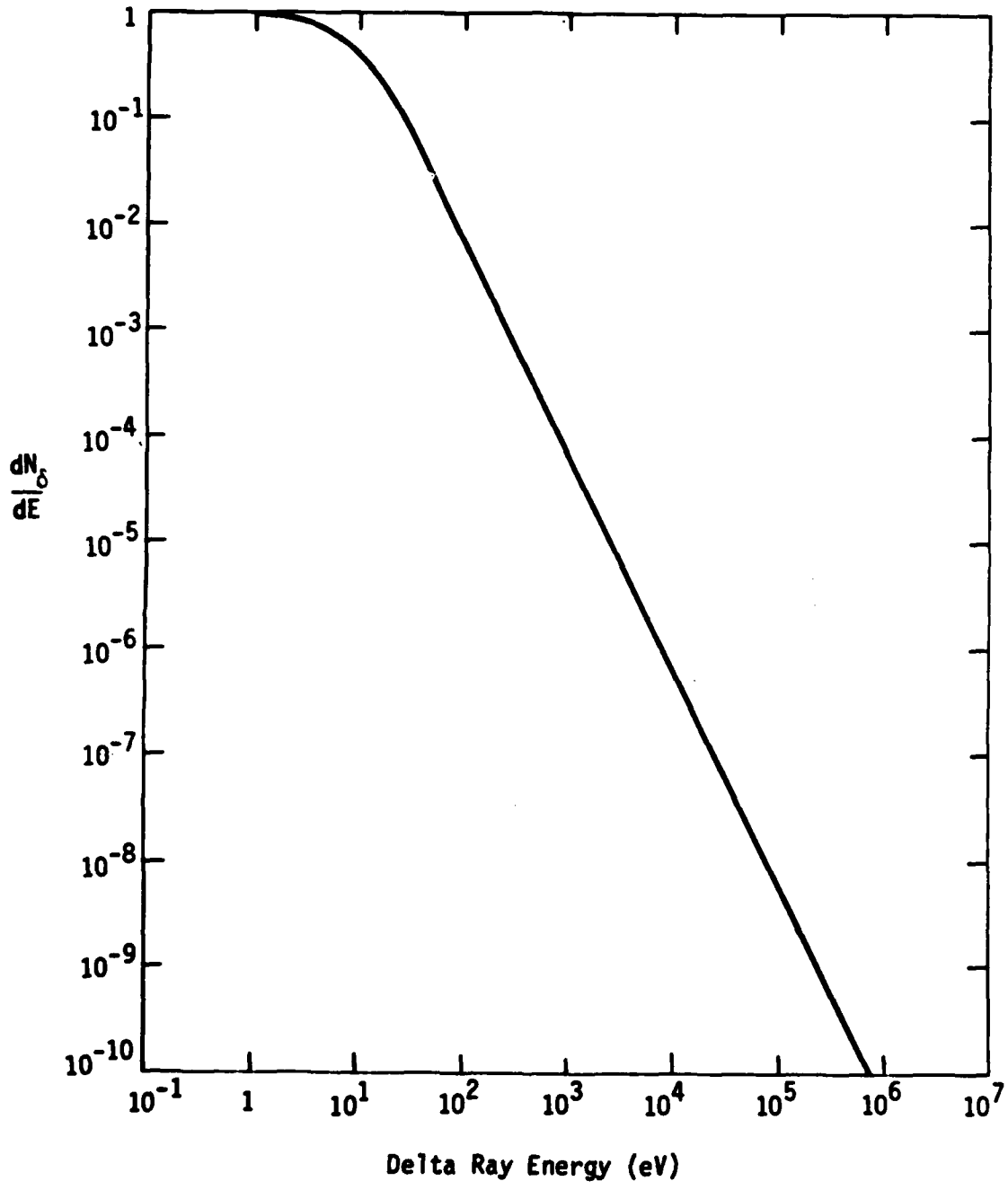

Figure 2. Distribution of delta rays with energy.
(Calculated for $\gamma \gtrsim 4$)

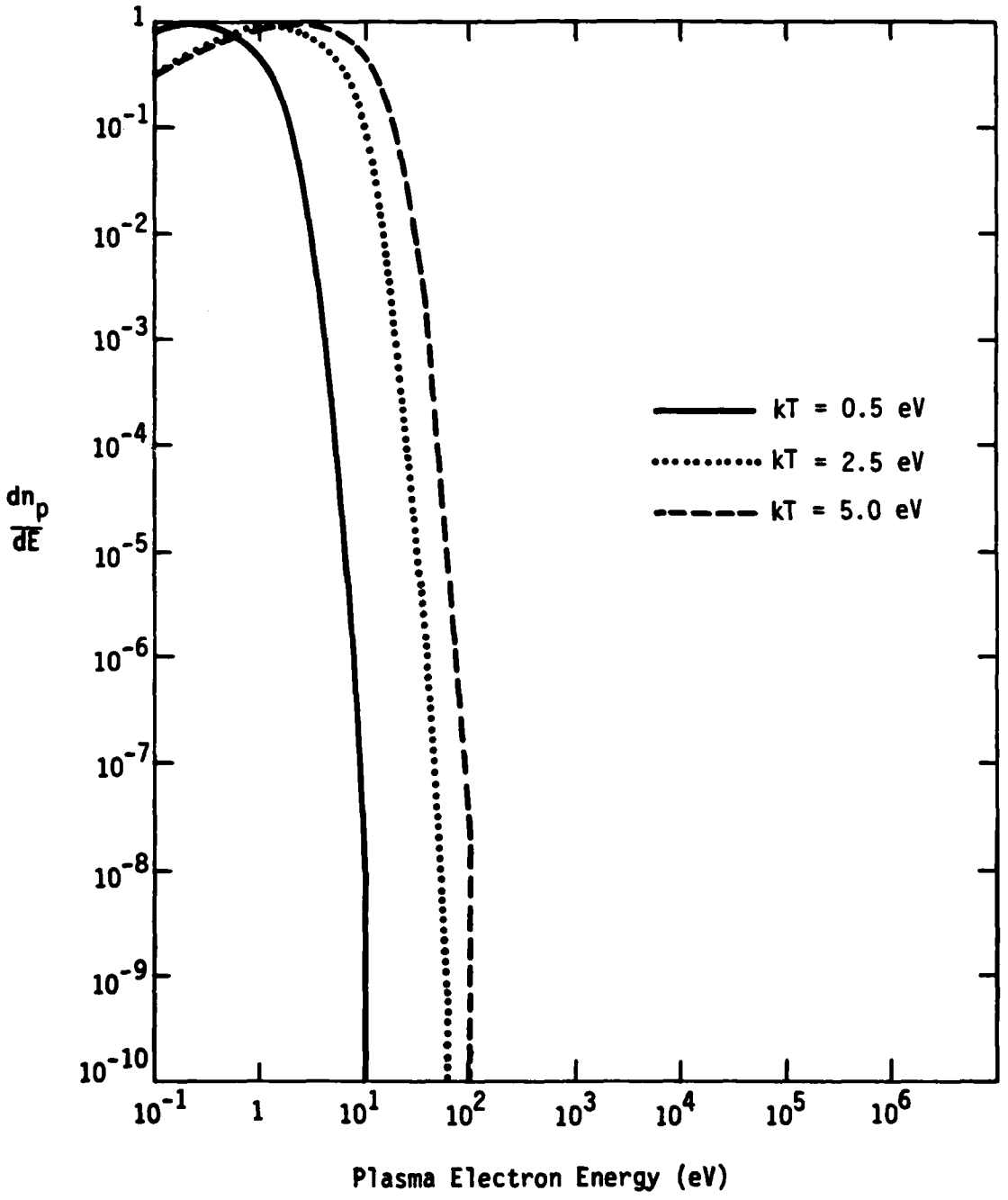

Figure 3. Distribution of plasma electrons with energy for three Maxwellian temperature distributions.

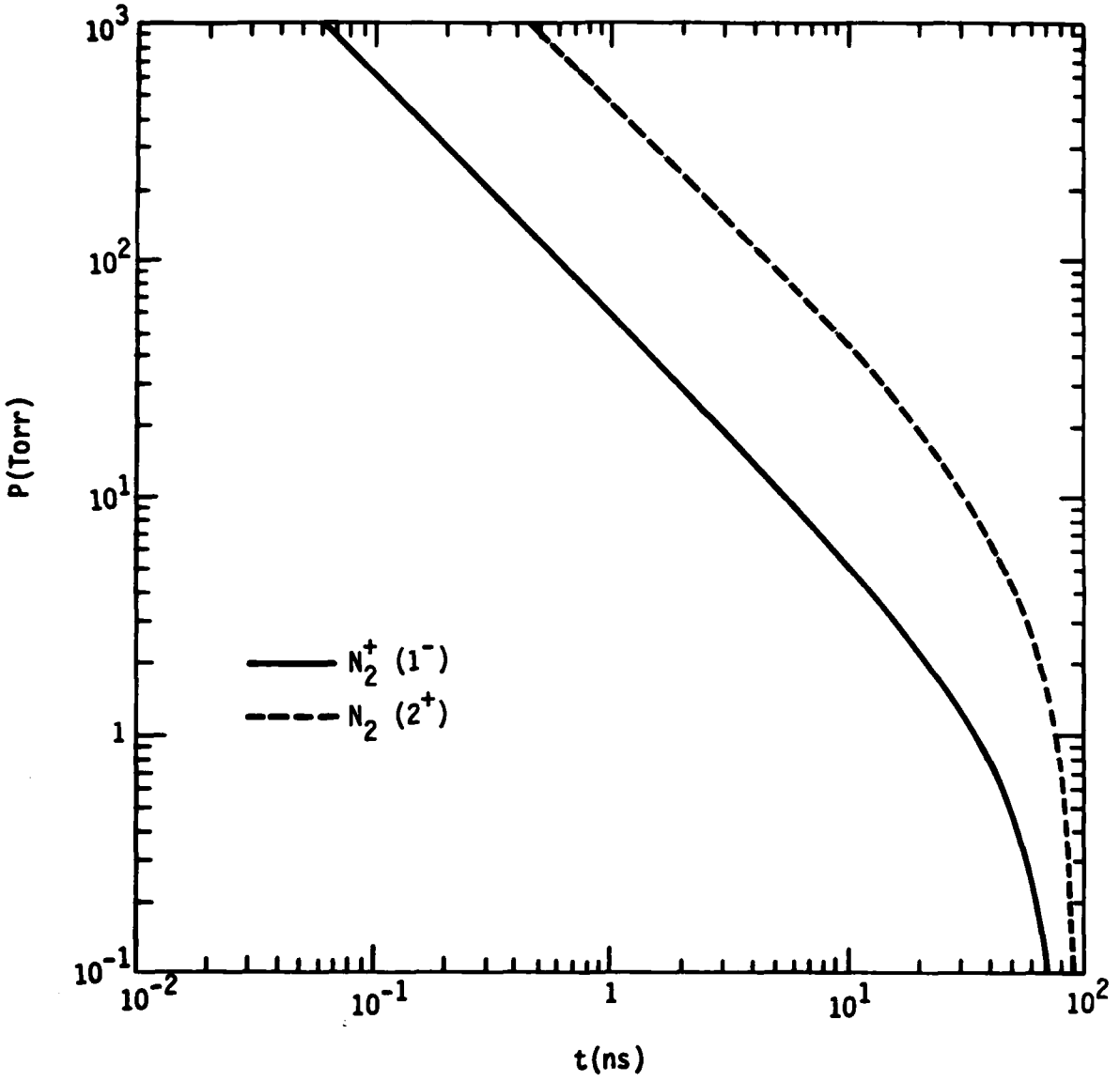

Figure 4. Pressure required for a given response time for two nitrogen bands.

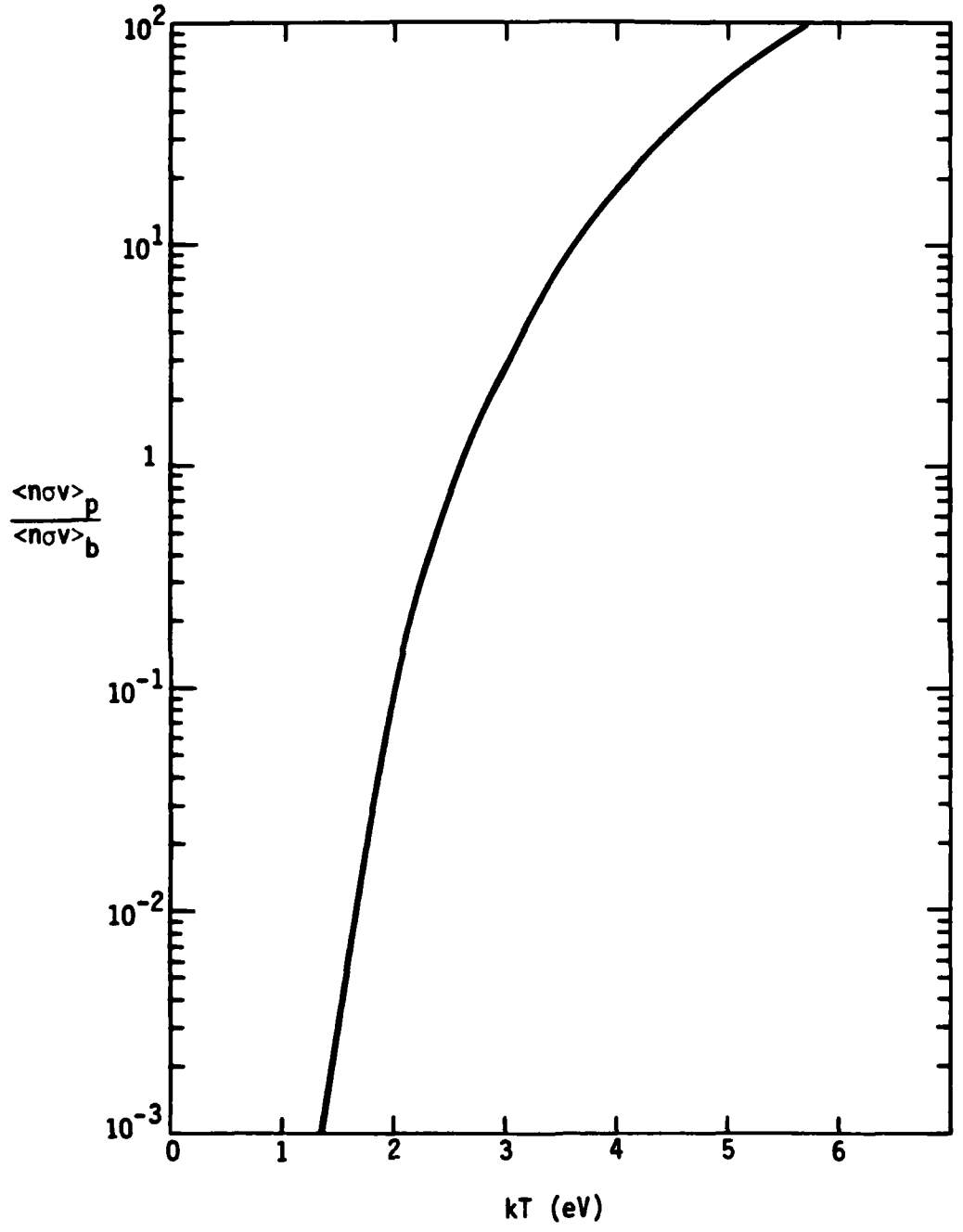

Figure 5. Ratio of $N_2^+(1^-)$ excitation caused by plasma electrons to beam electrons as a function of plasma temperature, assuming $n_p/n_b = 10^3$ and $E_b = 1.5$ MeV.

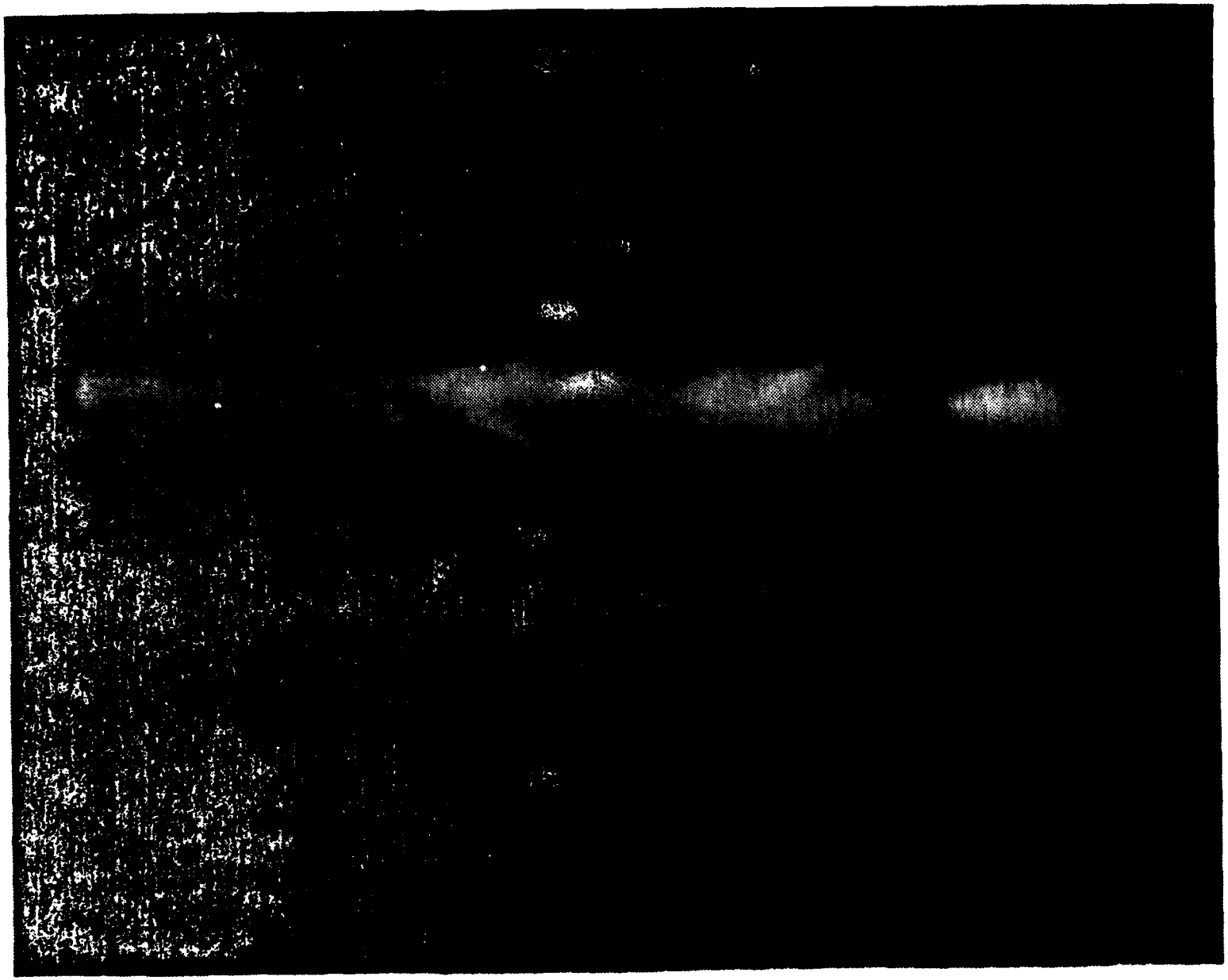

Figure 6. Open shutter photograph of FX-100 beam showing feathering.

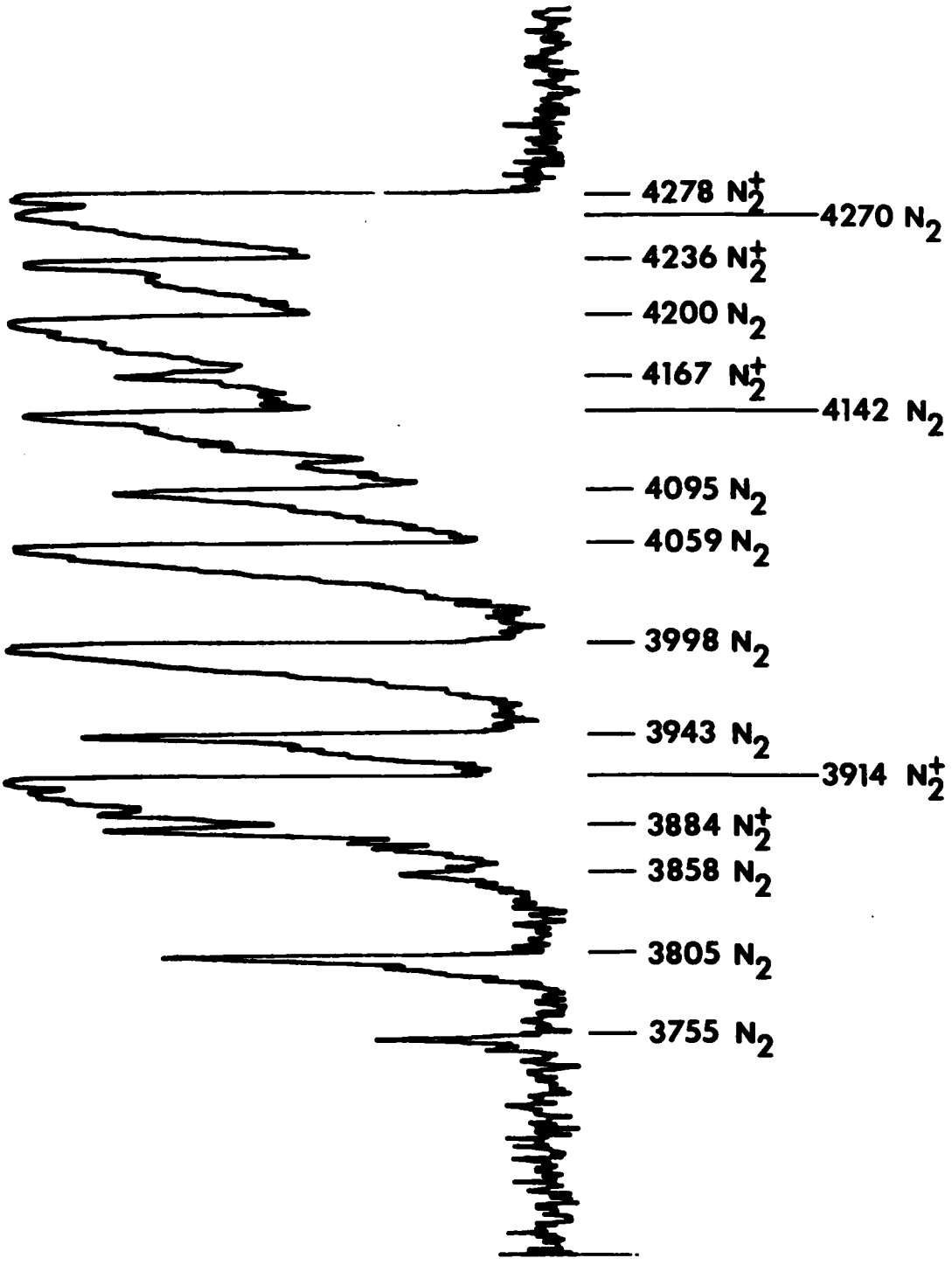

Figure 7. Densitometer scan of FX-100 spectra.

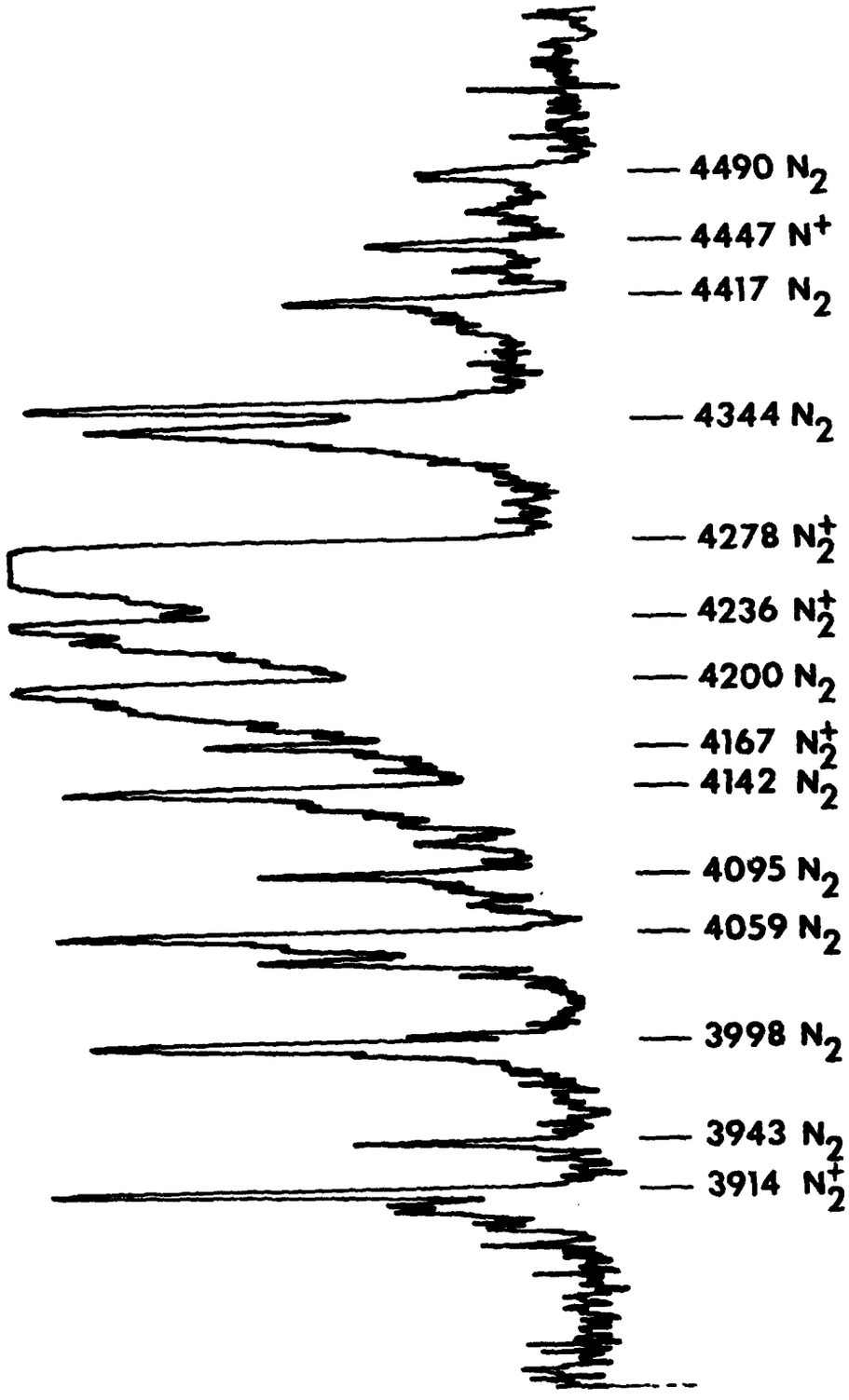

Figure 8. Densitometer scan of FX-100 spectra.

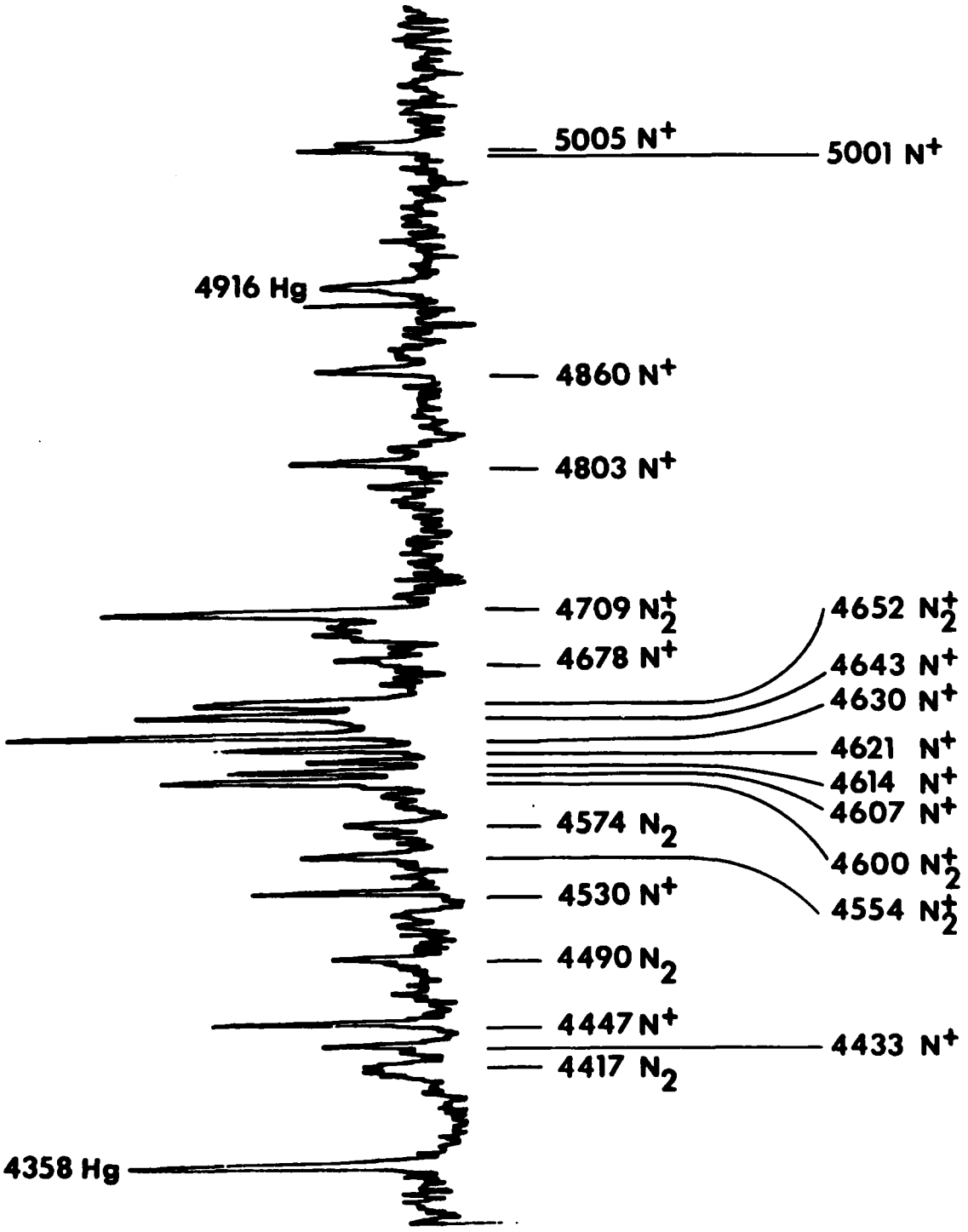

Figure 9. Densitometer scan of FX-100 spectra.

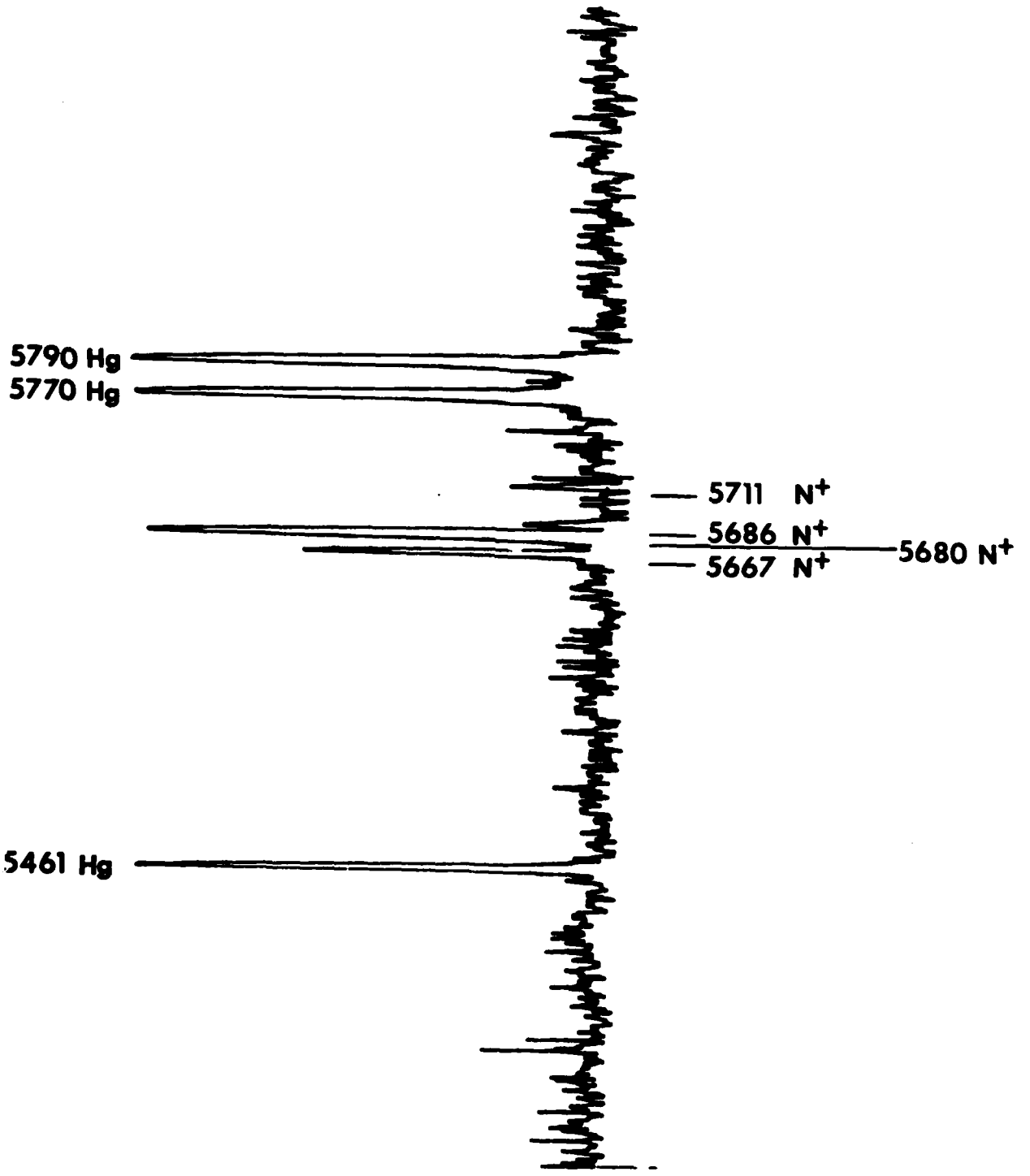

Figure 10. Densitometer scan of FX-100 spectra.

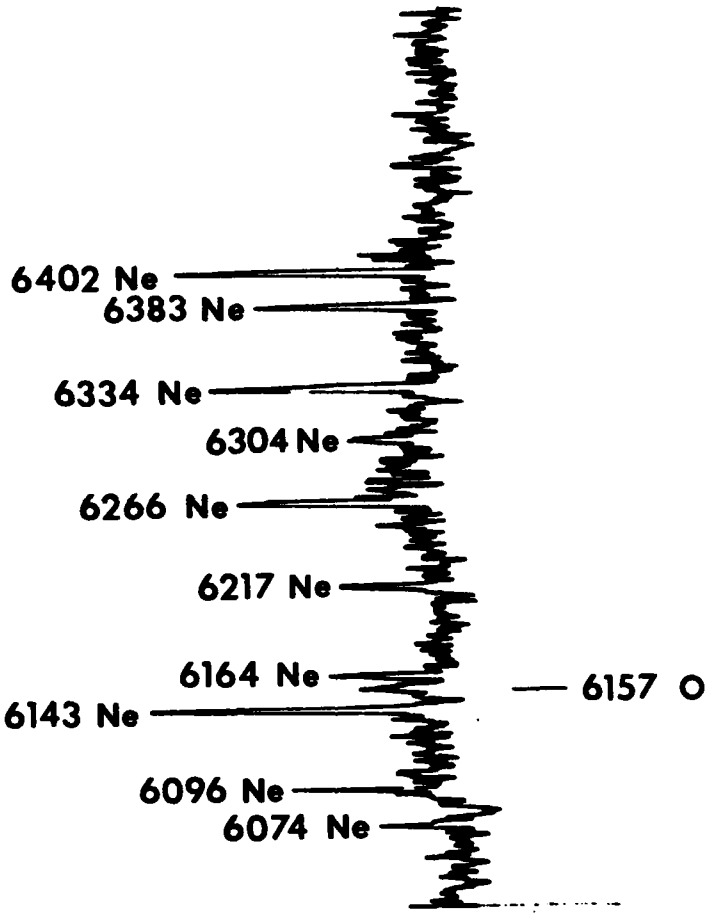

Figure 11. Densitometer scan of FX-100 spectra.

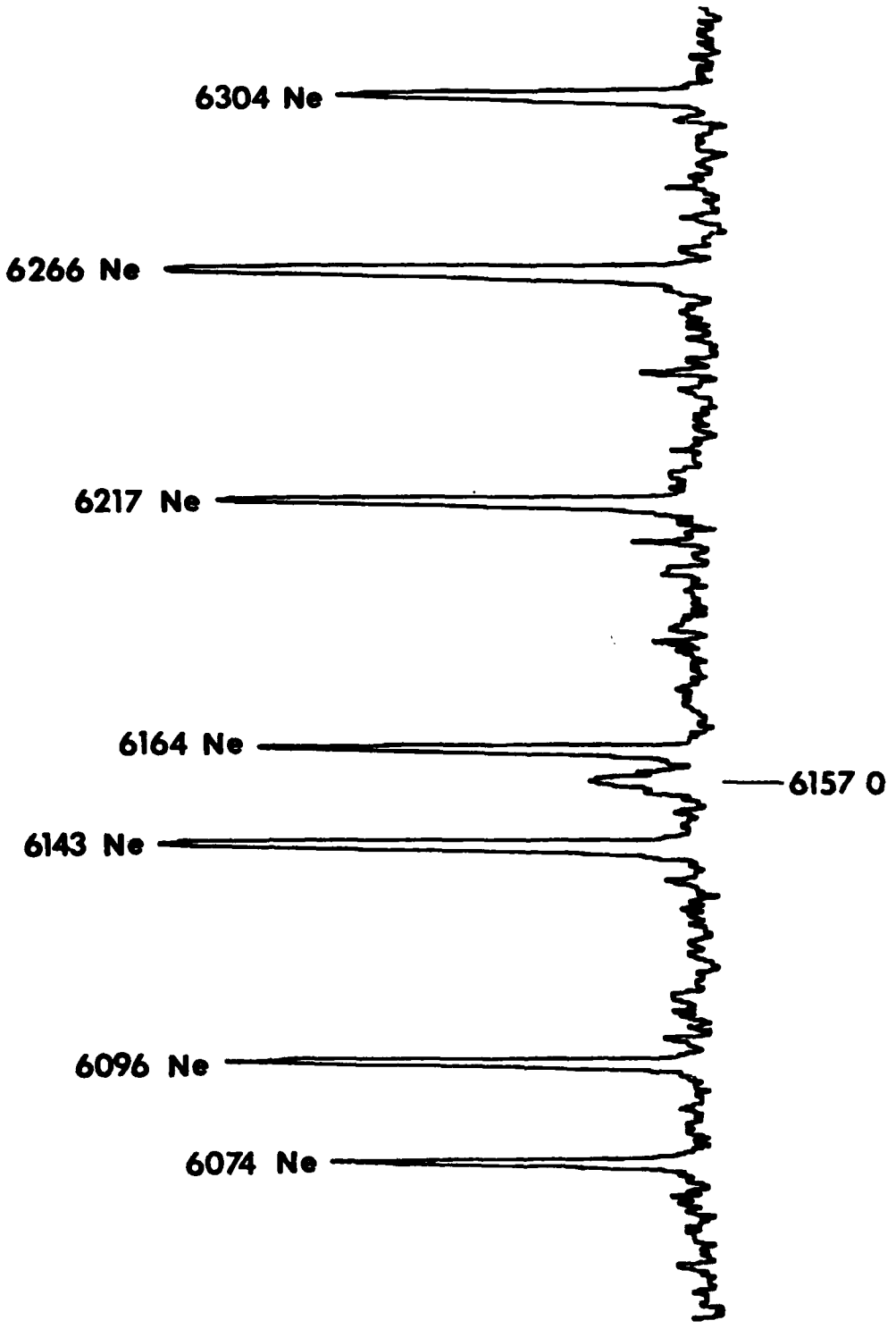

Figure 12. Detailed densitometer scan of oxygen line.

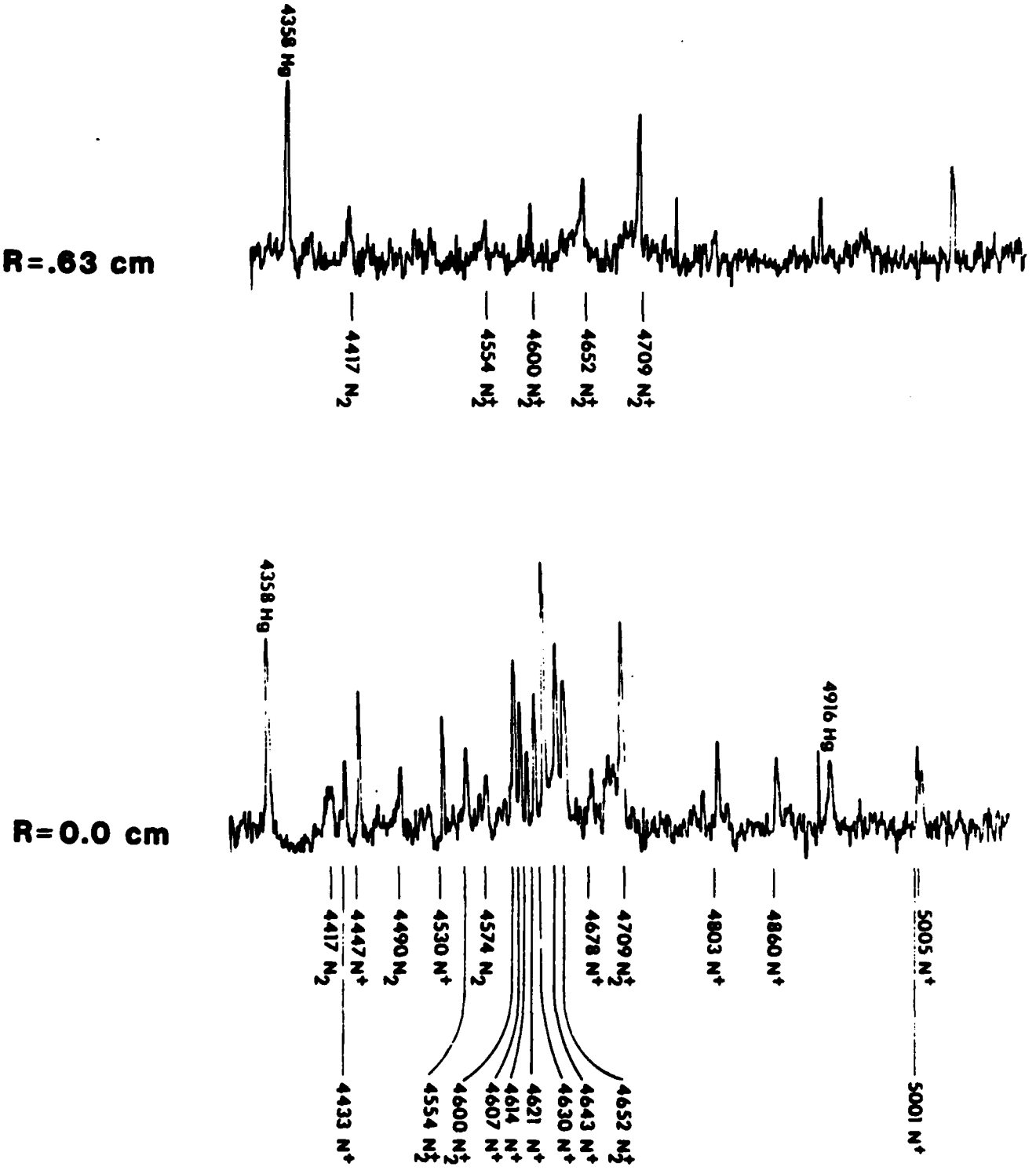

Figure 13. Densitometer scan of FX-100 spectra off axis and on axis.

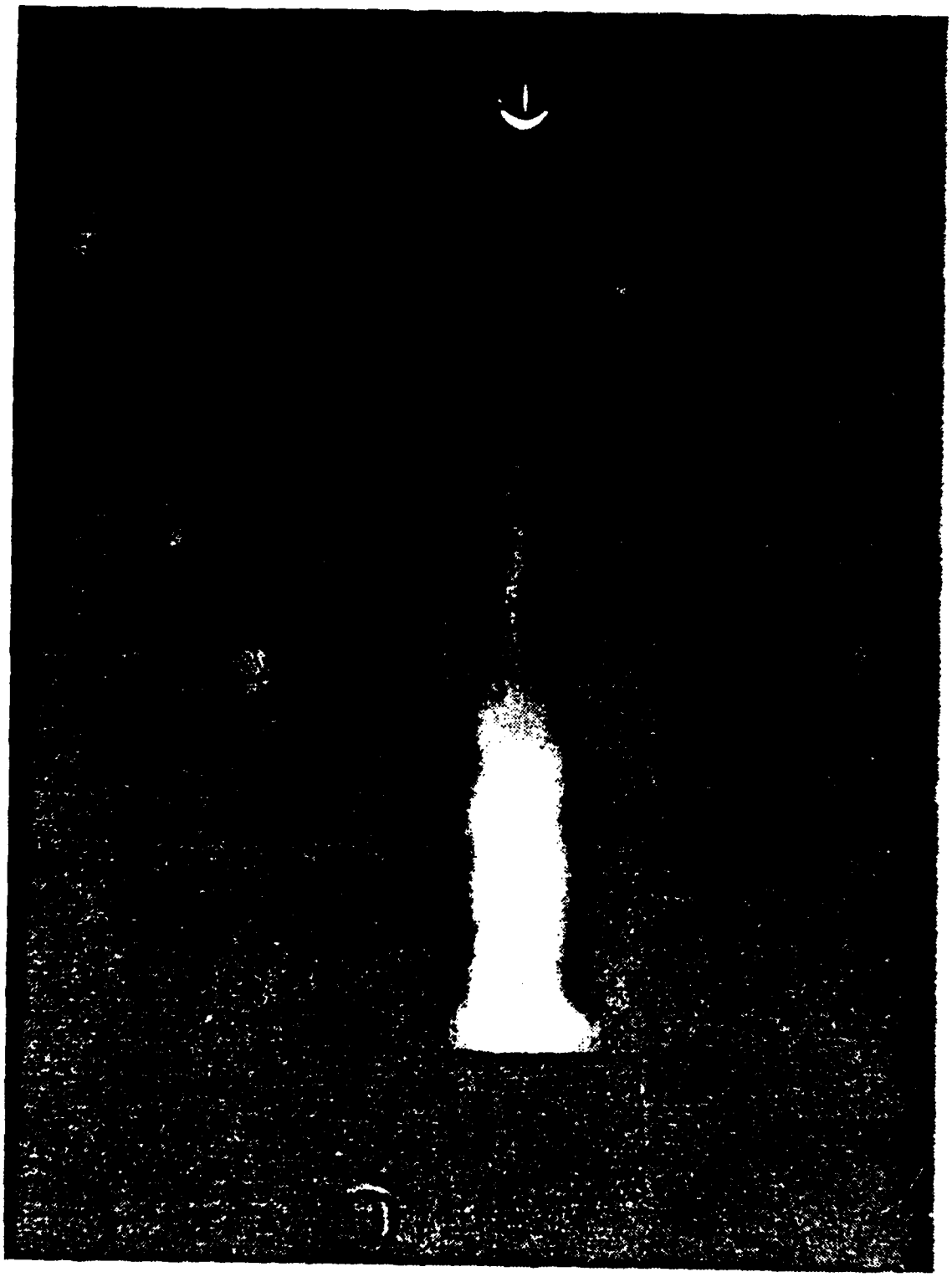

Figure 14. Streak photograph of beam at .35 Torr.

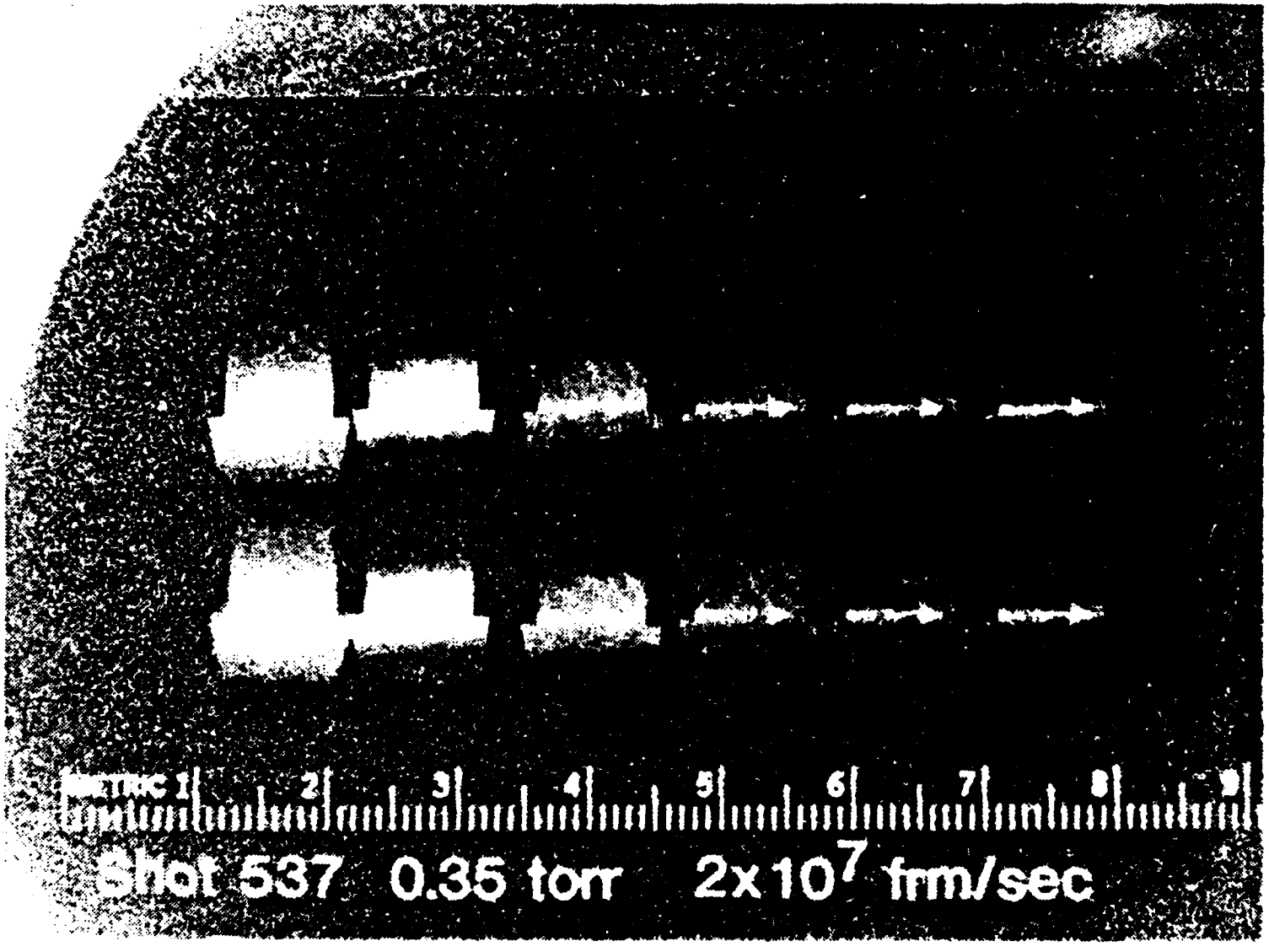

Figure 15. Framing photograph of FX-100 beam at .35 Torr.

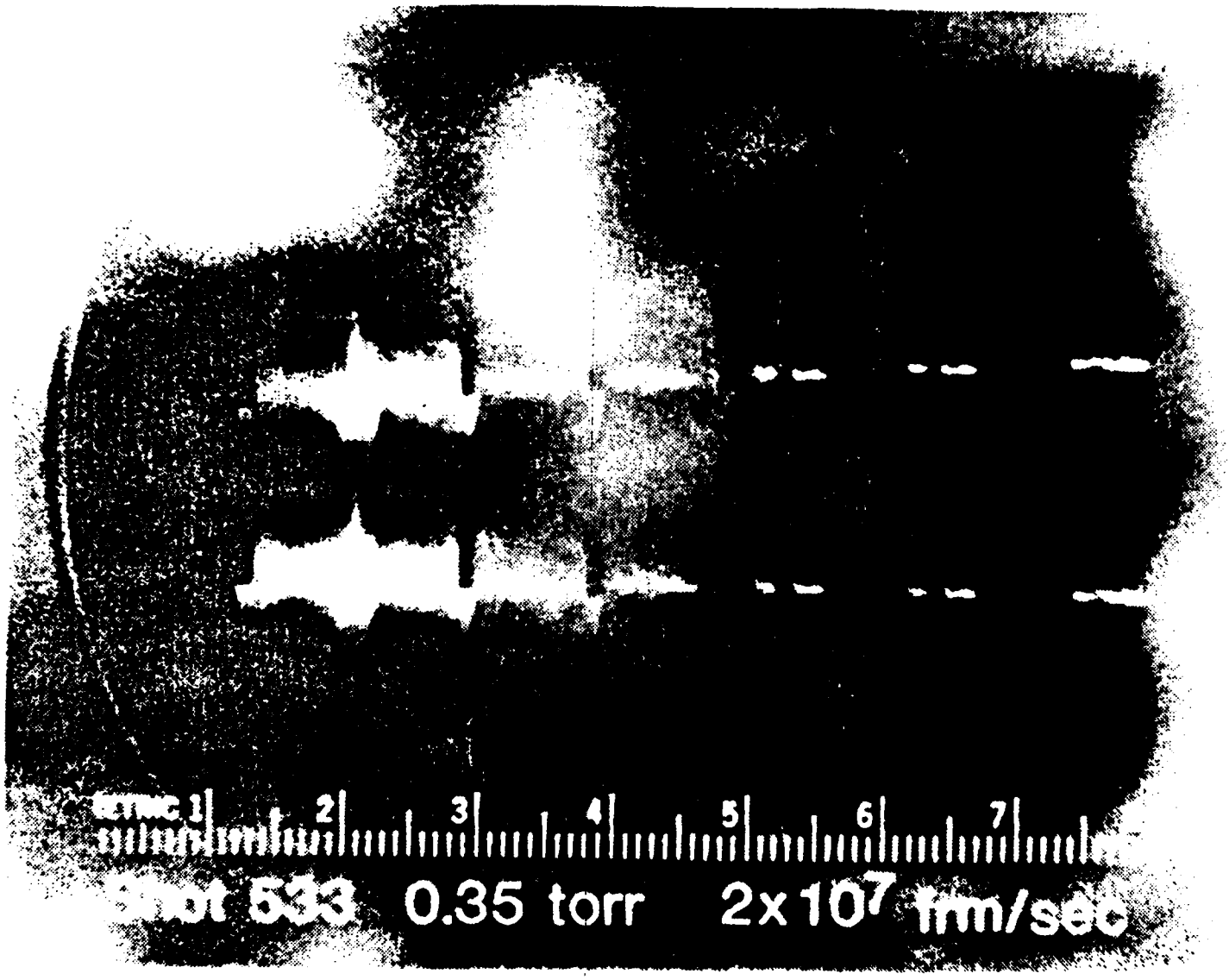

Figure 16. Framing photograph of FX-100 beam at .35 Torr.

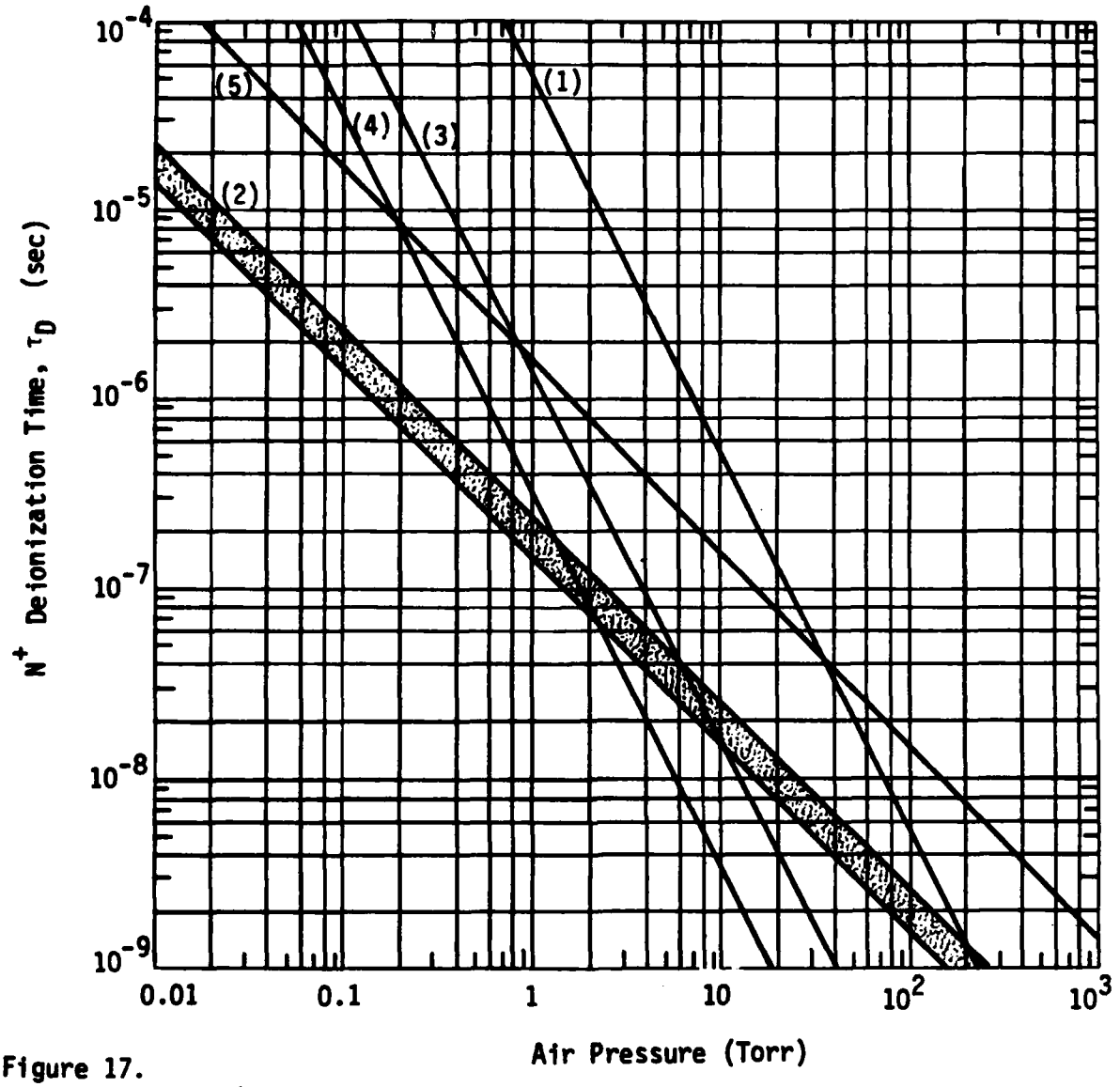

Figure 17.
Persistance of N^+ ions in air resulting from the following deionization reactions:

(1) $N^+ + 2N_2 \rightarrow N_3^+ + N_2$ ($T_g = 0.025$ eV; $\tau_D \propto n_a^{-2} T_g$)

(2) $N^+ + O_2 \rightarrow \begin{cases} O_2^+ + N \\ NO^+ + O \\ NO + O^+ \end{cases}$ (0.025 eV $< T_g < 1.0$ eV; $\tau_D \propto n_a^{-1} T_g^{0.57}$)

(3) $e + M + N^+ \rightarrow M + N$ ($T_e = 0.025$; $n_e = 0.1\, n_a$; $\tau_D \propto n_e^{-1} n_a^{-1} T_e^{2.5}$)

(4) $e + e + N^+ \rightarrow e + N$ ($T_e = 0.025$; $n_e = 0.1\, n_a$; $\tau_D \propto n_e^{-2} T_e^{4.5}$)

(5) $e + N^+ \rightarrow N + h\nu$ ($T_e = 0.025$; $n_e = 0.1\, n_a$; $\tau_D \propto n_e^{-1} T_e^{0.5}$)

REFERENCES

1. T. J. Fessenden, R. J. Briggs, J. C. Clark, E. J. Lauer, and D. O. Trimble, Lawrence Livermore National Laboratory Report UCID-17840 (1978).

2. R. B. Miller, Sandia National Laboratory Report SAND-79-2129 (1979).

3. R. B. Fiorito, E. W. Fordham, J. R. Greig, R. E. Pechacek, J. D. Sethian, R. Fernsler, and J. Halle, Naval Research Laboratory Memorandum Report 4557, (1981).

4. R. M. Hill, K. Y. Tang, B. E. Perry, D. J. Eckstrom, and D. L. Huestis, SRI International Report MP80-41 (1980).

5. A. M. Frank, S. S. Yu, and J. M. Masmitsu, Lawrence Livermore National Laboratory Report (1982).

6. T. J. Fessenden, W. L. Atkinson, W. A. Barletta, J. F. Campbell, J. C. Clark, L. D. Clendenen, R. B. Fiorito, A. M. Frank, F. D. Lee, H. A. Koehler, and K. W. Struve, Lawrence Livermore National Laboratory Report UCID-19245 (1981).

7. G. Davidson and R. O'Niel, J. Chem. Phys. 41, 3946 (1964).

8. M. N. Hirsch, E. Poss, and P. N. Eisner, Phys. Rev. A1, 1615 (1970).

9. H. A. Bethe and J. Ashkin, in Experimental Nuclear Physics, Vol. I, ed. by E. Segre, (1953).

10. P. Millet, Y. Salamero, H. Brunet, J. Galy, D. Blane, and J. L. Teyssier, J. Chem. Phys. 58, 5893 (1973).

11. G. A. Baraff and S. J. Buchsbaum, Phys. Rev. 130, 1007 (1963).

12. G. W. Sutter and A. Sherman, Engineering Magnetohydrodynamics, (McGraw-Hill, N.Y., 1965), pp. 125-210.

13. S. Brown, Basic Data of Plasma Physics, (Wiley, N.Y. 1959).

14. A. W. Ali, Naval Research Laboratory Memorandum Report 4619, (1981) and references therein.

15. R. W. P. McWhirter, in Plasma Diagnostic Techniques, ed. by R. H. Huddlestone and S. L. Leonard, (Academic Press, N.Y., 1965), pp. 208-214 and references therein.

APPENDIX C

APPENDIX C

CHANNEL TEMPERATURE DETERMINATION

The singly ionized atomic nitrogen and neutral atomic oxygen emissions observed in some low pressure electron beam propagation studies (FX-100, VISHNU) are related to the beam channel temperature after the beam has passed. The goal of this study was to gain a better understanding of the neutral oxygen emission at 615.7 nm and the feathered structure associated with it (Fig. 1). Out of this came the identification of reliable nitrogen ionic lines for time resolved channel temperature determination. Because the available spectra were time integrated, an accurate determination of the temperature using line ratios was not possible, although rough (± 15%) averages were made.

To review earlier optical emission work,[1] experimental data from the FX-100 electron beam (1.5 MeV, 40 kA, 120 ns, .35 Torr) show:

1) N^+ and O emissions have a much smaller radius than either the beam or the N_2 and N_2^+ emissions,

2) N_2 and N_2^+ emission are quenched at roughly the end of the beam pulse,

3) N^+ and O emissions start at roughly the end of the beam and are long lived, i.e., longer than the .6 microseconds recorded by the framing camera,

4) O emissions occurred at pressures between .1 and .8 Torr (roughly the propagation window).

The electron beam spectra are very similar to spectra of lightning channels (20,000 - 25,000°K) and of laser produced channels (20,000 - 28,000°K). Table 1 lists the lines spectroscopically observed and used in

N^+ LINES

λ(Å)	EXCITATION ENERGY (cm^{-1})	gf	REMARKS
3995	174213	1.89	Prueitt, obscured
4041	211332	17.43	Prueitt, obscured
4433	211428	8.19	Vignetted
4447	187092	1.93	Vignetted
4530	211403	4.69	
4623.2	170637	3.03	
(4630)	170667	1.34	
4678	211491	2.70	
4803	187493	.76	Low Intensity
4860	—	—	Forbidden Transition
5001	—	—	Mixture of 3 Multiplets
5005	—	—	^3D-^3F, ^5P-^5P, ^3P-^3S
5679.4	166616	4.07	
(5680)	166679	1.90	Prueitt

forming line ratios plus the lines at 399.5 nm and 404.1 nm recommended by Prueitt[2] in lightning studies. These two were obscured by N_2 bands in the time integrated spectra. Some lines were not used for temperature determination because of vignetting, low intensity or overlapping multiplets with different parent states. All the others are good for temperature measurements, having both high intensity and spanning a broad range of excitation energies. Those parenthetical wavelength entries refer to the brightest line from the multiplet average listed just above.

From the available lines and multiplets at 4530, 4632.2 4678 and 5679.4 A four intensity ratios were formed: I(4530)/I(4623.2), I(4530)/I(5679.4), I(4678)/I(4623.2) and I(4678)/I(5679.4). These line ratios take advantage of the large difference in excitation energies of the upper states. Because the spectra are time integrated accurate temperature measurements cannot be made. Even average temperatures can be misleading. As the channel cools, the lines originating from the highest lying states stop radiating, but the lines from the lower lying states continue to radiate. The effect is to integrate the light from lower states longer than the higher states, augmenting the intensity of lower states. Line ratios of these will then give an apparent temperature lower than the average temperature of the channel while the higher state was radiating. Nevertheless, an average temperature from these four line ratios was 22,400°K ± 15%. This agrees well with a temperature estimate of ~2 eV made from ohmic heating of the channel.

At this time two points should be made. First, the time integrated temperature determined above contains only limited information. Time dependent spectra are really needed to determine the channel temperature properly, and in this respect, the time integrated spectra were useful in identifying suitable N^+ lines. Secondly, even though these spectra were time integrated no N lines were detected. As the temperature drops, N^+

lines stop and N lines start radiating. However, their intensity is low and they are undetected relative to the N^+ lines. This is unfortunate since at full atmospheric pressure much lower channel temperatures are expected, temperatures too low to excite the more readily seen N^+ lines.

At roughly T = 2 eV, the state responsible for the neutral oxygen emission is not in equilibrium with the observed N^+ states. This can be seen from the following. O_2 has a lower dissociation energy than N_2 and O a lower ionization energy than N. Hence, if in equilibrium, oxygen should be in a higher, not lower ionization state. Thus, the 615.7 nm radiation probably arises from recombination of $O^+ + e$, with the O^+ in equilibrium, although no O^+ emissions exist to verify this. Alternatively, the O emission could be from later times and lower temperatures than the N^+ emissions.

The interpretation of the physical processes involved is that after the beam passes, the fields collapse and heat the plasma. This turns on the N^+ and O emissions which continue until the temperature is sufficiently low. The energy deposited in the plasma is in part determined by the gas pressure. At pressures above the propagation window, the density is up so the energy per particle is down. At pressures below the propagation window, poor propagation (smaller fields and larger channels) also makes the energy per particle low. This interpretation explains the observations made earlier, and why the FX-100 experiments, which have a propagation window at a comparatively low pressure, consistently observed the oxygen emission (red, 615.7 nm).

In summary, the N^+ and O emissions are related to the channel temperature. The O (615.7 nm) emission is a qualitative indicator of ~ 2 eV temperatures. The N^+ is a quantitative indicator with many lines (λ = 399.5, 404.1, 453.0, 463.0, 467.8 and 568.0 nm) suitable for time resolved temperature measurements.

REFERENCES

1. L. A. Wright, C. A. Ekdahl, R. F. Benjamin, and T. P. Starke, "Optical Emission from Intense Relativistic Electron Beam Excited Air," AMRC-R-326 (Mission Research Corporation, Albuquerque, 1981); C. A. Ekdahl, "Beam Propagation Experimental Study," AMRC-R-352 (Mission Research Corporation, Albuquerque, 1982).

2. Prueitt, M. L., "The Excitation Temperature of Lightning," J. Geophys. Res. 68, 803 (1963).

AD-A133 310 BEAM PROPAGATION EXPERIMENTAL STUDY(U) MISSION RESEARCH 3/4
CORP ALBUQUERQUE NM R J ADLER ET AL. APR 83 AMRC-R-466
AFOSR-TR-83-0743 F49620-81-C-0016

UNCLASSIFIED F/G 20/7 NL

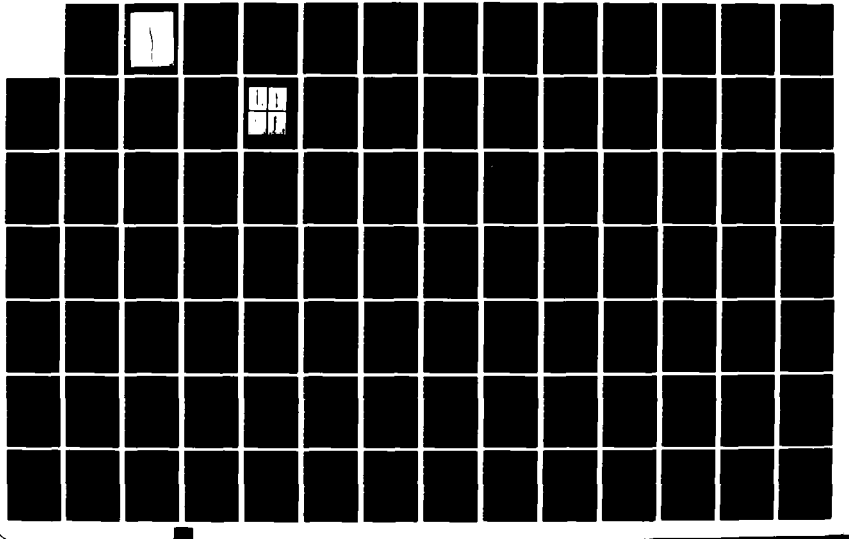

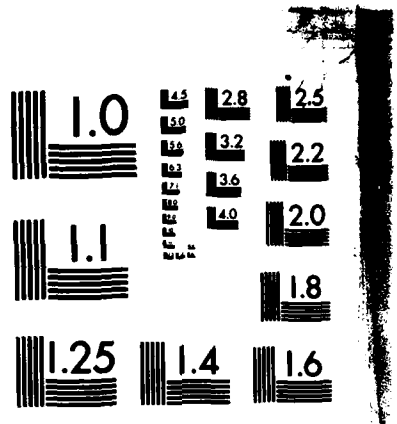

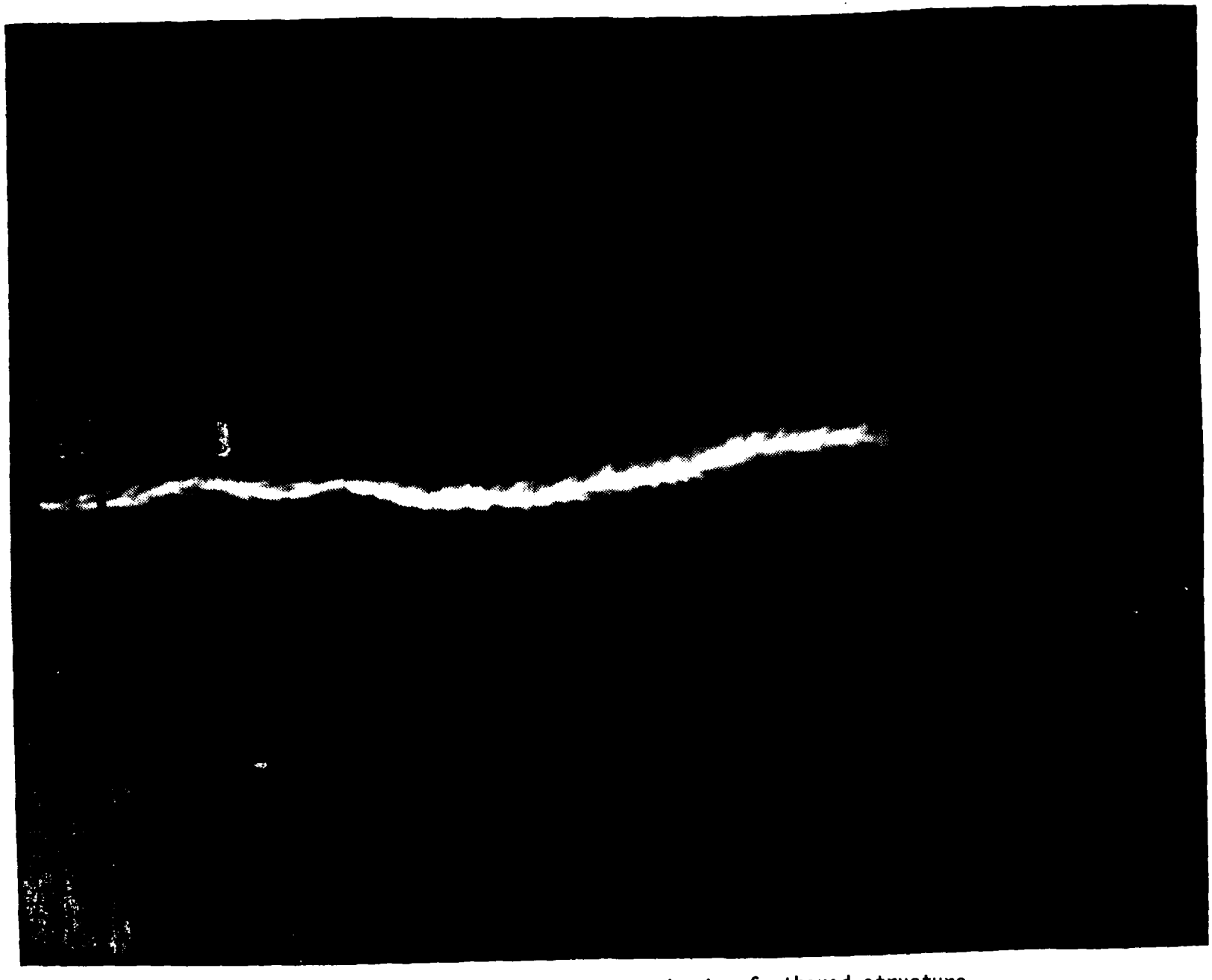

Figure 1. VISHNU beam propagation at low pressure showing feathered structure.

APPENDIX D

APPENDIX D
TICKLER ANALYSIS

An important problem in any study of beam instabilities is the initial perturbation. In this note we discuss the self-excited magnetic tickler option as a candidate for perturbing the beam for hose instability studies. The geometry is shown in Fig. 1, where a pickup loop (inductance L) is coupled to a capacitor of capactiance C. We first consider a beam current of the form $I = I_0(1 - e^{-\alpha t})$. The voltage induced will be distributed between L and C, and is given by $(d/dt) \int B_\theta \, dr dz \sim V$ or

$$V \sim \frac{\mu_0 I_0 \alpha \ell}{2\pi} \ell n \, b/a \, e^{-\alpha t} \tag{1}$$

The equivalent circuit is an L-C resonator (we ignore damping for the moment)

$$V = L\ddot{Q} + Q/C \tag{2}$$

where Q is the capacitor charge. Let $q = \mathscr{L}[Q]$, the Laplace transform of the charge with initial conditions $Q(0) = \dot{Q}(0) = 0$.

The Laplace transform of (2) is

$$\left[\frac{\mu_0 I_0 \alpha \ell \ell n \, b/a}{2\pi}\right] \left(\frac{1}{s + \alpha}\right) = L s^2 q + \frac{1}{C} q \tag{3}$$

resulting in

$$q = \frac{A}{(s + \alpha)(s^2 + \omega^2)}$$

$$= \frac{A(s - \alpha)}{\omega^2 + \alpha^2} \left[\frac{1}{s^2 - \alpha^2} - \frac{1}{s^2 + \omega^2}\right] \tag{4}$$

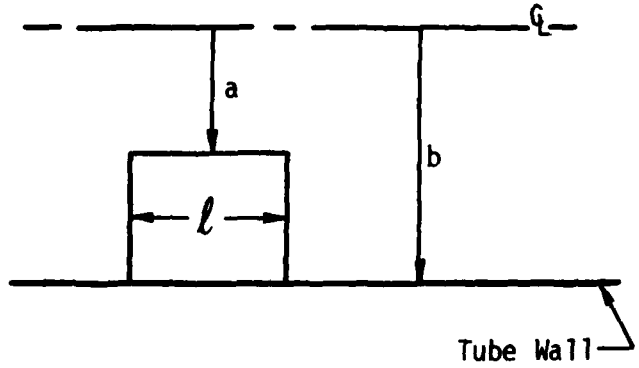

Figure 1.

where $A = \mu_0 I\ \alpha\ \ell\ \ell n\ (b/a)/2\pi L$.

We invert the above expression for q as

$$Q = \frac{A}{\omega^2 + \alpha^2} \left[e^{-\alpha t} + \frac{\alpha}{\omega} \sin\omega t - \cos\omega t \right] \tag{5}$$

The current of the tickler I_t is given by

$$I_t = \frac{A}{\omega^2 + \alpha^2} \left[\alpha(\cos\omega t - e^{-\alpha t}) - \omega \sin\omega t \right] \tag{6}$$

Using the vector potential of a square current loop[1] in free space, we can calculate the total impulse applied to the beam.

If y is the distance of a particle from the system centroid, the impulse is found to be

$$\delta p_y = \frac{e\ \ell\ (b - a)}{(a - x)\ (b - x)} \quad \frac{\mu_0\ I_t}{4\pi} \tag{7}$$

Similarly, the pitch angle is

$$\phi = \delta p_y / p_z \sim \frac{\ell\ (b - a)}{(a - x)\ (b - x)} \quad \frac{\mu_0\ I_t}{4\pi\ \gamma mc} \tag{8}$$

Substituting the expression for I_t into (8) we find

$$\phi = \frac{\ell\,(b-a)}{(a-x)\,(b-x)} \left[\frac{\mu_0\, I\, \alpha\, \ell\, \ell n\, b/a}{2\pi L}\right] \left[\frac{\mu_0}{4\pi\, \gamma mc}\right]$$

$$\times \left[\alpha\,(\cos\omega t - e^{-\alpha t}) - \omega \sin\omega t\right] \frac{1}{(\omega^2 + \alpha^2)}$$

$$= \frac{\ell\,(b-a)}{(a-x)\,(b-x)} \left[\frac{\mu_0\, \alpha\, \ell\, \ell n\, b/a}{2\pi\, L\, (\omega^2 + \alpha^2)}\right] \frac{I}{I_A}$$

$$\times \left[\alpha\,(\cos\omega t - e^{-\alpha t}) - \omega \sin\omega t\right]$$

$$\approx \frac{\ell\,(b-a)}{(a-x)\,(b-x)} \left(\frac{\alpha}{\omega}\right)\left(\frac{\mu_0\, \ell\, \ell n\, b/a}{2\pi\, L}\right) \frac{I}{I_A} \sin\omega t \qquad (9)$$

Thus, we have made an analytic estimate of perturbations due to at least one tickler geometry. The perturbation amplitudes for typical parameters vary from .2 - 5 mm.

REFERENCES

1. R. J. Adler, "Beam Transverse Motion Due to Asymmetric Accelerating Modules," AMRC-N-158, February 1981.

APPENDIX E

APPENDIX E

SECURITY CLASSIFICATION OF THIS PAGE (When Data Entered)

REPORT DOCUMENTATION PAGE		READ INSTRUCTIONS BEFORE COMPLETING FORM
1. REPORT NUMBER	2. GOVT ACCESSION NO.	3. RECIPIENT'S CATALOG NUMBER
4. TITLE (and Subtitle) Particle Simulations of FX-100 Beam Propagation and Comparison with Experiment		5. TYPE OF REPORT & PERIOD COVERED Interim Report 6. PERFORMING ORG. REPORT NUMBER AMRC-R-187
7. AUTHOR(s) Thomas Hughes Carl Ekdahl Brendan Godfrey		8. CONTRACT OR GRANT NUMBER(s) F49620-81-C-0016
9. PERFORMING ORGANIZATION NAME AND ADDRESS Mission Research Corporation 1400 San Mateo Boulevard, S.E., Suite A Albuquerque, New Mexico 87108		10. PROGRAM ELEMENT, PROJECT, TASK AREA & WORK UNIT NUMBERS
11. CONTROLLING OFFICE NAME AND ADDRESS Air Force Office of Scientific Research Bolling Air Force Base Washington, D.C. 20332		12. REPORT DATE January 1982 13. NUMBER OF PAGES 14
14. MONITORING AGENCY NAME & ADDRESS(if different from Controlling Office)		15. SECURITY CLASS (of this report) Unclassified 15a. DECLASSIFICATION/DOWNGRADING SCHEDULE
16. DISTRIBUTION STATEMENT (of this Report)		
17. DISTRIBUTION STATEMENT (of the abstract entered in Block 20, if different from Report)		
18. SUPPLEMENTARY NOTES		
19. KEY WORDS (Continue on reverse side if necessary and identify by block number) Electron beam propagation Particle simulations		
20. ABSTRACT (Continue on reverse side if necessary and identify by block number) The propagation code CPROP and the linear theory code KMRAD are used to simulate the FX-100 beam propagating in air. When avalanching is significant, return current tends to concentrate on axis and defocuses the beam head. A strong filamentation instability accompanies large return current fractions. We attempt to correlate these results with the experimental data.		

DD FORM 1 JAN 73 1473 EDITION OF 1 NOV 65 IS OBSOLETE

SECURITY CLASSIFICATION OF THIS PAGE (When Data Entered)

CONTENTS

SECTION		PAGE
I	INTRODUCTION	3
II	NUMERICAL RESULTS	5
III	SUMMARY	13
	REFERENCES	14

LIST OF ILLUSTRATIONS

FIGURE		PAGE
1	Initialization of CPROP at 0.4 Torr. Part (a) shows contours of the beam current density $J_b(\rho,z)$ in units of 17 kA/cm^2. The values of the contours, labeled by A, B, C, D, E, F, G, are linearly spaced. The z coordinate is in cm. The radial coordinate ρ is related to the physical coordinate r by $\rho = a\ln(1 + r/a)$ where a is the Bennett radius in cm. The Bennett radius is at $\rho = 2.2$. In (b), (c), (d), (e) phase plots of the beam are depicted. The current and voltage ramps in (a) and (e), respectively, are approximately those of the experiment.	4
2	Contour plots of the fields E_z, E_r, in units of 0.51 MV/cm, the B_θ field in units of $0.51 \times 10^4/3$ gauss, the z component of the net current density J_{net}, and the conductivity σ in units of $3 \times 10^{10}/4\pi$ sec^{-1}, at an air pressure of 0.4 Torr. Avalanching is included in the conductivity model.	6
3	Contour plots of J_{net}, B_θ, and σ with the same normalization as in Fig. 2, also at 0.4 Torr. The avalanching term in the conductivity model has been removed.	8
4	Open shutter photographs of the FX-100 beam at various air pressures (p). The beam is propagating from left to right. In (a), (c) and (d), the camera is positioned 13 cm downstream from the diode. In (b), it is 4.4 m downstream.	9
5	Contour plots of J_{net}, B_θ and σ at 0.125 Torr. Avalanching is included.	11
6	Phase plots of beam after traveling two meters through air at 0.4 Torr, showing nose erosion. Cf. Fig. 1.	12

I. INTRODUCTION

Theoretical investigations in support of the FX-100 experiments have relied on two existing MRC computer codes: CPROP, which is a propagation code, and KMRAD, a linear theory code. The usefulness of these codes is hampered by lack of an air conductivity model whose known range of validity encompasses the 0.1 - 2.0 Torr regime. At present, CPROP uses a conductivity model developed for use at pressures in the range 10^2 - 10^3 Torr.[1] The validity of this model at pressures in the neighborhood of 1 Torr is certainly questionable, but its degree of inaccuracy is unknown. We shall interpret our numerical results in this light and seek to extract information which will guide future efforts.

The CPROP model for the beam is straightforward. The beam is initialized with current and voltage ramps close to those measured experimentally, and is given a Bennett profile in radius (Fig. 1). Due to computing expense and computer core limitations only the first 15 ns of the pulse were simulated. At each location in z (direction of propagation) the beam particles were assigned an emittance based on an approximate formula for the scattering produced by the titanium anode foil.[2] The initialization of the code is completed by computing the self-consistent fields, conductivity, and return current in the frozen field approximation[3] (the initialization is the only stage at which this approximation is used by CPROP).

The code KMRAD requires the input of a beam equilibrium and conductivity profile. It provides linear growth rates and is much cheaper to run than CPROP. It simulates only the body of the pulse and cannot deal with the head of the beam.

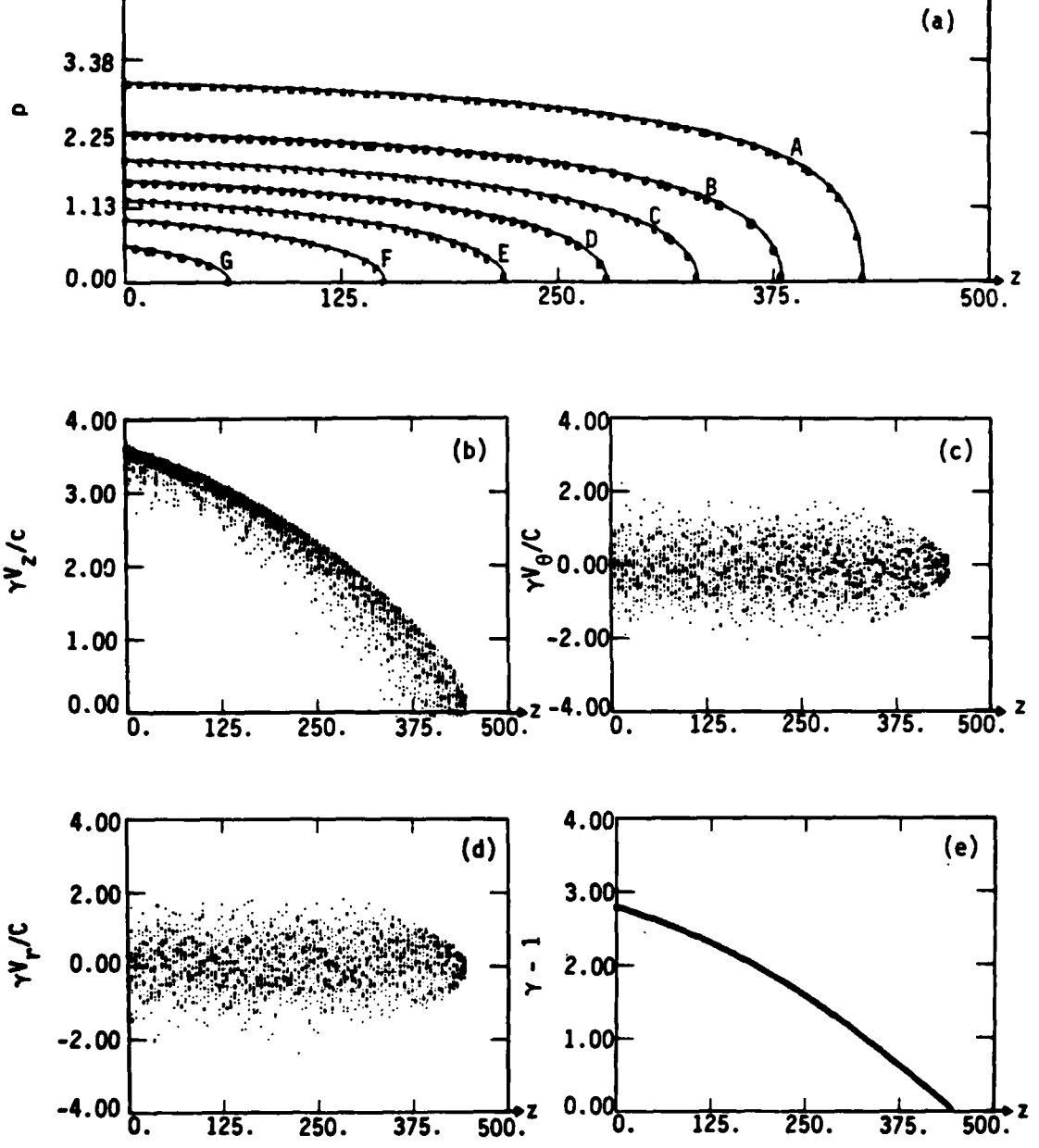

Figure 1. Initialization of CPROP at 0.4 Torr. Part (a) shows contours of the beam current density $J_b(\rho,z)$ in units of 17 kA/cm^2. The values of the contours, labeled by A, B, C, D, E, F, G, are linearly spaced. The z coordinate is in cm. The radial coordinate ρ is related to the physical coordinate r by $\rho = a\ln(1 + r/a)$ where a is the Bennett radius in cm. The Bennett radius is at $\rho = 2.2$. In (b), (c), (d), (e) phase plots of the beam are depicted. The current and voltage ramps in (a) and (e), respectively, are approximately those of the experiment.

II. NUMERICAL RESULTS

The result of initializing CPROP at a pressure of 0.4 Torr, which is in the experimental propagation window, is shown in Fig. 2. This figure shows the presence of both an electrostatic radial and an inductive longitudinal electric field at the head of the beam where the conductivity is lowest. Comparing Fig. 2 with Fig. 3, we see that the avalanching these fields produce have a large effect on the magnitude and profile of the return current. In Fig. 2, the return current fraction obtained is f ≈ 80% and the return current is more peaked on axis than the beam current so that the B_θ field peaks near the wall instead of at the Bennett radius. When the particles are "let go," the beam expands out radially and loses almost one third of the particles to the wall before contracting. Most of these lost particles come from the nose of the beam. The beam continues to bounce but few particles are subsequently lost. It has been suggested[4] that at low pressures, avalanching will not occur on a significant scale because of the long mean free path of secondary electrons. With avalanching turned off in CPROP, we obtain f ≈ 35% and the return current has approximately the same radial profile as the beam. If propagated, this beam will start to pinch inward. The experimental evidence tends to favor the inclusion of avalanching in the conductivity model. At pressures near 0.35 Torr, return current fractions of 80 - 95% are observed near the diode. Furthermore, several open shutter photographs taken near the diode (Fig. 4a) show some of the beam blowing off radially.

The large conductivity produced by avalanching leads to a long magnetic decay time for the monopole return current, $\tau \sim 900$ ns (the pulse length is about 120 ns). This means that the resistive instabilities most likely to develop are those with short transverse wavelength $\lambda_\perp$, i.e. filamentary instabilities, since the magnetic decay time is proportional to $\lambda_\perp^2$. The linearized simulation code KMRAD was used to look for such instabilities. The open shutter photographs seem to indicate that the fine structure in the beam is azimuthally symmetric so we set m=0

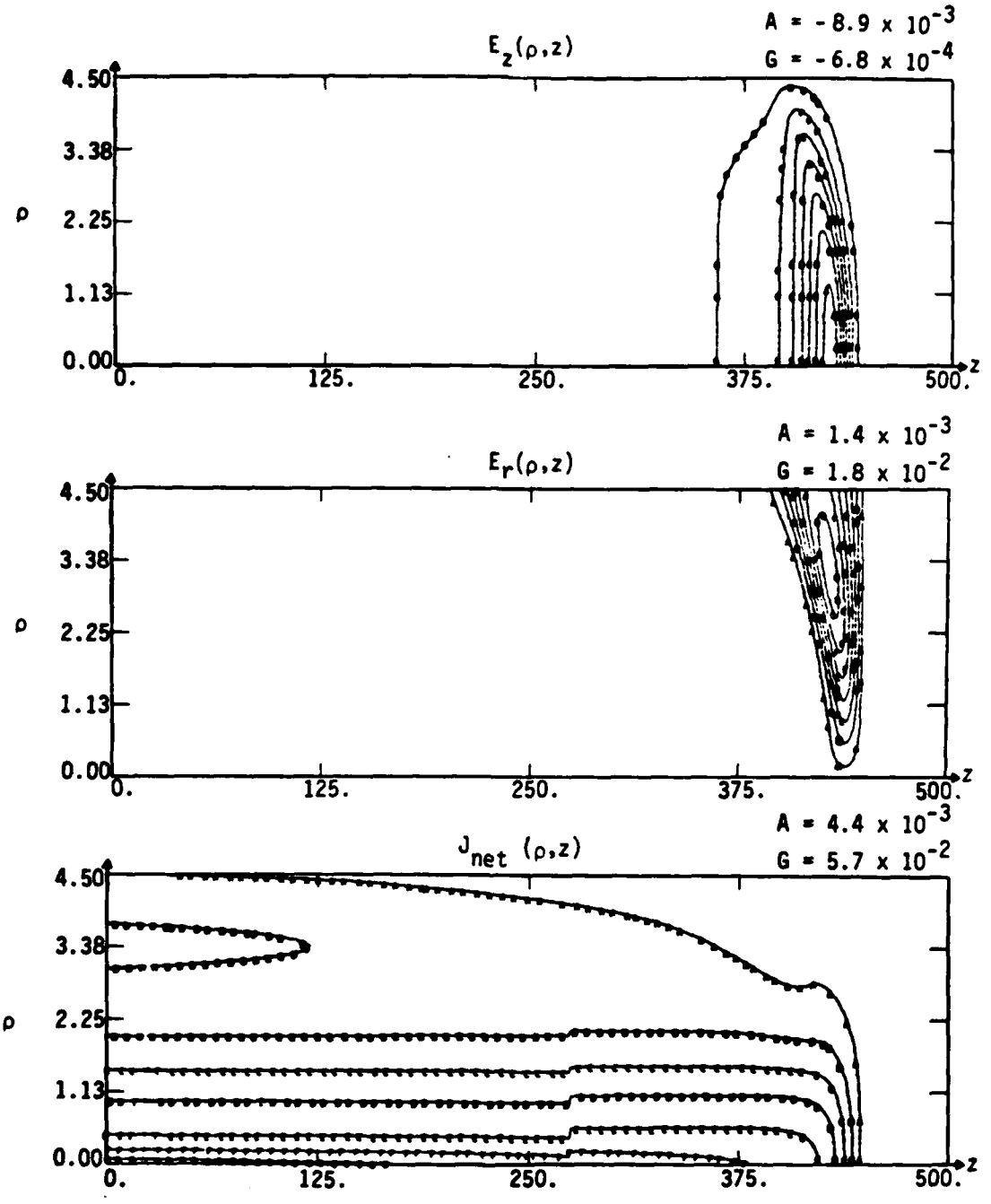

Figure 2. Contour plots of the fields E_z, E_r, in units of 0.51 MV/cm, the B_θ field in units of 0.51 x $10^4/3$ gauss, the z component of the net current density J_{net}, and the conductivity σ in units of 3 x $10^{10}/4\pi$ sec^{-1}, at an air pressure of 0.4 Torr. Avalanching is included in the conductivity model.

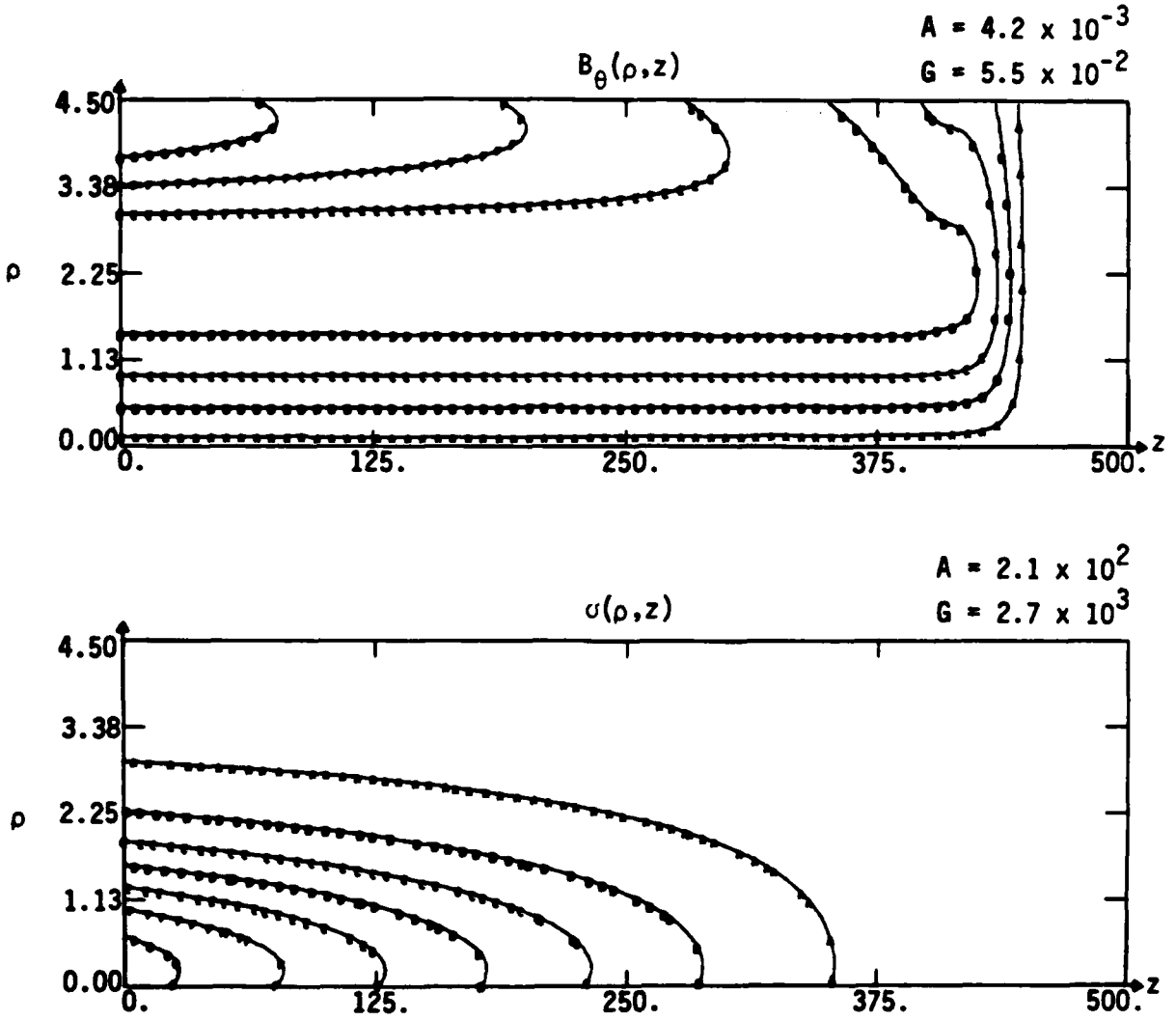

Figure 2 (continued).

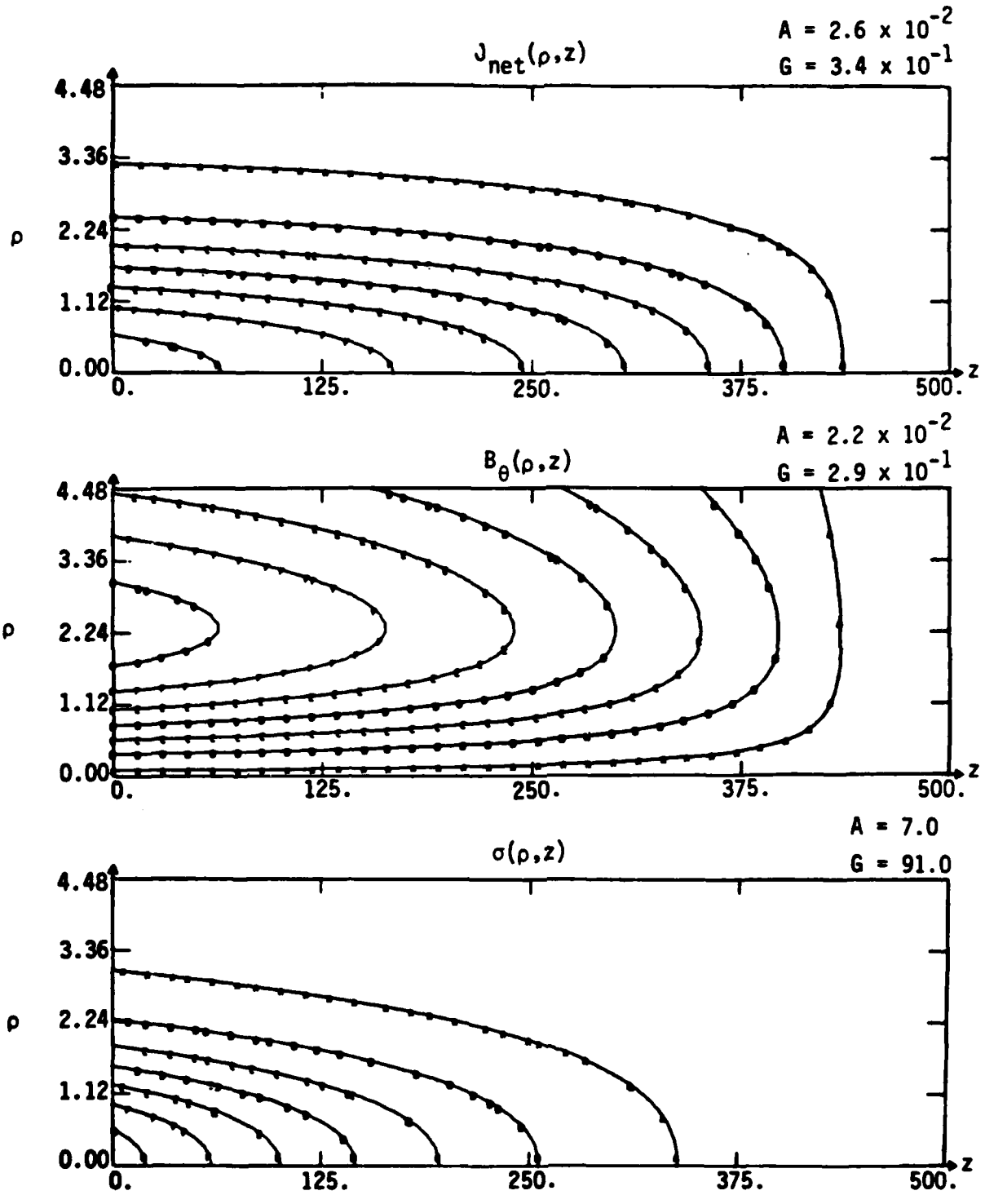

Figure 3. Contour plots of J_{net}, B_θ, and σ with the same normalization as in Fig. 2, also at 0.4 Torr. The avalanching term in the conductivity model has been removed.

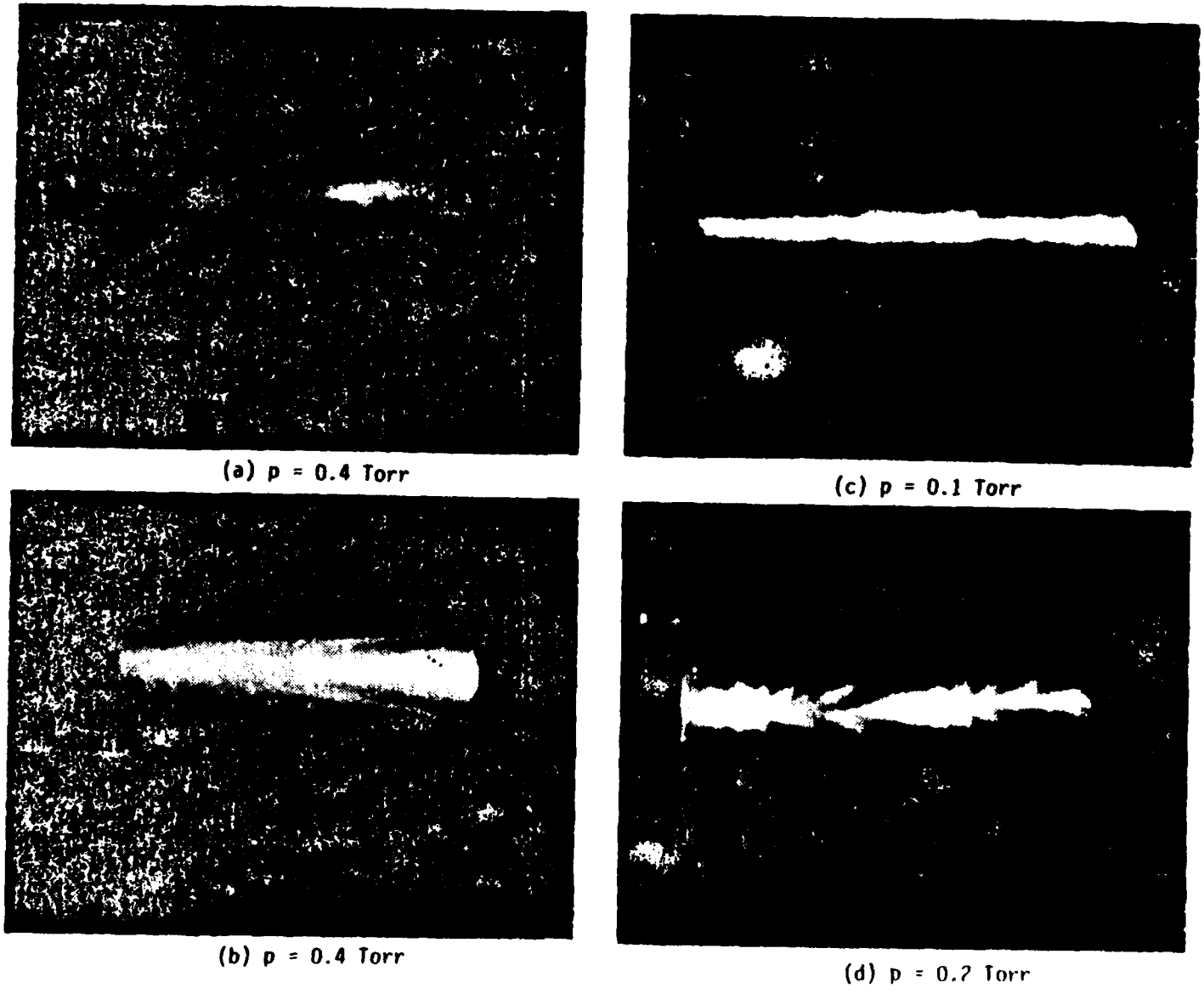

(a) p = 0.4 Torr

(c) p = 0.1 Torr

(b) p = 0.4 Torr

(d) p = 0.2 Torr

Figure 4. Open shutter photographs of the FX-100 beam at various air pressures (p). The beam is propagating from left to right. In (a), (c) and (d), the camera is positioned 13 cm downstream from the diode. In (b), it is 4.4 m downstream.

in the simulations. We chose a return current fraction of 95% and the return current and conductivity profiles were assumed to follow the beam profile. The magnitude of the conductivity was taken from CPROP. We found growth rates on the order of 2×10^8 sec^{-1}, with a transverse wavelength of 0.8 - 1 cm (The beam Bennett radius is 3 cm). The growth rates are largest for $k_z << k_\perp$ which corresponds to low real frequencies, and low group velocities. The latter implies that the number of e-foldings which the instability can undergo is roughly $N_\gamma \approx \gamma\tau_p$, where γ is the growth-rate and τ_p is the pulse length. Assuming that our estimate of the growth rate is reasonable, then $N_\gamma \approx 20$ can be attained, which would allow the instability to develop strongly. However, while these calculations are suggestive, the experimental data is not detailed enough to allow us to rule out other explanations for the fine structure seen both in the open shutter (Figs. 4b, 4d) and streak photographs.

At lower pressures, in the neighborhood of 0.1 Torr, CPROP predicts return current fractions of about 70%, and a return current profile close to that of the beam current (Fig. 5). When propagated, the beam collapses to a smaller radius than its initial one of 3 cm. This behavior is qualitatively similar to that observed experimentally. The measured return current fraction is about 45% and the open shutter photographs (Fig. 4c) show a pinched beam with a radius of about 2 cm.

No significant nose erosion is seen experimentally. CPROP predicts that at $p = 0.4$ Torr, the beam loses about 1 meter in propagating the first 2 meters, as we see by comparing Figs. 1 and 6. This erosion is at the limit of the experimental precision. The steepening of the longitudinal beam current profile in Fig. 6 gives rise to an increase in the amplitude of E_z at the beam head by a factor of six over its value at $t = 0$ (Fig. 2). This does not lead to a dramatic increase in the erosion rate however since the beam energy γ also increases as one moves back from the head.

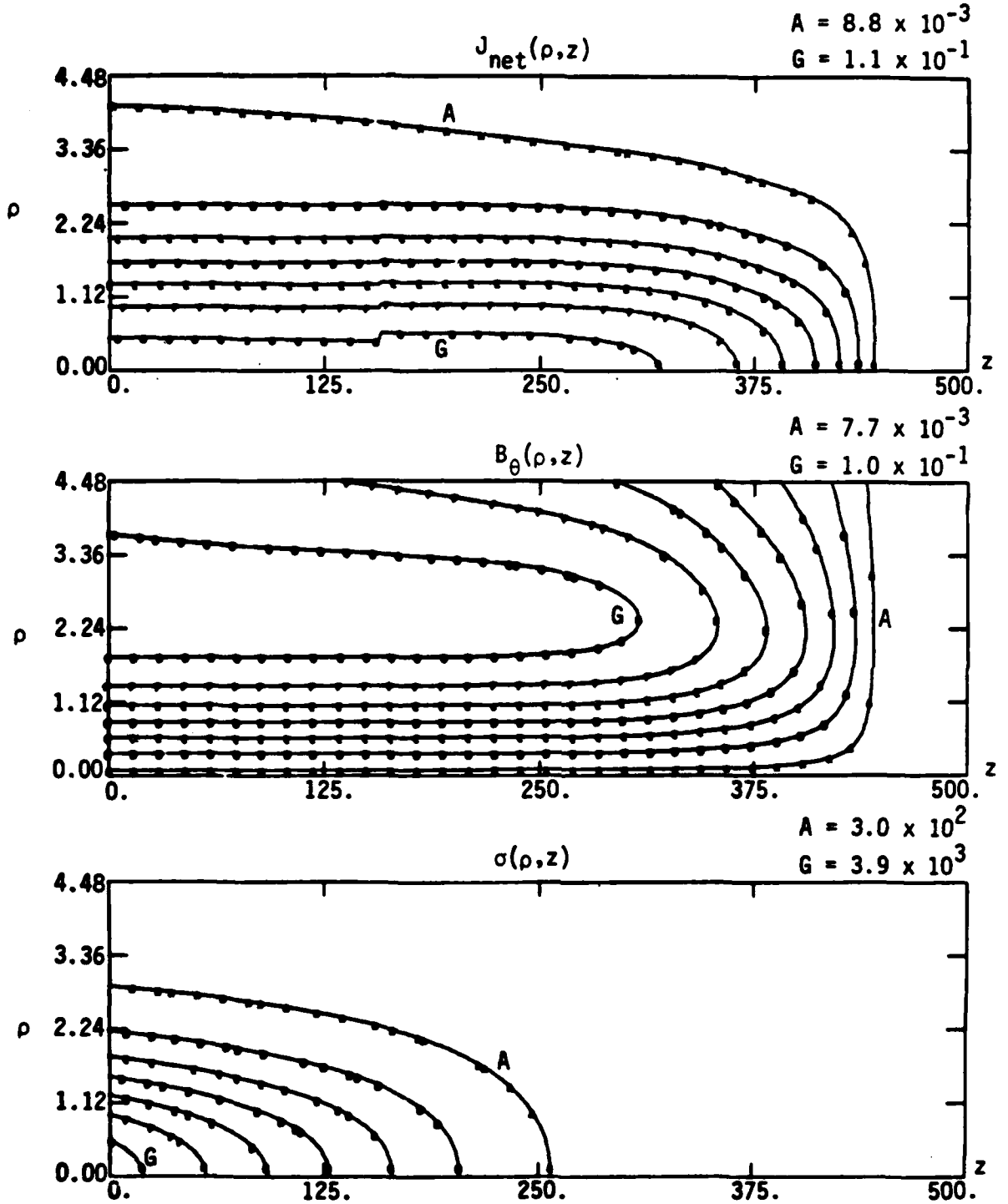

Figure 5. Contour plots of J_{net}, B_θ and σ at 0.125 Torr. Avalanching is included.

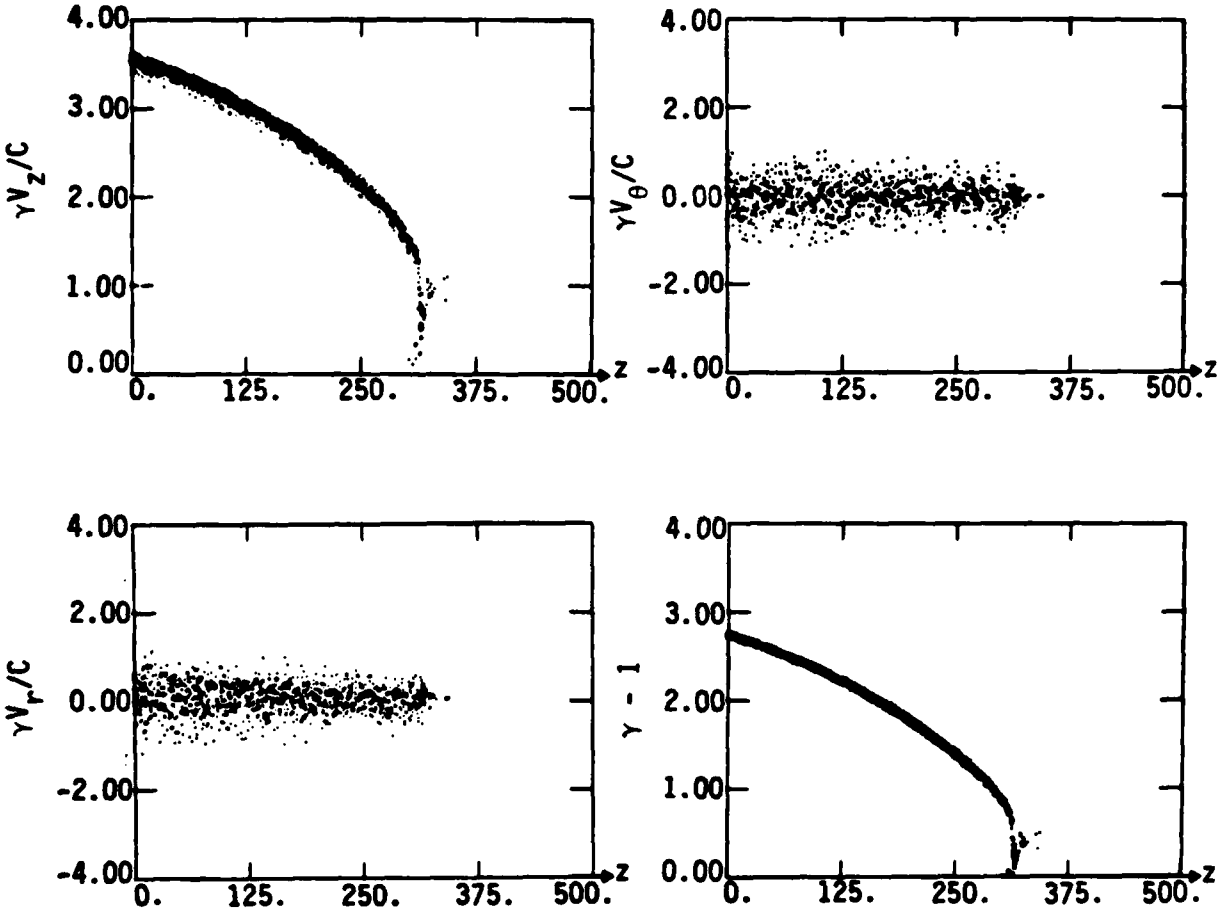

Figure 6. Phase plots of beam after traveling two meters through air at 0.4 Torr, showing nose erosion. Cf. Fig. 1.

III. SUMMARY

We have used the simulation codes CPROP and KMRAD to attempt to explain some of the phenomena seen in the FX-100 experiments. Since we have doubts about the appropriateness of the conductivity model employed, our conclusions are tentative. The simulations show that:

(1) The large return current fractions measured experimentally near 0.4 Torr and above are consistent with the presence of avalanching.

(2) At 0.4 Torr and above, avalanching causes the return current to concentrate on axis, and this may be responsible for the radial blowing-off of some of the beam seen in open shutter photographs.

(3) Resistive filamentation instabilities driven by the large return current fraction may be the source of the fine structure seen in open shutter and streak photographs at 0.2 - 0.4 Torr.

(4) Near 0.1 Torr the return current profile tends to follow the beam current profile.

To put the above conclusions on a more secure footing, an improved conductivity model is essential. In addition, more carefully controlled experimental conditions would benefit future work. In the present series of experiments, the beam exhibited diverse behavior on different shots under apparently identical conditions.

ACKNOWLEDGMENT

We would like to thank Dr. Winston Bostick and Mr. Ray Lemke for useful conversations.

REFERENCES

1. F. W. Chambers, UCID-18302, Lawrence Livermore National Laboratory (1979).

2. L. E. Thode, private communication.

3. E. P. Lee, UCID-17826, Lawrence Livermore National Laboratory (1976).

4. R. J. Briggs, UCID-19187, Lawrence Livermore National Laboratory (1981).

APPENDIX F

APPENDIX F

SECURITY CLASSIFICATION OF THIS PAGE (When Data Entered)

REPORT DOCUMENTATION PAGE		READ INSTRUCTIONS BEFORE COMPLETING FORM
1. REPORT NUMBER	2. GOVT ACCESSION NO.	3. RECIPIENT'S CATALOG NUMBER
4. TITLE (and Subtitle) ELECTRON BEAM TRANSPORT IN A SMALL APERTURE FARADAY CUP		5. TYPE OF REPORT & PERIOD COVERED Interim Report
		6. PERFORMING ORG. REPORT NUMBER AMRC-N-185
7. AUTHOR(s) D. J. Sullivan C. A. Ekdahl		8. CONTRACT OR GRANT NUMBER(s) F49620-81-C-0016
9. PERFORMING ORGANIZATION NAME AND ADDRESS MISSION RESEARCH CORPORATION 1400 San Mateo Blvd. S. E., Suite A Albuquerque, New Mexico 87108		10. PROGRAM ELEMENT PROJECT, TASK AREA & WORK UNIT NUMBERS
11. CONTROLLING OFFICE NAME AND ADDRESS Air Force Office of Scientific Research Bolling Air Force Base Washington, D. C. 20332		12. REPORT DATE January 1982 13. NUMBER OF PAGES 65
14. MONITORING AGENCY NAME & ADDRESS(if different from Controlling Office)		15. SECURITY CLASS. (of this report) Unclassified 15a. DECLASSIFICATION DOWNGRADING SCHEDULE

16. DISTRIBUTION STATEMENT (of this Report)

Approved for public release; distribution unlimited.

17. DISTRIBUTION STATEMENT (of the abstract entered in Block 20, if different from Report)

18. SUPPLEMENTARY NOTES

19. KEY WORDS (Continue on reverse side if necessary and identify by block number)

Electron Beam Diagnostics
Electron Monte-Carlo Transport Calculations
Faraday Cup

20. ABSTRACT (Continue on reverse side if necessary and identify by block number)

The Monte Carlo transport code CYCLTRAN is used to study electron transport and scattering in a Faraday cup consisting of a small cross section coaxial cable surrounded concentrically by a massive carbon block. Electrons impinging on the center wire of the coax generate a signal proportional to the electron beam current. As expected, it is found that the effective cross section of the wire is greater than its geometrical cross section due to scattering of primaries into it. The cross section is only slightly modified by production

DD FORM 1 JAN 73 1473 EDITION OF 1 NOV 65 IS OBSOLETE

SECURITY CLASSIFICATION OF THIS PAGE (When Data Entered)

20. and deposition of secondary electrons in the form of knockons. These effects are dependent on electron beam energy.

TABLE OF CONTENTS

	Page
ABSTRACT	1
PROBLEM CONFIGURATION	2
CODE RESULTS	2
ACKNOWLEDGEMENT	4
REFERENCES	6
APPENDIX A	7
APPENDIX B	15

ABSTRACT

The Monte Carlo transport code CYLTRAN is used to study electron transport and scattering in a Faraday cup consisting of a small cross section coaxial cable surrounded concentrically by a massive carbon block. Electrons impinging on the center wire of the coax generate a signal proportional to the electron beam current. As expected, it is found that the effective cross section of the wire is greater than its geometrical cross section due to scattering of primaries into it. The cross section is only slightly modified by production and deposition of secondary electrons in the form of knockons. These effects are dependent on electron beam energy.

PROBLEM CONFIGURATION

The design of a small aperture Faraday cup to measure electron beam current is given in Figure 1. It consists of a UT-47 coaxial cable embedded in a cylindrically shaped massive carbon block. In experiments, the block is sufficiently large in axial and radial extent to stop all primary and secondary electrons. Figure 1 depicts the accurate coaxial cable dimensions. However, the carbon block shown was utilized in code runs to minimize necessary computer time. The length is sufficient to effectively stop all electrons up to 4 MeV - the maximum energy tested. Because we were not interested in electrons scattered outward, the block radius was set equal to the beam radius.

CODE RESULTS

The Monte Carlo transport code CYLTRAN was used in this study. It is particularly suitable, because it can calculate both electron and photon transport in cylindrical geometry. The problem may involve up to five materials each consisting of a maximum of ten elements without code modification. The problem cylinder may be zoned axially and radially into 100 compartments, if necessary. CYLTRAN is detailed in Reference 1.

Data on materials used in the Faraday cup pertaining to beam stopping power, range and radiation yield up to a maximum beam energy of 4 MeV is compiled in Appendix A. It is generated based on material density, composition, and tabulated cross sections for the various elements.

The largest obstacle in producing statistically significant results from this problem was the exceedingly small ratio of the area of the central wire, which generates the signal, to the beam area. That ratio is $.367 \times 10^{-3}$. The beam is assumed to have a uniform current density and is monoenergetic. Increasing the particle substep size in zones comprising

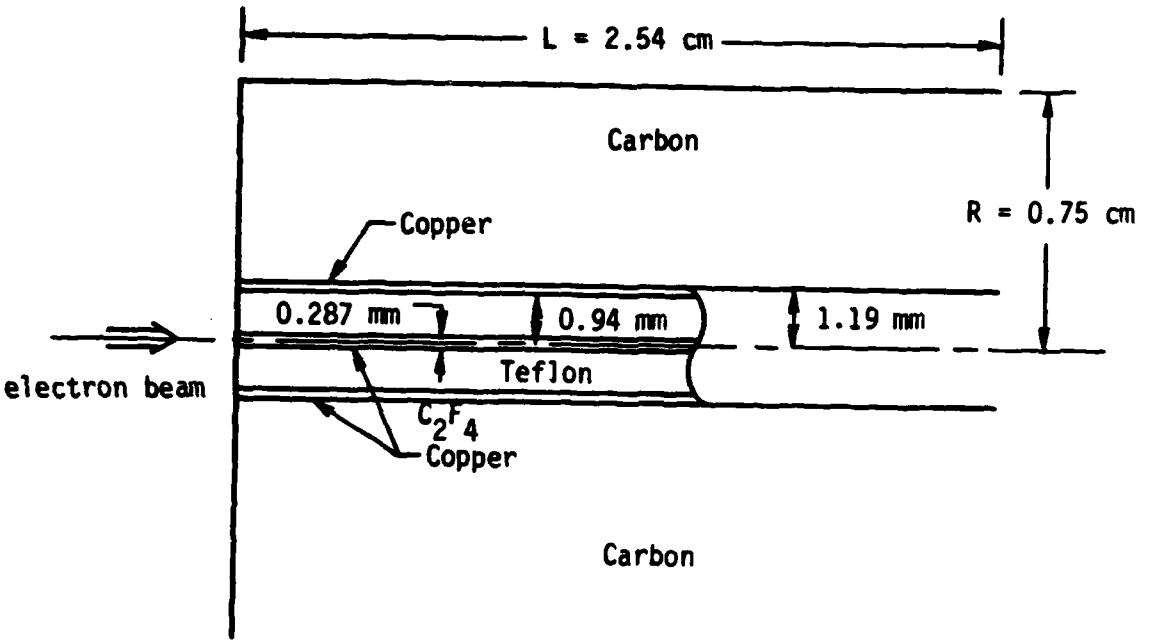

Figure 1. Physical dimensions and material composition of a small aperture Faraday cup. The electron beam in uniformly distributed over the entire cross sectional area.

the coaxial cable improved the statistics only marginally. Eventually, ten batches of 3000 particles were utilitzed. Further statistical improvement could be obtained by increasing the number of primaries. However, the increased accuracy was not deemed necessary for the present application.

The main purpose of this study was to determine the amount of charge deposited in the central wire due to scattering and secondary electron producton versus that predicted from its cross section area. Electrons with energies greater than approximately 10 keV were followed. It was found that the number of electrons deposited was several times larger than could be explained by purely geometric considerations. This is the result of the higher density of copper in relation to the other materials present in the problem. The higher density results in a shorter range and larger stopping power for electrons in the wire than in carbon or Teflon. This effect was observed over the range of energies studied from 1 to 4 MeV. Results are presented in Figure 2. The error bars are too large to derive an exact energy dependence for the ratio of effective to geometric cross sections. However, it appears to be logarithmic in energy. Finally, it is noteworthy that although, depending on beam energy, five to ten secondary electrons are created for each primary electron, they insignificantly modify the charge distribution in the various zones. This indicates that on average the number of knockons created in a zone is equal to the number whose histories are terminated in that zone by dropping below the minimum energy level of 10 keV.

ACKNOWLEDGEMENT

The author is pleased to acknowledge helpful discussions with J. Mack of Los Alamos National Laboratory and J. A. Halbleib of Sandia National Laboratory on the use of the CYLTRAN code.

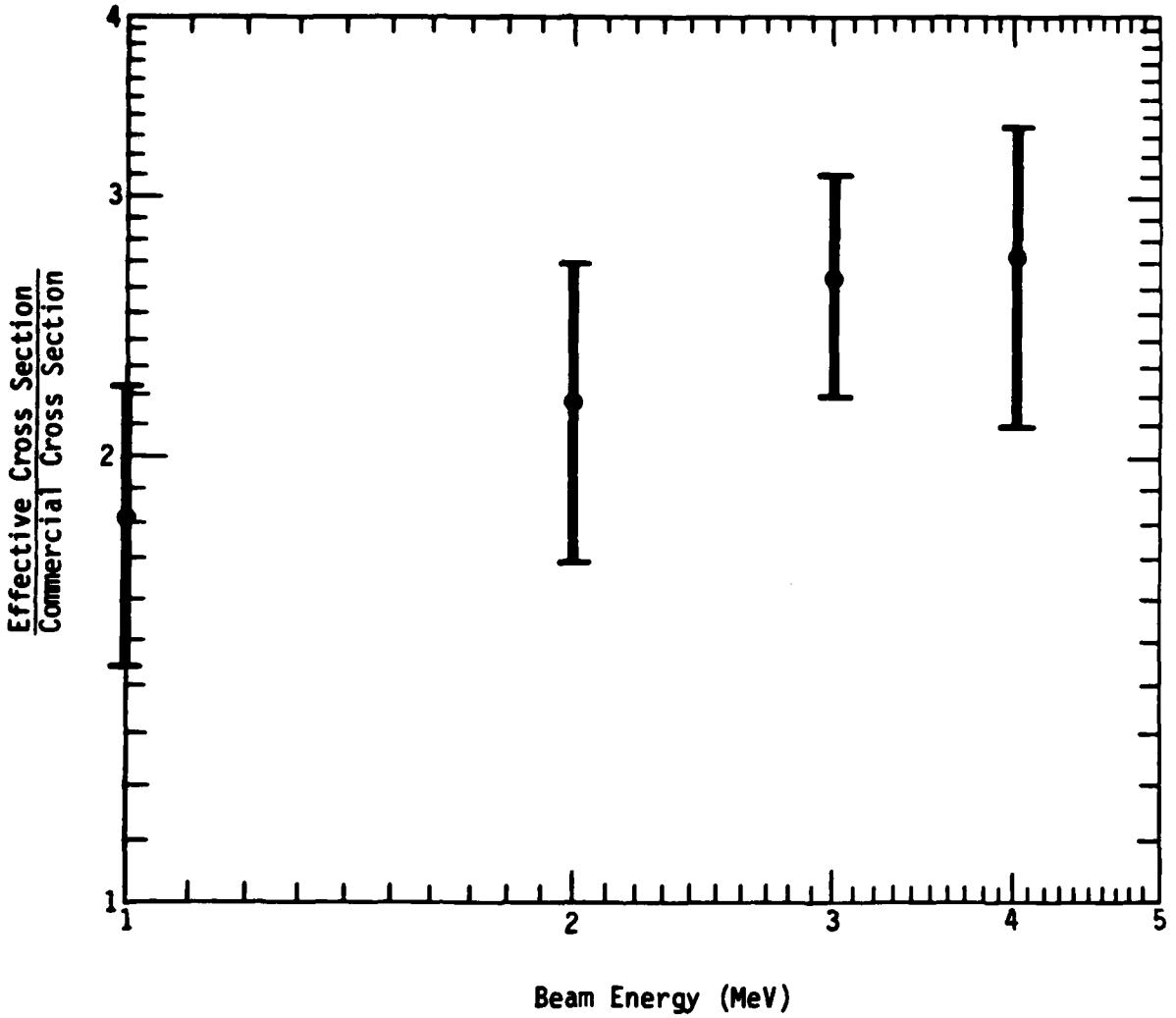

Figure 2. Ratio of effective to geometrical cross section versus electron beam energy.

REFERENCES

1. J. A. Halbleib Sr. and W. H. Vandevender, CYLTRAN: A Cylindrical-Geometry Multimaterial Electron/Photon Monte Carlo Transport Code, SAND 74-0030, Sandia National Laboratories, (1975), unpublished.

APPENDIX A

FARADAY CUP MATERIAL DATA

```
 1  324 mev electron beam into bare fx-100 faraday cup##
 2 g
 3 0 nael  ifre  isip  iaga  isub  inel  icyc  ncyc  nmax       emax
 4      1     5     0     1    50     1     1     8    64      .40000e+01
 5 0input data tape identification
 6  datatape-2 (rester-sigingar ph-rad corr), 54 sternheimer cots. 30 jan 8
 7 0detour        density
 8    .53000e+00    .89500e+01
 9 0
10 0range table
11 0      emax        ncyc        efac        nmax      t(nmax+1)      ncal      t(ncal)
12     .40000e+01         8    .91700e+00        64     .15625e-01        97     .97656e-03
13 0 jmax  lmax
14      1     1
15 0         z           a           w
16     29.00000    63.54006     1.00000
17 0        pi         pid
18    314.05142   314.05142
19 0 ----------parameters for density effect----------
20          pi           c           b          dm          x1          x0
21
22     314.05142    -4.37188      .15716     3.00000     3.00000      .20000
23     314.05142    -4.37188      .15716     3.00000     3.00000      .20000
24     .1372e+00   -.1410e+02    .7010e-01
25 1                                          electron results
26 0     effective z/a =  .45640     effective mean ionization potential =  314.05 ev     critical energy =   0.000 mev
27 0        energy          stopping power                    range    radiation    beta##2    density    rad/col    drange     dyield
28     n                collision radiation    total                      yield                  corr
29           mev       mev cm2/g mev cm2/g mev cm2/g   g/cm2                                   mev cm2/g                 g/cm2
30
31    97   .9766e-03   .473e+02  .180e-01  .473e+02  .103e-04 0.          .381e-02 0.          .388e-03 0.          0.
32    96   .1065e-02   .463e+02  .180e-01  .463e+02  .122e-04  .318e-04   .416e-02 0.          .388e-03  .188e-05   .338e-07
33    95   .1161e-02   .452e+02  .180e-01  .452e+02  .143e-04  .617e-04   .453e-02 0.          .387e-03  .211e-05   .378e-07
34    94   .1266e-02   .439e+02  .179e-01  .439e+02  .167e-04  .991e-04   .494e-02 0.          .400e-03  .236e-05   .424e-07
35    93   .1381e-02   .425e+02  .179e-01  .425e+02  .193e-04  .117e-03   .538e-02 0.          .422e-03  .265e-05   .476e-07
36    92   .1506e-02   .411e+02  .179e-01  .411e+02  .223e-04  .143e-03   .587e-02 0.          .437e-03  .299e-05   .536e-07
37    91   .1642e-02   .396e+02  .179e-01  .396e+02  .257e-04  .168e-03   .640e-02 0.          .453e-03  .338e-05   .606e-07
38    90   .1791e-02   .380e+02  .179e-01  .381e+02  .295e-04  .192e-03   .697e-02 0.          .471e-03  .383e-05   .686e-07
39    89   .1953e-02   .365e+02  .179e-01  .365e+02  .339e-04  .216e-03   .760e-02 0.          .490e-03  .435e-05   .779e-07
40    88   .2130e-02   .348e+02  .178e-01  .350e+02  .388e-04  .240e-03   .828e-02 0.          .512e-03  .495e-05   .886e-07
41    87   .2323e-02   .334e+02  .178e-01  .334e+02  .445e-04  .263e-03   .903e-02 0.          .535e-03  .564e-05   .101e-06
42    86   .2533e-02   .319e+02  .178e-01  .319e+02  .509e-04  .287e-03   .984e-02 0.          .560e-03  .644e-05   .115e-06
43    85   .2762e-02   .304e+02  .178e-01  .304e+02  .583e-04  .311e-03   .107e-01 0.          .588e-03  .737e-05   .132e-06
44    84   .3012e-02   .289e+02  .178e-01  .289e+02  .667e-04  .335e-03   .117e-01 0.          .617e-03  .843e-05   .151e-06
45    83   .3285e-02   .275e+02  .178e-01  .275e+02  .764e-04  .360e-03   .127e-01 0.          .649e-03  .967e-05   .172e-06
46    82   .3582e-02   .261e+02  .178e-01  .261e+02  .875e-04  .385e-03   .139e-01 0.          .683e-03  .111e-04   .198e-06
47    81   .3906e-02   .248e+02  .178e-01  .248e+02  .100e-03  .411e-03   .151e-01 0.          .719e-03  .128e-04   .227e-06
48    80   .4260e-02   .235e+02  .178e-01  .235e+02  .115e-03  .438e-03   .165e-01 0.          .758e-03  .147e-04   .261e-06
49    79   .4645e-02   .222e+02  .178e-01  .222e+02  .132e-03  .467e-03   .179e-01 0.          .801e-03  .169e-04   .300e-06
50    78   .5066e-02   .210e+02  .178e-01  .210e+02  .151e-03  .496e-03   .195e-01 0.          .846e-03  .195e-04   .346e-06
51    77   .5524e-02   .199e+02  .178e-01  .199e+02  .174e-03  .527e-03   .213e-01 0.          .894e-03  .224e-04   .399e-06
52    76   .6024e-02   .188e+02  .177e-01  .188e+02  .200e-03  .560e-03   .232e-01 0.          .946e-03  .259e-04   .460e-06
53    75   .6570e-02   .177e+02  .177e-01  .177e+02  .230e-03  .594e-03   .252e-01 0.          .100e-02  .298e-04   .530e-06
54    74   .7164e-02   .167e+02  .177e-01  .167e+02  .264e-03  .630e-03   .275e-01 0.          .106e-02  .346e-04   .612e-06
55    73   .7812e-02   .157e+02  .177e-01  .158e+02  .304e-03  .668e-03   .298e-01 0.          .112e-02  .400e-04   .708e-06
56    72   .8520e-02   .148e+02  .177e-01  .148e+02  .350e-03  .708e-03   .325e-01 0.          .119e-02  .462e-04   .818e-06
57    71   .9291e-02   .140e+02  .177e-01  .140e+02  .404e-03  .752e-03   .354e-01 0.          .126e-02  .535e-04   .946e-06
58    70   .1013e-01   .132e+02  .177e-01  .132e+02  .466e-03  .798e-03   .386e-01 0.          .134e-02  .620e-04   .109e-05
59    69   .1105e-01   .124e+02  .176e-01  .124e+02  .538e-03  .846e-03   .419e-01 0.          .142e-02  .718e-04   .127e-05
60    68   .1205e-01   .116e+02  .176e-01  .117e+02  .621e-03  .898e-03   .455e-01 0.          .151e-02  .832e-04   .147e-05
```

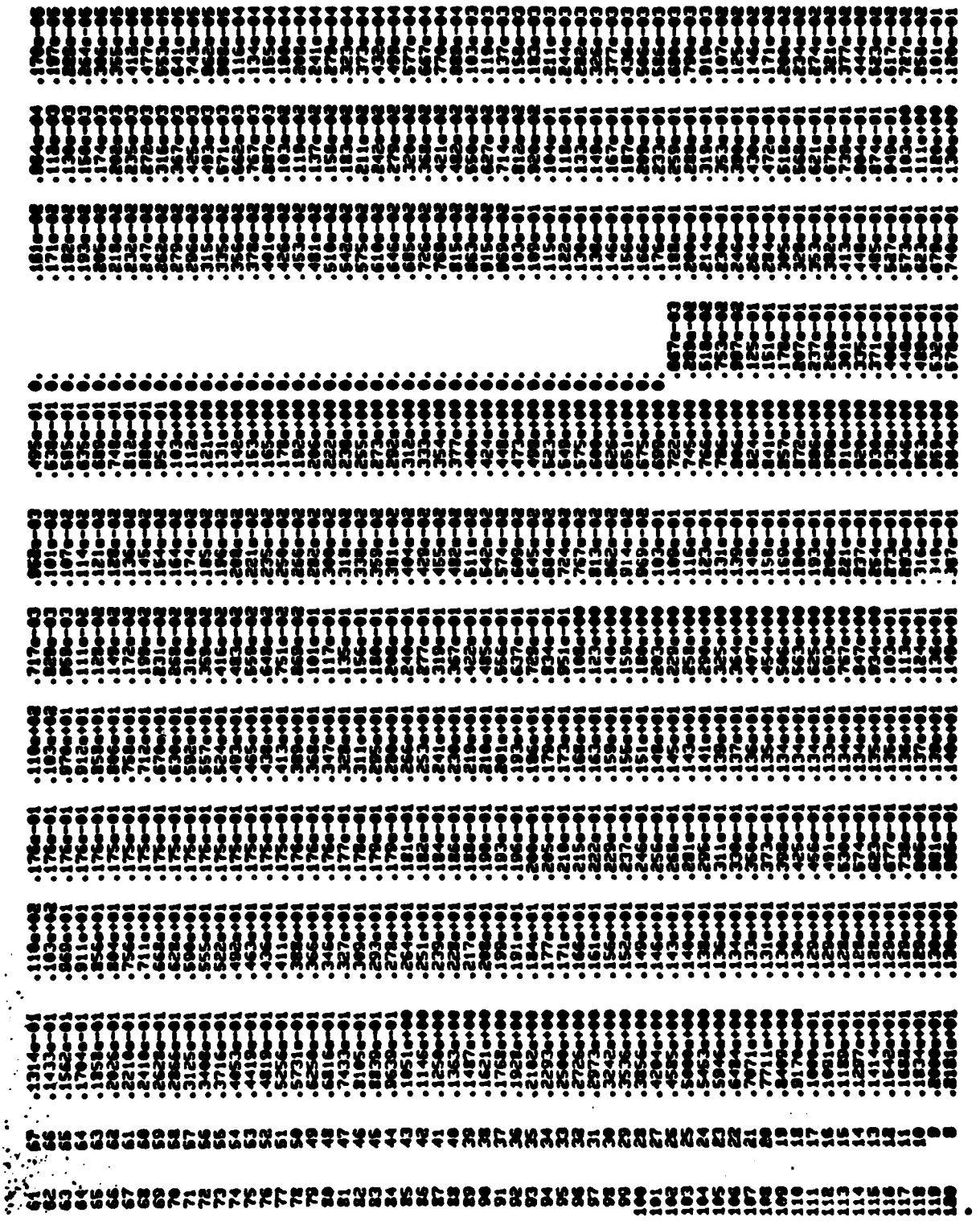

```
 121    7   .2378e+01   .131e+01   .106e+00   .142e+01   .163e+01   .386e-01   .969e+00   .625e-01   .899e-01   .140e+00   .142e-01
 122    6   .2594e+01   .132e+01   .116e+00   .143e+01   .178e+01   .428e-01   .973e+00   .674e-01   .885e-01   .151e+00   .168e-01
 123    5   .2828e+01   .132e+01   .128e+00   .146e+01   .196e+01   .463e-01   .977e+00   .728e-01   .968e-01   .163e+00   .198e-01
 124    4   .3084e+01   .133e+01   .141e+00   .147e+01   .212e+01   .501e-01   .980e+00   .778e-01   .106e+00   .175e+00   .234e-01
 125    3   .3364e+01   .134e+01   .156e+00   .150e+01   .231e+01   .543e-01   .983e+00   .834e-01   .116e+00   .188e+00   .278e-01
 126    2   .3668e+01   .135e+01   .178e+00   .152e+01   .251e+01   .588e-01   .985e+00   .898e-01   .128e+00   .202e+00   .331e-01
 127    1   .4000e+01   .136e+01   .198e+00   .155e+01   .273e+01   .637e-01   .987e+00   .952e-01   .140e+00   .216e+00   .388e-01
 128 0
 129 0 nset  ibrw  isip  iaga  iaub  imol  iayc  nayc  nmax       emax
 130     2     5     0     1    14     1     1     8    64     .40000e+01                              TEFLON
 131 0input data tape identification
 132  datatape-2 (rester-sigingar ph-rad corr), 64 sternheimer sets. 30 jan 8
 133 0detour       density
 134    .81500e+00   .23000e+01
 135 0
 136 0range table
 137 0     emax       nayc       efac       nmax     t(nmax+1)    ncal     t(ncal)
 138     .40000e+01      8    .81700e+00     64     .15625e-01    97     .97656e-03
 139 0 jmax   lmax
 140     2     1
 141 0      z          a          w
 142      6.00000    12.01115      .24000
 143      9.00000    18.99840      .76000
 144 0     pi         pid
 146     88.28321    88.28321
 146 0 ----------parameters for density effect----------
 147        pi          c          b          dm          xi          x0
 148
 149     88.28321    -3.14158      .38072     3.00000     2.00000      .20000
 150     88.28321    -3.14158      .38072     3.00000     2.00000      .20000
 151    .1443e+00  -.1863e+02   .7371e-01
 152 1                                                  electron reactio
 153 0     effective z/a =  .47992     effective mean ionization potential =   88.28 ev     critical energy =   0.000 mev
 154 0        energy                stopping power                    range    radiation    beta2#2    density    rad/col    drange     dyield
 155      n                collision radiation    total                          yield                    corr
 156           mev       mev cm2/g mev cm2/g mev cm2/g   g/cm2                                          mev cm2/g              g/cm2
 157
 158     97   .9766e-03   .988e+02   .582e-02   .988e+02   .494e-05 0.          .381e-02 0.          .589e-04 0.          0.
 159     96   .1065e-02   .937e+02   .581e-02   .937e+02   .586e-05   .588e-05   .416e-02 0.          .620e-04   .918e-06   .534e-08
 160     95   .1161e-02   .888e+02   .581e-02   .888e+02   .692e-05   .989e-05   .453e-02 0.          .654e-04   .108e-05   .614e-08
 161     94   .1266e-02   .840e+02   .580e-02   .840e+02   .813e-05   .146e-04   .494e-02 0.          .690e-04   .122e-05   .707e-08
 162     93   .1381e-02   .794e+02   .579e-02   .795e+02   .954e-05   .193e-04   .538e-02 0.          .728e-04   .140e-05   .814e-08
 163     92   .1506e-02   .751e+02   .579e-02   .751e+02   .112e-04   .239e-04   .587e-02 0.          .771e-04   .162e-05   .938e-08
 164     91   .1642e-02   .708e+02   .578e-02   .708e+02   .130e-04   .285e-04   .640e-02 0.          .815e-04   .187e-05   .108e-07
 165     90   .1791e-02   .668e+02   .577e-02   .668e+02   .152e-04   .331e-04   .697e-02 0.          .863e-04   .216e-05   .125e-07
 166     89   .1953e-02   .630e+02   .576e-02   .630e+02   .177e-04   .378e-04   .760e-02 0.          .914e-04   .250e-05   .144e-07
 167     88   .2130e-02   .593e+02   .575e-02   .593e+02   .206e-04   .424e-04   .828e-02 0.          .969e-04   .289e-05   .166e-07
 168     87   .2323e-02   .558e+02   .573e-02   .558e+02   .239e-04   .472e-04   .903e-02 0.          .103e-03   .335e-05   .192e-07
 169     86   .2533e-02   .525e+02   .572e-02   .525e+02   .278e-04   .521e-04   .984e-02 0.          .109e-03   .388e-05   .822e-07
 170     85   .2762e-02   .494e+02   .571e-02   .494e+02   .323e-04   .571e-04   .107e-01 0.          .116e-03   .450e-05   .257e-07
 171     84   .3012e-02   .464e+02   .569e-02   .464e+02   .375e-04   .622e-04   .117e-01 0.          .123e-03   .522e-05   .298e-07
 172     83   .3285e-02   .436e+02   .567e-02   .436e+02   .436e-04   .675e-04   .127e-01 0.          .130e-03   .606e-05   .344e-07
 173     82   .3582e-02   .409e+02   .565e-02   .409e+02   .506e-04   .731e-04   .138e-01 0.          .138e-03   .704e-05   .399e-07
 174     81   .3906e-02   .384e+02   .564e-02   .384e+02   .588e-04   .788e-04   .151e-01 0.          .147e-03   .818e-05   .462e-07
 175     80   .4260e-02   .360e+02   .561e-02   .360e+02   .683e-04   .848e-04   .165e-01 0.          .156e-03   .951e-05   .535e-07
 176     79   .4645e-02   .338e+02   .559e-02   .338e+02   .794e-04   .911e-04   .179e-01 0.          .166e-03   .111e-04   .620e-07
 177     78   .5066e-02   .317e+02   .557e-02   .317e+02   .923e-04   .977e-04   .195e-01 0.          .176e-03   .129e-04   .718e-07
 178     77   .5524e-02   .297e+02   .555e-02   .297e+02   .107e-03   .105e-03   .213e-01 0.          .187e-03   .150e-04   .832e-07
 179     76   .6024e-02   .278e+02   .553e-02   .278e+02   .125e-03   .112e-03   .232e-01 0.          .199e-03   .174e-04   .964e-07
 180     75   .6570e-02   .260e+02   .550e-02   .260e+02   .146e-03   .120e-03   .253e-01 0.          .211e-03   .203e-04   .112e-06
```

181	74	.7164e-02	.244e+02	.547e-02	.844e+02	.169e-03	.128e-03	.876e-01	0.	.885e-03	.238e-04	.130e-06	
182	73	.7812e-02	.228e+02	.545e-02	.820e+02	.196e-03	.136e-03	.898e-01	0.	.238e-03	.876e-04	.160e-06	
183	72	.8520e-02	.213e+02	.542e-02	.814e+02	.228e-03	.146e-03	.325e-01	0.	.254e-03	.321e-04	.174e-06	
184	71	.9291e-02	.200e+02	.540e-02	.800e+02	.265e-03	.155e-03	.354e-01	0.	.270e-03	.374e-04	.800e-06	
185	70	.1013e-01	.187e+02	.537e-02	.187e+02	.309e-03	.186e-03	.385e-01	0.	.287e-03	.436e-04	.834e-06	
186	69	.1105e-01	.175e+02	.534e-02	.175e+02	.360e-03	.176e-03	.419e-01	0.	.306e-03	.507e-04	.872e-06	
187	68	.1205e-01	.164e+02	.532e-02	.164e+02	.419e-03	.188e-03	.465e-01	0.	.326e-03	.592e-04	.315e-06	
188	67	.1314e-01	.153e+02	.529e-02	.153e+02	.488e-03	.200e-03	.496e-01	0.	.346e-03	.690e-04	.366e-06	
189	66	.1433e-01	.143e+02	.526e-02	.143e+02	.568e-03	.213e-03	.530e-01	0.	.368e-03	.804e-04	.424e-06	
190	65	.1562e-01	.134e+02	.524e-02	.134e+02	.662e-03	.227e-03	.585e-01	0.	.391e-03	.937e-04	.488e-06	
191	64	.1704e-01	.125e+02	.521e-02	.125e+02	.771e-03	.242e-03	.636e-01	0.	.417e-03	.109e-03	.571e-06	
192	63	.1858e-01	.117e+02	.519e-02	.117e+02	.898e-03	.257e-03	.689e-01	0.	.443e-03	.127e-03	.663e-06	
193	62	.2026e-01	.110e+02	.517e-02	.110e+02	.105e-02	.274e-03	.748e-01	0.	.472e-03	.148e-03	.709e-06	
194	61	.2210e-01	.103e+02	.515e-02	.103e+02	.122e-02	.292e-03	.812e-01	0.	.502e-03	.173e-03	.892e-06	
195	60	.2410e-01	.968e+01	.513e-02	.968e+01	.142e-02	.310e-03	.880e-01	0.	.534e-03	.202e-03	.104e-05	
196	59	.2628e-01	.898e+01	.511e-02	.898e+01	.166e-02	.330e-03	.954e-01	0.	.568e-03	.236e-03	.120e-05	
197	58	.2866e-01	.841e+01	.508e-02	.842e+01	.193e-02	.352e-03	.103e+00	0.	.605e-03	.274e-03	.139e-05	
198	57	.3125e-01	.788e+01	.507e-02	.788e+01	.225e-02	.374e-03	.112e+00	0.	.644e-03	.319e-03	.162e-05	
199	56	.3408e-01	.738e+01	.506e-02	.739e+01	.262e-02	.398e-03	.121e+00	0.	.685e-03	.371e-03	.188e-05	
200	55	.3716e-01	.692e+01	.505e-02	.693e+01	.305e-02	.424e-03	.131e+00	0.	.729e-03	.431e-03	.218e-05	
201	54	.4053e-01	.649e+01	.504e-02	.650e+01	.355e-02	.451e-03	.142e+00	0.	.776e-03	.502e-03	.253e-05	
202	53	.4419e-01	.609e+01	.503e-02	.610e+01	.414e-02	.480e-03	.153e+00	0.	.826e-03	.583e-03	.294e-05	
203	52	.4819e-01	.572e+01	.503e-02	.572e+01	.481e-02	.511e-03	.165e+00	0.	.879e-03	.678e-03	.341e-05	
204	51	.5256e-01	.537e+01	.503e-02	.538e+01	.560e-02	.544e-03	.178e+00	0.	.935e-03	.787e-03	.395e-05	
205	50	.5731e-01	.505e+01	.503e-02	.506e+01	.651e-02	.579e-03	.192e+00	0.	.995e-03	.913e-03	.459e-05	
206	49	.6250e-01	.475e+01	.504e-02	.476e+01	.757e-02	.616e-03	.206e+00	0.	.106e-02	.106e-02	.532e-05	
207	48	.6816e-01	.448e+01	.505e-02	.448e+01	.880e-02	.655e-03	.222e+00	0.	.113e-02	.123e-02	.618e-05	
208	47	.7433e-01	.422e+01	.506e-02	.423e+01	.102e-01	.697e-03	.238e+00	0.	.120e-02	.142e-02	.716e-05	
209	46	.8105e-01	.398e+01	.508e-02	.399e+01	.119e-01	.742e-03	.255e+00	0.	.127e-02	.164e-02	.831e-05	
210	45	.8839e-01	.376e+01	.510e-02	.377e+01	.137e-01	.789e-03	.273e+00	0.	.136e-02	.189e-02	.964e-05	
211	44	.9639e-01	.356e+01	.513e-02	.357e+01	.159e-01	.840e-03	.292e+00	0.	.144e-02	.218e-02	.112e-04	
212	43	.1051e+00	.337e+01	.517e-02	.338e+01	.184e-01	.893e-03	.312e+00	0.	.153e-02	.252e-02	.130e-04	
213	42	.1146e+00	.320e+01	.521e-02	.320e+01	.213e-01	.950e-03	.333e+00	0.	.163e-02	.289e-02	.150e-04	
214	41	.1250e+00	.304e+01	.526e-02	.304e+01	.247e-01	.101e-02	.354e+00	0.	.173e-02	.332e-02	.174e-04	
215	40	.1363e+00	.289e+01	.532e-02	.290e+01	.285e-01	.107e-02	.377e+00	0.	.184e-02	.381e-02	.202e-04	
216	39	.1487e+00	.275e+01	.539e-02	.276e+01	.328e-01	.114e-02	.400e+00	0.	.196e-02	.437e-02	.234e-04	
217	38	.1621e+00	.263e+01	.547e-02	.263e+01	.378e-01	.122e-02	.424e+00	0.	.208e-02	.499e-02	.271e-04	
218	37	.1768e+00	.251e+01	.556e-02	.252e+01	.435e-01	.129e-02	.448e+00	0.	.221e-02	.570e-02	.315e-04	
219	36	.1928e+00	.241e+01	.567e-02	.241e+01	.500e-01	.137e-02	.473e+00	0.	.235e-02	.649e-02	.365e-04	
220	35	.2102e+00	.231e+01	.579e-02	.232e+01	.574e-01	.146e-02	.498e+00	0.	.251e-02	.738e-02	.423e-04	
221	34	.2293e+00	.222e+01	.593e-02	.223e+01	.658e-01	.155e-02	.523e+00	0.	.267e-02	.838e-02	.491e-04	
222	33	.2500e+00	.214e+01	.608e-02	.215e+01	.753e-01	.165e-02	.549e+00	0.	.284e-02	.949e-02	.570e-04	
223	32	.2726e+00	.207e+01	.626e-02	.208e+01	.860e-01	.176e-02	.575e+00	0.	.302e-02	.107e-01	.661e-04	
224	31	.2973e+00	.200e+01	.646e-02	.201e+01	.981e-01	.187e-02	.600e+00	0.	.322e-02	.121e-01	.768e-04	
225	30	.3242e+00	.194e+01	.668e-02	.195e+01	.112e+00	.199e-02	.626e+00	0.	.344e-02	.136e-01	.893e-04	
226	29	.3536e+00	.189e+01	.694e-02	.190e+01	.127e+00	.212e-02	.651e+00	0.	.367e-02	.153e-01	.104e-03	
227	28	.3856e+00	.184e+01	.723e-02	.185e+01	.144e+00	.226e-02	.675e+00	0.	.392e-02	.171e-01	.121e-03	
228	27	.4204e+00	.180e+01	.755e-02	.181e+01	.163e+00	.241e-02	.699e+00	0.	.420e-02	.191e-01	.141e-03	
229	26	.4585e+00	.176e+01	.792e-02	.177e+01	.184e+00	.257e-02	.722e+00	.708e-03	.450e-02	.213e-01	.165e-03	
230	25	.5000e+00	.172e+01	.834e-02	.173e+01	.208e+00	.274e-02	.745e+00	.310e-02	.484e-02	.237e-01	.193e-03	
231	24	.5453e+00	.169e+01	.880e-02	.170e+01	.235e+00	.293e-02	.766e+00	.665e-02	.520e-02	.264e-01	.226e-03	
232	23	.5946e+00	.166e+01	.933e-02	.167e+01	.264e+00	.313e-02	.786e+00	.835e-02	.561e-02	.293e-01	.265e-03	
233	22	.6484e+00	.164e+01	.992e-02	.165e+01	.296e+00	.335e-02	.806e+00	.112e-01	.605e-02	.324e-01	.312e-03	
234	21	.7071e+00	.162e+01	.106e-01	.163e+01	.332e+00	.359e-02	.824e+00	.142e-01	.654e-02	.358e-01	.367e-03	
235	20	.7711e+00	.160e+01	.113e-01	.161e+01	.371e+00	.385e-02	.841e+00	.174e-01	.708e-02	.395e-01	.433e-03	
236	19	.8408e+00	.159e+01	.122e-01	.160e+01	.415e+00	.414e-02	.857e+00	.208e-01	.768e-02	.436e-01	.511e-03	
237	18	.9170e+00	.157e+01	.131e-01	.158e+01	.463e+00	.446e-02	.872e+00	.244e-01	.834e-02	.478e-01	.606e-03	
238	17	.1000e+01	.156e+01	.142e-01	.158e+01	.515e+00	.481e-02	.886e+00	.282e-01	.908e-02	.524e-01	.717e-03	
239	16	.1091e+01	.156e+01	.154e-01	.157e+01	.573e+00	.519e-02	.898e+00	.322e-01	.989e-02	.575e-01	.850e-03	
240	15	.1188e+01	.155e+01	.167e-01	.157e+01	.638e+00	.560e-02	.910e+00	.364e-01	.108e-01	.630e-01	.101e-02	

```
241    14   .1287e+01   .156e+01   .182e-01   .156e+01   .704e+00   .887e-02   .988e+00   .498e-01   .118e-01   .887e-01   .188e-02
242    13   .1414e+01   .154e+01   .199e-01   .156e+01   .778e+00   .857e-02   .938e+00   .456e-01   .129e-01   .758e-01   .143e-02
243    12   .1542e+01   .154e+01   .218e-01   .157e+01   .861e+00   .714e-02   .938e+00   .506e-01   .141e-01   .818e-01   .171e-02
244    11   .1682e+01   .154e+01   .239e-01   .157e+01   .950e+00   .775e-02   .946e+00   .558e-01   .155e-01   .891e-01   .204e-02
245    10   .1834e+01   .155e+01   .263e-01   .157e+01   .105e+01   .844e-02   .953e+00   .613e-01   .170e-01   .970e-01   .243e-02
246     9   .2000e+01   .156e+01   .289e-01   .158e+01   .115e+01   .919e-02   .959e+00   .671e-01   .187e-01   .105e+00   .291e-02
247     8   .2181e+01   .155e+01   .318e-01   .158e+01   .127e+01   .100e-01   .964e+00   .731e-01   .205e-01   .115e+00   .348e-02
248     7   .2378e+01   .156e+01   .351e-01   .159e+01   .138e+01   .109e-01   .968e+00   .794e-01   .225e-01   .124e+00   .416e-02
249     6   .2594e+01   .156e+01   .387e-01   .160e+01   .153e+01   .119e-01   .973e+00   .860e-01   .248e-01   .135e+00   .498e-02
250     5   .2828e+01   .157e+01   .428e-01   .161e+01   .167e+01   .131e-01   .977e+00   .929e-01   .273e-01   .146e+00   .596e-02
251     4   .3084e+01   .157e+01   .473e-01   .162e+01   .183e+01   .143e-01   .980e+00   .100e+00   .301e-01   .158e+00   .714e-02
252     3   .3364e+01   .158e+01   .524e-01   .163e+01   .200e+01   .157e-01   .983e+00   .108e+00   .331e-01   .172e+00   .855e-02
253     2   .3668e+01   .159e+01   .578e-01   .164e+01   .219e+01   .171e-01   .985e+00   .115e+00   .365e-01   .186e+00   .102e-01
254     1   .4000e+01   .158e+01   .648e-01   .166e+01   .238e+01   .188e-01   .987e+00   .123e+00   .403e-01   .201e+00   .123e-01
255 0
256 0 nset  itrw  izip  iegn  isub  insl  iegc  negc  nmax       emax
257      3     5     0     1     3     1     1     8    64      .40000e+01                                  CARBON
258 0input data tape identification
259  datatape-2 (reuter-nginger ph-rad corr), 54 sternheimer sets. 30 jun 6
260 0dateur       density
261   .87000e+00   .19000e+01
262 0
263 0range table
264 0     emax       negc       efac       nmax     t(nmax+1)    ncal      t(ncal)
265    .40000e+01      8    .91700e+00      64     .15625e-01     97     .97656e-03
266 0 jmax  lmax
267      1     1
268 0       z          a          w
269      6.00000    12.01115    1.00000
270 0      pi         pid
271     78.00000    78.00000
272 0 ----------------------parameters for density effect----------------------
273         pi          c           b          dm          xi          x0
274
275     78.00000    -3.04489      .36414     3.00000     2.00000      .20000
276     78.00000    -3.04489      .36414     3.00000     2.00000      .20000
277    .1502e+00  -.1688e+02   .7872e-01
278 1                                                  electron results
279 0     effective z/a =  .48954     effective mean ionization potential =   78.00 ev     critical energy =   0.000 mev
280 0        energy          stopping power                 range    radiation    beta**2    density   rad/col    drange     dyield
281      x                collision radiation   total                  yield                  corr
282           mev        mev cm2/g mev cm2/g mev cm2/g    g/cm2                              mev cm2/g              g/cm2
283
284     97   .9768e-03   .100e+03   .466e-02   .100e+03   .453e-05 0.          .381e-02 0.          .423e-04 0.          0.
285     96   .1065e-02   .102e+03   .455e-02   .102e+03   .537e-05   .308e-05   .416e-02 0.          .446e-04   .848e-06   .384e-08
286     95   .1161e-02   .966e+02   .454e-02   .966e+02   .634e-05   .710e-05   .453e-02 0.          .470e-04   .971e-06   .441e-08
287     94   .1266e-02   .913e+02   .453e-02   .913e+02   .746e-05   .105e-04   .494e-02 0.          .496e-04   .118e-05   .508e-08
288     93   .1381e-02   .862e+02   .452e-02   .862e+02   .876e-05   .130e-04   .538e-02 0.          .524e-04   .129e-05   .585e-08
289     92   .1506e-02   .814e+02   .451e-02   .814e+02   .102e-04   .172e-04   .587e-02 0.          .554e-04   .149e-05   .674e-08
290     91   .1642e-02   .767e+02   .450e-02   .767e+02   .120e-04   .205e-04   .640e-02 0.          .586e-04   .173e-05   .777e-08
291     90   .1791e-02   .723e+02   .448e-02   .723e+02   .140e-04   .238e-04   .697e-02 0.          .620e-04   .200e-05   .897e-08
292     89   .1953e-02   .681e+02   .447e-02   .681e+02   .163e-04   .271e-04   .760e-02 0.          .656e-04   .231e-05   .103e-07
293     88   .2130e-02   .640e+02   .446e-02   .640e+02   .190e-04   .306e-04   .828e-02 0.          .695e-04   .268e-05   .119e-07
294     87   .2323e-02   .602e+02   .443e-02   .602e+02   .221e-04   .339e-04   .903e-02 0.          .736e-04   .311e-05   .138e-07
295     86   .2533e-02   .566e+02   .442e-02   .566e+02   .257e-04   .374e-04   .984e-02 0.          .780e-04   .360e-05   .159e-07
296     85   .2762e-02   .532e+02   .440e-02   .532e+02   .298e-04   .409e-04   .107e-01 0.          .827e-04   .418e-05   .184e-07
297     84   .3012e-02   .499e+02   .438e-02   .499e+02   .347e-04   .446e-04   .117e-01 0.          .877e-04   .485e-05   .213e-07
298     83   .3285e-02   .469e+02   .436e-02   .469e+02   .403e-04   .484e-04   .127e-01 0.          .930e-04   .564e-05   .246e-07
299     82   .3588e-02   .440e+02   .434e-02   .440e+02   .469e-04   .524e-04   .138e-01 0.          .987e-04   .655e-05   .285e-07
300     81   .3908e-02   .412e+02   .432e-02   .412e+02   .546e-04   .564e-04   .151e-01 0.          .106e-03   .762e-05   .330e-07
```

301	80	.4880e-02	.386e+02	.489e-02	.387e+02	.634e-04	.607e-04	.185e-01	0.	.111e-03	.888e-06	.381e-07
302	79	.4645e-02	.362e+02	.427e-02	.362e+02	.737e-04	.652e-04	.179e-01	0.	.118e-03	.103e-04	.448e-07
303	78	.5066e-02	.339e+02	.425e-02	.339e+02	.857e-04	.699e-04	.196e-01	0.	.125e-03	.120e-04	.511e-07
304	77	.6524e-02	.318e+02	.423e-02	.318e+02	.997e-04	.748e-04	.213e-01	0.	.133e-03	.140e-04	.588e-07
305	76	.6024e-02	.297e+02	.420e-02	.298e+02	.116e-03	.800e-04	.232e-01	0.	.141e-03	.163e-04	.688e-07
306	75	.6570e-02	.278e+02	.418e-02	.278e+02	.135e-03	.854e-04	.252e-01	0.	.150e-03	.190e-04	.784e-07
307	74	.7164e-02	.261e+02	.416e-02	.261e+02	.157e-03	.912e-04	.275e-01	0.	.159e-03	.221e-04	.888e-07
308	73	.7812e-02	.244e+02	.413e-02	.244e+02	.183e-03	.972e-04	.299e-01	0.	.170e-03	.257e-04	.107e-06
309	72	.8520e-02	.228e+02	.411e-02	.228e+02	.213e-03	.104e-03	.325e-01	0.	.180e-03	.300e-04	.124e-06
310	71	.9291e-02	.213e+02	.409e-02	.213e+02	.248e-03	.111e-03	.354e-01	0.	.192e-03	.350e-04	.143e-06
311	70	.1013e-01	.199e+02	.407e-02	.200e+02	.288e-03	.118e-03	.385e-01	0.	.204e-03	.408e-04	.166e-06
312	69	.1106e-01	.187e+02	.404e-02	.187e+02	.336e-03	.125e-03	.419e-01	0.	.217e-03	.476e-04	.193e-06
313	68	.1205e-01	.174e+02	.402e-02	.174e+02	.391e-03	.134e-03	.455e-01	0.	.231e-03	.555e-04	.224e-06
314	67	.1314e-01	.163e+02	.400e-02	.163e+02	.456e-03	.142e-03	.495e-01	0.	.246e-03	.647e-04	.260e-06
315	66	.1433e-01	.152e+02	.398e-02	.153e+02	.532e-03	.151e-03	.538e-01	0.	.261e-03	.754e-04	.301e-06
316	65	.1562e-01	.143e+02	.396e-02	.143e+02	.620e-03	.161e-03	.585e-01	0.	.278e-03	.880e-04	.350e-06
317	64	.1704e-01	.133e+02	.395e-02	.133e+02	.722e-03	.172e-03	.635e-01	0.	.296e-03	.103e-03	.406e-06
318	63	.1858e-01	.125e+02	.393e-02	.125e+02	.842e-03	.183e-03	.689e-01	0.	.315e-03	.120e-03	.471e-06
319	62	.2026e-01	.117e+02	.391e-02	.117e+02	.981e-03	.195e-03	.748e-01	0.	.336e-03	.140e-03	.547e-06
320	61	.2210e-01	.109e+02	.390e-02	.109e+02	.114e-02	.207e-03	.812e-01	0.	.357e-03	.163e-03	.635e-06
321	60	.2410e-01	.102e+02	.389e-02	.102e+02	.133e-02	.221e-03	.880e-01	0.	.381e-03	.190e-03	.738e-06
322	59	.2628e-01	.955e+01	.387e-02	.955e+01	.155e-02	.235e-03	.954e-01	0.	.406e-03	.221e-03	.857e-06
323	58	.2866e-01	.894e+01	.386e-02	.894e+01	.181e-02	.250e-03	.103e+00	0.	.432e-03	.257e-03	.996e-06
324	57	.3125e-01	.837e+01	.385e-02	.837e+01	.211e-02	.266e-03	.112e+00	0.	.460e-03	.300e-03	.116e-05
325	56	.3408e-01	.784e+01	.385e-02	.785e+01	.246e-02	.284e-03	.121e+00	0.	.491e-03	.349e-03	.134e-05
326	55	.3716e-01	.735e+01	.384e-02	.735e+01	.287e-02	.302e-03	.131e+00	0.	.523e-03	.406e-03	.156e-05
327	54	.4053e-01	.689e+01	.384e-02	.689e+01	.334e-02	.322e-03	.142e+00	0.	.557e-03	.473e-03	.182e-05
328	53	.4419e-01	.646e+01	.384e-02	.647e+01	.389e-02	.343e-03	.153e+00	0.	.594e-03	.550e-03	.211e-05
329	52	.4819e-01	.607e+01	.384e-02	.607e+01	.453e-02	.365e-03	.165e+00	0.	.633e-03	.639e-03	.245e-05
330	51	.5256e-01	.570e+01	.384e-02	.570e+01	.527e-02	.389e-03	.178e+00	0.	.674e-03	.742e-03	.285e-05
331	50	.5731e-01	.536e+01	.385e-02	.536e+01	.613e-02	.415e-03	.192e+00	0.	.718e-03	.861e-03	.331e-05
332	49	.6250e-01	.504e+01	.386e-02	.505e+01	.713e-02	.442e-03	.206e+00	0.	.766e-03	.998e-03	.384e-05
333	48	.6816e-01	.475e+01	.387e-02	.475e+01	.828e-02	.471e-03	.222e+00	0.	.815e-03	.116e-02	.447e-05
334	47	.7433e-01	.447e+01	.388e-02	.448e+01	.962e-02	.501e-03	.238e+00	0.	.868e-03	.134e-02	.519e-05
335	46	.8105e-01	.422e+01	.390e-02	.423e+01	.112e-01	.534e-03	.255e+00	0.	.925e-03	.155e-02	.603e-05
336	45	.8839e-01	.399e+01	.393e-02	.399e+01	.130e-01	.569e-03	.273e+00	0.	.985e-03	.179e-02	.700e-05
337	44	.9639e-01	.377e+01	.396e-02	.378e+01	.150e-01	.606e-03	.292e+00	0.	.105e-02	.206e-02	.813e-05
338	43	.1051e+00	.357e+01	.399e-02	.358e+01	.174e-01	.646e-03	.312e+00	0.	.112e-02	.238e-02	.944e-05
339	42	.1146e+00	.339e+01	.403e-02	.339e+01	.201e-01	.688e-03	.333e+00	0.	.119e-02	.273e-02	.110e-04
340	41	.1250e+00	.322e+01	.407e-02	.322e+01	.233e-01	.732e-03	.354e+00	0.	.127e-02	.314e-02	.127e-04
341	40	.1363e+00	.306e+01	.412e-02	.306e+01	.269e-01	.780e-03	.377e+00	0.	.135e-02	.360e-02	.148e-04
342	39	.1487e+00	.291e+01	.418e-02	.292e+01	.310e-01	.830e-03	.400e+00	0.	.143e-02	.413e-02	.171e-04
343	38	.1621e+00	.278e+01	.425e-02	.278e+01	.357e-01	.884e-03	.424e+00	0.	.153e-02	.472e-02	.199e-04
344	37	.1768e+00	.266e+01	.432e-02	.266e+01	.411e-01	.941e-03	.448e+00	0.	.163e-02	.539e-02	.231e-04
345	36	.1928e+00	.255e+01	.441e-02	.255e+01	.473e-01	.100e-02	.473e+00	0.	.173e-02	.614e-02	.268e-04
346	35	.2102e+00	.244e+01	.451e-02	.245e+01	.542e-01	.107e-02	.498e+00	0.	.184e-02	.699e-02	.311e-04
347	34	.2293e+00	.235e+01	.462e-02	.235e+01	.622e-01	.114e-02	.523e+00	0.	.197e-02	.793e-02	.362e-04
348	33	.2500e+00	.226e+01	.474e-02	.227e+01	.712e-01	.121e-02	.549e+00	0.	.209e-02	.898e-02	.420e-04
349	32	.2726e+00	.219e+01	.488e-02	.219e+01	.813e-01	.129e-02	.575e+00	0.	.223e-02	.101e-01	.488e-04
350	31	.2973e+00	.212e+01	.506e-02	.212e+01	.927e-01	.137e-02	.600e+00	0.	.238e-02	.114e-01	.568e-04
351	30	.3242e+00	.206e+01	.523e-02	.206e+01	.106e+00	.146e-02	.626e+00	0.	.255e-02	.129e-01	.662e-04
352	29	.3536e+00	.200e+01	.543e-02	.200e+01	.120e+00	.156e-02	.651e+00	0.	.272e-02	.145e-01	.771e-04
353	28	.3856e+00	.194e+01	.566e-02	.195e+01	.136e+00	.166e-02	.675e+00	0.	.291e-02	.162e-01	.899e-04
354	27	.4204e+00	.190e+01	.592e-02	.191e+01	.154e+00	.177e-02	.699e+00	0.	.318e-02	.181e-01	.105e-03
355	26	.4585e+00	.186e+01	.622e-02	.186e+01	.175e+00	.189e-02	.722e+00	.868e-03	.335e-02	.202e-01	.123e-03
356	25	.5000e+00	.182e+01	.656e-02	.183e+01	.197e+00	.202e-02	.745e+00	.378e-02	.360e-02	.225e-01	.144e-03
357	24	.5453e+00	.179e+01	.698e-02	.179e+01	.222e+00	.217e-02	.766e+00	.678e-02	.388e-02	.250e-01	.168e-03
358	23	.5946e+00	.176e+01	.734e-02	.176e+01	.250e+00	.232e-02	.786e+00	.984e-02	.418e-02	.278e-01	.198e-03
359	22	.6484e+00	.173e+01	.781e-02	.174e+01	.281e+00	.249e-02	.806e+00	.138e-01	.453e-02	.308e-01	.231e-03
360	21	.7071e+00	.171e+01	.834e-02	.171e+01	.315e+00	.267e-02	.824e+00	.187e-01	.489e-02	.340e-01	.276e-03

361	20	.7711e+00	.169e+01	.894e-02	.170e+01	.362e+00	.887e-02	.841e+00	.803e-01	.530e-02	.378e-01	.384e-03
362	19	.8409e+00	.167e+01	.961e-02	.168e+01	.394e+00	.308e-02	.857e+00	.841e-01	.575e-02	.413e-01	.383e-03
363	18	.9178e+00	.166e+01	.104e-01	.167e+01	.439e+00	.332e-02	.872e+00	.881e-01	.625e-02	.455e-01	.454e-03
364	17	.1000e+01	.165e+01	.112e-01	.166e+01	.489e+00	.359e-02	.886e+00	.923e-01	.681e-02	.498e-01	.530e-03
365	16	.1091e+01	.164e+01	.122e-01	.165e+01	.544e+00	.387e-02	.898e+00	.967e-01	.742e-02	.547e-01	.630e-03
366	15	.1189e+01	.163e+01	.132e-01	.164e+01	.604e+00	.419e-02	.910e+00	.414e-01	.810e-02	.599e-01	.760e-03
367	14	.1297e+01	.163e+01	.144e-01	.164e+01	.669e+00	.454e-02	.920e+00	.462e-01	.886e-02	.655e-01	.905e-03
368	13	.1414e+01	.162e+01	.157e-01	.164e+01	.741e+00	.493e-02	.930e+00	.514e-01	.970e-02	.716e-01	.108e-02
369	12	.1542e+01	.162e+01	.172e-01	.164e+01	.819e+00	.536e-02	.938e+00	.567e-01	.106e-01	.781e-01	.129e-02
370	11	.1682e+01	.162e+01	.189e-01	.164e+01	.904e+00	.582e-02	.946e+00	.624e-01	.117e-01	.851e-01	.154e-02
371	10	.1834e+01	.162e+01	.208e-01	.165e+01	.996e+00	.634e-02	.953e+00	.683e-01	.128e-01	.928e-01	.184e-02
372	9	.2000e+01	.163e+01	.229e-01	.165e+01	.110e+01	.692e-02	.959e+00	.746e-01	.141e-01	.101e+00	.220e-02
373	8	.2181e+01	.163e+01	.252e-01	.166e+01	.121e+01	.755e-02	.964e+00	.810e-01	.155e-01	.110e+00	.263e-02
374	7	.2378e+01	.163e+01	.278e-01	.166e+01	.133e+01	.825e-02	.969e+00	.877e-01	.170e-01	.119e+00	.315e-02
375	6	.2594e+01	.164e+01	.307e-01	.167e+01	.145e+01	.902e-02	.973e+00	.948e-01	.187e-01	.129e+00	.378e-02
376	5	.2828e+01	.165e+01	.339e-01	.168e+01	.160e+01	.987e-02	.977e+00	.102e+00	.206e-01	.140e+00	.453e-02
377	4	.3084e+01	.165e+01	.375e-01	.169e+01	.175e+01	.108e-01	.980e+00	.110e+00	.227e-01	.152e+00	.543e-02
378	3	.3364e+01	.166e+01	.415e-01	.170e+01	.191e+01	.119e-01	.983e+00	.118e+00	.251e-01	.165e+00	.651e-02
379	2	.3668e+01	.166e+01	.460e-01	.171e+01	.209e+01	.130e-01	.985e+00	.126e+00	.276e-01	.179e+00	.781e-02
380	1	.4000e+01	.167e+01	.509e-01	.172e+01	.228e+01	.143e-01	.987e+00	.134e+00	.305e-01	.193e+00	.937e-02

APPENDIX B

Tabulated CYLTRAN Output for 1, 2, 3, and 4 MeV Monoenergetic Electron Beams Into a Small Aperture Faraday Cup

```
595 lines. (120a)
  1 @o c t o b e r  1 4 , 1 9 7 6  v e r s i o n
  2 @ nmat  mati
  3       1     3
  4 @ nmat  ntab
  5       1     1
  6 @npair  ntax
  7      25    41
  8 @gamma ray cross section data
  9 @energies (mev)
 10  1000.000000  800.000000  600.000000  500.000000  400.000000  300.000000
 11   200.000000  150.000000  100.000000   80.000000   60.000000   50.000000
 12    40.000000   30.000000   20.000000   15.000000   10.000000    8.000000
 13     6.000000    5.000000    4.000000    3.000000    2.000000    1.500000
 14     1.000000     .800000     .600000     .500000     .400000     .300000
 15      .200000     .150000     .100000     .080000     .060000     .050000
 16      .040000     .030000     .020000     .015000     .010000
 17 @total attenuation coefficients (cm2/g)
 18      .133015     .115792     .097314     .087552     .077436     .067025
 19      .056529     .051401     .046420     .044377     .042060     .040625
 20      .038802     .036353     .033322     .031958     .030918     .030686
 21      .030945     .031565     .032919     .035741     .041882     .047769
 22      .058536     .065369     .075103     .082004     .091659     .107638
 23      .146661     .205315     .421761     .705562    1.487422    2.456969
 24     4.613069   10.492178   33.180213   73.691769  215.150145
 25 @ratio of scattering plus pair production to total attenuation coefficients
 26      .999999     .999998     .999997     .999996     .999995     .999992
 27      .999986     .999979     .999965     .999955     .999936     .999920
 28      .999895     .999849     .999747     .999641     .999422     .999249
 29      .998956     .998721     .998371     .997787     .996538     .995083
 30      .991319     .987487     .978709     .969185     .949887     .903104
 31      .762317     .594141     .321116     .201461     .100774     .062778
 32      .034460     .015642     .005116     .002345     .000818
 33 @ratio of scattering to scattering plus pair production attenuation coefficients
 34      .001662     .002382     .003765     .005007     .007046     .010778
 35      .018909     .027362     .044314     .056913     .077841     .094684
 36      .120290     .163683     .248185     .323842     .453488     .536768
 37      .651019     .722340     .882503     .886979     .963836     .991964
 38     1.000000
 39 @k shell ionization data
 40 @binding energy (mev), photoeffect efficiency and fluorescent efficiency
 41      .008981     .871336     .392853
 42 @k x-ray energies (mev)
 43      .008150     .008150     .008150     .008150
 44 @k x-ray accumulated relative intensities
 45     1.000000    1.000000    1.000000    1.000000
 46 @auger electron energies (mev)
 47      .008150     .008150     .008150
 48 @auger electron accumulated relative intensities
 49     1.000000    1.000000    1.000000
 50 @ nmat  ntab
 51       2     1
 52 @npair  ntax
 53      25    41
 54 @gamma ray cross section data
 55 @energies (mev)1000.000000  800.000000  600.000000  500.000000  400.000000  300.000000
 57   200.000000  150.000000  100.000000   80.000000   60.000000   50.000000
 58    40.000000   30.000000   20.000000   15.000000   10.000000    8.000000
 59     6.000000    5.000000    4.000000    3.000000    2.000000    1.500000
 60     1.000000     .800000     .600000     .500000     .400000     .300000
```

```
      .200000     .150000     .100000     .080000     .060000     .050000
      .040000     .030000     .020000     .015000     .010000
@total attenuation coefficients (cm2/g)
      .042664     .037443     .031861     .028924     .025899     .022819
      .019298     .018399     .018998     .018885     .020888     .026802
      .024515     .026632     .029693     .034451     .042729     .049688
      .061023     .067886     .077309     .083599     .091601     .102329
      .117953     .129244     .146076     .157139     .177347     .197927
      .240815     .359073     .869633    1.932250    6.538229
@ratio of scattering plus pair production to total attenuation coefficients
    1.000000    1.000000    1.000000    1.000000    1.000000    1.000000
    1.000000     .999999     .999999     .999999     .999998     .999998
     .999985     .999980     .999980     .999980     .999980     .999988
     .999908     .999868     .999775     .999673     .999458     .998892
     .996690     .992470     .974912     .951171     .888740     .819442
     .694128     .480603     .205262     .094029     .028300
@ratio of scattering to scattering plus pair production attenuation coefficients
     .005449     .007745     .012092     .015937     .022153     .033290
     .056784     .080393     .125794     .158022     .208788     .247184
     .301520     .383491     .513893     .607020     .731386     .793818
     .863227     .899113     .933997     .965506     .990010     .997897
    1.000000
@k shell ionization data
@binding energy (mev), photoeffect efficiency and fluorescent efficiency
     .000687     .831990     .003376
@k x-ray energies (mev)
     .000687     .000687     .000687     .000687
@k x-ray accumulated relative intensities
    1.000000    1.000000    1.000000    1.000000
@auger electron energies (mev)
     .000687     .000687     .000687
@auger electron accumulated relative intensities
    1.000000    1.000000    1.000000
@ nmat  ntab
     3     1
@mpair  mtax
    25    41
@gamma ray cross section data
@energies (mev)
 1000.000000  800.000000  600.000000  500.000000  400.000000  300.000000
  200.000000  150.000000  100.000000   80.000000   60.000000   50.000000
    6.000000    5.000000    4.000000    3.000000    2.000000    1.500000
    1.000000     .800000     .600000     .500000     .400000     .300000
     .200000     .150000     .100000     .080000     .060000     .050000
     .040000     .030000     .020000     .015000     .010000
@total attenuation coefficients (cm2/g)
     .047459     .040496     .033058     .028154     .025144     .021091
     .017198     .015493     .014218     .013934     .013862     .013935
     .014112     .014480     .015476     .016765     .019512     .021495
     .024631     .027011     .030385     .035532     .044349     .051688
     .063513     .070654     .080455     .086995     .095307     .106425
     .122475     .133783     .149253     .157712     .169540     .178754
     .194556     .232360     .307554     .719228    2.228837
@ratio of scattering plus pair production to total attenuation coefficients
    1.000000    1.000000    1.000000    1.000000    1.000000    1.000000
    1.000000    1.000000    1.000000    1.000000     .999999     .999999
     .999998     .999999     .999998     .999998     .999997     .999997
```

```
      .959996     .999986     .999988     .999999     .999890     .999880
      .999123     .997987     .993163     .986454     .967663     .944418
      .894285     .773848     .479415     .262940     .086410
0ratio of scattering to scattering plus pair production attenuation coefficients
      .005099     .007454     .012130     .016458     .023751     .037489
      .068025     .099356     .158345     .198381     .258494     .382099
      .361954     .449719     .584721     .675399     .786023     .838082
      .894243     .922718     .950047     .974365     .992814     .998465
     1.000000
0k shell ionization data
0binding energy (mev), photoeffect efficiency and fluorescent efficiency
      .000284     .958303     .000382
0k x-r0000Edrgies.000884     .000284     .000284
0k x-ray accumulated relative intensities
     1.000000    1.000000    1.000000    1.000000
0auger electron energies (mev)
      .000284     .000284     .000284
0auger electron accumulated relative intensities
     1.000000    1.000000    1.000000
1number of sets on datapac tape =   3
0input from datapac

  331 mev electron beam into bare fx-100 faraday cup##
0 nrun  itra  izip  iaga  isub  inel  icyc  ncyc  nmax       emax            emin            rmax          lmat
     1     5     0     1     7     1     1     8    64  1.0000000e+00  3.9062500e-03  6.2492930e-01     1
 dataprep data for datapac set   1    64    33     7   121  6.249293e-01
0 nrun  itra  izip  iaga  isub  inel  icyc  ncyc  nmax       emax            emin            rmax          lmat
     2     5     0     1     3     1     1     8    64  1.0000000e+00  3.9062500e-03  5.1516960e-01     2

 dataprep data for datapac set   2    64    33     3   121  5.151696e-01
0 nrun  itra  izip  iaga  isub  inel  icyc  ncyc  nmax       emax            emin            rmax          lmat
     3     5     0     1     3     1     1     8    64  1.0000000e+00  3.9062500e-03  4.8893680e-01     1

 dataprep data for datapac set   3    64    33     3   121  4.889368e-01

 collision / total de/dx ratios for datapac set   3

 cumulative bremsstrahlung cross sections for datapac set   3

 cumulative bremsstrahlung angular distributions for datapac set   3

 langauss - equiprobable endpoints for interpolation

 k x-ray production for datapac set   3

 photoelectron angular distributions

 pair electron energy division distribution (lead)
1
0 nrun   inc istrg  inok  inel iphot  ibed  idos  ipun itape
     1     1     1     1     2     1     1     1     2     2
0 zone  material  left plane  right plane  inner cylinder  outer cylinder    ecut        ptcz
     1     1     0.          .25400e+01     0.              .14350e-01    .100e-01   0.
     2     2     0.          .25400e+01      .14350e-01     .94000e-01    .100e-01   0.
     3     1     0.          .25400e+01      .94000e-01     .11900e+00    .100e-01   0.
     4     3     0.          .25400e+01      .11900e+00     .75000e+00    .100e-01   0.
0incident electrons
```

```
 81 0electron collision and radiation energy loss straggling
 82 0knock-on electron production
 83 0no coupled inelastic scattering deflections
 84 0bremsstrahlung and characteristic x-ray quanta followed
 85 0bremsstrahlung intrinsic angle of emission from tabulated distribution
 186 0photon-produced particles followed
 187 0 iunt  lmax  itmk  jmax  ipmk jpmax  inmk  kmax  ibnk kpmax
 188      2     1     1    20     1    20     1     6     1     6
 189 0 imax  nsmx  iflux  acyc  isrun
 190  30000     4     2    -1100000000000000000
 191 0888888888888888 the standard error estimates are based on    10 batches of  3000 histories 888888888888888
 192 0       tin        tcut       tpcut      cthin      sorcin
 193      1.00000      .01000      .01000    1.00000      .74900
 194 0       tsave                           tmfac       rlen       qblk
 195       .01000                          10.00000      .50000    1.00000
 196 0electron energy classifications (mev)
 197       .95000      .90000      .85000      .80000      .75000      .70000
 198       .65000      .60000      .55000      .50000      .45000      .40000
 199       .35000      .30000      .25000      .20000      .15000      .10000
 200       .05000      .01000
 201 0photon energy classifications (mev)
 202       .95000      .90000      .85000      .80000      .75000      .70000
 203       .65000      .60000      .55000      .50000      .45000      .40000
 204       .35000      .30000      .25000      .20000      .15000      .10000
 205       .05000      .01000
 206 0electron obliquity classifications (degrees)
 207     30.00000    60.00000    90.00000   120.00000   150.00000   180.00000
 208 0electron azimuth classifications (degrees)
 209    180.00000
 210 0photon obliquity classifications (degrees)
 211     30.00000    60.00000    90.00000   120.00000   150.00000   180.00000
 212 0photon azimuth classifications (degrees)
 213    180.00000
 214 0ntfst       rgmax     scale skale      tcut       tpcut      tfcut       tsave      dlim       bnus       xnus
 215      1      .62493e+00      1     1      .01000      .01000     0.00000      .01000     1.00000      0.0        0.0
 216 0k x-ray quanta not followed in material      1
 217 0ntfst       rgmax     scale skale      tcut       tpcut      tfcut       tsave      dlim       bnus       xnus
 218      1      .51517e+00      1     1      .01000      .01000     0.00000      .01000     1.00000      0.0        0.0
 219 0k x-ray quanta not followed in material      2
 220 0ntfst       rgmax     scale skale      tcut       tpcut      tfcut       tsave      dlim       bnus       xnus
 221      1      .48894e+00      1     1      .01000      .01000     0.00000      .01000     1.00000      0.0        0.0
 222 0k x-ray quanta not followed in material      3
 223 0annihilation quanta followed
 224 1the problem is 100  per cent complete.  time to finish is       0.000 seconds. average time per batch is       103.122
 225 0average source energy = 1.0000e+00 mev
 226 0      isran          ire          irc
 227  000000000000000000 5405677252600465 1546362076272651
 228 0     ------------------------------------ histories ------------------------------------     rej       --- steps ----
 229      prim      sec     knock      p e      pair      com     auger      brem       rad      xray      land      prim        sec
 230     30000   148524   148141      301         0       82         0      1408      4483         0      7007   1421941    1418193
 231 0                          energy (mev)       ave energy (mev)      number/primary      number generated
 232  first knock (above tcut)     1.4620e-01          3.1105e-02          4.7003e+00          141009
 233  total knock (above tcut)     1.5037e-01          3.0451e-02          4.9380e+00          148141
 234  photo-electron               2.2994e-04          1.9766e-02          1.1633e-02             349
 235  pair                         0.                  0.                  0.                       0
 236  compton                      1.3276e-04          1.2848e-02          1.0333e-02             310
 237  auger                        0.                  0.                  0.                       0
 238  first bremsstrahlung         3.6363e-03          2.8730e-02          1.2657e-01            3797
 239  total bremsstrahlung         3.7052e-03          2.4845e-02          1.4913e-01            4474
 240  k x-ray                      0.                  0.                  0.                       0
```

```
 annihilation quanta          0.                    0.                    0.                    0
uncattered primary photons number and energy
 0.       99 0.       99
number coefficients - knock-ons, photon descendants
                                                  transmission
 0.       99
 0.       99
                                                   reflection
  .34e-02 11
 0.       99
                                                  lateral escape
  .11e-02 19
 0.       99
                                              number and energy coefficients
                                                  transmission
            cylinder dimensions          ---------- electron ----------      ---------- photon ----------
           length(cm)  radius(cm)        number      energy      counts      number      energy      counts

             .254e+01    .750e+00  0.       99 0.       99          0   .14e-02 10  .20e-03 15        124
                                                  reflection
            cylinder dimensions          ---------- electron ----------      ---------- photon ----------
           length(cm)  radius(cm)        number      energy      counts      number      energy      counts

             .254e+01    .750e+00   .38e-01  6  .15e-01  7       1094   .75e-02  5  .40e-03  4        299
                                                 lateral escape
            cylinder dimensions          ---------- electron ----------      ---------- photon ----------
           length(cm)  radius(cm)        number      energy      counts      number      energy      counts

             .254e+01    .750e+00   .10e+00  2  .58e-01  2       3096   .26e-01  4  .25e-02  5       1278
1                                             energy deposition
                                    (normalized to one incident particle)
                                                                                    energy deposition (mev)
      zone      material     mass(gm)   volume(cc)                      prim        knock        g-sec          to
tal

         1            1       .1471e-01      .1843e-02                 .7493e-03 17  -.1012e-04 99   .2511e-05 43   .7
417e-03 17
         2            2       .1584e+00      .6886e-01                 .1185e-01  3  -.2764e-05 99   .8798e-05 37   .1
186e-01  3
         3            1       .3803e+00      .4249e-01                 .1437e-01  2  -.3922e-05 99   .1666e-03  8   .1
454e-01  2
         4            3       .8314e+01      .4376e+01                 .8967e+00  0  -.4589e-03 12   .2256e-03 10   .8
968e+00  0
0                                                          total        .9237e+00  0  -.4757e-03 12   .4035e-03  7   .9
238e+00  0
0                                             charge distribution
                                    (normalized to one incident particle)
0                                                                                   electrons
      zone      material     zl         zr          r1          r0          prim        knock        g-sec        total
         1            1     0.          .254e+01   0.          .144e-01    .67e-03 21  .33e-04 99 0.       99  .70e-03 2
7
         2            2     0.          .254e+01    .144e-01    .840e-01    .10e-01  4 -.10e-03 99  .33e-04 99  .99e-02
5
         3            1     0.          .254e+01    .840e-01    .119e+00    .18e-01  4 -.67e-04 99 -.67e-04 67  .18e-01
4
         4            3     0.          .254e+01    .119e+00    .750e+00    .84e+00  0 -.46e-02  9  .33e-04 99  .83e+00
0
0                                                    total                  .86e+00  0 -.48e-02  9  .27e-18 67  .86e+00
0
```

energy spectra of transmitted electrons
(number/mev, normalized to one incident particle)

e (mev)		length= 2.5400		
1.0000	.9500	0.		99
.9500	.9000	0.		99
.9000	.8500	0.		99
.8500	.8000	0.		99
.8000	.7500	0.		99
.7500	.7000	0.		99
.7000	.6500	0.		99
.6500	.6000	0.		99
.6000	.5500	0.		99
.5500	.5000	0.		99
.5000	.4500	0.		99
.4500	.4000	0.		99
.4000	.3500	0.		99
.3500	.3000	0.		99
.3000	.2500	0.		99
.2500	.2000	0.		99
.2000	.1500	0.		99
.1500	.1000	0.		99
.1000	.0500	0.		99
.0500	.0100	0.		99

energy spectra of reflected electrons
(number/mev, normalized to one incident particle)

e (mev)		length= 2.5400		
1.0000	.9500	.27e-02		41
.9500	.9000	.67e-02		47
.9000	.8500	.15e-01		18
.8500	.8000	.13e-01		27
.8000	.7500	.22e-01		11
.7500	.7000	.25e-01		17
.7000	.6500	.25e-01		18
.6500	.6000	.31e-01		8
.6000	.5500	.45e-01		20
.5500	.5000	.46e-01		12
.5000	.4500	.61e-01		14
.4500	.4000	.62e-01		14
.4000	.3500	.58e-01		11
.3500	.3000	.60e-01		10
.3000	.2500	.47e-01		11
.2500	.2000	.48e-01		17
.2000	.1500	.55e-01		12
.1500	.1000	.37e-01		12
.1000	.0500	.36e-01		12
.0500	.0100	.42e-01		14

energy spectra of laterally escaping electrons
(number/mev, normalized to one incident particle)

e (mev)		length= 2.5400		
1.0000	.9500	.22e-01		17
.9500	.9000	.10e+00		8
.9000	.8500	.11e+00		11
.8500	.8000	.13e+00		8
.8000	.7500	.17e+00		7
.7500	.7000	.15e+00		9
.7000	.6500	.17e+00		5
.6500	.6000	.16e+00		6

.6000 -	.5500	.15e+00	5	
.5500 -	.5000	.13e+00	7	
.5000 -	.4500	.14e+00	10	
.4500 -	.4000	.11e+00	6	
.4000 -	.3500	.12e+00	9	
.3500 -	.3000	.10e+00	9	
.3000 -	.2500	.84e-01	12	
.2500 -	.2000	.83e-01	9	
.2000 -	.1500	.61e-01	15	
.1500 -	.1000	.43e-01	8	
.1000 -	.0500	.28e-01	20	
.0500 -	.0100	.11e-01	34	

angular distributions of transmitted and reflected electrons
(number/sr, normalized to one incident particle)

phi(deg)= 0.000

theta (deg)	180.000			
0.0000 - 30.0000	0.	99		
30.0000 - 60.0000	0.	99		
60.0000 - 90.0000	0.	99		
90.0000 -120.0000	.24e-02	6		
120.0000 -150.0000	.82e-02	7		
150.0000 -180.0000	.12e-01	8		

angular distributions of laterally escaping electrons
(number/sr, normalized to one incident particle)

phi(deg)= 0.000

theta (deg)	180.000	
0.0000 - 30.0000	.13e-01	9
30.0000 - 60.0000	.15e-01	3
60.0000 - 90.0000	.10e-01	4
90.0000 -120.0000	.60e-02	6
120.0000 -150.0000	.27e-02	8
150.0000 -180.0000	.67e-03	25

energy spectra and angular distributions of electrons transmitted and reflected
azimuthal interval is 0.00000 to 180.00000 degrees
(number/(mevsr), normalized to one particle)

e (mev)	theta= 0.000		30.000		60.000		90.000		120.000		150.000	
	30.000		60.000		90.000		120.000		150.000		180.000	
1.0000 - .9500	0.	99	0.	99	0.	99	0.	99	.29e-03	99	.24e-02	51
.9500 - .9000	0.	99	0.	99	0.	99	.42e-03	99	.20e-02	43	.79e-03	99
.9000 - .8500	0.	99	0.	99	0.	99	.13e-02	37	.41e-02	24	.16e-02	67
.8500 - .8000	0.	99	0.	99	0.	99	.15e-02	30	.29e-02	33	.16e-02	67
.8000 - .7500	0.	99	0.	99	0.	99	.23e-02	16	.52e-02	14	.32e-02	41
.7500 - .7000	0.	99	0.	99	0.	99	.21e-02	37	.52e-02	23	.79e-02	26
.7000 - .6500	0.	99	0.	99	0.	99	.21e-02	39	.58e-02	20	.55e-02	43
.6500 - .6000	0.	99	0.	99	0.	99	.11e-02	33	.78e-02	14	.12e-01	20
.6000 - .5500	0.	99	0.	99	0.	99	.28e-02	26	.99e-02	25	.17e-01	24
.5500 - .5000	0.	99	0.	99	0.	99	.21e-02	30	.13e-01	8	.12e-01	25
.5000 - .4500	0.	99	0.	99	0.	99	.32e-02	23	.13e-01	20	.26e-01	18
.4500 - .4000	0.	99	0.	99	0.	99	.53e-02	18	.13e-01	18	.19e-01	26
.4000 - .3500	0.	99	0.	99	0.	99	.49e-02	26	.11e-01	18	.21e-01	21
.3500 - .3000	0.	99	0.	99	0.	99	.42e-02	24	.12e-01	18	.23e-01	20
.3000 - .2500	0.	99	0.	99	0.	99	.21e-02	33	.96e-02	16	.21e-01	19
.2500 - .2000	0.	99	0.	99	0.	99	.28e-02	38	.12e-01	23	.14e-01	14
.2000 - .1500	0.	99	0.	99	0.	99	.21e-02	21	.14e-01	15	.20e-01	12
.1500 - .1000	0.	99	0.	99	0.	99	.30e-02	27	.87e-02	19	.95e-02	27
.1000 - .0500	0.	99	0.	99	0.	99	.15e-02	37	.93e-02	16	.12e-01	25
.0500 - .0100	0.	99	0.	99	0.	99	.37e-02	24	.87e-02	21	.12e-01	21

energy spectra and angular distributions of electrons laterally escaping
azimuthal interval is 0.00000 to 180.00000 degrees
(number/(mev*sr), normalized to one particle)

e (mev)	theta=	0.000		30.000		60.000		90.000		120.000		150.000	
		30.000		60.000		90.000		120.000		150.000		180.000	
1.0000 -	.9500	.16e-01	17	.35e-02	27	0.	99	.21e-03	99	0.	99	0.	99
.9500 -	.9000	.57e-01	10	.18e-01	14	.34e-02	31	.21e-03	99	0.	99	0.	99
.9000 -	.8500	.32e-01	10	.29e-01	15	.57e-02	22	.13e-02	27	0.	99	0.	99
.8500 -	.8000	.32e-01	19	.27e-01	10	.98e-02	22	.19e-02	39	.58e-03	67	0.	99
.8000 -	.7500	.32e-01	21	.32e-01	12	.15e-01	11	.40e-02	24	.20e-02	30	0.	99
.7500 -	.7000	.17e-01	31	.29e-01	9	.16e-01	13	.49e-02	15	.17e-02	27	0.	99
.7000 -	.6500	.18e-01	21	.26e-01	9	.22e-01	9	.79e-02	15	.14e-02	45	.79e-03	99
.6500 -	.6000	.17e-01	36	.23e-01	6	.16e-01	18	.11e-01	20	.35e-02	35	.79e-03	99
.6000 -	.5500	.95e-02	27	.19e-01	14	.17e-01	9	.11e-01	15	.43e-02	18	.79e-03	99
.5500 -	.5000	.87e-02	21	.13e-01	15	.20e-01	12	.83e-02	15	.20e-02	37	.79e-03	99
.5000 -	.4500	.55e-02	37	.14e-01	12	.17e-01	15	.11e-01	19	.49e-02	20	.79e-03	99
.4500 -	.4000	.32e-02	55	.11e-01	14	.12e-01	11	.85e-02	14	.70e-02	21	.79e-03	99
.4000 -	.3500	.40e-02	45	.12e-01	19	.13e-01	15	.93e-02	13	.58e-02	25	.79e-03	99
.3500 -	.3000	.16e-02	67	.11e-01	19	.10e-01	14	.10e-01	17	.41e-02	27	.16e-02	67
.3000 -	.2500	.40e-02	45	.58e-02	24	.87e-02	22	.83e-02	23	.55e-02	18	.16e-02	67
.2500 -	.2000	.24e-02	51	.49e-02	22	.95e-02	11	.87e-02	15	.43e-02	35	.32e-02	41
.2000 -	.1500	.24e-02	71	.61e-02	31	.72e-02	13	.53e-02	25	.23e-02	41	.79e-03	99
.1500 -	.1000	.79e-03	99	.38e-02	26	.40e-02	28	.45e-02	32	.29e-02	21	.79e-03	99
.1000 -	.0500	.16e-02	67	.20e-02	48	.23e-02	29	.34e-02	27	.17e-02	44	0.	99
.0500 -	.0100	.99e-03	99	.72e-03	67	.19e-02	43	.27e-03	99	.72e-03	67	0.	99

energy spectra of transmitted photons
(number/mev, normalized to one incident particle)

e (mev) length= 2.5400

1.0000 -	.9500	0.	99
.9500 -	.9000	0.	99
.9000 -	.8500	0.	99
.8500 -	.8000	0.	99
.8000 -	.7500	.47e-03	99
.7500 -	.7000	0.	99
.7000 -	.6500	0.	99
.6500 -	.6000	0.	99
.6000 -	.5500	0.	99
.5500 -	.5000	0.	99
.5000 -	.4500	0.	99
.4500 -	.4000	.79e-03	67
.4000 -	.3500	.18e-02	57
.3500 -	.3000	.81e-03	67
.3000 -	.2500	.12e-02	51
.2500 -	.2000	.18e-02	33
.2000 -	.1500	.22e-02	49
.1500 -	.1000	.51e-02	30
.1000 -	.0500	.61e-02	23
.0500 -	.0100	.96e-02	10

energy spectra of reflected photons
(number/mev, normalized to one incident particle)

e (mev) length= 2.5400

1.0000 -	.9500	0.	99
.9500 -	.9000	0.	99
.9000 -	.8500	0.	99
.8500 -	.8000	0.	99
.8000 -	.7500	0.	99
.7500 -	.7000	0.	99

```
481      .7000 -   .6500   0.          99
482      .6500 -   .6000   0.          99
483      .6000 -   .5500   0.          99
484      .5500 -   .5000   0.          99
485      .5000 -   .4500   0.          99
486      .4500 -   .4000   0.          99
487      .4000 -   .3500   0.          99
488      .3500 -   .3000    .66e-03    99
489      .3000 -   .2500    .61e-03    99
490      .2500 -   .2000    .24e-02    41
491      .2000 -   .1500    .32e-02    33
492      .1500 -   .1000    .12e-01    22
493      .1000 -   .0500    .37e-01    10
494      .0500 -   .0100    .12e+00    10
495                                  energy spectra of laterally escaping photons
496                                (number/mev, normalized to one incident particle)
497 ●      e (mev)  length=      2.5400
498
499    1.0000 -   .9500   0.          99
500      .9500 -   .9000   0.          99
501      .9000 -   .8500   0.          99
502      .8500 -   .8000    .58e-03    99
503      .8000 -   .7500   0.          99
504      .7500 -   .7000    .48e-03    99
505      .7000 -   .6500    .11e-02    99
506      .6500 -   .6000    .58e-03    99
507      .6000 -   .5500    .17e-02    51
508      .5500 -   .5000    .55e-02    26
509      .5000 -   .4500    .24e-02    41
510      .4500 -   .4000    .27e-02    34
511      .4000 -   .3500    .84e-02    30
512      .3500 -   .3000    .85e-02    27
513      .3000 -   .2500    .11e-01    34
514      .2500 -   .2000    .20e-01    14
515      .2000 -   .1500    .28e-01    20
516      .1500 -   .1000    .70e-01     7
517      .1000 -   .0500    .11e+00     6
518      .0500 -   .0100    .30e+00     5
519                          angular distributions of transmitted and reflected photon intensity
520                                (mev/sr, normalized to one incident particle)
521 ●            phi(deg)=  0.000
522      theta (deg)       180.000
523
524    0.0000 - 30.0000    .23e-03 15
525   30.0000 - 60.0000    .53e-05 82
526   60.0000 - 90.0000   0.          99
527   90.0000 -120.0000    .52e-04 13
528  120.0000 -150.0000    .77e-04 12
529  150.0000 -180.0000    .68e-04 22
530                          angular distributions of laterally escaping photon intensity
531                                (mev/sr, normalized to one incident particle)
532 ●            phi(deg)=  0.000
533      theta (deg)       180.000
534
535    0.0000 - 30.0000    .49e-03 13
536   30.0000 - 60.0000    .49e-03 10
537   60.0000 - 90.0000    .22e-03  9
538   90.0000 -120.0000    .62e-04 17
539  120.0000 -150.0000    .18e-04 37
540  150.0000 -180.0000    .18e-04 63
```

energy spectra and angular distributions of photons transmitted and reflected
azimuthal interval is 0.00000 to 180.00000 degrees
(number/(mev*sr), normalized to one particle)

e (mev)	theta=	0.000		30.000		60.000		90.000		120.000		150.000	
		30.000		60.000		90.000		120.000		150.000		180.000	
1.0000 -	.9500	0.	99	0.	99	0.	99	0.	99	0.	99	0.	99
.9500 -	.9000	0.	99	0.	99	0.	99	0.	99	0.	99	0.	99
.9000 -	.8500	0.	99	0.	99	0.	99	0.	99	0.	99	0.	99
.8500 -	.8000	0.	99	0.	99	0.	99	0.	99	0.	99	0.	99
.8000 -	.7500	.56e-03	99	0.	99	0.	99	0.	99	0.	99	0.	99
.7500 -	.7000	0.	99	0.	99	0.	99	0.	99	0.	99	0.	99
.7000 -	.6500	0.	99	0.	99	0.	99	0.	99	0.	99	0.	99
.6500 -	.6000	0.	99	0.	99	0.	99	0.	99	0.	99	0.	99
.6000 -	.5500	0.	99	0.	99	0.	99	0.	99	0.	99	0.	99
.5500 -	.5000	0.	99	0.	99	0.	99	0.	99	0.	99	0.	99
.5000 -	.4500	0.	99	0.	99	0.	99	0.	99	0.	99	0.	99
.4500 -	.4000	.94e-03	67	0.	99	0.	99	0.	99	0.	99	0.	99
.4000 -	.3500	.15e-02	51	.23e-03	99	0.	99	0.	99	0.	99	0.	99
.3500 -	.3000	.96e-03	67	0.	99	0.	99	0.	99	.29e-03	99	0.	99
.3000 -	.2500	.14e-02	51	0.	99	0.	99	.20e-03	99	0.	99	0.	99
.2500 -	.2000	.21e-02	33	0.	99	0.	99	.57e-03	51	.29e-03	99	0.	99
.2000 -	.1500	.27e-02	49	0.	99	0.	99	.38e-03	67	.56e-03	67	.78e-03	99
.1500 -	.1000	.60e-02	30	0.	99	0.	99	.17e-02	25	.19e-02	38	.31e-02	55
.1000 -	.0500	.65e-02	23	.28e-03	99	0.	99	.44e-02	15	.78e-02	17	.62e-02	24
.0500 -	.0100	.11e-01	10	0.	99	0.	99	.14e-01	15	.25e-01	12	.21e-01	24
integral (/sr)		.16e-02	10	.25e-04	67	0.	99	.91e-03	11	.15e-02	9	.14e-02	13

energy spectra and angular distributions of photons laterally escaping
azimuthal interval is 0.00000 to 180.00000 degrees
(number/(mev*sr), normalized to one particle)

e (mev)	theta=	0.000		30.000		60.000		90.000		120.000		150.000	
		30.000		60.000		90.000		120.000		150.000		180.000	
1.0000 -	.9500	0.	99	0.	99	0.	99	0.	99	0.	99	0.	99
.9500 -	.9000	0.	99	0.	99	0.	99	0.	99	0.	99	0.	99
.9000 -	.8500	0.	99	0.	99	0.	99	0.	99	0.	99	0.	99
.8500 -	.8000	0.	99	0.25e-03	99	0.	99	0.	99	0.	99	0.	99
.7500 -	.7000	.58e-03	99	0.	99	0.	99	0.	99	0.	99	0.	99
.7000 -	.6500	0.	99	.49e-03	99	0.	99	0.	99	0.	99	0.	99
.6500 -	.6000	0.	99	.25e-03	99	0.	99	0.	99	0.	99	0.	99
.6000 -	.5500	.62e-03	99	.25e-03	99	.18e-03	99	0.	99	0.	99	0.	99
.5500 -	.5000	.71e-03	99	.19e-02	31	.20e-03	99	0.	99	0.	99	0.	99
.5000 -	.4500	.55e-02	89	0.83e-03	99	0.56e-03	99	0.	99	0.	99	0.	99
.4500 -	.4000	.34e-02	44	.87e-03	56	.10e-02	45	0.	99	0.	99	0.	99
.4000 -	.3500	.17e-02	51	.23e-02	34	.58e-03	51	0.	99	0.	99	0.	99
.3500 -	.3000	.13e-02	67	.25e-02	40	.98e-03	45	0.	99	0.	99	.78e-03	99
.3000 -	.2500	.59e-02	42	.49e-02	17	.11e-02	46	.19e-03	99	0.	99	0.	99
.2500 -	.2000	.45e-02	40	.51e-02	30	.27e-02	36	.12e-02	51	0.	99	0.	99
.2000 -	.1500	.12e-01	20	.11e-01	11	.79e-02	15	.27e-02	29	0.	99	.64e-03	99
.1500 -	.1000	.19e-01	12	.18e-01	11	.12e-01	11	.50e-02	19	.18e-02	37	.79e-04	99
.1000 -	.0500	.40e-01	12	.47e-01	5	.33e-01	10	.15e-01	14	.28e-02	45	.35e-02	41
integral (/sr)		.42e-02	7	.43e-02	5	.27e-02	6	.11e-02	12	.20e-03	37	.21e-03	44

the number of ecs words used for statistics is 717

```
fix pc'o'output'lb,140'l1,60
01 lines. (120a)
 1 0o c t o b e r  1 4 , 1 9 7 6  v e r s i o n
 2 0 nmat  matl
 3       2       3
 4 0 nmat  ntab
 5       1       1
 6 0mpair  mtax
 7      25      41
 8 0gamma ray cross section data
 9 0energies (mev)
10  1000.000000  800.000000  600.000000  500.000000  400.000000  300.000000
11   200.000000  150.000000  100.000000   80.000000   60.000000   50.000000
12    40.000000   30.000000   20.000000   15.000000   10.000000    8.000000
13     6.000000    5.000000    4.000000    3.000000    2.000000    1.500000
14     1.000000     .800000     .600000     .500000     .400000     .300000
15      .200000     .150000     .100000     .080000     .060000     .050000
16      .040000     .030000     .020000     .015000     .010000
17 0total attenuation coefficients (cm2/g)
18      .133015     .115792     .097314     .087552     .077436     .067025
19      .056529     .051401     .046420     .044377     .042060     .040625
20      .038802     .036353     .033322     .031958     .030918     .030686
21      .030945     .031565     .032919     .035741     .041882     .047769
22      .058536     .065369     .075103     .082004     .091659     .107638
23      .146661     .205315     .421761     .705562    1.487422    2.456969
24     4.613069   10.492178   33.180213   73.691769  215.150145
25 0ratio of scattering plus pair production to total attenuation coefficients
26      .999999     .999998     .999997     .999996     .999995     .999992
27      .999986     .999979     .999965     .999955     .999936     .999920
28      .999895     .999849     .999747     .999641     .999422     .999249
29      .998956     .998721     .998371     .997787     .996538     .995083
30      .991319     .987487     .978709     .969185     .949887     .903104
32      .882860     .858642     .805116     .802805     .000878     .062778
33 0ratio of scattering to scattering plus pair production attenuation coefficients
34      .001662     .002382     .003765     .005007     .007046     .010778
35      .018909     .027362     .044314     .056913     .077841     .094684
36      .120290     .163683     .248185     .323842     .453488     .536768
37      .651019     .722340     .802503     .886979     .963836     .991964
38     1.000000
39 0k shell ionization data
40 0binding energy (mev), photoeffect efficiency and fluorescent efficiency
41      .008981     .871336     .392853
42 0k x-ray energies (mev)
43      .008150     .008150     .008150     .008150
48 0k xi=0.0000e+00 wall=1.000000 active=0.000000 ities=0.000000
46 0auger electron energies (mev)
47      .008150     .008150     .008150
48 0auger electron accumulated relative intensities
49     1.000000    1.000000    1.000000
50 0 nmat  ntab
51       2       1
52 0mpair  mtax
53      25      41
54 0gamma ray cross section data
55 0energies (mev)
56  1000.000000  800.000000  600.000000  500.000000  400.000000  300.000000
57   200.000000  150.000000  100.000000   80.000000   60.000000   50.000000
58    40.000000   30.000000   20.000000   15.000000   10.000000    8.000000
59     6.000000    5.000000    4.000000    3.000000    2.000000    1.500000
60     1.000000     .800000     .600000     .500000     .400000     .300000
.l44,46
44 0k x-ray accumulated relative intensities
46     1.000000    1.000000    1.000000    1.000000
```

```
      .200000     .150000     .100000     .080000     .060000     .050000
      .040000     .030000     .020000     .015000     .010000
@total attenuation coefficients (cm2/g)
      .042664     .037443     .031861     .028924     .025899     .022819
      .019793     .018395     .017194     .016805     .016488     .016362
      .016276     .016313     .016918     .017921     .020146     .021802
      .024515     .026632     .029693     .034451     .042729     .049688
      .061023     .067886     .077309     .083599     .091601     .102329
      .117953     .129244     .146076     .157139     .177347     .197927
      .240815     .359073     .869633    1.932250    6.538229
@ratio of scattering plus pair production to total attenuation coefficients
    1.000000    1.000000    1.000000    1.000000    1.000000    1.000000
    1.000000     .999999     .999999     .999999     .999998     .999998
     .999997     .999996     .999994     .999993     .999990     .999988
     .999985     .999983     .999979     .999974     .999962     .999947
     .999908     .999868     .999775     .999673     .999458     .998892
     .998688     .998400     .998062     .997629     .996200     .994442
@ratio of scattering to scattering plus pair production attenuation coefficients
     .005449     .007745     .012092     .015937     .022153     .033290
     .056784     .080393     .125794     .158022     .208788     .247184
     .301520     .383491     .513893     .607020     .731386     .793818
     .863227     .899113     .933997     .965506     .990010     .997897
    1.000000
@k shell ionization data
@binding energy (mev), photoeffect efficiency and fluorescent efficiency
     .000687     .831990     .003376
@k x-ray energies (mev)
     .000687     .000687     .000687     .000687
@k x-ray accumulated relative intensities
    1.000000    1.000000    1.000000    1.000000
@auger electron energies (mev)
     .000687     .000687     .000687
@auger electron accumulated relative intensities
    1.000000    1.000000    1.000000
@ nmat  ntab
     3     1
@npair  ntax
    25    41
@gamma ray cross section data
@energies (mev)
 1000.000000  800.000000  600.000000  500.000000  400.000000  300.000000
  200.000000  150.000000  100.000000   80.000000   60.000000   50.000000
    6.000000    5.000000    4.000000    3.000000    2.000000    1.500000
    1.000000     .800000     .600000     .500000     .400000     .300000
     .200000     .150000     .100000     .080000     .060000     .050000
     .040000     .030000     .020000     .015000     .010000
@total attenuation coefficients (cm2/g)
     .047459     .040496     .033058     .029154     .025144     .021091
     .017198     .015493     .014218     .013934     .013862     .013935
     .014112     .014480     .015476     .016765     .019512     .021495
     .024631     .027011     .030385     .035532     .044349     .051688
     .063513     .070654     .080455     .086895     .095307     .106425
     .122475     .133783     .149253     .157712     .169540     .178754
     .194556     .232360     .387554     .719226    2.228837
@ratio of scattering plus pair production to total attenuation coefficients
    1.000000    1.000000    1.000000    1.000000    1.000000    1.000000
    1.000000    1.000000    1.000000    1.000000     .999999     .999999
     .999998     .999998     .999998     .999998     .999997     .999997
```

```
      .999996     .999995     .999994     .999993     .999991     .999986
      .999976     .999966     .999942     .999915     .999859     .999710
      .999123     .997987     .993163     .986454     .967663     .944418
      .894285     .773048     .479415     .262940     .086410
@ratio of scattering to scattering plus pair production attenuation coefficients
      .005099     .007454     .012130     .016458     .023751     .037489
      .068025     .099356     .158345     .198381     .258494     .302099
      .361954     .449719     .584721     .675399     .786023     .838082
      .894243     .922718     .950047     .974365     .992814     .998465
     1.000000
@k shell ionization data
@binding energy (mev), photoeffect efficiency and fluorescent efficiency
      .000284     .958303     .000382
@k x-ray energies (mev)
      .000284     .000284     .000284     .000284
@k x-ray accumulated relative intensities
     1.000000    1.000000    1.000000    1.000000
@auger electron energies (mev)
      .000284     .000284     .000284
@auger electron accumulated relative intensities
     1.000000    1.000000    1.000000
1number of sets on datapac tape =   3
@input from datapac

  ##2 mev electron beam into bare fx-100 faraday cup##
@ nrun  itra  isip  isgn  isub  inal  icyc  ncyc  nmax       emax            emin            rmax        imat
     1     5     0     1    10     1     1     8    64  2.0000000e+00  7.8125000e-03  1.3637750e+00     1

 dataprep data for datapac set   1    64    33    10   121  1.363775e+00
@ nrun  itra  isip  isgn  isub  inal  icyc  ncyc  nmax       emax            emin            rmax        imat
     2     5     0     1     6     1     1     8    64  2.0000000e+00  7.8125000e-03  1.1525970e+00     2

 dataprep data for datapac set   2    64    33     6   121  1.152597e+00
@ nrun  itra  isip  isgn  isub  inal  icyc  ncyc  nmax       emax            emin            rmax        imat
     3     5     0     1     3     1     1     8    64  2.0000000e+00  7.8125000e-03  1.0971910e+00     1

 dataprep data for datapac set   3    64    33     3   121  1.097191e+00
 collision / total de/dx ratios for datapac set   3

 cumulative bremsstrahlung cross sections for datapac set   3

 cumulative bremsstrahlung angular distributions for datapac set   3

 langauss - equiprobable endpoints for interpolation

 k x-ray production for datapac set   3

 photoelectron angular distributions

 pair electron energy division distribution (lead)
1
@ nrun#   ine# istrg  inek  ine2 iphot  ibad  ides  ipu# itap#
@ zone  material  left plane  right plane  inner cylinder  outer cylinder    ecut        ptcs
     1        1     0.          .25400e+01     0.             .14350e-01    .100e-01   0.
     2        2     0.          .25400e+01      .14350e-01    .94000e-01    .100e-01   0.
     3        1     0.          .25400e+01      .94000e-01    .11900e+00    .100e-01   0.
     4        3     0.          .25400e+01      .11900e+00    .75000e+00    .100e-01   0.
@incident electrons
.t173,174
@ nrun#   ine# istrg  inek  ine2 iphot  ibad  ides  ipu# itap#
.t173,174
@ nrun   inc istrg  inek  inel iphot  ibad  ides  ipun itape
     2     1     1     1     2     1     1     1     2     2
```

```
 181 @electron collision and radiation energy loss straggling
 182 @knock-on electron production
 183 @no coupled inelastic scattering deflections
 184 @bremsstrahlung and characteristic x-ray quanta followed
 185 @bremsstrahlung intrinsic angle of emission from tabulated distribution
 186 @photon-produced particles followed
 187 @ iunt   lmax   itmk   jmax   ipnk jpmax   iemk   kmax   ibnk kpmax
 188       2      1      1     40      1     40      1      6      1      6
 189 @ imax   nzon iflux   ncyc   inran
 190   30000      4      2     -1100000000000000000
 191 @zzzzzzzzzzzzzz the standard error estimates are based on    10 batches of   3000 histories zzzzzzzzzzzzzz
 192 @     2.00000      1.00000      1.00000      1.00000      5.00000e-01
 193 @       tsave                                 tmfac        rlan         qblk
 194         .01000                               10.00000       .50000      1.00000
 195 @electron energy classifications (mev)
 196       1.95000      1.90000      1.85000      1.80000      1.75000      1.70000
 197       1.65000      1.60000      1.55000      1.50000      1.45000      1.40000
 198       1.35000      1.30000      1.25000      1.20000      1.15000      1.10000
 199       1.05000      1.00000       .95000       .90000       .85000       .80000
 200        .75000       .70000       .65000       .60000       .55000       .50000
 201        .45000       .40000       .35000       .30000       .25000       .20000
 202        .15000       .10000       .05000       .01000
 203 @photon energy classifications (mev)
 204       1.95000      1.90000      1.85000      1.80000      1.75000      1.70000
 205       1.65000      1.60000      1.55000      1.50000      1.45000      1.40000
 206       1.35000      1.30000      1.25000      1.20000      1.15000      1.10000
 207       1.05000      1.00000       .95000       .90000       .85000       .80000
 208        .45000       .40000       .35000       .30000       .25000       .20000
 209        .15000       .10000       .05000       .01000
 210 @electron obliquity classifications (degrees)
 211     30.00000     60.00000     90.00000    120.00000    150.00000    180.00000
 212 @electron azimuth classifications (degrees)
 213     180.00000
 214 @photon obliquity classifications (degrees)
 215     30.00000     60.00000     90.00000    120.00000    150.00000    180.00000
 216 @photon azimuth classifications (degrees)
 217     180.00000
 218 @ntfat         rgmax      scale skale       tcut       tpcut       tfcut       tsave       dlim       bnum       xnum
 219        1      .13638e+01      1      1      .01000      .01000     0.00000      .01000     1.00000      0.0        0.0
 220 @k x-ray quanta not followed in material      1
 221 @ntfat         rgmax      scale skale       tcut       tpcut       tfcut       tsave       dlim       bnum       xnum
 222        1      .11526e+01      1      1      .01000      .01000     0.00000      .01000     1.00000      0.0        0.0
 223 @k x-ray quanta not followed in material      2
 224 @ntfat         rgmax      scale skale       tcut       tpcut       tfcut       tsave       dlim       bnum       xnum
 225        1      .18972e+01      1      1      .01000      .01000     0.00000      .01000     1.00000      0.0        0.0
 226 @k x-ray quanta not followed in material      3
 227 @annihilation quanta followed
 228 1the problem is 100  per cent complete.  time to finish is       0.000 seconds. average time per batch is       171.432
 229 @average source energy = 2.0000e+00 mev
 230 @      inran          ira          irc
 231  000000000000000 2025166701752431 1241741267011501
 232 @    ------------------------------------ histories ------------------------------------      rej       --- steps ----
 233        prim       sec     knock       p-e       pair       com      ewgr      brem       rad      xray      land       prim       sec
 234       30000    289173    288171       718          0       284         0      3406      8358         0     11607    1488973    2960171
 235 @                          energy (mev)       ave energy (mev)       number/primary      number generated
 236  first knock (above tcut)      3.3275e-01          3.7391e-02            8.8993e+00            266978
 237  total knock (above tcut)      3.4670e-01          3.6893e-02            9.6057e+00            288171
 238  photo-electron                5.9255e-04          2.1264e-02            2.7867e-02               836
 239 .t192,193
 240 @      tin        tcut       tpcut      cthin      sercin
 241       2.00000      .01000      .01000     1.00000      .74900
 242
```

```
 pair                          0.                  0.                  0.                    0
 compton                       7.3042e-04          2.5871e-02          2.8233e-02          847
 auger                         0.                  0.                  0.                    0
 first bremsstrahlung          1.4196e-02          6.3640e-02          2.2307e-01         6692
 total bremsstrahlung          1.4458e-02          5.1963e-02          2.7823e-01         8347
 k x-ray                       0.                  0.                  0.                    0
 annihilation quanta           0.                  0.                  0.                    0
0unscattered primary photons number and energy
 0.       99 0.       99
0number coefficients - knock-ons, photon descendants
0                                                  transmission
 0.       99
 0.       99
0                                                   reflection
  .30e-02  8
 0.       99
0                                                  lateral escape
  .42e-02  8
0 .33e-04 99                                 number and energy coefficients
0            cylinder dimensions       ---------- electron ----------      ---------- photon ----------
           length(cm)  radius(cm)      number      energy      counts      number      energy      counts

             .254e+01    .750e+00  0.       99 0.       99          0   .65e-02  4  .79e-03  8        488
0                                                   reflection
0            cylinder dimensions       ---------- electron ----------      ---------- photon ----------
           length(cm)  radius(cm)      number      energy      counts      number      energy      counts

             .254e+01    .750e+00   .17e-01  4  .56e-02  5        516   .98e-02  6  .42e-03  8        436
0                                                  lateral escape
0            cylinder dimensions       ---------- electron ----------      ---------- photon ----------
           length(cm)  radius(cm)      number      energy      counts      number      energy      counts

             .254e+01    .750e+00   .22e+00  1  .11e+00  1       6701   .70e-01  2  .51e-02  3       3284
0 1                                                energy deposition
                                        (normalized to one incident particle)
0                                                                                    energy deposition (mev)
      zone      material     mass(gm)   volume(cc)                          prim        knock         g-sec          to
tal
         1            1       .1471e-01      .1643e-02                    .1528e-02 11  -.1773e-04 98   .1433e-04 51   .1
524e-02 10
         2            2       .1584e+00      .6886e-01                    .2151e-01  2  -.4305e-04 99   .2433e-04 36   .2
149e-01  3
         3            1       .3803e+00      .4249e-01                    .3678e-01  2   .5798e-04 99   .4412e-03 12   .3
728e-01  2
         4            3       .8314e+01      .4376e+01                    .1691e+01  0  -.1518e-02 10   .9326e-03  9   .1
690e+01  0
0                                                                total       .1750e+01  0  -.1521e-02 10   .1412e-02  7   .1
750e+01  0
0                                                  charge distribution
                                        (normalized to one incident particle)
0                                                                                    electrons
      zone      material     zi         zr          ri          r0          prim        knock         g-sec         total

         1            1     0.          .254e+01    0.          .144e-01    .80e-03 83  -.13e-03 99  0.       99   .67e-03 3
2
         2            2     0.          .254e+01     .144e-01    .540e-01    .89e-02  6  -.33e-04 99   .33e-04 99   .89e-02
3 0
```

```
                3          1     0.          .254e+01    .940e-01    .119e+00    .25e-01  2 -.20e-03 99 -.33e-04 99  .25e-01
 2
                4          3     0.          .254e+01    .119e+00    .750e+00    .73e+00  0 -.71e-02  7 -.33e-04 99  .72e+00

                                                 total                           .77e+00  0 -.75e-02  6 -.33e-04 99  .76e+00


                                                    energy spectra of transmitted electrons
                                                (number/mev, normalized to one incident particle)

      e (mev)  length=      2.5400

   2.0000 -  1.9500  0.       99
   1.9500 -  1.9000  0.       99
   1.9000 -  1.8500  0.       99
   1.8500 -  1.8000  0.       99
   1.8000 -  1.7500  0.       99
   1.7500 -  1.7000  0.       99
   1.7000 -  1.6500  0.       99
   1.6500 -  1.6000  0.       99
   1.6000 -  1.5500  0.       99
   1.5500 -  1.5000  0.       99
   1.5000 -  1.4500  0.       99
   1.4500 -  1.4000  0.       99
   1.4000 -  1.3500  0.       99
   1.3500 -  1.3000  0.       99
   1.3000 -  1.2500  0.       99
   1.2500 -  1.2000  0.       99
   1.2000 -  1.1500  0.       99
   1.1500 -  1.1000  0.       99
   1.1000 -  1.0500  0.       99
   1.0500 -  1.0000  0.       99
   1.0000 -   .9500  0.       99
    .9500 -   .9000  0.       99
    .9000 -   .8500  0.       99
    .8500 -   .8000  0.       99
    .8000 -   .7500  0.       99
    .7500 -   .7000  0.       99
    .7000 -   .6500  0.       99
    .6500 -   .6000  0.       99
    .6000 -   .5500  0.       99
    .5500 -   .5000  0.       99
    .5000 -   .4500  0.       99
    .4500 -   .4000  0.       99
    .4000 -   .3500  0.       99
    .3500 -   .3000  0.       99
    .3000 -   .2500  0.       99
    .2500 -   .2000  0.       99
    .2000 -   .1500  0.       99
    .1500 -   .1000  0.       99
    .1000 -   .0500  0.       99
    .0500 -   .0100  0.       99


                                                    energy spectra of reflected electrons
                                                (number/mev, normalized to one incident particle)

      e (mev)  length=      2.5400

   2.0000 -  1.9500  0.       99
   1.9500 -  1.9000  0.       99
   1.9000 -  1.8500   .13e-02 67
   1.8500 -  1.8000   .67e-03 99
   1.8000 -  1.7500   .80e-02 71
   1.7500 -  1.7000   .47e-02 43
```

361	1.7000 -	1.6500	.67e-03	99
362	1.6500 -	1.6000	0.	99
363	1.6000 -	1.5500	.67e-02	30
364	1.5500 -	1.5000	.47e-02	30
365	1.5000 -	1.4500	.27e-02	55
366	1.4500 -	1.4000	.60e-02	26
367	1.4000 -	1.3500	.67e-02	26
368	1.3500 -	1.3000	.40e-02	37
369	1.3000 -	1.2500	.93e-02	22
370	1.2500 -	1.2000	.67e-02	26
371	1.2000 -	1.1500	.40e-02	37
372	1.1500 -	1.1000	.80e-02	24
373	1.1000 -	1.0500	.67e-02	39
374	1.0500 -	1.0000	.67e-02	37
375	1.0000 -	.9500	.11e-01	17
376	.9500 -	.9000	.67e-02	21
377	.9000 -	.8500	.10e-01	25
378	.8500 -	.8000	.15e-01	22
379	.8000 -	.7500	.67e-02	45
380	.7500 -	.7000	.11e-01	29
381	.7000 -	.6500	.13e-01	23
382	.6500 -	.6000	.11e-01	18
383	.6000 -	.5500	.10e-01	18
384	.5500 -	.5000	.14e-01	28
385	.5000 -	.4500	.19e-01	16
386	.4500 -	.4000	.15e-01	17
387	.4000 -	.3500	.11e-01	15
388	.3500 -	.3000	.17e-01	16
389	.3000 -	.2500	.11e-01	14
390	.2500 -	.2000	.11e-01	23
391	.2000 -	.1500	.11e-01	23
392	.1500 -	.1000	.14e-01	26
393	.1000 -	.0500	.21e-01	18
394	.0500 -	.0100	.29e-01	11
395				
396				
397	e (mev)	length=	2.5400	
398				
399	2.0000 -	1.9500	.13e-02	67
400	1.9500 -	1.9000	.34e-01	9
401	1.9000 -	1.8500	.74e-01	10
402	1.8500 -	1.8000	.85e-01	12
403	1.8000 -	1.7500	.83e-01	9
404	1.7500 -	1.7000	.11e+00	6
405	1.7000 -	1.6500	.11e+00	7
406	1.6500 -	1.6000	.12e+00	9
407	1.6000 -	1.5500	.11e+00	7
408	1.5500 -	1.5000	.12e+00	8
409	1.5000 -	1.4500	.13e+00	8
410	1.4500 -	1.4000	.12e+00	9
411	1.4000 -	1.3500	.13e+00	5
412	1.3500 -	1.3000	.13e+00	9
413	1.3000 -	1.2500	.14e+00	4
414	1.2500 -	1.2000	.13e+00	7
415	1.2000 -	1.1500	.15e+00	7
416	1.1500 -	1.1000	.15e+00	5
417	1.1000 -	1.0500	.16e+00	5
418	1.0500 -	1.0000	.15e+00	8
419	1.0000 -	.9500	.14e+00	4
420	.9500 -	.9000	.14e+00	4

energy spectra of laterally escaping electrons
(number/mev, normalized to one incident particle)

```
 21     .9000 -   .8500    .15e+00  5
 22     .8500 -   .8000    .16e+00  7
 23     .8000 -   .7500    .13e+00  5
 24     .7500 -   .7000    .14e+00  7
 25     .7000 -   .6500    .16e+00  6
 26     .6500 -   .6000    .14e+00  6
 27     .6000 -   .5500    .14e+00  5
 28     .5500 -   .5000    .14e+00  6
 29     .5000 -   .4500    .13e+00  8
 30     .4500 -   .4000    .12e+00  5
 31     .4000 -   .3500    .99e-01  8
 32     .3500 -   .3000    .96e-01  8
 33     .3000 -   .2500    .77e-01  9
 34     .2500 -   .2000    .74e-01 11
 35     .2000 -   .1500    .72e-01 12
 36     .1500 -   .1000    .42e-01 12
 37     .1000 -   .0500    .36e-01 12
 38     .0500 -   .0100    .17e-01 20
 39                          angular distributions of transmitted and reflected electrons
 40                              (number/sr, normalized to one incident particle)
 41 0            phi(deg)=  0.000
 42     theta (deg)       180.000
 43
 44    0.0000 - 30.0000  0.       99
 45   30.0000 - 60.0000  0.       99
 46   60.0000 - 90.0000  0.       99
 47   90.0000 -120.0000   .13e-02 10

 48  120.0000 -150.0000   .37e-02  6
 49  150.0000 -180.0000   .53e-02  9
 50                          angular distributions of laterally escaping electrons
 51                            (number/sr, normalized to one incident particle)
 52 0            phi(deg)=  0.000
 53     theta (deg)       180.000
 54
 55    0.0000 - 30.0000   .43e-01  4
 56   30.0000 - 60.0000   .36e-01  2
 57   60.0000 - 90.0000   .21e-01  1
 58   90.0000 -120.0000   .95e-02  3
 59  120.0000 -150.0000   .37e-02  6
 60  150.0000 -180.0000   .99e-03 22
 61 0                      energy spectra and angular distributions of electrons transmitted and reflected
 62                          azimuthal interval is   0.00000 to 180.00000 degrees
 63                           (number/(mevtsr), normalized to one particle)
 64 0      e (mev)  theta=  0.000      30.000      60.000      90.000     120.000     150.000
 65                        30.000      60.000      90.000     120.000     150.000     180.000
 66
 67    2.0000 -  1.9500  0.       99 0.       99 0.       99 0.       99 0.       99 0.       99
 68    1.9500 -  1.9000  0.       99 0.       99 0.       99 0.       99 0.       99 0.       99
 69    1.9000 -  1.8500  0.       99 0.       99 0.       99 0.       99  .58e-03 67 0.       99
 70    1.8500 -  1.8000  0.       99 0.       99 0.       99  .21e-03 99 0.       99 0.       99
 71    1.8000 -  1.7500  0.       99 0.       99 0.       99  .42e-03 99 0.       99  .79e-03 99
 72    1.7500 -  1.7000  0.       99 0.       99 0.       99  .64e-03 51  .58e-03 99  .16e-02 67
 73    1.7000 -  1.6500  0.       99 0.       99 0.       99  .21e-03 99 0.       99 0.       99
 74    1.6500 -  1.6000  0.       99 0.       99 0.       99 0.       99 0.       99 0.       99
 75    1.6000 -  1.6500  0.       99 0.       99 0.       99  .11e-02 33  .87e-03 51  .16e-02 67
 76    1.6500 -  1.5000  0.       99 0.       99 0.       98  .85e-03 41  .58e-03 67  .79e-03 99
 77    1.5000 -  1.4500  0.       99 0.       98 0.       99  .21e-03 99  .87e-03 51 0.       99
 78    1.4500 -  1.4000  0.       99 0.       98 0.       98  .64e-03 71  .87e-03 51  .24e-02 51
 79    1.4000 -  1.3500  0.       98 0.       99 0.       99  .11e-02 54  .87e-03 51  .16e-02 67
 80    1.3500 -  1.3000  0.       99 0.       98 0.       99  .42e-03 67  .12e-02 55 0.       99
```

481	1.3000	-	1.2500	0.	99	0.	99	0.	99	.15e-02	37	.12e-02	55	.24e-02	51		
482	1.2500	-	1.2000	0.	99	0.	99	0.	99	.64e-03	51	.17e-02	27	.78e-03	99		
483	1.2000	-	1.1500	0.	99	0.	99	0.	99	0.	99	.12e-02	55	.16e-02	67		
484	1.1500	-	1.1000	0.	99	0.	99	0.	99	.64e-03	51	.17e-02	37	.24e-02	51		
485	1.1000	-	1.0500	0.	99	0.	99	0.	99	.85e-03	76	.58e-03	67	.32e-02	41		
486	1.0500	-	1.0000	0.	99	0.	99	0.	99	.21e-03	99	.14e-02	54	.32e-02	55		
487	1.0000	-	.9500	0.	99	0.	99	0.	99	.13e-02	51	.20e-02	30	.24e-02	71		
488	.9500	-	.9000	0.	99	0.	99	0.	99	.42e-03	67	.14e-02	33	.24e-02	51		
489	.9000	-	.8500	0.	99	0.	99	0.	99	.64e-03	51	.17e-02	51	.48e-02	61		
490	.8500	-	.8000	0.	99	0.	99	0.	99	.42e-03	99	.43e-02	25	.48e-02	37		
491	.8000	-	.7500	0.	99	0.	99	0.	99	.64e-03	71	.20e-02	48	0.	99		
492	.7500	-	.7000	0.	99	0.	99	0.	99	.11e-02	33	.29e-02	42	.16e-02	67		
493	.7000	-	.6500	0.	99	0.	99	0.	99	.64e-03	51	.35e-02	32	.32e-02	41		
494	.6500	-	.6000	0.	99	0.	99	0.	99	.64e-03	51	.29e-02	30	.32e-02	55		
495	.6000	-	.5500	0.	99	0.	99	0.	99	.64e-03	51	.35e-02	27	0.	99		
496	.5500	-	.5000	0.	99	0.	99	0.	99	.64e-03	99	.35e-02	21	.48e-02	37		
497	.5000	-	.4500	0.	99	0.	99	0.	99	.85e-03	55	.55e-02	15	.48e-02	37		
498	.4500	-	.4000	0.	99	0.	99	0.	99	.64e-03	51	.20e-02	37	.10e-01	26		
499	.4000	-	.3500	0.	99	0.	99	0.	99	.11e-02	33	.23e-02	17	.32e-02	41		
500	.3500	-	.3000	0.	99	0.	99	0.	99	.15e-02	30	.35e-02	36	.55e-02	30		
501	.3000	-	.2500	0.	99	0.	99	0.	99	.85e-03	41	.26e-02	20	.24e-02	51		
502	.2500	-	.2000	0.	99	0.	99	0.	99	.64e-03	51	.23e-02	31	.48e-02	37		
503	.2000	-	.1500	0.	99	0.	99	0.	99	0.	99	.32e-02	37	.40e-02	45		
504	.1500	-	.1000	0.	99	0.	99	0.	99	.64e-03	51	.26e-02	35	.71e-02	31		
505	.1000	-	.0500	0.	99	0.	99	0.	99	.19e-02	39	.41e-02	16	.63e-02	36		
506	.0500	-	.0100	0.	99	0.	99	0.	99	.29e-02	21	.43e-02	24	.12e-01	24		

energy spectra and angular distributions of electrons laterally escaping
azimuthal interval is 0.00000 to 180.00000 degrees
(number/(mevSsr), normalized to one particle)

e (mev)	theta=	0.000	30.000	60.000	90.000	120.000	150.000
		30.000	60.000	90.000	120.000	150.000	180.000

2.0000	-	1.9500	.16e-02	67	0.	99	0.	99	0.	99	0.	99	0.	99			
1.9500	-	1.9000	.34e-01	18	.17e-02	27	.21e-03	99	.21e-03	99	0.	99	0.	99			
1.9000	-	1.8500	.70e-01	10	.55e-02	23	.85e-03	41	0.	99	0.	99	0.	99			
1.8500	-	1.8000	.68e-01	8	.11e-01	23	.85e-03	55	0.	99	0.	99	0.	99			
1.8000	-	1.7500	.50e-01	12	.15e-01	12	.15e-02	30	.21e-03	99	0.	99	0.	99			
1.7500	-	1.7000	.64e-01	11	.20e-01	10	.23e-02	29	.42e-03	67	.29e-03	99	0.	99			
1.7000	-	1.6500	.55e-01	10	.23e-01	17	.30e-02	30	.42e-03	67	0.	99	0.	99			
1.6500	-	1.6000	.51e-01	11	.29e-01	11	.40e-02	24	0.	99	.29e-03	99	0.	99			
1.6000	-	1.5500	.45e-01	13	.23e-01	9	.62e-02	26	.85e-03	41	.58e-03	67	0.	99			
1.5500	-	1.5000	.42e-01	14	.28e-01	9	.64e-02	19	.11e-02	33	0.	99	0.	99			
1.5000	-	1.4500	.29e-01	22	.36e-01	8	.74e-02	21	.85e-03	41	.58e-03	67	0.	99			
1.4500	-	1.4000	.29e-01	19	.26e-01	16	.11e-01	14	.11e-02	45	.29e-03	99	0.	99			
1.4000	-	1.3500	.29e-01	20	.27e-01	10	.12e-01	10	.28e-02	26	.29e-03	99	0.	99			
1.3500	-	1.3000	.20e-01	30	.30e-01	12	.89e-02	16	.28e-02	20	.14e-02	45	0.	99			
1.3000	-	1.2500	.30e-01	31	.28e-01	9	.12e-01	12	.42e-02	18	.58e-03	67	0.	99			
1.2500	-	1.2000	.18e-01	21	.30e-01	8	.14e-01	12	.19e-02	35	.29e-03	99	0.	99			
1.2000	-	1.1500	.21e-01	17	.33e-01	9	.15e-01	13	.34e-02	17	.29e-03	99	0.	99			
1.1500	-	1.1000	.18e-01	18	.30e-01	8	.18e-01	10	.40e-02	30	.29e-03	99	0.	99			
1.1000	-	1.0500	.13e-01	20	.30e-01	11	.19e-01	9	.59e-02	17	.14e-02	61	.78e-03	99			
1.0500	-	1.0000	.21e-01	23	.24e-01	9	.19e-01	10	.53e-02	15	.87e-03	71	0.	99			
1.0000	-	.9500	.21e-01	14	.23e-01	13	.17e-01	7	.59e-02	22	.12e-02	55	0.	99			
.9500	-	.9000	.12e-01	20	.23e-01	10	.18e-01	7	.66e-02	13	.12e-02	55	0.	99			
.9000	-	.8500	.13e-01	21	.21e-01	12	.19e-01	10	.68e-02	15	.14e-02	45	.24e-02	51			
.8500	-	.8000	.10e-01	28	.20e-01	15	.21e-01	12	.10e-01	11	.35e-02	24	.79e-03	99			
.8000	-	.7500	.10e-01	26	.18e-01	12	.15e-01	6	.91e-02	13	.26e-02	26	0.	99			
.7500	-	.7000	.12e-01	20	.18e-01	13	.17e-01	9	.70e-02	18	.29e-02	33	.24e-02	71			
.7000	-	.6500	.78e-02	30	.20e-01	12	.18e-01	12	.12e-01	8	.43e-02	29	0.	99			
.6500	-	.6000	.66e-02	48	.20e-01	10	.17e-01	10	.85e-02	10	.32e-02	29	.16e-02	67			

```
;41
542    .6000 -   .5500   .95e-02 84  .18e-01 11  .16e-01  9  .79e-02 15  .49e-02 20 0.        99
543    .5500 -   .5000   .11e-01 24  .15e-01 14  .16e-01 12  .93e-02 16  .46e-02 33  .24e-02 51
544    .5000 -   .4500   .40e-02 33  .14e-01 15  .17e-01 15  .10e-01 12  .41e-02 40  .16e-02 67
545    .4500 -   .4000   .40e-02 45  .10e-01 12  .13e-01 10  .11e-01 13  .70e-02 19  .24e-02 51
546    .4000 -   .3500   .24e-02 71  .84e-02 16  .12e-01 10  .98e-02 10  .43e-02 33  .79e-03 99
547    .3500 -   .3000   .32e-02 55  .10e-01 11  .91e-02 16  .93e-02 13  .46e-02 25  .79e-03 99
548    .3000 -   .2500   .48e-02 51  .49e-02 30  .10e-01 13  .66e-02 23  .38e-02 20  .79e-03 99
549    .2500 -   .2000   .71e-02 26  .52e-02 25  .85e-02 14  .81e-02 13  .17e-02 37 0.        99
550    .2000 -   .1500   .32e-02 41  .43e-02 27  .81e-02 12  .76e-02 26  .41e-02 30  .79e-03 99
551    .1500 -   .1000   .79e-03 99  .32e-02 29  .40e-02 17  .38e-02 14  .32e-02 25  .24e-02 51
552    .1000 -   .0500   0.        99  .41e-02 30  .38e-02 16  .30e-02 32  .23e-02 31 0.        99
553    .0500 -   .0100   0.        99  .72e-03 99  .11e-02 55  .21e-02 25  .22e-02 44 0.        99
554 ●
555 ●                                    energy spectra of transmitted photons
556                                   (number/mev, normalized to one incident particle)
557 ●      e (mev)  length=      2.5400
558
559    2.0000 -  1.9500  0.        99
560    1.9500 -  1.9000  0.        99
561    1.9000 -  1.8500  0.        99
562    1.8500 -  1.8000  0.        99
563    1.8000 -  1.7500  0.        99
564    1.7500 -  1.7000  0.        99
565    1.8000 -  1.6500  0.        99
566    1.6500 -  1.6000  0.        99
567    1.6000 -  1.5500  0.        99
568    1.5500 -  1.5000   .52e-03 99
569    1.5000 -  1.4500  0.        99
570    1.4500 -  1.4000  0.        99
571    1.4000 -  1.3500   .10e-02 67
572    1.3500 -  1.3000  0.        99
573    1.3000 -  1.2500  0.        99
574    1.2500 -  1.2000   .47e-03 99
575    1.2000 -  1.1500   .50e-03 99
576    1.1500 -  1.1000  0.        99
577    1.1000 -  1.0500   .54e-03 99
578    1.0500 -  1.0000   .15e-02 51
579    1.0000 -   .9500   .99e-03 67
580     .9500 -   .9000   .15e-02 51
581     .9000 -   .8500   .48e-03 99
582     .8500 -   .8000   .13e-02 52
583     .8000 -   .7500   .90e-03 67
584     .7500 -   .7000   .24e-02 33
585     .7000 -   .6500   .88e-03 67
586     .6500 -   .6000   .23e-02 45
587     .6000 -   .5500   .90e-03 67
588     .5500 -   .5000   .15e-02 74
589     .5000 -   .4500   .33e-02 45
590     .4500 -   .4000   .27e-02 28
591     .4000 -   .3500   .45e-02 46
592     .3500 -   .3000   .37e-02 26
593     .3000 -   .2500   .62e-02 28
594     .2500 -   .2000   .87e-02 28
595     .2000 -   .1500   .17e-01 17
596     .1500 -   .1000   .15e-01 13
597     .1000 -   .0500   .22e-01 16
598     .0600 -   .0100   .35e-01  9
599 ●
600 ●                                    energy spectra of reflected photons
                                      (number/mev, normalized to one incident particle)
 ●      e (mev)  length=      2.5400
```

601	2.0000 -	1.9500	0.	99
602	1.9500 -	1.9000	0.	99
603	1.9000 -	1.8500	0.	99
604	1.8500 -	1.8000	0.	99
605	1.8000 -	1.7500	0.	99
606	1.7500 -	1.7000	0.	99
607	1.7000 -	1.6500	0.	99
608	1.6500 -	1.6000	0.	99
609	1.6000 -	1.5500	0.	99
610	1.5500 -	1.5000	0.	99
611	1.5000 -	1.4500	0.	99
612	1.4500 -	1.4000	0.	99
613	1.4000 -	1.3500	0.	99
614	1.3500 -	1.3000	0.	99
615	1.3000 -	1.2500	0.	99
616	1.2500 -	1.2000	0.	99
617	1.2000 -	1.1500	0.	99
618	1.1500 -	1.1000	0.	99
619	1.1000 -	1.0500	0.	99
620	1.0500 -	1.0000	0.	99
621	1.0000 -	.9500	0.	99
622	.9500 -	.9000	0.	99
623	.9000 -	.8500	0.	99
624	.8500 -	.8000	0.	99
625	.8000 -	.7500	0.	99
626	.7500 -	.7000	0.	99
627	.7000 -	.6500	0.	99
628	.6500 -	.6000	.64e-03	99
629	.6000 -	.5500	0.	99
630	.5500 -	.5000	.12e-02	67
631	.5000 -	.4500	.13e-02	67
632	.4500 -	.4000	.65e-03	99
633	.4000 -	.3500	.18e-02	51
634	.3500 -	.3000	.19e-02	51
635	.3000 -	.2500	.36e-02	37
636	.2500 -	.2000	.75e-02	31
637	.2000 -	.1500	.12e-01	18
638	.1500 -	.1000	.24e-01	21
639	.1000 -	.0500	.52e-01	10
640	.0500 -	.0100	.11e+00	5

641

642 energy spectra of laterally escaping photons
(number/mev, normalized to one incident particle)

643 0 e (mev) length= 2.5400

644

645	2.0000 -	1.9500	0.	99
646	1.9500 -	1.9000	0.	99
647	1.9000 -	1.8500	0.	99
648	1.8500 -	1.8000	0.	99
649	1.8000 -	1.7500	.58e-03	99
650	1.7500 -	1.7000	0.	99
651	1.7000 -	1.6500	0.	99
652	1.6500 -	1.6000	0.	99
653	1.6000 -	1.5500	0.	99
654	1.5500 -	1.5000	0.	99
655	1.5000 -	1.4500	0.	99
656	1.4500 -	1.4000	0.	99
657	1.4000 -	1.3500	.64e-03	99
658	1.3500 -	1.3000	.66e-03	99
659	1.3000 -	1.2500	.17e-02	51
660	1.2500 -	1.2000	.17e-02	51

```
 1.2000 -  1.1500  0.       99
 1.1500 -  1.1000   .16e-02 51
 1.1000 -  1.0500   .23e-02 55
 1.0500 -  1.0000   .27e-02 54
 1.0000 -   .9500   .44e-02 25
  .9500 -   .9000   .37e-02 67
  .9000 -   .8500   .57e-02 30
  .8500 -   .8000   .76e-02 36
  .8000 -   .7500   .72e-02 22
  .7500 -   .7000   .70e-02 29
  .7000 -   .6500   .77e-02 31
  .6500 -   .6000   .70e-02 40
  .6000 -   .5500   .15e-01 19
  .5500 -   .5000   .15e-01 20
  .5000 -   .4500   .15e-01 11
  .4500 -   .4000   .19e-01 15
  .4000 -   .3500   .25e-01 16
  .3500 -   .3000   .30e-01 15
  .3000 -   .2500   .46e-01 12
  .2500 -   .2000   .66e-01  9
  .2000 -   .1500   .95e-01  6
  .1500 -   .1000   .16e+00  8
  .1000 -   .0500   .29e+00  5
  .0500 -   .0100   .71e+00  3

                    angular distributions of transmitted and reflected photon intensity
                                (mev/sr, normalized to one incident particle)
            phi(deg)=  0.000
    theta (deg)      180.000

  0.0000 - 30.0000   .18e-02  8
 30.0000 - 60.0000   .24e-04 39
 60.0000 - 90.0000   .76e-06 89
 90.0000 -120.0000   .90e-04  9
120.0000 -150.0000   .19e-03 13
150.0000 -180.0000   .16e-03 14

                    angular distributions of laterally escaping photon intensity
                                (mev/sr, normalized to one incident particle)
            phi(deg)=  0.000
    theta (deg)      180.000

  0.0000 - 30.0000   .32e-02  9
 30.0000 - 60.0000   .18e-02  5
 60.0000 - 90.0000   .72e-03  4
 90.0000 -120.0000   .29e-03 12
120.0000 -150.0000   .99e-04 24
150.0000 -180.0000   .37e-04 40

                      energy spectra and angular distributions of photons transmitted and reflected
                                azimuthal interval is   0.00000 to 180.00000 degrees
                                 (number/(mevSsr), normalized to one particle)
     e (mev)  theta= 30.000      90.000      90.000     180.000     180.000     180.000

   2.0000 -  1.9500  0.       99 0.       99 0.       99 0.       99 0.       99 0.       99
   1.9500 -  1.9000  0.       99 0.       99 0.       99 0.       99 0.       99 0.       99
   1.9000 -  1.8500  0.       99 0.       99 0.       99 0.       99 0.       99 0.       99
   1.8500 -  1.8000  0.       99 0.       99 0.       99 0.       99 0.       99 0.       99
   1.8000 -  1.7500  0.       99 0.       99 0.       99 0.       99 0.       99 0.       99
   1.7500 -  1.7000  0.       99 0.       99 0.       99 0.       99 0.       99 0.       99
   1.7000 -  1.6500  0.       99 0.       99 0.       99 0.       99 0.       99 0.       99
   1.6500 -  1.6000  0.       99 0.       99 0.       99 0.       99 0.       99 0.       99
```

```
 721   1.6000 -  1.5500   0.          99 0.          99 0.          99 0.          99 0.          99 0.          99
 722   1.5500 -  1.5000    .68e-03 99 0.          99 0.          99 0.          99 0.          99 0.          99
 723   1.5000 -  1.4500   0.          99 0.          99 0.          99 0.          99 0.          99 0.          99
 724   1.4500 -  1.4000   0.          99 0.          99 0.          99 0.          99 0.          99 0.          99
 725   1.4000 -  1.3500    .12e-02 67 0.          99 0.          99 0.          99 0.          99 0.          99
 726   1.3500 -  1.3000   0.          99 0.          99 0.          99 0.          99 0.          99 0.          99
 727   1.3000 -  1.2500   0.          99 0.          99 0.          99 0.          99 0.          99 0.          99
 728   1.2500 -  1.2000    .56e-03 99 0.          99 0.          99 0.          99 0.          99 0.          99
 729   1.2000 -  1.1500    .60e-03 99 0.          99 0.          99 0.          99 0.          99 0.          99
 730   1.1500 -  1.1000   0.          99 0.          99 0.          99 0.          99 0.          99 0.          99
 731   1.1000 -  1.0500    .64e-03 99 0.          99 0.          99 0.          99 0.          99 0.          99
 732   1.0000 -  1.0000    .12e-02 67 0.          99 0.          99 0.          99 0.          99 0.          99
 734    .9500 -   .9000    .17e-02 51 0.          99 0.          99 0.          99 0.          99 0.          99
 735    .9000 -   .8500    .58e-03 99 0.          99 0.          99 0.          99 0.          99 0.          99
 736    .8500 -   .8000    .15e-02 52 0.          99 0.          99 0.          99 0.          99 0.          99
 737    .8000 -   .7500    .11e-02 67 0.          99 0.          99 0.          99 0.          99 0.          99
 738    .7500 -   .7000    .28e-02 33 0.          99 0.          99 0.          99 0.          99 0.          99
 739    .7000 -   .6500    .10e-02 67 0.          99 0.          99 0.          99 0.          99 0.          99
 740    .6500 -   .6000    .27e-02 45 0.          99 0.          99  .20e-03 99 0.          99 0.          99
 741    .6000 -   .5500    .11e-02 67 0.          99 0.          99 0.          99 0.          99 0.          99
 742    .5500 -   .5000    .00e-02 89 0.28e-03 99 0.          99 0.19e-03 99  .88e-03 89 0.          99
 744    .4500 -   .4000    .25e-02 33  .24e-03 99 0.          99 0.          99  .28e-03 99 0.          99
 745    .4000 -   .3500    .54e-02 46 0.          99 0.          99  .57e-03 51 0.          99 0.          99
 746    .3500 -   .3000    .44e-02 26 0.          99 0.          99 0.          99  .81e-03 51 0.          99
 747    .3000 -   .2500    .73e-02 26 0.          99 0.          99  .59e-03 51  .78e-03 51 0.          99
 748    .2500 -   .2000    .10e-01 28 0.          99 0.          99  .96e-03 62  .15e-02 37  .13e-02 67
 749    .2000 -   .1500    .19e-01 16  .46e-03 68 0.          99  .89e-03 34  .32e-02 32  .22e-02 51
 750    .1500 -   .1000    .18e-01 13 0.          99 0.          99  .23e-02 36  .50e-02 26  .57e-02 35
 751    .1000 -   .0500    .22e-01 15  .14e-02 41  .21e-03 99  .50e-02 24  .11e-01 11  .14e-01 19
 752    .0500 -   .0100    .37e-01  9  .15e-02 29  .47e-04 99  .85e-02 13  .25e-01  8  .34e-01 11
 753 0   integral (/sr)    .71e-02  4  .18e-03 24  .12e-04 84  .88e-03 10  .21e-02  8  .25e-02  8
 754 0                    energy spectra and angular distributions of photons laterally escaping
 755                                 azimuthal interval is   0.00000 to 180.00000 degrees
 756                                 (number/(mev*sr), normalized to one particle)
 757 0     e (mev)  theta= 0.000      30.000      60.000      90.000     120.000     150.000
 758                      30.000      60.000      90.000     120.000     150.000     180.000
 759
 760   2.0000 -  1.9500   0.          99 0.          99 0.          99 0.          99 0.          99 0.          99
 761   1.9500 -  1.9000   0.          99 0.          99 0.          99 0.          99 0.          99 0.          99
 762   1.9000 -  1.8500   0.          99 0.          99 0.          99 0.          99 0.          99 0.          99
 763   1.8500 -  1.8000   0.          99 0.          99 0.          99 0.          99 0.          99 0.          99
 764   1.8000 -  1.7500    .66e-03 99 0.          99 0.          99 0.          99 0.          99 0.          99
 765   1.7500 -  1.7000   0.          99 0.          99 0.          99 0.          99 0.          99 0.          99
 766   1.7000 -  1.6500   0.          99 0.          99 0.          99 0.          99 0.          99 0.          99
 767   1.6500 -  1.6000   0.          99 0.          99 0.          99 0.          99 0.          99 0.          99
 768   1.6000 -  1.5500   0.          99 0.          99 0.          99 0.          99 0.          99 0.          99
 769   1.5500 -  1.5000   0.          99 0.          99 0.          99 0.          99 0.          99 0.          99
 770   1.5000 -  1.4500   0.          99 0.          99 0.          99 0.          99 0.          99 0.          99
 771   1.4500 -  1.4000   0.          99 0.          99 0.          99 0.          99 0.          99 0.          99
 772   1.4000 -  1.3500   0.          99 0.          99  .21e-03 99 0.          99 0.          99 0.          99
 773   1.3500 -  1.3000    .67e-03 99 0.          99 0.          99 0.          99 0.          99 0.          99
 774   1.3000 -  1.2500    .61e-03 99  .48e-03 67 0.          99 0.          99 0.          99 0.          99
 775   1.2500 -  1.2000    .13e-02 67  .26e-03 99 0.          99 0.          99 0.          99 0.          99
 776   1.2000 -  1.1500   0.          99 0.          99 0.          99 0.          99 0.          99 0.          99
 777   1.1500 -  1.1000    .85e-03 99  .48e-03 67 0.          99 0.          99 0.          99 0.          99
 778   1.1000 -  1.0500    .72e-03 99  .73e-03 51 0.          99 0.          99 0.          99 0.          99
 779   1.0500 -  1.0000    .19e-02 51  .48e-03 67 0.          99 0.          99 0.          99 0.          99
 780   1.0000 -   .9500    .38e-02 45  .50e-03 67  .17e-03 99 0.          99 0.          99 0.          99
```

81	.9500 -	.9000	.21e-02	51	.53e-03	99	.21e-03	99	0.	99	0.	99	0.	99				
82	.9000 -	.8500	.14e-02	67	.15e-02	36	.34e-03	67	0.	99	0.	99	0.	99				
83	.8500 -	.8000	.24e-02	56	.13e-02	45	.41e-03	67	.38e-03	99	0.	99	0.	99				
84	.8000 -	.7500	.20e-02	51	.13e-02	34	.58e-03	51	.21e-03	99	0.	99	0.	99				
785	.7500 -	.7000	.41e-02	37	.10e-02	54	.36e-03	67	0.	99	0.	99	0.	99				
786	.7000 -	.6500	.36e-02	46	.99e-03	56	.75e-03	41	0.	99	0.	99	0.	99				
787	.6500 -	.6000	.12e-02	67	.15e-02	37	.61e-03	71	.19e-03	99	0.	99	0.	99				
788	.6000 -	.5500	.46e-02	37	.31e-02	20	.11e-02	36	0.	99	.29e-03	99	0.	99				
789	.5500 -	.5000	.66e-02	35	.26e-02	30	.83e-03	33	.17e-03	99	0.	99	0.	99				
790	.5000 -	.4500	.25e-02	42	.47e-02	17	.77e-03	55	0.	99	0.	99	0.	99				
791	.4500 -	.4000	.86e-02	32	.37e-02	18	.99e-03	44	.21e-03	99	0.	99	0.	99				
792	.4000 -	.3500	.87e-02	17	.34e-02	25	.26e-02	31	.55e-03	71	0.	99	0.	99				
793	.3500 -	.3000	.10e-01	25	.66e-02	19	.12e-02	43	.60e-03	51	.28e-03	99	0.	99				
794	.3000 -	.2500	.84e-02	21	.71e-02	19	.40e-02	22	.21e-02	30	.11e-02	75	.78e-03	99				
795	.2500 -	.2000	.20e-01	20	.96e-02	14	.49e-02	23	.34e-02	19	.73e-03	51	0.	99				
796	.2000 -	.1500	.25e-01	12	.17e-01	10	.74e-02	10	.35e-02	25	.83e-03	71	0.	99				
797	.1500 -	.1000	.35e-01	15	.24e-01	8	.14e-01	12	.72e-02	19	.16e-02	41	.70e-03	99				
798	.1000 -	.0500	.62e-01	8	.44e-01	4	.23e-01	5	.14e-01	19	.76e-02	27	.38e-02	36				
799	.0500 -	.0100	.14e+00	9	.11e+00	5	.62e-01	4	.36e-01	6	.16e-01	16	.46e-02	45				
800	integral (/sr)		.18e-01	4	.11e-01	3	.57e-02	2	.31e-02	6	.13e-02	13	.45e-03	35				

801 the number of ecs words used for statistics is 1317

```
output'tl,60
 3 ! nos. (120e)
 1 0e c t o b e r 1 4 , 1 9 7 6 v e r s i o n
 2 0 nmat  matl
 3      3      3
 4 0 nmat  ntab
 5      1      1
 6 0npair  ntax
 7     25     41
 8 0gamma ray cross section data
 9 0energies (mev)
10  1000.000000  800.000000  600.000000  500.000000  400.000000  300.000000
11   200.000000  150.000000  100.000000   80.000000   60.000000   50.000000
12    40.000000   30.000000   20.000000   15.000000   10.000000    8.000000
13     6.000000    5.000000    4.000000    3.000000    2.000000    1.500000
14     1.000000     .800000     .600000     .500000     .400000     .300000
15      .200000     .150000     .100000     .080000     .060000     .050000
16      .040000     .030000     .020000     .015000     .010000
17 0total attenuation coefficients (cm2/g)
18      .133015     .115792     .097314     .087552     .077436     .067025
19      .056529     .051401     .046420     .044377     .042060     .040625
20      .038802     .036353     .033322     .031958     .030918     .030686
21      .030945     .031565     .032919     .035741     .041882     .047769
22      .058536     .065369     .075103     .082004     .091659     .107638
23      .146661     .205315     .421761     .705562    1.487422    2.456969
24     4.613069   10.492178   33.188213   73.691769  215.150145
25 0ratio of scattering plus pair production to total attenuation coefficients
26      .999999     .999998     .999997     .999996     .999995     .999992
27      .999986     .999979     .999965     .999955     .999936     .999920
28      .999895     .999849     .999747     .999641     .999422     .999249
29      .998956     .998721     .998371     .997787     .996538     .995083
30      .991319     .987487     .978709     .969185     .949887     .903104
31      .762317     .594141     .321116     .201461     .100774     .062778
32      .034460     .015642     .005116     .002345     .000818
33 0ratio of scattering to scattering plus pair production attenuation coefficients
34      .001662     .002382     .003765     .005007     .007046     .010778
35      .018909     .027362     .044314     .056913     .077841     .094684
36      .120290     .163683     .248185     .323842     .453488     .536768
37      .651019     .722340     .802503     .886979     .963836     .991964
38     1.000000
39 0k shell ionization data
40 0binding energy (mev), photoeffect efficiency and fluorescent efficiency
41      .008981     .871336     .392853
42 0k x-ray energies (mev)
43      .008150     .008150     .008150     .008150
44 0k x-ray accumulated relative intensities
45     1.000000    1.000000    1.000000    1.000000
46 0auger electron energies (mev)
47      .008150     .008150     .008150
48 0auger electron accumulated relative intensities
49     1.000000    1.000000    1.000000
50 0 nmat  ntab
51      2      1
52 0npair  ntax
53     25     41
54 0gamma ray cross section data
56 0energies (mev)
56  1000.000000  800.000000  600.000000  500.000000  400.000000  300.000000
57   200.000000  150.000000  100.000000   80.000000   60.000000   50.000000
58    40.000000   30.000000   20.000000   15.000000   10.000000    8.000000
59     6.000000    5.000000    4.000000    3.000000    2.000000    1.500000
60     1.000000     .800000     .600000     .500000     .400000     .300000
```

```
      .200000     .150000     .100000     .080000     .060000     .050000
      .040000     .030000     .020000     .015000     .010000
@total attenuation coefficients (cm2/g)
      .042664     .037443     .031861     .028924     .025899     .022819
      .019793     .018395     .017194     .016805     .016488     .016362
      .028876     .026832     .028898     .030881     .033788     .039888
      .061023     .067886     .077309     .083599     .091601     .102329
      .117953     .129244     .146076     .157139     .177347     .197927
      .240815     .359073     .869633    1.932250    6.538229
@ratio of scattering plus pair production to total attenuation coefficients
    1.000000    1.000000    1.000000    1.000000    1.000000    1.000000
    1.000000     .999999     .999999     .999999     .999998     .999998
     .999997     .999996     .999994     .999993     .999990     .999988
     .999985     .999983     .999979     .999974     .999962     .999947
     .999908     .999868     .999775     .999673     .999458     .998892
     .996690     .992470     .974912     .951171     .888740     .819442
     .694128     .480603     .205262     .094029     .028300
@ratio of scattering to scattering plus pair production attenuation coefficients
     .005449     .007745     .012092     .015937     .022153     .033290
     .056784     .080393     .125794     .158022     .208788     .247184
     .301520     .383491     .513893     .607020     .731386     .793818
     .863227     .899113     .933997     .965506     .990010     .997897
    1.000000
@k shell ionization data
@binding energy (mev), photoeffect efficiency and fluorescent efficiency
     .000687     .831990     .003376
@k x-ray energies (mev)
     .000687     .000687     .000687     .000687
@k x-ray accumulated relative intensities
    1.000000    1.000000    1.000000    1.000000
@auger electron energies (mev)
     .000687     .000687     .000687
@auger electron accumulated relative intensities
    1.000000    1.000000    1.000000
@ nmat  ntab
     3     1
@npair  ntax
    25    41
@gamma ray cross section data
@energies (mev)
 1000.000000  800.000000  600.000000  500.000000  400.000000  300.000000
  200.000000  150.000000  100.000000   80.000000   60.000000   50.000000
   40.000000   30.000000   20.000000   15.000000   10.000000    8.000000
    6.000000    5.000000    4.000000    3.000000    2.000000    1.500000
    1.000000     .800000     .600000     .500000
 .400000      .300000
      .200000     .150000     .100000     .080000     .060000     .050000
      .040000     .030000     .020000     .015000     .010000
@total attenuation coefficients (cm2/g)
      .047459     .040496     .033058     .029154     .025144     .021081
      .017198     .015493     .014218     .013934     .013862     .013935
      .014112     .014480     .015476     .016765     .019512     .021495
      .024631     .027011     .030385     .035532     .044349     .051688
      .063513     .070654     .080456     .086995     .095307     .106425
      .122475     .133783     .149253     .157712     .169540     .178754
      .194556     .232360     .387554     .719226    2.228837
@ratio of scattering plus pair production to total attenuation coefficients
    1.000000    1.000000    1.000000    1.000000    1.000000    1.000000
    1.000000    1.000000    1.000000    1.000000     .999999     .999999
     .999998     .999998     .999998     .999998     .999997     .999997
..
```

```
 21      .996996      .999995      .999994      .999993      .999990      .999986
 22      .999976      .999966      .999942      .999915      .999859      .999710
 23      .999123      .997987      .993163      .986454      .967663      .944418
 24      .894285      .773048      .479415      .262940      .086410
25 0ratio of scattering to scattering plus pair production attenuation coefficients
 26      .005099      .007454      .012130      .016458      .023751      .037489
 27      .068025      .099356      .158345      .198381      .258494      .302099
 28      .361954      .449719      .584721      .675399      .786023      .838082
 29      .894243      .922718      .950047      .974365      .992814      .998465
 30     1.000000
31 0k shell ionization data
32 0binding energy (mev), photoeffect efficiency and fluorescent efficiency
 33      .000284      .958303      .000382
34 0k x-ray energies (mev)
 35      .000284      .000284      .000284      .000284
36 0k x-ray accumulated relative intensities
 37     1.000000     1.000000     1.000000     1.000000
38 0auger electron energies (mev)
 39      .000284      .000284      .000284
40 0auger electron accumulated relative intensities
 41     1.000000     1.000000     1.000000
42 1number of sets on datapac tape =   3
43 0input from datapac
44
45   333 mev electron beam into bare fx-100 faraday cup33
46 0 nrun  itra  isip  iaga  isub  inal  icyc  ncyc  nmax        emax          emin          rmax        imat
47      1     5     0     1    14     1     1     8    64  3.0000000e+00  1.1718750e-02  2.0655130e+00     1
48
49  dataprep data for datapac set   1    64    33    14   121  2.065513e+00
50 0 nrun  itra  isip  iaga  isub  inal  icyc  ncyc  nmax        emax          emin          rmax        imat
51      2     5     0     1     9     1     1     8    64  3.0000000e+00  1.1718750e-02  1.7789810e+00     2
52
53  dataprep data for datapac set   2    64    33     9   121  1.778981e+00
54 0 nrun  itra  isip  iaga  isub  inal  icyc  ncyc  nmax        emax          emin          rmax        imat
55      3     5     0     1     3     1     1     8    64  3.0000000e+00  1.1718750e-02  1.6970910e+00     1
56
57  dataprep data for datapac set   3    64    33     3   121  1.697091e+00
3689  collision / total de/dx ratios for datapac set   3
160
161  cumulative bremsstrahlung cross sections for datapac set   3
162
163  cumulative bremsstrahlung angular distributions for datapac set   3
164
165  langauss - equiprobable endpoints for interpolation
166
167  k x-ray production for datapac set   3
168
169  photoelectron angular distributions
170
171  pair electron energy division distribution (lead)
172 1
173 0 nrun   inc istrg  inok  inel iphot  ibad  idos  ipun itape
174      3     1     1     1     2     1     1     1     2     2
175 0 zone  material  left plane  right plane  inner cylinder  outer cylinder    ecut          ptcs
176      1     1     0.           .25400e+01     0.              .14350e-01    .100e-01    0.
177      2     2     0.           .25400e+01      .14350e-01     .84000e-01    .100e-01    0.
178      3     1     0.           .25400e+01      .84000e-01     .11900e+00    .100e-01    0.
179      4     3     0.           .25400e+01      .11900e+00     .75000e+00    .100e-01    0.
180 0incident electrons
```

```
 81 0electron collision and radiation energy loss straggling
 82 0knock-on electron production
 83 0no coupled inelastic scattering deflections
184 0bremsstrahlung and characteristic x-ray quanta followed
185 0bremsstrahlung intrinsic angle of emission from tabulated distribution
188 0photon-produced pair ionization multigroup  iunk  kmax  ibnk kpmax
188       2       1       1      30       1      30       1       6       1       6
189 0 imax  nson iflux  acyc  inran
190  30000     4       2    -1100000000000000000
191 0################ the standard error estimates are based on    10 batches of  3000 histories ################
192 0      tin         tcut        tpcut       cthin       sorcin
193      3.00000       .01000       .01000      1.00000       .74900
194 0################0electron cut-off energy below electron energy list. cut-off energy has been changed to en(nmax)##########
195 ####
196 0      tsave                                 tmfac         rlan        qblk
197        .01225                               10.00000       .50000     1.00000
198 0electron energy classifications (mev)
199      2.90000     2.80000     2.70000     2.60000     2.50000     2.40000
200      2.30000     2.20000     2.10000     2.00000     1.90000     1.80000
201      1.70000     1.60000     1.50000     1.40000     1.30000     1.20000
202      1.10000     1.00000      .90000      .80000      .70000      .60000
203       .50000      .40000      .30000      .20000      .10000      .01225
204 0photon energy classifications (mev)
205      2.90000     2.80000     2.70000     2.60000     2.50000     2.40000
206      2.30000     2.20000     2.10000     2.00000     1.90000     1.80000
207      1.70000     1.60000     1.50000     1.40000     1.30000     1.20000
208      1.10000     1.00000      .90000      .80000      .70000      .60000
209 0electr50000bliquity40000sification30000(degree20000      .10000      .01000
211     30.00000    60.00000    90.00000   120.00000   150.00000   180.00000
212 0electron azimuth classifications (degrees)
213    180.00000
214 0photon obliquity classifications (degrees)
215     30.00000    60.00000    90.00000   120.00000   150.00000   180.00000
216 0photon azimuth classifications (degrees)
217    180.00000
218 0ntfst        rqmax     scale skale      tcut        tpcut       tfcut       tsave       dlim        bnum        xnum
219 0k x-ray quan80656e+00llowed in material.01225       .01000     0.00000      .01225     1.00000      0.0         0.0
221 0ntfst        rqmax     scale skale      tcut        tpcut       tfcut       tsave       dlim        bnum        xnum
222       1      .17790e+01     1     1      .01225       .91000     0.00000      .01225     1.00000      0.0         0.0
223 0k x-ray quanta not followed in material     2
224 0ntfst        rqmax     scale skale      tcut        tpcut       tfcut       tsave       dlim        bnum        xnum
225       1      .16971e+01     1     1      .01225       .01000     0.00000      .01225     1.00000      0.0         0.0
226 0k x-ray quanta not followed in material     3
227 0annihilation quanta followed
228 1the problem is 100  per cent complete.  time to finish is       0.000 seconds. average time per batch is      204.419
229 0average source energy = 3.0000e+00 mev
230 0     inran           ira           irc
231  000000000000000000 1361516456813215 3061637164470405
232 0     ------------------------------------ histories ------------------------------------      rej       --- steps ----
233       prim      sec     knock      p e      pair      com     auger      brem       rad      xray      land      prim       sec
234      30000   333877   332549      841         0      487         0      5733     11950         0     11924   1382170   3492808
235 0                          energy (mev)      ave energy (mev)      number/primary      number generated
236  first knock (above tcut)     4.9781e-01          4.8828e-02           1.0179e+01            305368
237  total knock (above tcut)     5.1993e-01          4.6904e-02           1.1085e+01            332549
238  photo-electron               8.8340e-04          2.0138e-02           4.3867e-02              1316
239  pair                         0.                  0.                   0.                         0
240  compton                      2.0228e-03          4.2159e-02           4.7967e-02              1439
```

```
 241,384
  241  auger                          0.                  0.                  0.                  0
  242  first bremsstrahlung           3.2168e-02          1.0258e-01          3.1360e-01          9408
  243  total bremsstrahlung           3.2644e-02          9.2062e-02          3.9780e-01          11934
  244  k x-ray                        0.                  0.                  0.                  0
  245  annihilation quanta            0.                  0.                  0.                  0
  246 @unscattered primary photons number and energy
  247   0.       99 0.       99
  248 @number coefficients - knock-ons, photon descendents
  249 @
  250   0.       99                                        transmission
  252 00.       99
  253    .34e-02 15                                         reflection
  254   0.       99
  255 @
  256    .93e-02  4                                        lateral escape
  257    .17e-03 33
  258 @
  259 @                                                 number and energy coefficients
  260 @                                                      transmission
  261              cylinder dimensions          ---------- electron ----------      ---------- photon ----------
  262            length(cm)  radius(cm)         number      energy      counts      number      energy      counts
  263
  264 @            .254e+01    .750e+00  0.       99 0.       99           0   .15e-01  3  .18e-02  6       1054
  265 @                                                      reflection
  266              cylinder dimensions          ---------- electron ----------      ---------- photon ----------
  267            length(cm)  radius(cm)         number      energy      counts      number      energy      counts
  268
  269 @            .254e+01    .750e+00   .12e-01  8  .33e-02  8         357   .10e-01  5  .37e-03 15        487
  270 @                                                   lateral escape
  271              cylinder dimensions          ---------- electron ----------      ---------- photon ----------
  272            length(cm)  radius(cm)         number      energy      counts      number      energy      counts
  273
  274 1            .254e+01    .750e+00   .34e+00  1  .16e+00  1       10109   .12e+00  1  .76e-02  3       5557
  275                                                 energy deposition
  276 @                                      (normalized to one incident particle)
  277       zone      material     mass(gm)   volume(cc)                                  energy deposition (mev)
  278 tal                                                          prim          knock          g-sec          to
  279
  280          1
  281 072e-02  6         1        .1471e-01      .1643e-02                    .2085e-02  6  -.3671e-04 99   .2415e-04 52   .2
  282          2
  283 587e-01  2         2        .1584e+00      .6886e-01                    .3522e-01  2  -.2080e-03 63   .6222e-04 34   .3
  284          3
  285 024e-01  2         1        .3883e+00      .4249e-01                    .5941e-01  2   .1751e-03 94   .6613e-03  5   .6
  286          4
  287 386e+01  0         3        .8314e+01      .4376e+01                    .2387e+01  0  -.3417e-02  8   .2250e-02  8   .2
  288 @
  289 484e+01  0                                                  total        .2484e+01  0  -.3486e-02  5   .2998e-02  7   .2
  290 @
  291                                                  charge distribution
  292 @                                      (normalized to one incident particle)
  293       zone      material     zl         zr          rl          r0          electrons
  294                                                                            prim          knock          g-sec          total
  295          1         1      0.          .254e+01    0.          .144e-01    .97e-03 17   .33e-04 99 0.          99   .10e-02 2
  296 3
  297          2         2      0.          .254e+01     .144e-01   .940e-01    .12e-01  5  -.53e-03 58   .10e-03 51   .11e-01
  298 7
  299          3         1      0.          .254e+01     .940e-01   .119e+00    .28e-01  3   .17e-03 99  -.13e-03 55   .28e-01
  300 2
```

```
 4       3    0.          .254e+01   .119e+00   .750e+00   .62e+00  1 -.13e-01  4 -.13e-03 41  .61e+00

                                      total                          .66e+00  1 -.13e-01  3 -.17e-03 33  .65e+00

                                  energy spectra of transmitted electrons
                              (number/mev, normalized to one incident particle)

     e (mev)  length=      2.5400

   3.0000 -  2.9000  0.       99
   2.9000 -  2.8000  0.       99
   2.8000 -  2.7000  0.       99
   2.7000 -  2.6000  0.       99
   2.6000 -  2.5000  0.       99
   2.5000 -  2.4000  0.       99
   2.4000 -  2.3000  0.       99
   2.3000 -  2.2000  0.       99
   2.2000 -  2.1000  0.       99
   2.1000 -  2.0000  0.       99
   2.0000 -  1.9000  0.       99
   1.9000 -  1.8000  0.       99
   1.8000 -  1.7000  0.       99
   1.7000 -  1.6000  0.       99
   1.6000 -  1.5000  0.       99
   1.5000 -  1.4000  0.       99
   1.4000 -  1.3000  0.       99
   1.3000 -  1.2000  0.       99
   1.2000 -  1.1000  0.       99
   1.1000 -  1.0000  0.       99
   1.0000 -   .9000  0.       99
    .9000 -   .8000  0.       99
    .8000 -   .7000  0.       99
    .7000 -   .6000  0.       99
    .6000 -   .5000  0.       99
    .5000 -   .4000  0.       99
    .4000 -   .3000  0.       99
    .3000 -   .2000  0.       99
    .2000 -   .1000  0.       99
    .1000 -   .0122  0.       99

                                  energy spectra of reflected electrons
                              (number/mev, normalized to one incident particle)

     e (mev)  length=      2.5400

   3.0000 -  2.9000   .33e-03 98
   2.9000 -  2.8000   .67e-03 67
   2.8000 -  2.7000   .10e-02 71
   2.7000 -  2.6000   .33e-03 99
   2.6000 -  2.5000   .33e-03 99
   2.5000 -  2.4000   .20e-02 51
   2.4000 -  2.3000   .17e-02 45
   2.3000 -  2.2000   .33e-03 98
   2.2000 -  2.1000   .17e-02 45
   2.1000 -  2.0000   .67e-03 67
   2.0000 -  1.9000   .17e-02 45
   1.9000 -  1.8000   .23e-02 48
   1.8000 -  1.7000   .20e-02 37
   1.7000 -  1.6000   .47e-02 29
   1.6000 -  1.5000   .30e-02 39
   1.5000 -  1.4000   .37e-02 29
   1.4000 -  1.3000   .33e-02 30
   1.3000 -  1.2000   .37e-02 38
```

```
 1.2000 <  1.1000   .47e-02 22
 1.1000 -  1.0000   .43e-02 30
 1.0000 -   .9000   .47e-02 22
  .9000 -   .8000   .50e-02 15
  .8000 -   .7000   .50e-02 32
  .7000 -   .6000   .53e-02 23
  .6000 -   .5000   .67e-02 15
  .5000 -   .4000   .67e-02 31
  .4000 -   .3000   .53e-02 17
  .3000 -   .2000   .70e-02 18
  .2000 -   .1000   .93e-02 19
  .1000 -   .0122   .25e-01 18

                                  energy spectra of laterally escaping electrons
                                (number/ev, normalized to one incident particle)
0       e (ev)  length=      2.5400

  3.0000 -  2.9000   .37e-02 25
  2.9000 -  2.8000   .46e-01 10
  2.8000 -  2.7000   .60e-01  5
  2.7000 -  2.6000   .78e-01  6
  2.6000 -  2.5000   .87e-01  5
  2.5000 -  2.4000   .99e-01  7
  2.4000 -  2.3000   .98e-01  4
  2.3000 -  2.2000   .11e+00  5
  2.2000 -  2.1000   .11e+00  5
  2.1000 -  2.0000   .13e+00  5
  2.0000 -  1.9000   .13e+00  6
  1.9000 -  1.8000   .14e+00  6
  1.8000 -  1.7000   .14e+00  6
  1.7000 -  1.6000   .16e+00  5
  1.6000 -  1.5000   .15e+00  4
  1.5000 -  1.4000   .15e+00  5
  1.4000 -  1.3000   .15e+00  5
  1.3000 -  1.2000   .15e+00  5
  1.2000 -  1.1000   .16e+00  3
  1.1000 -  1.0000   .15e+00  5
  1.0000 -   .9000   .16e+00  3
   .9000 -   .8000   .14e+00  4
   .8000 -   .7000   .14e+00  3
   .7000 -   .6000   .13e+00  6
   .6000 -   .5000   .12e+00  5
   .5000 -   .4000   .11e+00  6
   .4000 -   .3000   .10e+00  5
   .3000 -   .2000   .88e-01  4
   .2000 -   .1000   .66e-01  9
   .1000 -   .0122   .40e-01 10

                                angular distributions of transmitted and reflected electrons
                                    (number/sr, normalized to one incident particle)
0                 phi(deg)=  0.000
     theta (deg)       180.000

   0.0000 - 30.0000  0.        99
  30.0000 - 60.0000  0.        99
  60.0000 - 90.0000  0.        99
  90.0000 -120.0000   .90e-03 12
 120.0000 -150.0000   .27e-02  9
 150.0000 -180.0000   .35e-02 13

                                  angular distributions of laterally escaping electrons
                                    (number/sr, normalized to one incident particle)
0                 phi(deg)=  0.000
```

```
 theta (deg)      180.000

  0.0000 - 30.0000   .77e-01  2
 30.0000 - 60.0000   .56e-01  2
 60.0000 - 90.0000   .29e-01  2
 90.0000 -120.0000   .13e-01  2
120.0000 -150.0000   .46e-02  7

                    energy spectra and angular distributions of electrons transmitted and reflected
                                azimuthal interval is   0.00000 to 180.00000 degrees
                                 (number/(mev*sr), normalized to one particle)

     e (mev)  theta=  0.000      30.000      60.000      90.000     120.000     150.000
                     30.000      60.000      90.000     120.000     150.000     180.000

  3.0000 -  2.9000  0.       99 0.       99 0.       99 0.       99  .14e-03 99 0.       99
  2.9000 -  2.8000  0.       99 0.       99 0.       99 0.       99  .29e-03 67 0.       99
  2.8000 -  2.7000  0.       99 0.       99 0.       99  .21e-03 67 0.       99  .40e-03 99
  2.7000 -  2.6000  0.       99 0.       99 0.       99  .11e-03 99 0.       98 0.       99
  2.6000 -  2.5000  0.       99 0.       99 0.       99 0.       99  .14e-03 99 0.       99
  2.5000 -  2.4000  0.       99 0.       99 0.       99  .42e-03 41  .29e-03 99 0.       99
  2.4000 -  2.3000  0.       99 0.       99 0.       99  .32e-03 51  .29e-03 67 0.       99
  2.3000 -  2.2000  0.       99 0.       99 0.       99  .11e-03 99 0.       99 0.       99
  2.2000 -  2.1000  0.       99 0.       99 0.       99  .11e-03 99  .43e-03 51  .40e-03 99
  2.1000 -  2.0000  0.       99 0.       99 0.       99  .11e-03 99 0.       98  .40e-03 99
  2.0000 -  1.9000  0.       99 0.       99 0.       99 0.       99  .58e-03 55  .40e-03 99
  1.9000 -  1.8000  0.       99 0.       99 0.       99  .21e-03 99  .58e-03 41  .40e-03 99
  1.8000 -  1.7000  0.       99 0.       99 0.       99  .21e-03 99  .58e-03 41 0.       99
  1.7000 -  1.6000  0.       99 0.       99 0.       99  .53e-03 33  .72e-03 45  .16e-02 55
  1.6000 -  1.5000  0.       99 0.       99 0.       99  .11e-03 99  .10e-02 48  .40e-03 99
  1.5000 -  1.4000  0.       99 0.       99 0.       99  .64e-03 37  .58e-03 41  .40e-03 99
  1.4000 -  1.3000  0.       99 0.       99 0.       99  .53e-03 45  .58e-03 55  .40e-03 99
  1.3000 -  1.2000  0.       99 0.       99 0.       99  .32e-03 51  .58e-03 41  .16e-02 41
  1.2000 -  1.1000  0.       99 0.       99 0.       99  .42e-03 41  .43e-03 51  .28e-02 30
  1.1000 -  1.0000  0.       99 0.       99 0.       99  .11e-03 99  .13e-02 35  .12e-02 51
  1.0000 -   .9000  0.       99 0.       99 0.       99  .42e-03 55  .10e-02 30  .12e-02 51
   .9000 -   .8000  0.       99 0.       99 0.       99  .21e-03 67  .12e-02 25  .20e-02 33
   .8000 -   .7000  0.       99 0.       99 0.       99  .32e-03 51  .13e-02 39  .12e-02 51
   .7000 -   .6000  0.       99 0.       99 0.       99  .11e-03 99  .12e-02 25  .28e-02 43
   .6000 -   .5000  0.       99 0.       99 0.       99  .53e-03 33  .12e-02 17  .28e-02 52
   .5000 -   .4000  0.       99 0.       99 0.       99  .53e-03 45  .14e-02 33  .20e-02 33
   .4000 -   .3000  0.       99 0.       99 0.       99  .21e-03 67  .16e-02 25  .12e-02 51
   .3000 -   .2000  0.       99 0.       99 0.       99  .42e-03 55  .16e-02 37  .24e-02 37
   .2000 -   .1000  0.       99 0.       99 0.       99  .64e-03 37  .26e-02 25  .16e-02 41
   .1000 -   .0122  0.       99 0.       99 0.       99  .13e-02 34  .58e-02 26  .86e-02 18

                    energy spectra and angular distributions of electrons laterally escaping
                                azimuthal interval is   0.00000 to 180.00000 degrees
                                 (number/(mev*sr), normalized to one particle)

     e (mev)  theta=  0.000      30.000      60.000      90.000     120.000     150.000
                     30.000      60.000      90.000     120.000     150.000     180.000

  3.0000 -  2.9000   .40e-02 26  .14e-03 99 0.       99 0.       99 0.       99 0.       99
  2.9000 -  2.8000   .50e-01 10  .13e-02 38  .32e-03 71 0.       99 0.       99 0.       99
  2.8000 -  2.7000   .57e-01  7  .48e-02 23  .53e-03 33 0.       99 0.       99 0.       99
  2.7000 -  2.6000   .64e-01  7  .96e-02 13  .64e-03 37 0.       99 0.       98 0.       99
  2.6000 -  2.5000   .61e-01  8  .14e-01  9  .85e-03 41  .32e-03 51 0.       99 0.       99
  2.5000 -  2.4000   .63e-01  6  .18e-01 13  .14e-02 38  .42e-03 41 0.       99 0.       99
  2.4000 -  2.3000   .53e-01  7  .20e-01 10  .21e-02 22  .21e-03 67  .28e-03 67 0.       99
  2.3000 -  2.2000   .42e-01  9  .26e-01  7  .41e-02 15  .32e-03 51 0.       99 0.       99
  2.2000 -  2.1000   .38e-01  9  .28e-01  6  .49e-02  8  .42e-03 55  .29e-03 67 0.       99
  2.1000 -  2.0000   .47e-01 11  .30e-01  6  .66e-02 12  .74e-03 57  .14e-03 99 0.       99
```

```
 81    2.0000 -  1.9000   .41e-01  9  .58e-01  7  .68e-02 13  .18e-02 23  .14e-03 99 0.       99
 82    1.9000 -  1.8000   .32e-01 11  .33e-01  8  .86e-02 13  .16e-02 20  .29e-03 67 0.       99
 83    1.8000 -  1.7000   .31e-01 10  .31e-01 12  .11e-01  8  .17e-02 21 0.
 84 0.      99
 84    1.7000 -  1.6000   .30e-01  8  .34e-01  6  .14e-01  9  .22e-02 21 0.       99 0.       99
 85    1.6000 -  1.5000   .22e-01 13  .31e-01  8  .16e-01  9  .24e-02 23  .10e-02 37  .40e-03 99
 86    1.5000 -  1.4000   .21e-01 12  .30e-01  7  .17e-01  8  .32e-02 22  .58e-03 41 0.       99
 87    1.4000 -  1.3000   .17e-01 12  .29e-01  6  .16e-01 10  .56e-02 12  .10e-02 48 0.       99
 88    1.3000 -  1.2000   .18e-01 21  .25e-01  8  .16e-01  7  .71e-02 13  .12e-02 25 0.       99
 89    1.2000 -  1.1000   .15e-01 17  .28e-01  6  .20e-01  6  .64e-02 12  .14e-02 26 0.       99
 90    1.1000 -  1.0000   .12e-01 16  .23e-01  5  .17e-01  7  .85e-02 13  .16e-02 29 0.       99
 91    1.0000 -   .9000   .12e-01 23  .21e-01  5  .20e-01  8  .98e-02  9  .36e-02 16 0.       99
 92     .9000 -   .8000   .11e-01 17  .17e-01 10  .16e-01  7  .99e-02 11  .26e-02 25  .40e-03 99
 93     .8000 -   .7000   .83e-02 18  .14e-01  8  .16e-01  8  .11e-01 12  .43e-02 19  .79e-03 67
 94     .7000 -   .6000   .75e-02 25  .12e-01 14  .16e-01  5  .10e-01 14  .38e-02 12  .12e-02 51
 95     .6000 -   .5000   .44e-02 37  .13e-01  9  .13e-01  9  .90e-02 13  .48e-02 13  .79e-03 67
 96     .5000 -   .4000   .44e-02 34  .13e-01 11  .13e-01 10  .84e-02 11  .39e-02 15  .79e-03 67
 97     .4000 -   .3000   .55e-02 28  .10e-01 12  .12e-01 11  .64e-02 14  .62e-02 17  .40e-03 99
 98     .3000 -   .2000   .16e-02 55  .67e-02 15  .92e-02 10  .94e-02  6  .45e-02  9  .28e-02 48
 99     .2000 -   .1000   .24e-02 37  .67e-02 25  .71e-02 14  .58e-02 14  .29e-02 28  .12e-02 51
100     .1000 -   .0122   .90e-03 67  .20e-02 44  .48e-02 15  .48e-02 13  .17e-02 33  .90e-03 67
101 0                                          energy spectra of transmitted photons
102                                          (number/mev, normalized to one incident particle)
103 0      e (mev)  length=      2.5400
104
105     3.0000 -  2.9000  0.       99
106     2.9000 -  2.8000  0.       99
107     2.8000 -  2.7000  0.       99
108     2.7000 -  2.6000   .28e-03 99
109     2.6000 -  2.5000  0.       99
110     2.5000 -  2.4000  0.       99
111     2.4000 -  2.3000   .27e-03 99
112     2.3000 -  2.2000   .28e-03 99
113     2.2000 -  2.1000  0.       99
114     2.1000 -  2.0000   .27e-03 99
115     2.0000 -  1.9000   .54e-03 67
116     1.9000 -  1.8000   .80e-03 51
117     1.8000 -  1.7000   .27e-03 99
118     1.7000 -  1.6000   .11e-02 55
119     1.6000 -  1.5000   .18e-02 48
120     1.5000 -  1.4000   .78e-03 51
121     1.4000 -  1.3000   .10e-02 41
122     1.3000 -  1.2000   .76e-03 51
123     1.2000 -  1.1000   .21e-02 31
124     1.1000 -  1.0000   .29e-02 25
125     1.0000 -   .9000   .32e-02 24
126      .9000 -   .8000   .36e-02 37
127      .8000 -   .7000   .34e-02 48
128      .7000 -   .6000   .44e-02 22
129      .6000 -   .5000   .62e-02 14
130      .5000 -   .4000   .82e-02 18
131      .4000 -   .3000   .12e-01 15
132      .3000 -   .2000   .18e-01  8
133      .2000 -   .1000   .29e-01  8
134      .1000 -   .0100   .58e-01  5
135 0                                          energy spectra of reflected photons
136                                          (number/mev, normalized to one incident particle)
137 0      e (mev)  length=      2.5400
138
139     2.0000 -  2.0000  0.       99
140     2.0000 -  2.0000  0.       99
```

541	2.8000 - 2.7000	0.		99
542	2.7000 - 2.6000	0.		99
543	2.6000 - 2.5000	0.		99
544	2.5000 - 2.4000	0.		99
545	2.4000 - 2.3000	0.		99
546	2.3000 - 2.2000	0.		99
547	2.2000 - 2.1000	0.		99
548	2.1000 - 2.0000	0.		99
549	2.0000 - 1.9000	0.		99
550	1.9000 - 1.8000	0.		99
551	1.8000 - 1.7000	0.		99
552	1.7000 - 1.6000	0.		99
553	1.6000 - 1.5000	0.		99
554	1.5000 - 1.4000	0.		99
555	1.4000 - 1.3000	0.		99
556	1.3000 - 1.2000	0.		99
557	1.2000 - 1.1000	.30e-03		99
558	1.1000 - 1.0000	.63e-03		67
559	1.0000 - .9000	.31e-03		99
560	.9000 - .8000	.32e-03		99
561	.8000 - .7000	.93e-03		72
562	.7000 - .6000	.29e-03		99
563	.6000 - .5000	.29e-03		99
564	.5000 - .4000	.18e-02		36
565	.4000 - .3000	.23e-02		37
566	.3000 - .2000	.55e-02		33
567	.2000 - .1000	.19e-01		9
568	.1000 - .0100	.75e-01		7
569				
570			energy spectra of laterally escaping photons	
571	e (mev) length=		(number/mev, normalized to one incident particle) 2.5400	
572				
573	3.0000 - 2.9000	0.		99
574	2.9000 - 2.8000	0.		99
575	2.8000 - 2.7000	0.		99
576	2.7000 - 2.6000	0.		99
577	2.6000 - 2.5000	.31e-03		99
578	2.5000 - 2.4000	0.		99
579	2.4000 - 2.3000	0.		99
580	2.3000 - 2.2000	.12e-02		77
581	2.2000 - 2.1000	.93e-03		51
582	2.1000 - 2.0000	.33e-03		99
583	2.0000 - 1.9000	.12e-02		57
584	1.9000 - 1.8000	.93e-03		51
585	1.8000 - 1.7000	.63e-03		67
586	1.7000 - 1.6000	.20e-02		37
587	1.6000 - 1.5000	.29e-02		21
588	1.5000 - 1.4000	.11e-02		41
589	1.4000 - 1.3000	.66e-02		15
590	1.3000 - 1.2000	.35e-02		40
591	1.2000 - 1.1000	.76e-02		19
592	1.1000 - 1.0000	.81e-02		19
593	1.0000 - .9000	.75e-02		22
594	.9000 - .8000	.11e-01		16
595	.8000 - .7000	.17e-01		17
596	.7000 - .6000	.20e-01		9
597	.6000 - .5000	.25e-01		13
598	.5000 - .4000	.30e-01		9
599	.4000 - .3000	.58e-01		10
600	.3000 - .2000	.86e-01		5

```
601     .80+0 -    1000    .21e+00  3
602     .10+0 -    .0100   .77e+00  1
603                          angular distributions of transmitted and reflected photon intensity
604                                (mev/sr, normalized to one incident particle)
605 ●            phi(deg)=  0.000
606      theta (deg)       180.000
607
608    0.0000 - 30.0000    .60e-02  6
609   30.0000 - 60.0000    .12e-03 32
610   60.0000 - 90.0000    .69e-05 49
611   90.0000 -120.0000    .10e-03 32
612  120.0000 -150.0000    .23e-03 13
613  150.0000 -180.0000    .30e-03 12
614                          angular distributions of laterally escaping photon intensity
615                                (mev/sr, normalized to one incident particle)
616 ●            phi(deg)=  0.000
617      theta (deg)       180.000
618
619    0.0000 - 30.0000    .89e-02  6
620   30.0000 - 60.0000    .38e-02  4
621   60.0000 - 90.0000    .14e-02  7
622   90.0000 -120.0000    .53e-03  6
623  120.0000 -150.0000    .19e-03 11
624  150.0000 -180.0000    .32e-04 23
625 ●                        energy spectra and angular distributions of photons transmitted and reflected
626                             azimuthal interval is   0.00000 to 180.00000 degrees
627                              (number/(mev*sr), normalized to one particle)
628 ●      e (mev)  theta=  0.000      30.000      60.000      90.000     120.000     150.000
629                        30.000      60.000      90.000     120.000     150.000     180.000
630
631    3.0000 -  2.9000  0.       99 0.       99 0.       99 0.       99 0.       99 0.       99
632    2.9000 -  2.8000  0.       99 0.       99 0.       99 0.       99 0.       99 0.       99
633    2.8000 -  2.7000  0.       99 0.       99 0.       99 0.       99 0.       99 0.       99
634    2.7000 -  2.6000  .33e-03  99 0.       99 0.       99 0.       99 0.       99 0.       99
635    2.6000 -  2.5000  0.       99 0.       99 0.       99 0.       99 0.       99 0.       99
636    2.5000 -  2.4000  0.       99 0.       99 0.       99 0.       99 0.       99 0.       99
637    2.4000 -  2.3000  .33e-03  99 0.       99 0.       99 0.       99 0.       99 0.       99
638    2.3000 -  2.2000  .33e-03  99 0.       99 0.       99 0.       99 0.       99 0.       99
639    2.2000 -  2.1000  0.       99 0.       99 0.       99 0.       99 0.       99 0.       99
640    2.1000 -  2.0000  .32e-03  99 0.       99 0.       99 0.       99 0.       99 0.       99
641    2.0000 -  1.9000  .64e-03  67 0.       99 0.       99 0.       99 0.       99 0.       99
642    1.9000 -  1.8000  .95e-03  51 0.       99 0.       99 0.       99 0.       99 0.       99
643    1.8000 -  1.7000  .32e-03  99 0.       99 0.       99 0.       99 0.       99 0.       99
644    1.7000 -  1.6000  .13e-02  55 0.       99 0.       99 0.       99 0.       99 0.       99
645    1.6000 -  1.5000  .22e-02  48 0.       99 0.       99 0.       99 0.       99 0.       99
646    1.5000 -  1.4000  .92e-03  51 0.       99 0.       99 0.       99 0.       99 0.       99
647    1.4000 -  1.3000  .12e-02  41 0.       99 0.       99 0.       99 0.       99 0.       99
648    1.3000 -  1.2000  .91e-03  51 0.       99 0.       99 0.       99 0.       99 0.       99
649    1.2000 -  1.1000  .21e-02  37  .13e-03 99 0.       99 0.       99  .13e-03 99 0.       99
650    1.1000 -  1.0000  .35e-02  25 0.       99 0.       99 0.       99  .27e-03 67 0.       99
651    1.0000 -   .9000  .35e-02  25  .11e-03 99 0.       99  .97e-04 99 0.       99 0.       99
652     .9000 -   .8000  .40e-02  37  .12e-03 99 0.       99  .10e-03 99 0.       99 0.       99
653     .8000 -   .7000  .33e-02  42  .26e-03 99 0.       99  .30e-03 72 0.       99 0.       99
654     .7000 -   .6000  .52e-02  22 0.       99 0.       99  .92e-04 99 0.       99 0.       99
655     .6000 -   .5000  .74e-02  14 0.       99 0.       99  .93e-04 99 0.       99 0.       99
656     .5000 -   .4000  .91e-02  15  .22e-03 69 0.       99  .95e-04 99  .48e-03 51  .64e-03 67
657     .4000 -   .3000  .13e-01  16  .44e-03 56 0.       99  .37e-03 56  .37e-03 51  .36e-03 99
658     .3000 -   .2000  .18e-01   9  .74e-03 37  .93e-04 99  .53e-03 56  .13e-02 29  .97e-03 52
659     .2000 -   .1000  .31e-01   6  .81e-03 40  .17e-03 68  .81e-03 29  .48e-02  9  .91e-02 19
660     .1000 -   .0100  .83e-01   5  .14e-02 26  .42e-03 41  .33e-02 14  .17e-01  9  .29e-01  9
```

```
 0    integral (/sr)   .17e-01  4  .41e-03 19  .64e-04 36  .55e-03 17  .22e-02  9  .37e-02  5
 0                          energy spectra and angular distributions of photons laterally escaping
                                 azimuthal interval is   0.00000 to 180.00000 degrees
                                  (number/(mev*sr), normalized to one particle)
 0      e (mev)  theta=  0.000      30.000      60.000      90.000     120.000     150.000
                        30.000      60.000      90.000     120.000     150.000     180.000

    3.0000 -  2.9000  0.        99 0.        99 0.        99 0.        99 0.        99 0.        99
    2.9000 -  2.8000  0.        99 0.        99 0.        99 0.        99 0.        99 0.        99
    2.8000 -  2.7000  0.        99 0.        99 0.        99 0.        99 0.        99 0.        99
    2.7000 -  2.6000  0.        99 0.        99 0.        99 0.        99 0.        99 0.        99
    2.6000 -  2.5000   .37e-03  99 0.        99 0.        99 0.        99 0.        99 0.        99
    2.5000 -  2.4000  0.        99 0.        99 0.        99 0.        99 0.        99 0.        99
    2.4000 -  2.3000  0.        99 0.        99 0.        99 0.        99 0.        99 0.        99
    2.3000 -  2.2000   .10e-02  71  .13e-03  99 0.        99 0.        99 0.        99 0.        99
    2.2000 -  2.1000   .11e-02  51 0.        99 0.        99 0.        99 0.        99 0.        99
    2.1000 -  2.0000  0.        99  .14e-03  99 0.        99 0.        99 0.        99 0.        99
    2.0000 -  1.9000   .32e-03  99  .26e-03  67  .10e-03  99 0.        99 0.        99 0.        99
    1.9000 -  1.8000   .75e-03  67  .13e-03  99 0.        99 0.        99 0.        99 0.        99
    1.8000 -  1.7000   .36e-03  99 0.        99 0.        99  .11e-03  99 0.        99 0.        99
    1.7000 -  1.6000   .14e-02  41  .25e-03  67  .92e-04  99 0.        99 0.        99 0.        99
    1.6000 -  1.5000   .31e-02  26  .13e-03  99 0.        99 0.        99 0.        99 0.        99
    1.5000 -  1.4000  0.        99  .49e-03  41 0.        99 0.        99 0.        99 0.        99
    1.4000 -  1.3000   .25e-02  22  .17e-02  23  .20e-03  67 0.        99 0.        99 0.        99
    1.3000 -  1.2000   .20e-02  50  .41e-03  70  .29e-03  51 0.        99 0.        99 0.        99
    1.2000 -  1.1000   .53e-02  29  .13e-02  25  .10e-03  99 0.        99 0.        99 0.        99
    1.1000 -  1.0000   .24e-02  22  .17e-02  23  .58e-03  45  .99e-04  99 0.        99 0.        99
    1.0000 -   .9000   .29e-02  46  .18e-02  16  .19e-03  67  .10e-03  99 0.        99 0.        99
     .9000 -   .8000   .56e-02  30  .14e-02  21  .86e-03  25  .94e-04  99 0.        99 0.        99
     .8000 -   .7000   .85e-02  20  .31e-02  26  .49e-03  33  .19e-03  67  .14e-03  99 0.        99
     .7000 -   .6000   .79e-02  17  .41e-02   9  .12e-02  33  .18e-03  67 0.        99 0.        99
     .6000 -   .5000   .10e-01  14  .38e-02  19  .21e-02  24  .30e-03  51  .14e-03  99 0.        99
     .5000 -   .4000   .85e-01  19  .88e-02  10  .32e-02  15  .88e-03  86  .88e-03  99 0.        99
     .3000 -   .2000   .23e-01  10  .16e-01   7  .76e-02  10  .35e-02  13  .15e-02  21 0.        99
     .2000 -   .0000   .59e+00   8  .82e+00   4  .65e-01   8  .88e-02  18  .37e-02  18  .88e-03 88
 0    integral (/sr)   .32e-01  3  .19e-01  2  .91e-02  3  .50e-02  5  .22e-02  7  .59e-03 18
 the number of scs words used for statistics is       1017
//
end

 all done
```

```
'cu.put'ti,;1\1\0
.03 (1no5. 1.20a)
  1 0o c t o b e r  1 4 , 1 9 7 6  v e r s i o n
  2 0 nsct  matl
  3       4     3
  4 0 nmat  ntab
  5       1     1
  6 0npair  ntax
  7      25    41
  8 0gamma ray cross section data
  9 0energies (mev)
 10  1000.000000  800.000000  600.000000  500.000000  400.000000  300.000000
 11   200.000000  150.000000  100.000000   80.000000   60.000000   50.000000
 12    40.000000   30.000000   20.000000   15.000000   10.000000    8.000000
 13     6.000000    5.000000    4.000000    3.000000    2.000000    1.500000
 14     1.000000     .800000     .600000     .500000     .400000     .300000
 15      .200000     .150000     .100000     .080000     .060000     .050000
 16      .040000     .030000     .020000     .015000     .010000
 17 0total attenuation coefficients (cm2/g)
 18      .133015     .115792     .097314     .087552     .077436     .067825
 19      .056529     .051401     .046420     .044377     .042060     .040625
 20      .038802     .036353     .033322     .031958     .030918     .030686
 21      .030945     .031565     .032919     .035741     .041882     .047769
 22      .058536     .065369     .075103     .082004     .091659     .107638
 23     4.688869   10.808378   33.080263   73.885968  215.088888    2.456969
 25 0ratio of scattering plus pair production to total attenuation coefficients
 26      .999999     .999998     .999997     .999996     .999995     .999992
 27      .999986     .999979     .999965     .999955     .999936     .999920
 28      .999895     .999849     .999747     .999641     .999422     .999249
 30      .998958     .998787     .998388     .997908     .997088     .996088
 32      .994460     .915642     .985116     .982345     .980818
 33 0ratio of scattering to scattering plus pair production attenuation coefficients
 34      .001662     .002382     .003765     .005007     .007046     .010778
 35      .018909     .027362     .044314     .056913     .077841     .094684
 36      .120290     .163683     .248185     .323842     .453488     .536768
 37      .651019     .722340     .882503     .886979     .963836     .991964
 38     1.000000
 39 0k shell ionization data
 40 0binding energy (mev), photoeffect efficiency and fluorescent efficiency
 41      .008981     .871336     .392853
 42 0k x-ray energies (mev)
 43      .008150     .008150     .008150     .008150
 44 0k x-ray accumulated relative intensities
 45     1.000000    1.000000    1.000000    1.000000
 46 0auger electron energies (mev)
 47      .008150     .008150     .008150
 48 0auger electron accumulated relative intensities
 49     1.000000    1.000000    1.000000
 50 0 nmat  ntab
 51       2     1
 52 0npair  ntax
 53      25    41
 54 0gamma ray cross section data
 55 0energies (mev)
 56  1000.000000  800.000000  600.000000  500.000000  400.000000  300.000000
 57   200.000000  150.000000  100.000000   80.000000   60.000000   50.000000
 58    40.000000   30.000000   20.000000   15.000000   10.000000    8.000000
 59     6.000000    5.000000    4.000000    3.000000    2.000000    1.500000
 60     1.000000     .800000     .600000     .500000     .400000     .300000
.123,24
 23      .148681     .206315     .421781     .705562    1.487422    2.456969
 24     4.613060   10.402178   33.180213   73.691789  215.150145
.181,121
```

```
 81     .0800000    .0300000    .0200000    .0080000    .0060000     .050000
 83 @total attenuation coefficients (cm2/g)
 84      .042664     .037443     .031861     .028924     .025899     .022819
 85      .019793     .018395     .017194     .016805     .016488     .016362
 86      .016276     .016313     .016918     .017921     .020146     .021802
 87      .024515     .026632     .029693     .034451     .042729     .049688
 88      .061023     .067886     .077309     .083599     .091601     .102329
 89      .117953     .129244     .146076     .157139     .177347     .197927
 90      .240815     .359073     .869633    1.932250    6.538229
 91 @ratio of scattering plus pair production to total attenuation coefficients
 92     1.000000    1.000000    1.000000    1.000000    1.000000    1.000000
 93     1.000000     .999999     .999999     .999999     .999998     .999998
 94      .999997     .999996     .999994     .999993     .999990     .999988
 95      .999985     .999983     .999979     .999974     .999962     .999947
 96      .999908     .999868     .999775     .999673     .999458     .998892
 97      .996690     .992470     .974912     .951171     .888740     .819442
 98      .694128     .480603     .285262     .094029     .028300
 99 @ratio of scattering to scattering plus pair production attenuation coefficients
100      .005449     .007745     .012092     .015937     .022153     .033290
101      .056784     .080393     .125794     .158022     .208788     .247184
102      .301520     .383491     .513893     .607020     .731386     .793818
103      .863227     .899113     .933997     .965506     .990010     .997897
104     1.000000
105 @k shell ionization data
106 @binding energy (mev), photoeffect efficiency and fluorescent efficiency
107      .000687     .831990     .003376
108 @k x-ray energies (mev)
109      .000687     .000687     .000687     .000687
110 @k x-ray accumulated relative intensities
111     1.000000    1.000000    1.000000    1.000000
112 @auger electron energies (mev)
113      .000687     .000687     .000687
114 @auger electron accumulated relative intensities
115     1.000000    1.000000    1.000000
116 @ nmat  ntab
117        3     1
118 @npair  ntax
119       25    41
120 @gamma ray cross section data
121 @energies (mev)
122  1000.000000  800.000000  600.000000  500.000000  400.000000  300.000000
123   200.000000  150.000000  100.000000   80.000000   60.000000   50.000000
124    40.000000   30.000000   20.000000   15.000000   10.000000    8.000000
                                                                          105     6.000000    5.000000    4.000000    3.000000    2
.000000    1.500000
126     1.000000     .800000     .600000     .500000     .400000     .300000
127      .200000     .150000     .100000     .080000     .060000     .050000
128      .040000     .030000     .020000     .015000     .010000
129 @total attenuation coefficients (cm2/g)
130      .047459     .040496     .033058     .029154     .025144     .021091
131      .017198     .015493     .014218     .013934     .013862     .013935
132      .024632     .027030     .030888     .036988     .048968     .061888
133      .063513     .070654     .080455     .086995     .095307     .106425
134      .122896     .232288     .389858     .758228    2.288880     .178754
135 @ratio of scattering plus pair production to total attenuation coefficients
136     1.000000    1.000000    1.000000    1.000000    1.000000     000000
137     1.000000    1.000000    1.000000    1.000000     .999999     .999999
138      .999999     .999999     .999998     .999998     .999997     .999997
139      .999996     .999995     .999994     .999993     .999990     .999986
```

```
 .999996     .999995     .999994     .999993     .999990     .999986
 .999978     .999966     .999948     .999915     .999859     .999710
 .999123     .997987     .993163     .986454     .967663     .944418
 .894285     .773048     .479415     .262940     .086410
@ratio of scattering to scattering plus pair production attenuation coefficients
 .005099     .007454     .012130     .016458     .023751     .037489
 .068025     .099356     .158345     .198381     .258494     .382099
 .361954     .449719     .584721     .675399     .786023     .838082
 .894243     .922718     .950047     .974385     .992814     .998465
1.000000
@k shell ionization data
@binding energy (mev), photoeffect efficiency and fluorescent efficiency
 .000284     .958303     .000382
@k x-ray energies (mev)
 .000284     .000284     .000284     .000284
@k x-ray accumulated relative intensities
1.000000    1.000000    1.000000    1.000000
@auger electron energies (mev)
 .000284     .000284     .000284
@auger electron accumulated relative intensities
1.000000    1.000000    1.000000
1number of sets on datapac tape =   3
@input from datapac

  334 mev electron beam into bare fx-100 faraday cup##
@ nrun  itra  isip  iagn  isub  inal  icyc  ncyc  nmax      emax            emin            rmax       lmat
     1     5     0     1    17     1     1     8    64  4.0000000e+00  1.5625000e-02  2.7291488e+00     1

 dataprep data for datapac set   1    64    33    17   121  2.729148e+00
@ nrun  itra  isip  iagn  isub  inal  icyc  ncyc  nmax      emax            emin            rmax       lmat
     2     5     0     1    11     1     1     8    64  4.0000000e+00  1.5625000e-02  2.3896380e+00     2

 dataprep data for datapac set   2    64    33    11   121  2.389638e+00
@ nrun  itra  isip  iagn  isub  inal  icyc  ncyc  nmax      emax            emin            rmax       lmat
     3     5     0     1     3     1     1     8    64  4.0000000e+00  1.5625000e-02  2.2837680e+00     1

 dataprep data for datapac set   3    64    33     3   121  2.283768e+00

 collision / total de/dx ratios for datapac set   3

 cumulative bremsstrahlung cross sections for datapac set   3

 cumulative bremsstrahlung angular distributions for datapac set   3

 tangense - equiprobable endpoints for interpolation

 k x-ray production for datapac set   3

 photoelectron angular distributions

 pair electron energy division distribution (lead)
@ nrun   inc istrg  inok  inol iphot  ibad  idos  ipun itape
     4     1     1     1     2     1     1     1     2     2
@ zone  material  left plane  right plane  inner cylinder  outer cylinder    ecut        ptcs
     1         1         0.   .25400e+01              0.      .14350e-01   .100e-01   0.
     2         2         0.   .25400e+01       .14350e-01      .94000e-01   .100e-01   0.
     3         1         0.   .25400e+01       .94000e-01      .11900e+00   .100e-01   0.
     4         3         0.   .25400e+01       .11900e+00      .75000e+00   .100e-01   0.
@incident electrons
```

```
181 @electron collision and radiation energy loss straggling
182 @knock-on electron production
183 @no coupled inelastic scattering deflections
188 @bremsstrahlung and rejected energy and bremsstrahlung angle sampled from scaled Bethe-Heitler distribution
186 @photon-produced particles followed
187 @ iunt   lmax   itmk   jmax   ipsk jpmax   ismk   kmax   ibnk kpmax
188       2      1      1     40      1     40      1      6      1      6
189 @ imax   nsmp iflux  acyc   iran
190  30000      4      2     -1100000000000000000
191 @#################### the standard error estimates are based on    10 batches of  3000 histories ##################
192 @     4.00000       .01000       .01000       .01000    sorced00
194 @#################electron cut-off energy below electron energy list. cut-off energy has been changed to em(nmax)##########
195 ####
196 @       tsave                                 tmfac        rlan        qblk
197         .01633                               10.00000       .50000     1.00000
198 @electron energy classifications (mev)
199       3.90000     3.80000     3.70000     3.60000     3.50000     3.40000
200       3.30000     3.20000     3.10000     3.00000     2.90000     2.80000
201       2.70000     2.60000     2.50000     2.40000     2.30000     2.20000
202       2.10000     2.00000     1.90000     1.80000     1.70000     1.60000
203       1.50000     1.40000     1.30000     1.20000     1.10000     1.00000
204        .90000      .80000      .70000      .60000      .50000      .40000
205        .30000      .20000      .10000      .01633
206 @photon energy classifications (mev)
207       3.90000     3.80000     3.70000     3.60000     3.50000     3.40000
208       3.30000     3.20000     3.10000     3.00000     2.90000     2.80000
209       2.70000     2.60000     2.50000     2.40000     2.30000     2.20000
210       2.10000     2.00000     1.90000     1.80000     1.70000     1.60000
211       1.50000     1.40000     1.30000     1.20000     1.10000     1.00000
212        .90000      .80000      .70000      .60000      .50000      .40000
213        .30000      .20000      .10000      .01000
214 @electron obliquity classifications (degrees)
215     30.00000    60.00000    90.00000   120.00000   150.00000   180.00000
216 @electron azimuth classifications (degrees)
217    180.00000
218 @photon obliquity classifications (degrees)
219     30.00000    60.00000    90.00000   120.00000   150.00000   180.00000
220 @photon azimuth classifications (degrees)
221    180.00000
222 @ntfst       rmax     scale skale      tcut      tpcut      tfcut      tsave       dlim       bnum       xnum
223         1   .27291e+01         1         1      .01633      .01000    0.00000      .01633    1.00000        0.0        0.0
224 @k x-ray quanta not followed in material      1
225 @ntfst       rmax     scale skale      tcut      tpcut      tfcut      tsave       dlim       bnum       xnum
226         1   .23896e+01         1         1      .01633      .01000    0.00000      .01633    1.00000        0.0        0.0
227 @k x-ray quanta not followed in material      2
228 @ntfst       rmax     scale skale      tcut      tpcut      tfcut      tsave       dlim       bnum       xnum
229         1   .22838e+01         1         1      .01633      .01000    0.00000      .01633    1.00000        0.0        0.0
230 @k x-ray quanta not followed in material      3
231 @annihilation quanta followed
232 1the problem is 100  per cent complete.  time to finish is       0.000 seconds. average time per batch is      208.338
233 @average source energy = 4.0000e+00 mev
234 @      inran          irn          irc
235  000000000000000 5264073242716201 6415365352001645
236 @     ------------------------------------ histories ------------------------------------      rej       --- steps ----
237       prim       sec      knock       p e       pair       com      auger       brem        rad       xray       land       prim        sec
238      30000    313094    311758       716          0       620          0       7925      14570          0       9747    1258552    3304719
239 @                                energy (mev)       ave energy (mev)      number/primary      number generated
240  first knock (above tcut)       6.3380e-01          6.6399e-02            9.5346e+00            286039
.t182,183
242 @      tin        tcut       tpcut      cthin      sorcin
243       4.00000      .01000      .01000     1.00000      .74900
```

```
 41 total knock (above tcut)     6.6193e-01          6.3697e-02          1.0392e+01          311758
 42 photo-electron               1.2560e-03          2.1085e-02          5.9567e-02            1787
 43 pair                         0.                  0.                  0.                       0
 44 compton                      3.5322e-03          5.3410e-02          6.6133e-02            1984
 45 auger                        0.                  0.                  0.                       0
 46 first bremsstrahlung         5.6152e-02          1.4605e-01          3.8447e-01           11534
 47 total bremsstrahlung         5.6837e-02          1.1716e-01          4.8513e-01           14554
 48 k x-ray                      0.                  0.                  0.                       0
 49 annihilation quanta          0.                  0.                  0.                       0
 50 @unscattered primary photons number and energy
 51  0.       99 0.       99
 52 @number coefficients - knock-ons, photon descendants
 53 @                                                transmission
 54   .33e-04 99
 55   .13e-03 41
 56 @                                                 reflection
 57   .27e-02 12
 58  0.       99
 59 @                                                lateral escape
 60   .16e-01  4
 61   .33e-03 30
 62 @                                          number and energy coefficients
 63 @                                                transmission
 64 @            cylinder dimensions       ---------- electron ----------      ---------- photon ----------
 65             length(cm)  radius(cm)      number      energy      counts      number      energy      counts
 66
 67               .254e+01    .750e+00   .17e-03 45  .29e-04 58         5   .27e-01  2  .28e-02  6       1786
 68 @                                                 reflection
 69 @            cylinder dimensions       ---------- electron ----------      ---------- photon ----------
 70             length(cm)  radius(cm)      number      energy      counts      number      energy      counts
 71
 72               .254e+01    .750e+00   .77e-02  6  .19e-02  6       232   .90e-02  6  .29e-03 14        456
 73 @                                                lateral escape
 74 @            cylinder dimensions       ---------- electron ----------      ---------- photon ----------
 75             length(cm)  radius(cm)      number      energy      counts      number      energy      counts
 76
 77               .254e+01    .750e+00   .44e+00  1  .20e+00  0     13159   .17e+00  2  .96e-02  3       7545
 78 1                                                energy deposition
 79                                        (normalized to one incident particle)
 80 @                                                                                  energy deposition (mev)
 81       zone      material     mass(gm)   volume(cc)                          prim        knock         g-sec          to
 82 tal
 83
 84          1           1       .1471e-01      .1643e-02                    .2863e-02  8  -.4870e-04 99   .3659e-04 31   .2
 85 851e-02  9
 86          2           2       .1584e+00      .6886e-01                    .4473e-01  3  -.2799e-03 66   .9692e-04 29   .4
 87 455e-01  3
 88          3           1       .3803e+00      .4249e-01                    .7962e-01  2   .2633e-03 99   .1080e-02  7   .8
 89 097e-01  2
 90          4           3       .8314e+01      .4378e+01                    .3023e+01  0  -.7369e-02  5   .3490e-02  7   .3
 91 018e+01  0
 92 @                                                        total            .3150e+01  0  -.7435e-02  4   .4703e-02  6   .3
 93 148e+01  0
 94 @                                                charge distribution
 95                                        (normalized to one incident particle)
 96 @                                                                        electrons
 97       zone      material     zl         zr          ri          r0          prim        knock       g-sec       total
 98
 99          1           1     0.          .254e+01   0.          .144e-01    .10e-02 23 -.10e-03 99  .33e-04 99  .97e-03 3
100 7
```

2	2	0.	.254e+01	.144e-01	.940e-01	.13e-01	6	-.53e-03	99	-.31e-04	99	.12e-01
3	1	0.	.254e+01	.940e-01	.119e+00	.27e-01	5	-.33e-03	99	-.23e-03	48	.26e-01
4	3	0.	.254e+01	.119e+00	.750e+00	.53e+00	0	-.19e-01	5	-.23e-03	57	.51e+00
			total			.57e+00	0	-.20e-01	4	-.47e-03	19	.55e+00

energy spectra of transmitted electrons
(number/mev, normalized to one incident particle)

e (mev) length= 2.5400

4.0000 - 3.9000	0.		99
3.9000 - 3.8000	0.		99
3.8000 - 3.7000	0.		99
3.7000 - 3.6000	0.		99
3.800000 -3.9000000	0.		9999
3.4000 - 3.3000	0.		99
3.3000 - 3.2000	0.		99
3.2000 - 3.1000	0.		99
3.1000 - 3.0000	0.		99
3.0000 - 2.9000	0.		99
2.9000 - 2.8000	0.		99
2.8000 - 2.7000	0.		99
2.7000 - 2.6000	0.		99
2.6000 - 2.5000	0.		99
2.5000 - 2.4000	0.		99
2.4000 - 2.3000	0.		99
2.3000 - 2.2000	0.		99
2.2000 - 2.1000	0.		99
2.1000 - 2.0000	0.		99
2.0000 - 1.9000	0.		99
1.9000 - 1.8000		.33e-03	99
1.8000 - 1.7000	0.		99
1.7000 - 1.6000	0.		99
1.6000 - 1.5000	0.		99
1.5000 - 1.4000	0.		99
1.4000 - 1.3000	0.		99
1.3000 - 1.2000	0.		99
1.2000 - 1.1000	0.		99
1.1000 - 1.0000	0.		99
1.0000 - .9000		.33e-03	99
.9000 - .8000	0.		99
.8000 - .7000	0.		99
.7000 - .6000	0.		99
.6000 - .5000	0.		99
.5000 - .4000		.33e-03	99
.4000 - .3000	0.		99
.3000 - .2000		.33e-03	99
.2000 - .1000		.33e-03	99
.1000 - .0163	0.		99

energy spectra of reflected electrons
(number/mev, normalized to one incident particle)

e (mev) length= 2.5400

4.0000 - 3.9000	0.		99
3.9000 - 3.8000	0.		99
3.8000 - 3.7000	0.		99
3.7000 - 3.6000		.33e-03	99

```
 351    3.6000 -  3.5000   .67e-03 39
 352    3.5000 -  3.4000   .33e-03 99
 353    3.4000 -  3.3000  0.        99
 354    3.3000 -  3.2000  0.        99
 355    3.2000 -  3.1000   .67e-03 67
 356    3.1000 -  3.0000   .67e-03 67
 357    3.0000 -  2.9000   .33e-03 99
 358    2.9000 -  2.8000   .10e-02 71
 359    2.8000 -  2.7000   .67e-03 67
 370    2.7000 -  2.6000   .33e-03 99
 371    2.6000 -  2.5000   .13e-02 55
 372    2.5000 -  2.4000   .13e-02 41
 373    2.4000 -  2.3000   .67e-03 67
 374    2.3000 -  2.2000   .10e-02 51
 375    2.2000 -  2.1000   .67e-03 67
 376    2.1000 -  2.0000   .13e-02 41
 377    2.0000 -  1.9000   .10e-02 71
 378    1.9000 -  1.8000   .13e-02 41
 379    1.8000 -  1.7000   .23e-02 43
 380    1.7000 -  1.6000   .30e-02 35
 381    1.6000 -  1.5000   .17e-02 45
 382    1.5000 -  1.4000   .20e-02 37
 383    1.4000 -  1.3000   .33e-02 21
 384    1.3000 -  1.2000   .17e-02 45
 385    1.2000 -  1.1000   .20e-02 27
 386    1.1000 -  1.0000   .33e-02 33
 388    1.0000 -   .9000   .37e-02 29
 389     .9000 -   .8000   .10e-02 51
 390     .8000 -   .7000   .33e-02 30
 391     .7000 -   .6000   .23e-02 37
 392     .6000 -   .5000   .47e-02 32
 393     .5000 -   .4000   .23e-02 30
 394     .4000 -   .3000   .47e-02 27
 395     .3000 -   .2000   .67e-02 22
 396     .2000 -   .1000   .67e-02 22
 398     .1000 -   .0163   .17e-01  8
                                    (number/energy/particle/electron)
 399 0      e (mev)  length=      2.5400
 400
 401    4.0000 -  3.9000   .33e-03 99
 402    3.9000 -  3.8000   .23e-01 11
 403    3.8000 -  3.6000   .99e-01 10
 405    3.6000 -  3.5000   .61e-01  5
 406    3.5000 -  3.4000   .63e-01  8
 407    3.4000 -  3.3000   .79e-01  9
 408    3.3000 -  3.2000   .95e-01  3
 409    3.2000 -  3.1000   .96e-01  5
 410    3.1000 -  3.0000   .97e-01  4
 411    3.0000 -  2.9000   .11e+00  8
 412    2.9000 -  2.8000   .11e+00  6
 413    2.8000 -  2.7000   .12e+00  5
 414    2.7000 -  2.6000   .12e+00  4
 415    2.6000 -  2.5000   .12e+00  4
 416    2.5000 -  2.4000   .12e+00  4
 417    2.4000 -  2.3000   .13e+00  4
 418    2.3000 -  2.2000   .14e+00  6
 419    2.2000 -  2.1000   .13e+00  6
 420    2.1000 -  2.0000   .14e+00  4
.t397,398
 397                                  energy spectra of laterally escaping electrons
 398                                (number/mev, normalized to one incident particle)
```

```
 2.1000 -  1.9000   .15e+00  3
 1.9000 -  1.8000   .15e+00  5
 1.8000 -  1.7000   .14e+00  5
 1.7000 -  1.6000   .14e+00  7
 1.6000 -  1.5000   .14e+00  4
 1.5000 -  1.4000   .16e+00  4
 1.4000 -  1.3000   .15e+00  4
 1.3000 -  1.2000   .15e+00  6
 1.2000 -  1.1000   .15e+00  3
 1.1000 -  1.0000   .15e+00  3
 1.0000 -   .9000   .15e+00  5
  .9000 -   .8000   .14e+00  5
  .8000 -   .7000   .14e+00  7
  .7000 -   .6000   .12e+00  9
  .6000 -   .5000   .12e+00  5
  .5000 -   .4000   .11e+00  6
  .4000 -   .3000   .10e+00  5
  .3000 -   .2000   .80e-01  5
  .2000 -   .1000   .64e-01  6
  .1000 -   .0163   .43e-01  6

                    angular distributions of transmitted and reflected electrons
                       (number/sr, normalized to one incident particle)
          phi(deg)=  0.000
  theta (deg)      180.000

  0.0000 - 30.0000   .12e-03 51
 30.0000 - 60.0000   .29e-04 67
 60.0000 - 90.0000  0.       99
 90.0000 -120.0000   .56e-03 13
120.0000 -150.0000   .18e-02  9
150.0000 -180.0000   .21e-02 15

                    angular distributions of laterally escaping electrons
                       (number/sr, normalized to one incident particle)
          phi(deg)=  0.000
  theta (deg)      180.000

  0.0000 - 30.0000   .11e+00  2
 30.0000 - 60.0000   .74e-01  1
 60.0000 - 90.0000   .35e-01  1
 90.0000 -120.0000   .16e-01  3
120.0000 -150.0000   .62e-02  3
150.0000 -180.0000   .11e-02 17
                    energy spectra and angular distributions of electrons transmitted and reflected
                       azimuthal interval is   0.00000 to 180.00000 degrees
                        (number/(mev*sr), normalized to one particle)
      e (mev)  theta=  0.000      30.000      60.000      90.000     120.000     150.000
                      30.000      60.000      90.000     120.000     150.000     180.000

 4.0000 -  3.9000  0.       99 0.       99 0.       99 0.       99 0.       99 0.       99
 3.9000 -  3.8000  0.       99 0.       99 0.       99 0.       99 0.       99 0.       99
 3.8000 -  3.7000  0.       99 0.       99 0.       99 0.       99 0.       99 0.       99
 3.7000 -  3.6000  0.       99 0.       99 0.       99 0.       99 0.       99  .40e-03 99
 3.6000 -  3.5000  0.       99 0.       99 0.       99 0.       99  .14e-03 99  .40e-03 99
 3.5000 -  3.4000  0.       99 0.       99 0.       99  .11e-03 99 0.       99 0.       99
 3.4000 -  3.3000  0.       99 0.       99 0.       99 0.       99 0.       99 0.       99
 3.3000 -  3.2000  0.       99 0.       99 0.       99 0.       99 0.       99 0.       99
 3.2000 -  3.1000  0.       99 0.       99 0.       99  .11e-03 99  .14e-03 99 0.       99
 3.1000 -  3.0000  0.       99 0.       99 0.       99  .11e-03 99  .14e-03 99 0.       99
 3.0000 -  2.9000  0.       99 0.       99 0.       99 0.       99  .14e-03 99 0.       99
 2.9000 -  2.8000  0.       99 0.       99 0.       99 0.       99  .14e-03 99  .79e-03 99
```

81	2.8000 -	2.7000	0.	99	0.	99	0.	99	0.	99	.14e-03	99	.40e-03	99		
82	2.7000 -	2.6000	0.	99	0.	99	0.	99	.11e-03	99	0.	99	0.	99		
83	2.6000 -	2.5000	0.	99	0.	99	0.	99	.32e-03	51	0.	99	.40e-03	99		
84	2.5000 -	2.4000	0.	99	0.	99	0.	99	.21e-03	67	.29e-03	67	0.	99		
85	2.4000 -	2.3000	0.	99	0.	99	0.	99	.11e-03	99	.14e-03	99	0.	99		
86	2.3000 -	2.2000	0.	99	0.	99	0.	99	0.	99	.29e-03	67	.40e-03	99		
87	2.2000 -	2.1000	0.	99	0.	99	0.	99	.11e-03	99	0.	99	.40e-03	99		
88	2.1000 -	2.0000	0.	99	0.	99	0.	99	.11e-03	99	.43e-03	51	0.	99		
89	2.0000 -	1.9000	0.	99	0.	99	0.	99	.21e-03	67	0.	99	.40e-03	99		
90	1.9000 -	1.8000	.40e-03	99	0.	99	0.	99	.11e-03	99	.14e-03	99	.79e-03	67		
91	1.8000 -	1.7000	0.	99	0.	99	0.	99	.11e-03	99	.72e-03	54	.40e-03	99		
92	1.7000 -	1.6000	0.	99	0.	99	0.	99	.21e-03	67	.87e-03	37	.40e-03	99		
93	1.6000 -	1.5000	0.	99	0.	99	0.	99	0.	99	.58e-03	55	.40e-03	99		
94	1.5000 -	1.4000	0.	99	0.	99	0.	99	.11e-03	99	.43e-03	51	.79e-03	67		
95	1.4000 -	1.3000	0.	99	0.	99	0.	99	.32e-03	51	.72e-03	33	.79e-03	67		
96	1.3000 -	1.2000	0.	99	0.	99	0.	99	.21e-03	67	.29e-03	99	.40e-03	99		
97	1.2000 -	1.1000	0.	99	0.	99	0.	99	.11e-03	99	.29e-03	67	.12e-02	51		
98	1.1000 -	1.0000	0.	99	0.	99	0.	99	.21e-03	67	.10e-02	48	.40e-03	99		
99	1.0000 -	.9000	0.	99	.14e-03	99	0.	99	0.	99	.43e-03	51	.79e-03	67		
100	.9000 -	.8000	0.	99	0.	99	0.	99	.32e-03	51	.87e-03	27	.79e-03	99		
101	.8000 -	.7000	0.	99	0.	99	0.	99	.11e-03	99	.29e-03	67	0.	99		
102	.8000 -	.6000	0.	99	0.	99	0.	99	0.	21e-03	89	.82e-03	94	.78e-03	87	
104	.5000 -	.4000	.40e-03	99	0.	99	0.	99	.21e-03	67	.12e-02	45	.16e-02	41		
105	.4000 -	.3000	0.	99	0.	99	0.	98	.21e-03	67	.72e-03	33	0.	99		
106	.3000 -	.2000	.40e-03	99	0.	99	0.	99	.42e-03	41	.10e-02	30	.12e-02	71		
107	.2000 -	.1000	0.	99	.14e-03	99	0.	99	.64e-03	44	.14e-02	26	.16e-02	55		
108	.1000 -	.0163	0.	99	0.	99	0.	99	.76e-03	44	.45e-02	16	.47e-02	30		

energy spectra and angular distributions of electrons laterally escaping
azimuthal interval is 0.00000 to 180.00000 degrees
(number/(mev*sr), normalized to one particle)

e (mev)	theta= 0.000	30.000	60.000	90.000	120.000	150.000	180.000

115	4.0000 -	3.9000	.40e-03	99	0.	99	0.	99	0.	99	0.	99	0.	99		
116	3.9000 -	3.8000	.26e-01	11	.43e-03	71	.11e-03	99	0.	99	0.	99	0.	99		
117	3.8000 -	3.7000	.41e-01	9	.72e-03	61	.11e-03	98	0.	99	0.	99	0.	99		
118	3.7000 -	3.6000	.60e-01	6	.29e-02	20	.32e-03	51	0.	99	.14e-03	99	0.	99		
119	3.6000 -	3.5000	.56e-01	6	.57e-02	14	.32e-03	71	.11e-03	99	0.	99	0.	99		
120	3.5000 -	3.4000	.53e-01	11	.71e-02	12	.64e-03	37	.11e-03	99	0.	99	0.	99		
121	3.4000 -	3.3000	.62e-01	12	.11e-01	13	.53e-03	45	.11e-03	99	0.	99	0.	99		
122	3.3000 -	3.2000	.69e-01	5	.15e-01	7	.74e-03	37	.11e-03	99	0.	99	0.	99		
123	3.2000 -	3.1000	.62e-01	10	.17e-01	5	.16e-02	23	.21e-03	67	0.	99	0.	99		
124	3.1000 -	3.0000	.59e-01	9	.18e-01	7	.12e-02	42	.32e-03	71	.14e-03	99	0.	99		
125	3.0000 -	2.9000	.56e-01	8	.22e-01	7	.28e-02	21	.11e-03	99	.14e-03	99	0.	99		
126	2.9000 -	2.8000	.53e-01	13	.25e-01	10	.33e-02	18	.42e-03	55	.14e-03	99	0.	99		
127	2.8000 -	2.7000	.46e-01	14	.29e-01	8	.32e-02	19	.64e-03	37	.14e-03	99	0.	99		
128	2.7000 -	2.6000	.40e-01	11	.27e-01	7	.62e-02	12	.53e-03	45	.14e-03	99	0.	99		
129	2.6000 -	2.5000	.42e-01	9	.30e-01	6	.55e-02	14	.53e-03	45	0.	99	0.	99		
130	2.5000 -	2.4000	.40e-01	8	.28e-01	6	.63e-02	9	.74e-03	37	.14e-03	99	0.	99		
131	2.4000 -	2.3000	.30e-01	14	.33e-01	6	.66e-02	10	.15e-02	27	.14e-03	99	0.	99		
132	2.3000 -	2.2000	.32e-01	12	.32e-01	8	.91e-02	11	.17e-02	23	0.	99	0.	99		
133	2.2000 -	2.1000	.29e-01	11	.30e-01	6	.88e-02	11	.17e-02	42	0.	99	0.	99		
134	2.1000 -	2.0000	.28e-01	10	.33e-01	9	.11e-01	10	.24e-02	26	.29e-03	67	0.	99		
135	2.0000 -	1.9000	.22e-01	9	.34e-01	8	.14e-01	11	.36e-02	22	.29e-03	99	0.	99		
136	1.9000 -	1.8000	.22e-01	13	.30e-01	5	.15e-01	10	.30e-02	13	.58e-03	55	0.	99		
137	1.8000 -	1.7000	.16e-01	24	.27e-01	10	.15e-01	7	.49e-02	16	.58e-03	55	.40e-03	99		
138	1.7000 -	1.6000	.17e-01	28	.27e-01	9	.14e-01	12	.47e-02	10	.10e-02	30	0.	99		
139	1.6000 -	1.5000	.17e-01	15	.25e-01	7	.16e-01	6	.47e-02	13	.13e-02	39	0.	99		
140	1.5000 -	1.4000	.17e-01	19	.28e-01	8	.16e-01	7	.83e-02	11	.19e-02	16	.40e-03	99		

541	1.4000 -	1.3000	.15e-01	13	.23e-01	16	.19e-01	7	.68e-02	11	.12e-02	45	0. 99
542	1.3000 -	1.2000	.15e-01	13	.22e-01	9	.19e-01	8	.75e-02	9	.32e-02	13	0. 99
543	1.2000 -	1.1000	.11e-01	17	.22e-01	4	.17e-01	8	.91e-02	14	.26e-02	20	.79e-03 67
544	1.1000 -	1.0000	.12e-01	14	.21e-01	6	.16e-01	8	.94e-02	11	.46e-02	18	.79e-03 99
545	1.0000 -	.9000	.13e-01	19	.21e-01	8	.17e-01	7	.94e-02	6	.38e-02	22	0. 99
546	.9000 -	.8000	.91e-02	26	.18e-01	9	.18e-01	8	.80e-02	13	.38e-02	25	.12e-02 71
547	.8000 -	.7000	.48e-02	43	.16e-01	13	.16e-01	6	.11e-01	11	.46e-02	15	.12e-02 51
548	.7000 -	.6000	.44e-02	29	.13e-01	12	.15e-01	9	.10e-01	12	.45e-02	20	0. 99
549	.6000 -	.5000	.71e-02	27	.11e-01	11	.13e-01	11	.11e-01	12	.68e-02	13	.12e-02 51
550	.5000 -	.4000	.32e-02	36	.11e-01	11	.12e-01	8	.10e-01	9	.46e-02	15	.32e-02 41
551	.4000 -	.3000	.12e-02	51	.91e-02	14	.11e-01	9	.11e-01	11	.41e-02	20	.79e-03 67
552	.3000 -	.2000	.40e-02	28	.70e-02	15	.82e-02	9	.75e-02	13	.46e-02	12	.40e-03 99
553	.2000 -	.1000	.16e-02	55	.48e-02	14	.79e-02	12	.59e-02	7	.35e-02	23	.40e-03 99
554	.1000 -	.0163	.19e-02	67	.31e-02	28	.53e-02	17	.30e-02	21	.35e-02	17	.47e-03 99

energy spectra of transmitted photons
(number/mev, normalized to one incident particle)

e (mev) length= 2.5400

4.0000 -	3.9000	0.		99
3.9000 -	3.8000	0.		99
3.8000 -	3.7000	0.		99
3.7000 -	3.6000	0.		99
3.6000 -	3.5000	0.		99
3.5000 -	3.4000	.29e-03		99
3.4000 -	3.3000	.28e-03		99
3.3000 -	3.2000	0.		99
3.2000 -	3.1000	.28e-03		99
3.1000 -	3.0000	.56e-03		99
3.0000 -	2.9000	.55e-03		67
2.9000 -	2.8000	.11e-02		41
2.8000 -	2.7000	.84e-03		71
2.7000 -	2.6000	.56e-03		67
2.6000 -	2.5000	.84e-03		71
2.5000 -	2.4000	.60e-03		67
2.4000 -	2.3000	.69e-03		54
2.3000 -	2.2000	0.		99
2.2000 -	2.1000	.83e-03		51
2.1000 -	2.0000	.16e-02		37
2.0000 -	1.9000	.21e-02		26
1.9000 -	1.8000	.80e-03		51
1.8000 -	1.7000	.27e-02		26
1.7000 -	1.6000	.22e-02		30
1.6000 -	1.5000	.78e-03		71
1.5000 -	1.4000	.31e-02		21
1.4000 -	1.3000	.23e-02		38
1.3000 -	1.2000	.28e-02		31
1.2000 -	1.1000	.24e-02		28
1.1000 -	1.0000	.33e-02		21
1.0000 -	.9000	.48e-02		23
.9000 -	.8000	.31e-02		33
.8000 -	.7000	.60e-02		22
.7000 -	.6000	.10e-01		18
.6000 -	.5000	.11e-01		15
.5000 -	.4000	.15e-01		15
.4000 -	.3000	.21e-01		15
.3000 -	.2000	.31e-01		9
.2000 -	.1000	.46e-01		5
.1000 -	.0100	.10e+00		5

energy spectra of reflected photons
(number/mev, normalized to one incident particle)

```
601 0      d (mev)  length=      2.5400
602
603     4.0000 -  3.9000  0.          99
604     3.9000 -  3.8000  0.          99
605     3.8000 -  3.7000  0.          99
606     3.7000 -  3.6000  0.          99
607     3.6000 -  3.5000  0.          99
608     3.5000 -  3.4000  0.          99
609     3.4000 -  3.3000  0.          99
610     3.3000 -  3.2000  0.          99
611     3.2000 -  3.1000  0.          99
612     3.1000 -  3.0000  0.          99
613     3.0000 -  2.9000  0.          99
614     2.9000 -  2.8000  0.          99
615     2.8000 -  2.7000  0.          99
616     2.7000 -  2.6000  0.          99
617     2.6000 -  2.5000  0.          99
618     2.5000 -  2.4000  0.          99
619     2.4000 -  2.3000  0.          99
620     2.3000 -  2.2000  0.          99
621     2.2000 -  2.1000  0.          99
622     2.1000 -  2.0000  0.          99
623     2.0000 -  1.9000  0.          99
624     1.9000 -  1.8000  0.          99
625     1.8000 -  1.7000   .31e-03 99
626     1.7000 -  1.6000  0.          99
627     1.6000 -  1.5000  0.          99
628     1.5000 -  1.4000  0.          99
629     1.4000 -  1.3000  0.          99
630     1.3000 -  1.2000   .59e-03 67
631     1.2000 -  1.1000   .33e-03 99
632     1.1000 -  1.0000  0.          99
633     1.0000 -   .9000   .61e-03 99
634      .9000 -   .8000   .63e-03 67
635      .8000 -   .7000   .62e-03 67
636      .7000 -   .6000   .30e-03 99
637      .6000 -   .5000   .58e-03 67
638      .5000 -   .4000   .62e-03 67
639      .4000 -   .3000   .29e-02 15
640      .3000 -   .2000   .59e-02 21
641      .2000 -   .1000   .19e-01 13
642      .1000 -   .0100   .63e-01  7
643
644
645 0      e (mev)  length=      2.5400
646
647     4.0000 -  3.9000  0.          99
648     3.9000 -  3.8000  0.          99
649     3.8000 -  3.7000  0.          99
650     3.7000 -  3.6000  0.          99
651     3.6000 -  3.5000  0.          99
652     3.5000 -  3.4000   .30e-03 99
653     3.4000 -  3.3000   .60e-03 67
654     3.3000 -  3.2000   .61e-03 67
655     3.2000 -  3.1000   .94e-03 51
656     3.1000 -  3.0000   .32e-03 99
657     3.0000 -  2.9000   .94e-03 51
658     2.9000 -  2.8000   .28e-03 99
659     2.8000 -  2.7000   .28e-03 99
660     2.7000 -  2.6000   .13e-02 41
```

energy spectra of laterally escaping photons
(number/mev, normalized to one incident particle)

```
 61    2.6000 -  2.5000   .98e-03 76
 62    2.5000 -  2.4000   .31e-03 99
 63    2.4000 -  2.3000   .86e-03 99
 64    2.3000 -  2.2000   .15e-02 54
 65    2.2000 -  2.1000   .19e-02 27
 66    2.1000 -  2.0000   .24e-02 40
 67    2.0000 -  1.9000   .22e-02 47
 68    1.9000 -  1.8000   .24e-02 25
 69    1.8000 -  1.7000   .53e-02 28
 70    1.7000 -  1.6000   .54e-02 22
 71    1.6000 -  1.5000   .38e-02 29
 72    1.5000 -  1.4000   .57e-02 23
 73    1.4000 -  1.3000   .12e-01 16
 74    1.3000 -  1.2000   .73e-02 17
 75    1.2000 -  1.1000   .93e-02 13
 76    1.1000 -  1.0000   .84e-02 18
 77    1.0000 -   .9000   .15e-01 12
 78     .9000 -   .8000   .21e-01 11
 79     .8000 -   .7000   .21e-01 10
 80     .7000 -   .6000   .35e-01 10
 81     .6000 -   .5000   .39e-01  8
 82     .5000 -   .4000   .49e-01  5
 83     .4000 -   .3000   .91e-01  4
 84     .3000 -   .2000   .15e+00  4
 85     .2000 -   .1000   .29e+00  4
 86     .1000 -   .0100   .98e+00  3
 87                        angular distributions of transmitted and reflected photon intensity
 88                              (mev/sr, normalized to one incident particle)
 89          phi(deg)=  0.000
 90     theta (deg)     180.000
 91
 92   0.0000 - 30.0000   .13e-01  6
 93  30.0000 - 60.0000   .14e-03 23
 94  60.0000 - 90.0000   .95e-05 39
 95  90.0000 -120.0000   .58e-04 33
 96 120.0000 -150.0000   .32e-03 18
 97 150.0000 -180.0000   .27e-03 21
 98                        angular distributions of laterally escaping photon intensity
 99                              (mev/sr, normalized to one incident particle)
100          phi(deg)=  0.000
101     theta (deg)     180.000
102
103   0.0000 - 30.0000   .17e-01  5
104  30.0000 - 60.0000   .63e-02  3
105  60.0000 - 90.0000   .19e-02  4
106  90.0000 -120.0000   .89e-03  6
107 120.0000 -150.0000   .33e-03  9
108 150.0000 -180.0000   .84e-04 17
109                     energy spectra and angular distributions of photons transmitted and reflected
110                              azimuthal interval is   0.00000 to 180.00000 degrees
111                               (number/(mev*sr), normalized to one particle)
112       e (mev)  theta=  0.000     30.000     60.000     90.000    120.000    150.000
113                       30.000     60.000     90.000    120.000    150.000    180.000
114
115    4.0000 -  3.9000  0.       99 0.      99 0.      99 0.      99 0.      99 0.      99
116    3.9000 -  3.8000  0.       99 0.      99 0.      99 0.      99 0.      99 0.      99
117    3.8000 -  3.7000  0.       99 0.      99 0.      99 0.      99 0.      99 0.      99
118    3.7000 -  3.6000  0.       99 0.      99 0.      99 0.      99 0.      99 0.      99
119    3.6000 -  3.5000  0.       99 0.      99 0.      99 0.      99 0.      99 0.      99
120    3.6000 -  3.4000   .34e-03 99 0.      99 0.      99 0.      99 0.      99 0.      99
```

721	3.4000	-	3.3000	.34e-03	99	0.		99	0.		99	0.		99	0.		99	0.		99
722	3.3000	-	3.2000	0.		99	0.		99	0.		99	0.		99	0.		99	0.		99
723	3.2000	-	3.1000	.33e-03	99	0.		99	0.		99	0.		99	0.		99	0.		99
724	3.1000	-	3.0000	.67e-03	99	0.		99	0.		99	0.		99	0.		99	0.		99
725	3.0000	-	2.9000	.65e-03	67	0.		99	0.		99	0.		99	0.		99	0.		99
726	2.9000	-	2.8000	.13e-02	41	0.		99	0.		99	0.		99	0.		99	0.		99
727	2.8000	-	2.7000	.10e-02	71	0.		99	0.		99	0.		99	0.		99	0.		99
728	2.7000	-	2.6000	.66e-03	67	0.		99	0.		99	0.		99	0.		99	0.		99
729	2.6000	-	2.5000	.99e-03	71	0.		99	0.		99	0.		99	0.		99	0.		99
730	2.5000	-	2.4000	.71e-03	67	0.		99	0.		99	0.		99	0.		99	0.		99
731	2.4000	-	2.3000	.82e-03	54	0.		99	0.		99	0.		99	0.		99	0.		99
732	2.3000	-	2.2000	0.		99	0.		99	0.		99	0.		99	0.		99	0.		99
733	2.2000	-	2.1000	.98e-03	51	0.		99	0.		99	0.		99	0.		99	0.		99
734	2.1000	-	2.0000	.20e-02	37	0.		99	0.		99	0.		99	0.		99	0.		99
735	2.0000	-	1.9000	.25e-02	26	0.		99	0.		99	0.		99	0.		99	0.		99
736	1.9000	-	1.8000	.95e-03	51	0.		99	0.		99	0.		99	0.		99	0.		99
737	1.8000	-	1.7000	.32e-02	26	0.		99	0.		99	0.		99	.13e-03		99	0.		99
738	1.7000	-	1.6000	.22e-02	37	.14e-03		99	0.		99	0.		99	0.		99	0.		99
739	1.6000	-	1.5000	.93e-03	71	0.		99	0.		99	0.		99	0.		99	0.		99
740	1.5000	-	1.4000	.36e-02	21	0.		99	0.		99	0.		99	0.		99	0.		99
741	1.4000	-	1.3000	.27e-02	38	0.		99	0.		99	0.		99	0.		99	0.		99
742	1.3000	-	1.2000	.31e-02	30	.11e-03		99	0.		99	0.		99	.26e-03		67	0.		99
743	1.2000	-	1.1000	.28e-02	28	0.		99	0.		99	0.		99	.14e-03		99	0.		99
744	1.1000	-	1.0000	.39e-02	21	0.		99	0.		99	0.		99	0.		99	0.		99
745	1.0000	-	.9000	.57e-02	23	0.		99	0.		99	0.		99	.27e-03		99	0.		99
746	.9000	-	.8000	.37e-02	33	0.		99	0.		99	.10e-03		99	.13e-03		99	0.		99
747	.8000	-	.7000	.71e-02	22	0.		99	0.		99	0.		99	.13e-03		99	.38e-03		99
748	.7000	-	.6000	.11e-01	15	.25e-03		67	0.		99	.96e-04		99	0.		99	0.		99
749	.6000	-	.5000	.13e-01	15	.13e-03		99	0.		99	0.		99	.25e-03		67	0.		99
750	.5000	-	.4000	.17e-01	15	.31e-03		52	0.		99	.10e-03		99	.13e-03		99	0.		99
751	.4000	-	.3000	.24e-01	15	.27e-03		67	0.		99	.28e-03		71	.88e-03		22	0.		99
752	.3000	-	.2000	.33e-01	8	.10e-02		24	.19e-03		67	.18e-03		67	.17e-02		19	.16e-02		53
753	.2000	-	.1000	.51e-01	6	.13e-02		40	.18e-03		68	.11e-02		27	.41e-02		16	.77e-02		22
754	.1000	-	.0100	.11e+00	4	.30e-02		17	.61e-03		57	.31e-02		17	.14e-01		12	.27e-01		12
755	integral (/sr)			.30e-01	3	.62e-03		15	.92e-04		44	.46e-03		12	.20e-02		9	.34e-02		12
756	energy spectra and angular distributions of photons laterally escaping																		
757	azimuthal interval is 0.00000 to 180.00000 degrees																		
758	(number/(mevtar), normalized to one particle)																		
759	e (mev) theta=			0.000		30.000		60.000		90.000		120.000		150.000					
760				30.000		60.000		90.000		120.000		150.000		180.000					
761																			
762	4.0000	-	3.9000	0.		99	0.		99	0.		99	0.		99	0.		99	0.		99
763	3.9000	-	3.8000	0.		99	0.		99	0.		99	0.		99	0.		99	0.		99
764	3.8000	-	3.7000	0.		99	0.		99	0.		99	0.		99	0.		99	0.		99
765	3.7000	-	3.6000	0.		99	0.		99	0.		99	0.		99	0.		99	0.		99
766	3.6000	-	3.5000	0.		99	0.		99	0.		99	0.		99	0.		99	0.		99
767	3.5000	-	3.4000	.36e-03	99	0.		99	0.		99	0.		99	0.		99	0.		99
768	3.4000	-	3.3000	.34e-03	99	.14e-03		99	0.		99	0.		99	0.		99	0.		99
769	3.3000	-	3.2000	0.		99	.27e-03		67	0.		99	0.		99	0.		99	0.		99
770	3.2000	-	3.1000	.73e-03	67	.14e-03		99	0.		99	0.		99	0.		99	0.		99
771	3.1000	-	3.0000	.38e-03	99	0.		99	0.		99	0.		99	0.		99	0.		99
772	3.0000	-	2.9000	.11e-02	51	0.		99	0.		99	0.		99	0.		99	0.		99
773	2.9000	-	2.8000	.33e-03	99	0.		99	0.		99	0.		99	0.		99	0.		99
774	2.8000	-	2.7000	.34e-03	99	0.		99	0.		99	0.		99	0.		99	0.		99
775	2.7000	-	2.6000	.11e-02	51	0.		99	0.		99	.11e-03		99	0.		99	0.		99
776	2.6000	-	2.5000	.11e-02	70	0.		99	0.		99	0.		99	0.		99	0.		99
777	2.5000	-	2.4000	.37e-03	99	0.		99	0.		99	0.		99	0.		99	0.		99
778	2.4000	-	2.3000	.10e-02	99	0.		99	0.		99	0.		99	0.		99	0.		99
779	2.3000	-	2.2000	.68e-03	67	.41e-03		99	0.		99	0.		99	0.		99	0.		99

```
 31    2.1000 -  2.0000   .14e-02 55  .53e-03 55 0.       99 0.       99 0.       99 0.       99
 32    2.0000 -  1.9000   .15e-02 41  .40e-03 71 0.       99 0.       99 0.       99 0.       99
 33    1.9000 -  1.8000   .21e-02 37  .26e-03 67 0.       99 0.       99 0.       99 0.       99
 34    1.8000 -  1.7000   .26e-02 44  .95e-03 30  .28e-03 51 0.       99 0.       99 0.       99
 35    1.7000 -  1.6000   .35e-02 33  .66e-03 54  .29e-03 51 0.       99 0.       99 0.       99
 36    1.6000 -  1.5000   .10e-02 51  .76e-03 51  .29e-03 70  .95e-04 99 0.       99 0.       99
 37    1.5000 -  1.4000   .28e-02 31  .15e-02 25 0.       99 0.       99 0.       99 0.       99
 38    1.4000 -  1.3000   .69e-02 23  .17e-02 39  .59e-03 37  .20e-03 67 0.       99 0.       99
 39    1.3000 -  1.2000   .54e-02 17  .92e-03 22  .19e-03 67 0.       99 0.       99 0.       99
 40    1.2000 -  1.1000   .46e-02 35  .13e-02 15  .30e-03 51  .49e-03 33 0.       99 0.       99
 41    1.1000 -  1.0000   .49e-02 31  .12e-02 31  .49e-03 33 0.       99 0.       99 0.       99
 42    1.0000 -   .9000   .67e-02 23  .29e-02 17  .69e-03 31  .99e-04 99  .14e-03 99 0.       99
 43     .9000 -   .8000   .10e-01 17  .35e-02 11  .13e-02 29  .94e-04 99 0.       99 0.       99
 44     .8000 -   .7000   .11e-01 22  .35e-02 12  .85e-03 26  .39e-03 41  .13e-03 99 0.       99
 45     .7000 -   .6000   .18e-01 13  .79e-02 13  .24e-02 30  .90e-03 80  .26e-03 67 0.       99
 46     .6000 -   .5000   .21e-01 10  .92e-02 13  .23e-02  9  .86e-03 26  .27e-03 67 0.       99
 47     .5000 -   .4000   .34e-01  9  .13e-01  7  .61e-02  7  .34e-02 16  .69e-03 61 0.       99
 48     .4000 -   .3000   .49e-01  7  .23e-01  7  .10e-01 10  .58e-02  9  .17e-02 36  .11e-02 51
 49     .3000 -   .2000   .80e-01  5  .49e-01  6  .18e-01  7  .13e-01  7  .66e-02 10  .12e-02 53
 50     .2000 -   .1000   .24e+00  5  .15e+00  4  .73e-01  3  .44e-01  4  .25e-01  6  .12e-01 23
 51     .1000 -   .0100   .15e+00  4  .10e+00  4  .44e-01  3  .26e-01  4  .15e-01  6  .13e-01 19
 52 0the ambbgrndf(eca)word50es04 for e860t01ic3 is1le-01 1317.65e-02  3  .33e-02  6  .13e-02 19
.t802,1
 52 0    integral (/sr)   .50e-01  4  .26e-01  3  .11e-01  3  .65e-02  3  .33e-02  6  .13e-02 19
 53  the number of eca words used for statistics is       1317
.end

 all done
%hp 0014.2046
```

APPENDIX G

APPENDIX G

SECURITY CLASSIFICATION OF THIS PAGE (When Data Entered)

REPORT DOCUMENTATION PAGE		READ INSTRUCTIONS BEFORE COMPLETING FORM
1. REPORT NUMBER	2. GOVT ACCESSION NO.	3. RECIPIENT'S CATALOG NUMBER
4. TITLE (and Subtitle) Monte Carlo Electron Beam Transport in Air		5. TYPE OF REPORT & PERIOD COVERED Interim Report 6. PERFORMING ORG. REPORT NUMBER AMRC-N-186
7. AUTHOR(s) D. J. Sullivan C. A. Ekdahl		8. CONTRACT OR GRANT NUMBER(s) F49620-81-C-0016
9. PERFORMING ORGANIZATION NAME AND ADDRESS Mission Research Corporation 1400 San Mateo Boulevard, S.E., Suite A Albuquerque, New Mexico 87108		10. PROGRAM ELEMENT, PROJECT, TASK AREA & WORK UNIT NUMBERS
11. CONTROLLING OFFICE NAME AND ADDRESS Air Force Office of Scientific Research Bolling Air Force Base Washington, DC 20332		12. REPORT DATE January 1982 13. NUMBER OF PAGES 24
14. MONITORING AGENCY NAME & ADDRESS(if different from Controlling Office)		15. SECURITY CLASS (of this report) Unclassified 15a. DECLASSIFICATION/DOWNGRADING SCHEDULE

16. DISTRIBUTION STATEMENT (of this Report)

17. DISTRIBUTION STATEMENT (of the abstract entered in Block 20, if different from Report)

Approved for Public Release; Distribution Unlimited

18. SUPPLEMENTARY NOTES

19. KEY WORDS (Continue on reverse side if necessary and identify by block number)

Electron Beam Transport
Monte Carlo Transport Calculations
Delta Rays

20. ABSTRACT (Continue on reverse side if necessary and identify by block number)

The Monte Carlo transport of a 1.5 MeV electron beam in low density and full atmosphere air is studied. At a pressure of 0.5 Torr virtually none of the beam is deflected in 10 meters due to classical scattering or bremsstrahlung. At 760 Torr the beam is scattered in less than 2 meters. The main purpose of this research was to determine the angular dependence of secondary electrons (delta rays) leaving the beam-air interaction region on their energy. At low pressure, excellent agreement is observed between code results and an analytical formula for the scattering angle as a function of delta ray energy

DD FORM 1 JAN 73 1473 EDITION OF 1 NOV 65 IS OBSOLETE

SECURITY CLASSIFICATION OF THIS PAGE (When Data Entered)

down to energies of a few tens of keV.

ABSTRACT

The Monte Carlo transport of a 1.5 MeV electron beam in low density and full atmosphere air is studied. At a pressure of 0.5 Torr virtually none of the beam is deflected in 10 meters due to classical scattering or bremsstrahlung. At 760 Torr the beam is scattered in less than 2 meters. The main purpose of this research was to determine the angular dependence of secondary electrons (delta rays) leaving the beam-air interaction region on their energy. At low pressure, excellent agreement is observed between code results and an analytical formula for the scattering angle as a function of delta ray energy down to energies of a few tens of keV.

PROBLEM CONFIGURATION

A monoenergetic 1.5 MeV electron beam of radius 3.8 cm is injected into a cylindrical column of air 10 cm in radius and 10 meters deep. The air is composed of 79% Nitrogen, 20 % oxygen and 1% Argon. The low pressure simulation at 0.5 Torr is sectioned into 80 zones in an attempt to determine where the beam energy is deposited. The high pressure run at 760 Torr is divided into 2 zones from 0 to 2, and 2 to 10 meters. The primary purpose of this was to reduce computer running time, because we were mainly interested in the angular distribution of delta rays (secondary electrons) as a function of their energy. At high pressure, however, the angular dependence was unobtainable.

RESULTS

The Monte Carlo transport code CYLTRAN was used in this study. It is particularly suitable, because it can calculate both electron and photon transport in cylindrical geometry. The problem may involve up to five materials each consisting of a maximum of ten elements without code modification. The problem cylinder may be zoned axially and radially into 100 compartments, if necessary. CYLTRAN is detailed in Reference 1.

Data on air at 0.5 Torr pertaining to beam stopping power, range and radiation yield up to a maximum beam energy of 1.5 MeV is compiled in Appendix A. It is generated based on material density, composition, and tabulated cross sections for the various elements. Transport data for the electron beam in 0.5 Torr air is also given in Appendix A. It shows that all of the electron beam is transmitted. Only those zones within the beam path have any energy from primary electrons deposited in them. Total energy deposition from primary and secondary electrons is .10%. No charge deposition due to primaries is recorded. Charge loss from secondaries leaving the beam volume is .7%. The 500,000 incident beam electrons generate only 3440 secondary electrons - all knockons. This results in rather

AD-A133 310 BEAM PROPAGATION EXPERIMENTAL STUDY(U) MISSION RESEARCH 4/4
CORP ALBUQUERQUE NM R J ADLER ET AL. APR 83 AMRC-R-466
AFOSR-TR-83-0743 F49620-81-C-0016

UNCLASSIFIED F/G 20/7 NL

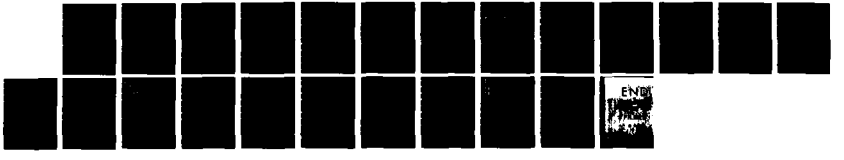

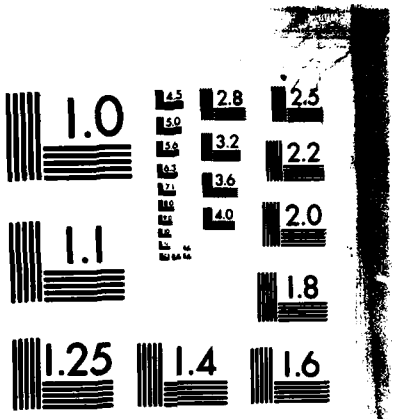

poor statistics for delta ray production and angular dependence on energy. Nevertheless, those points which can be plotted show excellent agreement with an already existing, well-known formula for the angular dependence of delta rays. The equation which was derived from momentum and energy conservation, is

$$\cos\theta = \frac{w}{E}\left(\frac{E + 2mc^2}{w + 2mc^2}\right)^{1/2} \qquad (1)$$

where E is the primary electron energy and w and θ are the delta ray energy and scattering angle. Equation (1) and the points derived from the CYLTRAN program are given in Figure 1.

A second run at full atmospheric pressure was made. CYLTRAN results at this higher pressure are given in Appendix B. In contrast with the prior results, all beam electrons are scattered with virtually all escaping the air cylinder laterally in less than 2 meters. A small percentage (< .2%) are reflected, but none are stopped in the cylinder volume. On average each primary deposits 9.1% of its energy to create .7 knockons/primary. Note, however, that delta rays which are created with energy of less than 10 keV are ignored, so that this number is an underestimate. Because the vast majority of the beam electrons are escaping laterally along with those deltas with sufficient energy to escape the cylinder, it is impossible to determine delta ray angular dependence on energy. Each 10° angular bin has electrons of all possible energies (1.5 MeV to 10 keV) in it. A code update which provides separate data on escaping primary and secondary electrons will be necessary to resolve this problem.

ACKNOWLEDGEMENT

The author is pleased to acknowledge helpful discussions with J. Mack of Los Alamos National Laboratory and J. A. Halbleib of Sandia National Laboratory on the use of the CYLTRAN code.

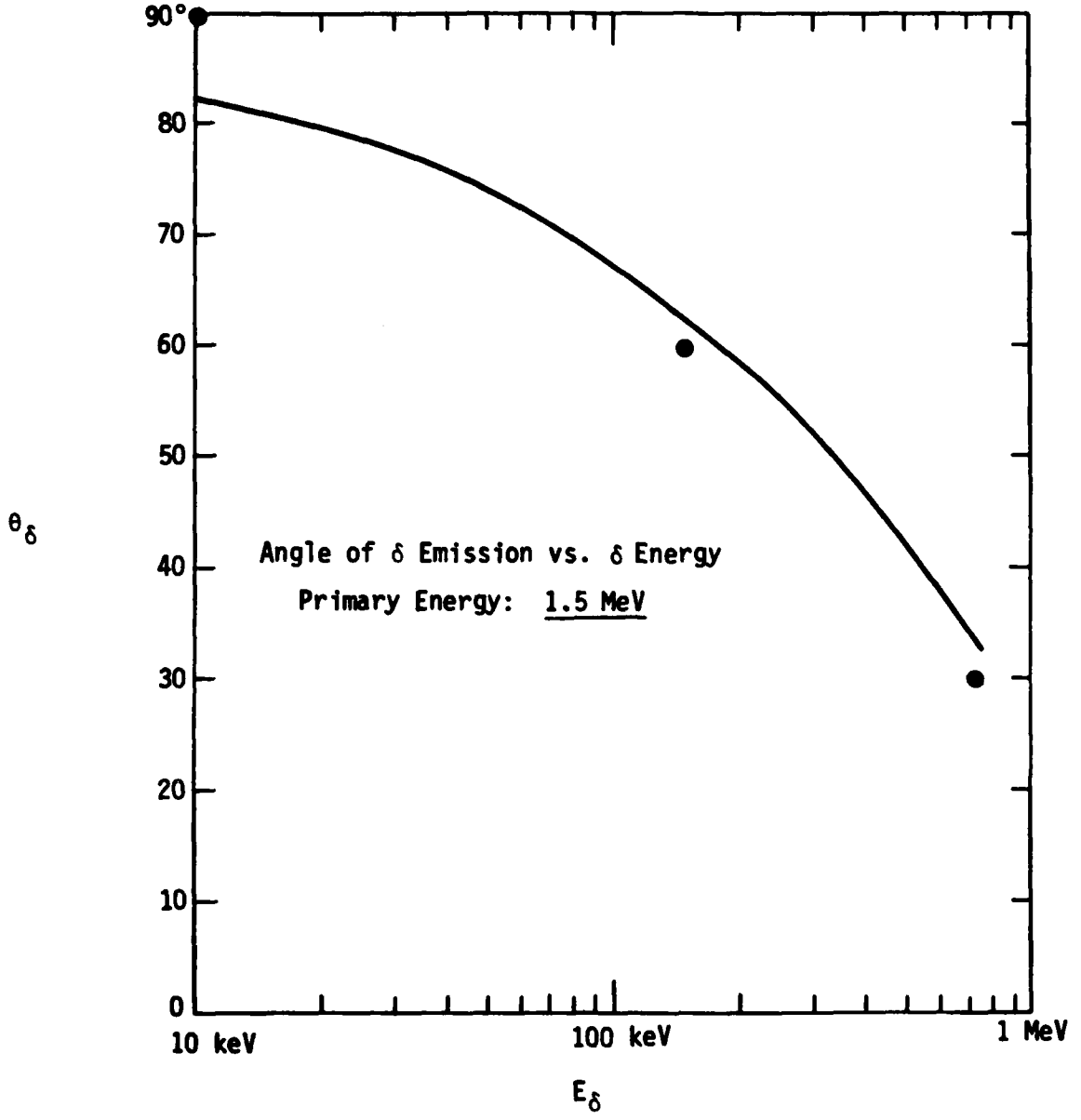

Figure 1. Angular dependence of delta rays on their energy for a 1.5 MeV beam. The solid line results from Equation (1). The points are based on CYLTRAN for air at 0.5 Torr.

REFERENCES

1. J. A. Halbleib Sr. and W. H. Vandevender, CYLTRAN: A Cylindrical-Geometry Multimaterial Electron/Photon Monte Carlo Transport Code, SAND 74-0030, Sandia National Laboratories, (1975), unpublished.

APPENDIX A

AIR PROPERTIES AND 1.5 MeV ELECTRON BEAM TRANSPORT AT 0.5 TORR

```
**1.0 MEV [illegible] BEAM INTO .0 TORR AIR**
0
0 NGET  ITRN  IZIP  IGEN  IRAD  IHEL  ICYC  NCYC  NMAX        EMAX
     1     5     0     1     3     1     1     0    64      .10000E+01
0INPUT DATA TAPE IDENTIFICATION
 DATATAPE-2 (HESTER-AIGINGER PH-RAD CORR), 64 STERNHEIMER SETS. 30 JAN 8
0VECTOUR          DENSITY
   .83000E-00    .64012E-00
0
GRANGE TABLE
0      EMAX        NCYC       EFAC       NMAX     TINMAX+1)   NCAL      TINCAL)
   .10000E+01        0     .01700E+00     64     .0000[illegible]E-02    88     .64083E-03
0 JMAX  LMAX
    3     1
0         Z            A            W
     7.00000     14.00670      .75500
     8.00000     15.99930      .23120
    18.00000     39.94700      .01280
0       PI          PID
    85.64100     85.64100
0  --------------------PARAMETERS FOR DENSITY EFFECT--------------------
         PI           C            A           XM           X1           MS

    85.64100   -17.00[illegible]      .21003      3.00000      5.0000[illegible]      3.3000[illegible]
    85.64100   -17.00[illegible]      .21003      3.00000      5.0000[illegible]      3.3000[illegible]
   .1500E+00  -.1007E+02    .7000E-01
1                                                     ELECTRON RESULTS
0     EFFECTIVE Z/A =  .49919     EFFECTIVE MEAN IONIZATION POTENTIAL =   86.0[illegible] EV     CRITICAL ENERGY =   0.000 MEV
0       ENERGY                  STOPPING POWER                RANGE    RADIATION     BETA**2    DENSITY    RAD/COL    GRANGE     DYIELD
    N                    COLLISION RADIATION    TOTAL                    YIELD                      CORR
           MEV          MEV CM2/G MEV CM2/G MEV CM2/G    G/CM2                                  MEV CM2/G               G/CM2

   86   [illegible]
   85   [illegible]
   84   [illegible]
   83   [illegible]
   82   [illegible]
   81   [illegible]
   80   [illegible]
   79   [illegible]
   78   [illegible]
   77   [illegible]
   76   [illegible]
   75   [illegible]
   74   [illegible]
   73   [illegible]
   72   [illegible]
   71   [illegible]
   70   [illegible]
   69   [illegible]
   68   [illegible]
   67   [illegible]
   66   [illegible]
   65   [illegible]
   64   [illegible]
   63   [illegible]
   62   [illegible]
   61   [illegible]
   60   [illegible]
   59   [illegible]
   58   [illegible]
   57   [illegible]
   56   [illegible]
   55   [illegible]
```

```
   54   [illegible]
   53   [illegible]
   52   [illegible]
   51   [illegible]
   50   [illegible]
   49   [illegible]
   48   [illegible]
   47   [illegible]
   46   [illegible]
   45   [illegible]
   44   [illegible]
   43   [illegible]
   42   [illegible]
   41   [illegible]
   40   [illegible]
   39   [illegible]
   38   [illegible]
   37   [illegible]
   36   [illegible]
   35   [illegible]
   34   [illegible]
   33   [illegible]
   32   [illegible]
   31   [illegible]
   30   [illegible]
   29   [illegible]
   28   [illegible]
   27   [illegible]
   26   [illegible]
   25   [illegible]
   24   [illegible]
   23   [illegible]
   22   [illegible]
   21   [illegible]
   20   [illegible]
   19   [illegible]
   18   [illegible]
   17   [illegible]
   16   [illegible]
   15   [illegible]
   14   [illegible]
   13   [illegible]
   12   [illegible]
   11   [illegible]
   10   [illegible]
    9   [illegible]
    8   [illegible]
    7   [illegible]
    6   [illegible]
    5   [illegible]
    4   [illegible]
    3   [illegible]
    2   [illegible]
    1   .1500E+01   .166E+01   .199E-01   .168E+01   .701E+00   .617E-02   .835E+00 0.        .[illegible]E-01   .7[illegible]E-01   .1[illegible]E-02
```

```
OCTOBER 14 ,1976 VERSION
0 NSET  NATL
          1
0 NMAT  NMAD
          1
GMPAIR  NTAB
       95    1
GAMMA RAY CROSS SECTION DATA
ENERGIES (MEV)
 1000.000000  500.000000  300.000000  200.000000  100.000000  80.000000
  60.000000   50.000000   40.000000   30.000000   20.000000  15.000000
  10.000000    8.000000    6.000000    5.000000    4.000000   3.000000
   2.000000    1.500000    1.000000     .800000     .600000    .500000
    .400000     .300000     .200000     .150000     .100000    .080000
    .060000     .050000     .040000     .030000     .020000    .015000
TOTAL ATTENUATION COEFFICIENTS (CM2/G)
     .039183     .038744     .038000     .037402     .036782    .036488
     .036088     .035773     .035471     .035182     .034906    .034780
     .034787     .034584     .034400     .034237     .034086    .033960
     .033837     .033737     .033651     .033577     .033517    .033488
     .033464     .033462     .033466     .033475     .033497    .033537
     .033597     .033737     .033937     .034237     .034637    .035137
     .035737     .036437     .037237     .038137     .039137    .040237
     .041437     .042737     .044137     .045637     .047237    .048937
     .050737     .052637     .054637     .056737     .058937    .061237
     .063637     .066137     .068737     .071437     .074237    .077137
     .080137     .083237     .086437     .089737     .093137    .096637
     .100237     .103937     .107737     .111637     .115637    .119737
     .123937     .128237     .132637     .137137     .141737    .146437
     .151237     .156137     .161137     .166237     .171437    .176737
     .182137     .187637     .193237     .198937     .204737    .210637
     .216637     .222737     .228937     .235237     .241637    .248137
     .254737     .261437     .268237     .275137     .282137    .289237
     .296437     .303737     .311137     .318637     .326237    .333937
     .341737     .349637     .357637     .365737     .373937    .382237
     .390637     .399137     .407737     .416437     .425237    .434137
     .443137     .452237     .461437     .470737     .480137    .489637
     .499237     .508937     .518737     .528637     .538637    .548737
     .558937     .569237     .579637     .590137     .600737    .611437
     .622237     .633137     .644137     .655237     .666437    .677737
     .689137     .700637     .712237     .723937     .735737    .747637
     .759637     .771737     .783937     .796237     .808637    .821137
     .833737     .846437     .859237     .872137     .885137    .898237
     .911437     .924737     .938137     .951637     .965237    .978937
     .992737    1.006637    1.020637    1.034737    1.048937   1.063237
    1.077637    1.092137    1.106737    1.121437    1.136237   1.151137
    1.166137    1.181237    1.196437    1.211737    1.227137   1.242637
    1.258237    1.273937    1.289737    1.305637    1.321637   1.337737
    1.353937    1.370237    1.386637    1.403137    1.419737   1.436437
    1.453237    1.470137    1.487137    1.504237    1.521437   1.538737
    1.556137    1.573637    1.591237    1.608937    1.626737   1.644637
    1.662637    1.680737    1.698937    1.717237    1.735637   1.754137
    1.772737    1.791437    1.810237    1.829137    1.848137   1.867237
    1.886437    1.905737    1.925137    1.944637    1.964237   1.983937
    2.003737    2.023637    2.043637    2.063737    2.083937   2.104237
    2.124637    2.145137    2.165737    2.186437    2.207237   2.228137
    2.249137    2.270237    2.291437    2.312737    2.334137   2.355637
    2.377237    2.398937    2.420737    2.442637    2.464637   2.486737
    2.508937    2.531237    2.553637    2.576137    2.598737   2.621437
    2.644237    2.667137    2.690137    2.713237    2.736437   2.759737
    2.783137    2.806637    2.830237    2.853937    2.877737   2.901637
    2.925637    2.949737    2.973937    2.998237    3.022637   3.047137
    3.071737    3.096437    3.121237    3.146137    3.171137   3.196237
    3.221437    3.246737    3.272137    3.297637    3.323237   3.348937
    3.374737    3.400637    3.426637    3.452737    3.478937   3.505237
    3.531637    3.558137    3.584737    3.611437    3.638237   3.665137
    3.692137    3.719237    3.746437    3.773737    3.801137   3.828637
    3.856237    3.883937    3.911737    3.939637    3.967637   3.995737
    4.023937    4.052237    4.080637    4.109137    4.137737   4.166437
    4.195237    4.224137    4.253137    4.282237    4.311437   4.340737
    4.370137    4.399637    4.429237    4.458937    4.488737   4.518637
    4.548637    4.578737    4.608937    4.639237    4.669637   4.700137
    4.730737    4.761437    4.792237    4.823137    4.854137   4.885237
    4.916437    4.947737    4.979137    5.010637    5.042237   5.073937
    5.105737    5.137637    5.169637    5.201737    5.233937   5.266237
    5.298637    5.331137    5.363737    5.396437    5.429237   5.462137
    5.495137    5.528237    5.561437    5.594737    5.628137   5.661637
    5.695237    5.728937    5.762737    5.796637    5.830637   5.864737
    5.898937    5.933237    5.967637    6.002137    6.036737   6.071437
    6.106237    6.141137    6.176137    6.211237    6.246437   6.281737
    6.317137    6.352637    6.388237    6.423937    6.459737   6.495637
    6.531637    6.567737    6.603937    6.640237    6.676637   6.713137
    6.749737    6.786437    6.823237    6.860137    6.897137   6.934237
    6.971437    7.008737    7.046137    7.083637    7.121237   7.158937
    7.196737    7.234637    7.272637    7.310737    7.348937   7.387237
    7.425637    7.464137    7.502737    7.541437    7.580237   7.619137
    7.658137    7.697237    7.736437    7.775737    7.815137   7.854637
    7.894237    7.933937    7.973737    8.013637    8.053637   8.093737
    8.133937    8.174237    8.214637    8.255137    8.295737   8.336437
    8.377237    8.418137    8.459137    8.500237    8.541437   8.582737
    8.624137    8.665637    8.707237    8.748937    8.790737   8.832637
    8.874637    8.916737    8.958937    9.001237    9.043637   9.086137
    9.128737    9.171437    9.214237    9.257137    9.300137   9.343237
    9.386437    9.429737    9.473137    9.516637    9.560237   9.603937
    9.647737    9.691637    9.735637    9.779737    9.823937   9.868237
    9.912637    9.957137    1.000137    1.044737    1.089437   1.134237
    1.179137    1.224137    1.269237    1.314437    1.359737   1.405137
    1.450637    1.496237    1.541937    1.587737    1.633637   1.679637
    1.725737    1.771937    1.818237    1.864637    1.911137   1.957737
    2.004437    2.051237    2.098137    2.145137    2.192237   2.239437
    2.286737    2.334137    2.381637    2.429237    2.476937   2.524737
    2.572637    2.620637    2.668737    2.716937    2.765237   2.813637
    2.862137    2.910737    2.959437    3.008237    3.057137   3.106137
    3.155237    3.204437    3.253737    3.303137    3.352637   3.402237
    3.451937    3.501737    3.551637    3.601637    3.651737   3.701937
    3.752237    3.802637    3.853137    3.903737    3.954437   4.005237
    4.056137    4.107137    4.158237    4.209437    4.260737   4.312137
    4.363637    4.415237    4.466937    4.518737    4.570637   4.622637
    4.674737    4.726937    4.779237    4.831637    4.884137   4.936737
    4.989437    5.042237    5.095137    5.148137    5.201237   5.254437
    5.307737    5.361137    5.414637    5.468237    5.521937   5.575737
    5.629637    5.683637    5.737737    5.791937    5.846237   5.900637
    5.955137    6.009737    6.064437    6.119237    6.174137   6.229137
    6.284237    6.339437    6.394737    6.450137    6.505637   6.561237
    6.616937    6.672737    6.728637    6.784637    6.840737   6.896937
    6.953237    7.009637    7.066137    7.122737    7.179437   7.236237
    7.293137    7.350137    7.407237    7.464437    7.521737   7.579137
    7.636637    7.694237    7.751937    7.809737    7.867637   7.925637
    7.983737    8.041937    8.100237    8.158637    8.217137   8.275737
    8.334437    8.393237    8.452137    8.511137    8.570237   8.629437
    8.688737    8.748137    8.807637    8.867237    8.926937   8.986737
    9.046637    9.106637    9.166737    9.226937    9.287237   9.347637
    9.408137    9.468737    9.529437    9.590237    9.651137   9.712137
    9.773237    9.834437    9.895737    9.957137   10.018637  10.080237
   10.141937   10.203737   10.265637   10.327637   10.389737  10.451937
   10.514237   10.576637   10.639137   10.701737   10.764437  10.827237
   10.890137   10.953137   11.016237   11.079437   11.142737  11.206137
   11.269637   11.333237   11.396937   11.460737   11.524637  11.588637
   11.652737   11.716937   11.781237   11.845637   11.910137  11.974737
   12.039437   12.104237   12.169137   12.234137   12.299237  12.364437
   12.429737   12.495137   12.560637   12.626237   12.691937  12.757737
   12.823637   12.889637   12.955737   13.021937   13.088237  13.154637
   13.221137   13.287737   13.354437   13.421237   13.488137  13.555137
   13.622237   13.689437   13.756737   13.824137   13.891637  13.959237
   14.026937   14.094737   14.162637   14.230637   14.298737  14.366937
   14.435237   14.503637   14.572137   14.640737   14.709437  14.778237
   14.847137   14.916137   14.985237   15.054437   15.123737  15.193137
   15.262637   15.332237   15.401937   15.471737   15.541637  15.611637
   15.681737   15.751937   15.822237   15.892637   15.963137  16.033737
   16.104437   16.175237   16.246137   16.317137   16.388237  16.459437
   16.530737   16.602137   16.673637   16.745237   16.816937  16.888737
   16.960637   17.032637   17.104737   17.176937   17.249237  17.321637
   17.394137   17.466737   17.539437   17.612237   17.685137  17.758137
   17.831237   17.904437   17.977737   18.051137   18.124637  18.198237
   18.271937   18.345737   18.419637   18.493637   18.567737  18.641937
   18.716237   18.790637   18.865137   18.939737   19.014437  19.089237
   19.164137   19.239137   19.314237   19.389437   19.464737  19.540137
   19.615637   19.691237   19.766937   19.842737   19.918637  19.994637
   20.070737   20.146937   20.223237   20.299637   20.376137  20.452737
   20.529437   20.606237   20.683137   20.760137   20.837237  20.914437
   20.991737   21.069137   21.146637   21.224237   21.301937  21.379737
   21.457637   21.535637   21.613737   21.691937   21.770237  21.848637
   21.927137   22.005737   22.084437   22.163237   22.242137  22.321137
   22.400237   22.479437   22.558737   22.638137   22.717637  22.797237
   22.876937   22.956737   23.036637   23.116637   23.196737  23.276937
   23.357237   23.437637   23.518137   23.598737   23.679437  23.760237
   23.841137   23.922137   24.003237   24.084437   24.165737  24.247137
   24.328637   24.410237   24.491937   24.573737   24.655637  24.737637
   24.819737   24.901937   24.984237   25.066637   25.149137  25.231737
   25.314437   25.397237   25.480137   25.563137   25.646237  25.729437
   25.812737   25.896137   25.979637   26.063237   26.146937  26.230737
   26.314637   26.398637   26.482737   26.566937   26.651237  26.735637
   26.820137   26.904737   26.989437   27.074237   27.159137  27.244137
   27.329237   27.414437   27.499737   27.585137   27.670637  27.756237
   27.841937   27.927737   28.013637   28.099637   28.185737  28.271937
   28.358237   28.444637   28.531137   28.617737   28.704437  28.791237
   28.878137   28.965137   29.052237   29.139437   29.226737  29.314137
   29.401637   29.489237   29.576937   29.664737   29.752637  29.840637
   29.928737   30.016937   30.105237   30.193637   30.282137  30.370737
   30.459437   30.548237   30.637137   30.726137   30.815237  30.904437
   30.993737   31.083137   31.172637   31.262237   31.351937  31.441737
   31.531637   31.621637   31.711737   31.801937   31.892237  31.982637
   32.073137   32.163737   32.254437   32.345237   32.436137  32.527137
   32.618237   32.709437   32.800737   32.892137   32.983637  33.075237
   33.166937   33.258737   33.350637   33.442637   33.534737  33.626937
   33.719237   33.811637   33.904137   33.996737   34.089437  34.182237
   34.275137   34.368137   34.461237   34.554437   34.647737  34.741137
   34.834637   34.928237   35.021937   35.115737   35.209637  35.303637
   35.397737   35.491937   35.586237   35.680637   35.775137  35.869737
   35.964437   36.059237   36.154137   36.249137   36.344237  36.439437
   36.534737   36.630137   36.725637   36.821237   36.916937  37.012737
   37.108637   37.204637   37.300737   37.396937   37.493237  37.589637
   37.686137   37.782737   37.879437   37.976237   38.073137  38.170137
   38.267237   38.364437   38.461737   38.559137   38.656637  38.754237
   38.851937   38.949737   39.047637   39.145637   39.243737  39.341937
   39.440237   39.538637   39.637137   39.735737   39.834437  39.933237
   40.032137   40.131137   40.230237   40.329437   40.428737  40.528137
   40.627637   40.727237   40.826937   40.926737   41.026637  41.126637
   41.226737   41.326937   41.427237   41.527637   41.628137  41.728737
   41.829437   41.930237   42.031137   42.132137   42.233237  42.334437
   42.435737   42.537137   42.638637   42.740237   42.841937  42.943737
   43.045637   43.147637   43.249737   43.351937   43.454237  43.556637
   43.659137   43.761737   43.864437   43.967237   44.070137  44.173137
   44.276237   44.379437   44.482737   44.586137   44.689637  44.793237
   44.896937   45.000737   45.104637   45.208637   45.312737  45.416937
   45.521237   45.625637   45.730137   45.834737   45.939437  46.044237
   46.149137   46.254137   46.359237   46.464437   46.569737  46.675137
   46.780637   46.886237   46.991937   47.097737   47.203637  47.309637
   47.415737   47.521937   47.628237   47.734637   47.841137  47.947737
   48.054437   48.161237   48.268137   48.375137   48.482237  48.589437
   48.696737   48.804137   48.911637   49.019237   49.126937  49.234737
   49.342637   49.450637   49.558737   49.666937   49.775237  49.883637
   49.992137   50.100737   50.209437   50.318237   50.427137  50.536137
   50.645237   50.754437   50.863737   50.973137   51.082637  51.192237
   51.301937   51.411737   51.521637   51.631637   51.741737  51.851937
   51.962237   52.072637   52.183137   52.293737   52.404437  52.515237
   52.626137   52.737137   52.848237   52.959437   53.070737  53.182137
   53.293637   53.405237   53.516937   53.628737   53.740637  53.852637
   53.964737   54.076937   54.189237   54.301637   54.414137  54.526737
   54.639437   54.752237   54.865137   54.978137   55.091237  55.204437
   55.317737   55.431137   55.544637   55.658237   55.771937  55.885737
   55.999637   56.113637   56.227737   56.341937   56.456237  56.570637
   56.685137   56.799737   56.914437   57.029237   57.144137  57.259137
   57.374237   57.489437   57.604737   57.720137   57.835637  57.951237
   58.066937   58.182737   58.298637   58.414637   58.530737  58.646937
   58.763237   58.879637   58.996137   59.112737   59.229437  59.346237
   59.463137   59.580137   59.697237   59.814437   59.931737  60.049137
   60.166637   60.284237   60.401937   60.519737   60.637637  60.755637
   60.873737   60.991937   61.110237   61.228637   61.347137  61.465737
   61.584437   61.703237   61.822137   61.941137   62.060237  62.179437
   62.298737   62.418137   62.537637   62.657237   62.776937  62.896737
   63.016637   63.136637   63.256737   63.376937   63.497237  63.617637
   63.738137   63.858737   63.979437   64.100237   64.221137  64.342137
   64.463237   64.584437   64.705737   64.827137   64.948637  65.070237
   65.191937   65.313737   65.435637   65.557637   65.679737  65.801937
   65.924237   66.046637   66.169137   66.291737   66.414437  66.537237
   66.660137   66.783137   66.906237   67.029437   67.152737  67.276137
   67.399637   67.523237   67.646937   67.770737   67.894637  68.018637
   68.142737   68.266937   68.391237   68.515637   68.640137  68.764737
   68.889437   69.014237   69.139137   69.264137   69.389237  69.514437
   69.639737   69.765137   69.890637   70.016237   70.141937  70.267737
   70.393637   70.519637   70.645737   70.771937   70.898237  71.024637
   71.151137   71.277737   71.404437   71.531237   71.658137  71.785137
   71.912237   72.039437   72.166737   72.294137   72.421637  72.549237
   72.676937   72.804737   72.932637   73.060637   73.188737  73.316937
   73.445237   73.573637   73.702137   73.830737   73.959437  74.088237
   74.217137   74.346137   74.475237   74.604437   74.733737  74.863137
   74.992637   75.122237   75.251937   75.381737   75.511637  75.641637
   75.771737   75.901937   76.032237   76.162637   76.293137  76.423737
   76.554437   76.685237   76.816137   76.947137   77.078237  77.209437
   77.340737   77.472137   77.603637   77.735237   77.866937  77.998737
   78.130637   78.262637   78.394737   78.526937   78.659237  78.791637
   78.924137   79.056737   79.189437   79.322237   79.455137  79.588137
   79.721237   79.854437   79.987737   80.121137   80.254637  80.388237
   80.521937   80.655737   80.789637   80.923637   81.057737  81.191937
   81.326237   81.460637   81.595137   81.729737   81.864437  81.999237
   82.134137   82.269137   82.404237   82.539437   82.674737  82.810137
   82.945637   83.081237   83.216937   83.352737   83.488637  83.624637
   83.760737   83.896937   84.033237   84.169637   84.306137  84.442737
   84.579437   84.716237   84.853137   84.990137   85.127237  85.264437
   85.401737   85.539137   85.676637   85.814237   85.951937  86.089737
   86.227637   86.365637   86.503737   86.641937   86.780237  86.918637
   87.057137   87.195737   87.334437   87.473237   87.612137  87.751137
   87.890237   88.029437   88.168737   88.308137   88.447637  88.587237
   88.726937   88.866737   89.006637   89.146637   89.286737  89.426937
   89.567237   89.707637   89.848137   89.988737   90.129437  90.270237
   90.411137   90.552137   90.693237   90.834437   90.975737  91.117137
   91.258637   91.400237   91.541937   91.683737   91.825637  91.967637
   92.109737   92.251937   92.394237   92.536637   92.679137  92.821737
   92.964437   93.107237   93.250137   93.393137   93.536237  93.679437
   93.822737   93.966137   94.109637   94.253237   94.396937  94.540737
   94.684637   94.828637   94.972737   95.116937   95.261237  95.405637
   95.550137   95.694737   95.839437   95.984237   96.129137  96.274137
   96.419237   96.564437   96.709737   96.855137   97.000637  97.146237
   97.291937   97.437737   97.583637   97.729637   97.875737  98.021937
   98.168237   98.314637   98.461137   98.607737   98.754437  98.901237
   99.048137   99.195137   99.342237   99.489437   99.636737  99.784137
   99.931637  100.079237  100.226937  100.374737  100.522637 100.670637
  100.818737  100.966937  101.115237  101.263637  101.412137 101.560737
  101.709437  101.858237  102.007137  102.156137  102.305237 102.454437
  102.603737  102.753137  102.902637  103.052237  103.201937 103.351737
  103.501637  103.651637  103.801737  103.951937  104.102237 104.252637
  104.403137  104.553737  104.704437  104.855237  105.006137 105.157137
  105.308237  105.459437  105.610737  105.762137  105.913637 106.065237
  106.216937  106.368737  106.520637  106.672637  106.824737 106.976937
  107.129237  107.281637  107.434137  107.586737  107.739437 107.892237
  108.045137  108.198137  108.351237  108.504437  108.657737 108.811137
  108.964637  109.118237  109.271937  109.425737  109.579637 109.733637
  109.887737  110.041937  110.196237  110.350637  110.505137 110.659737
  110.814437  110.969237  111.124137  111.279137  111.434237 111.589437
  111.744737  111.900137  112.055637  112.211237  112.366937 112.522737
  112.678637  112.834637  112.990737  113.146937  113.303237 113.459637
  113.616137  113.772737  113.929437  114.086237  114.243137 114.400137
  114.557237  114.714437  114.871737  115.029137  115.186637 115.344237
  115.501937  115.659737  115.817637  115.975637  116.133737 116.291937
  116.450237  116.608637  116.767137  116.925737  117.084437 117.243237
  117.402137  117.561137  117.720237  117.879437  118.038737 118.198137
  118.357637  118.517237  118.676937  118.836737  118.996637 119.156637
  119.316737  119.476937  119.637237  119.797637  119.958137 120.118737
  120.279437  120.440237  120.601137  120.762137  120.923237 121.084437
  121.245737  121.407137  121.568637  121.730237  121.891937 122.053737
  122.215637  122.377637  122.539737  122.701937  122.864237 123.026637
  123.189137  123.351737  123.514437  123.677237  123.840137 124.003137
  124.166237  124.329437  124.492737  124.656137  124.819637 124.983237
  125.146937  125.310737  125.474637  125.638637  125.802737 125.966937
  126.131237  126.295637  126.460137  126.624737  126.789437 126.954237
  127.119137  127.284137  127.449237  127.614437  127.779737 127.945137
  128.110637  128.276237  128.441937  128.607737  128.773637 128.939637
  129.105737  129.271937  129.438237  129.604637  129.771137 129.937737
  130.104437  130.271237  130.438137  130.605137  130.772237 130.939437
  131.106737  131.274137  131.441637  131.609237  131.776937 131.944737
  132.112637  132.280637  132.448737  132.616937  132.785237 132.953637
  133.122137  133.290737  133.459437  133.628237  133.797137 133.966137
  134.135237  134.304437  134.473737  134.643137  134.812637 134.982237
  135.151937  135.321737  135.491637  135.661637  135.831737 136.001937
  136.172237  136.342637  136.513137  136.683737  136.854437 137.025237
  137.196137  137.367137  137.538237  137.709437  137.880737 138.052137
  138.223637  138.395237  138.566937  138.738737  138.910637 139.082637
  139.254737  139.426937  139.599237  139.771637  139.944137 140.116737
  140.289437  140.462237  140.635137  140.808137  140.981237 141.154437
  141.327737  141.501137  141.674637  141.848237  142.021937 142.195737
  142.369637  142.543637  142.717737  142.891937  143.066237 143.240637
  143.415137  143.589737  143.764437  143.939237  144.114137 144.289137
  144.464237  144.639437  144.814737  144.990137  145.165637 145.341237
  145.516937  145.692737  145.868637  146.044637  146.220737 146.396937
  146.573237  146.749637  146.926137  147.102737  147.279437 147.456237
  147.633137  147.810137  147.987237  148.164437  148.341737 148.519137
  148.696637  148.874237  149.051937  149.229737  149.407637 149.585637
  149.763737  149.941937  150.120237  150.298637  150.477137 150.655737
  150.834437  151.013237  151.192137  151.371137  151.550237 151.729437
  151.908737  152.088137  152.267637  152.447237  152.626937 152.806737
  152.986637  153.166637  153.346737  153.526937  153.707237 153.887637
  154.068137  154.248737  154.429437  154.610237  154.791137 154.972137
  155.153237  155.334437  155.515737  155.697137  155.878637 156.060237
  156.241937  156.423737  156.605637  156.787637  156.969737 157.151937
  157.334237  157.516637  157.699137  157.881737  158.064437 158.247237
  158.430137  158.613137  158.796237  158.979437  159.162737 159.346137
  159.529637  159.713237  159.896937  160.080737  160.264637 160.448637
  160.632737  160.816937  161.001237  161.185637  161.370137 161.554737
  161.739437  161.924237  162.109137  162.294137  162.479237 162.664437
  162.849737  163.035137  163.220637  163.406237  163.591937 163.777737
  163.963637  164.149637  164.335737  164.521937  164.708237 164.894637
  165.081137  165.267737  165.454437  165.641237  165.828137 166.015137
  166.202237  166.389437  166.576737  166.764137  166.951637 167.139237
  167.326937  167.514737  167.702637  167.890637  168.078737 168.266937
  168.455237  168.643637  168.832137  169.020737  169.209437 169.398237
  169.587137  169.776137  169.965237  170.154437  170.343737 170.533137
  170.722637  170.912237  171.101937  171.291737  171.481637 171.671637
  171.861737  172.051937  172.242237  172.432637  172.623137 172.813737
  173.004437  173.195237  173.386137  173.577137  173.768237 173.959437
  174.150737  174.342137  174.533637  174.725237  174.916937 175.108737
  175.300637  175.492637  175.684737  175.876937  176.069237 176.261637
  176.454137  176.646737  176.839437  177.032237  177.225137 177.418137
  177.611237  177.804437  177.997737  178.191137  178.384637 178.578237
  178.771937  178.965737  179.159637  179.353637  179.547737 179.741937
  179.936237  180.130637  180.325137  180.519737  180.714437 180.909237
  181.104137  181.299137  181.494237  181.689437  181.884737 182.080137
  182.275637  182.471237  182.666937  182.862737  183.058637 183.254637
  183.450737  183.646937  183.843237  184.039637  184.236137 184.432737
  184.629437  184.826237  185.023137  185.220137  185.417237 185.614437
  185.811737  186.009137  186.206637  186.404237  186.601937 186.799737
  186.997637  187.195637  187.393737  187.591937  187.790237 187.988637
  188.187137  188.385737  188.584437  188.783237  188.982137 189.181137
  189.380237  189.579437  189.778737  189.978137  190.177637 190.377237
  190.576937  190.776737  190.976637  191.176637  191.376737 191.576937
  191.777237  191.977637  192.178137  192.378737  192.579437 192.780237
  192.981137  193.182137  193.383237  193.584437  193.785737 193.987137
  194.188637  194.390237  194.591937  194.793737  194.995637 195.197637
  195.399737  195.601937  195.804237  196.006637  196.209137 196.411737
  196.614437  196.817237  197.020137  197.223137  197.426237 197.629437
  197.832737  198.036137  198.239637  198.443237  198.646937 198.850737
  199.054637  199.258637  199.462737  199.666937  199.871237 200.075637
  200.280137  200.484737  200.689437  200.894237  201.099137 201.304137
  201.509237  201.714437  201.919737  202.125137  202.330637 202.536237
  202.741937  202.947737  203.153637  203.359637  203.565737 203.771937
  203.978237  204.184637  204.391137  204.597737  204.804437 205.011237
  205.218137  205.425137  205.632237  205.839437  206.046737 206.254137
  206.461637  206.669237  206.876937  207.084737  207.292637 207.500637
  207.708737  207.916937  208.125237  208.333637  208.542137 208.750737
  208.959437  209.168237  209.377137  209.586137  209.795237 210.004437
  210.213737  210.423137  210.632637  210.842237  211.051937 211.261737
  211.471637  211.681637  211.891737  212.101937  212.312237 212.522637
  212.733137  212.943737  213.154437  213.365237  213.576137 213.787137
  213.998237  214.209437  214.420737  214.632137  214.843637 215.055237
  215.266937  215.478737  215.690637  215.902637  216.114737 216.326937
  216.539237  216.751637  216.964137  217.176737  217.389437 217.602237
  217.815137  218.028137  218.241237  218.454437  218.667737 218.881137
  219.094637  219.308237  219.521937  219.735737  219.949637 220.163637
  220.377737  220.591937  220.806237  221.020637  221.235137 221.449737
  221.664437  221.879237  222.094137  222.309137  222.524237 222.739437
  222.954737  223.170137  223.385637  223.601237  223.816937 224.032737
  224.248637  224.464637  224.680737  224.896937  225.113237 225.329637
  225.546137  225.762737  225.979437  226.196237  226.413137 226.630137
  226.847237  227.064437  227.281737  227.499137  227.716637 227.934237
  228.151937  228.369737  228.587637  228.805637  229.023737 229.241937
  229.460237  229.678637  229.897137  230.115737  230.334437 230.553237
  230.772137  230.991137  231.210237  231.429437  231.648737 231.868137
  232.087637  232.307237  232.526937  232.746737  232.966637 233.186637
  233.406737  233.626937  233.847237  234.067637  234.288137 234.508737
  234.729437  234.950237  235.171137  235.392137  235.613237 235.834437
  236.055737  236.277137  236.498637  236.720237  236.941937 237.163737
  237.385637  237.607637  237.829737  238.051937  238.274237 238.496637
  238.719137  238.941737  239.164437  239.387237  239.610137 239.833137
  240.056237  240.279437  240.502737  240.726137  240.949637 241.173237
  241.396937  241.620737  241.844637  242.068637  242.292737 242.516937
  242.741237  242.965637  243.190137  243.414737  243.639437 243.864237
  244.089137  244.314137  244.539237  244.764437  244.989737 245.215137
  245.440637  245.666237  245.891937  246.117737  246.343637 246.569637
  246.795737  247.021937  247.248237  247.474637  247.701137 247.927737
  248.154437  248.381237  248.608137  248.835137  249.062237 249.289437
  249.516737  249.744137  249.971637  250.199237  250.426937 250.654737
  250.882637  251.110637  251.338737  251.566937  251.795237 252.023637
  252.252137  252.480737  252.709437  252.938237  253.167137 253.396137
  253.625237  253.854437  254.083737  254.313137  254.542637 254.772237
  255.001937  255.231737  255.461637  255.691637  255.921737 256.151937
  256.382237  256.612637  256.843137  257.073737  257.304437 257.535237
  257.766137  257.997137  258.228237  258.459437  258.690737 258.922137
  259.153637  259.385237  259.616937  259.848737  260.080637 260.312637
  260.544737  260.776937  261.009237  261.241637  261.474137 261.706737
  261.939437  262.172237  262.405137  262.638137  262.871237 263.104437
  263.337737  263.571137  263.804637  264.038237  264.271937 264.505737
  264.739637  264.973637  265.207737  265.441937  265.676237 265.910637
  266.145137  266.379737  266.614437  266.849237  267.084137 267.319137
  267.554237  267.789437  268.024737  268.260137  268.495637 268.731237
  268.966937  269.202737  269.438637  269.674637  269.910737 270.146937
  270.383237  270.619637  270.856137  271.092737  271.329437 271.566237
  271.803137  272.040137  272.277237  272.514437  272.751737 272.989137
  273.226637  273.464237  273.701937  273.939737  274.177637 274.415637
  274.653737  274.891937  275.130237  275.368637  275.607137 275.845737
  276.084437  276.323237  276.562137  276.801137  277.040237 277.279437
  277.518737  277.758137  277.997637  278.237237  278.476937 278.716737
  278.956637  279.196637  279.436737  279.676937  279.917237 280.157637
  280.398137  280.638737  280.879437  281.120237  281.361137 281.602137
  281.843237  282.084437  282.325737  282.567137  282.808637 283.050237
  283.291937  283.533737  283.775637  284.017637  284.259737 284.501937
  284.744237  284.986637  285.229137  285.471737  285.714437 285.957237
  286.200137  286.443137  286.686237  286.929437  287.172737 287.416137
  287.659637  287.903237  288.146937  288.390737  288.634637 288.878637
  289.122737  289.366937  289.611237  289.855637  290.100137 290.344737
  290.589437  290.834237  291.079137  291.324137  291.569237 291.814437
  292.059737  292.305137  292.550637  292.796237  293.041937 293.287737
  293.533637  293.779637  294.025737  294.271937  294.518237 294.764637
  295.011137  295.257737  295.504437  295.751237  295.998137 296.245137
  296.492237  296.739437  296.986737  297.234137  297.481637 297.729237
  297.976937  298.224737  298.472637  298.720637  298.968737 299.216937
  299.465237  299.713637  299.962137  300.210737  300.459437 300.708237
  300.957137  301.206137  301.455237  301.704437  301.953737 302.203137
  302.452637  302.702237  302.951937  303.201737  303.451637 303.701637
  303.951737  304.201937  304.452237  304.702637  304.953137 305.203737
  305.454437  305.705237  305.956137  306.207137  306.458237 306.709437
  306.960737  307.212137  307.463637  307.715237  307.966937 308.218737
  308.470637  308.722637  308.974737  309.226937  309.479237 309.731637
  309.984137  310.236737  310.489437  310.742237  310.995137 311.248137
  311.501237  311.754437  312.007737  312.261137  312.514637 312.768237
  313.021937  313.275737  313.529637  313.783637  314.037737 314.291937
  314.546237  314.800637  315.055137  315.309737  315.564437 315.819237
  316.074137  316.329137  316.584237  316.839437  317.094737 317.350137
  317.605637  317.861237  318.116937  318.372737  318.628637 318.884637
  319.140737  319.396937  319.653237  319.909637  320.166137 320.422737
  320.679437  320.936237  321.193137  321.450137  321.707237 321.964437
  322.221737  322.479137  322.736637  322.994237  323.251937 323.509737
  323.767637  324.025637  324.283737  324.541937  324.800237 325.058637
  325.317137  325.575737  325.834437  326.093237  326.352137 326.611137
  326.870237  327.129437  327.388737  327.648137  327.907637 328.167237
  328.426937  328.686737  328.946637  329.206637  329.466737 329.726937
  329.987237  330.247637  330.508137  330.768737  331.029437 331.290237
  331.551137  331.812137  332.073237  332.334437  332.595737 332.857137
  333.118637  333.380237  333.641937  333.903737  334.165637 334.427637
  334.689737  334.951937  335.214237  335.476637  335.739137 336.001737
  336.264437  336.527237  336.790137  337.053137  337.316237 337.579437
  337.842737  338.106137  338.369637  338.633237  338.896937 339.160737
  339.424637  339.688637  339.952737  340.216937  340.481237 340.745637
  341.010137  341.274737  341.539437  341.804237  342.069137 342.334137
  342.599237  342.864437  343.129737  343.395137  343.660637 343.926237
  344.191937  344.457737  344.723637  344.989637  345.255737 345.521937
  345.788237  346.054637  346.321137  346.587737  346.854437 347.121237
  347.388137  347.655137  347.922237  348.189437  348.456737 348.724137
  348.991637  349.259237  349.526937  349.794737  350.062637 350.330637
  350.598737  350.866937  351.135237  351.403637  351.672137 351.940737
  352.209437  352.478237  352.747137  353.016137  353.285237 353.554437
  353.823737  354.093137  354.362637  354.632237  354.901937 355.171737
  355.441637  355.711637  355.981737  356.251937  356.522237 356.792637
  357.063137  357.333737  357.604437  357.875237  358.146137 358.417137
  358.688237  358.959437  359.230737  359.502137  359.773637 360.045237
  360.316937  360.588737  360.860637  361.132637  361.404737 361.676937
  361.949237  362.221637  362.494137  362.766737  363.039437 363.312237
  363.585137  363.858137  364.131237  364.404437  364.677737 364.951137
  365.224637  365.498237  365.771937  366.045737  366.319637 366.593637
  366.867737  367.141937  367.416237  367.690637  367.965137 368.239737
  368.514437  368.789237  369.064137  369.339137  369.614237 369.889437
  370.164737  370.440137  370.715637  370.991237  371.266937 371.542737
  371.818637  372.094637  372.370737  372.646937  372.923237 373.199637
  373.476137  373.752737  374.029437  374.306237  374.583137 374.860137
  375.137237  375.414437  375.691737  375.969137  376.246637 376.524237
  376.801937  377.079737  377.357637  377.635637  377.913737 378.191937
  378.470237  378.748637  379.027137  379.305737  379.584437 379.863237
  380.142137  380.421137  380.700237  380.979437  381.258737 381.538137
  381.817637  382.097237  382.376937  382.656737  382.936637 383.216637
  383.496737  383.776937  384.057237  384.337637  384.618137 384.898737
  385.179437  385.460237  385.741137  386.022137  386.303237 386.584437
  386.865737  387.147137  387.428637  387.710237  387.991937 388.273737
  388.555637  388.837637  389.119737  389.401937  389.684237 389.966637
  390.249137  390.531737  390.814437  391.097237  391.380137 391.663137
  391.946237  392.229437  392.512737  392.796137  393.079637 393.363237
  393.646937  393.930737  394.214637  394.498637  394.782737 395.066937
  395.351237  395.635637  395.920137  396.204737  396.489437 396.774237
  397.059137  397.344137  397.629237  397.914437  398.199737 398.485137
  398.770637  399.056237  399.341937  399.627737  399.913637 400.199637
  400.485737  400.771937  401.058237  401.344637  401.631137 401.917737
  402.204437  402.491237  402.778137  403.065137  403.352237 403.639437
  403.926737  404.214137  404.501637  404.789237  405.076937 405.364737
  405.652637  405.940637  406.228737  406.516937  406.805237 407.093637
  407.382137  407.670737  407.959437  408.248237  408.537137 408.826137
  409.115237  409.404437  409.693737  409.983137  410.272637 410.562237
  410.851937  411.141737  411.431637  411.721637  412.011737 412.301937
  412.592237  412.882637  413.173137  413.463737  413.754437 414.045237
  414.336137  414.627137  414.918237  415.209437  415.500737 415.792137
  416.083637  416.375237  416.666937  416.958737  417.250637 417.542637
  417.834737  418.126937  418.419237  418.711637  419.004137 419.296737
  419.589437  419.882237  420.175137  420.468137  420.761237 421.054437
  421.347737  421.641137  421.934637  422.228237  422.521937 422.815737
  423.109637  423.403637  423.697737  423.991937  424.286237 424.580637
  424.875137  425.169737  425.464437  425.759237  426.054137 426.349137
  426.644237  426.939437  427.234737  427.530137  427.825637 428.121237
  428.416937  428.712737  429.008637  429.304637  429.600737 429.896937
  430.193237  430.489637  430.786137  431.082737  431.379437 431.676237
  431.973137  432.270137  432.567237  432.864437  433.161737 433.459137
  433.756637  434.054237  434.351937  434.649737  434.947637 435.245637
  435.543737  435.841937  436.140237  436.438637  436.737137 437.035737
  437.334437  437.633237  437.932137  438.231137  438.530237 438.829437
  439.128737  439.428137  439.727637  440.027237  440.326937 440.626737
  440.926637  441.226637  441.526737  441.826937  442.127237 442.427637
  442.728137  443.028737  443.329437  443.630237  443.931137 444.232137
  444.533237  444.834437  445.135737  445.437137  445.738637 446.040237
  446.341937  446.643737  446.945637  447.247637  447.549737 447.851937
  448.154237  448.456637  448.759137  449.061737  449.364437 449.667237
  449.970137  450.273137  450.576237  450.879437  451.182737 451.486137
  451.789637  452.093237  452.396937  452
```

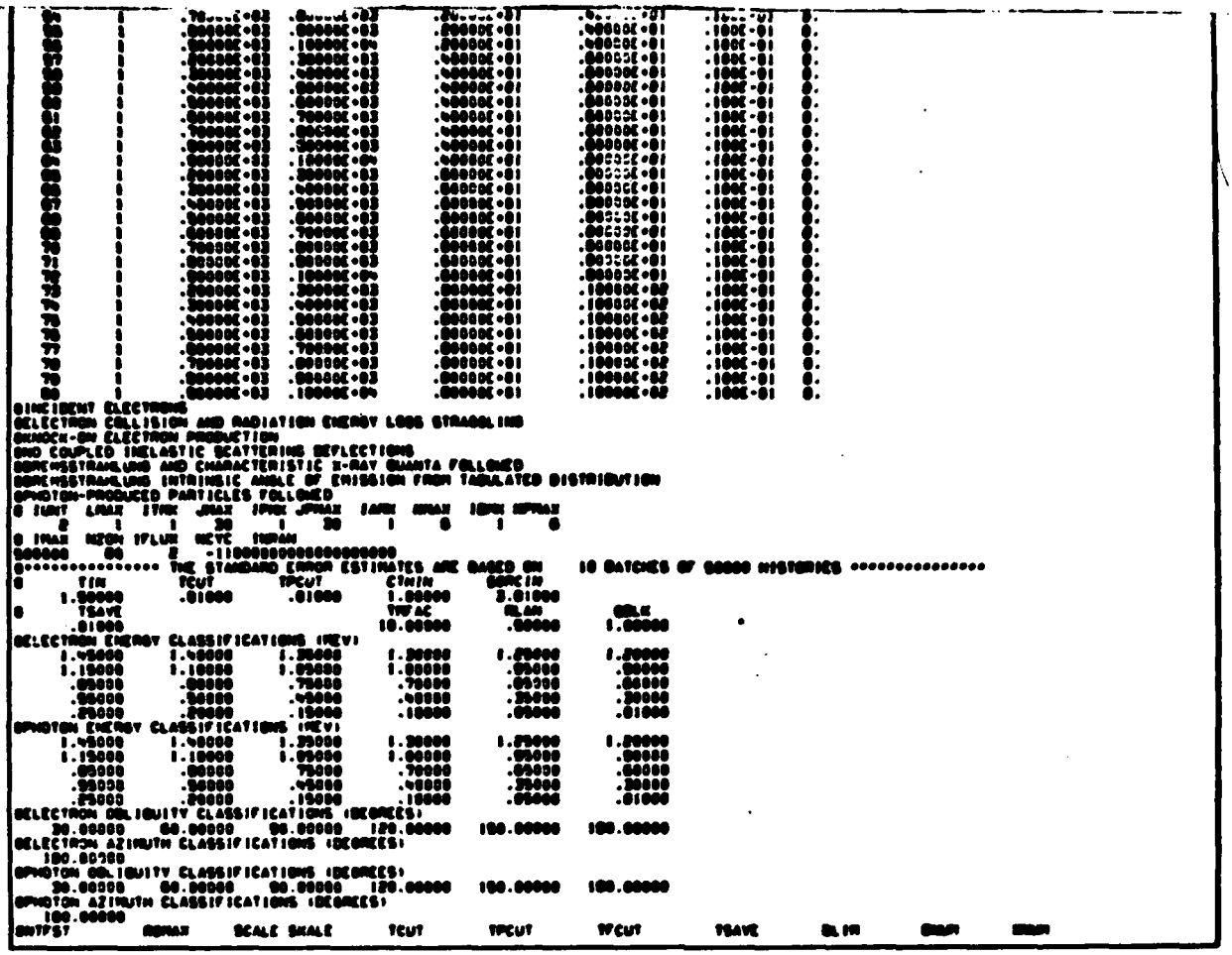

```
 INCIDENT ELECTRONS
 ELECTRON COLLISION AND RADIATION ENERGY LOSS STRAGGLING
 KNOCK-ON ELECTRON PRODUCTION
 AND COUPLED INELASTIC SCATTERING REFLECTIONS
 BREMSSTRAHLUNG AND CHARACTERISTIC X-RAY QUANTA FOLLOWED
 BREMSSTRAHLUNG INTRINSIC ANGLE OF EMISSION FROM TABULATED DISTRIBUTION
 BPHOTON-PRODUCED PARTICLES FOLLOWED
```

```
 ELECTRON ENERGY CLASSIFICATIONS (MEV)
 PHOTON ENERGY CLASSIFICATIONS (MEV)
 ELECTRON OBLIQUITY CLASSIFICATIONS (DEGREES)
 ELECTRON AZIMUTH CLASSIFICATIONS (DEGREES)
 PHOTON OBLIQUITY CLASSIFICATIONS (DEGREES)
 PHOTON AZIMUTH CLASSIFICATIONS (DEGREES)
```

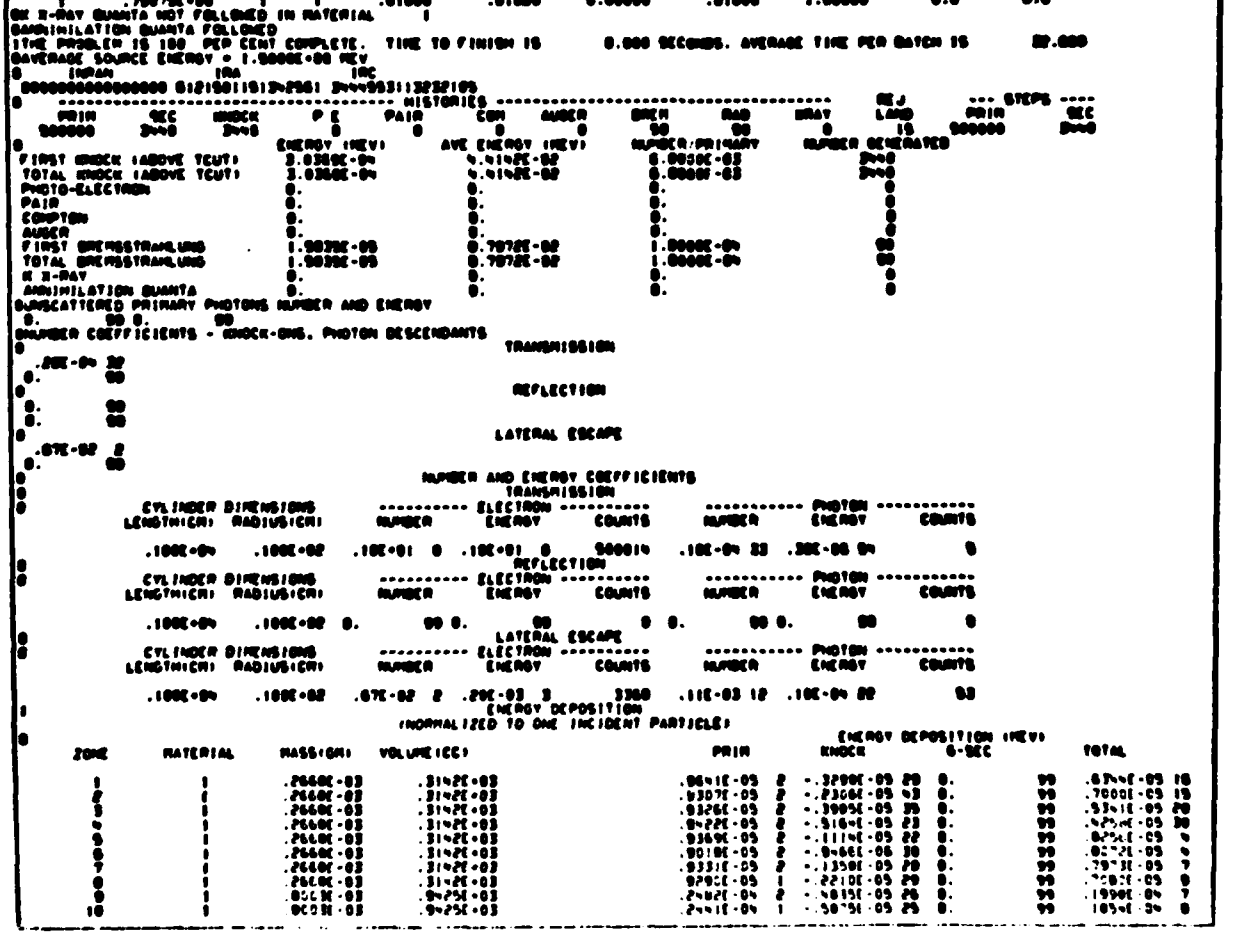

```
 BX X-RAY QUANTA NOT FOLLOWED IN MATERIAL
 BANNIHILATION QUANTA FOLLOWED
 THE PROBLEM IS 100  PER CENT COMPLETE.  TIME TO FINISH IS       0.000 SECONDS. AVERAGE TIME PER BATCH IS
 BAVERAGE SOURCE ENERGY = 1.0000E+00 MEV
```

```
 FIRST KNOCK (ABOVE TCUT)
 TOTAL KNOCK (ABOVE TCUT)
 PHOTO-ELECTRON
 PAIR
 COMPTON
 AUGER
 FIRST BREMSSTRAHLUNG
 TOTAL BREMSSTRAHLUNG
 K X-RAY
 ANNIHILATION QUANTA
 BBACKSCATTERED PRIMARY PHOTONS NUMBER AND ENERGY
 BNUMBER COEFFICIENTS - KNOCK-ONS, PHOTON DESCENDANTS
                                        TRANSMISSION
                                        REFLECTION
                                        LATERAL ESCAPE
                                NUMBER AND ENERGY COEFFICIENTS
                                      TRANSMISSION
```



```
                                      REFLECTION
```



```
                                    LATERAL ESCAPE
```



```
                                ENERGY DEPOSITION
                          (NORMALIZED TO ONE INCIDENT PARTICLE)
```

ENERGY DEPOSITION
(NORMALIZED TO ONE INCIDENT PARTICLE)

ZONE	MATERIAL	MASS(GM)	VOLUME(CC)	ENERGY DEPOSITION (MEV) PRIM	KNOCK	δ-REC	TOTAL
1	1	.3201E-02	.3770E+00	.0000E-00 1	-.1000E-00 11 0.	00	.7000E-00 1
2	1	.3201E-02	.3770E+00	.0000E-00 1	-.1000E-00 12 0.	00	.7000E-00 2
3	1	.3201E-02	.3770E+00	.0000E-00 0	-.2337E-00 13 0.	00	.7000E-00 3
4	1	.3201E-02	.3770E+00	.0000E-00 0	-.2337E-00 14 0.	00	.7000E-00 4
5	1	.3201E-02	.3770E+00	.0000E-00 1	-.2337E-00 15 0.	00	.7000E-00 5
6	1	.5335E-02	.6283E+00	0. 00	.1537E-07 12 0.	00	.1537E-07 12
7	1	.5335E-02	.6283E+00	0. 00	.1728E-07 20 0.	00	.1728E-07 20
8	1	.5335E-02	.6283E+00	0. 00	.1575E-07 19 0.	00	.1575E-07 19
9	1	.5335E-02	.6283E+00	0. 00	.1567E-07 17 0.	00	.1567E-07 17
10	1	.5335E-02	.6283E+00	0. 00	.1783E-07 19 0.	00	.1783E-07 19
11	1	.5335E-02	.6283E+00	0. 00	.1787E-07 0 0.	00	.1787E-07 0
12	1	.5335E-02	.6283E+00	0. 00	.1612E-07 13 0.	00	.1612E-07 13
13	1	.5335E-02	.6283E+00	0. 00	.1561E-07 18 0.	00	.1561E-07 18
14	1	.7470E-02	.8796E+00	0. 00	.1777E-07 17 0.	00	.1777E-07 17
15	1	.7470E-02	.8796E+00	0. 00	.1893E-07 25 0.	00	.1893E-07 25
16	1	.7470E-02	.8796E+00	0. 00	.1624E-07 16 0.	00	.1624E-07 16
17	1	.7470E-02	.8796E+00	0. 00	.1149E-07 16 0.	00	.1149E-07 16
18	1	.7470E-02	.8796E+00	0. 00	.1770E-07 17 0.	00	.1770E-07 17
19	1	.7470E-02	.8796E+00	0. 00	.1985E-07 13 0.	00	.1985E-07 13
20	1	.7470E-02	.8796E+00	0. 00	.1972E-07 18 0.	00	.1972E-07 18
21	1	.7470E-02	.8796E+00	0. 00	.1944E-07 18 0.	00	.1944E-07 18
22	1	.9554E-02	.1131E+00	0. 00	.2027E-07 21 0.	00	.2027E-07 21
23	1	.9554E-02	.1131E+00	0. 00	.1226E-07 16 0.	00	.1226E-07 16
24	1	.9554E-02	.1131E+00	0. 00	.1390E-07 17 0.	00	.1390E-07 17
25	1	.9554E-02	.1131E+00	0. 00	.1912E-07 15 0.	00	.1912E-07 15
26	1	.9554E-02	.1131E+00	0. 00	.1605E-07 18 0.	00	.1605E-07 18
27	1	.9554E-02	.1131E+00	0. 00	.1440E-07 18 0.	00	.1440E-07 18
28	1	.9554E-02	.1131E+00	0. 00	.1935E-07 18 0.	00	.1935E-07 18
			TOTAL	.1750E-02 0 -.3030E-03 3 0.		00	.1899E-02 1

CHARGE DISTRIBUTION
(NORMALIZED TO ONE INCIDENT PARTICLE)

ZONE	MATERIAL	A	Z0	Z1	Z2	ELECTRONS PRIM	KNOCK	δ-REC	TOTAL
1	1	0.	.0000E+00	0.	.0000E+01	0.	00 -.00E-00 10 0.	00	.00E-00 10
2	1	.2500E+00	.0000E+00	0.	.2000E+01	0.	00 -.00E-00 10 0.	00	.00E-00 10
3	1	.5000E+00	.7500E+00	0.	.2000E+01	0.	00 -.00E-00 10 0.	00	.00E-00 10
4	1	.7500E+00	.1000E+01	0.	.2000E+01	0.	00 -.00E-00 10 0.	00	.00E-00 10
5	1	.1000E+01	.1250E+01	0.	.2000E+01	0.	00 -.00E-00 10 0.	00	.00E-00 10
6	1	.1250E+01	.1500E+01	0.	.2000E+01	0.	00 -.00E-00 10 0.	00	.00E-00 10
7	1	.1500E+01	.1750E+01	0.	.2000E+01	0.	00 -.00E-00 10 0.	00	.00E-00 10
8	1	.1750E+01	.2000E+01	0.	.2000E+01	0.	00 -.00E-00 10 0.	00	.00E-00 10
9	1	0.	.2500E+00	.2000E+01	.4000E+01	0.	00 -.11E-03 13 0.	00	.11E-03 13
10	1	.2500E+00	.5000E+00	.2000E+01	.4000E+01	0.	00 -.14E-03 13 0.	00	.14E-03 13
11	1	.5000E+00	.7500E+00	.2000E+01	.4000E+01	0.	00 -.12E-03 10 0.	00	.12E-03 10
12	1	.7500E+00	.1000E+01	.2000E+01	.4000E+01	0.	00 -.14E-03 10 0.	00	.14E-03 10
13	1	.1000E+01	.1250E+01	.2000E+01	.4000E+01	0.	00 -.12E-03 10 0.	00	.12E-03 10
14	1	.1250E+01	.1500E+01	.2000E+01	.4000E+01	0.	00 -.92E-04 13 0.	00	.92E-04 13
15	1	.1500E+01	.1750E+01	.2000E+01	.4000E+01	0.	00 -.11E-03 13 0.	00	.11E-03 13
16	1	.1750E+01	.2000E+01	.2000E+01	.4000E+01	0.	00 -.18E-03 10 0.	00	.18E-03 10
17	1	0.	.2500E+00	.4000E+01	.6000E+01	0.	00 0.	00 0.	00 0.
18	1	.2500E+00	.5000E+00	.4000E+01	.6000E+01	0.	00 0.	00 0.	00 0.
19	1	.5000E+00	.7500E+00	.4000E+01	.6000E+01	0.	00 0.	00 0.	00 0.
20	1	.7500E+00	.1000E+01	.4000E+01	.6000E+01	0.	00 0.	00 0.	00 0.
21	1	.1000E+01	.1250E+01	.4000E+01	.6000E+01	0.	00 0.	00 0.	00 0.
22	1	.1250E+01	.1500E+01	.4000E+01	.6000E+01	0.	00 0.	00 0.	00 0.
23	1	.1500E+01	.1750E+01	.4000E+01	.6000E+01	0.	00 0.	00 0.	00 0.
24	1	.1750E+01	.2000E+01	.4000E+01	.6000E+01	0.	00 0.	00 0.	00 0.
25	1	0.	.2500E+00	.6000E+01	.8000E+01	0.	00 0.	00 0.	00 0.
26	1	.2500E+00	.5000E+00	.6000E+01	.8000E+01	0.	00 0.	00 0.	00 0.
27	1	.5000E+00	.7500E+00	.6000E+01	.8000E+01	0.	00 0.	00 0.	00 0.
28	1	.7500E+00	.1000E+01	.6000E+01	.8000E+01	0.	00 0.	00 0.	00 0.
29	1	.1000E+01	.1250E+01	.6000E+01	.8000E+01	0.	00 0.	00 0.	00 0.
30	1	.1250E+01	.1500E+01	.6000E+01	.8000E+01	0.	00 0.	00 0.	00 0.
31	1	.1500E+01	.1750E+01	.6000E+01	.8000E+01	0.	00 0.	00 0.	00 0.
32	1	.1750E+01	.2000E+01	.6000E+01	.8000E+01	0.	00 0.	00 0.	00 0.
33	1	0.	.2500E+00	.8000E+01	.1000E+02	0.	00 0.	00 0.	00 0.
34	1	.2500E+00	.5000E+00	.8000E+01	.1000E+02	0.	00 0.	00 0.	00 0.
35	1	.5000E+00	.7500E+00	.8000E+01	.1000E+02	0.	00 0.	00 0.	00 0.
36	1	.7500E+00	.1000E+01	.8000E+01	.1000E+02	0.	00 0.	00 0.	00 0.
37	1	.1000E+01	.1250E+01	.8000E+01	.1000E+02	0.	00 0.	00 0.	00 0.
38	1	.1250E+01	.1500E+01	.8000E+01	.1000E+02	0.	00 0.	00 0.	00 0.
39	1	.1500E+01	.1750E+01	.8000E+01	.1000E+02	0.	00 0.	00 0.	00 0.
40	1	.1750E+01	.2000E+01	.8000E+01	.1000E+02	0.	00 0.	00 0.	00 0.
41	1	.2000E+01	.3000E+01	0.	.2000E+01	0.	99 -.20E-03 10 0.	99	.20E-03 10
42	1	.3000E+01	.4500E+01	0.	.2000E+01	0.	99 -.17E-03 9 0.	99	.17E-03 9
43	1	.4000E+01	.6000E+01	0.	.2000E+01	0.	99 -.19E-03 9 0.	99	.19E-03 9
44	1	.5000E+01	.8000E+01	0.	.2000E+01	0.	99 -.18E-03 12 0.	99	.18E-03 12
45	1	.6000E+01	.9000E+01	0.	.2000E+01	0.	99 -.21E-03 7 0.	99	.21E-03 7
46	1	.7000E+01	.1050E+02	0.	.2000E+01	0.	99 -.23E-03 13 0.	99	.23E-03 13
47	1	.8000E+01	.1200E+02	0.	.2000E+01	0.	99 -.18E-03 10 0.	99	.18E-03 10

ZONE	MATERIAL	ZL	ZU	RI	RO	ELECTRONS PRIM	SHOCK	δ-SEC	TOTAL
91	1	.4000E+03	.5000E+03	.2000E+01	.4000E+01	0.	00 -.40E-03	6 0.	00 -.40E-03 6
92	1	.5000E+03	.6000E+03	.2000E+01	.4000E+01	0.	00 -.40E-03	6 0.	00 -.40E-03 6
93	1	.6000E+03	.7000E+03	.2000E+01	.4000E+01	0.	00 -.81E-03	7 0.	00 -.81E-03 7
94	1	.7000E+03	.8000E+03	.2000E+01	.4000E+01	0.	00 -.40E-03	7 0.	00 -.40E-03 7
95	1	.8000E+03	.9000E+03	.2000E+01	.4000E+01	0.	00 -.40E-03	7 0.	00 -.40E-03 7
96	1	.9000E+03	.1000E+04	.2000E+01	.4000E+01	0.	00 -.97E-03	7 0.	00 -.97E-03 7
97	1	.1000E+04	.1100E+04	.4000E+01	.4000E+01	0.	00 0.	00 0.	00 0. 00
98	1	.1100E+04	.1200E+04	.4000E+01	.4000E+01	0.	00 0.	00 0.	00 0. 00
99	1	.1200E+04	.1300E+04	.4000E+01	.4000E+01	0.	00 0.	00 0.	00 0. 00
90	1	.1300E+04	.1400E+04	.4000E+01	.4000E+01	0.	00 0.	00 0.	00 0. 00
81	1	.1400E+04	.1500E+04	.4000E+01	.4000E+01	0.	00 0.	00 0.	00 0. 00
82	1	.1500E+04	.1600E+04	.4000E+01	.4000E+01	0.	00 0.	00 0.	00 0. 00
83	1	.1600E+04	.1700E+04	.4000E+01	.4000E+01	0.	00 0.	00 0.	00 0. 00
84	1	.1700E+04	.1800E+04	.4000E+01	.4000E+01	0.	00 0.	00 0.	00 0. 00
85	1	.1800E+04	.1900E+04	.4000E+01	.4000E+01	0.	00 0.	00 0.	00 0. 00
86	1	.1900E+04	.2000E+04	.4000E+01	.4000E+01	0.	00 0.	00 0.	00 0. 00
87	1	.2000E+04	.2100E+04	.4000E+01	.4000E+01	0.	00 0.	00 0.	00 0. 00
88	1	.2100E+04	.2200E+04	.4000E+01	.4000E+01	0.	00 0.	00 0.	00 0. 00
89	1	.2200E+04	.2300E+04	.4000E+01	.4000E+01	0.	00 0.	00 0.	00 0. 00
70	1	.2300E+04	.2400E+04	.4000E+01	.4000E+01	0.	00 0.	00 0.	00 0. 00
71	1	.2400E+04	.2500E+04	.4000E+01	.4000E+01	0.	00 0.	00 0.	00 0. 00
72	1	.2500E+04	.2600E+04	.4000E+01	.4000E+01	0.	00 0.	00 0.	00 0. 00
73	1	.2600E+04	.2700E+04	.4000E+01	.1000E-02	0.	00 0.	00 0.	00 0. 00
74	1	.2700E+04	.2800E+04	.4000E+01	.1000E-02	0.	00 0.	00 0.	00 0. 00
75	1	.2800E+04	.2900E+04	.4000E+01	.1000E-02	0.	00 0.	00 0.	00 0. 00
76	1	.2900E+04	.3000E+04	.4000E+01	.1000E-02	0.	00 0.	00 0.	00 0. 00
77	1	.3000E+04	.3100E+04	.4000E+01	.1000E-02	0.	00 0.	00 0.	00 0. 00
78	1	.3100E+04	.3200E+04	.4000E+01	.1000E-02	0.	00 0.	00 0.	00 0. 00
79	1	.3200E+04	.3300E+04	.4000E+01	.1000E-02	0.	00 0.	00 0.	00 0. 00
80	1	.3300E+04	.3400E+04	.4000E+01	.1000E-02	0.	00 0.	00 0.	00 0. 00
			TOTAL			0.	00 -.80E-02	2 0.	00 -.80E-02 2

ENERGY SPECTRA OF TRANSMITTED ELECTRONS
(NUMBER/REV, NORMALIZED TO ONE INCIDENT PARTICLE)

E (REV) LENGTH= 1000.0000

1.5000 - 1.4500	.20E-02	0	
1.4500 - 1.4000	.60E-03	23	
1.4000 - 1.3500	.40E-04	97	
1.3500 - 1.3000	.20E-03	33	
1.3000 - 1.2500	.12E-03	91	
1.2500 - 1.2000	.40E-04	98	
1.2000 - 1.1500	.80E-04	97	
1.1500 - 1.1000	.40E-04	98	
1.1000 - 1.0500	.40E-04	98	
1.0500 - 1.0000	.80E-04	97	
1.0000 - .9500	.40E-04	98	
.9500 - .9000	.80E-04	97	
.9000 - .8500	0.		98
.8500 - .8000	0.		98
.8000 - .7500	0.		98
.7500 - .7000	0.		98
.7000 - .6500	.40E-04		98
.6500 - .6000	.40E-04		98
.6000 - .5500	0.		98
.5500 - .5000	.40E-04		98
.5000 - .4500	0.		98

J 8

J 8

K 8

K 8

.4500 - .4000	0.		98
.4000 - .3500	0.		98
.3500 - .3000	0.		98
.3000 - .2500	0.		98
.2500 - .2000	0.		98
.2000 - .1500	0.		98
.1500 - .1000	.12E-03	71	
.1000 - .0500	.40E-04	99	
.0500 - .0100	.36E-03	22	

ENERGY SPECTRA OF REFLECTED ELECTRONS
(NUMBER/REV, NORMALIZED TO ONE INCIDENT PARTICLE)

E (REV) LENGTH= 1000.0000

1.5000 - 1.4500	0.		98
1.4500 - 1.4000	0.		98
1.4000 - 1.3500	0.		98
1.3500 - 1.3000	0.		98
1.3000 - 1.2500	0.		98
1.2500 - 1.2000	0.		98
1.2000 - 1.1500	0.		98
1.1500 - 1.1000	0.		98
1.1000 - 1.0500	0.		98
1.0500 - 1.0000	0.		98
1.0000 - .9500	0.		98
.9500 - .9000	0.		98
.9000 - .8500	0.		98
.8500 - .8000	0.		98
.8000 - .7500	0.		98
.7500 - .7000	0.		98
.7000 - .6500	0.		98
.6500 - .6000	0.		98
.6000 - .5500	0.		98
.5500 - .5000	0.		98
.5000 - .4500	0.		98
.4500 - .4000	0.		98
.4000 - .3500	0.		98
.3500 - .3000	0.		98
.3000 - .2500	0.		98
.2500 - .2000	0.		98
.2000 - .1500	0.		98
.1500 - .1000	0.		98
.1000 - .0500	0.		98
.0500 - .0100	0.		98

ENERGY SPE... ...TRON ESCAPING ELECTRONS
(NUMBER/REV, NO... ...ZED TO ONE INCIDENT PARTICLE)

E (REV) LENGTH= 1000.0000

1.5000 - 1.4500	0.		98
1.4500 - 1.4000	0.		98
1.4000 - 1.3500	0.		98
1.3500 - 1.3000	0.		98
1.3000 - 1.2500	0.		98
1.2500 - 1.2000	0.		98
1.2000 - 1.1500	0.		98
1.1500 - 1.1000	0.		98
1.1000 - 1.0500	0.		98
1.0500 - 1.0000	0.		98
1.0000 - .9500	0.		98
.9500 - .9000	0.		98
.9000 - .8500	0.		98
.8500 - .8000	0.		98
.8000 - .7500	0.		98
.7500 - .7000	.15E-03	41	
.7000 - .6500	.15E-03	41	

```
    .0000 -    .0000   .12E-03 91
    .0000 -    .0000   .12E-03 71
    .0000 -    .0000   .88E-03 48
    .0000 -    .0000   .48E-03 87
    .0000 -    .0000   .14E-02 32
    .0000 -    .0000   .28E-02 17
    .0000 -    .0000   .88E-02 27
    .0000 -    .0000   .12E-02 25
    .0000 -    .0000   .28E-02  9
    .0000 -    .0000   .14E-02 15
    .0000 -    .0000   .14E-01  9
    .0000 -    .0100   .14E-00  2
                        ANGULAR DISTRIBUTIONS OF TRANSMITTED AND REFLECTED ELECTRONS
                          (NUMBER/SR, NORMALIZED TO ONE INCIDENT PARTICLE)
0          PHI(DEG)=  0.000
    THETA (DEG)      180.000

  0.0000 -  30.0000   .12E+01  0
 30.0000 -  60.0000   .28E-02 71
 60.0000 -  90.0000   .70E-05 20
 90.0000 - 120.0000  0.       00
120.0000 - 150.0000  0.       00
150.0000 - 180.0000  0.       00
                        ANGULAR DISTRIBUTIONS OF LATERALLY ESCAPING ELECTRONS
                          (NUMBER/SR, NORMALIZED TO ONE INCIDENT PARTICLE)
0          PHI(DEG)=  0.000
    THETA (DEG)      180.000

  0.0000 -  30.0000  0.       00
 30.0000 -  60.0000  .14E-03  9
 60.0000 -  90.0000  .13E-02  2
 90.0000 - 120.0000  .17E-03  4
120.0000 - 150.0000  0.       00
150.0000 - 180.0000  0.       00
0                   ENERGY SPECTRA AND ANGULAR DISTRIBUTIONS OF ELECTRONS TRANSMITTED AND REFLECTED
                      AZIMUTHAL INTERVAL IS   0.00000 TO 180.00000 DEGREES
                      (NUMBER/(MEV*SR), NORMALIZED TO ONE PARTICLE)
0     E (MEV)  THETA=  0.000      30.000      60.000      90.000     120.000     150.000
                      30.000      60.000      90.000     120.000     150.000     180.000

  1.5000 -  1.4000  .6%E-02  0 0.       00 0.       00 0.       00 0.       00 0.       00
  1.4000 -  1.4000  .71E-03 23 0.       00 0.       00 0.       00 0.       00 0.       00
  1.4000 -  1.3500  .88E-04 07 0.       00 0.       00 0.       00 0.       00 0.       00
  1.3500 -  1.3000  .2%E-03 33 0.       00 0.       00 0.       00 0.       00 0.       00
  1.3000 -  1.2500  .17E-03 51 0.       00 0.       00 0.       00 0.       00 0.       00
  1.2500 -  1.2000  .48E-04 00 0.       00 0.       00 0.       00 0.       00 0.       00
  1.2000 -  1.1500  .8%E-04 07 0.       00 0.       00 0.       00 0.       00 0.       00
  1.1500 -  1.1000  .48E-04 00 0.       00 0.       00 0.       00 0.       00 0.       00
  1.1000 -  1.0500  .48E-04 00 0.       00 0.       00 0.       00 0.       00 0.       00
  1.0500 -  1.0000  .8%E-04 07 0.       00 0.       00 0.       00 0.       00 0.       00
  1.0000 -   .9500  .48E-04 00 0.       00 0.       00 0.       00 0.       00 0.       00
   .9500 -   .9000  .8%E-04 07 0.       00 0.       00 0.       00 0.       00 0.       00
   .9000 -   .8500 0.       00 0.       00 0.       00 0.       00 0.       00 0.       00
   .8500 -   .8000 0.       00 0.       00 0.       00 0.       00 0.       00 0.       00
   .8000 -   .7500 0.       00 0.       00 0.       00 0.       00 0.       00 0.       00
   .7500 -   .7000 0.       00 0.       00 0.       00 0.       00 0.       00 0.       00
   .7000 -   .6500 0.       00 0.       00  .17E-04 00 0.       00 0.       00 0.       00
   .6500 -   .6000 0.       00 0.       00  .17E-04 00 0.       00 0.       00 0.       00
   .6000 -   .5500 0.       00 0.       00 0.       00 0.       00 0.       00 0.       00
   .5500 -   .5000 0.       00 0.       00  .17E-04 00 0.       00 0.       00 0.       00
   .5000 -   .4500 0.       00 0.       00 0.       00 0.       00 0.       00 0.       00
   .4500 -   .4000 0.       00 0.       00 0.       00 0.       00 0.       00 0.       00
   .4000 -   .3500 0.       00 0.       00 0.       00 0.       00 0.       00 0.       00
```

L 2 L 2

2 # 2

```
   .3500 -   .3000 0.       00 0.       00 0.       00 0.       00 0.       00 0.       00
   .3000 -   .2500 0.       00 0.       00 0.       00 0.       00 0.       00 0.       00
   .2500 -   .2000 0.       00 0.       00 0.       00 0.       00 0.       00 0.       00
   .2000 -   .1500 0.       00 0.       00 0.       00 0.       00 0.       00 0.       00
   .1500 -   .1000 0.       00 0.       00 0.       00  .38E-04 71 0.       00 0.       00
   .1000 -   .0500 0.       00 0.       00 0.       00  .13E-04 00 0.       00 0.       00
   .0500 -   .0100 0.       00 0.       00 0.       00  .11E-03 22 0.       00 0.       00
0                   ENERGY SPECTRA AND ANGULAR DISTRIBUTIONS OF ELECTRONS LATERALLY ESCAPING
                      AZIMUTHAL INTERVAL IS   0.00000 TO 180.00000 DEGREES
                      (NUMBER/(MEV*SR), NORMALIZED TO ONE PARTICLE)
0     E (MEV)  THETA=  0.000      30.000      60.000      90.000     120.000     150.000
                      30.000      60.000      90.000     120.000     150.000     180.000

  1.5000 -  1.4000  0.       00 0.       00 0.       00 0.       00 0.       00 0.       00
  1.4000 -  1.4000  0.       00 0.       00 0.       00 0.       00 0.       00 0.       00
  1.4000 -  1.3500  0.       00 0.       00 0.       00 0.       00 0.       00 0.       00
  1.3500 -  1.3000  0.       00 0.       00 0.       00 0.       00 0.       00 0.       00
  1.3000 -  1.2500  0.       00 0.       00 0.       00 0.       00 0.       00 0.       00
  1.2500 -  1.2000  0.       00 0.       00 0.       00 0.       00 0.       00 0.       00
  1.2000 -  1.1500  0.       00 0.       00 0.       00 0.       00 0.       00 0.       00
  1.1500 -  1.1000  0.       00 0.       00 0.       00 0.       00 0.       00 0.       00
  1.1000 -  1.0500  0.       00 0.       00 0.       00 0.       00 0.       00 0.       00
  1.0500 -  1.0000  0.       00 0.       00 0.       00 0.       00 0.       00 0.       00
  1.0000 -   .9500  0.       00 0.       00 0.       00 0.       00 0.       00 0.       00
   .9500 -   .9000  0.       00 0.       00 0.       00 0.       00 0.       00 0.       00
   .9000 -   .8500  0.       00 0.       00 0.       00 0.       00 0.       00 0.       00
   .8500 -   .8000  0.       00 0.       00 0.       00 0.       00 0.       00 0.       00
   .8000 -   .7500  0.       00 0.       00 0.       00 0.       00 0.       00 0.       00
   .7500 -   .7000  0.       00 0.       00  .70E-04 41 0.       00 0.       00 0.       00
   .7000 -   .6500  0.       00 0.       00  .70E-04 41 0.       00 0.       00 0.       00
   .6500 -   .6000  0.       00 0.       00  .5%E-04 21 0.       00 0.       00 0.       00
   .6000 -   .5500  0.       00 0.       00  .5%E-04 21 0.       00 0.       00 0.       00
   .5500 -   .5000  0.       00 0.       00  .12E-03 40 0.       00 0.       00 0.       00
   .5000 -   .4500  0.       00 0.       00  .17E-03 21 0.       00 0.       00 0.       00
   .4500 -   .4000  0.       00 0.       00  .18E-03 32 0.       00 0.       00 0.       00
   .4000 -   .3500  0.       00 0.       00  .12E-03 27 0.       00 0.       00 0.       00
   .3500 -   .3000  0.       00 0.       00  .38E-03 32 0.       00 0.       00 0.       00
   .3000 -   .2500  0.       00 0.       00  .%8E-03 24 0.       00 0.       00 0.       00
   .2500 -   .2000  0.       00 0.       00  .63E-03 25 0.       00 0.       00 0.       00
   .2000 -   .1500  0.       00 0.       00  .%%E-03 18  .%2E-03 15 0.       00 0.       00
   .1500 -   .1000  0.       00 0.       00 0.       00  .14E-02 12 0.       00 0.       00
   .1000 -   .0500  0.       00 0.       00 0.       00  .%3E-02  5 0.       00 0.       00
   .0500 -   .0100  0.       00  .20E-03 35  .38E-01  2  .%2E-02  % 0.       00 0.       00
0                   ENERGY SPECTRA OF TRANSMITTED PHOTONS
                      (NUMBER/MEV, NORMALIZED TO ONE INCIDENT PARTICLE)
0     E (MEV)  LENGTH=   1000.0000

  1.5000 -  1.4000  0.       00
  1.4000 -  1.4000  0.       00
  1.4000 -  1.3500  0.       00
  1.3500 -  1.3000  0.       00
  1.3000 -  1.2500  0.       00
  1.2500 -  1.2000  0.       00
  1.2000 -  1.1500  0.       00
  1.1500 -  1.1000  0.       00
  1.1000 -  1.0500  0.       00
  1.0500 -  1.0000  0.       00
  1.0000 -   .9500  0.       00
   .9500 -   .9000  0.       00
   .9000 -   .8500  0.       00
   .8500 -   .8000  0.       00
   .8000 -   .7500  0.       00
   .7500 -   .7000  0.       00
   .7000 -   .6500  0.       00
```

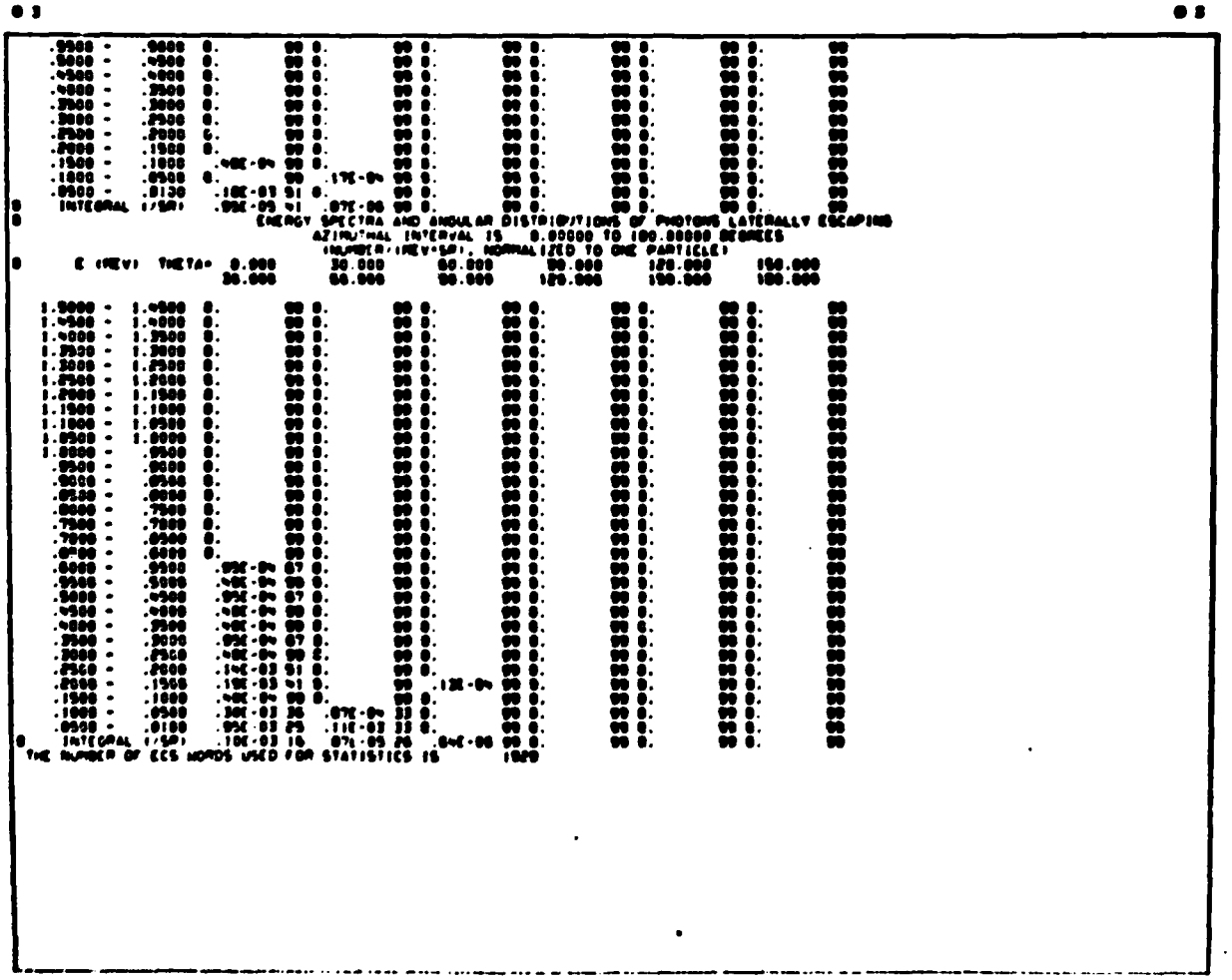

APPENDIX B

AIR PROPERTIES AND 1.5 MeV ELECTRON BEAM TRANSPORT AT 760 TORR

```
 **1.0 MEV PX100 BEAM INTO 760 TORR AIR**
0
0 NSET  ITYN  IZIP  IGGN  IGAD  INEL  ICYC  NCYC  EMAX        EMAX
     1     0     0     1    GA     1     1     0   0%    .100000E+01
0INPUT DATA TAPE IDENTIFICATION
 DATATAPE-2 (RESTER-AIGINGER PH-GAD CORR!, 0% STERNHEIMER DETS. 20 JAN 6
0SECTOUR          DENSITY
   .000000E+00    .100007E-02
0
0RANGE TABLE
0     EMAX          NCYC          EFAC          XMAX      T(XMAX+1)      RCAL      T(RCAL)
    .100000E+01       0     .017000E+00       0%     .0000+E-02       00     .0+0002E-03
0 JMAX  LMAX
     3     1
0        Z             A             M
     7.00000      14.00070       .70000
     8.00000      15.99930       .80120
    10.00000      20.0+700       .91300
0        P1            P1D
    00.0+100      00.0+100
0  ----------PARAMETERS FOR DENSITY EFFECT----------
        P1            C             0             0M            X1            X0

    00.0+100   -10.00+00       .01003     3.00000     0.00000     1.00000
    00.0+100   -10.00+00       .01003     3.00000     0.00000     1.00000
   .1000E+00   -.1007E+02    .7000E-01
1                                   ELECTRON RESULTS
0     EFFECTIVE Z/A =  .+0014     EFFECTIVE MEAN IONIZATION POTENTIAL =    00.0+ EV     CRITICAL ENERGY =    0.000 MEV
0          ENERGY          STOPPING POWER                    RANGE     RADIATION     BETA**2    DENSITY     RAD/COL     RANGE      YIELD
                      COLLISION RADIATION     TOTAL                      YIELD                    CORR
   N        MEV        MEV CM2/G MEV CM2/G MEV CM2/G                                            MEV CM2/G                 G/CM2
  00    .0+00E-03    .100E+03    .0+0E-02    .100E+03    .+01E-05 0.                 .371E-02 0.          .010E-0+ 0.          0.
  00    .1030E-02    .000E+02    .0+0E-02    .000E+02    .030E-05    .+0+E-05    .+0+E-02 0.          .0+7E-0+    .000E-05    .+00E-00
  0+    .1130E-02    .0+0E+02    .0+0E-02    .0+0E+02    .035E-05    .0720E-05    .+01E-02 0.          .077E-0+    .0+0E-05    .027E-00
  03    .1230E-02    .000E+02    .0+0E-02    .000E+02    .7+3E-05    .1000E-0+    .+000E-02 0.         .000E-0+    .111E-05    .0++E-00
  02    .13+3E-02    .0+0E+02    .0+0E-02    .0+0E+02    .071E-05    .1700E-0+    .+02+E-02 0.         .0+2E-0+    .1200E-05    .007E-00
  01    .1+00E-02    .700E+02    .0+3E-02    .000E+02    .100E-0+    .211E-0+    .+071E-02 0.         .070E-0+    .1+0E-05    .01?E-00
  00    .1507E-02    .700E+02    .0+0E-02    .700E+02    .110E-0+    .2+1E-0+    .+12+E-02 0.         .710E-0+    .171E-05    .0?:E-00
  7+    .170E-02     .710E+02    .0+1E-02    .710E+02    .130E-0+    .202E-0+    .+170E-02 0.         .750E-0+    .197E-05    .107E-07
  70    .1000E-02    .071E+02    .0300E-02   .071E+02    .1+0E-0+    .533E-0+    .+200E-02 0.         .000+E-0+   .2200E-05    .122E-07
  77    .2072E-02    .032E+02    .0300E-02   .032E+02    .100E-0+    .37+E-0+    .+000E-02 0.         .051E-0+    .2+0+E-05    .1+2E-07
  70    .2250E-02    .000E+02    .0370E-02   .000E+02    .210E-0+    .+10E-0+    .+070E-02 0.         .002E-0+    .3200E-05    .1000E-07
  75    .2+0+E-02    .0+50E+02   .0320E-02   .0+50E+02   .250E-0+    .+50E-0+    .+007E-02 0.         .0000E-0+   .3+0+E-05    .1007E-07
  7+    .2007E-02    .0200E+02   .0330E-02   .0200E+02   .2000E-0+   .0+02E-0+   .+10+E-01 0.         .101E-03    .+11E-05    .2220E-07
  73    .2030E-02    .+000E+02   .0320E-02   .+000E+02   .3+3E-0+    .0+70E-0+   .+11+E-01 0.         .107E-03    .+77E-05    .2+0+E-07
  72    .3105E-02    .+05E+02    .0330E-02   .+05E+02    .3000E-0+   .0002E-0+   .+2+E-01 0.         .1+0E-03    .000E-05    .2000E-07
  71    .3+0+E-02    .+30E+02    .0300E-02   .+30E+02    .+02E-0+    .0+1E-0+    .+300E-01 0.         .1+0E-03    .0+3E-05    .3+3E-07
  70    .3700E-02    .+00E+02    .0200E-02   .+00E+02    .+37E-0+    .002E-0+    .++7E-01 0.         .120E-03    .+7+E-05    .3+3E-07
  00    .+1+3E-02    .300+E+02   .0202E-02   .300+E+02   .02+E-0+    .0++E-0+    .+00E-01 0.         .13+E-03    .0000E-05    .+02E-07
  00    .+010E-02    .3000E+02   .0210E-02   .3000E+02   .025E-0+    .0700E-0+   .+170E-01 0.         .1+0E-03    .+10E-0+    .0+7E-07
  07    .+007E-02    .3300E+02   .0100E-02   .3300E+02   .0+2E-0+    .0007E-0+   .+100E-01 0.         .100E-03    .+17E-0+    .010E-07
  00    .0373E-02    .3100E+02   .0100E-02   .3100E+02   .075E-0+    .017E-0+    .+007E-01 0.         .103E-03    .+37E-0+    .707E-07
  05    .0050E-02    .2000E+02   .0+1E-02   .2000E+02   .11+E-03    .0001E-0+   .+200E-01 0.         .170E-03    .1000E-0+   .010E-07
  0+    .0300E-02    .2770E+02   .0+11E-02   .2700E+02   .1300E-03   .1000E-03   .++50E-01 0.         .100+E-03   .1050E-0+   .0+0E-07
  03    .0000E-02    .2000E+02   .0+00E-02   .2000E+02   .1+0+E-03   .1120E-03   .+007E-01 0.         .100E-03    .2150E-0+   .110E-00
  02    .7000E-02    .2+3E+02    .0+0E-02    .2+3E+02    .170E-03    .1100E-03   .+001E-01 0.         .2000E-03   .+50E-0+    .10?E-00
  01    .0200E-02    .2200E+02   .0+0+E-02   .2200E+02   .200E-03    .1270E-03   .+170E-01 0.         .2210E-03   .+00E-0+    .1+00E-00
  00    .0030E-02    .2130E+02   .0+01E-02   .2130E+02   .2+2E-03    .1300E-03   .++00E-01 0.         .2350E-03   .+01E-0+    .1710E-00
  00    .0000E-02    .2000E+02   .0+10E-02   .2000E+02   .2+0E-03    .1++0E-03   .+370E-01 0.         .2+50E-03   .+07E-0+    .1000E-00
  00    .1070E-01    .1000E+02   .0+00E-02   .1000E+02   .320E-03    .1+0+E-03   .+000E-01 0.         .2000E-03   .+03E-0+    .2130E-00
  07    .1172E-01    .1700E+02   .0+03E-02   .1700E+02   .300E-03    .1+0+E-03   .++3E-01 0.          .200E-03    .++0E-0+    .2+7E-00
  00    .1270E-01    .1030E+02   .0+01E-02   .1030E+02   .++5E-03    .1700E-03   .+02+E-01 0.         .2010E-03   .0200E-0+   .3100E-00
  00    .1300E-01    .1000E+02   .0+00E-02   .1000E+02   .510E-03    .1000E-03   .+02+E-01 0.         .3200E-03   .7300E-0+   .3500E-00
```

```
 Jl                                                                                                                                  Jl
 Kl                                                                                                                                  Kl
  0+    .1020E-01    .1+3E+02    .+000E-02    .1+3E+02    .+0+E-03    .1000E-03    .+000E-01 0.         .3+1E-03    .0000E-0+    .+17E-00
  03    .1007E-01    .133E+02    .+0+0E-02    .133E+02    .700E-03    .2110E-03    .+100E-01 0.         .3+0E-03    .+007E-0+    .+03E-00
  02    .1007E-01    .1200E+02   .+01E-02    .1200E+02   .0200E-03   .2+0+E-03    .+070E-01 0.         .3000E-03   .1100E-03    .0+1E-00
  01    .1071E-01    .117E+02    .+700E-02    .117E+02    .0000E-03   .2300E-03    .+720E-01 0.         .+100E-03   .13+E-03    .0+1E-00
  00    .21+0E-01    .1000E+02   .+77E-02    .1000E+02   .1111E-02   .2+0+E-03    .+700E-01 0.         .+27E-02    .1+00E-03    .7+0+E-00
  +0    .23+0+E-01   .102E+02    .+700E-02   .102E+02    .1300E-02   .2700E-03    .+000E-01 0.         .+07E-03    .10+0E-03    .077E-00
  +0    .2000E-01    .007E+01    .+7+E-02    .007E+01    .1010E-02   .2000E-03    .+030E-01 0.         .+07+-03    .21+0E-03    .1020E-00
  07    .2707E-01    .0000E+01   .+72E-02    .0300E+01   .1700E-02   .3000E-03    .+010E+00 0.         .+27E-03    .2+2E-03    .1100E-00
  00    .3033E-01    .030E+01    .+7+1E-02   .0+0E+01    .2000E-02   .3200E-03    .1000E+00 0.         .+00E-03    .2000E-03    .1370E-00
  00    .3315E-01    .700E+01    .+700E-02   .7+7E+01    .2300E-02   .3+7E-03     .1100E+00 0.         .+07E-03    .333E-03     .1500E-00
  0+    .3015E-01    .737E+01    .+00+E-02   .737E+01    .2700E-02   .3000E-03    .1200E+00 0.         .0300E-03   .3000E-03    .1050E-00
  03    .3000E-01    .0+1E+01    .+000E-02   .0+1E+01    .3200E-02   .3030E-03    .1300E+00 0.         .0777E-03   .+52E-03     .0100E-00
  02    .+200E-01    .0+0E+01    .+07E-02    .0+0E+01    .3700E-02   .3+00E-03    .1+00E+00 0.         .+20E-03    .0330E-03    .0+70E-00
  01    .+007E-01    .000E+01    .+07E-02    .000E+01    .+200E-02   .+000E-03    .1+10E+00 0.         .700E-03    .0+1E-03     .0+03E-00
  00    .0110E-01    .072E+01    .+07E-02    .072E+01    .+12E-02    .+7+0E-03    .1700E+00 0.         .0+17E-03   .0700E-03    .2300E-00
  30    .0070E-01    .037E+01    .+07E-02    .030E+01    .+2+E-02    .+000E-03    .1070E+00 0.         .0700E-03   .0+3E-03     .2+3E-00
  30    .0070E-01    .0000E+01   .+000E-02   .000E+01    .+02E-02    .+030E-03    .1000E+00 0.         .0+0E-03    .0+5E-03     .++3E-00
  37    .0+2E-01     .+70E+01    .+00E-02    .+70E+01    .+07E-02    .+070E-03    .2100E+00 0.         .0000E-03   .1+0E-02     .0+0E-00
  30    .7200E-01    .+00E+01    .+7+1E-02   .+00E+01    .0300E-02   .+030E-03    .2230E+00 0.         .1000E-02   .1300E-02    .0100E-00
  35    .7000E-01    .+02E+01    .+72E-02    .+02E+01    .1000E-01   .0+00E-03    .2+00E+00 0.         .110E-02    .1+00E-02    .7000E-00
  3+    .0507E-01    .+000E+01   .+7+E-02    .+000E+01   .1200E-01   .0002E-03    .2070E+00 0.         .1100E-02   .1720E-02    .0+21E-00
  33    .0370E-01    .370E+01    .+700E-02   .370E+01    .1+00E-01   .7300E-03    .2000E+00 0.         .1200E-02   .2003E-02    .0030E-00
  32    .1022E-00    .3+00E+01   .+01E-02    .3+00E+01   .1000E-01   .7010E-03    .3000E+00 0.         .1300E-02   .2110E-02    .0110E-00
  31    .1110E-00    .3300E+01   .+05+E-02   .3+0E+01    .1050E-01   .0327E-03    .3250E+00 0.         .1+30E-02   .2050E-02    .1200E-00
  30    .1210E-00    .3220E+01   .+000E-02   .3200E+01   .2200E-01   .0005E-03    .3+7E+00 0.          .1500E-02   .3050E-02    .1+00E-00
  00    .1320E-00    .3000E+01   .+05+E-02   .307E+01    .2070E-01   .0+2E-03     .3700E+00 0.         .1000E-02   .3500E-02    .1720E-00
  00    .1+00E-00    .2010E+01   .0002E-02   .2002E+01   .3012E-01   .1000E-02    .3000E+00 0.         .1720E-02   .+010E-02    .2000E-00
  07    .1077E-00    .270E+01    .+000E-02   .270E+01    .3+7E-01    .1070E-02    .+100E+00 7.         .1030E-02   .+500E-02    .2320E-00
  00    .1710E-00    .2000E+01   .+100E-02   .2000E+01   .3000E-01   .1130E-02    .++00E+00 0.         .1000E-02   .+2+0E-02    .2000E-00
  00    .1070E-00    .2+0+E+01   .+07+E-02   .2+0E+01    .+500E-01   .1210E-02    .+000E+00 0.         .2070E-02   .+00+E-02    .3120E-00
  07    .2000E-00    .2+0+E+01   .+300E-02   .2+0E+01    .+200E-01   .1200E-02    .+000E+00 0.         .2210E-02   .0+0.E-02    .3+2E-00
  03    .2230E-00    .2030E+01   .+3+1E-02   .2030E+01    .0+0E-01   .1370E-02    .+100E+00 0.         .2330E-02   .+72E-02     .+200E-00
  02    .2+3E+00     .2200E+01   .+300+E-02   .2200E+01   .0+0E-01   .1+0E-02     .+1+E+00 0.          .2+50E-02   .0720E-02    .+000E-00
  01    .2050E+00    .2100E+01   .+01E-02    .2100E+01   .7010E-01   .1550E-02    .+000E+00 0.         .2000E-02   .0000E-02    .0070E-00
  00    .2000E+00    .2110E+01   .+000E-02   .2100E+01   .0002E-01   .1050E-02    .+000E+00 0.         .2000E-02   .1120E-01    .0550E-00
  10    .2150E+00    .2000E+01   .+0+0E-02   .2000E+01   .1030E+00   .1700E-02    .+100E+00 0.         .3030E-02   .1000E-01    .0700E-00
  10    .2+30E+00    .1000E+01   .0+3E-02    .1000E+01   .1170E+00   .1070E-02    .0+3E+00 0.          .3+0E-02    .1010E-01    .0010E-00
  17    .2750E+00    .1020E+01   .0+00E-02   .1020E+01   .1330E+00   .1000E-02    .0007E+00 0.         .3+00E-02   .1050E-01    .1000E-00
  10    .+000E+00    .1000E+01   .0700E-02   .1000E+01   .1500E+00   .2120E-02    .0010E+00 0.         .3700E-02   .1770E-01    .1200E-00
  15    .+0+0E+00    .1050E+01   .7300E-02   .1050E+01   .1700E+00   .2200E-02    .7100E+00 0.         .3000E-02   .1000E-01    .1+10E-00
  1+    .+000E+00    .1010E+01   .7700E-02   .1000E+01   .1020E+00   .2+10E-02    .7370E+00 0.         .+250E-02   .2020E-01    .1000E-00
  13    .0300E+00    .1700E+01   .0120E-02   .1700E+01   .2170E+00   .2500E-02    .7500E+00 0.         .+570E-02   .2++0E-01    .1030E-00
  12    .0700E+00    .1750E+01   .0030E-02   .1700E+01   .2++0E+00   .2730E-02    .7000E+00 0.         .+010E-02   .2710E-01    .2200E-00
  11    .0307E+00    .1730E+01   .0100E-02   .1700E+01   .2770E+00   .2900E-02    .0030E+00 0.         .+200E-02   .3000E-01    .2000E-00
  10    .0070E+00    .1710E+01   .0750E-02   .1720E+01   .3070E+00   .3100E-02    .0100E+00 0.         .+710E-02   .3310E-01    .3120E-00
   0    .7500E+00    .1000E+01   .1000E-01   .1700E+01   .3+3E+00    .3300E-02    .0300E+00 0.         .0170E-02   .3++0E-01    .3070E-00
   0    .0170E+00    .1000E+01   .1120E-01   .1000E+01   .3030E+00   .3+30E-02    .0+20E+00 0.         .0+70E-02   .+020E-01    .+330E-00
   7    .0010E+00    .1070E+01   .1210E-01   .1000E+01   .3270E+00   .3000E-02    .0070E+00 0.         .0720E-02   .+100E-01    .+110E-00
   0    .0720E+00    .1000E+01   .1300E-01   .1070E+01   .+750E+00   .+200E-02    .0010E+00 0.         .0700E-02   .++01E-01    .0000E-00
   0    .1001E+00    .1000E+01   .1+10E-01   .1070E+01   .+200E+00   .++50E-02    .0000E+00 0.         .0+50E-02   .+070E-01    .0+1E-00
   +    .1157E+00    .1050E+01   .1+30E-01   .1070E+01   .+500E+00   .+000E-02    .0000E+00 0.         .1010E-01   .0+70E-01    .0100E-00
   3    .1201E+00    .1050E+01   .1+70E-01   .1070E+01   .+0+0E+00   .0+17E-02    .0017E+00 0.         .1000E-01   .0+03E-01    .0100E-00
   2    .1370E+01    .1000E+01   .1020E-01   .1070E+01   .7100E+00   .0700E-02    .0+7E+00 0.          .1100E-01   .0+03E-01    .1100E-02
   1    .1500E+01    .1000E+01   .1000E-01   .1000E+01   .7010E+00   .0+17E-02    .0+50E+00 0.         .1200E-01   .7+3E-01    .1+20E-02
```

```
0 MEDI  MATL
    1     1
0 MEAT  MTAB
    1     1
EXPAND  MTAB
    20    21
COMPTON RAY CROSS SECTION DATA
ENERGIES (MEV)
 1000.000000  500.000000  200.000000  100.000000  80.000000  60.000000
  40.000000  30.000000  20.000000  10.000000  8.000000  6.000000
   4.000000  3.000000  2.000000  1.000000  .800000  .600000
    .400000  .300000  .200000  .100000  .080000  .060000
    .040000  .030000  .020000  .010000  .010000
TOTAL ATTENUATION COEFFICIENTS (CM2/G)
    .03[illegible]  .03[illegible]  .03[illegible]  .03[illegible]  .03[illegible]  .03[illegible]
    .018000  .017[illegible]  .018[illegible]  .018[illegible]  .018[illegible]  .018[illegible]
    .018787  .018[illegible]  .018[illegible]  .017[illegible]  .03[illegible]  .03[illegible]
    .03[illegible]  .03[illegible]  .03[illegible]  .03[illegible]  .03[illegible]  .03[illegible]
    .03[illegible]  .03[illegible]  .03[illegible]  .03[illegible]  .03[illegible]  .03[illegible]
    .03[illegible]  .03[illegible]  .03[illegible]  .03[illegible]  .03[illegible]  .03[illegible]
    .03[illegible]  .03[illegible]  .03[illegible]  .03[illegible]  .03[illegible]  .03[illegible]
RATIO OF SCATTERING PLUS PAIR PRODUCTION TO TOTAL ATTENUATION COEFFICIENTS
    1.000000  1.000000  1.000000  1.000000  1.000000  1.000000
    1.000000  .000000  .000000  .000000  .000000  .000000
    .000000  .000007  .000000  .000000  .000002  .000001
    .000000  .000007  .000000  .000000  .000071  .000000
    .000001  .000002  .000033  .000787  .000000  .000173
    .007529  .00[illegible]  .001270  .003011  .019011  .001312
    .787000  .001102  .00[illegible]  .100030  .030870
RATIO OF SCATTERING TO SCATTERING PLUS PAIR PRODUCTION ATTENUATION COEFFICIENTS
    .007[illegible]  .000010  .01[illegible]  .010170  .000033  .030002
    .003000  .000027  .130070  .171[illegible]  .00[illegible]  .00[illegible]
    .323021  .[illegible]  .[illegible]  .02000[illegible]  .[illegible]  .012171
    .777030  .000[illegible]  .0[illegible]  .000000  .000000  .000130
    1.000000
EK SHELL IONIZATION DATA
BINDING ENERGY (MEV), PHOTOEFFECT EFFICIENCY AND FLUORESCENT EFFICIENCY
    .003203  .111013  .070[illegible]
EK X-RAY ENERGIES (MEV)
    .003203  .003203  .003203  .003203
EK X-RAY ACCUMULATED RELATIVE INTENSITIES
    1.000000  1.000000  1.000000  1.000000
AUGER ELECTRON ENERGIES (MEV)
    .003203  .003203  .003203
AUGER ELECTRON ACCUMULATED RELATIVE INTENSITIES
    1.000000  1.000000  1.000000
NUMBER OF SETS ON DATAPAC TAPE =   1
INPUT FROM DATAPAC

  **1.0 MEV PHIDU BEAM INTO 700 TORR AIR**
0 NRUN  ITRN  IZIP  IGEN  ISAD  INAL  ICYC  NCYC  NMAX      EMAX          EMIN          XMAX          LMAT
    1     0     0     1    50     1     1     0    0+  1.00000000E+00  5.00037500E-03  7.00752300E-01     3

 DATAPREP DATA FOR DATAPAC SET   1   0+   33   50   121  7.007523E-01

 COLLISION / TOTAL BE/BR RATIOS FOR DATAPAC SET   1

 CUMULATIVE BREMSSTRAHLUNG CROSS SECTIONS FOR DATAPAC SET   1

 CUMULATIVE BREMSSTRAHLUNG ANGULAR DISTRIBUTIONS FOR DATAPAC SET   1
```

0 2 0 2 0 3

E 2 E 2 E 3

```
 LANGAUSS - EQUIPROBABLE ENDPOINTS FOR INTERPOLATION

 K X-RAY PRODUCTION FOR DATAPAC SET   1

 PHOTOELECTRON ANGULAR DISTRIBUTIONS

 PAIR ELECTRON ENERGY DIVISION DISTRIBUTION (LEAD)
1
0 NRUN   IMC ISTRB  INDX  INEL IPHOT  IGAD  IDES  IPUN ITAPE
    1     1     1     1     0     1     1     1     2     2
0 ZONE   MATERIAL  LEFT PLANE  RIGHT PLANE  INNER CYLINDER  OUTER CYLINDER    ECUT       PTCZ
    1     1     0.          .000000E+03    0.              .100000E+02    .100E-01   0.
    0     1     .000000E+03  .100000E+04    0.              .100000E+02    .100E-01   0.
0INCIDENT ELECTRONS
0ELECTRON COLLISION AND RADIATION ENERGY LOSS STRAGGLING
0KNOCK-ON ELECTRON PRODUCTION
0MC COUPLED INELASTIC SCATTERING DEFLECTIONS
0BREMSSTRAHLUNG AND CHARACTERISTIC X-RAY QUANTA FOLLOWED
0BREMSSTRAHLUNG INTRINSIC ANGLE OF EMISSION FROM TABULATED DISTRIBUTION
0PHOTON-PRODUCED PARTICLES FOLLOWED
0 IUNT  LMAX  ITRK  JMAX  IPHK  JPHX  IAPK  KMAX  IBRK  KPHX
    0     1     1    30     1    30     1    10     1    10
0 IMAX  NION IFLUX  NCYC  INRAN
 50000     0     0    -1100000000000000000
0**************** THE STANDARD ERROR ESTIMATES ARE BASED ON    10 BATCHES OF  5000 HISTORIES ****************
0      TIN         TCUT        TPCUT       CTMIN       SORCIN
     1.00000      .01000      .01000      1.00000     3.01000
0      TSAVE                            TMFAC       RLAN        GBLK
       .01000                           10.00000      .50000     1.00000
0ELECTRON ENERGY CLASSIFICATIONS (MEV)
     1.40000     1.40000     1.20000     1.20000     1.20000     1.20000
     1.10000     1.10000     1.05000     1.00000      .95000      .90000
      .85000      .80000      .75000      .70000      .65000      .60000
      .55000      .50000      .45000      .40000      .35000      .30000
      .25000      .20000      .15000      .10000      .05000      .01000
0PHOTON ENERGY CLASSIFICATIONS (MEV)
     1.40000     1.40000     1.20000     1.20000     1.20000     1.20000
     1.10000     1.10000     1.05000     1.00000      .95000      .90000
      .85000      .80000      .75000      .70000      .65000      .60000
      .55000      .50000      .45000      .40000      .35000      .30000
      .25000      .20000      .15000      .10000      .05000      .01000
0ELECTRON OBLIQUITY CLASSIFICATIONS (DEGREES)
    10.00000    20.00000    30.00000    40.00000    50.00000    60.00000
    70.00000    80.00000    90.00000   100.00000   110.00000   120.00000
   130.00000   140.00000   150.00000   160.00000   170.00000   180.00000
0ELECTRON AZIMUTH CLASSIFICATIONS (DEGREES)
   180.00000
0PHOTON OBLIQUITY CLASSIFICATIONS (DEGREES)
    10.00000    20.00000    30.00000    40.00000    50.00000    60.00000
    70.00000    80.00000    90.00000   100.00000   110.00000   120.00000
   130.00000   140.00000   150.00000   160.00000   170.00000   180.00000
0PHOTON AZIMUTH CLASSIFICATIONS (DEGREES)
   180.00000
0NFST       PCMAX      SCALE SKALE       TCUT        TPCUT       TPCJT       TSAVE       DLIM        EMUN        XMUN
    1      .79[illegible]+00     1     1      .01000      .01000     0.00000      .01000     1.00000     0.0         0.0
0K X-RAY QUANTA NOT FOLLOWED IN MATERIAL     1
0ANNIHILATION QUANTA FOLLOWED
1THE PROBLEM IS 100  PER CENT COMPLETE.  TIME TO FINISH IS       0.000 SECONDS. AVERAGE TIME PER BATCH IS      196.787
0AVERAGE SOURCE ENERGY = 1.00000E+00 MEV
0     INPAN          IPA          IMC
 0000000CCCC000000 53[illegible]1[illegible]3[illegible]1[illegible]3[illegible]
0     ---------- HISTORIES ----------                    REJ       --- STEPS ---
      PRIM       SEC      KNOCK      P E      PAIR       COM      AUGER      BREM       RAD       XRAY       LAND       PRIM       SEC
     50000    3[illegible]+0+     [illegible]      0         0         1         0       589      1100         0       1093      81440     [illegible]
```

	ENERGY (MEV)	AVE ENERGY (MEV)	NUMBER/PRIMARY	NUMBER GENERATED
FIRST KNOCK (ABOVE TCUT)	0.0000E-02	4.1000E-02	0.0100E-01	2x99x
TOTAL KNOCK (ABOVE TCUT)	0.0000E-02	4.0000E-02	7.2300E-01	20100
PHOTO-ELECTRON	2.0770E-05	1.4070E-02	0.0000E-04	11
PAIR	0.	0.	0.	0
COMPTON	0.1200E-07	0.0347E-02	4.0000E-00	2
AUGER	0.	0.	0.	0
FIRST BREMSSTRAHLUNG	1.0317E-03	0.0000E-02	1.0000E-02	027
TOTAL BREMSSTRAHLUNG	1.0322E-03	7.4100E-02	0.2100E-02	1100
K X-RAY	0.	0.	0.	0
ANNIHILATION QUANTA	0.	0.	0.	0

UNSCATTERED PRIMARY PHOTONS NUMBER AND ENERGY

0. 00 0. 00

SHAPIRO COEFFICIENTS - KNOCK-ONS, PHOTON DESCENDANTS

TRANSMISSION

0. 00

0. 00

REFLECTION

.90E-02 10

0. 00

LATERAL ESCAPE

.40E-01 1

0. 00

NUMBER AND ENERGY COEFFICIENTS

TRANSMISSION

CYLINDER DIMENSIONS		ELECTRON			PHOTON		
LENGTH(CM)	RADIUS(CM)	NUMBER	ENERGY	COUNTS	NUMBER	ENERGY	COUNTS
.100E+04	.100E+02	0.	00	0	.17E-04 00	.00E-05 00	1

REFLECTION

CYLINDER DIMENSIONS		ELECTRON			PHOTON		
LENGTH(CM)	RADIUS(CM)	NUMBER	ENERGY	COUNTS	NUMBER	ENERGY	COUNTS
.100E+04	.100E+02	.10E-02 14	.13E-03 3%	00	.27E-04 07	.41E-00 75	2

LATERAL ESCAPE

CYLINDER DIMENSIONS		ELECTRON			PHOTON		
LENGTH(CM)	RADIUS(CM)	NUMBER	ENERGY	COUNTS	NUMBER	ENERGY	COUNTS
.100E+04	.100E+02	.10E+01 0	.01E+00 0	00000	.11E-01 0	.11E-02 0	000

ENERGY DEPOSITION

(NORMALIZED TO ONE INCIDENT PARTICLE)

ZONE	MATERIAL	MASS(GM)	VOLUME(CC)	ENERGY DEPOSITION (MEV) PRIM	KNOCK	G-SEC	TOTAL
1	1	.0110E+02	.0203E+05	.1304E+00 0	-.0027E-02 2	.2051E-05 25	.1273E+00 0
2	1	.3074E+03	.0512E+00	.1000E-03 19	-.0500E-05 07	.4725E-06 00	.1407E-03 19
			TOTAL	.1300E+00 0	-.0023E-02 2	.4823E-05 27	.1270E+00 0

CHARGE DISTRIBUTION

(NORMALIZED TO ONE INCIDENT PARTICLE)

ZONE	MATERIAL	ZL	ZR	RI	RO	ELECTRONS PRIM	KNOCK	G-SEC	TOTAL
1	1	0.	.200E+03	0.	.100E+02	0. 00	-.40E-01 2	0. 00	-.40E-01 2
2	1	.200E+03	.100E+04	0.	.100E+02	0. 00	-.00E-04 01	0. 00	-.00E-04 01
			TOTAL			0. 00	-.40E-01 2	0. 00	-.40E-01 2

ENERGY SPECTRA OF TRANSMITTED ELECTRONS

(NUMBER/MEV, NORMALIZED TO ONE INCIDENT PARTICLE)

0 E (MEV) LENGTH= 1000.0000

1.5000 -	1.4500	0.	00
1.4500 -	1.4000	0.	00
1.4000 -	1.3500	0.	00
1.3500 -	1.3000	0.	00
1.3000 -	1.2500	0.	00

0 2 0 2 0 2 0 2

1.2500 -	1.2000	0.	00
1.2000 -	1.1500	0.	00
1.1500 -	1.1000	0.	00
1.1000 -	1.0500	0.	00
1.0500 -	1.0000	0.	00
1.0000 -	.9500	0.	00
.9500 -	.9000	0.	00
.9000 -	.8500	0.	00
.8500 -	.8000	0.	00
.8000 -	.7500	0.	00
.7500 -	.7000	0.	00
.7000 -	.6500	0.	00
.6500 -	.6000	0.	00
.6000 -	.5500	0.	00
.5500 -	.5000	0.	00
.5000 -	.4500	0.	00
.4500 -	.4000	0.	00
.4000 -	.3500	0.	00
.3500 -	.3000	0.	00
.3000 -	.2500	0.	00
.2500 -	.2000	0.	00
.2000 -	.1500	0.	00
.1500 -	.1000	0.	00
.1000 -	.0500	0.	00
.0500 -	.0100	0.	00

ENERGY SPECTRA OF REFLECTED ELECTRONS

(NUMBER/MEV, NORMALIZED TO ONE INCIDENT PARTICLE)

0 E (MEV) LENGTH= 1000.0000

1.5000 -	1.4500	.10E-02 71	
1.4500 -	1.4000	.40E-03 00	
1.4000 -	1.3500	0.	00
1.3500 -	1.3000	0.	00
1.3000 -	1.2500	0.	00
1.2500 -	1.2000	0.	00
1.2000 -	1.1500	0.	00
1.1500 -	1.1000	0.	00
1.1000 -	1.0500	0.	00
1.0500 -	1.0000	0.	00
1.0000 -	.9500	0.	00
.9500 -	.9000	0.	00
.9000 -	.8500	0.	00
.8500 -	.8000	0.	00
.8000 -	.7500	0.	00
.7500 -	.7000	0.	00
.7000 -	.6500	0.	00
.6500 -	.6000	0.	00
.6000 -	.5500	0.	00
.5500 -	.5000	0.	00
.5000 -	.4500	0.	00
.4500 -	.4000	0.	00
.4000 -	.3500	0.	00
.3500 -	.3000	0.	00
.3000 -	.2500	0.	00
.2500 -	.2000	0.	00
.2000 -	.1500	0.	00
.1500 -	.1000	.24E-02 37	
.1000 -	.0500	.04E-02 71	
.0500 -	.0100	.20E-01 14	

ENERGY SPECTRA OF LATERALLY ESCAPING ELECTRONS

(NUMBER/MEV, NORMALIZED TO ONE INCIDENT PARTICLE)

0 E (MEV) LENGTH= 1000.0000

```
 1.4000 -  1.3000   .01E+01  1
 1.3000 -  1.2000   .00E+01  1
 1.2000 -  1.1000   .14E+01  1
 1.1000 -  1.0000   .74E+00  2
 1.0000 -  1.0000   .91E+00  5
 1.1000 -  1.0000   .00E+00  4
 1.0000 -  1.0000   .18E+00  5
 1.0000 -  1.0000   .07E-01  5
 1.0000 -   .9000   .40E-01 13
  .9000 -   .8000   .30E-01 10
  .8000 -   .8000   .10E-01 14
  .8000 -   .8000   .12E-01 10
  .8000 -   .7000   .10E-01  9
  .7000 -   .7000   .00E-00 13
  .7000 -   .8000   .13E-01 14
  .8000 -   .8000   .10E-01 17
  .8000 -   .8000   .10E-01 10
  .8000 -   .8000   .01E-01 11
  .8000 -   .4000   .07E-01  9
  .4000 -   .3000   .00E-01  9
  .3000 -   .3000   .00E-01 10
  .3000 -   .2000   .03E-01  9
  .2000 -   .2000   .00E-01  4
  .2000 -   .2000   .00E-01  5
  .2000 -   .1000   .12E+00  7
  .1000 -   .1000   .10E+00  3
  .1000 -   .0000   .00E+00  0
  .0000 -   .0100   .14E+00  9

                ANGULAR DISTRIBUTIONS OF TRANSMITTED AND REFLECTED ELECTRONS
                    (NUMBER/SR, NORMALIZED TO ONE INCIDENT PARTICLE)

          PHI(DEG)=  0.000
    THETA (DEG)     180.000

  0.0000 -  10.0000   0.        00
 10.0000 -  20.0000   0.        00
 20.0000 -  30.0000   0.        00
 30.0000 -  40.0000   0.        00
 40.0000 -  50.0000   0.        00
 50.0000 -  60.0000   0.        00
 60.0000 -  70.0000   0.        00
 70.0000 -  80.0000   0.        00
 80.0000 - 100.0000   0.        00
100.0000 - 110.0000   .10E-03 35
110.0000 - 120.0000   .04E-03 37
120.0000 - 130.0000   .03E-03 35
130.0000 - 140.0000   .40E-03 01
140.0000 - 150.0000   .02E-03 31
150.0000 - 160.0000   .43E-03 47
160.0000 - 170.0000   .42E-03 01
170.0000 - 180.0000   .42E-03 07

                ANGULAR DISTRIBUTIONS OF LATERALLY ESCAPING ELECTRONS
                    (NUMBER/SR, NORMALIZED TO ONE INCIDENT PARTICLE)

          PHI(DEG)=  0.000
    THETA (DEG)     180.000

  0.0000 -  10.0000   .00E+00  2
 10.0000 -  20.0000   .14E+01  1
 20.0000 -  30.0000   .04E+00  1
 30.0000 -  40.0000   .20E+00  2
 40.0000 -  50.0000   .44E-01  3
 50.0000 -  60.0000   .10E-01  3
 60.0000 -  70.0000   .11E-01  4
```



```
 70.0000 -  80.0000   .70E-02  5
 80.0000 -  90.0000   .00E-02  7
 90.0000 - 100.0000   .40E-02  5
100.0000 - 110.0000   .31E-02  9
110.0000 - 120.0000   .02E-02  5
120.0000 - 130.0000   .17E-02 12
130.0000 - 140.0000   .10E-02 12
140.0000 - 150.0000   .00E-03 13
150.0000 - 160.0000   .39E-03 31
160.0000 - 170.0000   .14E-03 00
170.0000 - 180.0000   .42E-03 07

                ENERGY SPECTRA AND ANGULAR DISTRIBUTIONS OF ELECTRONS TRANSMITTED AND REFLECTED
                    AZIMUTHAL INTERVAL IS    0.00000 TO 180.00000 DEGREES
                    (NUMBER/(MEV*SR), NORMALIZED TO ONE PARTICLE)

     E (MEV)  THETA=  0.000      10.000      20.000      30.000      40.000      50.000      60.000      70.000      80.000
                     10.000      20.000      30.000      40.000      50.000      60.000      70.000      80.000      90.000

 1.5000 -  1.4000   0.        00 0.        00 0.        00 0.        00 0.        00 0.        00 0.        00 0.        00 0.        00
 1.4000 -  1.4000   0.        00 0.        00 0.        00 0.        00 0.        00 0.        00 0.        00 0.        00 0.        00
 1.4000 -  1.3000   0.        00 0.        00 0.        00 0.        00 0.        00 0.        00 0.        00 0.        00 0.        00
 1.3000 -  1.2000   0.        00 0.        00 0.        00 0.        00 0.        00 0.        00 0.        00 0.        00 0.        00
 1.2000 -  1.2000   0.        00 0.        00 0.        00 0.        00 0.        00 0.        00 0.        00 0.        00 0.        00
 1.2000 -  1.1000   0.        00 0.        00 0.        00 0.        00 0.        00 0.        00 0.        00 0.        00 0.        00
 1.1000 -  1.1000   0.        00 0.        00 0.        00 0.        00 0.        00 0.        00 0.        00 0.        00 0.        00
 1.1000 -  1.0000   0.        00 0.        00 0.        00 0.        00 0.        00 0.        00 0.        00 0.        00 0.        00
 1.0000 -  1.0000   0.        00 0.        00 0.        00 0.        00 0.        00 0.        00 0.        00 0.        00 0.        00
 1.0000 -   .9000   0.        00 0.        00 0.        00 0.        00 0.        00 0.        00 0.        00 0.        00 0.        00
  .9000 -   .8000   0.        00 0.        00 0.        00 0.        00 0.        00 0.        00 0.        00 0.        00 0.        00
  .8000 -   .8000   0.        00 0.        00 0.        00 0.        00 0.        00 0.        00 0.        00 0.        00 0.        00
  .8000 -   .8000   0.        00 0.        00 0.        00 0.        00 0.        00 0.        00 0.        00 0.        00 0.        00
  .8000 -   .7000   0.        00 0.        00 0.        00 0.        00 0.        00 0.        00 0.        00 0.        00 0.        00
  .7000 -   .7000   0.        00 0.        00 0.        00 0.        00 0.        00 0.        00 0.        00 0.        00 0.        00
  .7000 -   .8000   0.        00 0.        00 0.        00 0.        00 0.        00 0.        00 0.        00 0.        00 0.        00
  .8000 -   .8000   0.        00 0.        00 0.        00 0.        00 0.        00 0.        00 0.        00 0.        00 0.        00
  .8000 -   .8000   0.        00 0.        00 0.        00 0.        00 0.        00 0.        00 0.        00 0.        00 0.        00
  .8000 -   .4000   0.        00 0.        00 0.        00 0.        00 0.        00 0.        00 0.        00 0.        00 0.        00
  .4000 -   .3000   0.        00 0.        00 0.        00 0.        00 0.        00 0.        00 0.        00 0.        00 0.        00
  .3000 -   .3000   0.        00 0.        00 0.        00 0.        00 0.        00 0.        00 0.        00 0.        00 0.        00
  .3000 -   .2000   0.        00 0.        00 0.        00 0.        00 0.        00 0.        00 0.        00 0.        00 0.        00
  .2000 -   .2000   0.        00 0.        00 0.        00 0.        00 0.        00 0.        00 0.        00 0.        00 0.        00
  .2000 -   .1000   0.        00 0.        00 0.        00 0.        00 0.        00 0.        00 0.        00 0.        00 0.        00
  .1000 -   .0000   0.        00 0.        00 0.        00 0.        00 0.        00 0.        00 0.        00 0.        00 0.        00
  .0000 -   .0100   0.        00 0.        00 0.        00 0.        00 0.        00 0.        00 0.        00 0.        00 0.        00

                ENERGY SPECTRA AND ANGULAR DISTRIBUTIONS OF ELECTRONS TRANSMITTED AND REFLECTED
                    AZIMUTHAL INTERVAL IS    0.00000 TO 180.00000 DEGREES
                    (NUMBER/(MEV*SR), NORMALIZED TO ONE PARTICLE)

     E (MEV)  THETA= 90.000     100.000     110.000     120.000     130.000     140.000     150.000     160.000     170.000
                    100.000     110.000     120.000     130.000     140.000     150.000     160.000     170.000     180.000

 1.5000 -  1.4000   0.        00 0.        00 0.        00 0.        00 .10E-02 67 .64E-03 00 0.        00 0.        00 0.        00
 1.4000 -  1.4000   0.        00 0.        00 0.        00 .45E-03 00 0.        00 0.        00 0.        00 0.        00 0.        00
 1.4000 -  1.3000   0.        00 0.        00 0.        00 0.        00 0.        00 0.        00 0.        00 0.        00 0.        00
 1.3000 -  1.2000   0.        00 0.        00 0.        00 0.        00 0.        00 0.        00 0.        00 0.        00 0.        00
 1.2000 -  1.2000   0.        00 0.        00 0.        00 0.        00 0.        00 0.        00 0.        00 0.        00 0.        00
 1.2000 -  1.1000   0.        00 0.        00 0.        00 0.        00 0.        00 0.        00 0.        00 0.        00 0.        00
 1.1000 -  1.1000   0.        00 0.        00 0.        00 0.        00 0.        00 0.        00 0.        00 0.        00 0.        00
 1.1000 -  1.0000   0.        00 0.        00 0.        00 0.        00 0.        00 0.        00 0.        00 0.        00 0.        00
 1.0000 -  1.0000   0.        00 0.        00 0.        00 0.        00 0.        00 0.        00 0.        00 0.        00 0.        00
 1.0000 -   .9000   0.        00 0.        00 0.        00 0.        00 0.        00 0.        00 0.        00 0.        00 0.        00
  .9000 -   .8000   0.        00 0.        00 0.        00 0.        00 0.        00 0.        00 0.        00 0.        00 0.        00
  .8000 -   .8000   0.        00 0.        00 0.        00 0.        00 0.        00 0.        00 0.        00 0.        00 0.        00
  .8000 -   .8000   0.        00 0.        00 0.        00 0.        00 0.        00 0.        00 0.        00 0.        00 0.        00
  .8000 -   .7000   0.        00 0.        00 0.        00 0.        00 0.        00 0.        00 0.        00 0.        00 0.        00
  .7000 -   .7000   0.        00 0.        00 0.        00 0.        00 0.        00 0.        00 0.        00 0.        00 0.        00
  .7000 -   .8000   0.        00 0.        00 0.        00 0.        00 0.        00 0.        00 0.        00 0.        00 0.        00
  .8000 -   .8000   0.        00 0.        00 0.        00 0.        00 0.        00 0.        00 0.        00 0.        00 0.        00
  .8000 -   .8000   0.        00 0.        00 0.        00 0.        00 0.        00 0.        00 0.        00 0.        00 0.        00
  .8000 -   .4000   0.        00 0.        00 0.        00 0.        00 0.        00 0.        00 0.        00 0.        00 0.        00
  .4000 -   .3000   0.        00 0.        00 0.        00 0.        00 0.        00 0.        00 0.        00 0.        00 0.        00
  .3000 -   .3000   0.        00 0.        00 0.        00 0.        00 0.        00 0.        00 0.        00 0.        00 0.        00
  .3000 -   .2000   0.        00 0.        00 0.        00 0.        00 0.        00 0.        00 0.        00 0.        00 0.        00
  .2000 -   .2000   0.        00 0.        00 0.        00 0.        00 0.        00 0.        00 0.        00 0.        00 0.        00
  .2000 -   .1000   0.        00 0.        00 0.        00 0.        00 0.        00 0.        00 0.        00 0.        00 0.        00
  .1000 -   .1000   0.        00 0.        00 0.        00 0.        00 0.        00 0.        00 0.        00 0.        00 0.        00
  .1000 -   .0000   0.        00 0.        00 0.        00 0.        00 0.        00 0.        00 0.        00 0.        00 0.        00
  .0000 -   .0100   0.        00 0.        00 0.        00 0.        00 0.        00 0.        00 0.        00 0.        00 0.        00
```

ENERGY SPECTRA AND ANGULAR DISTRIBUTIONS OF ELECTRONS LATERALLY ESCAPING
AZIMUTHAL INTERVAL IS 0.00000 TO 180.00000 DEGREES
(NUMBER/(MEV*SR), NORMALIZED TO ONE PARTICLE)

E (MEV)	THETA= 0.000	10.000	20.000	30.000	40.000	50.000	60.000	70.000	80.000
	10.000	20.000	30.000	40.000	50.000	60.000	70.000	80.000	90.000
1.0000 - 1.4000	.8XE-02 67	.8XE+00 10	.8XE+00 9	.8XE+00 9	.8XE-01 6	.4XE-01 10	.1XE-01 10	.8XE-02 67	
1.4000 - 1.4000	.8XE+01 0	.8XE+01 1	.8XE+01 1	.1XE+01 0	.2XE+00 7	.7XE-01 0	.3XE-01 10	.1XE-01 13	.1XE-01 10
1.4000 - 1.3000	.4XE+01 0	.4XE+01 0	.4XE+01 0	.1XE+00 0	.4XE-01 10	.2XE-01 12	.8XE-02 20	.4XE-02 20	
1.3000 - 1.3000	.2XE+01 0	.9XE+01 0	.2XE+01 0	.9XE+00 0	.8XE-01 10	.2XE-01 12	.9XE-02 20	.3XE-02 20	
1.3000 - 1.2000	.1XE+01 0	.2XE+01 0	.1XE+01 0	.2XE+00 0	.9XE-01 0	.1XE-01 21	.6XE-02 20	.1XE-02 33	.8XE-02 51
1.2000 - 1.2000	.6XE+00 0	.1XE+01 0	.6XE+00 0	.1XE+00 0	.8XE-01 10	.4XE-02 33	.2XE-02 37	.1XE-02 71	0.
1.2000 - 1.1000	.3XE+00 10	.6XE+00 0	.3XE+00 0	.6XE-01 0	.1XE-01 14	.7XE-02 27	.1XE-02 41	.2XE-02 33	0.
1.1000 - 1.1000	.1XE+00 14	.3XE+00 0	.1XE+00 7	.4XE-01 11	.8XE-02 27	.4XE-02 20	.1XE-02 67	0.	.3XE-03
1.1000 - 1.0000	.6XE-01 10	.1XE+00 7	.1XE+00 0	.2XE-01 10	.8XE-02 23	0.	.8XE-03 67	.3XE-03	0.
1.0000 - 1.0000	.1XE-01 00	.8XE-01 10	.4XE-01 17	.2XE-01 0	.2XE-02 45	.8XE-03 67	0.	0.	0.
1.0000 - .9000	.8XE-01 61	.4XE-01 10	.2XE-01 10	.1XE-01 30	.2XE-02 00	.4XE-03 00	0.	0.	0.
.9000 - .9000	.1XE-01 41	.2XE-01 20	.2XE-01 20	.8XE-02 20	.2XE-02 00	.1XE-02 51	0.	.3XE-03	0.
.9000 - .8000	.4XE-02 00	.1XE-01 27	.1XE-01 23	.6XE-02 33	0.	0.	0.	0.	.3XE-03
.8000 - .8000	0.	.1XE-01 30	.8XE-02 20	.3XE-02 31	.1XE-02 00	0.	.4XE-03 00	.3XE-03	0.
.8000 - .7000	.6XE-02 67	.4XE-02 31	.2XE-02 10	.2XE-02 41	.2XE-02 45	0.	0.	0.	0.
.7000 - .7000	.4XE-02 00	.2XE-02 37	.1XE-02 33	.3XE-02 37	.1XE-02 20	0.	0.	0.	0.
.7000 - .6000	0.	.3XE-02 30	.3XE-02 41	.2XE-02 20	.4XE-02 20	.1XE-02 51	.1XE-02 71	0.	0.
.6000 - .6000	0.	.2XE-02 37	.2XE-02 41	.1XE-02 20	.3XE-02 37	.3XE-02 30	.4XE-03 00	.3XE-03 00	0.
.6000 - .6000	.4XE-02 00	0.	.2XE-02 31	.2XE-02 31	.1XE-02 20	.2XE-02 33	.2XE-02 00	.2XE-02 67	.2XE-02 00
.6000 - .5000	0.	.2XE-02 67	.1XE-02 00	.1XE-01 00	.2XE-02 00	.4XE-02 20	.4XE-02 20	.3XE-02 00	.2XE-02 00
.5000 - .5000	0.	.2XE-02 67	.1XE-02 44	.2XE-02 17	.2XE-02 10	.2XE-02 23	.3XE-02 20	.1XE-02 51	.1XE-02 51
.5000 - .4000	0.	.4XE-02 51	.4XE-02 33	.2XE-02 17	.2XE-02 10	.2XE-02 10	.2XE-02 23	.1XE-02 46	.2XE-02 45
.4000 - .3000	0.	.6XE-02 41	.6XE-02 33	.3XE-02 20	.2XE-02 10	.2XE-02 10	.2XE-02 10	.2XE-02 27	.1XE-02 33
.3000 - .2500	0.	.8XE-02 41	.3XE-02 41	.1XE-01 20	.1XE-01 20	.1XE-01 10	.1XE-01 20	.8XE-02 23	.2XE-02 33
.2500 - .2000	.8XE-02 67	.1XE-01 33	.1XE-01 33	.1XE-01 17	.7XE-02 20	.1XE-01 12	.1XE-01 21	.1XE-01 13	.2XE-02 28
.2000 - .1500	.4XE-02 00	.4XE-02 51	.2XE-02 20	.1XE-01 20	.1XE-01 19	.2XE-02 11	.1XE-01 10	.1XE-01 16	.1XE-01 13
.1500 - .1000	0.	.2XE-02 67	.2XE-02 45	.1XE-01 20	.1XE-01 20	.2XE-02 11	.1XE-01 10	.1XE-01 20	.2XE-02 13
.1000 - .0500	.4XE-02 00	.2XE-02 37	.4XE-02 45	.1XE-01 20	.2XE-02 20	.2XE-02 11	.2XE-01 10	.2XE-01 20	.1XE-01 10
.0500 - .0100	0.	.1XE-02 00	.1XE-02 00	.2XE-02 20	.1XE-01 20	.1XE-01 27	.1XE-01 00	.1XE-01 20	.1XE-01 00

ENERGY SPECTRA AND ANGULAR DISTRIBUTIONS OF ELECTRONS LATERALLY ESCAPING
AZIMUTHAL INTERVAL IS 0.00000 TO 180.00000 DEGREES
(NUMBER/(MEV*SR), NORMALIZED TO ONE PARTICLE)

E (MEV)	THETA= 90.000	100.000	110.000	120.000	130.000	140.000	150.000	160.000	170.000
	100.000	110.000	120.000	130.000	140.000	150.000	160.000	170.000	180.000
1.0000 - 1.4000	.2XE-02 37	.1XE-02 33	.1XE-02 00	0.	00	0.	00	.6XE-03 00	0.	00	0.	00	0.	00
1.4000 - 1.4000	.8XE-02 20	.3XE-02 40	.8XE-03 67	.6XE-03 67	.6XE-03 00	.6XE-03 00	0.	00	0.	00	0.	00	0.	00
1.4000 - 1.3000	.2XE-02 44	.1XE-02 40	.4XE-03 00	.4XE-03 00	.4XE-03 00	0.	00	0.	00	0.	00	0.	00	0.	00

1.3000 - 1.3000	.8XE-02 43	.3XE-03 00	.4XE-03 00	0.	00	0.	00	.6XE-03 00	0.	00	0.	00	0.	00	0.	00	0.	00	0.
1.3000 - 1.2500	.1XE-02 71	.3XE-03 00	.8XE-03 67	0.	00	0.	00	0.	00	0.	00	0.	00	0.	00	0.	00	0.	00
1.2500 - 1.2000	.1XE-02 00	0.	00	.4XE-03 00	.4XE-03 00	0.	00	0.	00	0.	00	0.	00	0.	00	0.	00	0.	00
1.2000 - 1.1500	.3XE-03 00	0.	00	0.	00	.4XE-03 00	0.	00	0.	00	0.	00	0.	00	0.	00	0.	00	0.
1.1500 - 1.1000	0.	.7XE-03 67	0.	00	0.	00	0.	00	0.	00	0.	00	0.	00	0.	00	0.	00	0.
1.1000 - 1.0500	.3XE-03 00	0.	00	0.	00	0.	00	0.	00	0.	00	0.	00	0.	00	0.	00	0.	00
1.0500 - 1.0000	0.	00	0.	00	0.	00	0.	00	0.	00	0.	00	0.	00	0.	00	0.	00	0.
1.0000 - .9500	0.	00	0.	00	0.	00	0.	00	0.	00	0.	00	0.	00	0.	00	0.	00	0.
.9500 - .9000	0.	00	0.	00	0.	00	0.	00	0.	00	0.	00	0.	00	0.	00	0.	00	0.
.9000 - .8500	0.	00	0.	00	0.	00	0.	00	0.	00	0.	00	0.	00	0.	00	0.	00	0.
.8500 - .8000	0.	00	0.	00	0.	00	0.	00	0.	00	0.	00	0.	00	0.	00	0.	00	0.
.8000 - .7500	0.	.3XE-03 00	0.	00	0.	00	0.	00	0.	00	0.	00	0.	00	0.	00	0.	00	0.
.7500 - .7000	0.	00	0.	00	0.	00	0.	00	0.	00	0.	00	0.	00	0.	00	0.	00	0.
.7000 - .6500	0.	00	0.	00	0.	00	0.	00	0.	00	0.	00	0.	00	0.	00	0.	00	0.
.6500 - .6000	0.	00	0.	00	0.	00	0.	00	0.	00	0.	00	0.	00	0.	00	0.	00	0.
.6000 - .5500	0.	00	0.	00	0.	00	0.	00	0.	00	0.	00	0.	00	0.	00	0.	00	0.
.5500 - .5000	0.	00	0.	00	0.	00	0.	00	0.	00	0.	00	0.	00	0.	00	0.	00	0.
.5000 - .4500	0.	00	0.	00	0.	00	0.	00	0.	00	0.	00	0.	00	0.	00	0.	00	0.
.4500 - .4000	.1XE-02 71	.3XE-03 00	0.	00	0.	00	.3XE-03 00	0.	00	0.	00	0.	00	0.	00	0.	00	0.	00
.4000 - .3500	0.	.3XE-03 00	.8XE-03 00	0.	00	0.	00	.6XE-03 00	0.	00	0.	00	0.	00	0.	00	0.	00	0.
.3500 - .3000	.1XE-02 33	.7XE-03 67	.4XE-03 00	.4XE-03 00	0.	00	0.	00	0.	00	0.	00	0.	00	0.	00	0.	00	0.
.3000 - .2500	.1XE-02 51	.7XE-03 67	.4XE-03 00	.4XE-03 00	0.	00	0.	00	0.	00	0.	00	0.	00	0.	00	0.	00	0.
.2500 - .2000	.6XE-02 20	.4XE-02 21	.2XE-02 22	.6XE-03 00	.6XE-03 00	0.	00	0.	00	0.	00	0.	00	0.	00	0.	00	0.	00
.2000 - .1500	.9XE-02 15	.6XE-02 27	.3XE-02 27	.4XE-02 31	.3XE-02 44	0.	00	.6XE-03 00	0.	00	0.	00	0.	00	0.	00	0.	00	0.
.1500 - .1000	.1XE-01 10	.1XE-01 14	.9XE-02 14	.7XE-02 25	.4XE-02 31	.9XE-02 20	.2XE-02 51	.1XE-02 00	.4XE-02 00	0.	00	0.	00	0.	00	0.	00	0.	00
.1000 - .0500	.2XE-01 10	.1XE-01 10	.1XE-01 10	.1XE-01 9	.1XE-01 20	.7XE-02 27	.2XE-02 51	.1XE-02 00	0.	00	0.	00	0.	00	0.	00	0.	00	0.
.0500 - .0100	.1XE-01 0	.1XE-01 10	.1XE-01 23	.9XE-02 17	.1XE-01 20	.9XE-02 00	0.	00	0.	00	0.	00	0.	00	0.	00	0.	00	0.

ENERGY SPECTRA OF TRANSMITTED PHOTONS
(NUMBER/MEV, NORMALIZED TO ONE INCIDENT PARTICLE)

E (MEV) LENGTH= 1000.0000

1.0000 - 1.4000	0.	00	
1.4000 - 1.4000	0.	00	
1.4000 - 1.3000	0.	00	
1.3000 - 1.3000	0.	00	
1.3000 - 1.2500	0.	00	
1.2500 - 1.2000	0.	00	
1.2000 - 1.1500	0.	00	
1.1500 - 1.1000	0.	00	
1.1000 - 1.0500	0.	00	
1.0500 - 1.0000	0.	00	
1.0000 - .9500	0.	00	
.9500 - .9000	0.	00	
.9000 - .8500	0.	00	
.8500 - .8000	0.	00	
.8000 - .7500	0.	00	
.7500 - .7000	0.	00	
.7000 - .6500	0.	00	
.6500 - .6000	0.	00	
.6000 - .5500	0.	00	
.5500 - .5000	0.	00	
.5000 - .4500	0.	00	
.4500 - .4000	0.	00	
.4000 - .3500	0.	00	
.3500 - .3000	0.	00	
.3000 - .2500	0.	00	
.2500 - .2000	.3XE-03 00		
.2000 - .1500	0.	00	
.1500 - .1000	0.	00	
.1000 - .0500	0.	00	
.0500 - .0100	0.	00	

ENERGY SPECTRA OF REFLECTED PHOTONS
(NUMBER/MEV, NORMALIZED TO ONE INCIDENT PARTICLE)

E (MEV) LENGTH= 1000.0000

1.5000 -	1.4000	0.	99
1.4000 -	1.4000	0.	99
1.4000 -	1.3000	0.	99
1.3000 -	1.3000	0.	99
1.3000 -	1.2000	0.	99
1.2000 -	1.2000	0.	99
1.2000 -	1.1000	0.	99
1.1000 -	1.1000	0.	99
1.1000 -	1.0000	0.	99
1.0000 -	.9000	0.	99
.9000 -	.9000	0.	99
.9000 -	.8000	0.	99
.8000 -	.8000	0.	99
.8000 -	.7000	0.	99
.7000 -	.7000	0.	99
.7000 -	.6000	0.	99
.6000 -	.6000	0.	99
.6000 -	.5000	0.	99
.5000 -	.5000	0.	99
.5000 -	.4000	0.	99
.4000 -	.4000	0.	99
.4000 -	.3000	0.	99
.3000 -	.3000	0.	99
.3000 -	.2000	0.	99
.2000 -	.2000	0.	99
.2000 -	.1000	0.	99
.1000 -	.1000	0.	99
.0000 -	.0100	.00E-03	97

ENERGY SPECTRA OF LATERALLY ESCAPING PHOTONS
(NUMBER/REV, NORMALIZED TO ONE INCIDENT PARTICLE)

E (MEV) LENGTH= 1000.0000

1.5000 -	1.4000	0.	99
1.4000 -	1.4000	0.	99
1.4000 -	1.3000	0.	99
1.3000 -	1.3000	.40E-03	99
1.3000 -	1.2000	0.	99
1.2000 -	1.2000	.40E-03	99
1.2000 -	1.1000	.40E-03	99
1.1000 -	1.1000	.40E-03	99
1.1000 -	1.0000	.40E-03	99
1.0000 -	1.0000	.40E-03	99
1.0000 -	.9000	.40E-03	99
.9000 -	.9000	0.	99
.9000 -	.8000	.10E-02	91
.8000 -	.8000	0.	99
.8000 -	.7000	.80E-03	99
.7000 -	.7000	.10E-02	91
.7000 -	.6000	.12E-02	91
.6000 -	.6000	.80E-03	31
.6000 -	.5000	.24E-02	49
.5000 -	.5000	.12E-02	91
.5000 -	.4000	.40E-03	17
.4000 -	.4000	.40E-03	37
.4000 -	.3000	.80E-03	22
.3000 -	.3000	.88E-03	39
.3000 -	.2000	.88E-03	25
.2000 -	.2000	.88E-03	10
.2000 -	.1000	.10E-01	10
.1000 -	.1000	.10E-01	13
.1000 -	.0000	.44E-01	0

L 2 R 2

.0000 -	.0100	.12E+00	7

ANGULAR DISTRIBUTIONS OF TRANSMITTED AND REFLECTED PHOTON INTENSITY
(MEV/SR, NORMALIZED TO ONE INCIDENT PARTICLE)

PHI(DEG)= 0.000

THETA (DEG) 180.000

0.0000 -	10.0000	.44E-04	99
10.0000 -	20.0000	0.	99
20.0000 -	30.0000	0.	99
30.0000 -	40.0000	0.	99
40.0000 -	50.0000	0.	99
50.0000 -	60.0000	0.	99
60.0000 -	70.0000	0.	99
70.0000 -	80.0000	0.	99
80.0000 -	90.0000	0.	99
90.0000 -	100.0000	0.	99
100.0000 -	110.0000	0.	99
110.0000 -	120.0000	0.	99
120.0000 -	130.0000	0.	99
130.0000 -	140.0000	0.	99
140.0000 -	150.0000	0.	99
150.0000 -	160.0000	0.	99
160.0000 -	170.0000	0.	99
170.0000 -	180.0000	.00E-99	73

ANGULAR DISTRIBUTIONS OF LATERALLY ESCAPING PHOTON INTENSITY
(MEV/SR, NORMALIZED TO ONE INCIDENT PARTICLE)

PHI(DEG)= 0.000

THETA (DEG) 180.000

0.0000 -	10.0000	.38E-02	17
10.0000 -	20.0000	.18E-02	12
20.0000 -	30.0000	.88E-03	17
30.0000 -	40.0000	.72E-03	28
40.0000 -	50.0000	.12E-03	24
50.0000 -	60.0000	.48E-04	38
60.0000 -	70.0000	.44E-04	83
70.0000 -	80.0000	.18E-04	88
80.0000 -	90.0000	.88E-05	82
90.0000 -	100.0000	.72E-06	81
100.0000 -	110.0000	.88E-06	70
110.0000 -	120.0000	.22E-06	88
120.0000 -	130.0000	.17E-06	87
130.0000 -	140.0000	.22E-06	88
140.0000 -	150.0000	.44E-06	88
150.0000 -	160.0000	0.	99
160.0000 -	170.0000	0.	99
170.0000 -	180.0000	0.	99

ENERGY SPECTRA AND ANGULAR DISTRIBUTIONS OF PHOTONS TRANSMITTED AND REFLECTED
AZIMUTHAL INTERVAL IS 0.0000 TO 180.00000 DEGREES
(NUMBER/(MEV*SR), NORMALIZED TO ONE PARTICLE)

E (MEV)	THETA=	0.000 10.000	10.000 20.000	20.000 30.000	30.000 40.000	40.000 50.000	50.000 60.000	60.000 70.000	70.000 80.000	80.000 90.000	
1.5000 -	1.4000	0.	99	0.	99	0.	99	0.	99	0.	99
1.4000 -	1.4000	0.	99	0.	99	0.	99	0.	99	0.	99
1.4000 -	1.3000	0.	99	0.	99	0.	99	0.	99	0.	99
1.3000 -	1.3000	0.	99	0.	99	0.	99	0.	99	0.	99
1.3000 -	1.2000	0.	99	0.	99	0.	99	0.	99	0.	99
1.2000 -	1.2000	0.	99	0.	99	0.	99	0.	99	0.	99
1.2000 -	1.1000	0.	99	0.	99	0.	99	0.	99	0.	99
1.1000 -	1.1000	0.	99	0.	99	0.	99	0.	99	0.	99
1.1000 -	1.0000	0.	99	0.	99	0.	99	0.	99	0.	99
1.0000 -	.9000	0.	99	0.	99	0.	99	0.	99	0.	99

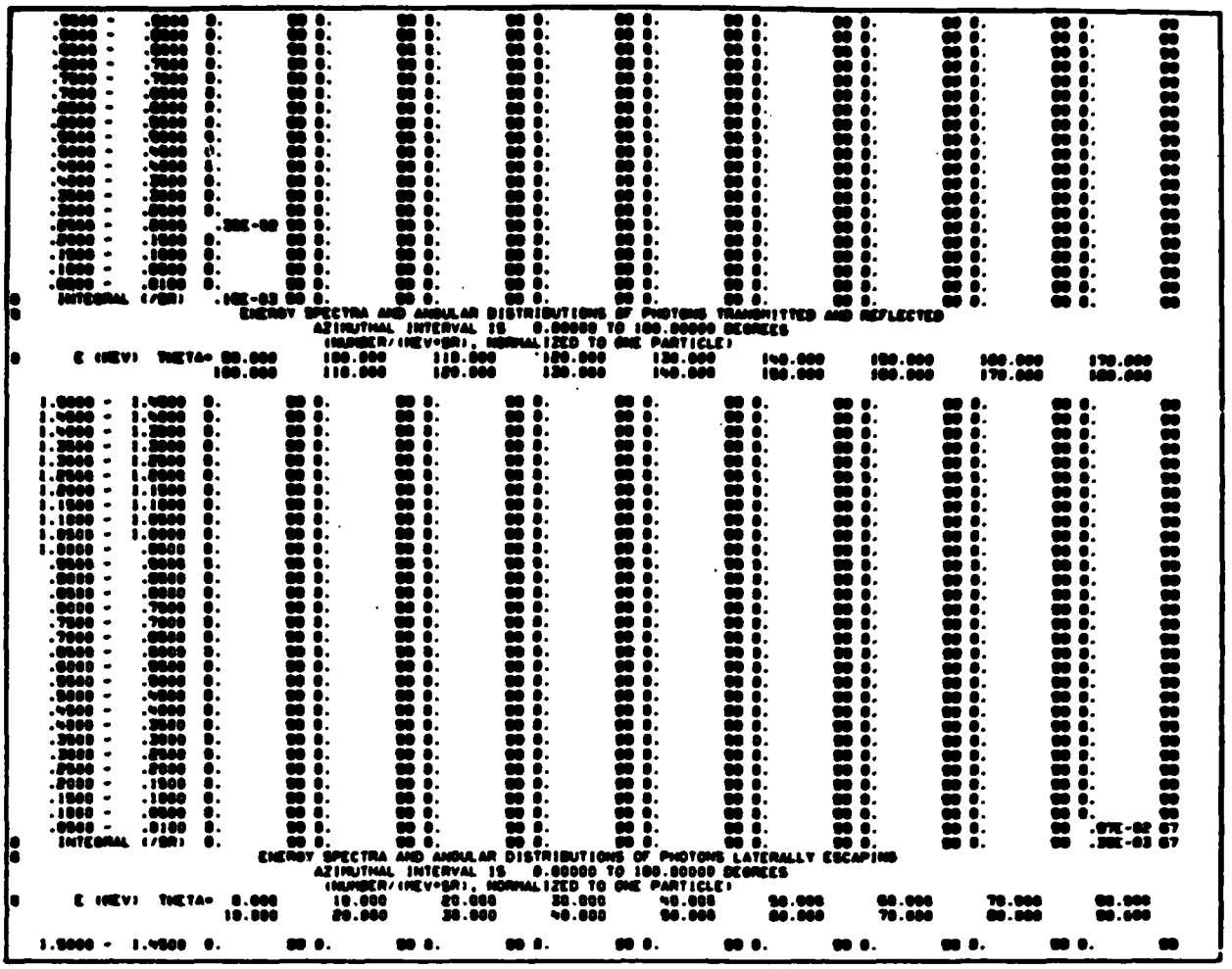

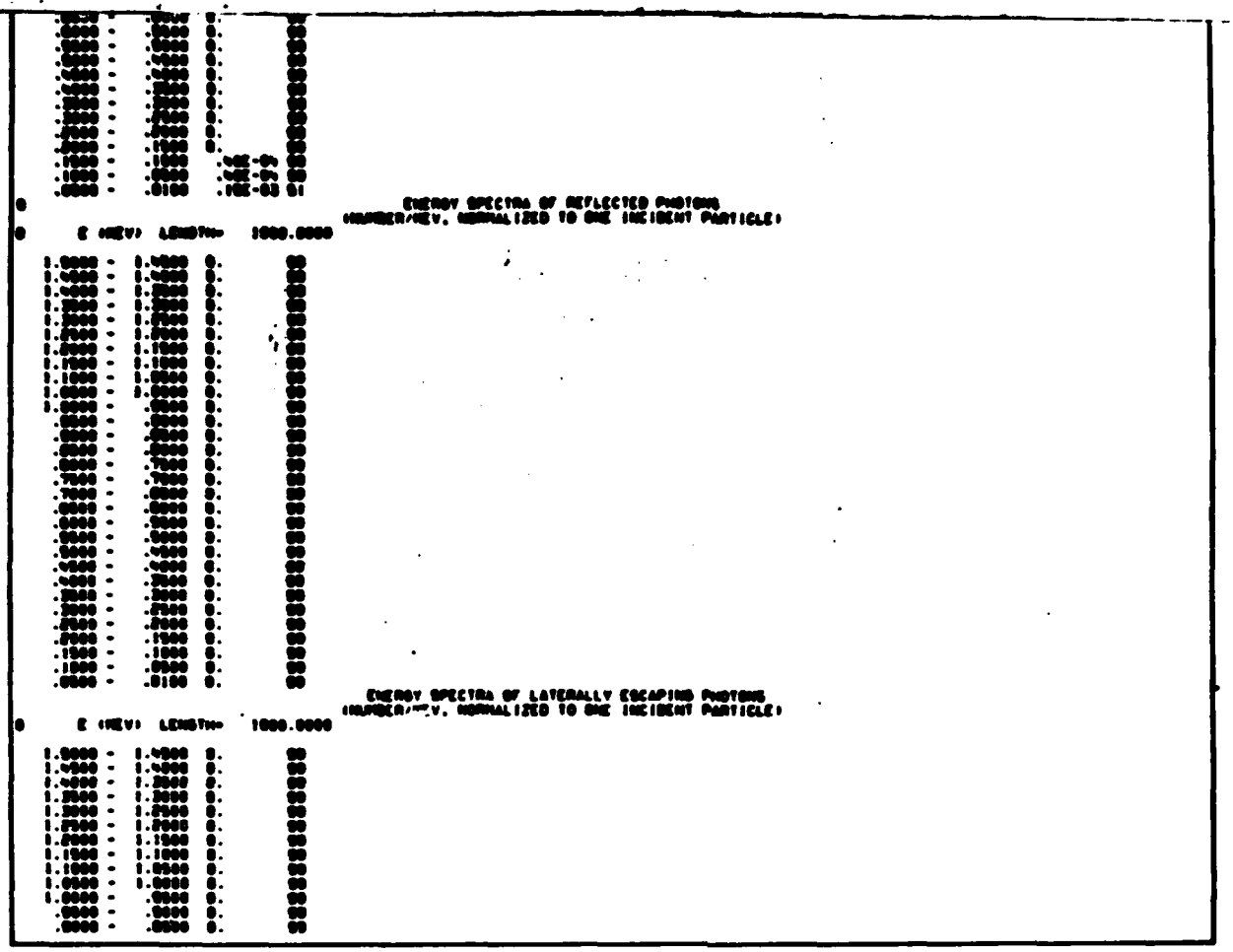

ENERGY SPECTRA OF REFLECTED PHOTONS
(NUMBER/MEV, NORMALIZED TO ONE INCIDENT PARTICLE)

E (MEV) LENGTH= 1000.0000

ENERGY SPECTRA OF LATERALLY ESCAPING PHOTONS
(NUMBER/MEV, NORMALIZED TO ONE INCIDENT PARTICLE)

E (MEV) LENGTH= 1000.0000

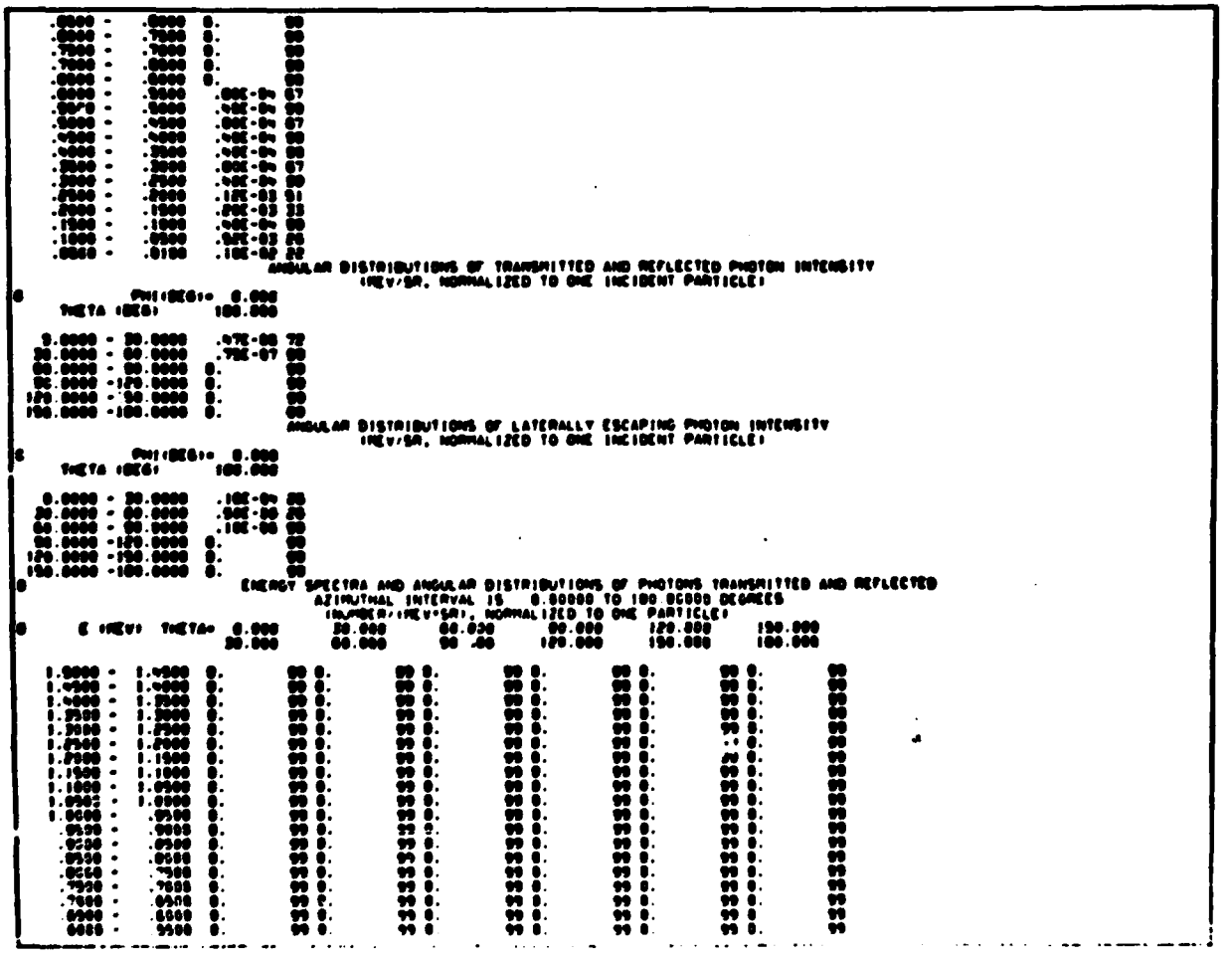

ANGULAR DISTRIBUTIONS OF TRANSMITTED AND REFLECTED PHOTON INTENSITY
(MEV/SR, NORMALIZED TO ONE INCIDENT PARTICLE)

PHI (DEG)= 0.000

THETA (DEG) 180.000

ANGULAR DISTRIBUTIONS OF LATERALLY ESCAPING PHOTON INTENSITY
(MEV/SR, NORMALIZED TO ONE INCIDENT PARTICLE)

PHI (DEG)= 0.000

THETA (DEG) 180.000

ENERGY SPECTRA AND ANGULAR DISTRIBUTIONS OF PHOTONS TRANSMITTED AND REFLECTED
AZIMUTHAL INTERVAL IS 0.00000 TO 180.0000 DEGREES
(NUMBER/(MEV*SR)), NORMALIZED TO ONE PARTICLE)

E (MEV) THETA= 0.000 30.000 60.000 90.000 120.000 150.000 180.000

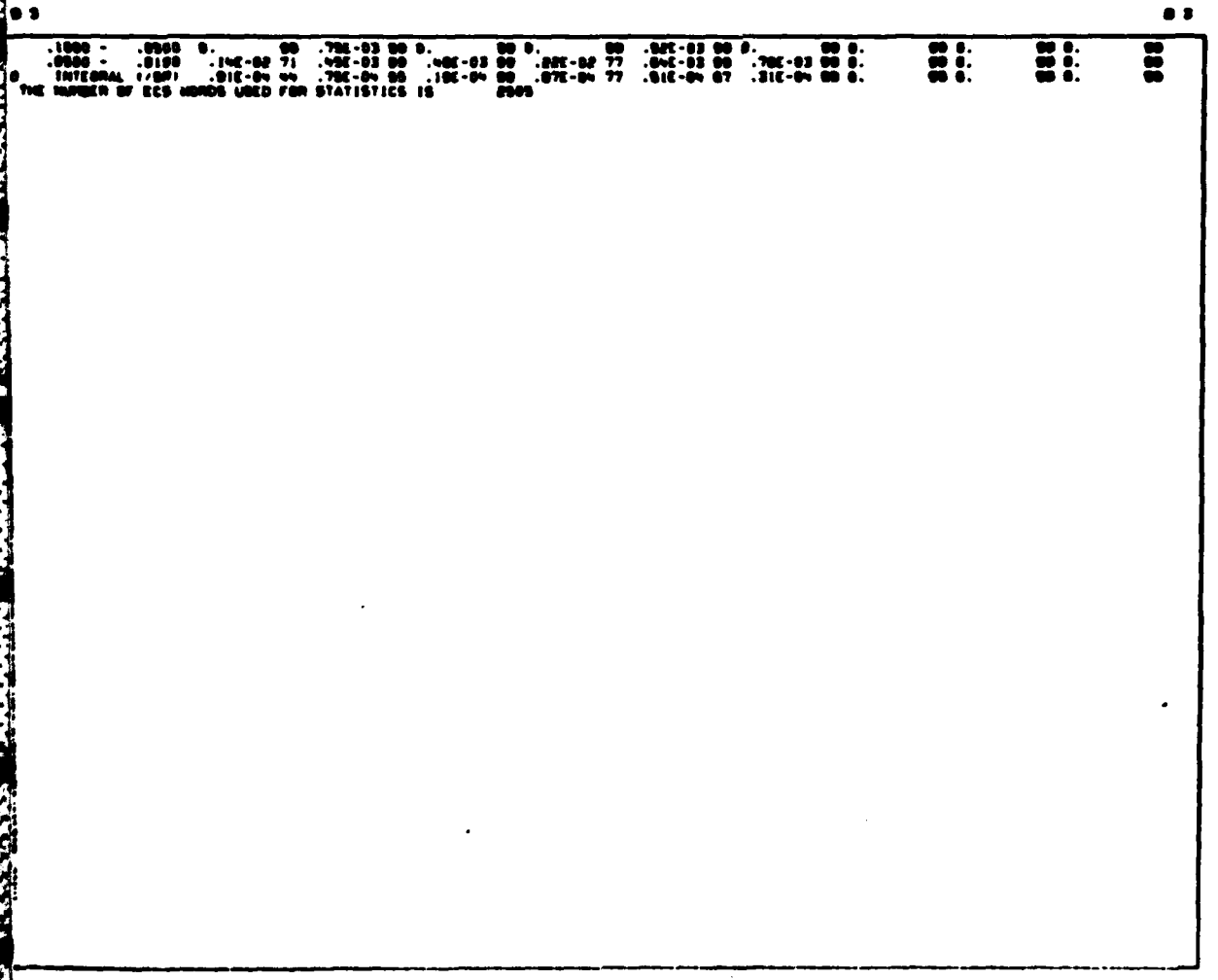
.1000 - .0500 0. 00 .70E-03 00 0. 00 0. 00 .52E-03 00 0. 00 0. 00 0. 00
.0500 - .0100 .14E-02 71 .95E-03 00 .40E-03 00 .82E-02 77 .04E-03 00 .70E-03 00 0. 00 0. 00 0. 00
0 INTEGRAL (/DT) .01E-04 00 .70E-04 00 .10E-04 00 .07E-04 77 .01E-04 67 .31E-04 00 0. 00 0. 00 0. 00
THE NUMBER OF ECG WORDS USED FOR STATISTICS IS 2005

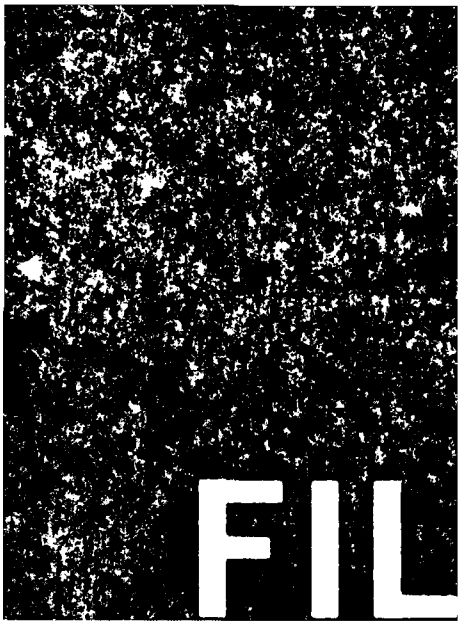
FIL